The University Of Sheffield.

Bioactive surfaces for the delivery of nerve growth factor and brain derived neurotrophic factor and its effects in neurite outgrowth

Ana Maria Sandoval Castellanos

A thesis submitted in partial fulfilment of the requirements for the degree of Doctor of Philosophy

The University of Sheffield
Faculty of Engineering
Department of Materials Science and Engineering

July 2021

Acknowledgments

“We can only be said to be alive in those moments when our heart are conscious of our treasures”

-Thorton Wilder-

There are not enough or right words to express my gratitude, even though the wise words from Mr Wilder are close enough,…Until I find them:

!!!Muchas gracias!!!

Prof John Haycock Dr Frederik Claeyssens

Dr Andrea Sandoval Castellanos, David Ramos Rodriguez, Sara Memarpour, Dr Alejandra Peñuelas, Ana Isabel Casas, Xavier Sanuy, Mom, Dad, Ana Jimenez, Sergio Rodriguez, Dr Mehri Behbehani, Dr Deborah Hammond, Dr Ahtasham Raza, Dr Harriet Drouin, Erika Alvarez, Paulina Martin del Campo, Ma. Jose Minakata, Carlos Santillanes.

CONACyT, thanks for your financial support.

Table of Contents

Abbreviations

2 dimensional	2D
3 dimensional	3D
Amine groups	NH_2^+
Analysis of variance	ANOVA
Basic fibroblast growth factor	bFGF
Brain derived neurotrophic factor	BDNF
Central Nervous System	CNS
Ciliary neurotrophic factor	CNTF
4', 6-diamidino-2-phenylindole	DAPI
Distilled water	dH_2O
Dichloromethane	DCM
Dorsal root ganglia	DRG
Dulbecco's Modified Eagle's Medium	DMEM
Extracellular matrix	ECM
Embryonic development day	EDD
Epidermal growth factor	EGF
Enzyme-linked immunosorbent assay	ELISA
Formaldehyde	FA

Food and drug administration	FDA
Glycosaminoglycan	GAG
Glial cell-derived neurotrophic factor	GDNF
Nerve guide conduit	NGC
Nerve growth factor	NGF
Nerve growth factor plus brain derived neurotrophic factor	NGF plus BDNF
Neurotrophin 3	NT-3
Neurotrophin 4/5	NT-4/5
P 75 neurotrophin receptor	$P75^{NRT}$
Phosphate buffered saline	PBS
Polycaprolactone	PCL
Peripheral nervous system	PNS
Polystyrene	PS
Radio frequency generator	RF generator
Stromal cell-derived factor	SDF-1
Scanning electron microscopy	SEM
Tissue Culture Plastic	TCP
Tyrosine kinase receptor A	TkrA
Tyrosine kinase receptor B	TkrB
Tetramethylrhodamine isothiocyanate	TRITC
Ultraviolet	UV

Vascular endothelial growth factor	VEGF
X- ray photoelectron spectroscopy	XPS

Figure index

Table index

Equation index

Publications and presentations

- Publications

Sandoval-Castellanos AM, Claeyssens F, Haycock JW. Biomimetic delivery of NGF and BDNF to enhance neurite outgrowth. Biotechnology and Bioengineering. 2020; vol. 117, no. 10, pp. 3124-3135. https://doi.org/10.1002/bit.27466

Schuh C.M.A.P., **Sandoval-Castellanos AM**., De Gregorio C., Contreras-Kallens P., Haycock J.W. (2020) The Role of Schwann Cells in Peripheral Nerve Function, Injury, and Repair. In: Gimble J., Marolt Presen D., Oreffo R., Redl H., Wolbank S. (eds) Cell Engineering and Regeneration. Reference Series in Biomedical Engineering. Springer, Cham.

- Publications in review

Sandoval-Castellanos AM, Claeyssens F, Haycock JW. Bioactive 3D scaffolds for the delivery of NGF and BDNF to improve nerve regeneration. Submitted to Frontiers in Materials, July 2021.

- Oral presentation

1. Bioactive surface as a platform for the delivery of immobilised NGF and BDNF and the effect in neurite outgrowth. 11th World Biomaterials Congress 2020. 11th December - 15th December 2020. Online.

- Poster presentation

1. Biomaterial surface functionalization for sustained delivery of NGF and BDNF to stimulate neurite growth. 6th World Congress of the Tissue Engineering and Regenerative Medicine International Society (TERMIS 2021). 15th November – 19th November 2021 in Maastricht, The Netherlands.
2. Bioactive 3D scaffolds for the delivery of neurotrophins to improve neurite outgrowth and induce Schwann cell migration. 6th World Congress of the Tissue Engineering and Regenerative Medicine International Society

(TERMIS 2021). 15th November – 19th November 2021 in Maastricht, The Netherlands.

3. Delivery of immobilised NGF and BDNF via a bioactive surface to enhance neurite outgrowth. Biomaterials and Tissue Engineering Group conference 2020. 17th December 2020. Online (+90 seconds presentation).

4. A comparative study to evaluate bioactive surfaces to deliver NGF and BDNF on neuronal cells. Biomaterials and Tissue Engineering Group conference 2019. 16th December 2019 in York, England.

5. A comparative study to evaluate bioactive surfaces to deliver NGF and BDNF on neuronal cells. Tissue and Cell Engineering Society and United Kingdom Society of Biomaterials Conference 2019. 11th – 13th June 2019 in Nottingham, England.

6. A Comparative Study to Evaluate Bioactive Surfaces to deliver NGF and BDNF on Nerve Cell Behaviour. Biomaterials and Tissue Engineering Group conference 2018. 17th December 2018 in Sheffield, England (+90 seconds presentation).

7. Transient Immobilisation and Release of Nerve Growth Factor in a Modified Heparin / Allylamine Surface to Promote Neurite Outgrowth. Tissue and Cell Engineering Society Conference 2018. 2nd-4th July 2018 in Keele, England.

8. Transient Immobilisation and Release of Nerve Growth Factor in a Modified Heparin / Allylamine Surface to Promote Neurite Outgrowth. Biomaterials and Tissue Engineering Group conference 2017. 18th December 2017 in Leeds, England (+90 seconds presentation).

Chapter 1 Introduction

Peripheral nerve injury is a severe condition that affects the quality of life of a patient as sensory and motor function are impaired. Current treatments include end-to-end suturing and end-to-side suturing of the injured nerve to restore function. The gold standard treatment for larger peripheral nerve injuries is the use of autografts, however, these are limited by donor site morbidity and size mismatches. Alternatively, allografts and xenografts have also been tried, but they might promote immunological responses that lead to rejection. To overcome these disadvantages, a hollow tube called nerve guide conduit (NGC) has been designed and fabricated, with natural and synthetic polymers, to aid peripheral nerve repair by connecting the proximal and distal stumps. Nonetheless, nerve guide conduits are limited to repair nerve gaps shorter than 20 mm.

Research has focused on innovating the design of NGCs to improve their performance in a variety of ways. For example, topographical cues, such as channels and intraluminal fibres, have been included inside the lumen of the NGC. Even though promising results have been obtained, for both *in vitro* and *in vivo* evaluation, the regeneration potential of these NGCs is still not enough, as it has been recognized that peripheral regeneration is a complex process in which different cells and molecules play a significant role to achieve complete functional regeneration. For this reason, chemical cues have been added to NGCs.

Chemical cues added to NGCs include mainly growth factors, peptides, and extracellular matrix components, such as collagen and laminin. These molecules have been incorporated into NGCs through different approaches, such as coatings on the inner wall, matrices filling the lumen, microspheres, adding the molecules within the wall of the NGC, and immobilisation, either on the wall or onto intraluminal fibres. Growth factors, such as nerve growth factor (NGF), brain derived neurotrophic factor (BDNF), glial cell-derived neurotrophic factor (GDNF), neurotrophin-3 (NT-3), and ciliary neurotrophic factor (CNTF), play an important role during peripheral nerve repair, therefore, these have been included in NGC to enhance neurite outgrowth and

Schwann cell migration. Nevertheless, techniques to add these growth factors usually involve the use of solvents, which decrease the bioactivity of the growth factors. Thus, a method to introduce growth factors to NGCs that extends their half-life and preserves their bioactivity would be a promising approach to enhance neurite outgrowth and Schwann cell migration during nerve repair.

The use of heparin has been reported to extend the half-life of growth factors as well as maintaining their bioactivity. Usually, heparin is bound covalently on different polymer surfaces, however, this technique could impair the bioactivity of heparin as covalent binding techniques also use solvents. Hence, binding heparin through electrostatic interactions to polymeric surfaces is an encouraging alternative. Heparin is a negatively charged glycosaminoglycan, thus, binding it to a positively charged surface would be the path to follow. Plasma deposition is a widely used technique to modify the surface of a material, making it hydrophilic or hydrophobic, depending on the application. Furthermore, plasma can be used to modify the charge on polymeric surfaces, either to encourage cell adhesion and proliferation of cells, or to bind other charged functional groups to the surface.

Therefore, by using plasma deposition technique on a surface, it is possible to bind heparin, and then to bind growth factors, which would create a bioactive surface capable of acting as a local delivery system of growth factors. Specifically, growth factors such as NGF and BDNF can be used to aid neurite outgrowth and Schwann cell migration during nerve repair. This bioactive surface would deliver growth factors in a sustained manner, avoiding undesirable high burst release. Furthermore, taking advantage of the flexibility of the plasma deposition technique, this bioactive surface could be fabricated on the surface of any polymer of choice, regardless of the shape, which would make this bioactive surface an attractive delivery system to adapt to any polymeric scaffold.

The work in this thesis consisted of, firstly, fabricating the bioactive surface on a commercially available amine (NH_2^+) coated plates (positively charged), to which heparin was bound (NH_2^+ + Heparin). Then, NGF, BDNF, or a combination of NGF plus BDNF, at different concentrations, were immobilised on heparin by electrostatic

interactions (NH_2^+ + Heparin + Immobilised NGF, NH_2^+ + Heparin + Immobilised BDNF, and NH_2^+ + Heparin + Immobilised NGF plus BDNF). Contact angle and XPS analysis were used to characterise the bioactive surface and to confirm the presence of heparin. ELISA was performed to characterise the release of NGF and BDNF from the bioactive surface.

The bioactive surface was then evaluated using NG108-15 neuronal cells and PC12 adh neuronal cells, finding that immobilised NGF and BDNF encouraged significant neurite outgrowth. Later, this bioactive surface was tested using dorsal root ganglia (DRG) and primary Schwann cells to evaluate neurite outgrowth and Schwann cell migration. The result of these experiments revealed that immobilised NGF at 1 ng/mL encouraged the growth of the longest neurites, in comparison to other test and control groups.

Positive results were achieved so far, hence, it was important to implement this bioactive surface to an approach that, in the future, could be implemented in an NGC. Thus, this bioactive surface was added to polycaprolactone (PCL) electrospun fibres. To achieve this, plasma deposition was used to add positively charged amine (NH_2^+) functional groups on the surface of PCL electrospun scaffolds. Then, heparin was bound to the NH_2^+, and finally, NGF, BDNF, and a combination of NGF plus BDNF, at different concentrations, were immobilised onto the PCL + NH_2^+ + Heparin surface.

XPS analysis was performed to confirm the successful addition of NH_2^+ and heparin. Moreover, ELISA showed that there was a sustained delivery of NGF and BDNF from the bioactive surface for up to21 days. Additionally, XPS analysis revealed that heparin was still present on the bioactive surface after 3 months of incubation at 4°C and 21°C.

Furthermore, DRG were seeded on these PCL + NH_2^+ + Heparin + Immobilised NGF/BDNF/NGF plus BDNF scaffolds and neurite outgrowth and Schwann cell migration were evaluated. The results of this experiment revealed that PCL + NH_2^+ + Heparin + Immobilised NGF 1 ng/mL encouraged the longest neurite outgrowth as well as the furthest Schwann cell migration in comparison to other test groups, control groups, and importantly, to other results found in the literature.

Even though PCL + NH_2^+ + Heparin + Immobilised BDNF did not encourage the longest neurite outgrowth, this surface stimulated the growth of longer neurites in comparison to when the bioactive surface was fabricated on flat, commercially available NH_2^+ coated plates, revealing that topological and chemical cues further improve the growth of neurites and migration of Schwann cells. Nevertheless, PCL + NH_2^+ + Heparin + Immobilised NGF plus BDNF did not stimulate an accumulative effect regarding neurite outgrowth and Schwann cell migration.

In conclusion, the bioactive surface NH_2^+ + Heparin + Immobilised NGF/BDNF/NGF plus BDNF was successfully fabricated on PCL electrospun fibres. Then, it was found that NGF and BDNF were delivered in a sustained manner for 21 days. In addition, it was found that by immobilising a relatively low concentration of NGF (1 ng/mL), neurite length of 3 mm was achieved *in vitro*. Therefore, the use of this bioactive surface on PCL electrospun fibres makes this approach directly applicable and scalable for improving the function of NGCs.

Chapter 2 Literature review

Peripheral nerve injuries are a major cause of physical disability, leading to the loss of sensory and motor functions [1]–[4]. Peripheral nerve injuries cost $150 billion dollars annually to the United States' health service [1], where $7 billion are expended annually on nerve graft procedures (ca. 50,000) [2]. Peripheral nerve injuries are caused by traumatic injuries such as penetrating injury, ischemia, traction, compression, crush, thermal and electrical shock [1], [2]. Even though some nerve injuries heal without any surgical intervention, some other nerve injuries need surgery to minimize neurological deficits [1]. Axon regeneration is not a fast process, which occurs at a speed of 85 μm/day [5]. Hence, injuries greater than 3 cm fail to regenerate and to achieve functionality, because the response and performance of Schwann cells to peripheral nerve injuries is time-dependent [2], [4]. The survival of Schwann cells in the distal stump is reduced within 8 weeks of injury. Therefore, after this time, Schwann cells undergo apoptosis [2]. Nevertheless, surgical treatment can be performed after years from the injury, with good results [6].

Peripheral nerve injury is a traumatic injury [4]. However, before revising the current treatments and research to improve nerve repair, an overview of peripheral nerve anatomy and repair process will be reviewed.

2.1 Peripheral nervous system: anatomy overview

The nervous system sustains and coordinates the function of the human body by chemical and electrical means, sending messages to and from organs and cells [7]. The nervous system is composed of two subsystems, the central nervous system (CNS), which comprises the spinal cord and the brain; and the peripheral nervous system (PNS), which includes all the nervous system but the brain and the spinal cord [1], [7] (Figure 1).

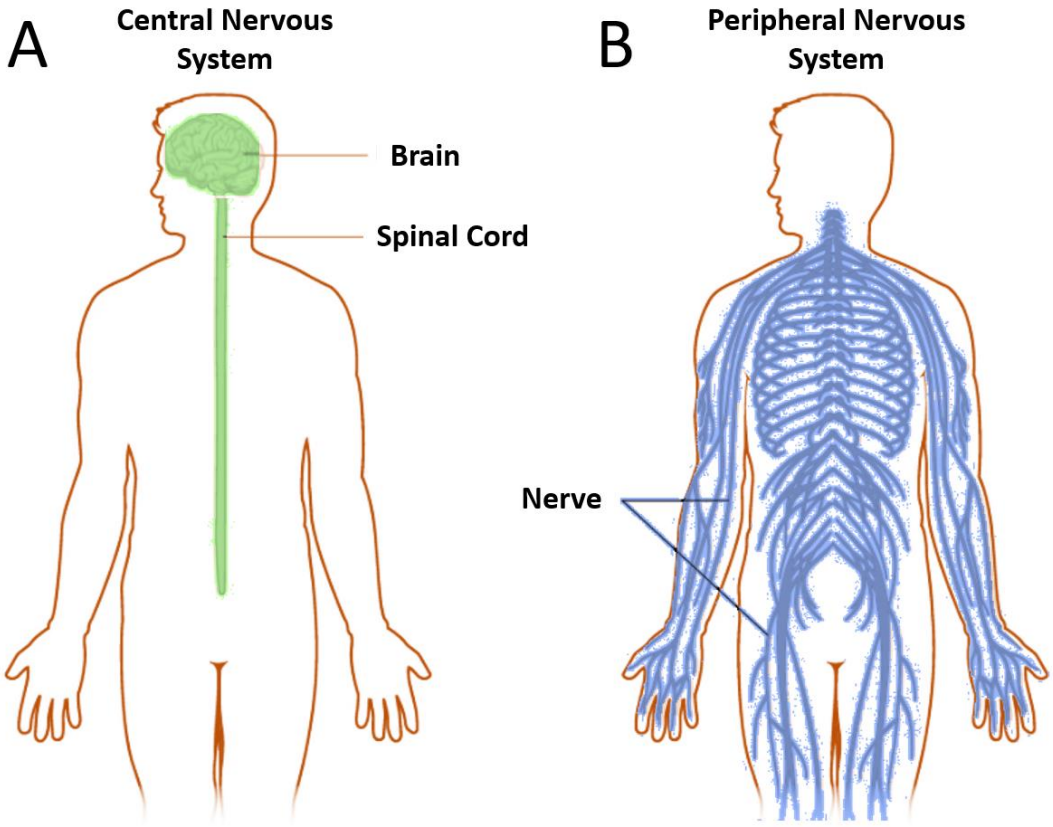

Figure 1. Nervous system schematic. The nervous system is composed of the central nervous system (A) and the peripheral nervous system (B).

The PNS is comprised of nerves and ganglia (Figure *2*). A nerve is a bundle of axons/neurites or nerve fibers enclosed in fibrous connective tissue. Ganglia, which is plural for ganglion, are swellings of the nerve where the cell bodies of neurons are contained [7]. By function, the PNS is divided into motor and sensory divisions [1], [7]:

- The sensory division transmits sensory signals from different receptors to the CNS. The visceral sensory division transmits signals from the thoracic and abdominal cavities (e.g., heart, lungs). The somatic sensory division transmits signals from receptors in the muscles, skin, and bones [7].
- The motor division transmits signals from the CNS to muscles and glands to implement the body's response to stimuli around and within. The autonomic

nervous system, also known as visceral motor division, transmits to smooth muscle, cardiac muscle, and glands. This division has two divisions: sympathetic division, which prepares the body for action, and the parasympathetic division, which allows energy intake by stimulating digestion. The somatic motor division transmits signals to skeletal muscles [7].

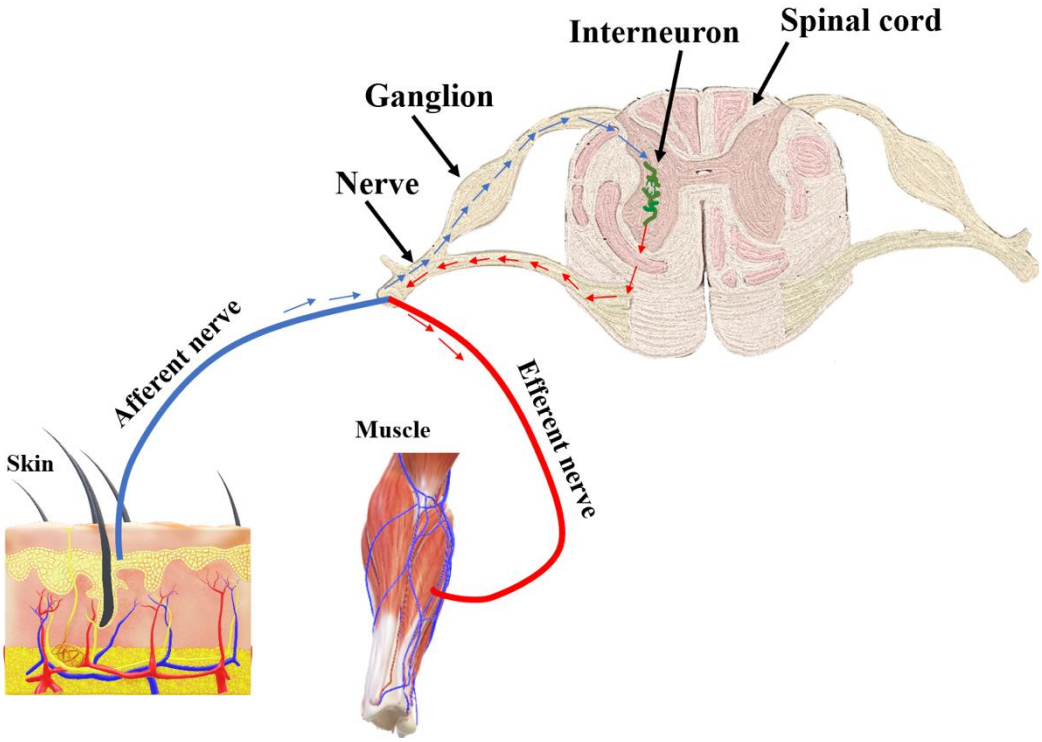

Figure 2. Diagram of the components of the peripheral nervous system. The components are the ganglion (singular for ganglia) and nerve. Drawing adapted from Saladin, 2014 [7].

The functional cell of the nervous system is the neuron (Figure *3*). The structure of the neurons consists of its neurosoma or cell body, where the control centre is; dendrites, which receive signals from other neurons; and the axon or nerve fibre, which transmits signals from the neurosoma to distant parts of the body [2], [7]. The cytoplasm and the membrane of the axon are called axoplasm and axolemma respectively (Figure 4) [7]. The dimensions of the neurosoma range between 5 and 135 µm in diameter (in humans); the diameter of the axon range from 1 to 20 µm and can measure from a few millimetres to more than a meter in length [7]. At the distal end of the axon, terminal

branches extend and form a synapse or junction with another neuron, gland cell or muscle cell via their synaptic knob [7].

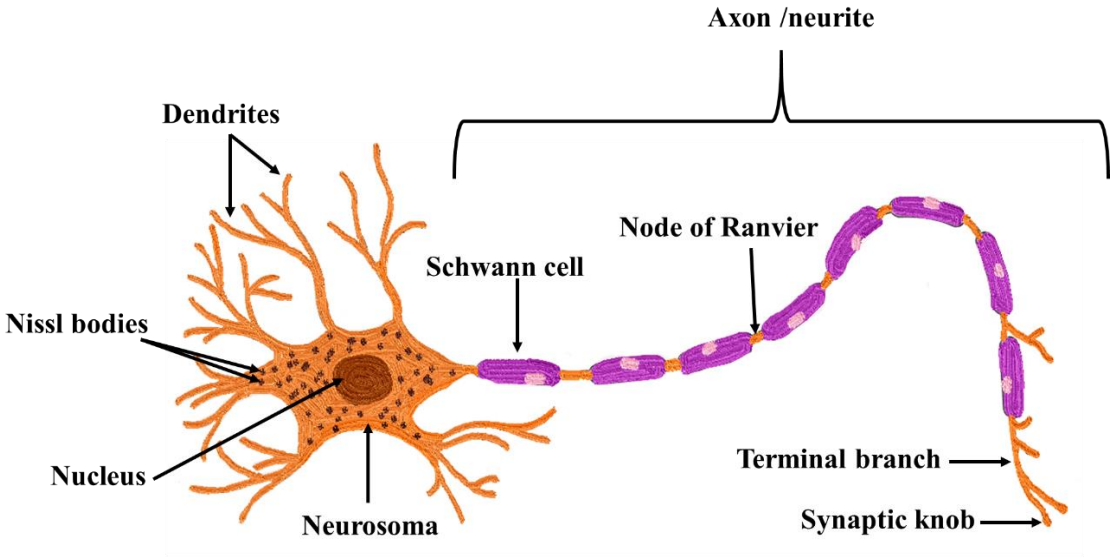

Figure 3. Diagram of a neuron. The structure of the neuron is comprised of the cell body or neurosoma, dendrites, axon or neurite. The synaptic knob, which is part of the axon, connects to another neuron, or other cell, for example, a muscle cell. Diagram based on Saladin, 2014 [7].

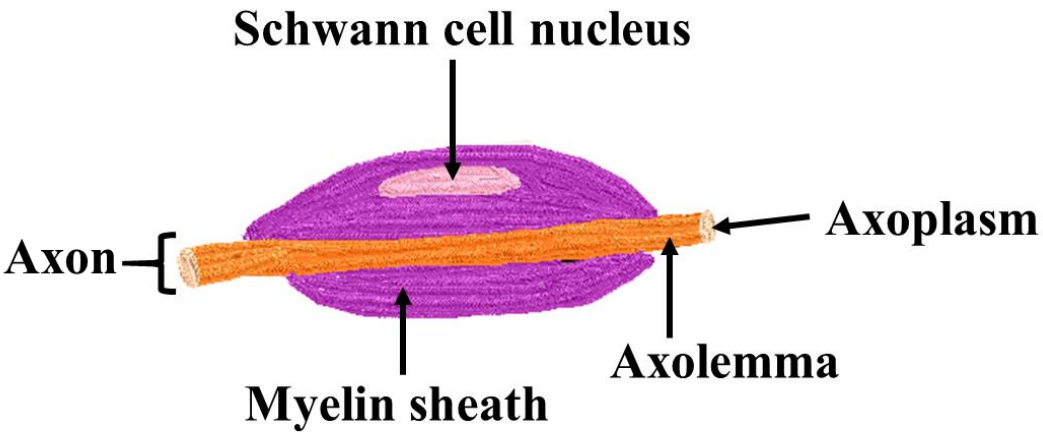

Figure 4. Schematic of the components of the axon: the axoplasm and the axolemma, which are the cytoplasm and the membrane of the axon. Moreover, Schwann cell covers the axon, forming a myelin sheath. However, not all Schwann cells form a myelin sheath around the axon and not all axons are covered by Schwann cells. Diagram adapted from Saladin, 2014 [7].

Neurons can be classified by their structure or by their function. According to their structure, neurons are classified as follows: multipolar neuron, which are the ones that have two or more dendrites and one axon; bipolar neurons, which have one dendrite and one axon; unipolar neurons, which have a single process coming from the neurosoma and then it branches to form a T; anaxonic neurons, which have many dendrite but no axon, enabling communication over short distances [7].

According to their function, neurons are classified as sensory neurons, interneurons and motor neurons. Sensory neurons detect stimuli, for example heat, light, and transmits this information to the CNS. Interneurons are found in the CNS. They receive signals from other neurons which they process, retrieve and store to decide on how the body should respond to external stimuli. Motor neurons send signals responding to the external stimuli from the CNS to muscle cells or gland cells [1], [7].

Apart from neurons, the PNS is composed of neuroglia or glial cells. One of these glial cells are Schwann cells, which give directional guidance to neurons, eliminates cellular debris after nerve injury, a process mainly controlled by macrophages, and form the neurilemma around nerve fibers [1], [7]–[9]. Moreover, Schwann cells wrap repeatedly around a nerve fiber, producing a myelin sheath between the nerve fiber and the neurilemma [10]. The myelin sheath insulates the nerve fiber and it is composed of 80% lipid and 20% protein [7], [11].

As it requires many Schwann cells to cover one nerve fiber, the myelin sheath is not continuous. The gap between the myelin sheaths is called the node of Ranvier [7]. The nodes of Ranvier expose small, but regular, segments of the axon. These structures are rich in sodium and potassium ion channels and function according to the action potential of the axon [10]. However, as Schwann cells can be non-myelinating type and myelinating type, not all nerve fibers have a myelin sheath. For these nerve fibers, Schwann cells do not wrap repeatedly around the nerve fiber [7], [12].

The speed of a signal along a nerve fiber depends on the diameter of such nerve fiber and the presence of myelin sheath as the conduction of the signal happens along the surface of the nerve fiber. For small unmyelinated fibers (diameter 2-4 μm), the speed of the signal is of 0.5-2.0 m/s; for small myelinated fibers (diameter 2-4 μm), the signal

speed is of 3-15 m/s; and for large myelinated fibers (diameter up to 20 µm) the signal speed is of 120 m/s [7], [12].

The other type of glia present in the PNS are satellite cells, which covers the soma of neurons localized in the ganglia, regulating its chemical environment and providing electrical insulation [7], [13].

All these structures are collectively enclosed by the endoneurium, loose connective tissue composed of collagen fibres, which covers each nerve fiber and Schwann cell. Then, the nerve fibers are assembled in fascicles, enclosed by the perineurium [1], [2], [7]. The perineurium is comprised of squamous epithelium [7]. Then, various fascicles are packed together and enclosed by the epineurium, comprising the nerve. The epineurium is composed of irregular fibrous connective tissue, and shields the nerve against injuries [1], [7]. Moreover, the ganglion is covered on the continuous epineurium of the nerve [7], as observed in Figure 5.

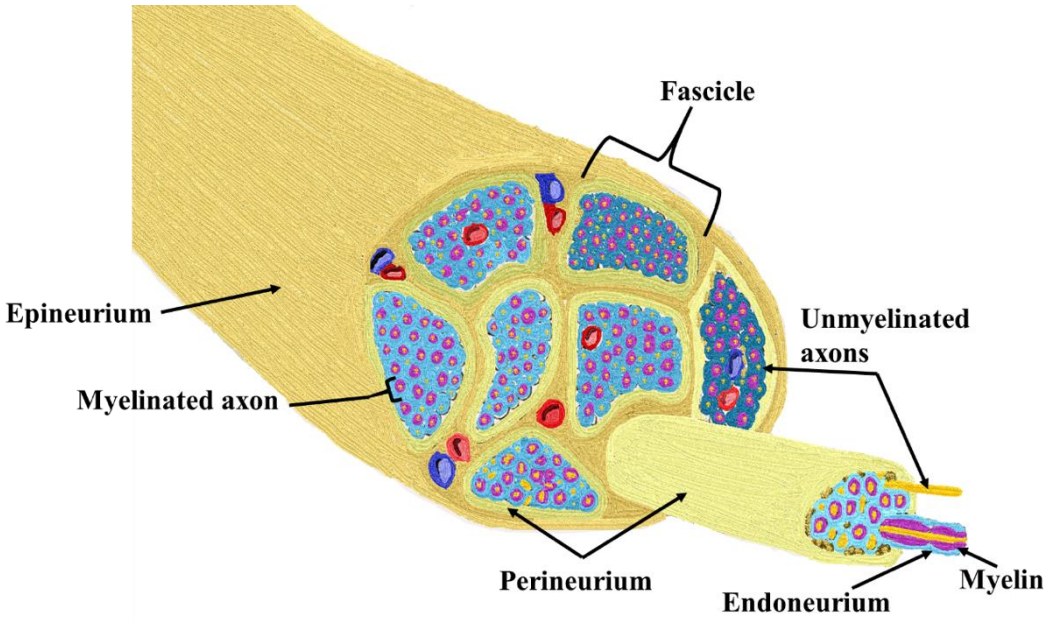

Figure 5. Diagram of the nerve and its components. The endoneurium enclosed the individual myelinated and unmyelinated axons; the perineurium covers the fascicle, which is composed of axons; the epineurium encloses the nerve trunk, which contains various fascicles [1]. Diagram based on Saladin 2014 [7].

2.2Peripheral nerve injury: causes and consequences

Peripheral nerve injury (PNI) significantly impacts the quality of life of 1 in 1,000 patients as it affects the health of nerves, leading to disability [1], [14]. Peripheral nerve dysfunctions are caused by traumatic or non-traumatic events, such as autoimmune disorders (e.g. Guillain-Barré syndrome [15]), drug-induced, infectious, deficiency-related, metabolic or genetic [16]. Furthermore, as the severity of the injury varies, the treatments are also variable [16]. Nevertheless, current treatments do not encourage a significant improvement in nerve repair after injury [17]. Moreover, there are different types and causes of PNI. Nerve compression injuries are caused by pressure on a nerve trunk. These injuries affect nerves that cross over or pass between rigid structures such as bones [18].

Compression neuropathy, or nerve compression syndrome, are present in a wide variety of disorders, for example, carpal tunnel syndrome (median nerve), meralgia paraesthetica (lateral cutaneous nerve), cubital tunnel syndrome (ulnar nerve), tarsal tunnel syndrome (tibial nerve), sciatica syndrome (sciatic nerve) [18], [19] . Moreover, compression neuropathies are frequent in patients that hold a single position during long periods [16].

Stretch and crush damage also cause nerve injury [16], [20]. Nerve crush injuries are caused by applying a significant force to the nerve, for example, with a blunt object or as a consequence of a large impact, such as a car accident [21]. Even though the severity among crush injuries differ, Wallerian degeneration occurs and, therefore, axon continuity is lost. However, as the integrity of the endoneurium, perineum and epineurium are not compromised, regeneration of axons happens allowing functional recovery [16], [22]. Nevertheless, neuroma formation and fibrosis are usually observed, preventing axonal regeneration. Stretch forces also damage peripheral nerves causing nerve injuries. When the stretching forces increase, the elasticity of the nerve is exceeded, causing the disruption of endoneurium, perineum, epineurium, axons and myelin sheaths [23], [24]. Studies have shown that by elongating the rat sciatic nerve by 8%, intraneural pressure increases and blood flow decreases, whereas nerve conduction velocity is not reduced [25]. One example of a stretch injury is the neonatal Erb-Duhenne palsy, which is a paralysis of the arm caused from tearing the

brachial plexus during birth [26]. Other examples of stretch injury may happen when a heavy object falls onto the shoulder, causing the tearing of the brachial plexus. Moreover, most of these stretch injuries are caused by car accidents [16], [27], [28].

Peripheral nerves are also injured by transection or laceration. Transection injuries are caused by knife wounds, metal shards, wood splinters, glass shard, gunshot [29], [30]. Additionally, peripheral nerves could be transected during surgical procedures. These transection injuries cause the complete loss of the nerve continuity, making it the most severe injury, as it causes a complete loss of sensory and motor function [30]. Even though full recovery is never achieved after a transection injury, the possibility of functional recovery is greater when the distance between proximal stump and distal stump is shorter [16].

There are two classifications for peripheral nerve injury: Seddon classification and Sunderland classification [31], [32], which are summarized in Table 1.b. Seddon classified the severity of the damaged nerve according to his observations of trauma cases: neuropraxia, the compression injury is repaired, segmental demyelination may be observed; axonotmesis, the epineurium, perineurium and endoneurium of the nerve were not damaged but axon continuity is lost; neurotmesis, complete transection of the nerve occurs [1], [16], [33]. Sunderland classified nerve injuries based on their histopathological characteristics: grade I is when the compression injury is repaired (Seddon's neuropraxia); grade II is when the integrity of the nerve is not compromised, but the continuity of the axons is lost and demyelination occurs (Seddon's axonotmesis); grade III, the perineurium is not damaged, but the axons and the endoneurium are damaged; grade IV, the epineurium is not damaged, but the axons, perineurium and endoneurium are damaged; grade V is the complete transection of the nerve (Seddon's neurotmesis) [1], [16], [31].

Table 1. Peripheral nerve injury's classification according to Sudden and Sunderland. Schematic representation based on Nadi and Midha, 2018 [34] and Menorca et al. 2013 [21].

Peripheral nerve injury classification		Characteristics	Schematic representation
Seddon's	Sunderland's		
Neuropraxia	I	A brief deficiency of motor function, but compression injury is repaired. Nerve and axon continuity is conserved. Recovery is from days to weeks [1], [16], [31]	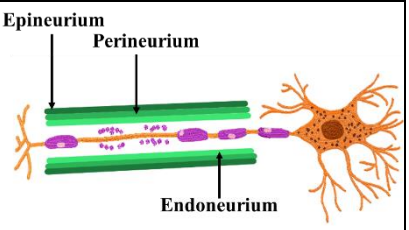
Axonotmesis	II	Crush and stretch injuries. Axon continuity is lost, but epineurium, perineurium and endoneurium are not damaged. Rate of regeneration is approx. 1 mm/day [1], [16], [31]	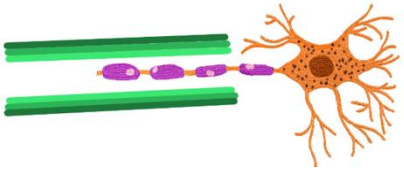
-	III	Crush and stretch injuries. The continuity of the axon and endoneurium is lost. Perineurium and epineurium are in good conditions [1], [31]	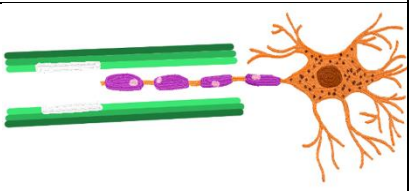
-	IV	Crush and stretch injuries. The continuity of endoneurium, perineurium and axon is lost. Epineurium is not damaged [1], [31].	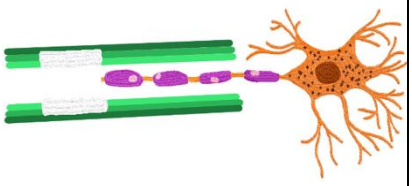
Neurotmesis	V	Knife wounds, wood splinters, metal shards injuries. It is the most severe injury, as it is the complete transection of the nerve: total loss of nerve continuity. It creates a physical gap between the distal and proximal end. Recovery from 3 to 4 weeks after injury [1], [16], [31]	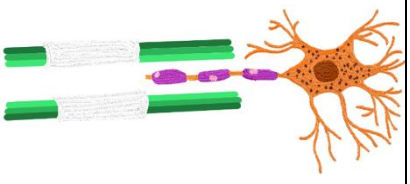

2.3 Peripheral nerve injury: mechanism of regeneration after injury

After peripheral nerve injury, the distal components of the injured axons degenerate, and go through Wallerian degeneration [3]. Retrograde reaction and Wallerian degeneration occur in parallel, forming a microenvironment that benefits neurite regrowth and elongation, allowing reinnervation and function recovery [3]. Axons in the PNS, when damaged and if the neurosoma is intact, can regenerate. Schwann cells of the neurilemma release neurotrophins that encourage axon outgrowth: nerve growth factor (NGF), brain derived neurotrophic factor (BDNF), glial cell-derived neurotrophic factor (GDNF) and ciliary neurotrophic factor (CNTF) [16]. Schwann cells form Bands of Bünger that lead the regenerating axon to its target location [7]. If the process is successful, the synaptic contact is reestablished; if not, neurons fail to find the target location and undergo apoptosis. A Schematic representation of Wallerian degeneration and axon regeneration is shown in Figure 6.

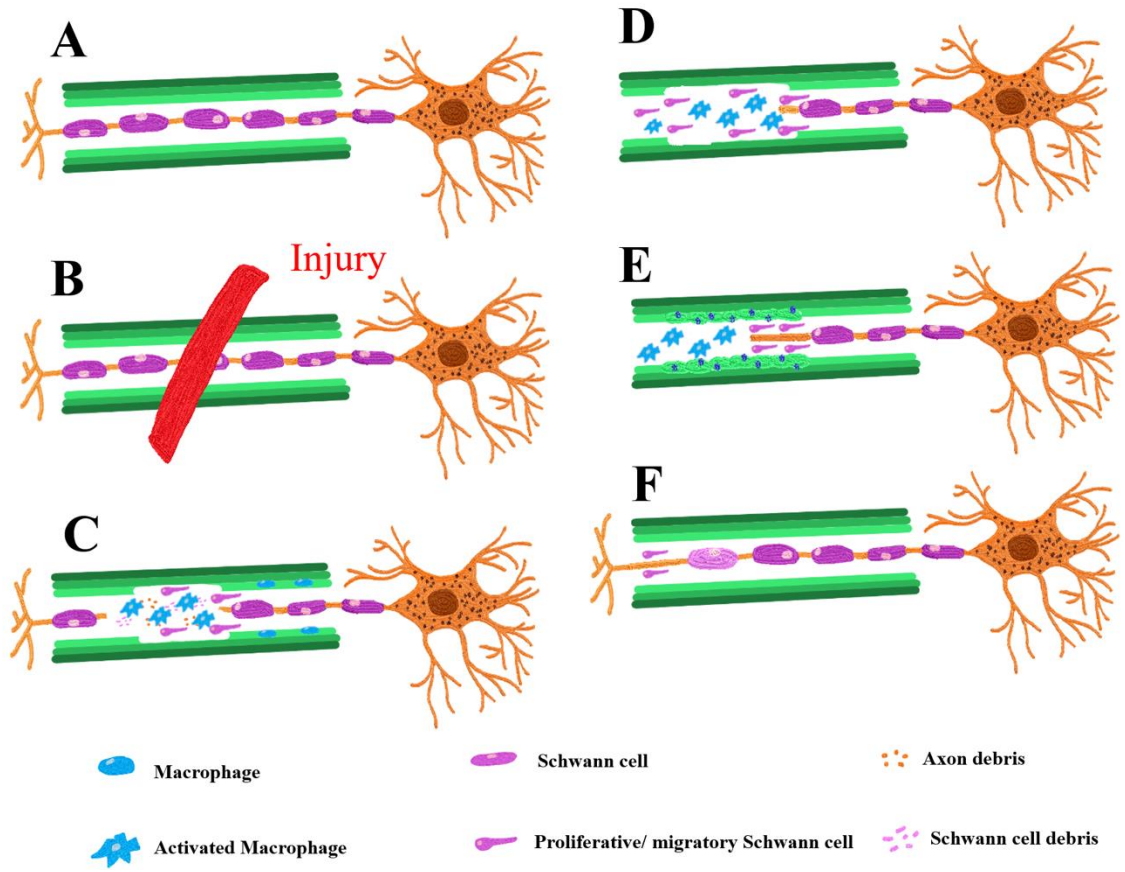

Figure 6. Schematic of Wallerian degeneration and nerve repair. A) When a nerve is healthy, its normal function is not compromised. However, B) when an injury occurs, some cellular components undergo apoptosis. C) Then, Schwann cells recruit macrophages, which then are activated and start to phagocytose myelin and axonal debris. D) Schwann cells stimulate the production of NGF, BDNF, GDNF and CNTF to encourage Schwann cell proliferation and migration. E) Furthermore, Schwann cells align to form Bands of Büngner, which encourage axonal regrowth and endoneurial regeneration. F) Before functional recovery is completed, axonal regrowth, remyelination and functional re-innervation need to happen [15], [16]. Schematic based on Caillaud et al. [16].

In order for peripheral nerves to regenerate, injured axons, Schwann cells, macrophages and endoneurial fibroblasts form a microenvironment which encourages regrowth of the proximal axon ending. When peripheral nerves are injured, the transected axon is disconnected from its soma, leading to the loss of nerve conductivity, which causes loss of sensation, muscle weakness, pain and a biological response to repair the injured nerve [35]. If the injury is close to the soma or if the injury is large, it may cause neuronal death. Nevertheless, if the injury is distant to the

soma, axons may regenerate. For this to occur, first, the axons in the distal nerve ending need to degenerate. This process is known as Wallerian degeneration [15], [36].

Wallerian degeneration is the process to degenerate axons, preparing the biological environment for nerve regeneration [15], [16], [36]. Firstly, the axoplasma and axolemma are disintegrated, producing myelin and axonal debris. Macrophages in the nerve tissue differentiate into active macrophages, which then phagocyte cellular debris [15], [36]. As Schwann cells are a source of monocyte chemoattractant protein-1, they act as recruiters of monocytes to the site of injury [37]. Additionally, mRNA translation is activated in axons in the proximal stump, which encourages the formation of importin-phosphorylated extracellular regulated protein kinase 1/2 vimentin protein complex. This protein complex is transported retrogradely by protein dynein to the soma, informing the neuron about the axonal damage [16]. Then, the neurons increase their volume and disintegrate the endoplasmic reticulum, stimulating protein synthesis [16], [38]. Moreover, messenger RNAs for antioxidant proteins (heme oxygenase 1, Nrf2) are increased within the first hour after injury [39], [40]. The growing axon elongates randomly oriented filopodia; then, they acquire directionality due to the upregulating expression of actin and myosin within the soma [41].

Two days after the injury, monocytes differentiate into activated macrophages and aid phagocytosis of myelin and axonal debris; this process occurs at least for two weeks. Moreover, this phagocytosis process is determined by the expression of galactoside-binding protein of macrophages galectin-3, which aids Schwann cells to eliminate myelin debris [15], [16], [38]. Injured Schwann cells encourage changes in protein expression at the site of injury. When Schwann cells lose contact with the injured axon, it promotes retraction of the myelin sheath, generating ovoid structures. These ovoid structures emerge two days after injury and remain for up to 3 weeks [16], [42], [43]. In addition to the loss of contact between Schwann cells and injured axons, Schwann cells change from a myelinating to a non-myelinating phenotype and start to proliferate, down-regulating the expression of myelin protein zero and peripheral myelin protein 22 [11].

Macrophages, aside from phagocyting myelin and axonal debris, secrete interleukin-1 (IL-1) which encourages Schwann cells to express NGF, inducing autocrine-stimulated proliferation and growth of Schwann cells, reaching its maximum mitotic activity at day 4 after injury [16]. Macrophages also encourage the expression of transforming growth factor beta (TGF-β) and insulin-like growth factor (IGF), which encourages mitotic activity not only in Schwann cells but also in fibroblasts [44]. Furthermore, macrophages produce apolipoprotein E, which supports myelin restoration. Additionally to the activity of the macrophages, the production of various proteins is upregulated to assist neuronal growth. These proteins are BDNF, GDNF, growth-associated protein- 43 (GAP-43), calcitonin gene-related peptide (CGRP), c-jun, vasoactive intestinal peptide (VIP), substance P and somatostatin [16], [45].

From day 3 to day 7 after injury, at the end of the proximal stump, a growth cone is formed. Neurotrophins stimulate the attraction and repulsion of the filopodia, as netrins and ephrins guide the regrowing axon [46]. However, the growth of the growth cone might be inhibited by the effects of collapsing 1, which causes the growth cone to collapse, or by the appearance of scar tissue. To impede the formation of scar tissue, and hence, to prevent the growth of the growth cone, the growth cone releases plasminogen activators and proteases to degrade scar tissue. Moreover, these molecules degrade any interaction between cells or cell-matrix that obstruct the growth of the growth cone [47].

Schwann cells secrete neurotrophins which change the neuronal gene expression to encourage axonal growth. For example, Schwann cells stimulated the expression of NGF, which promotes Schwann cell proliferation and axonal growth . At this stage, not only Schwann cells proliferate and migrate to the lesion site, but also endoneurial fibroblast. Both cell types form a bridge between the proximal and distal segment. This bridge is called neuroma, and it attempts to reconnect both segments [16], [48]. Moreover, when Schwann cells migrate to the distal segment, they align in columns forming Bands of Büngner, which assist endoneurial regeneration and axonal regrowth, as they act as physical guidance to the regenerating axon [15], [16]. Furthermore, Schwann cells stimulate the production of laminin and fibronectin, which are later incorporated into the extracellular matrix of the endoneurium. These

proteins aid the adhesion between the growth cone and the basal lamina of the endoneurium [49], [50].

Before functional recovery is completed, axonal regrowth, remyelination and functional re-innervation need to occur. As NGF and CNTF are secreted to encourage axonal growth, neuregulin-1 (NRG1) I and III, and acetylcholine, which are produced by the growing axon, stimulates the change in Schwann cell phenotype: from a non-myelinating to a myelinating phenotype [16], [51], [52]. These changes happen between three and four weeks after injury [16]. Additionally, the expression of apolipoprotein D, apolipoprotein E, cathepsin B, which are proteins involved in lipid metabolism, and the secretion of proteins involved in cellular maturation, including myelin reconstruction (tropomyosin 4-α, tropomyosin 3-γ, galectin 3) are upregulated [53]. Nerve fibers seem normal after three months. However, the endoneurium is divided into compartments by fibroblast, which later differentiate into perineurial cells. These compartments are then developed, forming the original fascicles in the nerve [54].

2.4 Current strategies for nerve regeneration

For short gap nerve injuries (<5 mm), inherent axon regeneration may occur [55]. Nevertheless, for larger gap nerve injuries (>5 mm), direct suturing is a common surgical procedure to reconnect the proximal and distal ends of the severed nerve. Direct suturing may be a satisfactory treatment if the number of sutures to use is low and the segments of the nerve are aligned [14], [56]–[58]. This treatment is limited for gaps shorter than 10 mm because this surgical procedure could introduce tension into the nerve, causing blood flow to decrease in the injury area, preventing nerve regeneration [14], [56], [59]–[61]. Other surgical approach is terminal lateral neurorrhaphy or end-to-side, used when direct suturing cannot be performed. However, it also causes the drawbacks mentioned for direct suturing [60], [62]. For this reason, for larger gaps (>10 mm) and for complete nerve transections, using a nerve autograft is the gold standard treatment [14], [56], [57], [59]–[61], [63]–[65].

The current gold standard to treat peripheral nerve injuries, when the nerve is completely transected, is the implantation of an autograft [16]. This autograft is harvested from another part of the body, for example, from the calf region. One of the most used autografts is a sensory nerve, called the sural nerve [16]. Other nerves that are used are lateral or medial antebrachial nerves, superficial cutaneous nerves [56], [63], [64]. However, outcomes following autograft repair are limited and less than 25% recover motor function [60], [63], [66]. Furthermore, the use of autografts carries a significant risk of donor site morbidity including, neuroma and scar formation, neuropathic pain, as well as the loss of function (from where the autograft was taken) and has the disadvantage of having multiple surgeries. In addition, availability of nerve autografts is limited, and with mismatching diameter, the regenerating nerve process would be impaired [56], [57], [59], [60], [64], [65], [67], [68].

To overcome some of the disadvantages of using autografts, the use of allografts (graft of the same species) or xenografts (graft of a different species) was explored. However, to use allografts or xenografts, the patient needed to be immunosuppressed. And, even with immunosuppression, it is possible to have rejection and risk of infection [65], [69], [70]. The design and development of polymeric scaffolds (natural or synthetic) for peripheral nerve generation has been proposed as an alternative for

autografts, allografts, and xenografts. These scaffolds should aim to achieve full functional recovery, both of sensory and motor function [59], [64], [71].

The use of tubular polymeric scaffolds, named nerve guide conduits (NGCs), are being studied and developed as an alternative to aid nerve repair, as this tubular device could bridge the nerve gap, guiding the regenerating axon to its target [2], [16], [72]. These NGCs have been developed using either natural or synthetic materials, some of which have the approval of the Food and Drug Administration (FDA) for their commercial use (Table *2*) [70], [72]. The most common natural materials used for the fabrication of NGCs include collagen, chitosan, porcine small intestinal submucosa, gelatin, hyaluronic acid, fibrin, and silk fibroin [2], [70]. Synthetic materials that have been used in research to develop NGCs include polylactic acid (PLA), polycaprolactone (PCL), polyglycolic acid (PGA), poly lactide-caprolactone (PLCL), poly-hydroxbutyrate (PHB), and polylactic-co-glycolic acid (PLGA) [2], [14], [63], [70], [73].

Table 2. NGCs approved by the FDA for commercial use. These NGCs are fabricated either with natural and/ or synthetic materials [2], [70], [72], [74], [75].

Material Origin	Commercial name	Material	Characteristic
Natural	NeuraGen ®	Collagen type I	Bridges up to 20 mm gap
	NeuraGen ® 3D	Collagen type I and glycosaminoglycagen	Degradation within 12 months
	NeuroMatrix™ /Neuroflex ™	Collagen type I	Degradation after 7 months
	CovaC ortho-nerve	Collagen type I	Non-degradable
	Reaxon® plus	Chitosan	Degradation within 3 months
	AxoGuard ™	Porcine small intestinal submucosa	Vascularisation occurs
Synthetic	Neurolac ®	Poly-DL-lactide-co-ε-caprolactone (PDLLA/CL)	Bridges up to a 20 mm gap
	Neurotube ®	Polyglycolic acid (PGA)	Degradation within 6 months
	SaluBridge ™/ SaluTunnel™	Polyvinyl alcohol hydrogel	Non-degradable
Natural and synthetic	Nerbridge ™	PGA and collagen type I and III	Degradation within 4 months

Even though these NGCs have shown axonal outgrowth, myelin formation and functional recovery, these NGCs are limited to aid repair in nerve gaps shorter than 20 mm [2], [14], [63], [76]. This limitation may be due to their simple design, as they are a hollow tube, leading to an inappropriate extracellular matrix (ECM) formation, low infiltration and activation of neurotrophic factors, and deficient Schwann cell migration [14], [56], [63]. Therefore, research has been expanded to improve NGCs by incorporating topographical, biological or chemical cues [2], [70], [72], [76]–[79].

2.5 Research to address peripheral nerve regeneration

To improve the performance of NGCs, studies have modified the design of these NGCs to further encourage neurite outgrowth, Schwann cell migration and, thus, nerve regeneration. Such modifications include the incorporation of cells into the NGC, addition of intraluminal guidance, microchannels and growth factors [56], [63], [80]–[84].

2.5.1 Incorporation of cells inside NGCs

As Schwann cells are the main cells that support nerve repair after injury, Schwann cells have been seeded with NGCs to improve their performance [78], [85]. Schwann cells, during Wallerian degeneration, migrate and form Bands of Büngner to guide the growing neurites [2], [78], [86]. Moreover, Schwann cells secrete ECM molecules, signaling molecules and growth factors that support nerve regeneration [2], [78].

NGCs seeded with Schwann cells encouraged the growth of longer neurites and the development of a higher number of neurites. Furthermore, NGCs with Schwann cells enhanced conduction velocity and myelin density [2], [70]. For example, Liu et al. seeded Schwann cells at one end of a 3D microchannel and demonstrated that DRG grew neurites into this 3D microchannel [87]. In addition, Schwann cells had been transfected to increase the production of NGF or BDNF, where results showed neurite outgrowth higher than the controls [88], [89].

Nevertheless, the use of Schwann cells has limitations, such as tissue availability, donor site morbidity, long culture times for cell expansion, viability once the Schwann

cells are transplanted [2], [70], [78], [84], [90]. Furthermore, the use of allogenic Schwann cells would elicit an immune response and future rejection of Schwann cells [70], [78]. To overcome the limitations of the use of Schwann cells, researchers have focused their attention in obtaining another source for Schwann cells. Therefore, they have studied stem cells.

Stem cells have been studied as an alternative to encourage nerve regeneration [2]. These include embryonic stem cells (ESC), induced pluripotent stem cells (iPSC), mesenchymal stem cells (MSC), adipose derived stem cells (ADSC) and neural stem cells (NSC) [2], [78], [84], [90]. Regardless of which stem cells are used, all of them are differentiated into Schwann cells [70], [78]. Stem cells have been delivered with NGCs and using gelatin microspheres [90]. However, the use of stem cells, even though they have shown promising results, are limited by ethical regulations, painful and complexity of harvesting, uncontrolled differentiation, risk of tumourogenicity, immunogenicity [78], [90]. Therefore, other strategies are being developed.

2.5.2 Architectural features for NGCs: topographical cues

The use of hollow NGCs has encouraged nerve regeneration in short injury gaps. However, challenges regarding wrong target innervations and neurites misdirection were encountered [78]. Therefore, topographical cues are being assessed alone and in combination with NGCs to overcome hollow NGCs limitations. It is well known that cell growth, proliferation and attachment is improved by micron and nano features [78], [91], [92].

For applications related to peripheral nerve regeneration, surface spatial cues such as roughness, grooved size, pore size, and orientation have been studied for their effects on cell adhesion, proliferation, differentiation, and axonal guidance [93], [94]. Although the mechanism of cell adhesion as a function of surface topography is not yet fully understood, it is known that other relevant material properties such as wettability and chemical composition are also key to induce cell attachment [93], [95]. Hence, NGCs had been designed with complex micro and nano features to enhance neurite outgrowth. Figure 7 shows an overview of the architectural features that can be added to NGCs.

Extrusion and stereolithography (SLA) are the most commonly used techniques to fabricate NGCs with micro and nano features in the inner wall [78], [96], [97]. For example, Field et al. used SLA for the fabrication of NGCs with grooves in its inner wall [96]. Furthermore, Zhu et al. also used SLA technique for the fabrication of NGCs with different designs: hollow tube, microchannel tube, and branched tube [97]. A 6 mm microchannel tube was tested *in vivo* in a mouse sciatic nerve model, showing that function recovery was achieved [97].

In addition, micropatterning and coatings are also incorporated in the inner wall of the NGC. Yao el al. introduced laminin-coated or collagen I-coated micropatterns in a PLGA guide, which showed aligned neurite outgrowth on the 5 µm grooves in comparison to the 10 µm grooves [98]. Sun et al. fabricated grooves in PCL NGCs, showing that primary Schwann cells and NG108-15 neuronal cells grew in alignment with the 5 µm grooves [99]. Furthermore, Rajnicek et al., fabricated 1 µm grooves from quartz using SLA, demonstrating that hippocampal neurites grew aligned with the grooves [100].

Moreover, neurite outgrowth was enhanced when aligned micro and nanofibers were introduced inside the NGCs [66], [70], [78], [92], [101]–[103]. Daud et al. electrospun aligned PCL fibres and seeded DRG on them [104]. The results of this work showed that neurite outgrowth was oriented along the parallel fibres [104]. Furthermore, Behbehani et al. introduced aligned PCL fibres inside a polyethylene glycol (PEG) conduit, revealing that neurite outgrowth was enhanced, and that neurite growth was oriented [105]. In addition, in an *in vivo* study from Daly et al. collagen fibres were introduced inside a collagen NGC [106]. This study showed that neurite outgrowth and Schwann cell migration were stimulated, with reduced neurite mismatch at the distal target [106]. Wang et al. electrospun PLLA fibres with different diameters (1325 nm, 759 nm, and 293 nm) and evaluated neurite outgrowth and Schwann cell migration [107]. The findings were that neurite length and Schwann cell migration were significantly longer in 1325 nm and 759 nm fibres in comparison to neurite length in 293 nm [107].

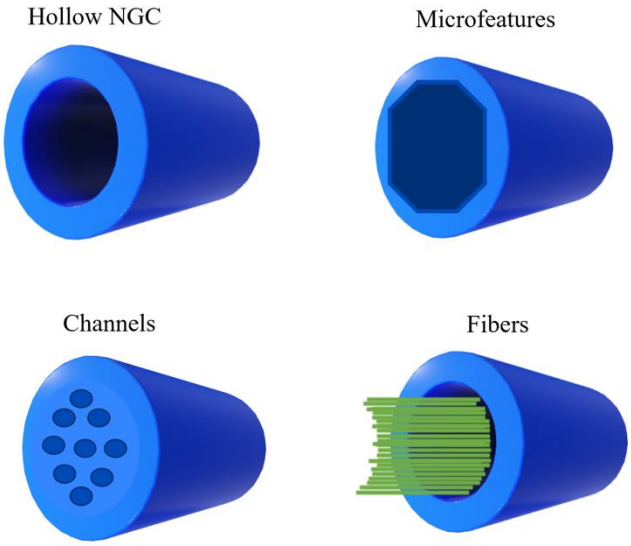

Figure 7. Schematic representation of architectural cues that can be added to NGCs

Different methods have been used to fabricate fibres, such as dry, wet, melt, gel and electrospinning [108]. Dry spinning consists of extruding a polymer solution through a needle into air, where fibres are obtained as the solvent evaporates supported by hot air [108]. For wet spinning, a polymer solution is extruded from a needle to a chemical bath, where the polymer is precipitated due a chemical reaction forming fibres by solidification [108]. Melt spinning involves extruding a polymer melt through a needle to form fibres while cooling [108]. Gel spinning forms fibres by spinning a gel polymer, where the fibres are air dried and then are cooled in a liquid bath [108]. These spinning techniques produce fibres with a diameter ranging from 10 µm to 100 µm, and cannot reach diameters lower than 10 µm [108]. Electrospinning is a technique where fibres are formed by spinning a polymer solution using an external electric field [108]. With electrospinning, fibre diameter could reach the nanoscale [102], [108].

Electrospinning is an advanced manufacturing technique developed during the first decades of the 20th century, but became characterised until the 1960s by Sir Geoffery Ingram Taylor [109]. However, this technique was not popularised until the early 1990s with an increase of research groups reporting the fabrication of nanofibers for several applications [110]. The electrospun fibrous membranes have attractive

characteristics for biomedical applications due to their high surface to volume ratio, their versatility regarding fibre diameter (10 nm to 10 μm), and high interconnectivity [111].

The electrospinning technique requires a polymer solution into which an electrostatic force is applied to create a polymer jet that travels towards a grounded collector. As the polymer solution is being ejected from a capillary and a pendant drop is formed, the electrostatic force starts to deform the drop into a cone shape known as Taylor cone. Once the electrostatic charge raises the threshold of the surface tension holding the droplet, a charged jet of polymer starts to flow towards the grounded collector. As the polymer jet moves towards the collector, the solvent evaporates and the fibres are deposited into the collector [112].

The basic electrospinning setup consists of a syringe containing the polymer solution, a pump to control the polymer flow from the syringe, a metallic needle, a voltage supply, and a metallic collector. Variations on this setup can be used on specific applications to control fibre alignment [113], microarchitecture [114], or for drug delivery applications [115]. Figure 8 shows a schematic of a basic electrospinning setup. The parameters of the electrospinning process play a critical role in defining key aspects of the fibre such as diameter and morphology. These parameters can be divided into process, solution, and environmental parameters. Table 3 shows a summary of the electrospinning parameters and their effects on fibre structure [116].

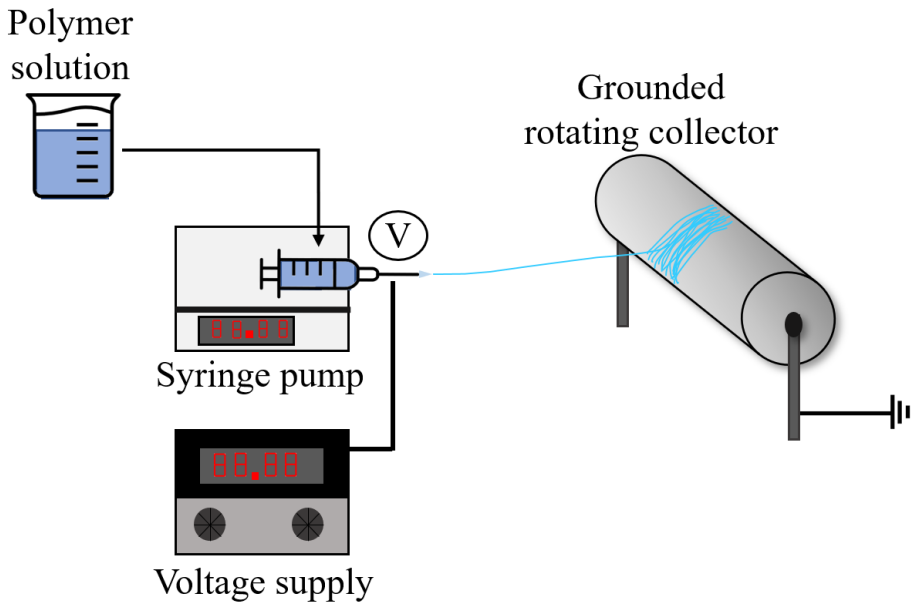

Figure 8. Schematic representation of a basic electrospinning set up. The set up consists of a syringe pump, voltage supply and a grounded collector, which can be static or rotating.

Table 3. Electrospinning parameters and their effects on fibre structure [116]–[118].

Electrospinning parameter	**Variable**	**Effect on fiber structure**
Process	Voltage	Controls fibre diameter and mainly controls formation of Taylor cone
	Flow rate	Controls fibre diameter and it can create beaded fibers if is too high
	Capillary–collector distance	Controls fibre diameter and small role on fiber deposition within collector. Beaded fibers if distance is too short.
Solution	Polymer concentration	Limits formation of Taylor cone (due to viscosity) and control fibre diameter
	Solvent volatility	Controls presence of microtexture on fibers
	Solution conductivity	Controls fibre diameter and its distribution across the fibrous membrane
Environmental	Temperature	Relates to solvent volatility and viscosity and controls fibre diameter
	Humidity	Relates to solvent volatility and controls fibre diameter.

Blend electrospinning, coaxial electrospinning and emulsion electrospinning are techniques that have been developed to encapsulate and deliver relevant molecules for biomedical applications such as drugs, growth factors, genes, and proteins [119]. Coaxial electrospinning requires to simultaneously electrospun two polymer solutions (usually with different hydrophilic profiles) through different channels into one

capillary to generate composite fibers with a core-shell structure. In contrast, blend electrospinning involves the mixing of the polymer solution with the drug followed by a conventional electrospinning method. Different strategies to introduce the drug have been implemented such as drug-loaded nanoparticles or microspheres, introducing another blend of polymer with the drug, and creating an emulsion of both polymer and drug by introducing different solvents (known as emulsion electrospinning) [112], [120], [121].

In general, electrospun fibres prepared by either blend or coaxial electrospinning show a burst release profile that is mostly used for rapid delivery rather than for extended periods of time [103]. However, new developments in electrospinning have allowed for a more controlled release using different polymer blends such as the work published by Kenawy et al. in which PLA and poly(ethylene-co-vinyl acetate) were used to produce a sustained release of tetracycline HCl [122]. Furthermore, controlled release of heparin [123], VEGF [124], and NGF [125] has been successfully achieved by blend or coaxial electrospinning. However, there is still controversy about the loss in bioactivity or decrease in the short-life of drugs loaded into electrospun fibres due to interactions with the solvent [126], [127].

2.5.3 Addition of chemical cues to NGCs

Even though NGCs with architectural features enhance and guide the regeneration of neurites and Schwann cell migration, nerve regeneration is still not satisfactory [86], [128]. Therefore, the inclusion of chemical cues might be a good alternative to enhance NGCs performance. Specifically, the addition of neurotrophic factors into the NGC would improve neurite outgrowth and Schwann cell migration as neurotrophic factors aid peripheral nerve regeneration after injury [128]–[130].

2.5.3.1 Nerve growth factor and brain derived neurotrophic factor

Neurotrophic factors are a family of growth factors that regulate survival, function, development and repair of the nervous system, both central and peripheral systems [131]–[133]. This family is subdivided in three groups: neurotrophins, that include

nerve growth factor (NGF), brain derived neurotrophic factor (BDNF), neurotrophin-3 (NT-3), and neurotrophin-4/5 (NT-4/5) [131], [133], [134]; neurokines, which include ciliary neurotrophic factor (CNTF) and leukemia inhibitory factor (LIF); and the transforming growth factor-β group (TGF- β), that includes TGF- β1, TGF- β2, TGF- β and glial-cell derived neurotrophic factor (GDNF) [131], [133], [134].

NGF is a 26 kDa homodimeric protein, which binds to two different transmembrane receptors: a 140 kDa high affinity tyrosine kinase receptor A (TrkA) and a 75 kDa low affinity receptor p75 neurotrophin receptor ($p75^{NRT}$) [86], [133]. NGF stimulates sensory and sympathetic neuron survival, neurite outgrowth and Schwann cell migration, regulation of peptides and neurotransmitters [2], [77], [86], [132], [133], [135]. NGF expression in the PNS increases after nerve injury [86], [133].

BDNF is a 13.5-14 kDa homodimeric protein [136]–[138]. The expression of BDNF in the CNS is higher than in the PNS. Nevertheless, after peripheral nerve injury, expression of BDNF is upregulated by motor neurons, DRG and Schwann cells [86], [133], [137]. Furthermore, BDNF binds to two transmembrane receptors, the 145 kDa TrkB and $p75^{NRT}$ [77], [86], [133], [137], [139]. BDNF promotes cell survival, differentiation, neurite outgrowth, remyelination (through $p75^{NRT}$ of Schwann cells), and regulates function and neuromuscular synapses [2], [77], [132], [133], [140], [141]. Nevertheless, BDNF may cause inhibitory responses when activating $p75^{NRT}$ [77].

When NGF and BDNF bind to TrkA and TrkB respectively, autophosphorylation occurs and intracellular signalling pathways are activated. These pathways include the phosphatidylinositol-3 kinase/protein kinase B (PI3K/Akt) and mitogen activated protein kinase/ extracellular receptor kinase (MAPK/ERK, also known as MEK) pathways, which stimulate cell survival, function, proliferation, migration, differentiation and neurite outgrowth [137], [138], [141]–[143]. Activation of MEK above threshold might be toxic. However, basal activity will promote neuronal survival [141]. Additionally, PI3K/Akt increase actin expression and microtubule reorganisation for neurite outgrowth [131], [137]. The general binding mechanism of NGF and BDNF is shown in Figure 9.

P75^{NRT}, a member of the tumour necrosis factor receptor family, binds to NGF, BDNF, NT-3 and NT4/5 [134], [137]. This receptor may elicit positive and negative signals, for example, by regulating RhoA, it may stimulate remyelination after injury or, might inhibit neurite outgrowth [137], [143]. Furthermore, if NGF binds only to p75^{NRT}, apoptosis signals are activated [142]. When either NGF or BDNF bind to both receptors Trk and p75^{NRT}, signals are differently combined to promote specific functions [134], [144]. For example, the effect of BDNF in neurite outgrowth depends on the expression levels of TrkB and (or) p75^{NRT} in neurons [141]. Furthermore, when NGF binds to TrkA and p75^{NRT}, cell viability is controlled by apoptosis [134].

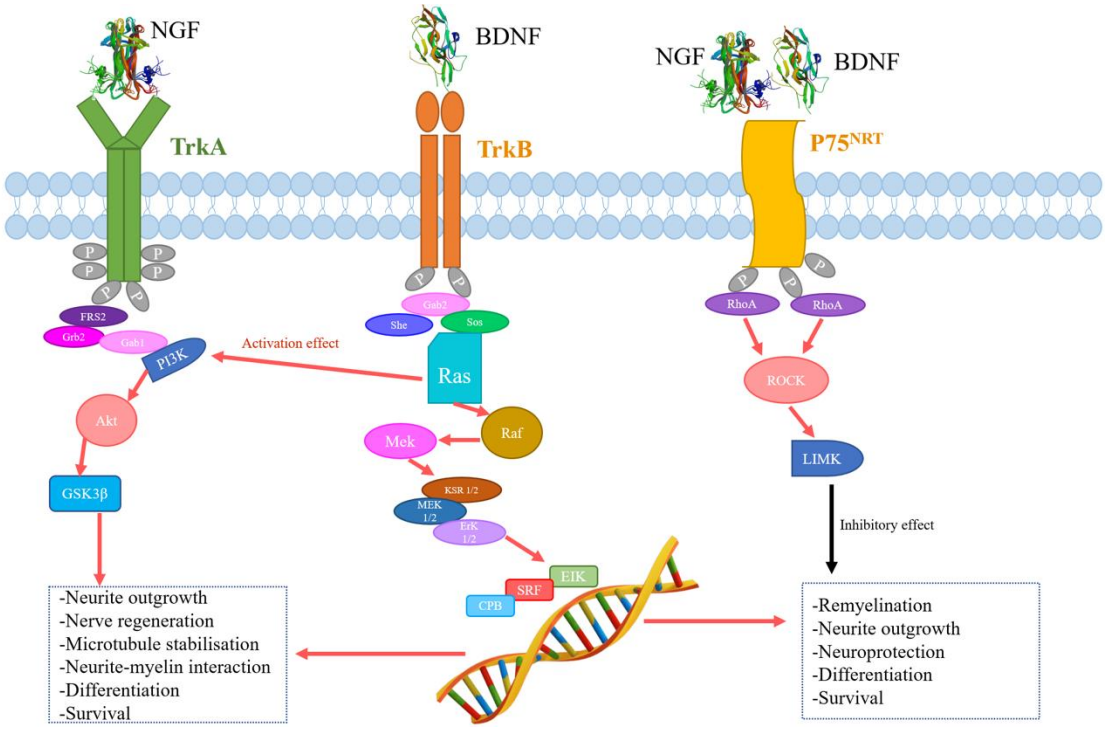

Figure 9. Representation of the general binding mechanism and signalling pathways of NGF and BDNF. When NGF and BDNF bind to their respective Trk receptors, signalling pathways are activated, which encourage cell survival, proliferation, differentiation, neurite outgrowth, synaptic plasticity, neurotransmitter release. Based on [138], [143]. NGF and BDNF images from the RCSB PDB [145], [146].

As NGF and BDNF are two important neurotrophins that aid neurite outgrowth, cell survival and differentiation after peripheral nerve injury, NGF and BDNF have been used in the clinic to treat chronic ulcerations and diabetic neuropathy [143]. Even though the outcomes were positive, the side effects, such as myalgia and hyperalgesia in the injection site, surpassed the outcome of the treatment [135]. Furthermore, NGF and BDNF had also been used in clinical trials for HIV-associated peripheral neuropathy, brain injury, glaucoma, macular degeneration, Alzheimer's disease, Parkinson's disease, using dosages ranging from 0.03 to 1 μg/kg [135], [138], [142], [143]. Side effects were also reported: hyperalgesia at injection site, pain, myalgia, weight loss, local burning [135], [142]. Besides these side effects, other drawbacks such as the invasiveness of the method to deliver neurotrophins, the lack of guarantee that neurotrophins would be deliver at site of injury without affecting other areas, inadequate neurotrophins doses, neurotrophin degradation [138], [143], [147] make this treatment deficient.

Currently, research has been conducted to find a treatment that overcomes the disadvantages aforementioned. This research has included growth factors into the NGCs, focusing on extending the neurotrophins half-life, searching for the optimal neurotrophin dose, and on the continued application of neurotrophins in the injury site to aid nerve regeneration [143].

2.5.3.2 Inclusion of neurotrophins into NGCs

Although NGCs support nerve regeneration in short injury gaps, sufficient functional recovery from complete transected nerves in injury gaps longer than 20 mm might need the use of exogenous growth factors [128]. Hence, research has designed growth factors delivery systems to be included in an NGC. These delivery systems include the use of the wall of the NGC, microspheres seeded into the wall/lumen of the NGC, matrices loaded inside the lumen of the NGC, immobilisation of growth factors, aligned fibres inside the lumen of the NGC, from which the growth factor might be released [2], [78], [128], [148], [149] (Figure 10). Furthermore, immobilisation of growth factors is achieved by chemical or physical interactions, such as electrostatic interactions (physical adsorption) and covalent binding [150].

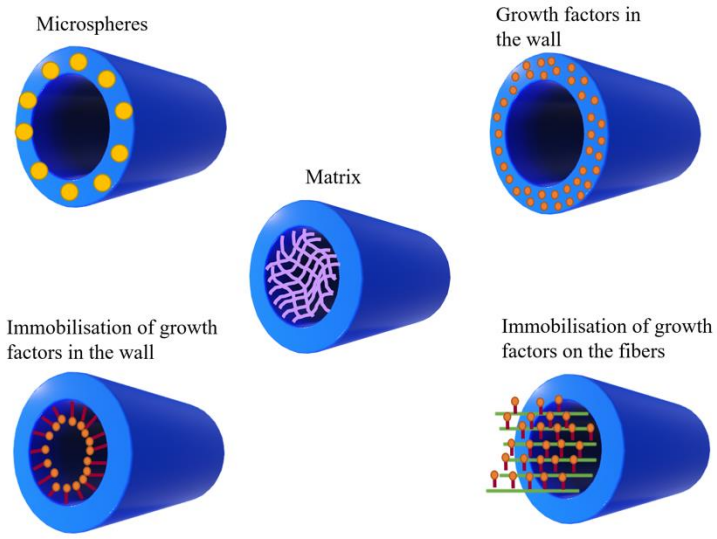

Figure 10. Schematic showing strategies to add growth factors into an NGC

Loading growth factors into the wall of an NGC is an approach for the later delivery of growth factors at the site of nerve injury. For example, Piotrowicz and Shoichet coated NGF directly into the wall of the poly(2-hydroxyethyl methacrylate-co-methyl methacrylate) and showed that NGF was completely released by day 1 [151]. Utley et al. covalently added BDNF to a collagen NGC and showed that functional recovery was achieved in a rat sciatic model [152]. Additionally, Chen et al. covalently bound NGF to a gelatin-tricalcium phosphate membrane, where the initial burst release of NGF was 60% [153]. Chang fabricated a porous PCL conduit to which gelatin solution was injected. Then, this solution was crosslinked with genipin to then bind NGF [154]. This conduit was tested *in vivo* in a rat sciatic nerve model and showed that more myelinated neurites were developed [154].

Matrices fabricated with collagen, laminin, heparin and alginate are frequently used to load NGF, BDNF, bFGF or VEGF. These matrices are then placed inside the lumen of the NGC [128], [155]. Depending on the nature of the material to fabricate the matrix, the matrix could bind growth factors by covalent binding or electrostatic interactions [128]. For example, Li et al. designed a heparin-poloxamer hydrogel loaded with NGF and bFGF (by electrostatic interactions) to improved peripheral nerve regeneration in a rat model [156]. Furthermore, Sakiyama-Elbert and Hubbell loaded NGF to a heparin-fibrin based matrix, and found that NGF and heparin bound

even though the duration of that binding was short [157]. Santos et al. loaded NGF, BDNF and NT-3 in a collagen matrix inside a silicon NGC to enhance nerve regeneration in a sciatic nerve model [158]. These matrices decrease initial growth factor burst release due to their viscous nature, nevertheless, this property might impede neurite outgrowth and Schwann cell migration [128].

Microspheres are being studied for the delivery of growth factors [2], [128]. This approach facilitates the loading of different growth factors, fabricating a specific microsphere type [2], [128]. Moreover, microspheres may be fabricated with different degradation properties to control growth factor dosing [2], [128]. Microspheres could be loaded into the lumen or into the wall of the NGC. If microspheres are loaded in the lumen, these can be in suspension or in a hydrogel [2], [128]. Zhang et al. encapsulated erythropoietin or NGF in PLGA microspheres, and found their potential to aid nerve regeneration in a rat sciatic nerve model [159]. Moreover, Yu et al. evaluated NGF loaded microspheres on nerve regeneration in a crush injury model [160]. Furthermore, Xu et al. encapsulated NGF in a phosphoester and ethylene terephthalate microsphere. NGF microspheres were loaded in the lumen of an NGC and implanted in a rat sciatic nerve model, which showed a higher number of developed neurites in comparison to the control [161]. Nevertheless, disadvantages on using this method include the complexity in protein encapsulation, and to preserve the bioactivity of the growth factor, as this is hampered by solvents (e.g., dichloromethane) used during the encapsulation process.

Furthermore, fibres have been also studied to deliver growth factors. For example, Whitehead et al. encapsulated NGF in PLGA microspheres which then were added to a methacrylated hyaluronic acid which was subsequently electrospun to fabricate aligned fibres [79]. DRG evaluation on the fibres revealed that NGF delivered from the PLGA microspheres and methacrylated hyaluronic acid fibres improved neurite outgrowth [79]. Moreover, Liu et al. encapsulated NGF and GDNF in PDLLA and PLGA fibres, respectively, using emulsion electrospinning [162]. Tests with PC12 neuronal cells showed that NGF and GDNF encouraged longer neurite lengths [162]. Ma et al. prepared a collagen-binding domain (CBD) to immobilise VEGF into collagen fibres. Then, these VEGF-CBD-collagen fibres were introduced to a collagen

NGC, which was tested in a rat sciatic nerve model [163]. This study showed that recovery of nerve function was higher compared to control groups [163]. In addition, Dinis et al. added NGF and CNTF to a silk solution to fabricate align electrospun fibers [164]. DRG evaluation showed Schwann cell migration and aligned neurite outgrowth [164]. Also, Guex et al. covalently immobilised VEGF on an oxygen plasma treated electrospun PCL scaffold, showing that proliferation of endothelial cells was increased [165].

Even though positive results have been shown of nerve regeneration using different methods to add growth factors, loss in bioactivity or decreased short half-life due to interactions with the solvent used [126], [127] are limitations, therefore leading to the study of an alternative approach to incorporate growth factors with a solvent-free method. Loading molecules by electrostatic interactions and affinity binding domains are promising methods for the addition of growth factors to a delivery system. Collagen and laminin domains were used to bind NGF and CNTF to collagen scaffolds and laminin-collagen fibres to support nerve regeneration in a rat sciatic nerve model [78], [149]. Furthermore, as all growth factors have a heparan sulphate proteoglycan (HSPG) binding domain [143], and the structure of heparin is similar to heparan sulphate [166], heparin would be an ideal candidate to test to bind growth factors, and therefore, fabricate a bioactive surface that would work as a delivery system.

2.5.3.3 Heparin

Heparin is a linear polysaccharide, member of the glycosaminoglycans (GAGs) family, composed of a uronate residue and a D-glucosamine residue [166]. Its uronate residues are mostly α-L-iduronate and its D-glucosamine residues are N-sulfated [166]. Heparin is composed, at least 70% of the disaccharide L-iduronate-2-O-sulfate D-glucosamine N,6-sulfate [166]–[168]. Schematic representation of the disaccharide unit of heparin is shown in Figure 11. As heparin has a high content of sulfates, it has higher charge and it has the strongest growth factor binding site in comparison to other GAGs [166], [167], [169], [170].

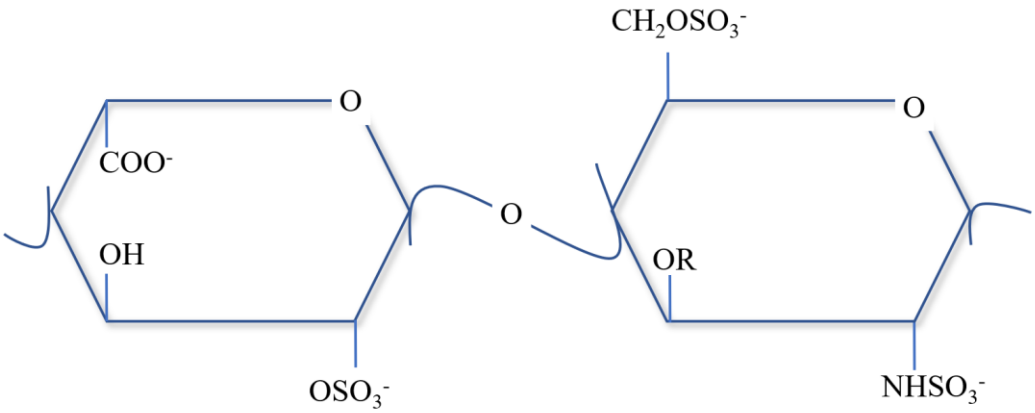

Figure 11. Schematic diagram of the main disaccharide unit of heparin L-iduronate-2-O-sulfate D-glucosamine N,6-sulfate.

The most conventional use of heparin is as an anticoagulant because it prevents thrombus formation by binding and activating the serine protease inhibitor antithrombin [166], [171]–[173]. Nevertheless, heparin could cause thrombocytopenia as a consequence of extended exposure [172]. Therefore, heparin has been immobilised to polymers to fabricate haemocompatible medical devices, for example, Pandiyaraj et al. immobilised heparin on polyethylene terephthalate films to improve anti-thrombogenic properties, such as platelet adhesion [174].

Furthermore, research has shown that negatively charged heparin is able to bind to different growth factors, through their positively charged amino acid residues lysine and arginine, extracellular matrix proteins (fibronectin, laminin), and to different receptors activating intercellular signalling [166]. For example, heparin binds to VEGF or bFGF to encourage angiogenesis [166], [175], [176].

As heparin binds different growth factors, this GAG could be used to bind neurotrophins to a biomaterial. For example, heparin was bound to a modified version on antithrombin III-heparin binding domain contained in a fibrin matrix, and then GDNF was bound to heparin. Results showed that this matrix stimulated nerve regeneration in a rat sciatic nerve model [177], [178].

Heparin has been covalently bound to different polymeric surfaces. Usually, heparin is covalently bound to protein using (1-ethyl-3-(3-dimethylamino-propyl)) carbodiimide (EDC) [179]. For example, Zhu et al. covalently immobilised a chitosan/heparin complex on a PLA surface using EDC and a solution of 4-azidobenzoic acid [180]. Liao et al. covalently immobilised heparin to a decellularised artery using EDC [181]. Nonetheless, covalent binding techniques could modify the functionality of heparin [182], therefore, binding heparin by electrostatic interactions is a promising approach.

Layer-by-layer film assembly technique has been used to electrostatically bind molecules. This technique consists of depositing polycationic and polyanionic polymers from aqueous solution to create alternating charged layers [81]. Kreke et al. prepared a poly(allylamine hydrochloride) (PAH) solution and a heparin solution and created a film that consisted of 10 bilayers on silicon wafers, demonstrating that these films encouraged cell adhesion [81]. Moreover, Elahi et al. prepared 1.5 and 2.5 bilayers on silk fibroin using PAH and poly(acrylic acid) (PAA) and added heparin on the PAH layer, showing that this device improved haemocompatibility [183]. However, layer-by-layer technique might change the mechanical properties, such as tensile strength and elongation at break. Furthermore, if the topography of the substrate wants to be preserved, layer-by-layer technique might interfere with this [184], [185]. Plasma deposition technique has been used to functionalise surfaces to improve cell adhesion properties [186]. Furthermore, if plasma deposition can add positively charge functional groups on the surface of a material, therefore, heparin could be bound by electrostatic interactions.

2.5.3.4 Plasma deposition

The use of polymers in medical applications has been popularised due to their versatility to meet specific tissue engineered requirements of mechanical, chemical, and conductive properties. However, in order to achieve cell adhesion, which is critical for biomedical applications, most synthetic polymers require activation of their surface. Therefore, modifying the surface properties of a polymeric device without

altering the bulk properties is key [187]. Among the different techniques for surface treatment such as wet chemistry, UV irradiation, or self-assembly monolayers, plasma deposition is one of the most versatile and effective techniques [172].

Wet chemistry is a combination of techniques that generates functional groups on the surface of a polymer by using liquid reagents. The advantages of this approach over plasma deposition include the capacity of penetrating porous 3D substrates, the lack of specialized equipment, and the ability to perform *in situ* functionalization for specific applications. However, significant limitations of wet chemical techniques include non-specificity that produces a variety of oxygen-containing functional groups, chemical contamination, and low repeatability dependent on polymer molecular weight and crystallinity [172], [188].

UV irradiation uses a similar mechanism to plasma deposition as a polymer surface is exposed to UV light to generate reactive sites that can become functional groups by the exposure of a gas. The main difference of UV irradiation is that it is possible to control the depth of surface reactivity by changing the absorption coefficient through altering the wavelength of the UV source [172], [187], [189]. However, certain disadvantages had limited UV surface treatment. For example, the polymer needs to be photoactive to interact with the UV source and the ageing effect of the surface is stronger and most surfaces suffer from hydrophobic recovery over a period of time [190]. Additionally, exposure to UV has been reported to cause photooxidative degradation on certain polymers [191].

Self-assembled monolayers (SAMs) is a technique that creates a film by molecular assemblies formed by the adsorption of a surfactant on a polymer surface. This approach allows for the control of both head and tail functional groups but requires a deep understanding of the self-organization molecular hierarchy and the interfacial properties of the polymer. Although SAMs are commonly used for electronic devices, monolayers fabricated for biomedical applications include fatty acids and alkylsiloxanes [172], [192]–[194].

Plasma deposition is a fast reaction and waste-free surface treatment process that has been used to treat polymeric surfaces for medical applications. The reactions between

plasma and a polymer surface can be divided into 3 groups: surface reactions, plasma cleaning, and plasma polymerization [187]. The basic mechanism of plasma deposition is to expose the polymer surface to the plasma, a high energy state of matter in which charged particles, radical species, electrons, and neutral molecules are created from ionized gas. The ionized gas is typically obtained when the gas is excited by radio frequency, direct current, electrons from a hot filament discharge, or microwaves. Additionally, plasma deposition is often achieved using low-pressure systems (vacuum), although new developments have led to the use of atmospheric-pressure plasma [172], [195], [196].

Depending on the selected gas, specific surface properties can be achieved, for example, oxygen plasma increases the surface energy of a polymer surface, in contrast with fluorine plasma which decreases surface energy. Table 4 shows an overview of the use of plasma deposition for tissue engineering applications The general result from the plasma deposition is an insoluble, mechanically tough, and thermally stable film that can range from 100 Å to 1 μm [197]. However, the disadvantages of the plasma deposition treatment are related to not being able to control the amount of a particular functional group and that the process parameters are highly system-dependent [187].

Table 4. Plasma deposition as a surface treatment technique for tissue engineering applications.

Ionized gas	**Application**	**Ref**
Oxygen	Surface treatment of rapid prototyping polydimethylsiloxane (PDMS) microchannels to improve cell adhesion and electro osmotic flow.	[186]
	3D printed hydroxyapatite/gelatin/chitosan composite scaffolds were treated to improve bioactivity.	[198]
	Electrospun poly(ethylene oxide terephthalate)/poly(butylenee terephthalate) fibres treated to improve protein adsorption and induce osteogenic differentiation.	[199]
	Treatment of ultra high molecular weight polyethylene fibres to chemically graft PVA hydrogels for soft tissue applications.	[200]
Nitrogen	Amination of PVA hydrogel by H_2/N_2 plasma to increase surface wettability and cell attachment.	[201]
	Amine groups introduced to 3D surfaces to promote attachment, proliferation, and osteogenic differentiation of human adipose derived stem cells.	[202]
	Use of allylamine treated 2D surfaces for the delivery of growth factors to improve neurite outgrowth.	[203]
Argon	Chitosan membranes treated to increase surface hydrophilicity to improve human skin fibroblasts attachment and proliferation.	[204]
	Silk fibroin nanofibrous scaffolds treated to improve cell behaviour of human articular chondrocytes.	[205]
Fluorine	PDMS surface treated to maintain hydrophobic characteristics, improve biocompatibility, and reduce cytotoxicity.	[206]
	Biomedical-grade zirconia treated to create the more reactive zirconium oxyfluoride for dental applications	[207]

There are different forms in which the plasma reactor can be designed, and the process parameters differ among setups. Radiofrequency glow discharge (RFGD) plasma and direct current glow discharge (DCGD) plasma are some of the most common low-pressure plasma setups available. Both setups have a chamber in which to create a low-pressure environment. DCGD uses electrodes to create and direct a potential difference that produces higher ion bombardment towards the cathode and higher electron bombardment towards the anode [208]. In contrast, RFGD uses an internal or external electrode to create a discharge that can generate a stable large volume of plasma [196]. A schematic of a basic RFGD plasma setup is shown in Figure 12.

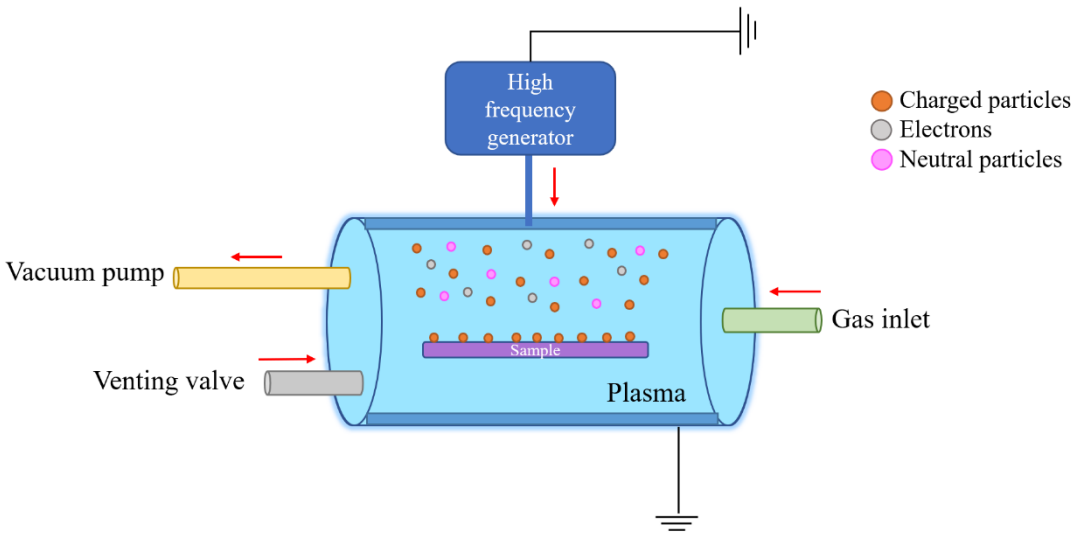

Figure 12. General configuration of a RFGD plasma setup. The sample is placed inside the chamber that is surrounded by an external RF generator. The discharge tube (chamber) is usually made of quartz or borosilicate. Once the chamber is sealed, a vacuum pump is used to create a low-pressure environment. The gas inlet is open after the vacuum is created to allow the gas to fill the entire chamber. After reaching a specific pressure threshold, the RF generator is activated, forming an ionized gas that creates a discharged glow inside the chamber. The exposure time varies according to the application. Finally, the venting valve is open to allow the system to recover atmospheric pressure. The general RFGD plasma parameters are 13.56 MHz with pressure during discharge between 10^{-3} and 100 Torr [196].

2.5.4 Bioactive surface for the delivery of NGF and BDNF

Plasma deposition has been used to bind heparin, either by covalent techniques or by electrostatic interactions. Cheng et al. functionalized PLL fibrous scaffolds using argon-ammonia plasmas. Then, heparin was covalently bound by EDC and N-hydroxysulfosuccinimide (NHS) [209]. Yang et al., modified stainless steel with poly(allylamine) plasma deposition and then covalently bound heparin by NHS and EDC [210]. Nevertheless, as mentioned before, covalent binding techniques use solvents that might cause the loss of bioactivity in heparin. Therefore, electrostatic interactions should be used to bind heparin to a surface.

The surface of a material can be functionalized by plasma deposition technique, by adding negatively charged or positively charged functional groups. For example, Mahoney et al. modified microtiter wells using allylamine plasma deposition. Then, a heparin solution was added to the wells and incubated overnight [211]. Results showed that heparin was bound to the surface [211]. Furthermore, Robinson et al. functionalised microwell plates using allylamine plasma deposition. Then, a heparin solution was added and incubated overnight. After, either tissue inhibitor of metalloproteinases 3 (TIMP-3) or osteoprotogerin (OPG) were bound to heparin [212]. Their results showed that allylamine was deposited on the surface, and that heparin and TIMP-3 or OPG were also on the surface [212]. Furthermore, another study by Robinson et al. reported the addition of amine (NH_2^+) functional groups on melt electrospun PCL scaffold by allylamine plasma deposition [213]. Then, heparin was added to the surface followed by FGF-2 immobilisation. Their results showed that NH_2^+ and FGF-2 were added to the surface. In addition, biological evaluation showed that keratinocytes and fibroblasts were proliferating and forming layers [213].

Therefore, a bioactive surface could be fabricated for the local and sustained delivery of neurotrophins. Plasma deposition would functionalise a surface with positively charged groups using allylamine ($C_3H_5NH_2$), to where heparin would bind. Then, neurotrophins, either NGF, BDNF or a combination of NGF plus BDNF would be added and immobilised to heparin by electrostatic interaction. As PCL is a biodegradable polyester, $(C_6H_{10}O_2)_n$ [214], the bioactive surface NH_2^+ + Heparin +

Immobilised NGF/BDNF/NGF plus BDNF could then be incorporated to PCL electrospun scaffolds.

2.6 Hypothesis

In summary, the nerve repair process is complex and cannot heal long injury gaps (> 5 mm). Therefore, exploring new alternatives for effective treatment of long gap nerve injuries is essential to improve the patient's quality of life. Based on the previous knowledge from our group [215], the following hypothesis was proposed:

Bioactive surfaces NH_2^+ + Heparin + Immobilised NGF, NH_2^+ + Heparin + Immobilised BDNF and NH_2^+ + Heparin + Immobilised NGF plus BDNF, fabricated by allylamine plasma deposition, heparin passive conjugation and immobilisation of NGF, BDNF or a combination of NGF plus BDNF would significantly encourage neurite outgrowth by the local and sustained delivery of neurotrophins.

Chapter 3 Aims and objectives

The aims of this thesis were:

- To develop a scalable bioactive surface that encourages neurite outgrowth, using amine groups NH_2^+, heparin and growth factors, specifically nerve growth factor (NGF) and brain derived neurotrophic factor (BDNF).
- To identify the optimal concentration of growth factors to use to maximise neurite outgrowth in dorsal root ganglia (DRG).

The objectives of this thesis were:

1. To fabricate and characterise the bioactive surface in tissue culture plastic (TCP).
2. Evaluate the effects of the bioactive surface (in TCP) when immobilised with NGF, BDNF and NGF plus BDNF on NG108-15 neuronal cell line and PC12 adh neuronal cell line.
3. Assess the effects of the bioactive surface (in TCP) when immobilised with NGF, BDNF and NGF plus BDNF on dorsal root ganglia (DRG).
4. To fabricate and characterise the bioactive surface in polycaprolactone (PCL) align electrospun fibres; and to evaluate the effects of the bioactive surface in PCL electrospun fibres in DRG.

Chapter 4 Materials and Methods

In this chapter, materials and methods used in this project are described. Additionally, each chapter describes their specific methodology used therein.

Please refer to Table 20 in the appendix for the catalogue number of all reagents used.

For simplicity, the culture medium used is described next:

- Culture medium: composed of Dulbecco's Modified Eagle's Medium (DMEM, Sigma, United Kingdom), 10% foetal bovine serum v/v (FBS, PAN Biotech, Germany), 1% L-glutamine v/v (200 mM, Sigma, United Kingdom), 1% penicillin-streptomycin v/v (P/S, 10,000 units penicillin / 10 mg/mL streptomycin, Sigma, United Kingdom), 0.25% amphotericin B v/v (250 µg/mL, Sigma, United Kingdom).
- Serum-free medium: composed of DMEM (Sigma, United Kingdom), 1% L-glutamine v/v (200 mM, Sigma, United Kingdom), 1% P/S v/v (10,000 units / 10 mg/mL, Sigma, United Kingdom), 0.25% amphotericin B v/v (250 µg/mL, Sigma, United Kingdom).
- Schwann cell isolation medium: MEM Eagle D-Valine (USBiological Life Sciences, USA), 1% L-glutamine v/v (200 mM, Sigma, United Kingdom), 10% FBS v/v (PAN Biotech, Germany), 0.25% amphotericin B v/v (250 µg/mL, Sigma, United Kingdom), 1% P/S v/v (10,000 units /10 mg/mL, Sigma, United Kingdom), 0.35% N2 supplement v/v (100x, 1 mM human transferrin, 0.0861 mM insulin recombinant, 0.002 mM progesterone, 10.01 mM putrescine, 0.00301 mM selenite, Invitrogen, United Kingdom), 0.15% v/v bovine pituitary extract (22 mg/mL, Sigma, United Kingdom), 0.01% v/v forskolin (10 mg/mL, Sigma-Aldrich, United Kingdom).

4.1 Fabrication and characterisation of bioactive surface

4.1.1 Adding heparin and growth factors to TCP + NH_2^+ surface

4.1.1.1 Heparin conjugation

A solution of heparin sodium salt from porcine intestinal mucosa (Sigma, United Kingdom) was prepared at a concentration of 50 µg/mL in phosphate buffered saline (PBS, Oxoid, United Kingdom). Then, the solution was filtered sterilized with a filter of 0.2 µm pore size (Filtropur S, Sarstedt AG & Co., Germany). The heparin solution was added to 96-well plates pre-coated with amine groups (TCP + NH_2^+, Becton Dickinson, BD PureCoat^{TM}, Belgium) and left overnight at room temperature. Finally, the heparin solution was discarded, and the surfaces washed one time with PBS. After performing this step, this surface became the bioactive surface TCP + NH_2^++ Heparin (Figure 13.C).

4.1.1.2 Immobilisation of nerve growth factor and brain derived neurotrophic factor.

Nerve growth factor (NGF, R&D systems, USA), brain derived neurotrophic factor (BDNF, R&D systems, USA) and combinations of NGF plus BDNF were immobilised onto the bioactive surface TCP + NH_2^+ + Heparin (prepared as described in section 4.1.1.1). Different concentrations of NGF, BDNF and NGF plus BDNF were prepared at concentrations of 1 pg/mL, 1 ng/mL, 10 ng/mL, 100 ng/mL and 1 µg/mL in sterile PBS. Each solution was added onto the bioactive surface and incubated for 5 hours at room temperature (Figure 13.D). Then, the solution was discarded, and the surface was washed one time with PBS. The bioactive surface with immobilised NGF and/or BDNF was now created (Figure 13.E). Figure 13 illustrates the design of the bioactive surface with immobilised neurotrophic factors.

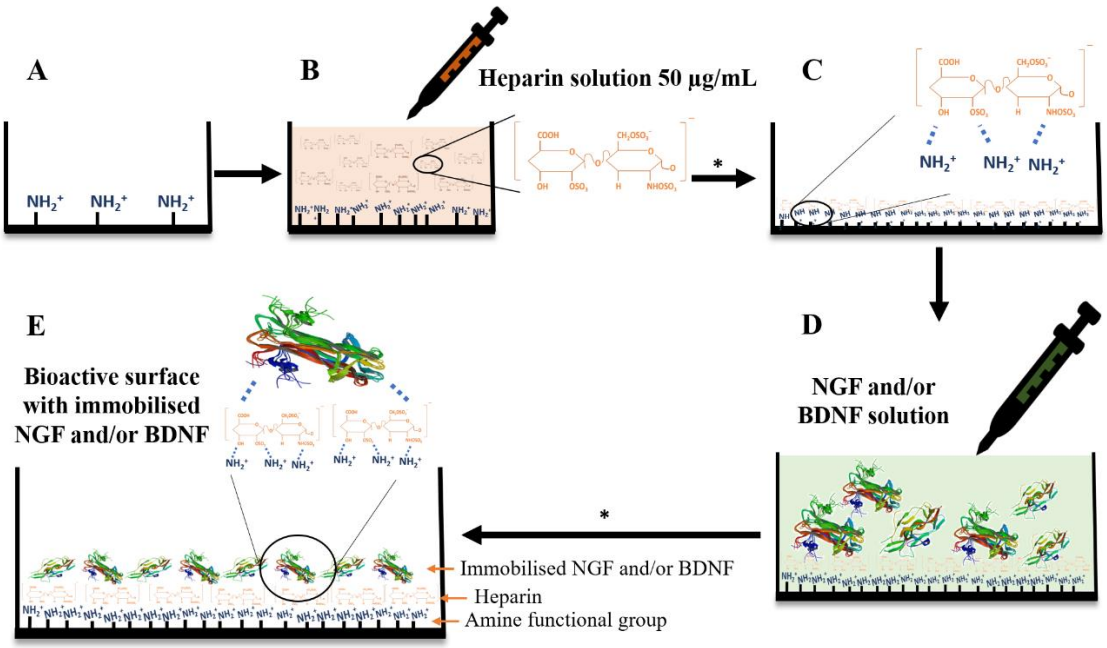

Figure 13. Schematic illustration of the fabrication of the bioactive surface with immobilised NGF and/or BDNF. A) TCP + NH_2^+ surface. B) A solution of heparin at 50 µg/mL was added. C) TCP + NH_2^+ + Heparin surface. D) NGF and/or BDNF solution was added. E) Bioactive surface with immobilised NGF and/or BDNF (TCP + NH_2^+ + Heparin + Immobilised NGF/BDNF). Each asterisk (*) above the arrows shows that at that step of fabrication, the surface was washed one time with PBS. NGF and BDNF images from the RCSB PDB [145], [146].

4.1.2 Surface characterisation

4.1.2.1 Water contact angle

Water contact angle was measured with Krüss GmbH drop shape analyzer-100 (DSA100) equipment by placing 5 µL of distilled water, from a 1 mL syringe (BD, United Kingdom) and 20-gauge needle (1 inch long Fisnar, USA) on top of the surface. Then, the contact angle of the bioactive surfaces was measured by sessile drop method and calculated with DSA100 software.

4.1.2.2 X-ray Photoelectron Spectroscopy (XPS) analysis

XPS analysis was performed at the Sheffield Surface Analysis Centre (The University of Sheffield, United Kingdom). Samples were interrogated to determine surface elemental composition (survey scans), carbon scans (C 1s), nitrogen scans (N 1s), and

sulphur scans (S 2p) using a Kratos Ultra instrument with a monochromated aluminium source (1486.6 eV). Elemental survey scans were collected between 1200 to 0 eV binding energy, 160 eV pass energy and 1 eV intervals. High resolution C 1s and N 1s scans were collected for all samples at 20 eV pass energy and 0.1 eV intervals. S 2p spectra were collected for samples containing heparin, at 20 eV pass energy, and 0.1 eV intervals. Two points per sample were analysed. The area of the analysis points was 700 µm by 300 µm. Data was processed and analysed using CasaXPS (version 2.3.19 PR 1.0, Casa Software Ltd).

4.1.2.3 Release profile of NGF and BDNF from bioactive surfaces

Methodology described in section 4.1.1 from this chapter was performed to prepare the bioactive surface with immobilised NGF or BDNF. Then, these bioactive surfaces were tested to investigate the release of NGF and BDNF from the bioactive surface. However, firstly, the quantity of NGF or BDNF bound to heparin needed to be calculated in order to quantify the percentage of growth factor released from the bioactive surface. In order to do this, the solution of NGF and BDNF which was removed after 5 hours of incubation (consequently called supernatant) was stored at -20°C for later enzyme-linked immunosorbent assay (ELISA).

In vitro release of NGF and BDNF was tested by incubating the bioactive surfaces immobilised with NGF or BDNF with 1 mL of PBS at 4°C and 37°C. Samples were taken at 1 hour, 24 hours, 48 hours, and 168 hours and kept at -20°C for ELISA assays [216], [217]. Standards for the calibration curve, provided as part of the kit, were prepared as serial dilutions in standard buffer. For samples taken from the supernatant and at 1 hour (both NGF and BDNF), 1:100 (1 µg/mL) and 1:10 (100 ng/mL and 10 ng/mL) dilutions were prepared with standard buffer to assure that the absorbance readings could be fitted inside the standard curve.

Firstly, standards and samples were added into the wells of the ELISA assay plate and incubated at room temperature for 2 hours and 30 minutes. Then, the samples and standards were discarded, and the plate rinsed with washing buffer (provided as part of the kit). Biotinylated antibody was added to the wells and incubated for1 hour at room temperature. The plate was then rinsed with washing buffer and Streptavidin-

HRP (horseradish peroxidase) was added. The wells were incubated for 45 minutes at room temperature. The plate was rinsed with washing buffer and 3,3',5,5'-tetramethylbenzidine (TMB) substrate was added and incubated for 30 minutes at room temperature, covered from light. Then, the stop solution was added. The absorbance was read at 450 nm using a Bio-Tek ELx 800 absorbance microplate reader and data was recorded using KC junior software 1.41.8 (Bio-Tek Instruments, USA).

4.2 *In vitro* studies with neuronal cell lines

4.2.1 General cell culture

Neuronal cell lines used in this thesis were handled using aseptic techniques and under sterile conditions in a class II biological safety cabinet (Airstream, ESCO Biotech, China). Cells were maintained in T-75 culture flasks (75 cm^2, Sarstedt, Germany) and incubated at 37°C and 5% CO_2. Cells were used within 10 passages. Culture medium and serum-free medium were pre-warmed at 37°C in a water bath prior to use. After pre-warming, growth factors were added to the culture medium or serum-free medium when needed.

4.2.1.1 Cell resurrection

Universal tube was prepared with 9 mL of warmed culture medium. Frozen cell vials were thawed in a 37°C water bath. Inside the biological safety cabinet II, cells were transferred to the universal tube. Then, the universal tube was centrifuged for 5 minutes at 1000 rpm. The supernatant was discarded, and the cell pellet was resuspended in 1 mL of warmed culture medium. A T-75 flask was prepared with 14 mL of warmed culture medium. The content of the universal tube was then transferred to the T-75 flask. Then, the T-75 flask was incubated overnight at 37°C, 5% CO_2. The next day, the culture medium was replaced with fresh, warmed culture medium. The cells in the flask were incubated until 80% - 90% confluency was reached.

4.2.1.2 Cell passaging

The T75 flask containing the cells was removed from the incubator and the cell culture medium was discarded. The cells were washed one time with PBS. Then, 5 mL of trypsin-ethylenediaminetetraacetic acid (Trypsin/ EDTA, ((0.5% wt/v) / (0.2% wt/v)), Sigma, United Kingdom) was added for 1 - 3 minutes. After inspecting that the cells were detached from the culture flask, 10 mL of culture medium was added to the T-75 flask. Then, the contents were transferred to a universal tube and centrifuged for 5 minutes at 1000 rpm. After, the supernatant was discarded, and the cell pellet resuspended in 1 mL of warmed culture medium. Then, 250 µL of cell suspension were transferred to a new T-75 flask with 15 mL of warmed culture medium. The T-75 flasks were incubated at 37°C, 5% CO_2 until confluency was reached before experiments were performed. Every 2 - 3 days, culture medium in the T-75 flasks was replaced.

4.2.1.3 Cell storage

Confluent cells from a T-75 flask were detached with Trypsin/EDTA, as described above (section 4.2.1.2). Then, the content was transferred to a universal tube and centrifuged for 5 minutes at 1000 rpm. The supernatant was discarded, and the pellet was resuspended with freezing medium (culture medium with 10% v/v dimethyl sulfoxide (DMSO, Alfa Aesar, United Kingdom). After, the cell suspension was transferred to cryo vials (1 mL per vial, Sarstedt, Germany). The cryo vials were placed in a freezer container (MrFrosty, Thermo Fisher, United Kingdom). This container was placed at a -80°C freezer. The cryo vials were kept at -80°C if they were used within 1 month, otherwise, the cryo vials were transferred to liquid nitrogen containers for long-term storage.

4.2.2 *In vitro* studies with NG108-15 neuronal cell line

An NG108-15 neuronal cell line (mouse neuroblastoma x rat glioma hybrid, cancerous. ECACC, United Kingdom) was seeded *in vitro* onto the bioactive surfaces (prepared as described in section 4.1.1) to evaluate the effects of the bioactive surface on neural length, percentage of neurons bearing neurites, maximum neurite length and

metabolic activity. Table 5 shows the bioactive surfaces that were prepared and later tested.

NG105-15 neuronal cells were detached with trypsin/EDTA from a T75 flask and centrifuged at 1000 rpm for 5 min. The supernatant was then discarded, and the cells were resuspended in cell culture medium. Cells were counted in a $1mm^2$ Neubauer cell counting chamber. Next, 500 cells were seeded per well in 150 µL of cell culture medium. These samples were incubated at 37 °C and 5% CO_2 for a total time of 7 days, where the culture medium was changed to serum-free medium with NGF, BDNF or NGF plus BDNF accordingly to Table 5, on day 2. For the bioactive surfaces with immobilised NGF, BDNF or NGF plus BDNF, serum-free medium with no growth factors was used. The experiment was performed three times independently. Each bioactive surface was tested in triplicate.

Table 5. Summary of the different surfaces and bioactive surfaces that were prepared, highlighting the delivery method of growth factor of each surface. NGF, BDNF and NGF plus BDNF solutions for immobilisation were prepared in PBS.

Surface	**Growth factor delivery method**	**NGF**	**BDNF**	**NGF plus BDNF**
TCP	In solution with culture medium	0 pg/mL	0 pg/mL	0 pg/mL
		1 pg/mL	1 pg/mL	1 pg/mL
		1 ng/mL	1 ng/mL	1 ng/mL
		10 ng/mL	10 ng/mL	10 ng/mL
		100 ng/mL	100 ng/mL	100 ng/mL
		1 µg/mL	1 µg/mL	1 µg/mL
TCP+NH_2^+	In solution with culture medium	0 pg/mL	0 pg/mL	0 pg/mL
		1 pg/mL	1 pg/mL	1 pg/mL
		1 ng/mL	1 ng/mL	1 ng/mL
		10 ng/mL	10 ng/mL	10 ng/mL
		100 ng/mL	100 ng/mL	100 ng/mL
		1 µg/mL	1 µg/mL	1 µg/mL
TCP+NH_2^++Heparin	In solution with culture medium	0 pg/mL	0 pg/mL	0 pg/mL
		1 pg/mL	1 pg/mL	1 pg/mL
		1 ng/mL	1 ng/mL	1 ng/mL
		10 ng/mL	10 ng/mL	10 ng/mL
		100 ng/mL	100 ng/mL	100 ng/mL
		1 µg/mL	1 µg/mL	1 µg/mL
TCP+NH_2^++Heparin	Immobilised on surface	0 pg/mL	0 pg/mL	0 pg/mL
		1 pg/mL	1 pg/mL	1 pg/mL
		1 ng/mL	1 ng/mL	1 ng/mL
		10 ng/mL	10 ng/mL	10 ng/mL
		100 ng/mL	100 ng/mL	100 ng/mL
		1 µg/mL	1 µg/mL	1 µg/mL

4.2.3 *In vitro* studies with PC12 adh neuronal cell line

A PC12 adh neuronal cell line (rat pheochromocytoma, cancerous, ATCC, USA) was seeded on bioactive surfaces prepared on pre-coated 96 well plates as described in section 4.1.1 and in Table *5*. PC12 adh neuronal cells were seeded *in vitro* to evaluate the effects of the bioactive surface on neural length, percentage of neurons bearing neurites, maximum neurite length and metabolic activity.

PC12 adh neuronal cells were detached with trypsin/EDTA from a T75 flask and centrifuged at 1000 rpm for 5 min. The supernatant was then discarded, and the cells were resuspended in cell culture medium. Cells were counted in a $1mm^2$ Neubauer cell counting chamber. Next, 700 cells were seeded per well in 150 µL of cell culture medium with NGF, BDNF or NGF plus BDNF accordingly to Table 5. These samples were incubated at 37 ℃ and 5% CO_2 for a total of 5 days. For the bioactive surfaces with immobilised NGF, BDNF or NGF plus BDNF, culture medium with no growth factors was used. The experiment was performed three times independently. Each bioactive surface was tested in triplicate.

4.2.4 Metabolic activity assay: MTS

CellTiter 96® AQ_{ueous} One Solution Cell Proliferation Assay (Promega, United Kingdom) was preformed to evaluate the effect of the bioactive surfaces on metabolic activity. This assay contains MTS, which is a tetrazolium compound [3-(4,5-dimethylthiazol-2-yl)-5-(3-carboxymethoxyphenyl)-2-(4-sulfophenyl)-2H tetrazolium] and an electron coupling reagent (phenazine ethosulfate, PES). Both come together in the same solution, which is used directly onto the samples. At day 7 (for NG108-15 neuronal cells) and at day 5 (for PC12 adh neuronal cells), 20% of CellTiter 96® AQ_{ueous} One Solution Cell Proliferation Assay solution (v/v) was added directly to the samples and incubated at 37 ℃ and 5% CO_2 for 4 hours and the samples were covered from light with aluminium foil. After the incubation period, the

absorbance was read at 490 nm with Bio-Tek ELx800 absorbance microplate reader and KC junior software 1.41.8 (Bio-Tek Instruments, USA).

4.2.5 Fixing and staining of NG108-15 and PC12 adh neuronal cell lines

A 3.7% solution of formaldehyde (FA, Sigma-Aldrich, United Kingdom) was added to each sample (30% v/v) and incubated for 15 minutes at room temperature as a pre-fixing step. Then, cell culture medium or serum free media with FA was discarded and 3.7% of FA was added and incubated for 45 minutes at room temperature. Then, FA was discarded, and the samples were washed one time with PBS. A 0.1% Triton X-100 solution in PBS (v/v) was added and incubated for 45 minutes at room temperature. After this incubation period, 0.1% Triton X-100 was discarded, and the samples washed 2 to 3 times with PBS. DAPI (4′,6-diamidino-2-phenylindole, 300mM, Sigma, United Kingdom) and phalloidin TRITC (Phalloidin–Tetramethyl rhodamine B isothiocyanate, Sigma-Aldrich, USA) solution (1:1000) in PBS was added to the samples and incubated for 1 hour at room temperature, covered from light with aluminium foil. The solution was discarded, and the samples washed 1 time with PBS. The samples were covered with PBS and stored at 4°C, covered from light with aluminium foil.

4.2.6 Epifluorescence microscopy

The images were obtained from the Inverted Olympus IX73 epifluorescent microscope and Micro-Manager 1.4.22 software (University of California, USA). A mercury lamp was used as a light source. To image DAPI and Phalloidin TRITC, excitation and emission wavelengths of λ_{ex} = 405 nm / λ_{em} = 450 nm and λ_{ex} = 540 nm / λ_{em} = 570 nm were used respectively.

Image J 1.52a software (National Institutes of Health, USA) [218] was used to measure the length of developed neurites and to count how many neurites were developed. Three images were taken per condition, and 10-15 neurites were measured to determine the averaged neurite length, averaged maximum neurite length and percentage of neurons bearing neurites. Background was subtracted (30-50 pixels) to enhance intensity and contrast.

4.2.7 Averaged neurite length calculations

For each image taken, 10-15 neurites were measured. The neurite was measured from the cell body to the tip of the neurite. Then, all neurites were averaged per condition, per repeat.

4.2.8 Averaged maximum neurite length calculations

For each image taken, 10-15 neurites were measured. The neurite was measured from the cell body to the tip of the neurite. The longest neurite was identified in each condition and then, it was averaged with the longest neurite from the other repeats (same condition).

4.2.9 Percentage of neurons bearing neurites calculations

For each image taken, 10-15 neurites were measured. Neurons with at least one neurite were counted as neurons bearing neurites. Neurons and neurons bearing neurites were counted per image and a percentage calculated according to Equation 1. An averaged value was calculated for the total of repeats.

$$\textit{Percentage of neurons bearing neurites (\%)} = \frac{\textit{number of neurons bearing neurites}}{\textit{Total number of neurons}} \times 100$$

Equation 1. Equation to calculate the percentage of neurons bearing neurites.

4.3 *In vitro* studies with primary cells

To evaluate the effects of the bioactive surface on primary neurons, chicken embryonic dorsal root ganglia (DRG) were utilised.

To study how the bioactive surface affect the migration of Schwann cells, these cells were isolated from DRGs.

4.3.1 Dorsal root ganglia dissection from chick embryos

Fertilised brown chicken eggs (Henry Stewart & Co Ltd, United Kingdom) were incubated at 37.5 ℃ and 50% – 70% humidity until embryonic development day 12 (EDD12) ((in compliance with UK Home Office Animals [Scientific Procedures] Act

1986 and definition of chicken as a Protected Animal from E14). The eggs were cracked in a biological safety cabinet to collect the embryo. The head of the chick embryo was removed with sharp surgical scissors. Then, the embryo was cleaned from its yolk, as seen in Figure 14.A, and its organs removed (Figure 14.B).

With the use of a dissecting microscope (Wild M3Z, Switzerland) and surgical tweezers, the DRG were dissected and placed in a petri dish with PBS and 10% P/S (v/v) (Figure 14.C) and any remains of the root were cut (Figure 14.D) [219]. DRGs were seeded at a density of one DRG per well on the bioactive surfaces in the prepared bioactive surfaces, as described in section 4.1.1. Firstly, they were seeded with a drop of 10 µL culture medium and then incubated at 37 ℃ for 1 hour to enhance adherence to the surface. Then, culture medium and NGF, BDNF or NGF plus BDNF was added as described in Table 6. For the bioactive surfaces with immobilised NGF, BDNF or NGF plus BDNF, culture medium with no growth factors was added. The DRGs were cultured for 7 days at 37 ℃ and 5% CO_2. Three independent tests were performed. Each bioactive surface was tested in triplicate.

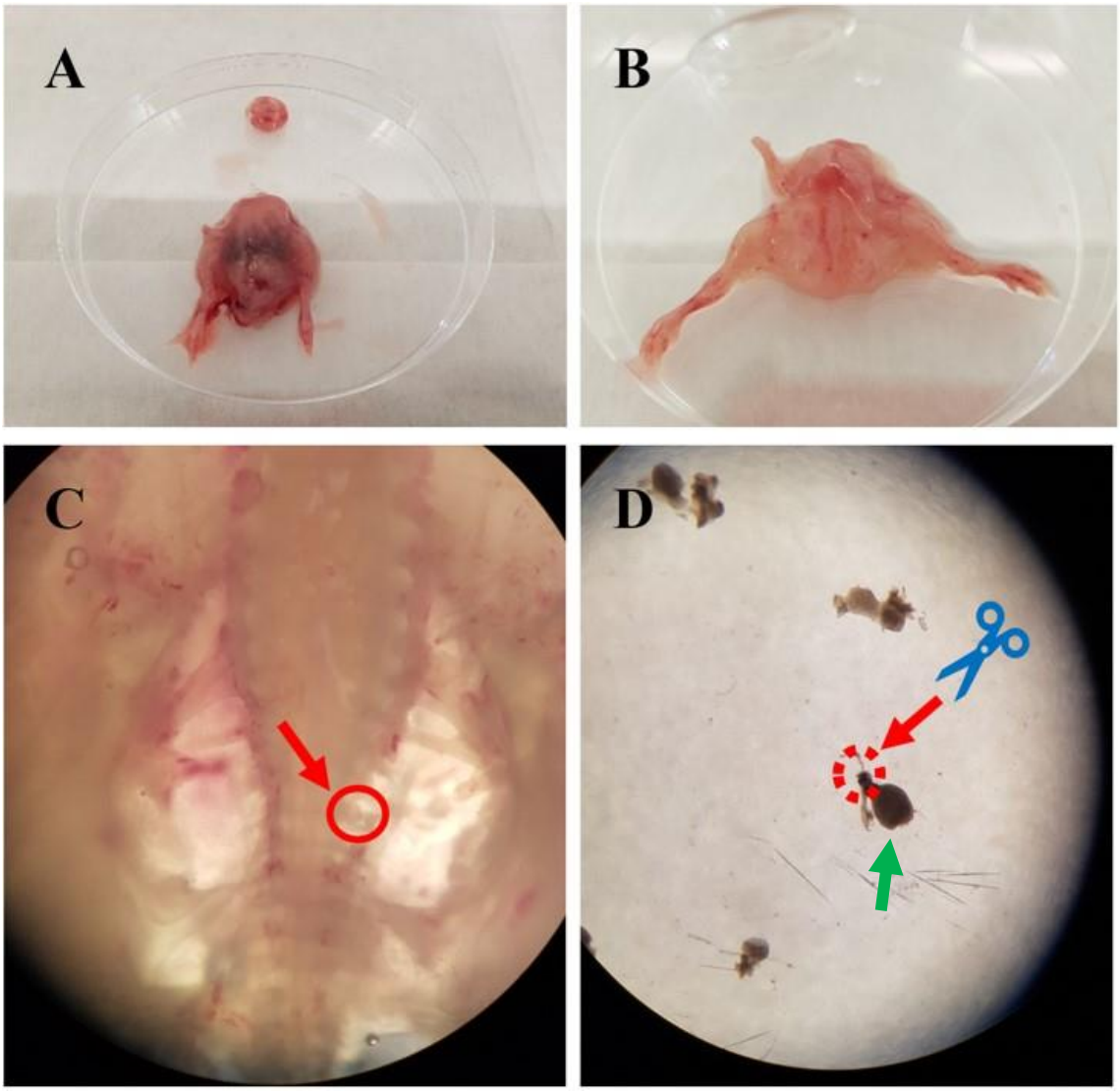

Figure 14. Photographs outlining dorsal root ganglia dissection from chick embryos EDD12. A) Chick embryo was cleaned from its yolk and the head was removed. B) The organs of the chick embryo were removed. C) View from the dissecting microscope. DRG is found next to the spinal cord (circled and signalled by arrow in red). D) DRG (green arrow) after being dissected from the chick embryo. Nerve root was cut (circled and signalled by arrow in red).

Table 6. The following surfaces were prepared, summarising the delivery method of growth factor for each surface. NGF, BDNF and NGF plus BDNF solutions for immobilisation were prepared in sterile PBS.

Surface	**Growth factor delivery method**	**NGF**	**BDNF**	**NGF plus BDNF**
TCP	In solution with culture medium	0 pg/mL	0 pg/mL	0 pg/mL
		1 µg/mL	1 µg/mL	1 µg/mL
TCP+NH_2^+	In solution with culture medium	0 pg/mL	0 pg/mL	0 pg/mL
		1 µg/mL	1 µg/mL	1 µg/mL
TCP+NH_2^++Heparin	In solution with culture medium	0 pg/mL	0 pg/mL	0 pg/mL
		1 µg/mL	1 µg/mL	1 µg/mL
TCP+NH_2^++Heparin	Immobilised on surface	0 pg/mL	0 pg/mL	0 pg/mL
		1 pg/mL	1 pg/mL	1 pg/mL
		1 ng/mL	1 ng/mL	1 ng/mL
		10 ng/mL	10 ng/mL	10 ng/mL
		100 ng/mL	100 ng/mL	100 ng/mL
		1 µg/mL	1 µg/mL	1 µg/mL

4.3.2 Primary Schwann cell isolation from DRG

The protocol described in section 4.3.1 was followed to retrieve DRG from chick embryos. Then, the protocol from Kaewkhaw et al., [220] to isolate primary Schwann cells from adult rat sciatic nerves was adapted to isolate primary Schwann cells from chick embryo DRG. DRG were placed in 10 mL trypsin and incubated at 37℃ and 5% CO_2 for 15 minutes. The cell solution was then centrifuged at 1600 rpm for 6 minutes. The supernatant was discarded, and the pellet resuspended in 2 mL of Schwann cell isolation medium. After, 1 mL of the cell suspension was transferred to a T-75 cell culture flask with 13 mL of Schwann cell isolation medium. This was done twice. The cells were incubated at 37℃ and 5% CO_2 for 24 hours. Then, 50% of the Schwann cells isolation medium was changed to culture medium. After 24 hours, culture medium was replaced with fresh normal culture medium. The cells were further incubated at 37℃ and 5% CO_2 until confluency was reached. Then, the cells were passaged 1:2, using cell culture medium. The cells were incubated at 37℃ and 5% CO_2.

4.3.3 Primary Schwann cell migration assay

Primary Schwann cells were detached from a T-75 culture flask by using 5 mL of trypsin/EDTA. Trypsin/EDTA was deactivated using culture medium. Then, the cell solution was collected and centrifuged for 6 minutes at 1600 rpm. The supernatant was discarded, and the pellet resuspended in culture medium. Stoppers (Figure 15.A) were placed on the bioactive surface, to create an area where Schwann cells would not adhere, as the stopper created a seal with the bioactive surface. (Figure 15.B-D). Bioactive surfaces were prepared following section 4.1.1 of this chapter. However, only concentrations of NGF 1 ng/mL, NGF 10 ng/mL, BDNF 1 ng/mL or BDNF 10 ng/mL were immobilised and investigated for Schwann cell migration. Schwann cells (10,000 cells) were seeded on the bioactive surface with culture medium and incubated at 37℃ and 5% CO_2. After 24 hours, the stoppers were removed, and an image taken of the area with no Schwann cells using an inverted Olympus IX73 epifluorescence microscope and Micro-Manager 1.4.22 software (University of California, USA). A LED lamp was used as a light source for brightfield imaging (Cairn Research, United Kingdom). As a positive control, Tumor Necrosis Factor-α

(TNF-α, Sigma, United Kingdom) was used at a concentration of 300 U/mL in PBS. This was added after images of day 0 were taken.

Image J 1.52a software (National Institutes of Health, USA) [218] was used to measure cell-free area at day 0, 1, 2, 5 and 7 using the oval tool. The value on day 0 was set as 0%, and thereafter, decrements in the cell-free area were calculated as a percentage of Schwann cell migration (Figure 16).

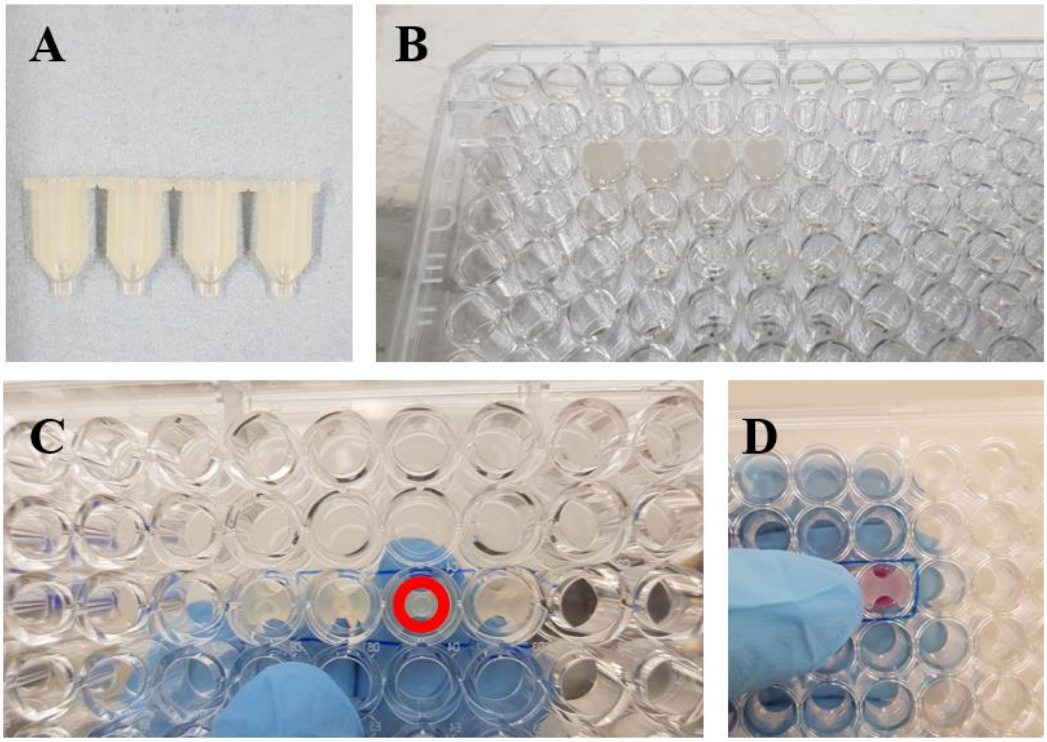

Figure 15. Set up for Schwann cell migration assay. A) Silicon stoppers; B) Stoppers in a 96-well plate; C) Images from the bottom of a 96-well plate with the stoppers, where a seal was observed between the stopper and the 96-well plate (circled in red); D) Top-view of the stopper, where a channel can be seen. This channel was used to introduce the tip of the micropipette for Schwann cell seeding.

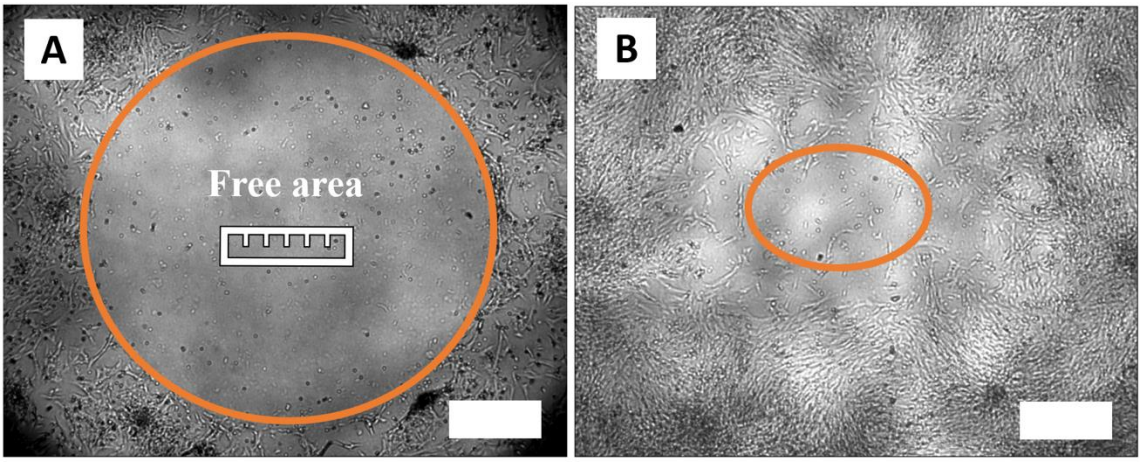

Figure 16. Schematic of how the cell-free area left by the stoppers was measured at day 0 (A). Then, decrements of this area were measured using the oval tool of Image J to calculate the migration percentage of Schwann cells (B). Scale bar = 500 µm.

4.3.4 Fixing and immunolabelling of DRGs and primary Schwann cells.

Immunolabelling was performed for β-III tubulin protein, to identify neurons and measure neurite outgrowth while S100-β protein was used to identify Schwann cells. DAPI was used to stain cell nuclei. Table 7 shows which primary (1°) and respective secondary (2°) antibodies were used to stain the DRG and primary Schwann cells.

Table 7. Primary (1°) and secondary (2°) antibodies used for immunolabeling of DRG, for β-III tubulin protein, and Schwann cells S100-β.

Structure	**1° antibody**	**Dilution factor of 1° antibody (in 1% BSA solution in PBS)**	**2° antibody**	**Dilution factor of 2° antibody (in 1% BSA solution in PBS)**
β-III tubulin protein (neurons and neurites)	Mouse Anti-β-III tubulin (Abcam, United Kingdom)	1:1000	Alexa Fluor 488 goat anti-mouse (Life technologies, USA)	1:400
S100-β protein (Schwann cells)	Rabbit Anti-S100-β (Dako, USA)	1:400	Alexa Fluor 546 goat anti-rabbit (Life technologies, USA)	1:400

First, culture medium was discarded from all samples. Cells were fixed with 3.7% FA for 30 minutes at room temperature. Then, FA was discarded, and the samples were washed one time with PBS. A solution of 0.1% Triton X-100 (v/v) with 3% bovine serum albumin (BSA, Sigma, United Kingdom) (w/v) in PBS was added and incubated for 1 hour at room temperature. This solution was then discarded, and the samples washed 2 - 3 times with PBS. After, a solution containing both 1° antibodies in 1% BSA (w/v) in PBS was added to each sample and left overnight at 4°C. Then, this solution was removed, and the samples washed one time with PBS. The 2° antibodies in 1% BSA (w/v) in PBS solution was added to the samples and incubated for 3 hours at room temperature protected from light with aluminium foil. The samples were then washed one time with PBS.

DAPI solution in PBS (1:1000) was added to each sample and incubated for 30 minutes at room temperature. Finally, DAPI solution was discarded, samples were washed one time with PBS, and stored at 4°C with PBS.

4.3.5 Epifluorescence microscopy and images analysis

DRG images were taken using an inverted Olympus IX73 epifluorescence microscope and Micro-Manager 1.4.22 software (University of California, USA). A mercury lamp was used as a light source. To image DAPI, Alexa Fluor-488 and Alexa Fluor-546, excitation and emission wavelengths of λ_{ex} = 405 nm / λ_{em} = 450 nm, λ_{ex} = 488 nm / λ_{em} = 525 nm, and λ_{ex} = 546 nm / λ_{em} = 570 were used, respectively.

Image J 1.52a software (National Institutes of Health, USA) [218] was used to measure the length of developed neurites and to count how many neurites were developed.

Neurites were measured from the DRG to the tip of the neurite. One image was taken per well. Three images were taken per condition, and 10-15 neurites were measured to determine the average neurite length and number of neurites. Background was subtracted (20-30 pixels) to enhance intensity and contrast.

Image J 1.52a software was also used to identify Schwann cell purity. Cells positive for S100-β protein were counted against the total number of cells, and a percentage was calculated to obtain the purity percentage of primary Schwann cells.

4.4 Fabrication and characterisation of polycaprolactone electrospun scaffolds, polycaprolactone spin-coated films and TCP well plates with bioactive surface

4.4.1 Fabrication of polycaprolactone electrospun scaffolds

A 20% w/v solution of polycaprolactone (PCL, Mn. 80,000 g/mol, Aldrich, United Kingdom) was prepared in a glass container with dichloromethane (DCM, Fisher Scientific, United Kingdom) as a solvent. The solution was left overnight at room temperature, in a fume cupboard, to dissolve.

The 20% PCL solution was loaded in a 1 mL syringe (Beckton Dickinson, BD, United Kingdom). A dispensing blunt needle of 20-gauge, (1 inch long, Fisnar, USA) was attached to the syringe and then placed in the syringe pump (AL 1000-220, World Precision Instruments, WPI, United Kingdom) as shown in Figure 17.A. A high voltage supply (Genvolt, United Kingdom) was used to set the required voltage (Figure 17.B). An overhead stirrer (RW20 digital, IKA) was used to rotate the collector as shown in Figure 17.D and Figure 17.E respectively. Aluminium foil was placed over the collector to facilitate the removal of the PCL electrospun scaffold. The volume used to electrospin was 1 mL each time. A new syringe and blunt needle were used each time. The parameters shown in Table 8 were set to achieve aligned PCL fibres to fabricate the PCL electrospun scaffold.

Table 8. Electrospinning parameters used for obtaining PCL electrospun scaffolds.

Parameter	
Distance between blunt needle and collector (Figure 17.C)	20 cm
Flow rate	6 mL/hr
Voltage	16-18 kV
Speed of collector	2,000 rpm

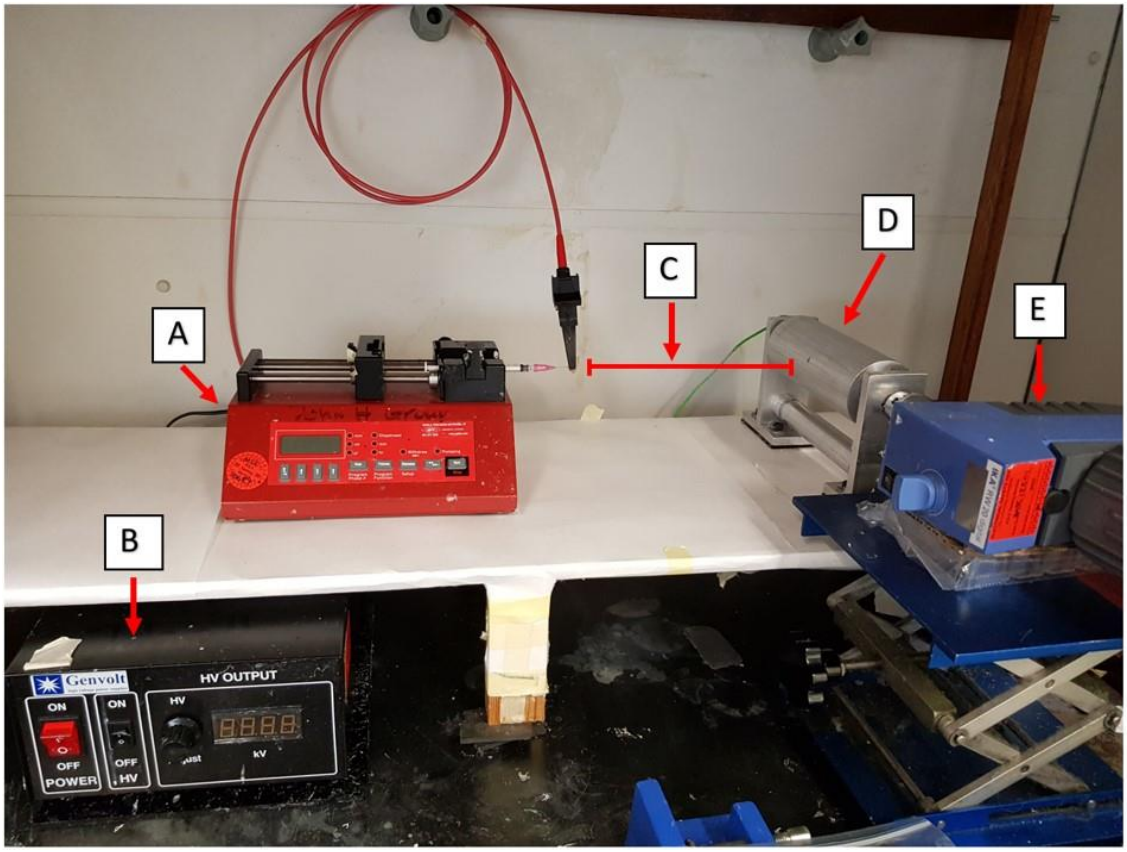

Figure 17. Electrospinning rig set up. A) syringe pump; B) high voltage supply; C) distance between the blunt needle and the collector; D) collector; e) overhead stirrer.

4.4.2 Fabrication of PCL spin-coated films

A 10% w/v solution of PCL (M_n 80,000 g/mol, Aldrich, United Kingdom) was prepared in a glass container with DCM (Fisher Scientific, United Kingdom) as a solvent. The solution was left overnight at room temperature, in a fume cupboard, to dissolve. Then, this solution was loaded in a 1 mL syringe (BD, United Kingdom). A dispensing blunt needle of 20-gauge, 1 inch long (Fisnar, USA) was set to the syringe.

A spin-coater (Laurell WS-400B-6NPP/Lite, USA) was set up to spin for 35 seconds at 3000 rpm. The lid of the spin-coater was opened, and a coverslip (13 mm diameter, Thermo Scientific, Germany) was placed inside the spin-coater. Then, 200 µL of the PCL solution was dispensed in the middle of the cover slip. The lid was closed, and the process was performed. When the sample was ready, the lid of the spin-coater was opened and the PCL film with the cover slip were retrieved.

4.4.3 Adding amine groups NH_2^+, heparin and growth factors to PCL electrospun scaffolds, PCL films, and TCP well plates

Plasma deposition was used to clean and add NH_2^+ on to polycaprolactone (PCL) electrospun scaffolds, PCL films, and TCP culture plates. Allylamine (Aldrich, United Kingdom) was the monomer used to obtain the NH_2^+ groups. The diameter and length of the glass vessel used were of 10.5 cm and 42.0 cm, respectively. This glass vessel was encircled by a coil of copper wire.

4.4.3.1 Air plasma cleaning

Air plasma cleaning was performed to clean the glass vessel and the PCL electrospun scaffold and PCL films from any chemical contamination. The cleaning of the glass vessel was done before the cleaning of the PCL electrospun scaffolds or PCL films.

Firstly, the cold trap (Figure 18.B) was filled up to 75% of its capacity with liquid nitrogen. Making sure that the lid was properly closed (Figure 18.H), the vacuum pump was turned on (Figure 18.A) to evacuate the plasma rig glass vessel (Figure 18.G) to $7x10^{-2}$ mBar. The equalisation valve (Figure 18.I) was open and adjusted to reach a steady pressure of $1.8x10^{-1}$ mBar. Then, the radio frequency generator of 13.56 MHz (RF generator, Figure 18.F) was turned on and the output power adjusted to 50 W. The air plasma deposition process began and was left for 30 minutes (Figure 19.A). After this time, the RF generator was turned off. The equalization valve and the isolation valve (Figure 18.C) were closed, and the vacuum pump turned off. The atmospheric valve (Figure 18.D) was open to reach atmospheric pressure to the glass vessel ($1x10^3$ mBar).

Then, the lid was opened and the PCL electrospun scaffolds or PCL films were placed inside the plasma rig glass vessel. The cold trap was refilled with liquid nitrogen, the isolation valve was opened, and the air plasma cleaning protocol was performed once more to clean the PCL electrospun scaffolds or PCL films from any contamination. The power used for this was 20 W. After this, the allylamine plasma deposition was performed.

4.4.3.2 Allylamine plasma deposition to add NH_2^+ on PCL electrospun scaffolds, PCL films and TCP well plates

The cold trap was filled up to 75% volume capacity with liquid nitrogen. Then, with the PCL electrospun scaffolds, PCL films or TCP well plates inside the glass vessel and the isolation valve open, the vacuum pump was turned on to evacuate the glass vessel to $8x10^{-3}$ mBar. The monomer flask (Figure 18.J), which contained allylamine, was attached to the equalisation valve. Then, the equalisation valve was opened and adjusted to reach a steady pressure of $2.2x10^{-2}$ mBar. Then, the RF generator was turned on and the output power adjusted to 10 W. The allylamine plasma polymerisation process was left for 10 minutes (Figure 19.B). After this time, the RF generator was turned off. The equalization valve and the isolation valve were closed, and the vacuum pump turned off. The atmospheric valve was opened to reach atmospheric pressure in the glass vessel. The monomer flask was then detached from the equalisation valve. The lid was opened, and the PCL + NH_2^+ scaffolds, PCL + NH_2^+ films or TCP + NH_2^+ well plates were removed.

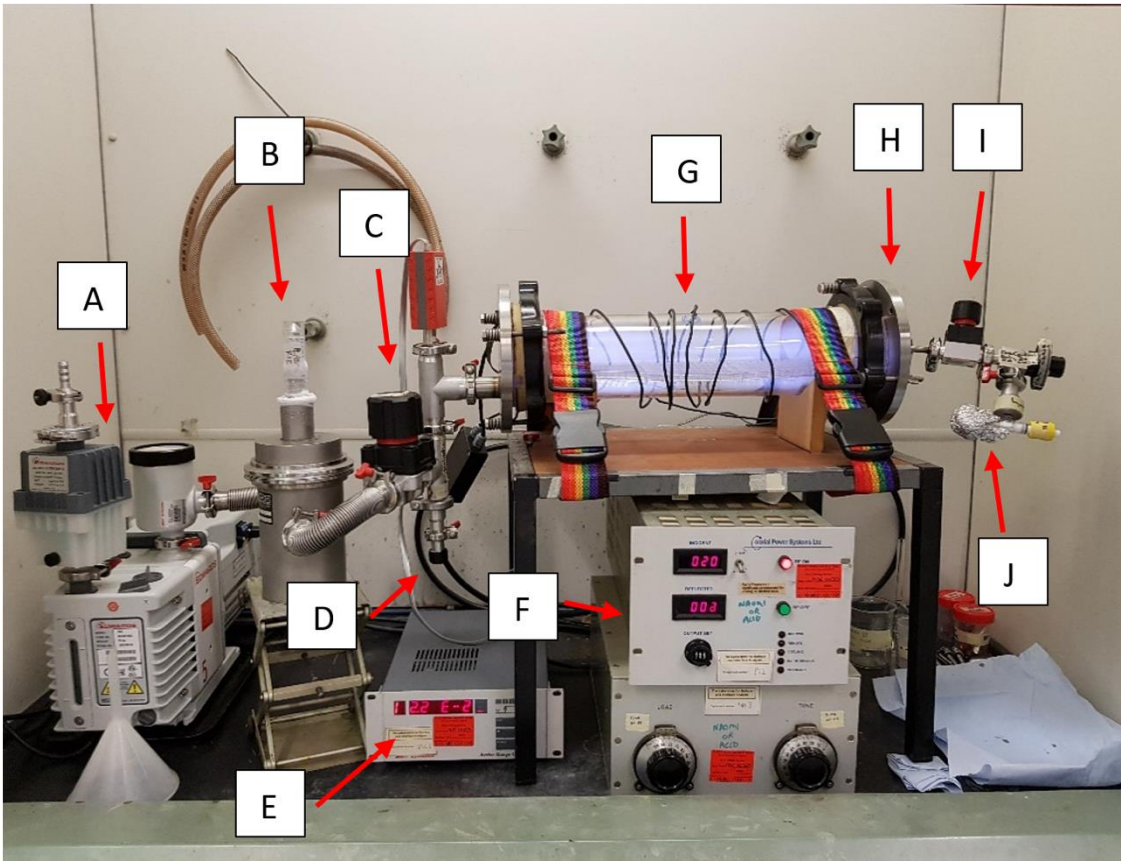

Figure 18. Plasma rig. The components are A) vacuum pump, B) cold trap, C) isolation valve, D) atmospheric valve, E) pressure monitor, F) radiofrequency generator, G) plasma rig chamber, H) lid of the chamber, I) equalisation valve, J) monomer flask.

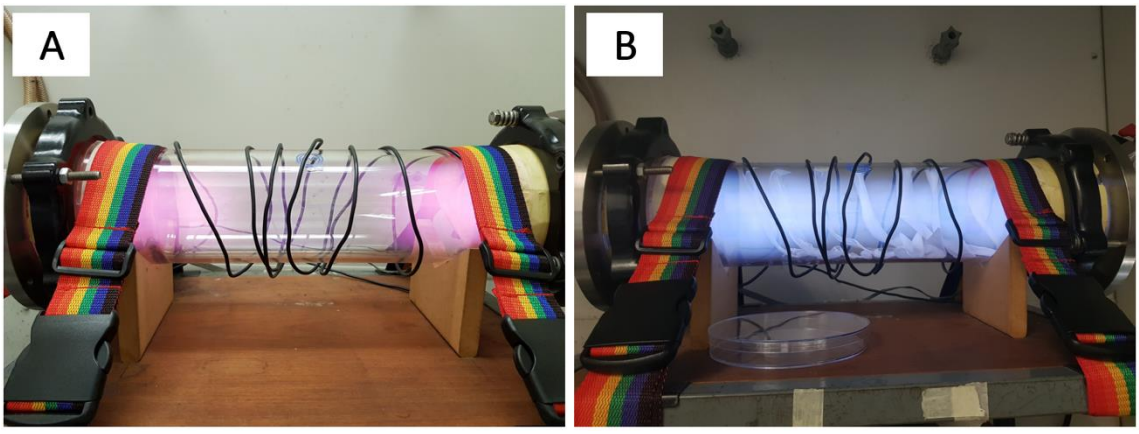

Figure 19. Difference in colour seen in the plasma rig glass vessel during A) air plasma cleaning and B) allylamine plasma deposition.

4.4.3.3 Heparin conjugation to PCL electrospun scaffolds, PCL films and TCP well plates

Heparin conjugation to PCL electrospun scaffolds, PCL films and TCP well plates was performed following the protocol described in section 4.1.1.1 of this chapter. Briefly, a heparin solution of 50 µg/mL was added to the PCL electrospun scaffolds, PCL films and TCP well plates and incubated overnight at room temperature. Then, the heparin solution was discarded, and the samples washed one time with PBS.

PCL films, PCL Air films, PCL + NH_2^+ films and PCL + NH_2^++ Heparin films were used for XPS analysis.

TCP, TCP + NH_2^+ and TCP + NH_2^+ + Heparin were used for a storage study described in section 4.4.7 of this chapter.

PCL + NH_2^+ scaffolds and PCL + NH_2^++ Heparin scaffolds were used for immobilisation of NGF, BDNF or NGF plus BDNF as described in section 4.4.3.3 of this chapter.

4.4.3.3 NGF, BDNF and NGF plus BDNF immobilisation to PCL electrospun scaffolds, and TCP well plates

After heparin conjugation, NGF, BDNF and NGF plus BDNF were immobilised to PCL + NH_2^+ scaffolds and PCL + NH_2^++ Heparin scaffolds. NGF plus BDNF were immobilised at a concentration of 1 ng/mL and 100 ng/mL only. NGF or BDNF was immobilised on TCP well plates at 1 ng/mL only. The immobilisation process followed the one described in section 4.1.1.2 of this chapter. Briefly, NGF or BDNF solutions of concentrations of 1 pg/mL, 1 ng/mL, 10 ng/mL, 100 ng/mL and 1 µg/mL were prepared and added to the samples. The samples were incubated for 5 hours at room temperature. Then, scaffolds were washed one time with PBS.

PCL electrospun scaffolds, PCL Air scaffolds, PCL + NH_2^+ scaffolds, PCL + NH_2^+ + Heparin scaffolds, PCL + NH_2^+ + Heparin + immobilised NGF/BDNF and were used to analyze neurite growth and Schwann cell migration from a seeded DRG.

TCP + NH_2^+ + Heparin + immobilised NGF/BDNF were used for a 21 days release profile, described in section 4.4.8 of this chapter.

4.4.4 Scanning Electron Microscopy analysis of PCL electrospun scaffolds

Scanning Electron Microscopy (SEM) was used to obtain images of the PCL electrospun scaffolds to measure the diameter and alignment of the fibres. Samples of the PCL electrospun scaffold were cut in 1x1 cm squares and placed on carbon adhesive tabs (Leit adhesive carbon tabs, Agar Scientific, United Kingdom). Then, the tabs were placed on aluminium pins (Agar Scientific, United Kingdom). To improve the quality of the image, all samples of PCL electrospun scaffolds were gold-coated (SC 500A, Emscope) before imaging with a field emission SEM (Sorby Centre, FE SEM JSM-6500F, Jeol Ltd., United Kingdom). Magnifications of 94x, 6000x and 10000x were used to obtain the images. The voltage used was 10 kV and the spot size was 3.5 nm.

4.4.5 Measurement of diameter and alignment of PCL electrospun scaffolds

Image J 1.52a software (National Institutes of Health, USA) [218] was used to measure the diameter and alignment of the fibres in the PCL electrospun scaffold. Three tests were run independently, and three PCL electrospun scaffolds chosen as samples. Three images were taken, and 10 PCL fibres were measured, per image. To determine the averaged diameter of the fibres, the straight tool of Image J was used. A straight line was drawn across the fibre, and then the diameter measured using the scale bar of the SEM image. The diameter values were taken from the measurement panel and averaged afterwards. To determine if the PCL electrospun scaffold was aligned, the angular difference between the PCL fibres was measured. Similarly, to the procedure used to determine the diameter of the fibre, the straight tool of Image J was used. A straight line was drawn along the PCL fibre, and the angle taken from the measurements panel. A 0° zero was defined to calculate the angular difference between the fibres. After the angles were calculated, an average was calculated.

4.4.6 X-ray Photoelectron Spectroscopy (XPS) analysis of PCL films

X-ray Photoelectron Spectroscopy (XPS) analysis was performed at the Sheffield Surface Analysis Centre (The University of Sheffield, United Kingdom). PCL film samples were interrogated to determine surface elemental composition (survey scans), carbon scans (C 1s), oxygen scans (O 1s), nitrogen scans (N 1s), and sulphur scans (S

2p) using a Kratos Ultra instrument with a monochromated aluminium source (1486.6 eV). Elemental survey scans were collected between 1200 to 0 eV binding energy, 160 eV pass energy and 1 eV intervals. High resolution C 1s, O 1s and N 1s scans were collected for all samples at 40 eV pass energy and 0.1 eV intervals. S 2p spectra was collected for samples containing heparin, at 40 eV pass energy, and 0.1 eV intervals. Two points per sample were analysed. The area of the analysis points was of 700 µm by 300 µm. Data was processed and analysed using CasaXPS (version 2.3.19 PR 1.0, Casa Software Ltd).

4.4.7 Storage of bioactive surfaces at different temperatures

Polystyrene (PS), TCP, TCP + NH_2^+ and TCP + NH_2^++ Heparin were stored at 4°C, room temperature (ca. 21°C) and 37°C for 24 hours, 1 month and 3 months. After storage periods, any changes in surface wettability were evaluated by water contact angle, as described in section 4.1.2.1 of this chapter.

4.4.8 Release profile of NGF or BDNF from bioactive surfaces for 21 days

TCP + NH_2^++ Heparin +immobilised NGF at 1 ng/mL and TCP + NH_2^++ Heparin + immobilised BDNF at 1 ng/mL were used to observe how much NGF or BDNF was released within 21 days.

After immobilisation of NGF or BDNF, bioactive surfaces were incubated at 37°C, with 1 mL of PBS for 21 days. Samples were taken at 1 hour, 24 hours, 48 hours, 168 hours (7 days), 240 hours (10 days), 336 hours (14 days), 408 hours (17 days), and 504 hours (21 days) and stored at -20°C for later quantification by ELISA. ELISA was performed as described in section 4.1.2.3 of this chapter.

4.5 Evaluation of bioactive surface on PCL electrospun scaffold on a neuronal cell line and primary cells

4.5.1 Crystal violet adhesion assay

PCL scaffold, PCL Air scaffold, PCL + NH_2^+ scaffold and PCL + NH_2^++ Heparin scaffold were tested to evaluate if NG108-15 neuronal cells adhered to them. Firstly, NG108-15 neuronal cells (1,500 cells) were seeded on each scaffold, which were placed inside a 24 well plate, with culture medium. The samples were incubated for 3 days at 37°C and 5% CO_2. Then, the samples were fixed with 3.7% FA. The scaffolds were then transferred to a new 24 well plate. A 0.2% crystal violet solution (w/v Sigma, United Kingdom, in 10% (v/v) ethanol (Fisher Scientific, United Kingdom)) was added to each sample and incubated for 10 minutes at room temperature. Then, the samples were rinsed one time with PBS. After, a 10% acetic acid solution (v/v Fisher Scientific, United Kingdom; in dH_2O) was added to each sample and used to elute the stain. The eluate was transferred to a 96-well plate, in triplicate, and the absorbance read at 630 nm using a Bio-Tek ELx 800 absorbance microplate reader and KC junior software 1.41.8 (Bio-Tek Instruments, USA). Three independent tests were performed, each sample was tested in triplicate.

4.5.2 Dorsal root ganglia seeding on PCL electrospun scaffolds

DRG were isolated as described earlier in this chapter, section 4.3.1. DRGs were seeded at a density of one DRG per PCL scaffold, PCL Air scaffold, PCL + NH_2^+ scaffold, and PCL + NH_2^++ Heparin scaffold. Then, culture medium and NGF, BDNF or NGF plus BDNF was added as described in Table 9. For the bioactive surface PCL + NH_2^++ Heparin with immobilised NGF, BDNF or NGF plus BDNF, one DRG per scaffold was seeded and culture medium with no growth factors was added. The DRG were cultured for 7 days at 37°C and 5% CO_2. Three independent tests were performed. Each sample was tested in triplicate.

Table 9. Summary of the different bioactive surfaces that were prepared, highlighting the delivery method of growth factor of each surface. NGF, BDNF and NGF plus BDNF solutions for immobilisation were prepared in sterile PBS.

Surface	**Growth factor delivery method**	**NGF**	**BDNF**	**NGF plus BDNF**
PCL electrospun scaffold (PCL)	In solution with culture medium	0 pg/mL	0 pg/mL	0 pg/mL
		1 µg/mL	1 µg/mL	1 µg/mL
Air plasma PCL electrospun scaffolds	In solution with culture medium	0 pg/mL	0 pg/mL	0 pg/mL
		1 µg/mL	1 µg/mL	1 µg/mL
PCL + NH_2^+	In solution with culture medium	0 pg/mL	0 pg/mL	0 pg/mL
		1 µg/mL	1 µg/mL	1 µg/mL
PCL + NH_2^++ Heparin	In solution with culture medium	0 pg/mL	0 pg/mL	0 pg/mL
		1 µg/mL	1 µg/mL	1 µg/mL
PCL + NH_2^++ Heparin	Immobilised on surface	0 pg/mL	0 pg/mL	0 pg/mL
		1 pg/mL	1 pg/mL	1 ng/mL
		1 ng/mL	1 ng/mL	100 ng/mL
		10 ng/mL	10 ng/mL	--
		100 ng/mL	100 ng/mL	--
		1 µg/mL	1 µg/mL	--

4.5.3 Fixing and immunolabelling of DRGs

Immunolabelling was performed for β-III tubulin protein, to identify neurons and measure neurite outgrowth and S100-β protein to identify Schwann cells. Immunolabelling was performed following the protocol described in section 4.3.4 of this chapter. Briefly, the samples were fixed using 3.7% FA. Then, 0.1% Triton X-100 with 3% BSA solution was added to the samples and incubated for 1 hour at room temperature. Primary antibodies (anti-β-III tubulin and anti-S100-β) in 1% BSA solution were added to the samples and incubated overnight at 4℃ (Table 7). Then, the solution was discarded and secondary antibodies in 1% BSA solution was added and incubated for 3 hours at 4℃. The samples were rinsed one time with PBS and then stored at 4℃ with PBS.

4.5.4 Lightsheet microscopy

Lightsheet microscopy was used to obtain images of the DRG seeded on bioactive surface PCL electrospun scaffolds. Z.1 lightsheet microscope (Carl Zeiss AG, Germany) and ZEN imaging software (Zen 9.2.8.54, Carl Zeiss, Germany) were used to obtain these images. Samples were cut longitudinally (Figure 20.A) and then mounted in 1% agarose solution (v/v, in dH_2O, Sigma-Aldrich, United Kingdom) inside glass capillaries (diameter 2.15 mm, Carl Zeiss AG, Germany). A plunger with Teflon tip (diameter 2 mm, Carl Zeiss AG, Germany) was used to insert the sample inside the glass capillaries. Then, capillaries were mounted inside a sample holder and placed inside the sample chamber, which was filled with dH_2O (Figure 20.B). Samples were localised and positioned in front of the objective. The objective used was a Zeiss W Plan-Apochromat 10x/ N.A. 0.5 for detection and two Zeiss LSFM 5x/ N.A. 0.1 for illumination. Alexa Fluor-488 and Alexa Fluor-546 were imaged using excitation and emission wavelengths of λ_{ex} = 488 nm / λ_{em} = 550 nm (short band filter), and λ_{ex} = 561 nm / λ_{em} = 545-590 nm (band pass filter) respectively. For each sample, various fields of view (longitudinally) were taken to capture all neurite outgrowth and Schwann cell migration. Each field of view was imaged in z-stack.

The z-stack was combined to produce a maximum projection intensity image using ZEN lite software (Carl Zeiss, Germany). Then, the maximum projection intensity

images were put together using the stitching tool in Image J [221]. Neurites (neurite bundle) were measured from DRG to the tip of the neurite. Schwann cells were measured from the DRG to the last Schwann cell (the one most distal from the DRG) [218]. Two images were taken per sample (upper half and lower half of the DRG, Figure 20.B). Three independent tests were performed. Each condition was tested in triplicate.

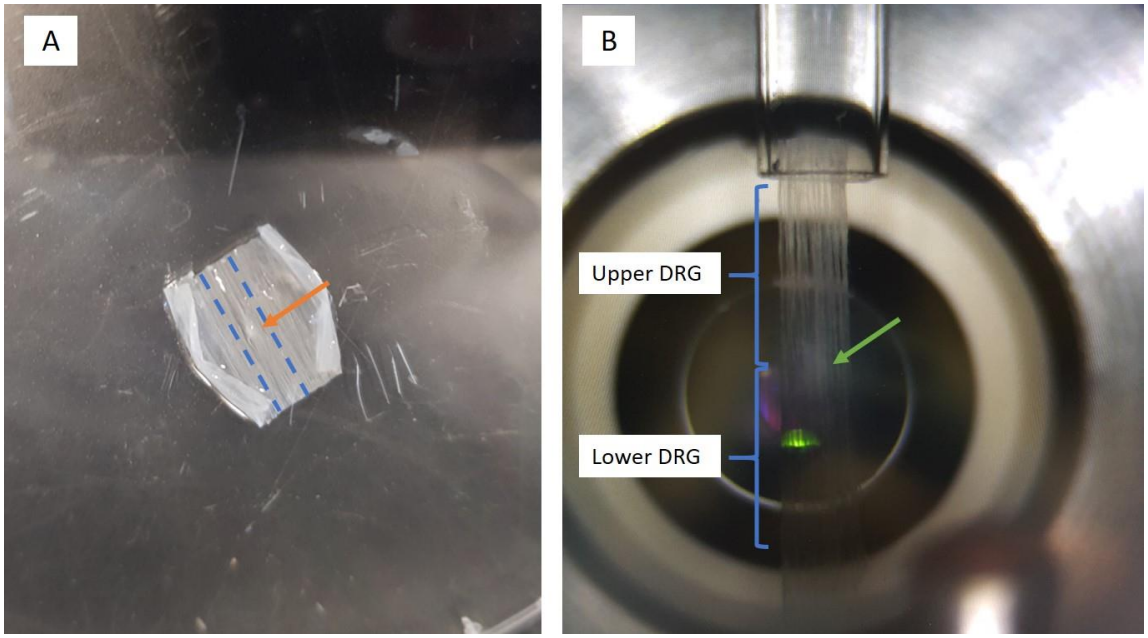

Figure 20. Preparation of DRG for lightsheet imaging. A) DRG on scaffold. Blue dashed lines highlight where the scaffold was cut. Orange arrow shows DRG B) DRG on scaffold, mounted with agarose, inside the sample chamber of the lightsheet microscope. Green arrow shows DRG. Blue brackets show upper DRG and lower DRG.

4.6 Statistical analysis

Analysis of variance (ANOVA) with Tukey multiple comparison post-test was performed to analyse statistical difference among the different conditions using GraphPad Prism 8.2.0 software (USA). A p value of < 0.05 was used to indicate if differences in data were significant.

Chapter 5 Fabrication and characterisation of a bioactive surface

The following experimental chapter has been partially taken from Sandoval-Castellanos et al., (2020) [203] which was published as an open access article under the terms of the Creative Commons Attribution License, allowing the use, distribution and reproduction of the material provided that it is properly cited.

5.1 Introduction

Cells interact directly to locally produced growth factors, responding to their stimuli with a specific cell behaviour; therefore, the use of a systemic delivery is impractical [222]. Moreover, systemic delivery of growth factors may cause adverse effects, for example, growth factors not arriving at the site of injury, inhibition of neurite outgrowth, and the further reduction of their half-lives [169], [217]. Immobilisation of growth factors on surfaces allows the retention and local delivery of these proteins at the site of injury, hence, they would be able to encourage cell differentiation, proliferation, and activity [222].

In addition, the immobilisation of growth factors could prevent undesirable adverse effects by controlling the release of the growth factors [169]. An initial high burst release is undesirable, as it may cause adverse effects, however, it is difficult to avoid [223]. For example, excessive initial nerve growth factor (NGF) dose can inhibit early neurite regeneration [217], [224] or may cause substantial branching of regenerating neurites, producing dysfunctional connections and inappropriate neuronal target reinnervations [217]. Previous failure in encouraging nerve regeneration using growth factors might have been due to a unsuitable delivery system [61]. For example, when growth factors were introduced in a nerve conduit, the outcome was not satisfactory due to aberrant neurite growth, resulting in mismatched connections between the nerve and the target [224]. This failure was attributed to an inappropriate growth factor dose and release kinetics at the injury site, undesired initial burst release and the use of a

single growth factor, instead of using various growth factors as occurring biologically [224]. Therefore, one of the steps to develop a bioactive surface for the delivery of growth factors, was to choose two growth factors that have an effect in nerve repair.

Nerve growth factor (NGF) is known for encouraging differentiation, function and survival of neurons in the peripheral nervous system. Additionally, after injury, NGF promotes neurite outgrowth, *in vitro* and *in vivo* [224]–[227]. Moreover, it has been used as a chemo-attractant to guide neurite growth [225]. Nevertheless, as with other growth factors, it has a short half-life *in vivo* [217], [226].

Additionally, brain derived neurotrophic factor (BDNF) is widely expressed in the brain and the central nervous system [141]. It promotes neuronal plasticity, morphogenesis and survival [137], [141]. For example, it is involved in the regeneration of the hippocampus [137]. Even though its name gives its primary location, it is not limited to be present in the central nervous system or in the brain. BDNF is also present in the peripheral nervous system, as it encourages neurite outgrowth after injury [51], [137]. It is synthesized by motor neurons, some dorsal root ganglia neurons and Schwann cells [137].

The optimal dosage of growth factors to encourage biological activity is still unknown, as there are no studies that define or characterise the delivery of different amounts of growth factors from the same delivery system [217], [224], [226]. However, it has been estimated to be from the picograms to nanograms range [226]. Therefore, an experimental range from picograms to nanograms was chosen to test the performance of the bioactive surface. It is important to design a delivery system capable of delivering an optimal amount of growth factors, avoiding its drawbacks, and that encourages neurite outgrowth and posterior nerve regeneration [226].

To directly adsorb neurotrophins to a biomaterial surface for delivery, coating into a solution of growth factors has disadvantages, for example, low loading and hence, limited supply and fast growth factor release [227]. Immobilisation of growth factors by introducing functional groups to bind them, has been studied to overcome these disadvantages [227]. Epidermal growth factor (EGF), and vascular endothelial growth factor (VEGF) are some of the growth factors that have been immobilised on

biomaterials for different applications [227]. Covalent and non-covalent immobilisation of growth factors have both been employed for the local delivery of growth factors. These strategies are promising approaches since they enhance the half-life and function of growth factors. Moreover, the chosen technique depends on how the functional groups can be presented and then bonded to growth factors [228]. Nevertheless, the disadvantage of covalent immobilisation is that, after performing this technique, it is difficult to use the whole potential of the growth factor [229]. For example, when NGF is covalently immobilised, its stability and bioactivity is reduced considerably [230]. To overcome this drawback, non-covalent immobilisation is a promising approach to maintain growth factor stability and bioactivity. The non-covalent immobilisation technique used in this work, utilises electrostatic interactions to bind NGF and BDNF to a biomaterial, creating a bioactive surface that encourages neurite outgrowth. This bioactive surface will be fabricated with amine functional groups and heparin. The reason for this is that amine functional groups are positively charged under physiological conditions, and can be used to bind growth factors or other biomolecules, such as heparin, as amine functional groups have high affinity for negatively charge biomolecules [210], [231]. Heparin is a sulphated glycosaminoglycan, rich in carboxyl, hydroxyl and sulphate groups which has binding affinity with diverse growth factors [169], [223]. Moreover, the half-life of growth factors is increased when they are bound to heparin [169]. This represents an advantage as the growth factors will be retained on the surface, maintaining bioactivity. Therefore, the work in this chapter will present the fabrication and characterisation of amine (NH_2^+) + Heparin + immobilised NGF and/or BDNF bioactive surfaces.

5.2 Aims and objectives

The aims of this chapter are:

1. Fabrication of a bioactive surface that contains amine groups NH_2^+, heparin, nerve growth factor or brain derived neurotrophic factor.
2. Characterisation of a bioactive surface that contains amine groups NH_2^+, heparin, nerve growth factor or brain derived neurotrophic factor.

The objectives of this chapter are:

1. Conjugate heparin to the surface that contains NH_2^+ in the surface.
2. Add nerve growth factor or brain derived neurotrophic factor to the NH_2^+ + Heparin bioactive surface.
3. Characterise the NH_2^+ bioactive surface and the NH_2^++ Heparin bioactive surface by water contact angle and XPS analysis.
4. Characterise the release of nerve growth factor and brain derived neurotrophic factor by ELISA assay from NH_2^++ Heparin + Immobilised NGF/BDNF bioactive surface.

5.3 Materials and Methods

5.3.1 Adding heparin and growth factors to TCP + NH_2^+ surface

5.3.1.1 Heparin conjugation

A solution of heparin sodium salt from porcine intestinal mucosa (Sigma, United Kingdom) was prepared at a concentration of 50 µg/mL in phosphate buffered saline (PBS, Oxoid, United Kingdom). Then, the solution was filter sterilized with a filter of 0.2 µm pore size (Filtropur S, Sarstedt AG & Co., Germany). The heparin solution was added to 96 pre-coated well plates with amine groups (TCP + NH_2^+, Becton Dickinson, BD PureCoat^{TM}, Belgium) and left overnight at room temperature. Then, the heparin solution was discarded, and the surfaces washed one time with PBS. After performing this step, this surface became the bioactive surface TCP + NH_2^++ Heparin (Figure 21.C).

5.3.1.2 Immobilisation of nerve growth factor and brain derived neurotrophic factor

Nerve growth factor (NGF, R&D systems, USA), brain derived neurotrophic factor (BDNF, R&D systems, USA) and combinations of NGF plus BDNF were immobilised onto the bioactive surface TCP + NH_2^+ + Heparin. Different concentrations of NGF, BDNF and NGF plus BDNF were prepared at concentrations of 1 pg/mL, 1 ng/mL, 10 ng/mL, 100 ng/mL and 1 µg/mL in sterile PBS. Each solution was added onto the bioactive surface and incubated for 5 hours at room temperature (Figure 21.D). Then, the solution was discarded, and the surface was washed one time with PBS. The bioactive surface with immobilised NGF and/or BDNF was now created (Figure 21.E). Figure 21 illustrates the design of the bioactive surface with immobilised neurotrophic factors.

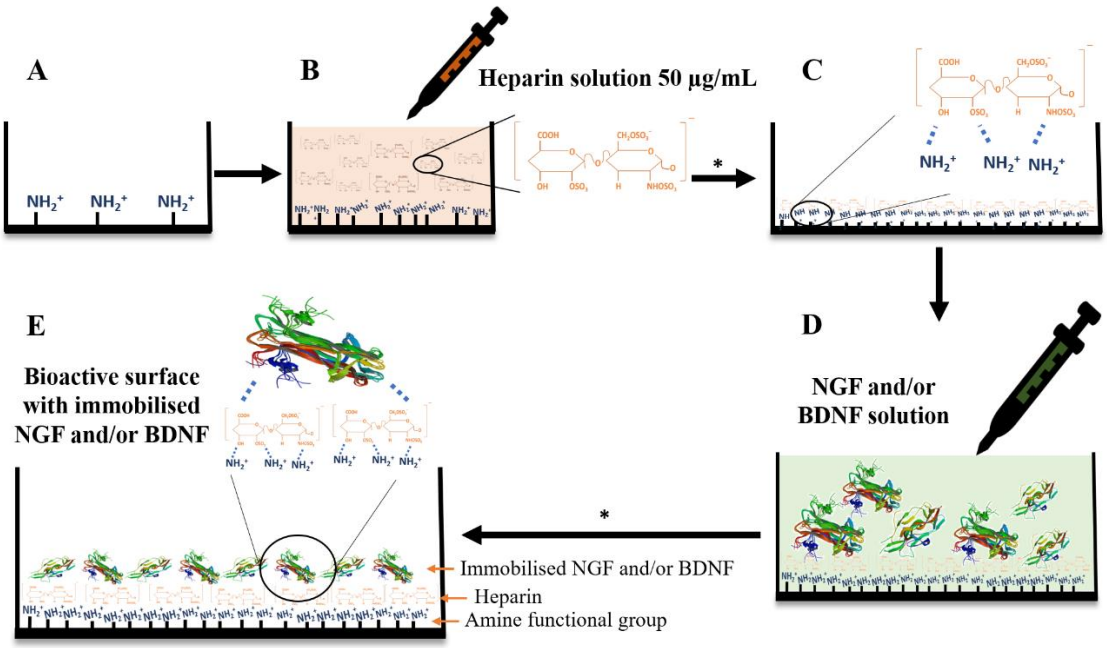

Figure 21. Diagram illustrating the fabrication of the bioactive surface with immobilised NGF and/or BDNF. A) TCP + NH_2^+ surface. B) A solution of heparin at 50 µg/mL was added. C) TCP + NH_2^+ + Heparin surface. D) NGF and/or BDNF solution was added. E) Bioactive surface with immobilised NGF and/or BDNF (TCP + NH_2^+ + Heparin + Immobilised NGF/BDNF). Each asterisk (*) shows that at that step of fabrication, the surface was washed one time with PBS. NGF and BDNF images from the RCSB PDB [145], [146].

5.3.2 Surface characterisation

5.3.2.1 Water contact angle

Water contact angle was measured with Krüss GmbH drop shape analyzer-100 (DSA100) equipment by placing 5 µL of distilled water, from a 1 mL syringe (BD, United Kingdom) and 20-gauge needle, (1 inch long, Fisnar, USA) on top of the surface. Then, the contact angle of the bioactive surfaces was measured by sessile drop method and calculated with DSA100 software.

Contact angle measures the angle formed between a liquid drop and a surface. This angle, θ, is determined by the equilibrium of the liquid drop under the solid-liquid (s-l), the solid-vapor (s-v) and liquid-vapour (l-v) interfacial tensions [232] (Figure 22). This equilibrium between these interfacial tensions, gives an angle θ that reveals information about the surface chemistry of a material [233].

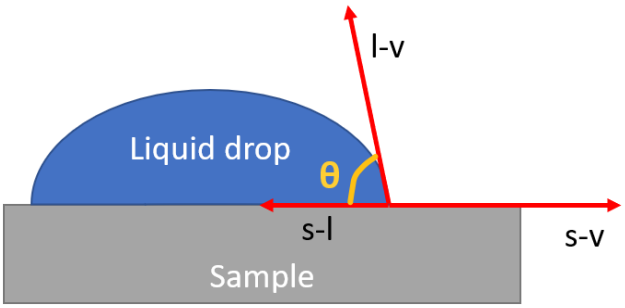

Figure 22. Diagram of the contact angle θ and the three interfacial tensions: liquid-vapour (l-v), solid-liquid (s-l), and solid-vapour (s-v). Adapted from [232].

5.3.2.2 X-ray Photoelectron Spectroscopy (XPS) analysis

XPS analysis was performed at the Sheffield Surface Analysis Centre (The University of Sheffield, United Kingdom). Samples were interrogated to determined surface elemental composition (survey scans), carbon scans (C 1s), nitrogen scans (N 1s), and sulphur scans (S 2p) using a Kratos Ultra instrument with a monochromated aluminium source (1486.6 eV). Elemental survey scans were collected between 1200 to 0 eV binding energy, 160 eV pass energy and 1 eV intervals. High resolution C 1s and N 1s scans were collected for all samples at 20 eV pass energy and 0.1 eV intervals. S 2p spectra were collected for samples containing heparin, at 20 eV pass energy, and 0.1 eV intervals. Two points per sample were analysed. The area of the analysis points was 700 µm by 300 µm. Data was processed and analysed using CasaXPS (version 2.3.19 PR 1.0, Casa Software Ltd).

XPS consists of irradiating a sample with a monoenergetic x-rays source followed by the analysis of the emitted electrons from the surface. This analysis plots the number of detected electrons per energy interval versus their binding energy, creating a spectrum. Each element has its own specific spectrum, hence, when a compound is analysed, its spectrum is the sum of the peaks of its components. Identification of chemical states of the components can be obtained, as they also have a unique spectrum. Further, the concentration of each component can be calculated from the peak area, which is expressed as a percentage [234].

5.3.2.3 Release profile of NGF and BDNF from bioactive surfaces

Methodology described in section 4.1.1 from chapter 4 materials and methods was performed to prepare the bioactive surface with immobilised NGF or BDNF. Then, these bioactive surfaces were tested to investigate the release of NGF and BDNF from the bioactive surface. However, firstly, the quantity of NGF or BDNF bound to heparin needed to be calculated in order to quantify the percentage of growth factor released from the bioactive surface. In order to do this, after the 5 hours incubation the solution of NGF and BDNF (called afterwards as supernatant) was stored at -20°C for later enzyme-linked immunosorbent assay (ELISA).

In vitro release of NGF and BDNF was tested by incubating the bioactive surfaces immobilised with NGF or BDNF with 1 mL of PBS at 4°C and 37°C. Samples were taken at 1 hour, 24 hours, 48 hours, and 168 hours and kept at -20°C for ELISA assays [216], [217]. Standards for the calibration curve were prepared as serial dilutions in standard buffer. For samples taken from the supernatant and at 1 hour (both NGF and BDNF), 1:100 (1 µg/mL) and 1:10 (100 ng/mL and 10 ng/mL) dilutions were prepared with standard buffer to assure that the absorbance readings could be fitted inside the standard curve.

Firstly, standards and samples were added into the wells of the ELISA assay plate and incubated at room temperature for 2 hours and 30 minutes. Then, the samples and standards were discarded, and the plate rinsed with washing buffer. Biotinylated antibody was added to the wells and incubated for 1 hour at room temperature. The plate was then rinsed with washing buffer and Streptavidin-HRP (horseradish peroxidase) was added. The wells were incubated for 45 minutes at room temperature. The plate was rinsed with washing buffer and 3,3’,5,5’-tetramethylbenzidine (TMB) substrate was added and incubated for 30 minutes at room temperature, covered from light. Then, the stop solution was added. The absorbance was read at 450 nm using a Bio-Tek ELx 800 absorbance microplate reader and data was recorded using KC junior software 1.41.8 (Bio-Tek Instruments, USA).

5.3.3 Statistical analysis

One-way analysis of variance (ANOVA) with a Tukey multiple comparison post-test was performed to identify statistical differences between conditions, using GraphPad Prism 8.2.0 software (USA). A p value of < 0.05 was considered significant.

5.4 Results

Bioactive surfaces were fabricated using methods described in section 5.3.1

5.4.1 Water contact angle characterisation of TCP, TCP+NH_2^+, TCP+NH_2^+ + Heparin surfaces

Water contact angle (section 5.3.2.1) was performed to measure and compare the contact angle formed between the droplet of water and the surface, as a relative measure of hydrophilicity [223]. Moreover, if a change in contact angle was noticed, it would give an indication of surface modification. As shown in Figure 23, the averaged contact angle of polystyrene (PS), TCP, TCP + NH_2^+ and TCP + NH_2^+ + Heparin was 98°, 70°, 43° and 39°, respectively. The decreased hydrophobicity is explained by the addition at the surface of charged functional groups, such as amine (NH_2^+) and sulphate, present in heparin. The lowest contact angle was found for TCP + NH_2^+ + Heparin surface. PS control was significantly different (****$p<0.0001$) compared to TCP+NH_2^+ and TCP+NH_2^++heparin surfaces. Moreover, TCP control was also significantly different when compared with TCP+NH_2^+ and TCP+NH_2^++heparin surfaces (***$p<0.001$, ****$p<0.0001$ respectively). Nevertheless, the contact angles between TCP+NH_2^+ and TCP+NH_2^++heparin were not significantly different. Figure 24 shows the shape of a droplet of water formed according to the surface they were on. These results indicated the hydrophilicity (or hydrophobicity) of each of the material, which changed after the surface modification.

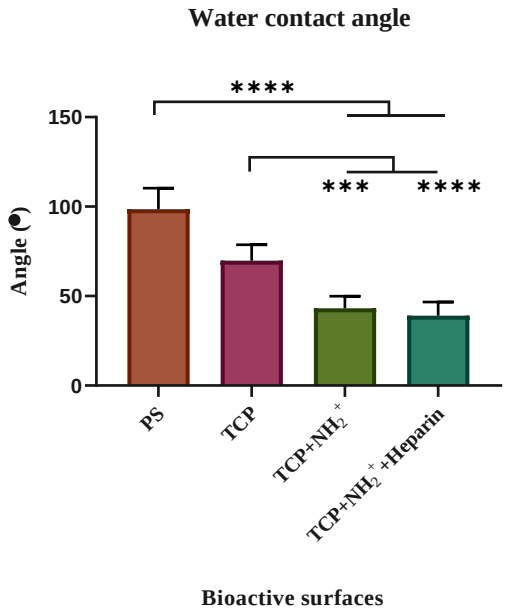

Figure 23. Water contact angle from each surface showing the significant difference ****p<0.0001 and ***p<0.001 among PS (98°), TCP (70°), TCP+NH_2^+ (43°) and TCP+NH_2^+ + Heparin (39°) surfaces. Bars represent the mean ± SD. N=3, n=3.

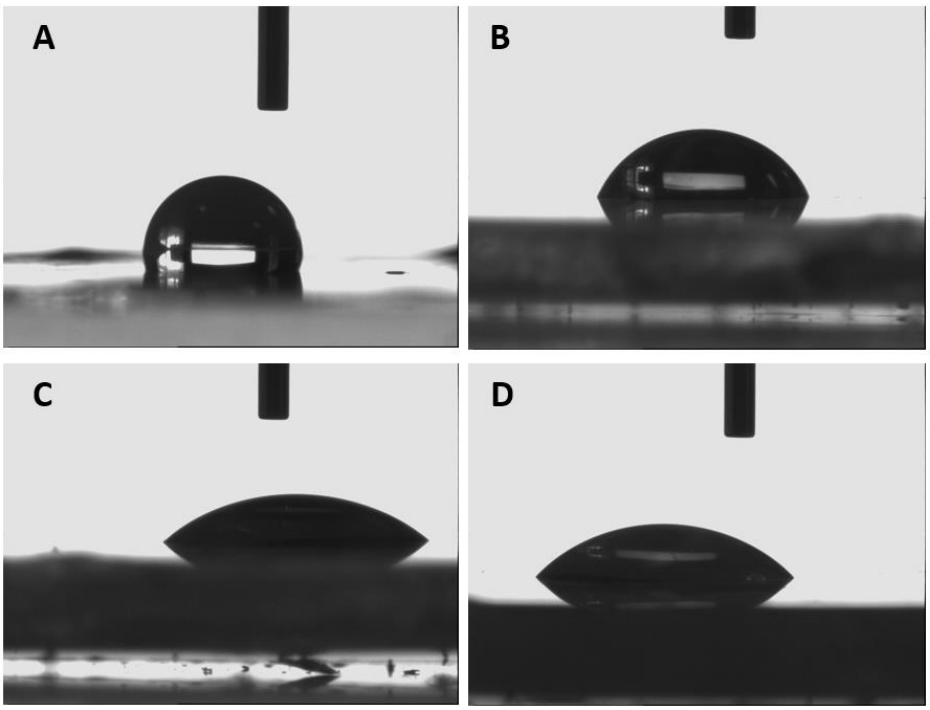

Figure 24. Water contact angle droplet shapes according to the surface they are on: A) PS, B) TCP, C) TCP+NH_2^+, D) TCP+NH_2^+ + Heparin.

5.4.2 X-ray Photoelectron Spectroscopy characterisation of TCP, TCP+NH_2^+, and TCP+NH_2^+ + Heparin surfaces

XPS analysis was used to determine the elemental composition of test surfaces after each modification. Figure 25 shows the spectra of the chemical survey scans of each of the modified surfaces. Figure 25.A corresponds to the survey scan of control TCP, which determined that its carbon content was 90.5%, and oxygen content was 9.45%. In comparison, TCP + NH_2^+ bioactive surface revealed a peak at 400 eV, confirming the presence of nitrogen, which composed 12.6% (Figure 25.B). The carbon and oxygen content of the TCP + NH_2^+ bioactive surface was 79% and 8.3% respectively. Furthermore, TCP + NH_2^+ + Heparin surface revealed a S 2p peak at 168 eV (Figure 25.C, signalled by arrow), revealing sulphur content in the bioactive surface. This sulphur content was 0.7%. Additionally, carbon, oxygen and nitrogen content were 75% (peak at 258 eV), 11.2% (550 eV), and 9.1% (400 eV) respectively [234]–[238].

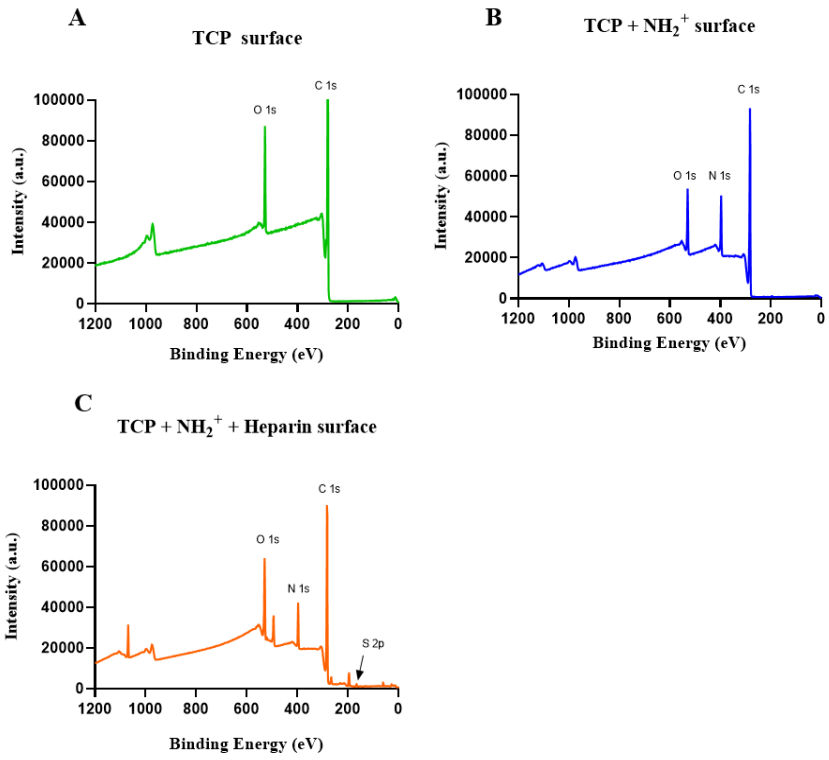

Figure 25. XPS survey scans of the surfaces after each modification. A) TCP surface control. B) TCP + NH_2^+ surface, where nitrogen peak can be seen at 400 eV. C) TCP + NH_2^+ + Heparin surface, where nitrogen peak can be seen at 400 eV, and sulphur peak is shown by the arrow at 168 eV.

The C 1s high resolution scans of the bioactive surfaces are compared in Figure 26. The peak at 285.0 eV corresponded to the hydrocarbon C-C/C-H contribution. The peaks at 286.5 eV and 288.0 eV were attributed to C-O and C=O contribution [239]–[242]. These peaks are comparable with those peaks present in TCP seen in literature [243], [244]. The scan of the TCP surface (Figure 26.A) showed 65.4% of C-C/C-H content. Additionally, the content of C-O and C=O was 8.9% and 1.8% respectively.

For the TCP + NH_2^+ bioactive surface (Figure 26.B), the percentage of C-C/C-H content was 68.6%. The contribution of the 286.5 eV peak increased up to 24% in comparison to the content of C-O from TCP surface (8.9%). This peak at 286.5 eV was also attributed to a C-N environment [240], [242], [245]–[247]. It can be concluded that the increase in atomic content at this 286.5 eV peak is due to the presence of nitrogen in the surface, as there is no nitrogen in the TCP surface, and the survey scan of TCP + NH_2^+ bioactive surface revealed the incorporation of nitrogen to the surface.

The C1s high resolution scan of TCP + NH_2^+ + Heparin is seen in Figure 26.C. The content of C-C/C-H, C-O/C-N and C=O was 69%, 25.4% and 6.6% respectively. The content of C-O/C-N contribution increased slightly in comparison to this same contribution in the TCP + NH_2^+ bioactive surface (from 24% to 25.4%). Moreover, this information is consistent with previous studies [248]–[250], where the high resolution C 1s scan did not show a great increase in the C-O contributions after heparin was added to the surface. This statement is also supported by the TCP + NH_2^+ + Heparin survey scan, where the oxygen content was 11.2%, which is higher compared to the 8.3% of oxygen content in the TCP + NH_2^+ bioactive surface.

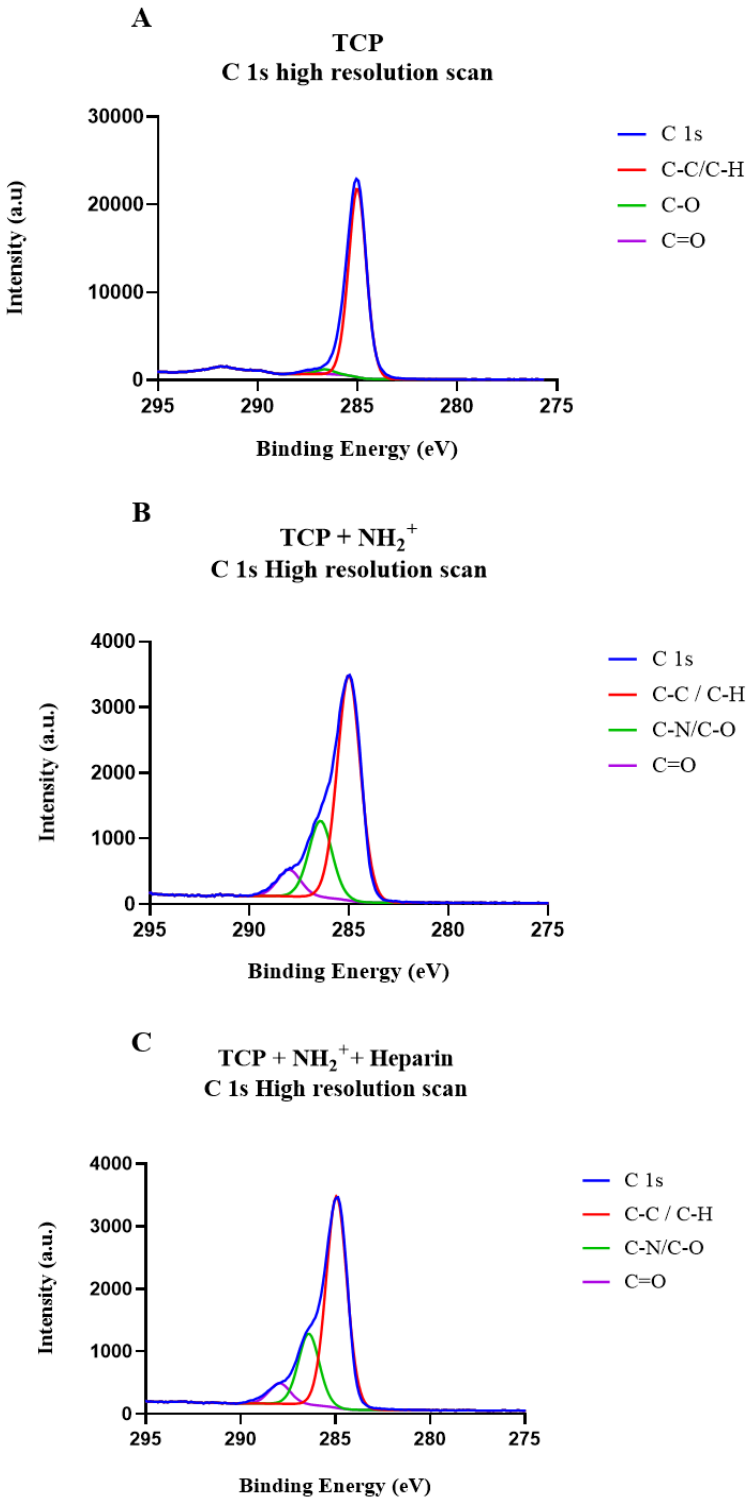

Figure 26. C 1s high resolution scans of the surfaces after each modification. C-C/C-H peak was detected at 285 eV, C-O/C-N peaks were detected at 286.5 eV and C=O peak was detected at 288 eV. A) TCP control. B) TCP + NH_2^+ surface. C) TCP + NH_2^+ + Heparin surface.

The N 1s high resolution scans of TCP + NH_2^+ and TCP + NH_2^+ + Heparin are shown in Figure 27. TCP + NH_2^+ bioactive surface showed a peak at 401.5 eV. Additionally, TCP + NH_2^+ + Heparin bioactive surface presented a peak at 400.9 eV. The presence of this peak in the N 1s high resolution scan confirmed the presence of -NH_2^+ in both TCP + NH_2^+ and TCP + NH_2^+ + Heparin bioactive surfaces [246], [247]. This peak shift is due to the chemical environment of the components of the surface.

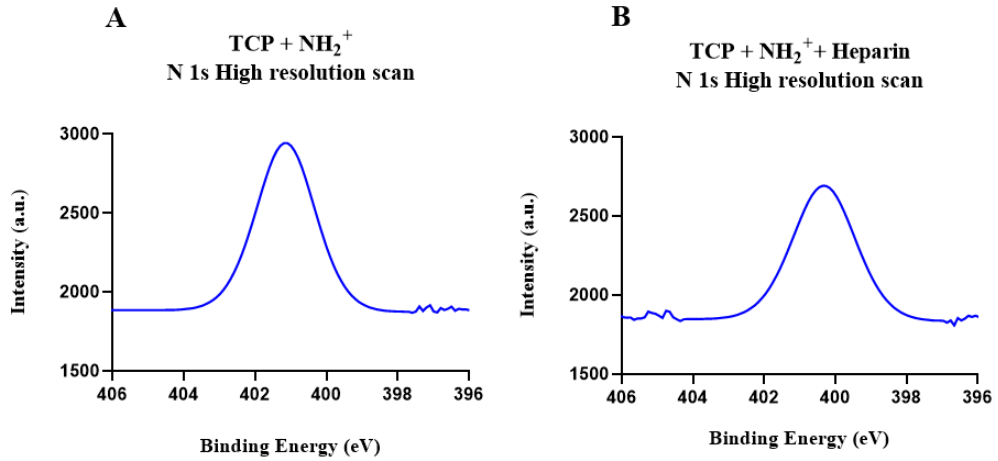

Figure 27. N 1s high resolution scan of A) TCP + NH_2^+ surface, and B) TCP + NH_2^+ + Heparin surface. The peak seen at ≈ 400 eV was attributed to -NH_2, confirming the presence of amine groups in the surfaces.

The S 2p high resolution spectrum of TCP + NH_2^+ + Heparin bioactive surface is shown in Figure 28. Two signals were identified, where each one is a spin orbit split doublet, S $2p^{3/2}$ and S $2p^{1/2}$ (2:1 ratio). These S $2p^{3/2}$ (168.2 eV) and S $2p^{1/2}$ (169.3 eV) peaks correspond to the -OSO_3 and -NSO_3 groups found in heparin [234], [251], [252]. Therefore, heparin was bound successfully to the TCP + NH_2^+ + Heparin bioactive surface.

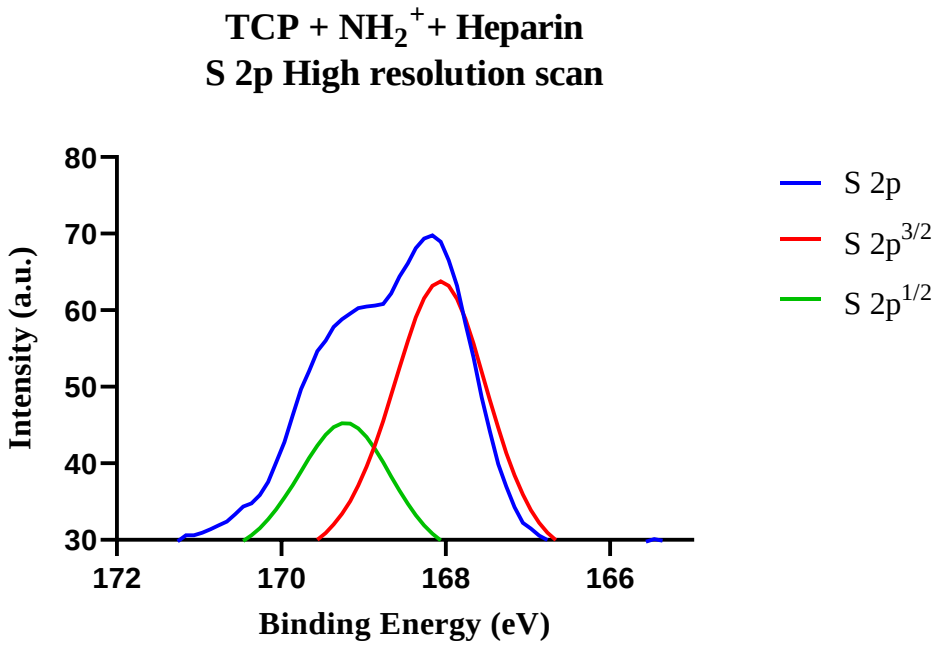

Figure 28. S 2p high resolution scan of TCP+NH_2^+ + Heparin surface. The S 2p peak shows a doublet in a 2:1 proportion of S $2p^{3/2}$ and S $2p^{1/2}$ (66.6% and 33.3% respectively) corresponding to -OSO_3 and -NSO_3 groups present in heparin.

5.4.3 Quantification of NGF and BDNF released from bioactive surface

5.4.3.1 NGF and BDNF bound to heparin on the surface of the bioactive surface

The concentration of NGF or BDNF remaining after 5 hours incubation period with TCP + NH_2^+ + Heparin was quantified by ELISA. This concentration represents the quantity of growth factor not bound to heparin. The total amount of growth factor in the solution prior immobilisation step minus the amount present in the supernatant would be the quantity of growth factor bound to heparin in the bioactive surface. Consequently, the quantity of growth factor bound to heparin was used to calculate the percentage of the released NGF or BDNF from the bioactive surface TCP + NH_2^+ + Heparin.

Figure 29 shows a bar graph with the percentage of NGF bound to heparin, calculated as described above. As seen in this graph, when NGF was immobilised on the bioactive surface with NGF 1 µg/mL, 97% of the total dose was bound to heparin on the bioactive surface. For bioactive surfaces immobilised with NGF 100 ng/mL and 10 ng/mL, 98% of NGF was bound to heparin. When bioactive surfaces were immobilised with NGF at 1 ng/mL, 99% of the total load was bound to heparin on the bioactive surface.

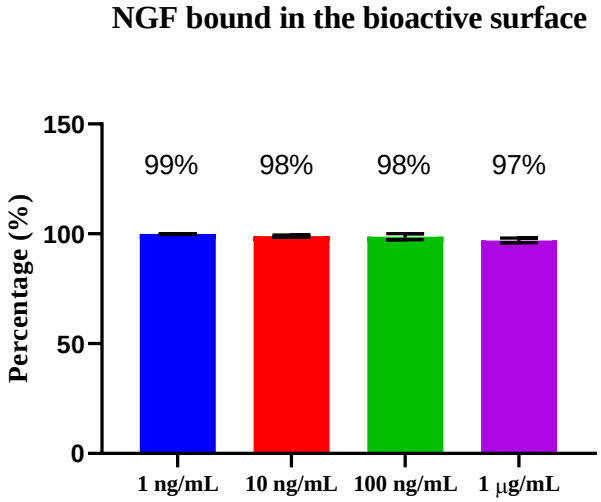

Figure 29. NGF bound to heparin on the bioactive surfaces. For each concentration of NGF immobilised, the quantity of NGF bound to the surface was calculated and represented as percentage. None of the results are statistically different from each other $p < 0.05$. Mean ± SD. N=2, n=4.

Figure 30 shows a bar graph with the percentage of BDNF bound to heparin, calculated as described above. It can be observed in the graph that 91% of BDNF was bound to heparin when the bioactive surface was immobilised with BDNF at 1 µg/mL. When the bioactive surface was immobilised with BDNF at 100 ng/mL, 86% of the total load was bound to heparin on the bioactive surface. Moreover, 85% of the total load was bound to heparin when the bioactive surfaces were immobilised with BDNF at 10 ng/mL and 1 ng/mL.

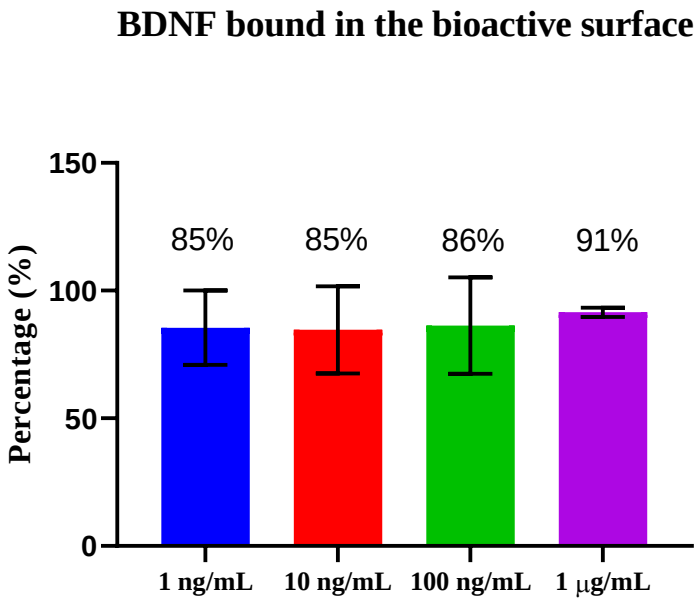

Figure 30. BDNF bound to heparin on the bioactive surfaces. For each concentration of BDNF immobilised, the quantity of BDNF bound to the surface was calculated. None of the results are statistically different from each other $p < 0.05$. Mean ± SD. N=2, n=4.

5.4.3.2 Quantification of released NGF from bioactive surface

Bioactive surfaces were fabricated as described in section 5.3.1. Furthermore, ELISA was used to quantify the release of neurotrophins as described in section 5.3.2.3. The quantity of NGF bound to heparin calculated in section 5.4.3.1 was used to calculate the percentage of the released NGF from the bioactive surface. A Calibration curve was also done (please see appendix, Figure 132, to see this graph).

The quantification of released NGF from the bioactive surface was evaluated over 168 hours at 37°C and 4°C, as shown in Figure 31 and Figure 32. None of the bioactive surfaces released NGF after1 hour incubation, either at 37°C or 4°C.

Release of NGF from bioactive surfaces immobilised with NGF incubated at 37°C are described first. At 24 hours, 0.03% of the total dose was detected for surfaces immobilised with NGF at 1µg/mL. For surfaces immobilised with NGF with 100 ng/mL, 1% and 0.04% were detected at 24 hours and 48 hours respectively. For surfaces immobilised with 10 ng/mL, NGF release was quantified at 24 hours and 48 hours, where 1% and 0.06% of total load was detected, respectively. Surfaces immobilised with NGF at the lower concentration of 1ng/mL did not show any NGF release at 1 hour, 24 hours or 48 hours. However, at 168 hours, 1% of total load of NGF was detected (Table 10).

When the bioactive surfaces immobilised with NGF were incubated at 4°C, the released NGF profile was different. For surfaces immobilised with NGF 1µg/mL, 0.003%, 0.007% and 0.02% of the total load was detected at 24 hours, 48 hours and 168 hours respectively. For surfaces immobilised with NGF 100 ng/mL, no growth factor release was detected until 168 hours, with 0.001% of the total load. At 48 hours, the release of NGF was 0.03% for surfaces immobilised with NGF 10 ng/mL. Moreover, for surfaces immobilised with NGF 1 ng/mL, 6% of the total dose was released at 24 hours. After that, no growth factor release was detected (Table 10).

Interestingly, when the bioactive surface immobilised with NGF at 1 µg/mL was incubated at 4°C, the bioactive surface released 0.02% (0.10 ng/mL) of NGF at 168 hours. In comparison, this same bioactive surface when incubated at 37°C,

released 0.03% (0.11 ng/mL) of NGF at 24 hours. This finding raises questions regarding how temperature might affect NGF release from the bioactive surface.

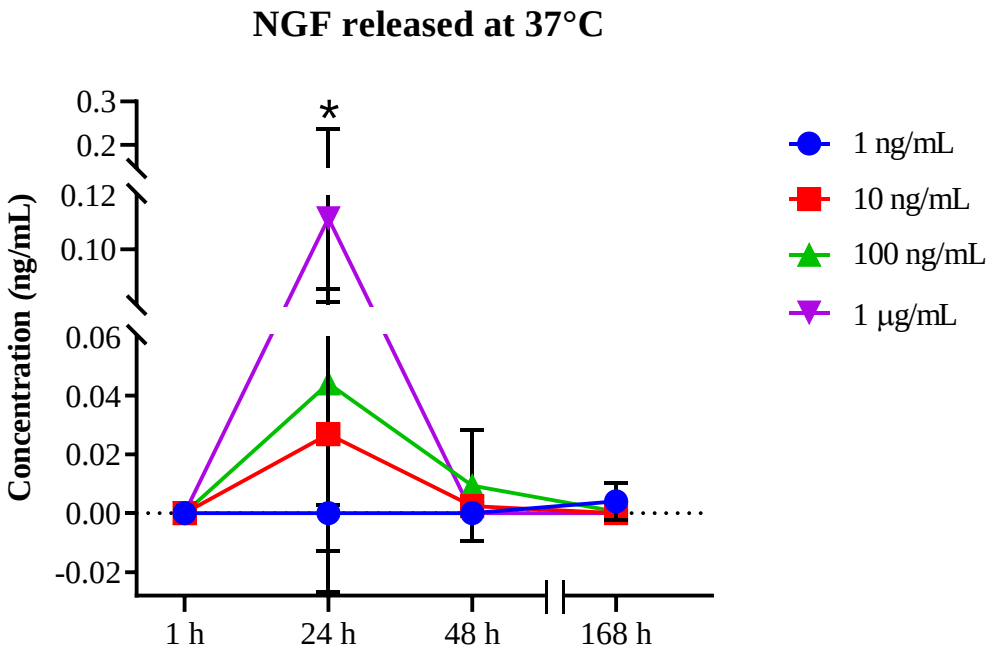

Figure 31. Concentration of NGF released from bioactive surface NH_2^+ + Heparin + Immobilised NGF incubated at 37°C within 168 hours (7 days). Mean ± SD. N = 2, n = 4.

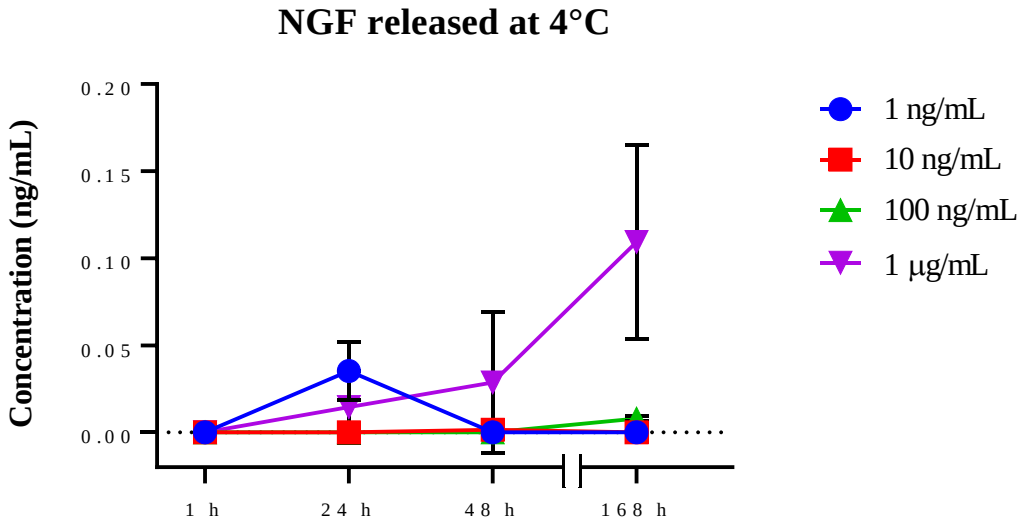

Figure 32. Concentration of NGF released from bioactive surface NH_2^+ + Heparin + Immobilised NGF incubated at 4°C within 168 hours (7 days). Mean ± SD. N = 2, n = 4.

Table 10. Released concentration, within 168 h at 37°C and 4°C, of NGF in ng/mL and its corresponding percentage (%) according to the initial load. Mean ± SD.

		Released Concentration (ng/mL) from bioactive surface/Released Percentage (%) from the total immobilized load							
		1 ng/mL		10 ng/mL		100 ng/mL		1 µg/mL	
		ng/mL	%	ng/mL	%	ng/mL	%	ng/mL	%
NGF at 37°C	1 h	0 ± 0	0	0 ± 0	0	0 ± 0	0	0 ± 0	0
	24 h	0 ± 0	0	0.027 ± 0.054	1	0.044 ± 0.041	1	0.115 ± 0.146	0.03
	48 h	0 ± 0	0	0.002 ± 0.002	0.06	0.009 ± 0.019	0.04	0 ± 0	0
	168 h	0.004 ± 0.004	1	0 ± 0	0	0 ± 0	0	0 ± 0	0
NGF at 4°C	1 h	0 ± 0	0	0 ± 0	0	0 ± 0	0	0 ± 0	0
	24 h	0.023 ± 0.03	6	0 ± 0	0	0 ± 0	0	0.015 ± 0.021	0.003
	48 h	0 ± 0	0	0.001 ± 0.001	0.03	0 ± 0	0	0.03 ± 0.04	0.007
	168 h	0 ± 0	0	0 ± 0	0	0.0003 ± 0.0005	0.001	0.015 ± 0.10	0.02

5.4.3.3 Quantification of released BDNF from bioactive surface

The quantity of BDNF bound to heparin calculated in section 4.3.1 was used to calculate the percentage of the released BDNF from the bioactive surface. A calibration curve was also done (please see appendix, Figure 133, to see this graph).

The quantification of released BDNF from the bioactive surface was evaluated over 168 hours of incubation at 37°C and 4°C, as shown in Figure 33 and Figure 34. Firstly, the release of BDNF from bioactive surfaces incubated at 37°C are described. For surfaces immobilised with BDNF with 1 µg/mL, 3% and 0.01% of the total dose was detected at 1 hour and 24 hours. Additionally, 0.06% and 0.01% release were measured at 48 hours and 168 hours respectively. The release of BDNF was also quantified at 1 hour, 24 hours, 48 hours and 168 hours from surfaces immobilised with 100 ng/mL resulting in 32%, 0.18%, 0.37% and 0.17% of initial load respectively. For surfaces immobilised with BDNF at 10 ng/mL, 35% (1 hour), 2.8% (24 hours), 1.2% (48 hours) and 1.5% (168 hours) of the initial BDNF load was measured. Bioactive

surfaces immobilised with BDNF at 1 ng/mL showed 25%, 30%, 11% and 31% of BDNF released at 1 hour, 24 hours, 48 hours and 168 hours respectively (Table 11).

The release of BDNF from bioactive surfaces with immobilised BDNF at 4°C was lower. Bioactive surfaces immobilised with BDNF at 1 µg/mL released 0.003%, 0.001% and 0.025% at 24 hours, 48 hours and 168 hours respectively. When bioactive surfaces immobilised with BDF at 100 ng/mL were measured, 3%, 0.01%, 0.02% and 0.01% of the initial load was released at 1 hour, 24 hours, 48 hours and 168 hours respectively. For bioactive surfaces immobilised with BDNF at 10 ng/mL, 0.02% (24 hours), 1% (48 hours) and 0.23% (168 hours) were detected. Moreover, for bioactive surfaces immobilised with BDNF at 1ng/mL, the released BDNF from the bioactive surface at 1 hour, 24 hours, 48 hours and 168 hours was 1.2%, 0.34%, 1% and 1% of the initial load respectively (Table 11).

For the bioactive surface immobilised with BDNF 100 ng/mL, the release of growth factor at 1 hour was 10 times less when this bioactive surface was incubated at 4°C than when it was incubated at 37°C. Therefore, this information suggested that the temperature affects the quantity of growth factor released from the bioactive surface.

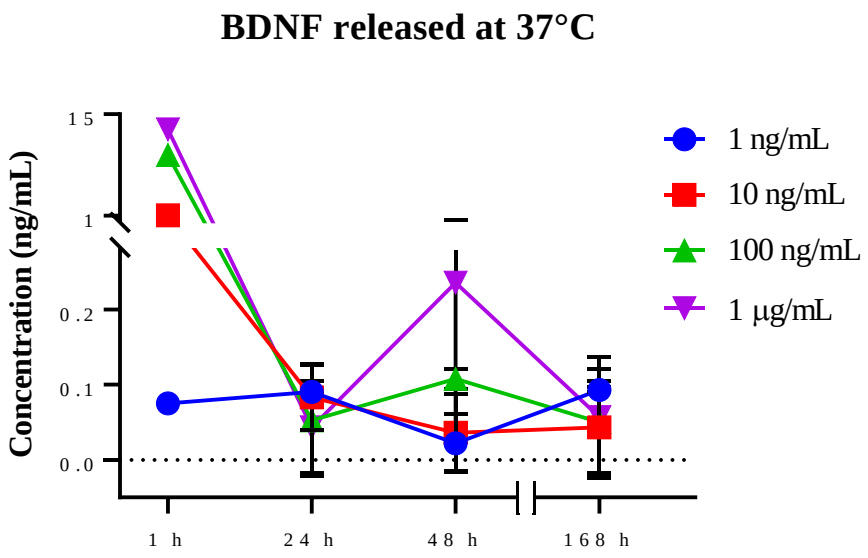

Figure 33. Concentration of BDNF released from bioactive surface NH_2^+ + Heparin + Immobilised BDNF incubated at 37°C within 168 hours (7 days). Mean ± SD. N = 2, n = 4.

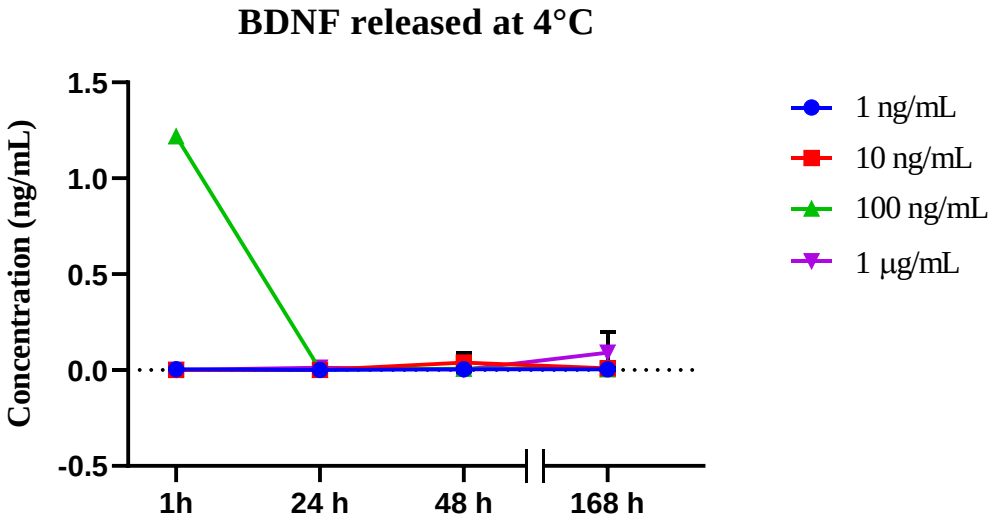

Figure 34. Concentration of BDNF released from bioactive surface NH_2^+ + Heparin + Immobilised BDNF incubated at 4°C within 168 hours (7 days). Mean ± SD. N = 2, n = 4.

Table 11. Released concentration, within 168 h at 37°C and 4°C, of BDNF in ng/mL and its corresponding percentage (%) according to the initial load. Mean ± SD.

		Released Concentration (ng/mL) from bioactive surface/Released Percentage (%) from the total immobilized load							
		1 ng/mL		10 ng/mL		100 ng/mL		1 µg/mL	
		ng/mL	%	ng/mL	%	ng/mL	%	ng/mL	%
BDNF at 37°C	1 h	0.075 ± 0	25	1.04 ± 0	35	9.35 ± 0	32	12.92 ± 0	3
	24 h	0.090 ± 0.008	30	0.083 ± 0.043	2.8	0.053 ± 0.074	0.18	0.043 ± 0.06	0.01
	48 h	0.033 ± 0.047	11	0.036 ± 0.050	1.2	0.108 ± 0.013	0.37	0.243 ± 0.18	0.06
	168 h	0.096 ± 0.003	31	0.043 ± 0.061	1.5	0.05 ± 0.071	0.17	0.049 ± 0.07	0.01
BDNF at 4°C	1 h	0.004 ± 0.003	1.2	0 ± 0	0	1.23 ± 0.86	3	0 ± 0	0
	24 h	0.001 ± 0.002	0.34	0.001 ± 0.001	0.02	0.003 ± 0.004	0.01	0.011 ± 0.005	0.003
	48 h	0.004 ± 0.005	1	0.002 ± 0.05	1	0.01 ± 0.01	0.02	0.002 ± 0.003	0.001
	168 h	0.004 ± 0.005	1	0.01 ± 0.012	0.23	0.003 ± 0.005	0.01	0.09 ± 0.11	0.025

5.5 Discussion

The main aim of this chapter was to fabricate and characterise bioactive surfaces that consisted of NH_2^+, heparin, NGF or BDNF. Fabrication was performed by adding a heparin solution onto a NH_2^+ surface. Then, NGF or BDNF were added to the NH_2^+ + Heparin bioactive surface, binding to heparin by electrostatic interactions. Contact angle and XPS analysis were conducted to characterise the bioactive surface NH_2^+ and NH_2^+ + Heparin. An ELISA was performed to evaluate the release of NGF and BDNF from the bioactive surface NH_2^+ + Heparin + Immobilised NGF or BDNF.

The main findings were that heparin was successfully adsorbed to the TCP + NH_2^+ bioactive surface as confirmed by water contact angle and the XPS analysis. Furthermore, NGF and BDNF were immobilised at different concentrations on the TCP + NH_2^+ + Heparin bioactive surface. Moreover, their release from the bioactive surface was detected and quantified by ELISA assay.

The technique used to incorporate heparin to the TCP + NH_2^+ bioactive surface was based on the knowledge that heparin, a negatively charged glycosaminoglycan, will bind electrostatically to the positively charged NH_2^+ amine group [211], [239]. Moreover, NGF and BDNF would be immobilised to the TCP + NH_2^+ + Heparin bioactive surface electrostatically and by means of their heparin binding domain.

Irrespective of the technique employed to modify surfaces or to immobilise biomolecules, XPS analysis and contact angle analysis are two frequently used techniques to characterise the surface of a material. XPS consists of irradiating a sample with a monoenergetic x-rays source followed by the analysis of the emitted electrons from the surface. Identification of chemical states of the components can be obtained, as they have a unique spectrum. Further, the concentration of each component can be calculated from the peak area, which is expressed as a percentage [234].

Moreover, contact angle has been used to investigate the wettability of materials and to follow how surface modification changes the surface chemistry of a material. For example, Lee et al., added carboxyl functional groups, amide groups and amine functional groups on polyethylene films. By contact angle, they concluded that the

wettability of the modified polyethylene (PE) increased in comparison with unmodified PE [239].

In the literature, different techniques for surface modification and addition of functional groups have been described. These techniques successfully bound or added a variety of biomolecules or other chemical substances to a diversity of materials. A common factor among these studies was the use of XPS and contact angle techniques to characterise the modification of the surface of the material. For example, Hopper et al., functionalised nanodiamond with amine groups in order to increase the adhesion properties of a material. Firstly, they coated a glass coverslip with acrylic acid by plasma deposition. Then, the nanodiamond surface was functionalised with 10-amino dec-1-ene by photochemical attachment using ultraviolet (UV) light. After, an amine functionalised nanodiamond solution was added to the glass coverslip-acrylic acid surface. Then, the samples were rinsed in distilled water and then with PBS prior to cell culture. XPS analysis confirmed the presence of amine groups as the survey scan showed 21.4% of nitrogen content. Additionally, the contact angle of the glass coverslip, glass coverslip-acrylic acid and glass coverslip-acrylic acid-amine functionalised nanodiamond was of 50°, 56° and 67° respectively. This data indicated a change in wettability on the surface as a consequence of the surface modification. This work focused on modifying a material by encouraging electrostatic interactions between a negatively charged acrylic acid and a positively charged 10-amino dec-1-ene, as they have carboxyl and amine groups, respectively [253].

Lee and Schmidt synthesised an amine functionalised polypyrrole by reducing 1-(2-cyanoethyl)pyrrole using $LiAlH_4$ to improve cell adhesion and electrical stimulation by the polypyrrole [231]. Similarly, to Hopper et al., Lee and Schmidt used contact angle and XPS analysis to confirm the addition of amine functional groups to polypyrrole films. The amine functionalised polypyrrole revealed an increased hydrophilicity in comparison to polypyrrole films as the contact angles were of 67.3° and 83.5° respectively. This change in wettability was attributed to the addition of amine groups to polypyrrole. Moreover, XPS analysis detected nitrogen content in the amine functionalised polypyrrole. The peak shown at 401.9 eV in the N 1s high

resolution spectra was attributed to amine functional groups present in the amine functionalised polypyrrole [231].

In contrast to Lee and Schmidt, Hopper et al., and the work presented in this thesis, Graisuwan et al., fabricated multilayers films using three derivatives of chitosan: N-sulfofurfuryl chitosan (SFC), N-[(2-hydroxyl-3-trimethylammonium)propyl] chitosan chloride (HTACC), and N-succinyl chitosan (SCC). These three derivatives of chitosan were paired either with polyacrylic acid (PAA) or poly(allylamine hydrochloride) (PAH) on a treated surface of poly(ethylene terephthalate) (t-PET). After hydrolysis by sodium hydroxide (NaOH) and hydrochloric acid (HCl), t-PET films were layer-by-layer dipped in a cation solution (2 mg/mL of either HTACC or PAH) and an anion solution (1 mg/mL of SCC or 2 mg/mL of either PAA or SFC) for 20 minutes at each step until 9 layers (odd number, positively charged surface layer) or 10 layers (even number, negatively charged surface layer) were assembled. Different combinations of films were fabricated, however, contact angle analysis revealed that, regarding the nature of the last layer, the positively charged surface layer was less hydrophilic than the films with a negatively charged surface layer. This difference in wettability was attributed to the negative charge of the carboxyl functional group over the positive charge of the amine groups [254]. However, this work did not show any numerical quantification of said measurement, so it cannot be concluded if the 9 layered films had a statistical difference when compared to the 10 layered films. Both functional groups were proven to improve the wettability of a surface they were present on.

In comparison, Zhu et al., modified polylactic acid (PLA) films with a chitosan/heparin complex to enhance cell adhesion properties of PLA. This surface modification was achieved by covalent immobilisation of chitosan on the PLA films. Chitosan powder, [1-ethyl-3-(3-dimethylamino-propyl)] carbodiimide (EDC) and 4-azidobenzoic acid were mixed with N,N,N',N'-tetramethylethylene diamine methanol (TEMED) solution. Then, this mixture was stirred for 72 hours and filtered. The Az-chitosan powder was dissolved in acetic acid/methoxyethanol to produce an Az-chitosan solution. This Az-chitosan solution was cast on PLA films and left to dry. Then, it was crosslinked with a UV lamp. A heparin solution (in acetate buffer

solution) was then added to the Az-chitosan-PLA film and it was incubated for 2 hours, achieving a heparin-Az-chitosan-PLA film. Chitosan was covalently immobilised to the PLA films by the photosensitive regent 4-azidobenzoic. Then, heparin was electrostatically bound to the positively charged chitosan [180]. To characterise their Az-chitosan-PLA film, Zhu et al., used XPS analysis and contact angle technique. The XPS analysis revealed a new peak, in comparison to control PLA film, at 400.28 eV, which was attributed to nitrogen, present in chitosan, bound to the PLA film. Moreover, an S 2p high resolution scan was obtained, revealing a sulphur peak at ca. 168 eV, suggesting that heparin was bound to the surface of hep-Az-chitosan-PLA film [180]. Contact angle analysis showed an increased hydrophilicity after each surface modification as PLA, Az-chitosan-PLA film and hep-Az-chitosan-PLA film had a contact angle of 65°, 48° and 40° respectively. The addition of chitosan and heparin changed the wettability of PLA films, as these molecules introduce a charge in the surface [180].

Heparin has also been bound to surfaces covalently. Yang et al., immobilised heparin on plasma allylamine-stainless steel films. Moreover, they demonstrated that heparin is well retained in allylamine. Firstly, allylamine was deposited by pulsed plasma deposition on the stainless steel films. Heparin was mixed with N-hydroxysuccinimide (NHS) and EDC to prepare a heparin solution. Then, the heparin solution was incubated with the allylamine-stainless steel films for 24 hours at 4°C. Heparin covalently bound to the -NH_2 amine functional groups present in the surface of the allylamine-stainless steel film. This was possible as allylamine has a high density of amine functional groups [210]. XPS analysis confirmed nitrogen content in the allylamine-stainless steel films and in the heparin-allylamine-stainless steel films. Additionally, contact angle decreased from 70.8°, on stainless steel, to 62.7° on allylamine-stainless steel. Moreover, the immobilisation of heparin in allylamine-stainless steel films also increases the surface hydrophilicity [210].

Comparably to Yang et al., and to Zhu et al., Wang et al., use covalent immobilisation technique to modify poly(lactic acid-co-glycolic acid) (PLGA) [255]. Chitosan was covalently immobilised to PLGA using EDC, NHS in a 2-morpholinoethane sulfonic acid (MES) buffer. Then, heparin, using the ECD-NHS-MES buffer, was covalently

immobilised to the chitosan-PLGA film. After 4 hours of incubation, the heparin-chitosan-PLGA film was rinsed with distilled water. XPS analysis revealed a peak at ca. 409 eV, which was attributed to the presence of amino groups (H-N-C=O) [255]. This is possible because the amine functional groups of the chitosan changed to amino groups, forming a covalent peptide linkage between chitosan and heparin. Additionally, an S 2p peak appeared in the survey scan, revealing that the surface had the sulphated groups found in heparin. This data confirmed the presence of heparin on the surface. Contact angle analysis showed that when the PLGA film was modified with chitosan, this film was more hydrophilic than the PLGA control. Furthermore, when heparin was immobilised on chitosan-PLGA films, the contact angle was lower compared to chitosan-PLGA films and the PLGA control [255]. This data indicated that the hydrophobicity of PLGA films was modified by the addition of amine groups from chitosan and sulphate groups and carboxyl groups from heparin.

In a complementary study, Liu et al., synthesised heparin-poly-L-lysine (PLL) nanoparticles and immobilised them on dopamine (DM) coated stainless steel. PLL, which is rich in amine functional groups, hence, it is positively charged, was mixed with negatively charged heparin to form heparin-PLL nanoparticles. These heparin-PLL nanoparticles were incubated for 12 hours at 20°C with the DM coated stainless steel samples to achieve nanoparticle immobilisation. DM has the ability to bind to amine groups, hence, DM bound to PLL allowing the immobilisation of the heparin-PLL nanoparticles to stainless steel [223]. XPS analysis revealed an S 2p peak at 168.8 eV, attributed to the sulphur content found in heparin. It is important to note that, from the original heparin solution of 10 mg/mL, only 0.9% of the total composition of the surface was sulphur. Additionally, an N 1s peak was shown at 400 eV, which was attributed to the presence of nitrogen on the surface. Contact angle was measured to change in hydrophilicity after the immobilisation of heparin-PLL nanoparticles. The heparin-PLL nanoparticle-DM-stainless steel sample was significantly more hydrophilic than the DM-stainless steel sample [223].

Moreover, Chen et al., immobilised heparin on silicone (PDMS) using poly(ethylene glycol) (PEG) and platinum-divinyltetramethylsisiloxane (Karstedt's Pt catalyst). Silicone samples were incubated with 2-methoxyethylene ether, α-allyl-ω-N-

succinimidyl carbonate PEG, and Karsteadt's Pt catalyst. Then, the modified silicon was rinsed and incubated for 6 hours with a heparin solution (10 mg/mL). Contact angle analysis revealed that the surface wettability was changed after each modification [248]. Control PDMS samples had an advancing contact angle of 120°. Modified PEG samples had a contact angle of 85°, whereas PEG-heparin surface had a contact angle of 48°. These results indicate that the surface became more hydrophilic after each surface modification. In addition, XPS analysis revealed an S 2p peak in the survey scan, which indicated the incorporation of sulphur content after heparin was added to the PEG modified surface. The sulphur content, attributed to heparin being immobilised in the PEG-heparin surface, was of 0.4%, representing approximately 0.68 μg/cm^2 of heparin in the PEG modified surface [248].

Interestingly, the method used by Chen et al., for the covalent immobilisation of heparin on silicon, by means of the reaction between PEG and PDMS, only bound 0.4% of sulphur on the surface [248]. This sulphur content came from the immobilised heparin; therefore, a low concentration of heparin was bound to the surface. It is important to notice that the heparin solution used in the covalent immobilisation process had a concentration of 10 mg/mL [248]. Comparatively, Liu et al., who also used a heparin solution of 10 mg/mL to electrostatically bind heparin to PLL, found that 0.91% of the surface composition was sulphur, which was attributed to heparin [223]. Both methods immobilised heparin on the surface, but electrostatic binding was more efficient for retaining heparin. In addition, the bioactive surface developed in this thesis immobilised, by electrostatic interactions, 50 μg/mL of negatively charged heparin to positively charged amine functional group, and XPS analysis revealed that 0.7% of sulphur was present in the modified surface. More information that would compare both methods would be needed. However, results found here suggested that heparin binding by electrostatic interactions is a more efficient method.

These findings raise the question of would the success of binding biomolecules increase when the biomolecules were immobilised by electrostatic means. This statement is supported by Mahoney et al., who non-covalently immobilised heparin on allylamine surfaces. Heparin solution (in PBS, 0-10 μg/well) was incubated on the allylamine surface overnight at room temperature. XPS analysis revealed a nitrogen

peak at 400 eV, confirming the presence of amines on the surface. Moreover, the Link_TSG6 binding assay showed that heparin bound to surfaces modified with allylamine. In addition, heparin was not found on surfaces without allylamine [211]. Heparin was bound to allylamine by electrostatic interactions because allylamine is positively charged, and heparin is negatively charged [211]. This work, which is similar to the one presented in this thesis, interrogates if heparin binds more efficiently to positively charged functionalities rather to negatively charged functionalities.

Kang et al. supported the hypothesis that more efficient binding is achieved when a negatively charged molecule is bound to a positively charged molecule instead of binding two negatively or two positively charged molecules [256]. Kang et al. covalently immobilised heparin on functionalised polyurethane (PU) samples with amine functional groups or carboxylic acid functional groups. Firstly, PU samples were modified with oxygen plasma deposition and then 1-acryloylbenzotriazole (AB) was polymerised on the surface (PU-AB) [256].

To add carboxylic acid functional groups on the PU-AB surface, this surface was incubated in a sodium hydroxide solution for 3 hours at room temperature. After the surfaces were rinsed, citric acid dissolved in an aqueous methanol solution was added to convert sodium carboxylate to carboxylic acid. Hence, they obtained the PU-COOH surface. For the addition of amine functional groups on PU-AB, this surface was incubated with ethylene diamine solution for 24 hours at room temperature [256]. In this manner they fabricated the PU-NH_2 surface.

To prepare PU-COOH surfaces with immobilised heparin, the PU-COOH surface was incubated with EDAC solution for 24 hours at 4°C. Then, the surface was rinsed with deionised water. Afterwards, the surface was incubated with heparin solution (in sodium citrate buffer) for 24 hours at 4°C. Then, the PU-C-Hep surface was obtained. In comparison, heparin solution in EDAC was incubated on PU-NH_2 surface for 24 hours at 4°C to obtain PU-N-Hep [256].

Contact angle of PU decreased from 69° to 52° after AB modification. Additionally, when carboxylic acid and amine functional groups were added to the surface, the contact angle decreased to 42° and 46°, respectively. When heparin was immobilised

to PU-COOH surface and PU- NH_2 , the contact angle was 42° and 43°, respectively [256]. Moreover, XPS analysis revealed that the sulphur content in PU-N-Hep (0.5%) was larger than the sulphur content in PU-C-Hep (0.1%) [256]. These results support the hypothesis that heparin has more affinity to bind to a positively charged surface than to a neutral or negatively charged surface.

These studies reinforce the use of positively charged functional groups to bind negatively charged functional groups or biomolecules, such as heparin. In addition, regardless of surface modification technique, XPS and contact angle techniques are widely used to characterise the surface of a material.

Having heparin on the surface is a paramount step to successfully immobilise growth factors. Moreover, it is important that these growth factors are retained on the surface to avoid an initial burst release that could compromise neurite outgrowth [169], [217], [224]. Different approaches had been studied to immobilise growth factors and to avoid or minimise an initial burst. Furthermore, ELISA has been frequently used to characterise growth factor content on the surface as they are released from that surface. ELISA recognises and quantifies proteins, antibodies, antigens, viruses and hormones. This assay uses antibodies and enzymes to detect the desired antigen, which are then quantified by colorimetry [257].

Photochemical techniques have been used to immobilise growth factors. Gomez and Schmidt reported on the immobilisation of NGF on the surface of polypyrrole (PPy) by UV exposure using polyallylamine and arylazido compound. Fluorescence microscopy was used to calculate the surface concentration of NGF on the PPY substrate and ELISA was performed to quantify the concentration of released NGF from the PPy substrate. Additionally, XPS was used to analyse the chemical changes in the PPy substrates after the modifications [227]. NGF photochemical immobilisation was performed as follows: N-4-(azidobenzoyloxy)succinimide was synthesised by adding a solution of dicyclohexylcarbodiimide in tetrahydrofuran to a solution of N-hydroxysuccinimide, and 4-azidobenzoic acid in tetrahydrofuran. Then,this solution was filtered and crystallised with isopropyl alcohol/ diisopropyl ether. After, a solution of polyallylamine (PAA) was added to a N-4-

(azidobenzoyloxy)succinimide solution in N,N-dimethylformamide and mixed for 24 hours at 4°C. The solution was filtered and washed with distilled water to obtain a photosensitive PAA-azido solution [227]. The solution was coated onto PPy substrates employing an UV lamp for 15 seconds. Then, after being washed with hydrochloric acid, this substrate was coated with a PAA solution, followed by the addition of NGF solution (0.5-2 µg in 50 µL of PBS). The substrates were treated with UV light for 15 seconds and then washed with PBS [227]. XPS analysis revealed a peak at 401.7 eV in the N 1s high resolution scan, which was attributed to the $C\text{-}N^+$ corresponding to PAA being present in the substrate. Fluorescence microscopy was performed to calculate the surface concentration of NGF on the PPy substrate. Only 100 ng of NGF were immobilised in an area of 1 cm^2, which corresponds to 5% of the initial load of NGF (2 µg). Moreover, ELISA revealed that at 6, 24, 48 and 72 hours, the averaged concentration of released NGF was 1.06 ng/mL[227]. NGF was immobilised on the surface by UV light activating the azido groups in the PAA-azido solution, enabling covalent bonds (N-H or C-N) between NGF and the PPy substrate [227]. This study revealed that the use of UV light for immobilising growth factors is not optimal, as most of the protein was lost or inactivated during the process.

Similarly, Kapur and Schoichet covalently immobilised NGF to poly-2-hydroxy-ethylmethacrylate (PHEMA) gels with NHS azido, using UV light [258]. By ELISA, only 30 ng of the initial load of 150 ng of NGF was detected on the PHEMA gels. Moreover, within the first measurement, 27.65 ng of NGF was detected, and 1.5 ng/mL was detected daily over the next three days [258]. According to Kapur and Schoichet, this amount is inadequate to encourage a biological response [258]. The explanation for the loss of NGF is that the UV light was very intense (23 W/cm^2 for 1 second) damaging NGF, as it compromised its structure and function [258].

As using UV light is not an appropriate method to immobilise growth factors, as it would affect the growth factor's biological activity, Madduri et al. designed a collagen nerve conduit to release glial cell line-derived neurotrophic factor (GDNF) alone or with NGF [224]. The collagen from the nerve conduits was crosslinked through a dehydro-thermal treatment (DHT, at 110°C and 20 mBar for 5 days). Then, either GDNF (40 ng/ collagen conduit) or GDNF in combination with NGF (40 ng GDNF +

40 ng NGF /collagen conduit) were loaded into the collagen nerve conduit. Then, the conduits were coated, using an ultrasonic spray nozzle, with polylactic-co-glycolic acid (PLGA, 50:50) to prevent diffusion of the growth factors [224].

ELISA analysis showed that non-crosslinked collagen conduits released high amounts of GDNF and NGF during the first three days: for GDNF, 9 ng/mL on day 1, 5 ng/mL on day 2 and 3 ng/mL on day 3; for when NGF and GDNF were co-immobilised: 4.5 ng/mL (GDNF) and 6.5 ng/mL (NGF) on day 1, 2.5 ng/mL and 4 ng/mL on day 2, and 2 ng/mL on day 3. In contrast, crosslinked collagen tubes did not exhibit a burst release: for GDNF, 1 ng/mL on day 1, 3 ng/mL on day 2 and 3 ng/mL on day 3; for when NGF and GDNF were co-immobilised: ca. 1 ng/mL on day 1, 1.5 ng/mL (GDNF) and 2 ng/mL (NGF) on day 2 and 3. Additionally, within 30 days, non-crosslinked collagen tubes released 83% and 78% of the initial load of NGF and GDNF respectively, whereas crosslinked collagen conduits released 56% of NGF and 68% of GDNF [224].

It was expected that the DHT treatment would decrease the growth factors release, as it crosslinks the collagen chains through the interactions of the carboxylic and amino functional groups of the collagen chains [224]. Physical crosslinking, specifically DHT treatment, avoids the use of cytotoxic reagents, which would impact cellular activity. However, DTH treatment also affects the mechanical properties of the material, for example, it denatures collagen, making the scaffold stiffer [259]. DHT as a technique to entrap growth factors may work, however, the success of this technique is dependent on the material, as this must have carboxyl and amino functional groups, so the crosslinking can take place. Moreover, the final application needs to be considered when using the DHT technique, as it changes the mechanical properties and the degradation rate of the material.

Other studies have also used crosslinking to entrap growth factors. Lee et al. designed an NGF delivery system, which consisted mainly of fibrin glue, to encourage nerve regeneration after dental injuries [260]. Firstly, a heparin conjugated fibrin gel was fabricated with heparin, fibrinogen, aprotinin, calcium chloride and thrombin. Then, 250 ng of NGF were added to the heparin-fibrin gel. The release profile of NGF from

this delivery system was measured by ELISA and samples were collected at 1, 3, 5, 7, 10 and 14 days [260]. By day 3, 0.46 ng/mL of NGF was released from the fibrin glue; and by day 5, 1 ng/mL was released. After day 5, the release of NGF was decreased until day 10, where all NGF was released [260]. Within 10 days, 250 ng of NGF were released from the fibrin glue, assuming that this initial load remained in the fibrin gel, as no test was performed to quantify the amount of NGF present in the glue. This delivery system was designed using the hypothesis that thrombin would reinforce the crosslinking of fibrin, hence decreasing the diffusion rate of NGF. Nevertheless, the targeted release rate was not achieved. In comparison, the work presented in this thesis showed that less than 6% of the immobilised NGF and was released after 7 days.

Neither photochemical nor physicochemical crosslinking techniques are suitable for the immobilisation and release of growth factors. Other studies have presented different approaches to accomplish immobilisation of growth factors. For example, Fine et al. added NGF and GDNF to ethylene-vinyl acetate (EVA) extruded conduits. Either 10 mg of NGF or GDNF, dissolved in 7.6 mL of water, were added to an EVA (in methylene chloride) and BSA solution. The solutions were mixed and sonicated to form an emulsion. Then, this polymer was frozen in liquid nitrogen and lyophilised for 48 hours. After the polymer was extruded to produce a conduit, it was left to dry under vacuum to remove all remaining solvent [61]. No quantification of growth factors was performed, however, the *in vitro* results showed that 1.817 mm (NGF) / 1.125 mm (GDNF) of neurite outgrowth, after 6 days, can be achieved using this delivery system with NGF. Furthermore, they concluded that the lack of success in previous studies regarding nerve outgrowth using growth factors were due to an inappropriate neurotrophic factor delivery system [61]. As this may be a good example for the delivery of growth factors, their lack of evidence of how much growth factor was retained in the EVA conduits after extrusion and how these growth factors were released from the delivery system does not support their statement that the lack of success in nerve outgrowth were due to an inappropriate delivery system of growth factors, as they did not characterise its delivery profile. Moreover, the high amount of NGF and GDNF (10 mg) represents a large investment that makes its manufacture more challenging to implement this delivery system to the clinic.

Additionally, Dinis et al. functionalised silk electrospun conduits with NGF and ciliary neurotrophic factor (CNTF). Silk solution was mixed with polyethylene oxide (PEO); then NGF and CNTF were reconstituted in PBS and added to the silk solution to obtain a functionalised spinning solution. NGF was added to the silk solution at a concentration of 100 ng/mL with or without CNTF at a concentration of 10 ng/mL. For the growth factor release study, functionalised silk conduits were incubated in sterile PBS at 37°C. Samples were collected after 1, 6, 24, 72, 168 (CNTF) and 240 hours (NGF) and stored at -80°C for later ELISA analysis. NGF released from the silk electrospun conduits was detected after 1 hour, at a concentration of 0.2 ng/mL. For 240 hours, NGF release was 0.4 ng/mL. CNTF released from the silk electrospun conduits was detected after 6 hours at a concentration of 0.2 ng/mL. At 24 hours and 168 hours, the release of CNTF was 0.5 ng/mL and 1.1 ng/mL, respectively [225]. Dinis et al. reported that 1% and 12% of NGF and CNTF respectively were released from the silk electrospun conduits [225]. However, they calculated this by assuming that all the original NGF (100 ng/mL) and CNTF (10 ng/mL) added to the silk solution remained after the electrospinning process. An ELISA determining the NGF and CNTF present at the silk electrospun conduit would support this assumption. Nevertheless, the low release of the growth factors from the silk electrospun conduit can be explained by the size and charge of NGF and CNTF, as their molecular weight are 27 kDa and 23 kDa, respectively; and at physiological pH both growth factors are charged positively. Both molecular weight and charge could hinder their diffusion from the silk electrospun conduit [225], [261]. This would explain why the release rate of both growth factors is different when compared to each other, as their molecular weight is different.

Furthermore, Hu et al. fabricated a polycaprolactone (PCL) electrospun nanofibrous scaffold by emulsion electrospinning, where PCL formed the shell and NGF and BSA were encapsulated in the core [226]. The emulsion electrospinning process used two phases, an inner water phase, which contained NGF and/or BSA; and the organic phase that comprised a PCL solution in chloroform with an emulsifying agent. Either alone or in combination, 8 µg of NGF and 8 mg of BSA were dissolved in 250 µL of distilled water. Then, this solution was added to the PCL solution. Afterwards, the emulsions

were mixed for 2 hours and used immediately for electrospinning [226]. ELISA analysis revealed that 60 pg of NGF were released from the PCL electrospun nanofiber scaffold (with no BSA) on the first day. After one day, NGF was no longer detected, suggesting that the growth factor was denatured or lost immunoreactivity during the preparation of the emulsion solution or during the electrospinning process. When NGF was encapsulated with BSA in the PCL solution, NGF was protected by BSA, therefore the NGF released from the scaffold was 0.81 ng within the first hour. After the initial burst release, by day 5, the NGF release was 1.5 ng. Then, NGF concentration was sustained for over 15 days. By day 28, NGF was not detectable by ELISA. Hu et al. suggested that the duration of NGF release could be related to a low initial NGF load concentration, which was 8 µg or 32 µg/mL [226]. However, they did not test the quantity of NGF in the emulsion or the quantity present in the PCL electrospun nanofiber scaffolds. Moreover, it has to be considered that another reason that NGF was not fully incorporated into the scaffold was that the emulsion was stirred for 2 hours, meaning that NGF was mechanically disturbed and in contact with an organic solvent, which could denature the protein [228]. In addition, by incorporating more NGF in the initial load concentration, the cost of manufacture would increase[165]. Furthermore, it is important to consider that a high concentration of growth factors may elicit an apoptotic signal instead of a survival signal [226].

Another approach should be considered to incorporate growth factors to a delivery system in order to avoid denaturation and loss of activity. Naka et la. coated nanoscale magnetic beads with NGF or BDNF to regulate survival and differentiation of neurons. NGF or BDNF solution at a concentration of 10 µg/mL was mixed with glutaraldehyde-activated nanoscale magnetic beads for 30 seconds in a bath sonicator. Then, this solution was incubated for 2 hours at room temperature. Afterwards, the growth factor-coated nanoscale magnetic beads were washed three times with PBS [262]. ELISA detected the binding of the growth factors to the nanoscale magnetic beads, revealing that more NGF was bound to the magnetic beads than BDNF, although no explanation or possible mechanism was given for this [262]. Interestingly, glutaraldehyde has been used as a crosslinking agent to bind proteins, as it forms covalent bonds with amine, thiols, phenols, and hydroxyl functional groups.

Nevertheless, the by-products of glutaraldehyde are toxic and elicit a negative effect in cells and tissue [263]. If these magnetic beads were to be implanted into a living system, it would cause adverse effects. Thus, reminding us that when designing a delivery system, the reagents or other chemicals used should not provoke any toxic effects in the long term.

In yet another different approach, Matsumoto et al. coated NGF or BDNF in carbon nanotubes using EDC reagent. Firstly, the carbon nanotubes were activated by adding amino groups. NGF or BDNF were mixed with EDC reagent at a concentration of 10 µg/mL and 100 µg/mL respectively, and then incubated with the carbon nanotubes for 2 hours at room temperature. Afterwards, sodium acetate solution was added to terminate the reaction. As a result, NGF/BDNF were covalently bound to the carbon nanotubes. ELISA confirmed that NGF and BDNF were immobilised on the carbon nanotubes. However, no quantification was done for the growth factors on the surface and neither for their release from the carbon nanotubes [264]. In addition, it is important to highlight that even though the growth factors were covalently immobilised, the initial load is too high, which leads to the question of what would be their biological effects.

Furthermore, Puleo et al. immobilised bone morphogenetic protein-4 (BMP-4) on titanium alloy by allylamine plasma deposition. After titanium alloy samples were all plasma treated to deposit amine groups on the surface, lysozyme (used as a model to study the effects of immobilisation) was immobilised following 3 different protocols [222]. For the adsorption protocol, amine-titanium alloy samples were incubated for 2 hours at room temperature with a lysozyme solution (5 mg/mL). For the one-step protocol the amine-titanium alloy sample was incubated with lysozyme solution, EDAC, NHS and 2-(N-morpholino)ethanesulfonic acid (MES) buffer. For the two-step protocol, amine groups from the amine-titanium alloy samples were converted to carboxyl groups by overnight incubation with succinic anhydride at room temperature. Then, samples were treated with EDAC and NHS solution in MES buffer for 2 hours at room temperature. After washing, samples were incubated with lysozyme solution for 2 hours [222]. For the adsorption protocol, no results were reported. For the one-step protocol, BCA (bicinchoninic acid) assay showed that lysozyme-amine-titanium

alloy samples retained 27% of lysozyme, where untreated titanium alloy samples retained 0 µg. In contrast, for the two-step protocol, 60% of lysozyme was immobilised on the amine-titanium alloy sample. One-step protocol retained a lower quantity of lysozyme in the surface in comparison to the two-step protocol. The main reason was, as the EDAC solution was mixed with the lysozyme solution in the same step, it crosslinked the protein, inactivating it or preventing access to its active site [222]. If this was the case, the bioactivity of the lysozyme might be reduced, not accomplishing any stimuli to the cells. Moreover, as the two-step protocol firstly incubated the EDAC solution and then incubated the lysozyme solution, crosslinking was avoided, and bioactivity might be achieved. Nevertheless, the EDAC solution may have left some by-products, causing further cytotoxicity. Neither of these issues were tested.

Additionally, Kim et al., immobilised basic fibroblast growth factor (bFGF) and/or NGF on PCL/Pluronic F127 microspheres using heparin. The quantity of growth factor immobilised on the microspheres and their release was assessed by ELISA. PCL/Pluronic F127 microspheres were incubated in heparin solution (1 mg/mL) for 3 hours at 4°C. Then, the heparin-PCL/Pluronic F127 microspheres were washed with water and incubated in an NGF or bFGF solution (200 ng/mL, in PBS) for 5 hours at room temperature. Afterwards, the growth factor-immobilised microspheres were washed three times with PBS [265]. By ELISA, the amount of growth factor immobilised on the microspheres was determined. NGF was immobilised at a concentration of 3.87 ng/ mg of microsphere, whereas bFGF was immobilised at 4.74 ng/mg. Moreover, growth factor immobilisation was assessed on microspheres with no heparin, revealing that the concentration at which NGF and bFGF were immobilised was 1.63 ng/mg and 1.89 ng/mg respectively. These findings suggested that heparin allowed a larger growth factor immobilisation. In addition, the release of NGF and bFGF from heparin-PCL/Pluronic F127 microspheres was 94% and 84% (of total loading amount) respectively within 28 days [265]. Moreover, the release of NGF after 10 days was 2.5 ng/mg, which corresponds to 65% of the initial immobilised NGF. In contrast, the release of NGF and bFGF from PCL/Pluronic F127 microspheres (no heparin) was 93% and 88%, respectively, after 7 days [265].

Heparin was immobilised by hydrogen bonding to PEG, present in Pluronic F127 [265]. These findings support the use of heparin as means to bind growth factors, because without heparin, the amount of growth factors present in the system would be smaller. Furthermore, NGF and bFGF were immobilised by the same technique, in the same conditions, but their final concentration on the microspheres was different. One explanation to this could be the molecular weight and charge of the growth factors, as suggested by Dinis et al. and Uebersax et al. [225], [261].

More research has been carried out using heparin to bind growth factors. Yang et al., immobilised human bone morphogenetic protein-2 (hBMP-2) and/or human growth and differentiation factor-5 (hGDF-5) on titanium discs using heparin [169]. Titanium discs were incubated and stirred in a sodium hydroxide (NaOH) solution for 48 hours at 80°C. This step was to add carboxyl (-COOH) groups to the titanium discs. Then, the discs were washed in distilled water and dried with nitrogen gas. Titanium-COOH discs were activated with 4-(4,6-Dimethoxy-1,3,5-triazin-2-yl)-4-methylmorpholinium chloride (DMT-MM) for one hour at room temperature. Afterwards, activated titanium-COOH discs were incubated with heparin solution for three days at room temperature. The hep-titanium discs were washed with distilled water and dried with nitrogen gas. Then, hBMP-2 (50 ng), heparin (10 mg) and hGDF-5 (50 ng) were incubated with the hep-titanium discs in 40 mL of PBS for 24 hours at 4°C. Then, the discs were washed with distilled water and dried with nitrogen gas [169]. The contact angle was decreased after the modifications, indicating that the growth factors were bound to the surface. The contact angle of titanium discs, hBMP-2-titanium, hGDF-5-titanium, and hBMP-2/hGDF-5-titanium, was 76 °, 58 °, 56 ° and 56° respectively. ELISA showed that the amount of growth factor retained after the fabrication process in the hBMP-2-titanium, hGDF-5-titanium, and hBMP-2/hGDF-5-titanium discs was 76%, 73% and 75% / 73% respectively. Moreover, the initial burst release (day one) of growth factors from hBMP-2-titanium, hGDF-5-titanium, and hBMP-2/hGDF-5-titanium discs was 12.5%, 4.5% and 13.5% / 3.2% respectively from their initial load. However, after the first day, a sustained released was observed, where the cumulated release was 50.5%, 47.8% and 45.2% / 36.4% respectively [169].

DMT-MM was needed to effectively bind heparin, as carboxyl functional groups would not bind the required heparin as reported by Kang et al. [256].

Furthermore, Gigliobianco et al. bound vascular endothelial growth factor (VEGF) to the surface of a scaffold fabricated from alternate layers of polyethyleneimine (PEI, positively charged) and heparin or PEI and polyacrylic acid coated on plasma polymerised poly-L-lactic acid (PLLA). Electrospun PLLA scaffolds were plasma polymerised with polyacrylic acid to add negatively charged carboxyl functional groups [266] onto the surface of PLLA [267]. Then, two different coatings were prepared using layer-by-layer techniques. The first coating consisted of PEI and heparin: the plasma treated PLLA scaffold was incubated in PEI solution for 30 minutes at room temperature. Then, the scaffolds were washed with deionised water and incubated in heparin solution for 30 minutes at room temperature. These steps were repeated 7 times and the last layer was always PEI [267]. The second coating consisted of PEI and polyacrylic acid: the plasma treated PLLA scaffold was incubated in PEI solution for 30 minutes at room temperature. Afterwards, the scaffold was incubated with polyacrylic acid solution for 30 minutes at room temperature. Then, the scaffold was washed with deionised water. These steps were also repeated 7 times, with being PEI the last layer. After the layer-by-layer coatings, the scaffolds were incubated with heparin solution overnight. Then, the scaffolds were incubated with a VEGF solution at a concentration of 2 ng/mL for 24 hours [267].

XPS spectra were used to evaluate sulphur content in the scaffold, as an indicator that heparin was bound to the scaffold. Moreover, ELISA was performed to study the binding of VEGF to the scaffolds, but not its release profile. XPS results showed that heparin was bound to the PEI-heparin scaffolds, with 0.53% sulphur content. In contrast, for the PEI-polyacrylic acid scaffolds, the sulphur content was 4.6%. This was attributed to the fact the PEI-polyacrylic acid scaffolds built the necessary charge to bind heparin, whereas PEI-heparin scaffolds did not [267]. However, another positively charged molecule could be used for coating and, possibly, obtain the same result as the PEI-polyacrylic scaffold. ELISA showed that VEGF was bound to PEI-polyacrylic acid scaffold, as 950 pg/cm^2 of VEGF was quantified. Unfortunately, VEGF content was not assessed in the PEI-heparin scaffolds, due to its low heparin

content. Nevertheless, it would be interesting to study the quantity of VEGF bound to this scaffold to see if a certain quantity of heparin is needed to bind more growth factor [267]. However, it is necessary to consider that acrylic acid is less biocompatible than heparin [267]. These findings showed that it is possible to bind heparin by electrostatic means to a positively charged surface, supporting the answer to one of the research questions of this thesis: that heparin will bind to a positively charged functional group NH_2^+, and that growth factors will bind to heparin. Moreover, these scaffolds coated using layer-by-layer technique needed at least 5 layers to successfully bind heparin to the scaffold [267]. The work presented in this thesis, only required an NH_2^+ surface to successfully bind heparin, and therefore, NGF and BDNF were able to bind to the surface through heparin.

It has been reported that the charge of the protein has an effect on its binding affinity to a charged molecule. In addition, the surface should have enough charge to bind molecules effectively. For example, Satriano et al. studied that at physiological pH 7.4, the isoelectric point of NGF is ca. 9, whereas the isoelectric point of BDNF is ca. 8. The evaluated gold surface is negatively charged at pH 7.4, hence, an attractive interaction, caused by electrostatic forces, can be deduced with both NGF and BDNF, as they both have positive charges at physiological pH [268]. Nevertheless, these isoelectric points change according to the origin and sequence of the protein that is used. Liu et al. reported that the isoelectric point of human BDNF was 9.1 [269]. Moreover, Harper et al. showed that the isoelectric point of bovine NGF and mouse NGF was of 9.5-10 and 9.3 respectively [270]. Therefore, it was important to corroborate the growth factor's data provided by the manufacturer to adequately report and explain the findings in this thesis.

According to the manufacturer, the isoelectric point of NGF was 8.81 (accession No. P25427), its molecular weight was 26.4 kDa and its sequence Ser122-Gly241 [136], [271]. In addition, the isoelectric point of BDNF was 9.59 (accession No. P23560), its molecular weight was 13.5 kDa and its sequence His129-Arg247 [136], [272]. Furthermore, arginine and lysine amino acids provide the positive charge of NGF and BDNF at physiological pH. The arginine and lysine content of NGF and BDNF are 14/18 and 11/11 respectively. According to Mascotti and Lohman, arginine has a

slightly higher affinity compared to lysine when they bind to the sulphate groups in heparin through hydrogen bonding [273]. In addition, another factor to consider is the degradation of both NGF and BDNF in PBS [269], [274], [275]. As these growth factors were incubated in PBS with the bioactive surface for 5 hours, it is expected that to a certain extent, the growth factors degraded.

Additionally, as can be seen in section 5.4.3.1, NGF was retained more on the bioactive surface than BDNF. The reason could be the isoelectric point of the molecules, hydrogen bonding between the growth factors and heparin, degradation of BDNF in PBS during incubation time, and the interactions dictated by the three-dimensional (3D) structure of the growth factors [276], as the availability of binding sites in the growth factors to create hydrogen bonds with heparin would change [228]. Therefore, even though BDNF has a higher isoelectric point compared to NGF, BDNF has a lower arginine and lysine content than NGF, which would explain why 97% - 99% of the initial load of NGF was retained on the bioactive surface, whereas the bioactive surface retained 85% - 91% of the initial load of BDNF.

Moreover, temperature and 3D structure of the neurotrophins would also explain the differences in release of NGF and BDNF from the bioactive surface. NGF and BDNF were immobilised on the bioactive surface at concentrations of 1 ng/mL, 10 ng/mL, 100 ng/mL and 1 µg/mL. These bioactive surfaces were incubated at 37°C and 4°C. The release of neurotrophins was different between these test conditions. This might be explained by the 3D structure of the neurotrophins and the concentration at which they were immobilised. If the concentration was low, the neurotrophin would bind to heparin without competing with another molecule for that same binding site and, even finding more binding sites, making the bond between the growth factor and the bioactive surface more stable [277]–[279]. However, if the concentration was higher, neurotrophins would compete with each other for heparin binding sites, making the bonding between the growth factor and heparin not as stable as it could be, with a possibility of creating aggregates. This hypothesis could explain to a certain extent why at higher concentrations of immobilised NGF or BDNF, the release was greater than in other conditions.

The maximum concentration at which NGF was released from the bioactive surface was 0.1 ng/mL, both at 37°C and 4°C. However, the timing at which this concentration was found was different (24 hours and 168 hours respectively). In comparison, the maximum concentration at which BDNF was released from the bioactive surface was 14 ng/mL at 37°C and 1.4 ng/mL at 4°C.

Based on the results on this thesis, regarding release of NGF and BDNF from bioactive surfaces, it is suggested that the bioactive surface acts as a stabiliser for both neurotrophins, and temperature may act as an on/off switch to break the bonds between heparin and the growth factors. Eng et al. evaluated the degradation of NGF in acetate buffer (pH 5.5) at 5°C and 37°C, finding that degradation was faster at 37°C than at 5°C [280]. They also elucidated that chemical stability decreased, as aggregation was found at 37°C, leading to degradation [280], [281]. This raises the question to whether growth factors would be stable at physiological pH. Nevertheless, according to Lam et al., and DeYoung et al., NGF can degrade rapidly at physiological pH if the neurotrophin is not stabilised [281], [282]. Furthermore, when NGF was in solution with PBS (with no stabiliser), its stability was reduced by at least 50%. Nevertheless, when NGF was in solution with PBS and Tween 20, its stability was maintained between 80% – 60% [73]. In addition, Polyakova et al. studied the stability of BDNF in solution with serum and ethylenediaminetetraacetic acid (EDTA)-plasma when stored at -80 °C and at room temperature [283]. Their findings suggested that BDNF was stable up to 6 months when stored at -80°C when it was in solution with both serum and EDTA-plasma. It also highlighted that BDNF was stable for up to 2 hours at room temperature, also in both serum and EDTA-plasma [283]. Furthermore, Callahan et al. also evaluated the stability of BDNF when in solution with histidine buffer with and without sodium chloride (NaCl), finding that BDNF maintained stability at 52°C when it was in solution with NaCl [284].

The stability of NGF and BDNF bound onto the bioactive surface NH_2^+ + Heparin has the potential of controlling the release of these neurotrophins, delivering an adequate dosage, at an appropriate time, which would encourage extensive neurite outgrowth. Which concentration of immobilised neurotrophin would be the most appropriate to achieve this will be evaluated in the following chapters.

5.6 Conclusion

The aim of this chapter was to fabricate and characterise a NH_2^+ + Heparin + Immobilised NGF/BDNF bioactive surface. This bioactive surface was fabricated by the adsorption of heparin onto a NH_2^+ surface by electrostatic interactions. NGF and BDNF were then added to the NH_2^+ + Heparin surface. These neurotrophins bond to heparin by electrostatic interactions.

Contact angle confirmed a change in wettability when heparin was added. Moreover, XPS analysis confirmed the presence of heparin on the NH_2^+ + Heparin bioactive surface. Furthermore, NGF and BDNF were successfully immobilised, at different concentrations, onto the NH_2^+ + Heparin bioactive surface. ELISA confirmed the presence and the release of the neurotrophins from the bioactive surface. Even though the NH_2^+ + Heparin + Immobilised NGF/BDNF were incubated at 4℃ and 37℃, revealing different release profiles for NGF and BDNF, ELISA still indicated the presence of the neurotrophins on the bioactive surfaces. Furthermore, it will be interesting to understand which concentration of neurotrophin would encourage the growth of larger neurites. This will be described and discussed in the next chapter.

In conclusion, the bioactive surface NH_2^+ + Heparin + Immobilised NGF/BDNF was successfully fabricated.

Chapter 6 Effects of bioactive surface on immortalised cell lines: NG108-15 neuronal cell line and PC12 adh neuronal cell line

6.1 Introduction

The effects of neurotrophins on neurite outgrowth and development are being studied in research, to evaluate their potential for improving nerve regeneration [77], [84]. Nerve growth factor (NGF), brain derived neurotrophic factor (BDNF), glial cell-derived neurotrophic factor (GDNF) and ciliary neurotrophic factor (CNTF) have been used for this purpose [61], [225], [285]–[287].

Even though neurotrophins have been introduced into nerve guide conduits (NGCs), nerve repair has not been successful, because of their short half-life, proteolytic degradation, and lack of diffusion [288]–[291]. Therefore, it is paramount to design a sustained delivery system for neurotrophins to enhance NGCs functionality [227], [229].

The development of bioactive surfaces, such as the one fabricated in chapter 5 of this thesis NH_2^+ + Heparin + Immobilised NGF, BDNF or NGF plus BDNF, will deliver neurotrophins more precisely, encouraging neurite outgrowth. The advantages of immobilising growth factors are that their half-life can be extended and that their bioactivity will not be lost [292]. Moreover, as the growth factor is immobilised, it will not be internalised by the cell, sustaining signaling for longer periods thus increasing their half-life [217], [292], [293]. Physical adsorption, crosslinking, covalent bonding, and entrapment are techniques used to immobilise neurotrophins [150].

Research has been performed to study the effects of immobilised growth factors. For example, Lee et al. loaded 250 ng and 500 ng of NGF into a heparin-fibrin gel. This delivery system encouraged neurite outgrowth of 40 μm in PC12 neuronal cells [260]. Furthermore, Oh et al. micropatterned 1 mg/mL of NGF in collagen sponges, and

found that 27.2% of PC12 neuronal cells developed neurites [294]. Bhang et al. immobilised NGF on a heparin surface, discovering that PC12 neuronal cells developed more neurites when NGF was immobilised than when it was in solution in culture media [292].

Additionally, growth factors have been co-immobilised to obtain an additive effect. Lequoy et al. co-immobilised epidermal growth factor (EGF) and vascular endothelial growth factor (VEGF) on a chondroitin sulfate coating [295]. The results obtained by Lequoy et al. showed that cell survival was improved compared to when each growth factor was immobilised alone [295]. Moreover, Kim et al. co-immobilised NGF and basic fibroblast growth factor (bFGF) on polycaprolactone/pluronic F127 microspheres and studied their effects on muscle derived stem cells [265]. Their findings showed that microspheres with both NGF and bFGF stimulated the development of more neurites in comparison to when the microspheres were immobilised with only one growth factor [265]. Furthermore, Naka et al. coated nanoscale magnetic beads with 10 µg/mL of NGF, BDNF, or NGF and BDNF and evaluated neurite outgrowth in PC12 neuronal cells [262]. Neurite extension was only found in cells cultured with NGF coated beads [262]. Nevertheless, BDNF has been known to also promote neurite growth [84].

Although the use of neurotrophins has been studied, there are no studies that define which is the optimal dose of neurotrophin to use and how frequently the neurotrophin should be administered [217]. For example, inappropriate target reinnervation and defective connections might result as a consequence of using high quantities of NGF [217], [296]. Moreover, Achyuta et al. suggested that there are a minimum number of TrkA receptors that must bind to NGF to initiate neurite outgrowth stimulation [229]. The appropriate dose and frequency of administration might be related to how the growth factors are being delivered. For example, the degradation of the material, or the degradation of the bond formed with a substrate or other molecule to which the growth factor was immobilised.

Therefore, in this chapter, an evaluation was performed regarding what would be the appropriate dose of immobilised NGF, BDNF, or NGF plus BDNF (1 pg/mL, 1 ng/mL, 10 ng/mL, 100 ng/mL and 1 µg/mL) to encourage the formation of longer neurites, in NG108-15 neuronal cells and in PC12 adh neuronal cells (an adherent variant of the PC12 cell line). Moreover, the bioactive surfaces NH_2^+ + Heparin + Immobilised NGF, NH_2^+ + Heparin + Immobilised BDNF, and NH_2^+ + Heparin + Immobilised NGF plus BDNF were assessed to evaluate how the bioactive surface affected the metabolic activity of the NG108-15 neuronal cell line and PC12 adh neuronal cell line.

6.2 Aims and objectives

The bioactive surfaces NH_2^+ + Heparin + Immobilised NGF, NH_2^+ + Heparin + Immobilised BDNF, and NH_2^+ + Heparin + Immobilised NGF plus BDNF were prepared on flat surface tissue culture plastic (TCP).

The aims of this chapter are:

1. Evaluate the effects of bioactive surface immobilised with NGF on NG108-15 neuronal cells.
2. Study the effects of bioactive surface immobilised with BDNF on NG108-15 neuronal cells.
3. Evaluate the effects of bioactive surface immobilised with NGF plus BDNF on NG108-15 neuronal cells.
4. Evaluate the effects of bioactive surface immobilised with NGF on PC12 adh neuronal cells.
5. Study the effects of bioactive surface immobilised with BDNF on PC12 adh neuronal cells.
6. Evaluate the effects of bioactive surface immobilised with NGF plus BDNF on PC12 adh neuronal cells.

The objectives of this chapter are:

1. Assess the metabolic activity of NG108-15 neuronal cells when cultured on bioactive surfaces immobilised with NGF, BDNF or NGF plus BDNF.
2. Calculate the average neurite length of NG108-15 neuronal cells when cultured on bioactive surfaces immobilised with NGF, BDNF or NGF plus BDNF.
3. Obtain the average maximum neurite length of NG108-15 neuronal cells when cultured on bioactive surfaces immobilised with NGF, BDNF or NGF plus BDNF.

4. Quantify the percentage of neurons bearing neurites of NG108-15 neuronal cells when cultured on bioactive surfaces immobilised with NGF, BDNF or NGF plus BDNF.

5. Assess the metabolic activity of PC12 adh cells when cultured on bioactive surfaces immobilised with NGF, BDNF or NGF plus BDNF.

6. Quantify the average neurite length of PC12 adh cells when cultured on bioactive surfaces immobilised with NGF, BDNF or NGF plus BDNF.

7. Obtain the average maximum neurite length of PC12 adh cells when cultured on bioactive surfaces immobilised with NGF, BDNF or NGF plus BDNF.

8. Calculate the percentage of neurons bearing neurites of PC12 adh cells when cultured on bioactive surfaces immobilised with NGF, BDNF or NGF plus BDNF.

6.3 Materials and methods

General cell culture methodology was performed as described in Chapter 4, in sections 4.2.1, 4.2.1.1, 4.2.1.2 and 4.2.1.3. Bioactive surfaces were prepared as described in chapter 5, section 5.3.1.

6.3.1 *In vitro* studies with NG108-15 neuronal cell lines

An NG108-15 neuronal cell line was seeded on TCP, NH_2^+, NH_2^+ + Heparin, and NH_2^+ + Heparin with immobilised NGF, BDNF or NGF plus BDNF surfaces *in vitro* to evaluate the effects of these bioactive surfaces on metabolic activity, neural length, maximum neurite length, and percentage of neurons bearing neurites. Detailed protocol was performed as described in chapter 4, section 4.2.2. Briefly, NG108-15 cell line cells were retrieved from a T-75 flask. Then, 500 cells were seeded per well in 150 µL of cell culture medium. The samples were incubated at 37°C and 5% CO_2 for 7 days, where the medium was changed to serum free medium with NGF, BDNF or NGF plus BDNF, according to Table 12, on day 2. For the bioactive surfaces with immobilised NGF, BDNF or NGF plus BDNF, serum-free medium with no growth factors was used. The experiment was performed 3 times independently; each condition was tested in triplicate.

6.3.2 *In vitro* studies with PC12 adherent neuronal cell line

A PC12 adherent (adh) neuronal cell line was seeded on TCP, NH_2^+, NH_2^+ + Heparin, and NH_2^+ + Heparin with immobilised NGF, BDNF or NGF plus BDNF surfaces *in vitro* to evaluate the effects of these bioactive surfaces on metabolic activity, neural length, maximum neurite length, and percentage of neurons bearing neurites. Detailed protocol was performed as described in chapter 4, section 4.2.3. Briefly, PC12 adh cell line cells were retrieved from a T-75 flask. Then, 700 cells were seeded per well in 150 µL of cell culture medium with NGF, BDNF or NGF plus BDNF according to Table 12. The samples were incubated at 37°C and 5% CO_2 for 5 days. For the bioactive surfaces with immobilised NGF, BDNF or NGF plus BDNF, culture medium with no growth factors was used. The experiment was performed 3 times independently; each condition was tested in triplicate.

Table 12. Summary of the different surfaces and bioactive surfaces that were prepared, indicating the delivery method of NGF, BDNF or NGF plus BDNF.

Surface	**Growth factor delivery method**	**NGF**	**BDNF**	**NGF plus BDNF**
TCP	In solution with culture medium	0 pg/mL	0 pg/mL	0 pg/mL
		1 pg/mL	1 pg/mL	1 pg/mL
		1 ng/mL	1 ng/mL	1 ng/mL
		10 ng/mL	10 ng/mL	10 ng/mL
		100 ng/mL	100 ng/mL	100 ng/mL
		1 µg/mL	1 µg/mL	1 µg/mL
NH_2^+	In solution with culture medium	0 pg/mL	0 pg/mL	0 pg/mL
		1 pg/mL	1 pg/mL	1 pg/mL
		1 ng/mL	1 ng/mL	1 ng/mL
		10 ng/mL	10 ng/mL	10 ng/mL
		100 ng/mL	100 ng/mL	100 ng/mL
		1 µg/mL	1 µg/mL	1 µg/mL
NH_2^++Heparin	In solution with culture medium	0 pg/mL	0 pg/mL	0 pg/mL
		1 pg/mL	1 pg/mL	1 pg/mL
		1 ng/mL	1 ng/mL	1 ng/mL
		10 ng/mL	10 ng/mL	10 ng/mL
		100 ng/mL	100 ng/mL	100 ng/mL
		1 µg/mL	1 µg/mL	1 µg/mL
NH_2^++Heparin	Immobilised on surface	0 pg/mL	0 pg/mL	0 pg/mL
		1 pg/mL	1 pg/mL	1 pg/mL
		1 ng/mL	1 ng/mL	1 ng/mL
		10 ng/mL	10 ng/mL	10 ng/mL
		100 ng/mL	100 ng/mL	100 ng/mL
		1 µg/mL	1 µg/mL	1 µg/mL

6.3.3 Metabolic activity assay: MTS

Detailed protocol was performed as described in chapter 4, section 4.2.4. Briefly, after total incubation period of the samples, 20% of CellTiter 96® AQ_{ueous} One Solution Cell Proliferation Assay solution (v/v) was added directly to the samples and incubated at 37°C and 5% CO_2 for 4 hours covered from light. After incubation time, the absorbance was read at 490 nm using a Bio-Tek ELx 800 absorbance microplate reader and KC junior software 1.41.8 (Bio-Tek Instruments, USA).

6.3.4 Fixing and staining of neuronal cell line

Cell culture medium was discarded, and 3.7% formaldehyde (FA) solution was added and incubated for 45 minutes at room temperature. Then, FA was discarded, and samples washed one time with PBS. After, 0.1% Triton X-100 was added and incubated for 45 minutes at room temperature. Triton X-100 was discarded, and the samples washed 2 - 3 times with PBS. DAPI and phalloidin-TRITC solution were added to the samples and incubated for 1 hour at room temperature. The solution was discarded, and the samples washed one time with PBS. The samples were covered with PBS and stored at 4 °C. Details were described in Chapter 4, section 4.2.5.

6.3.5 Epifluorescence microscopy

Images of the cells cultured on the bioactive surfaces were obtained from an Inverted Olympus IX73 Epifluorescent microscope and Micro-Manager 1.4.22 software. To image DAPI and phalloidin-TRITC, excitation and emission wavelengths of λ_{ex} = 405 nm / λ_{em} = 450 nm and λ_{ex} = 540 nm / λ_{em} = 570 nm were used respectively. Image J 1.52a [218] software was used to measure the length of developed neurites and to count how many neurites were developed. Neurite length was measured from the cell body to the tip of the neurite. Cells with at least one neurite were counted as cells bearing neurites and Equation 1 from chapter 4, section 4.2.9, was used to calculate the percentage of neurons bearing neurites. Three images were taken per condition, and 10-15 neurites were measured to determine the mean. The largest neurite from each repeat was counted and averaged for the maximum neurite length.

6.3.6 Statistical analysis

Two-way ANOVA analysis was performed following the Tukey procedure of multiple comparisons using GraphPad Prism 8.2.0 software. A p value of < 0.05 was used to indicate if the differences in the data were significant.

6.4 Results

6.4.1 Effects of bioactive surfaces on NG108-15 neuronal cell line cultures

6.4.1.1 Effects of Nerve Growth Factor

Metabolic activity was studied for NG108-15 neuronal cells cultured on TCP, NH_2^+, NH_2^+ + Heparin, and NH_2^+ + Heparin + Immobilised NGF. This assay was performed to evaluate any changes in metabolic activity of NG108-15 neuronal cells cultured on bioactive surfaces in comparison to TCP control. It was important to study any significant changes in the metabolic activity of the neuronal cells, because, if the metabolic activity was reduced, it was important to determine the cause of it, whether it was the bioactive surface, the concentration of NGF used or a combination of both.

The metabolic activity of NG108-15 neuronal cells was not significantly different when cultured on TCP, NH_2^+, NH_2^+ + Heparin, and NH_2^+ + Heparin + Immobilised NGF as shown in Figure 35. The metabolic activity of the neuronal cells did not change when NGF was in solution or immobilised onto the bioactive surface. Moreover, the information presented in Figure 35 also suggested that the metabolic activity did not change due to the surface where the neuronal cells were cultured on. These results show that neither the concentration of NGF used nor the surface where the neuronal cells were seeded changed the metabolic activity of the cells. Therefore, the bioactive surface and NGF did not decrease the metabolic activity of the NG108-15 neuronal cells *in vitro*.

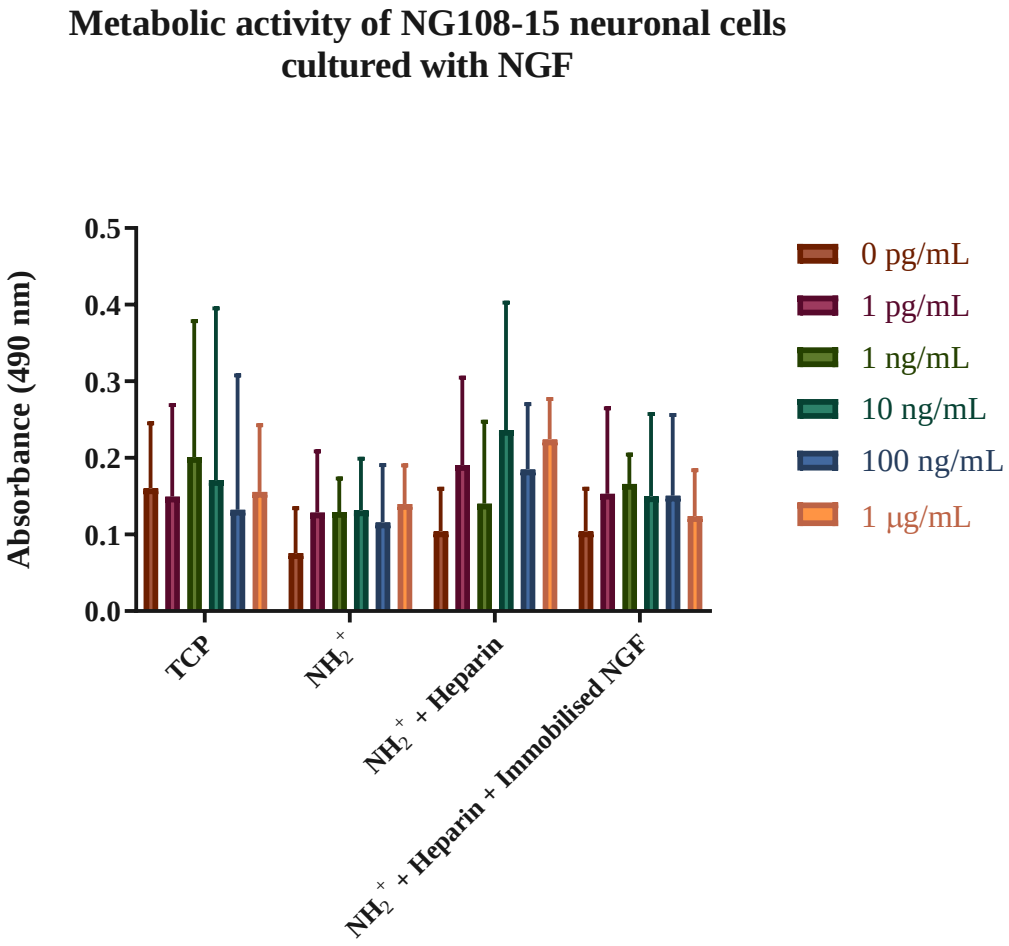

Figure 35. Metabolic activity of NG108-15 neuronal cells, measured with MTS assay at day 7, cultured onto different bioactive surfaces with NGF at different concentrations. NGF was present in culture medium in TCP, NH_2^+ and NH_2^+ + Heparin (controls). NGF was immobilised on NH_2^+ + Heparin (test). Two-way ANOVA statistical analysis was performed with Tukey procedure of multiple comparisons (*$p<0.05$). Mean ± SD. N=3, n=3.

Figure 36, Figure 37, Figure 38 and Figure 39 show NG108-15 neuronal cells cultured on different bioactive surfaces (TCP, NH_2^+, NH_2^+ + Heparin, and NH_2^+ + Heparin + Immobilised NGF respectively) at different concentrations of NGF. Developed neurites can be seen in all the images, with some highlighted with a yellow brace. DAPI was used to stain nuclei; phalloidin TRITC was used to stain the f-actin filaments of the cytoskeleton of the neurons, which includes the neurite. Regardless of the concentration used of NGF, either in solution in culture medium or immobilised, or the bioactive surface where the NG108-15 cells were seeded, neurites developed in all conditions, with no significant difference among them. These images are representative of average neurite length.

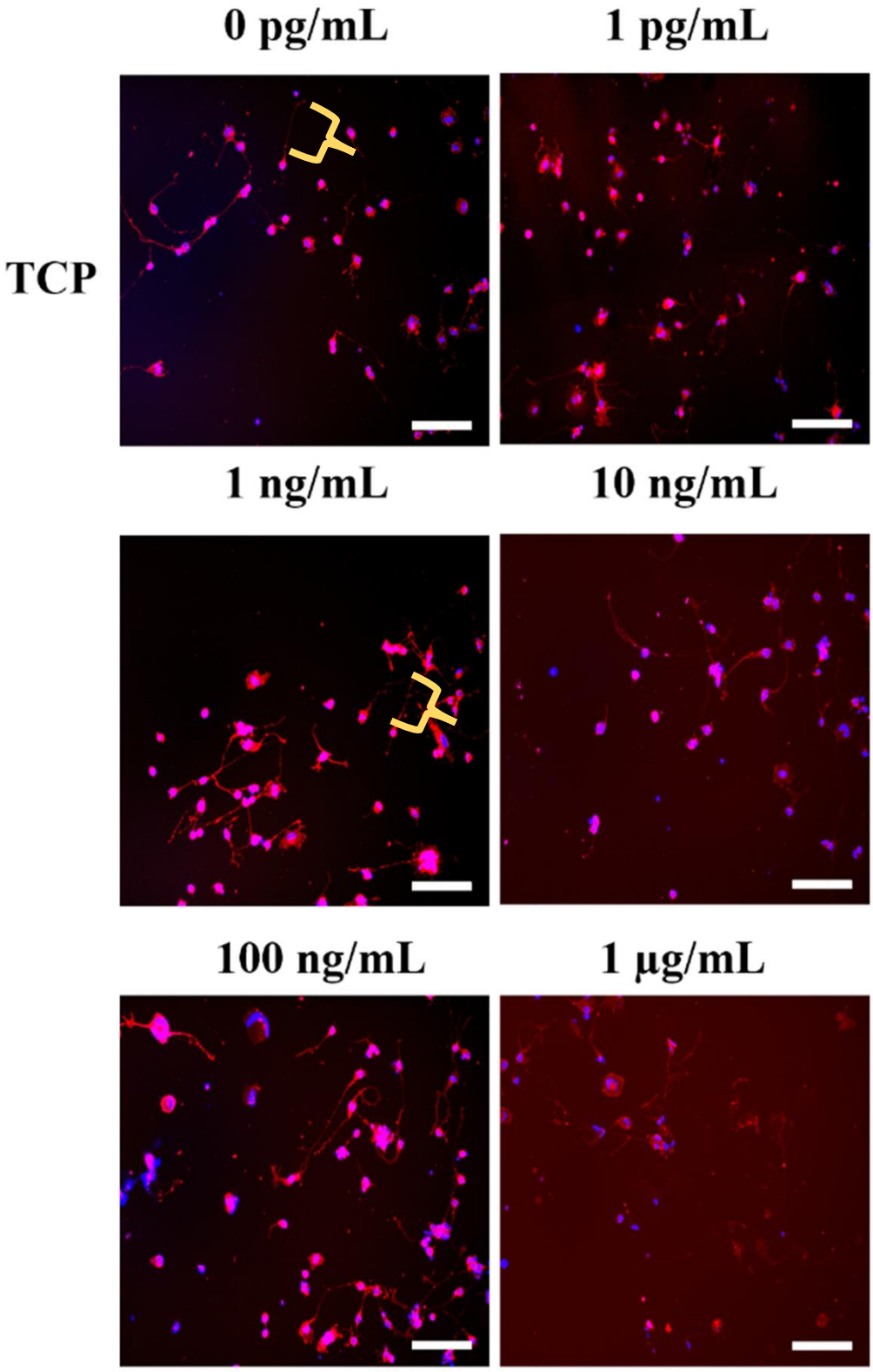

Figure 36. Epifluorescence images of NG108-15 neuronal cells cultured onto TCP with different concentrations of NGF. F-actin filaments are stained in red (phalloidin TRITC)., nuclei are stained in blue (DAPI). Scale bar = 200 µm.

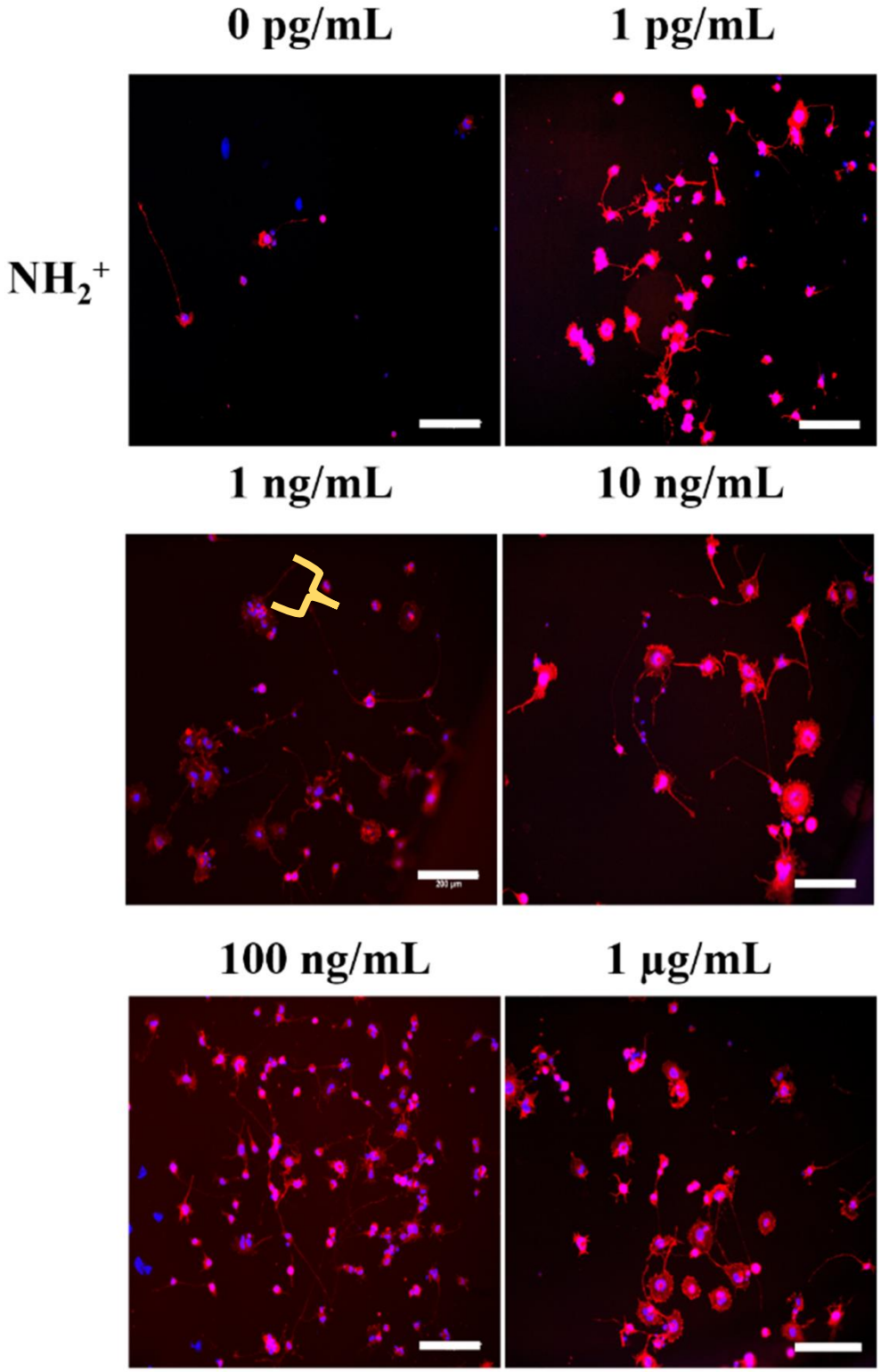

Figure 37. Epifluorescence images of NG108-15 neuronal cells cultured onto NH_2^+ with different concentrations of NGF. F-actin filaments are stained in red (phalloidin TRITC)., nuclei are stained in blue (DAPI). Scale bar = 200 µm.

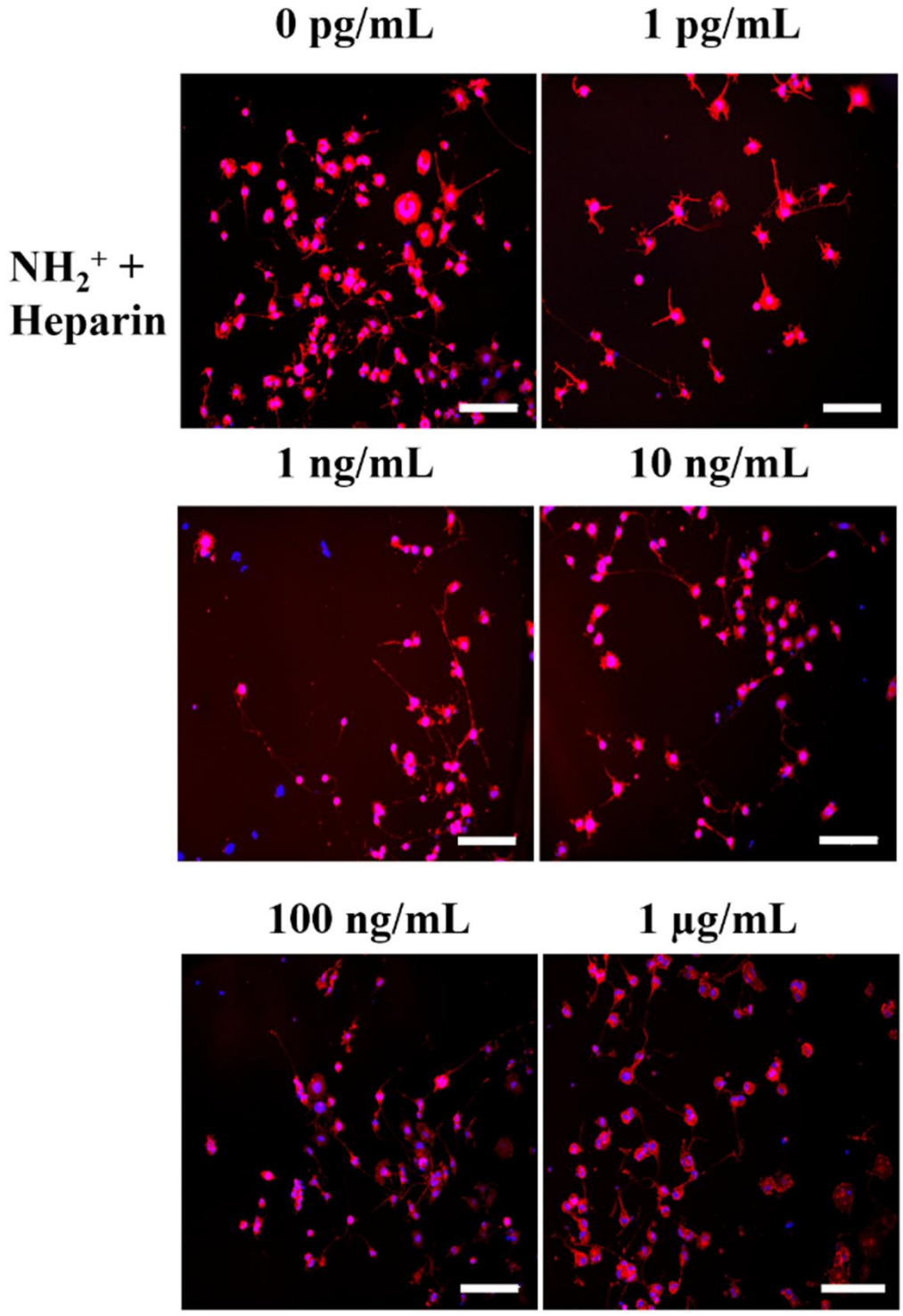

Figure 38. Epifluorescence images of NG108-15 neuronal cells cultured onto NH_2^+ + Heparin with different concentrations of NGF. F-actin filaments are stained in red (phalloidin TRITC)., nuclei are stained in blue (DAPI). Scale bar = 200 µm.

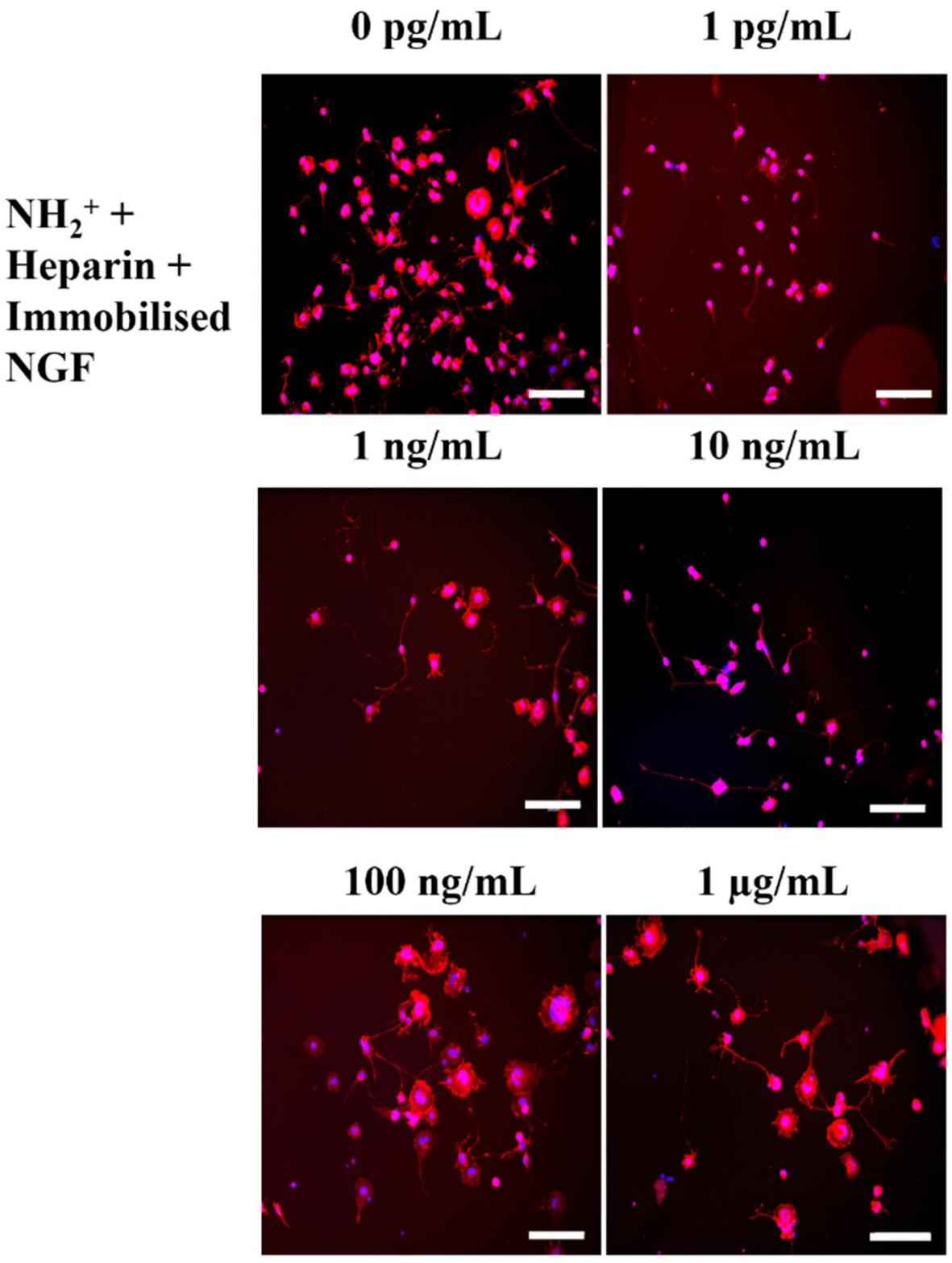

Figure 39. Epifluorescence images of NG108-15 neuronal cells cultured onto NH_2^+ + Heparin + Immobilised NGF with different concentrations of NGF. F-actin filaments are stained in red (phalloidin TRITC)., nuclei are stained in blue (DAPI). Scale bar = 200 µm.

Neurite length of NG108-15 neuronal cells was measured and averaged to obtain the averaged neurite length of NG108-15 neuronal cells seeded on TCP, NH_2^+, NH_2^+ + Heparin, and NH_2^+ + Heparin + Immobilised NGF. On average, the largest neurite was developed from neuronal cells cultured on NH_2^+ surface with soluble NGF at 1 µg/mL, its length was 134 ± 12 µm. The shortest neurite measured was 87 ± 20 µm, which was from neuronal cells cultured onto NH_2^+ surface. In addition, when NG108-15 neuronal cells were cultured onto TCP, the averaged neurite length was 120 ± 29 µm. In comparison, when NG108-15 neuronal cells were cultured on NH_2^+ + Heparin + Immobilised NGF at 1 µg/mL, the averaged neurite length was 128 ± 36 µm. However, as Figure 40 shows, there was no statistical difference between any samples, indicating that the bioactive surfaces and NGF, regardless of concentration, did not significantly affect neurite outgrowth of NG108-15 neuronal cells.

Average neurite length of NG108-15 neuronal cells cultured with NGF

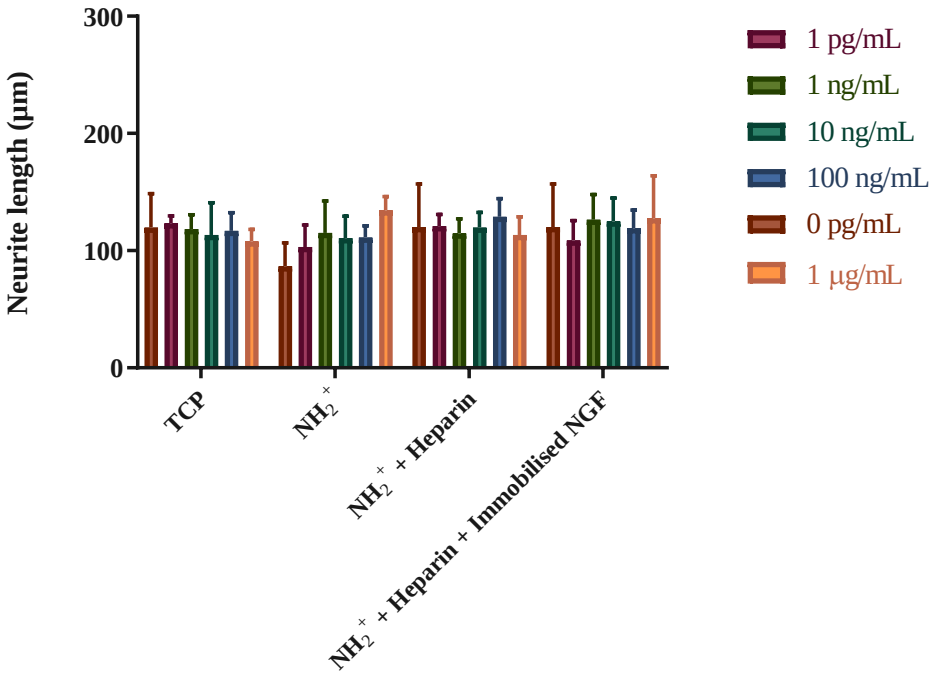

Figure 40. Average neurite length of NG108-15 neuronal cells when cultured on TCP, NH_2^+, NH_2^+ + Heparin, and NH_2^+ + Heparin + Immobilised NGF. NGF was added to the bioactive surfaces at different concentrations. Two-way ANOVA statistical analysis was performed with Tukey procedure of multiple comparisons (*$p<0.05$). Mean ± SD. N=3, n=3.

Figure 41 shows the averaged maximum neurite length measured from the NG108-15 neuronal cells cultured on TCP, NH_2^+, NH_2^+ + Heparin, and NH_2^+ + Heparin + Immobilised NGF. This measurement indicates the maximum neurite outgrowth reached under the test conditions. The average maximum neurite length was calculated by identifying the maximum neurite outgrowth from each condition, and then making an average from the values of each repeat. The shortest maximum neurite length was 170 ± 48 μm for NG108-15 neuronal cells cultured on NH_2^+ surface. The largest neurite length was 370 ± 116 μm for neuronal cells cultured on TCP with soluble NGF at a concentration of 1 pg/mL. Similarly, for neuronal cells seeded on NH_2^+ + Heparin + Immobilised NGF at 1 μg/mL, the averaged maximum neurite length was 365 ± 91 μm. Moreover, neuronal cells cultured on NH_2^+ surface with soluble NGF at 1 μg/mL and NH_2^+ + Heparin surface with soluble NGF at 1 μg/mL developed maximum neurite lengths of 314 ± 46 μm and 351 ± 130 μm respectively.

Interestingly, when NG108-15 neuronal cells were cultured on TCP, with soluble NGF at different concentrations, a trend towards a reduction in maximum neurite length was observed as the concentration of NGF increased, even though there was no significant difference. Firstly, the averaged maximum length of neuronal cells cultured on TCP was 332 ± 92 μm; when NG108-15 neuronal cells were cultured on TCP with soluble NGF at 1 pg/mL, the averaged maximum neurite length was 370 ± 116 μm; when the neuronal cells were cultured on TCP with soluble NGF at 1 μg/mL, the averaged maximum neurite length was 232 ± 60 μm. In comparison, when NGF was immobilised onto the bioactive surface NH_2^+ + Heparin, the averaged maximum neurite length of the NG108-15 neuronal cells increased as the concentration of NGF increased: from 265 ± 21 μm (immobilised NGF at 1 pg/mL), 275 ± 102 μm (immobilised NGF at 1 ng/mL), 290 ± 60 μm (immobilised NGF at 10 ng/mL), 339 ± 131 μm (immobilised NGF at 100 ng/mL) to 365 ± 91 μm (immobilised NGF at 1 μg/mL). Even though there was no significant difference between any samples, important information was obtained regarding the concentration of NGF used: increasing the concentration of soluble NGF delivered to cells on TCP decreased the average neurite length, but if a bioactive surface was used to immobilise NGF, increasing the concentration of NGF increased the maximum neurite length.

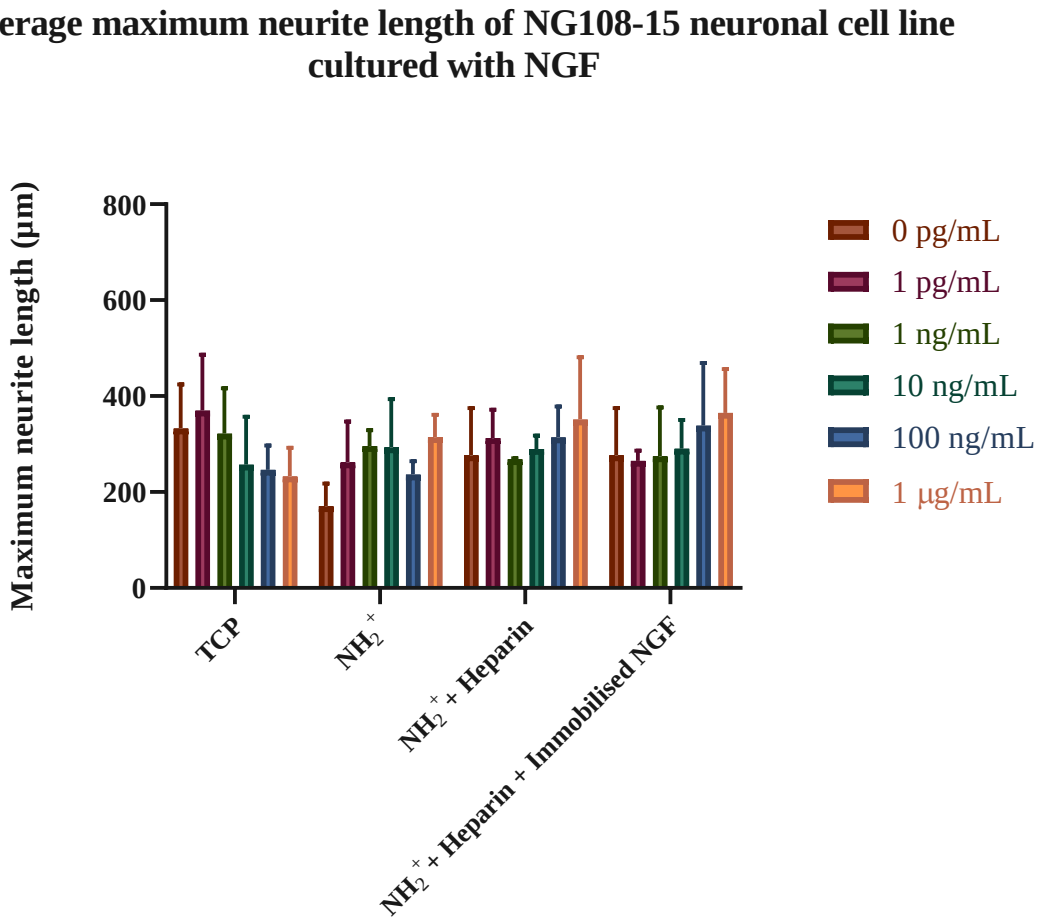

Figure 41. Average maximum neurite length of NG108-15 neuronal cells when culture on TCP, NH_2^+, NH_2^+ + Heparin (controls), and NH_2^+ + Heparin + Immobilised NGF (test). NGF was added to the bioactive surfaces at different concentrations. Two-way ANOVA statistical analysis was performed with Tukey procedure of multiple comparisons (*$p<0.05$). Mean ± SD. N=3, n=3.

The percentage of neurons bearing neurites was calculated for NG108-15 neuronal cells cultured on TCP, NH_2^+, NH_2^+ + Heparin, and NH_2^+ + Heparin + Immobilised NGF. The lowest percentage value of neurons bearing neurites was 20 ± 17% for neuronal cells cultured on NH_2^+ surface. The highest percentage of neurons bearing neurites was 51 ± 12% for neuronal cells seeded on TCP with soluble NGF at a concentration of 10 ng/mL. Control TCP revealed 35 ± 15% of neurons bearing neurites while bioactive surfaces with immobilised NGF at 1 µg/mL supported 35 ± 20% of neuronal cells bearing neurites. This suggests that high concentrations of immobilised NGF did not significantly affect neurite development. As Figure 42 shows, there was no significant difference between the samples regarding percentage of neurons bearing neurites, however, none of the conditions affected the development of neurites.

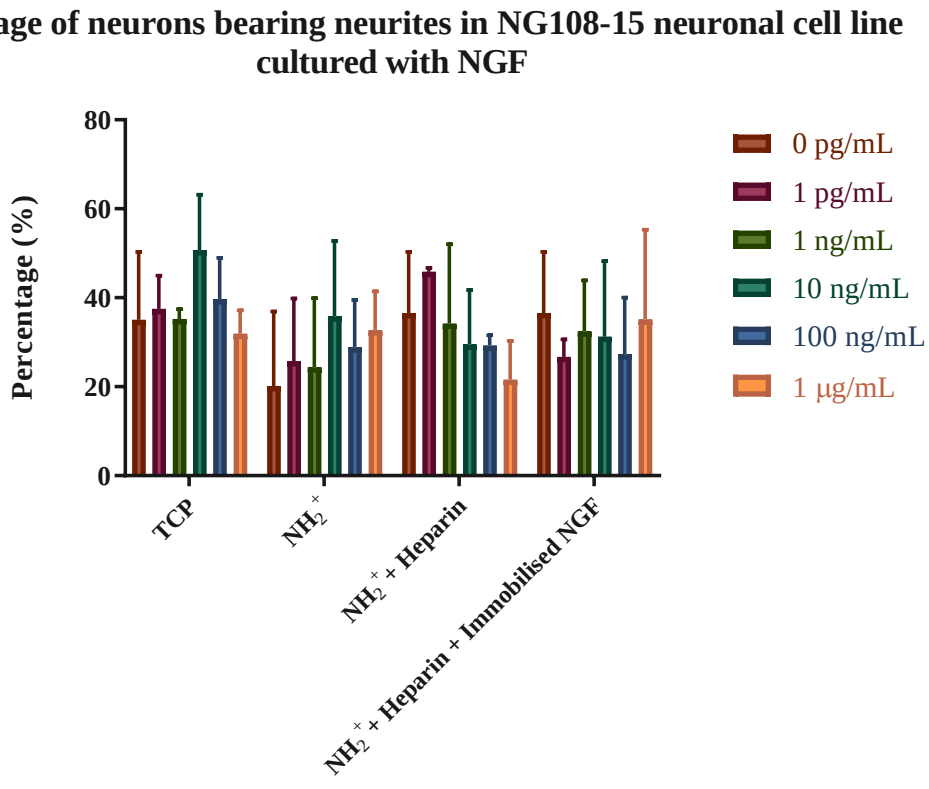

Figure 42. Percentage of neurons bearing neurites of NG108-15 neuronal cells when culture on TCP, NH_2^+, NH_2^+ + Heparin (controls), and NH_2^+ + Heparin + Immobilised NGF (test). NGF was added to the bioactive surfaces at different concentrations. Two-way ANOVA statistical analysis was performed with Tukey procedure of multiple comparisons (*$p<0.05$). Mean ± SD. N=3, n=3.

6.4.1.2 Effects of Brain Derived Neurotrophic Factor

Metabolic activity was also evaluated for NG108-15 neuronal cells cultured on TCP, NH_2^+, NH_2^+ + Heparin, and NH_2^+ + Heparin + Immobilised BDNF. This assay was used to observe any effect in the metabolic activity of NG108-15 neuronal cells that the bioactive surfaces could elicit. It was important to evaluate any changes in the metabolic activity of the NG108-15 neuronal cells when cultured with BDNF because if the metabolic activity was reduced, it was paramount to determine the cause of it: whether the bioactive surface or the concentration of BDNF used.

When NG108-15 neuronal cells were cultured on TCP with BDNF in solution at 1 µg/mL, the metabolic activity was significantly higher in comparison to the metabolic activity of the neuronal cells cultured on NH_2^+ with BDNF at 100 ng/mL and on NH_2^+ + Heparin with BDNF at 1 ng/mL and 100 ng/mL. Furthermore, when NG108-15 neuronal cells were cultured on NH_2^+ + Heparin + Immobilised BDNF at 1 µg/mL, the metabolic activity was significantly higher compared to neuronal cells cultured on NH_2^+ + Heparin with BDNF at 100 ng/mL. However, there was no significant difference in the metabolic activity of NG108-15 neuronal cells cultured on TCP with BDNF at 1 µg/mL and NH_2^+ + Heparin + Immobilised BDNF at 1 µg/mL. In addition, there was no significant reduction of the metabolic activity of the neuronal cells cultured on any of the bioactive surfaces NH_2^+ + Heparin + Immobilised BDNF with different concentrations of BDNF, as shown in Figure 43.

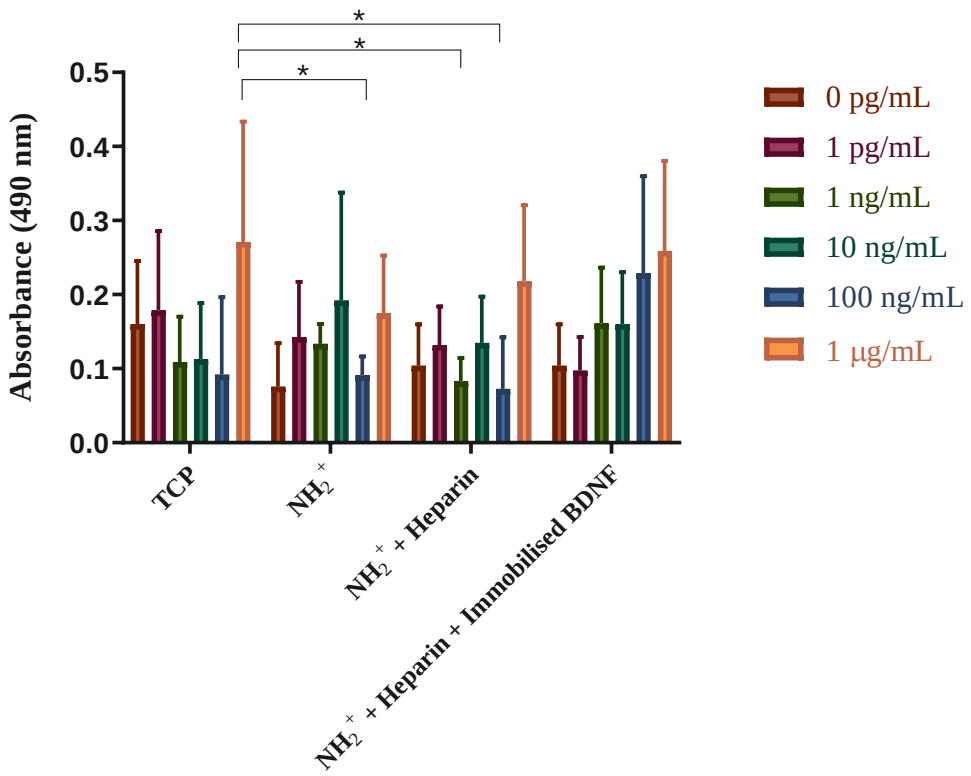

Figure 43. Metabolic activity of NG108-15 neuronal cells, measured with MTS assay at day 7, cultured on different bioactive surfaces with BDNF at different concentrations. BDNF was present in culture medium in TCP, NH_2^+ and NH_2^+ + Heparin (controls). BDNF was immobilised on NH_2^+ + Heparin (test). Two-way ANOVA statistical analysis was performed with Tukey procedure of multiple comparisons (*$p<0.05$). Mean ± SD. N=3, n=3.

Figure 44, Figure 45, Figure 46, Figure 47 show NG108-15 neuronal cells cultured on different bioactive surfaces (TCP, NH_2^+, NH_2^+ + Heparin, and NH_2^+ + Heparin + Immobilised BDNF respectively) at various concentrations of BDNF. Developed neurites can be seen in all the images with some highlighted with a yellow brace. DAPI was used to stain nuclei; phalloidin TRITC was used to stain the f-actin filaments of the cytoskeleton of the neuron, which includes the neurite. Regardless of the BDNF concentration or bioactive surface, NG108 neuronal cells developed neurites in all conditions. These images are representative of average neurite length.

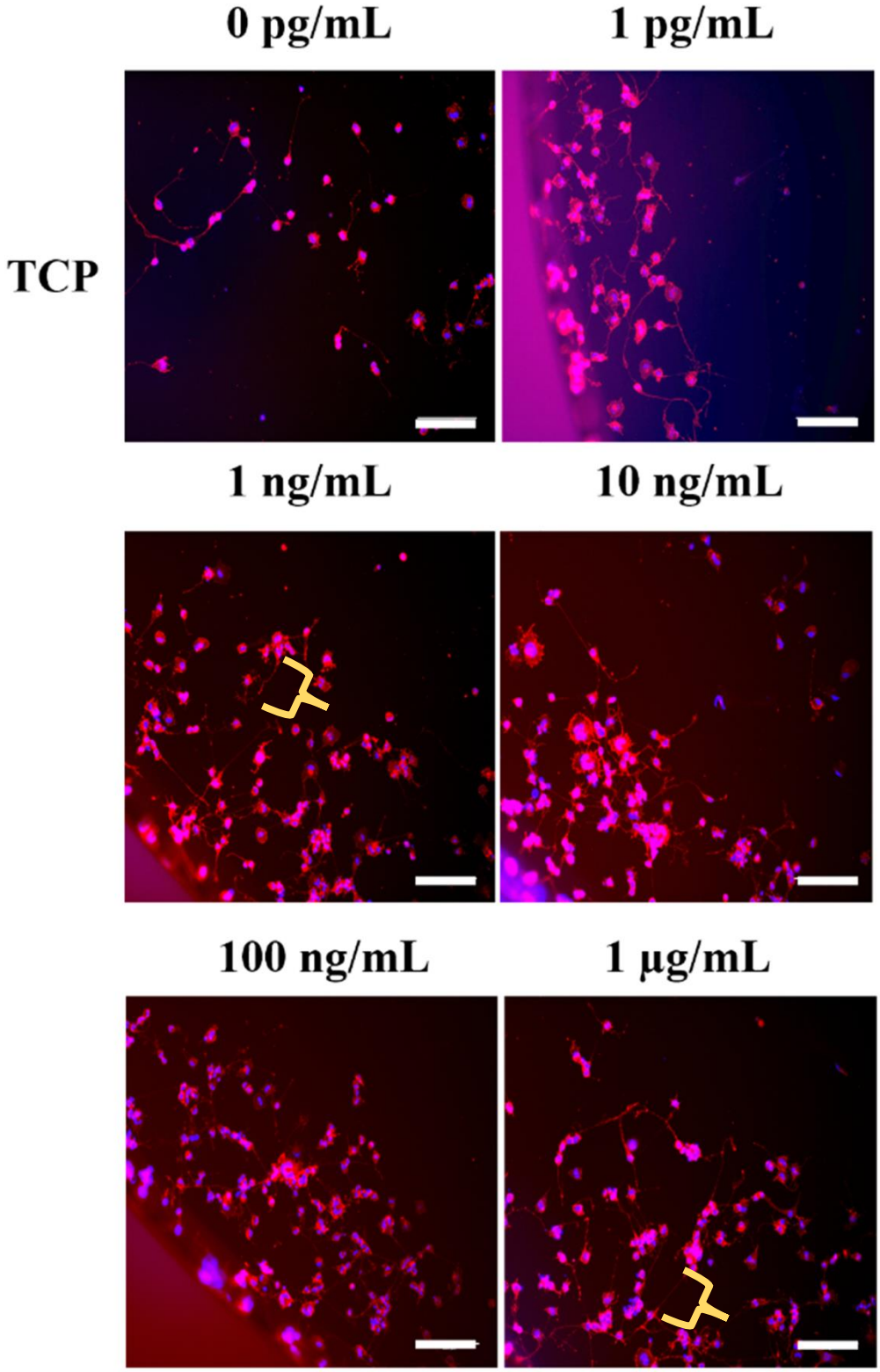

Figure 44. Epifluorescence images of NG108-15 neuronal cells cultured onto TCP with different concentrations of BDNF. F-actin filaments are stained in red (phalloidin TRITC)., nuclei are stained in blue (DAPI). Developed neurites can be seen in all the images with some highlighted with a yellow brace. Scale bar = 200 µm.

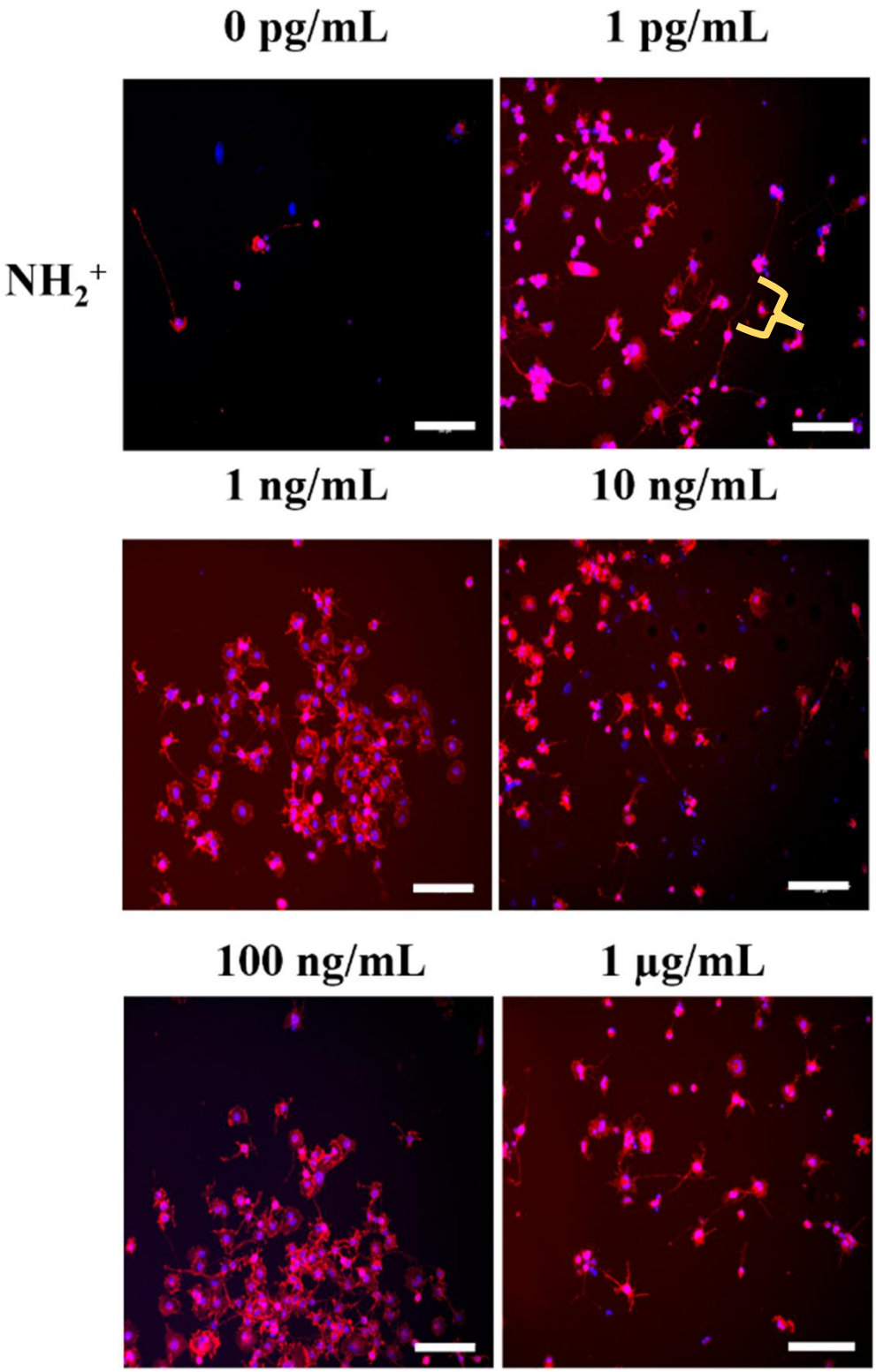

Figure 45. Epifluorescence images of NG108-15 neuronal cells cultured onto NH_2^+ with different concentrations of BDNF. F-actin filaments are stained in red (phalloidin TRITC)., nuclei are stained in blue (DAPI). Developed neurites can be seen in all the images with some highlighted with a yellow brace. Scale bar = 200 µm.

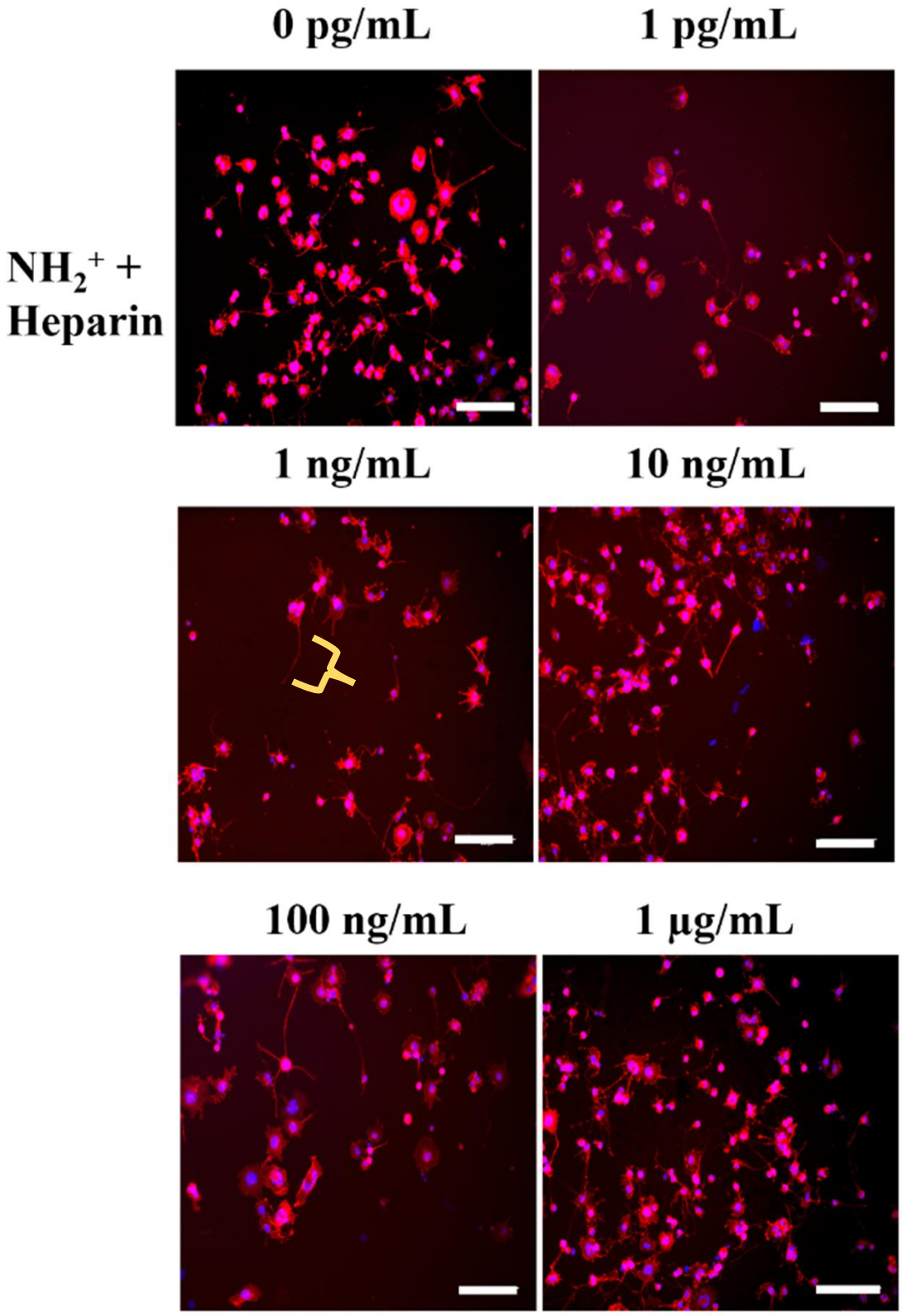

Figure 46. Epifluorescence images of NG108-15 neuronal cells cultured onto NH_2^+ + Heparin with different concentrations of BDNF. F-actin filaments are stained in red (phalloidin TRITC)., nuclei are stained in blue (DAPI). Developed neurites can be seen in all the images with some highlighted with a yellow brace. Scale bar = 200 µm.

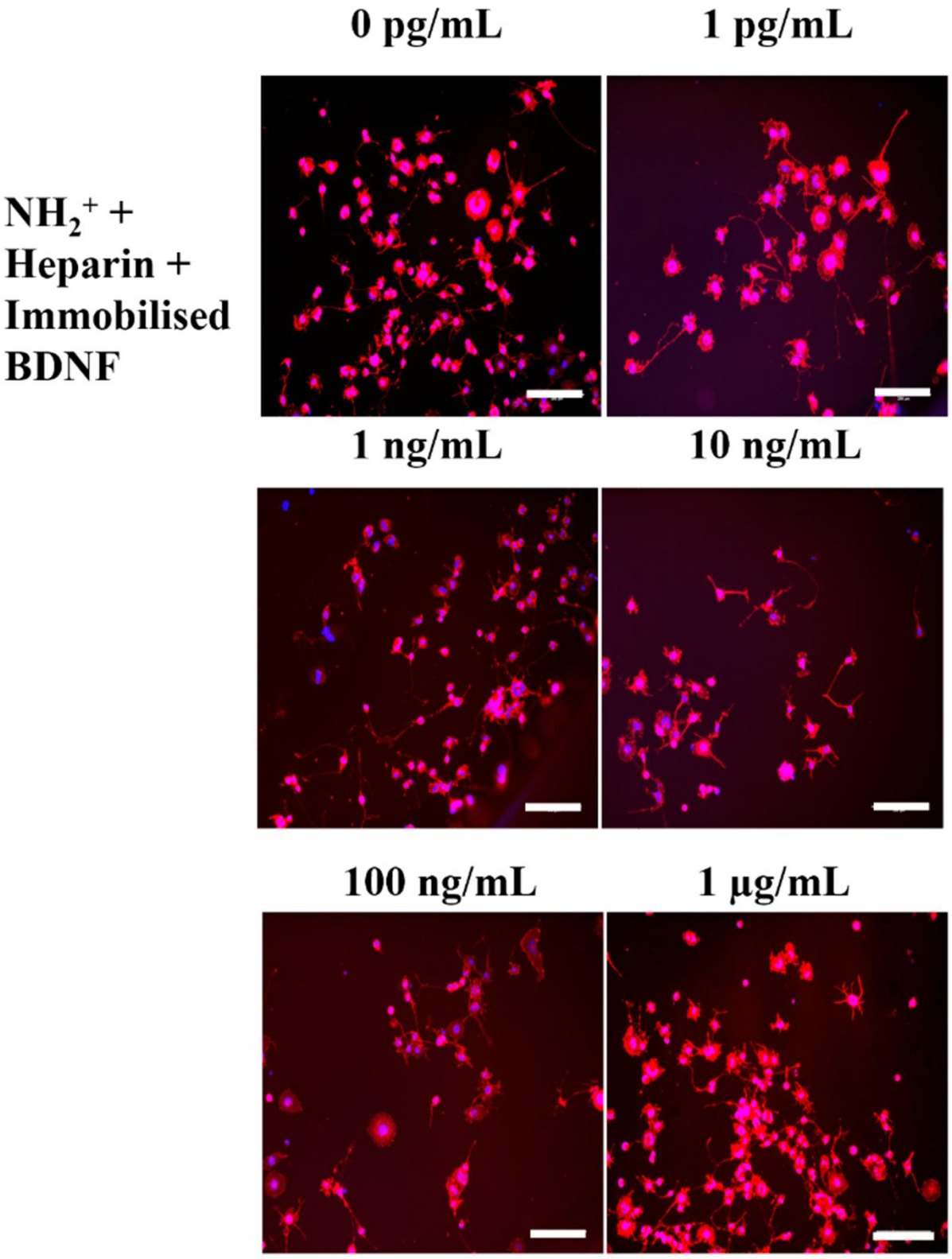

Figure 47. Epifluorescence images of NG108-15 neuronal cells cultured onto NH_2^+ + Heparin + Immobilised BDNF with different concentrations of BDNF. F-actin filaments are stained in red (phalloidin TRITC)., nuclei are stained in blue (DAPI). Developed neurites can be seen in all the images with some highlighted with a yellow brace. Scale bar = 200 µm.

The neurite length of NG108-15 neuronal cells was measured and averaged to obtain the averaged neurite length of NG108-15 neuronal cells cultured on TCP, NH_2^+, NH_2^+ + Heparin, and NH_2^+ + Heparin + Immobilised BDNF (Figure 48). On average, the longest neurite was 137 ± 19 µm for neuronal cells cultured on TCP with BDNF at 1 µg/mL. The shortest neurite was 36 ± 62 µm for neuronal cell cultures on TCP with BDNF at 10 ng/mL. There was a significant difference between these two groups (*$p<0.05$). No significant differences were found among other groups. The average neurite length of NG108-15 neuronal cells seeded on TCP was 119 ± 29 µm, whereas the average neurite length of the neuronal cells was 113 ± 20 µm when cultured on NH_2^+ + Heparin + Immobilised BDNF at 1 µg/mL. In addition, 129 ± 35 µm was the average neurite length of neuronal cells cultured on NH_2^+ + Heparin + Immobilised BDNF at 1 ng/mL.

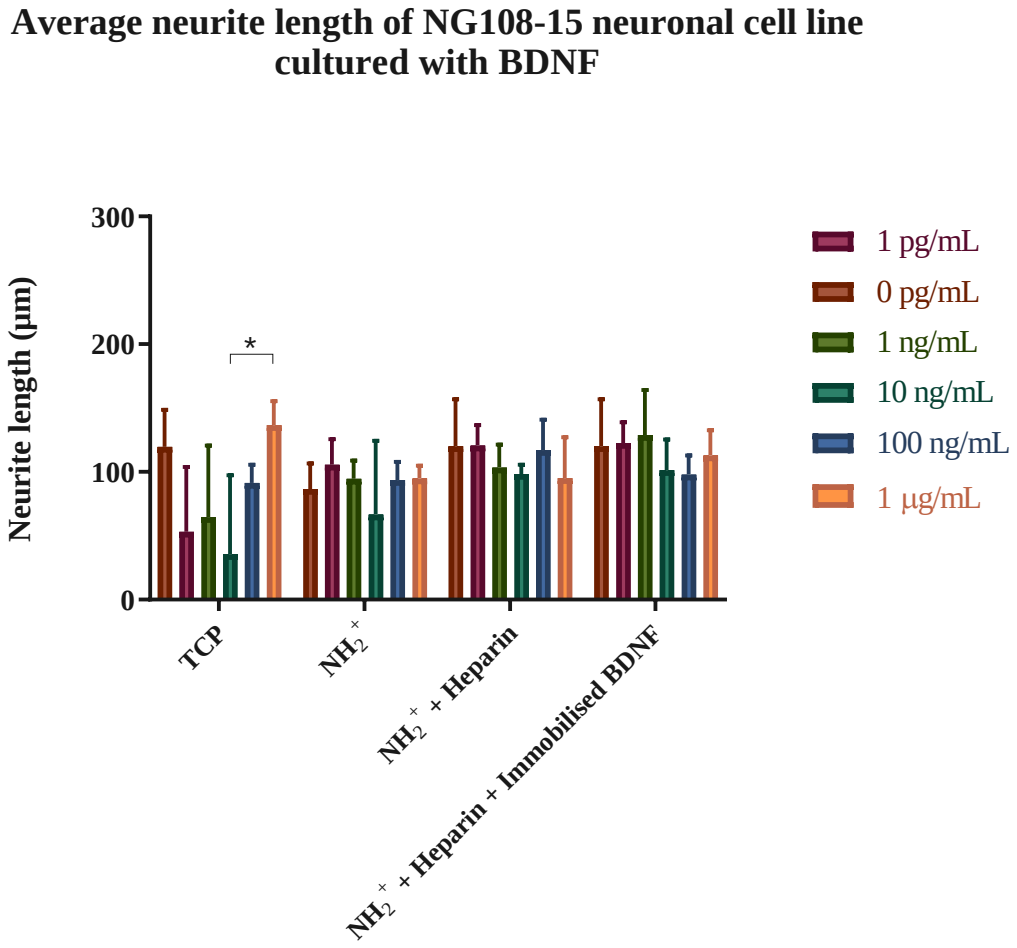

Figure 48. Average neurite length of NG108-15 neuronal cells when cultured on TCP, NH_2^+, NH_2^+ + Heparin (controls), and NH_2^+ + Heparin + Immobilised BDNF (test). BDNF was added to the bioactive surfaces at different concentrations. Two-way ANOVA statistical analysis was performed with Tukey procedure of multiple comparisons (*p<0.05). Mean ± SD. N=3, n=3.

The average maximum neurite length was measured to observe the maximum neurite outgrowth that the NG108-15 neuronal cells could develop. Figure 49 shows the average maximum neurite length of NG108-15 neuronal cells seeded on TCP, NH_2^+, NH_2^+ + Heparin, and NH_2^+ + Heparin + Immobilised BDNF. The longest averaged maximum neurite length was 335 ± 113 µm, measured from NG108-15 neuronal cells cultured on NH_2^+ + Heparin + Immobilised BDNF at 1 ng/mL. The shortest average maximum neurite length was 88 ± 152 µm, calculated from neuronal cells seeded on TCP with BDNF in solution at a concentration of 10 ng/mL. For neuronal cells seeded

on TCP with BDNF in solution at a concentration of 1 µg/mL, the average maximum neurite length was 331 ± 43 µm. In comparison, the average maximum neurite length of neuronal cells seeded on NH_2^+ + Heparin + Immobilised BDNF at 1 µg/mL was 269 ± 88 µm. There was no significant difference among the groups.

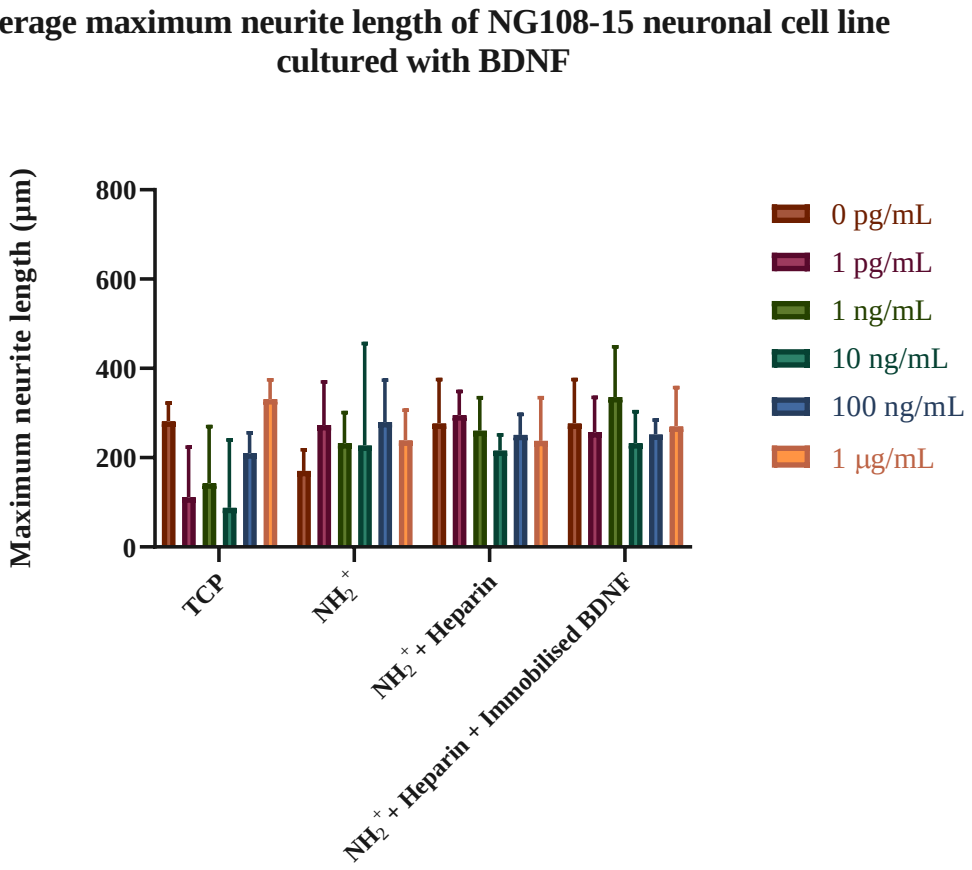

Figure 49. Average maximum neurite length of NG108-15 neuronal cells when cultured on TCP, NH_2^+, NH_2^+ + Heparin (controls), and NH_2^+ + Heparin + Immobilised BDNF (test). BDNF was added to the bioactive surfaces at different concentrations. Two-way ANOVA statistical analysis was performed with Tukey procedure of multiple comparisons (*$p<0.05$). Mean ± SD. N=3, n=3.

The percentage of neurons bearing neurites, shown in Figure 50, was calculated for NG108-15 neuronal cells cultured on TCP, NH_2^+, NH_2^+ + Heparin, and NH_2^+ + Heparin + Immobilised BDNF. The highest percentage of neurons bearing neurites was 38 ± 18% for neuronal cells cultured on NH_2^+ + Heparin with BDNF in solution at a concentration of 10 ng/mL. The lowest percentage was 7 ± 12% for NG108 neuronal cells cultured on TCP with soluble BDNF at a concentration of 10 ng/mL. Even though there were no significant differences between the control and test groups, the percentage of neurons beating neurites decreased slightly for the neuronal cells seeded on NH_2^+ + Heparin + Immobilised BDNF: from 36 ± 14% (0 pg/mL), 31 ± 5% (1 pg/mL), 31 ± 16% (1 ng/mL), 26 ± 8% (10 ng/mL), 27 ± 7% (100 ng/mL) to 24 ± 10% (1 µg/mL).

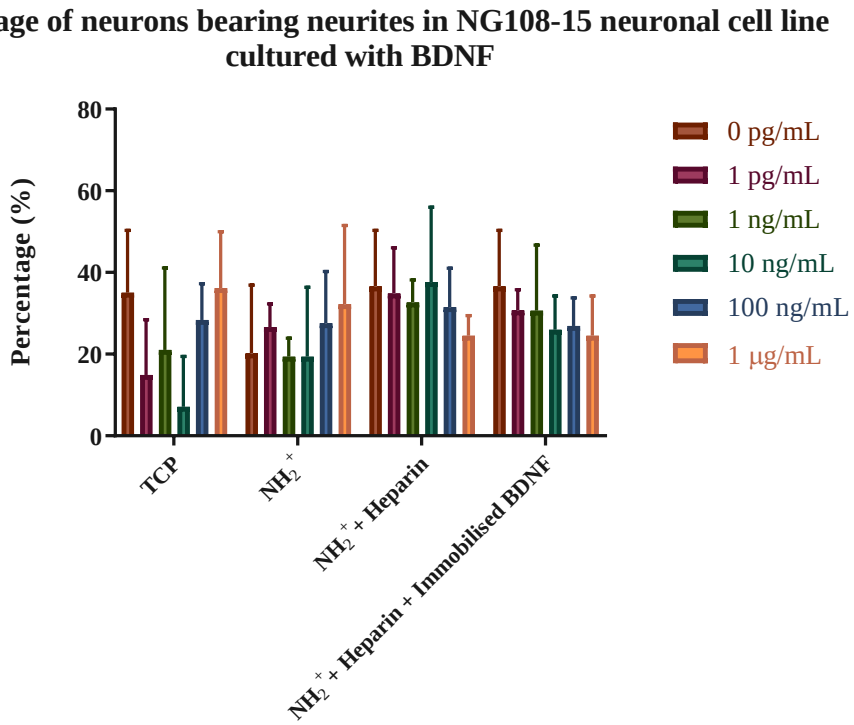

Figure 50. Percentage of neurons bearing neurites of NG108-15 neuronal cells when cultured on TCP, NH_2^+, NH_2^+ + Heparin (controls), and NH_2^+ + Heparin + Immobilised BDNF (test). BDNF was added to the bioactive surfaces at different concentrations. Two-way ANOVA statistical analysis was performed with Tukey procedure of multiple comparisons (*$p<0.05$). Mean ± SD. N=3, n=3.

6.4.1.3 Effects of Nerve Growth Factor plus Brain Derived Neurotrophic Factor

Metabolic activity was also assessed for NG108-15 neuronal cells cultured on TCP, NH_2^+, NH_2^+ + Heparin, and NH_2^+ + Heparin + Immobilised NGF plus BDNF. It was important to evaluate how the neuronal cells responded when they were cultured with both NGF and BDNF. The NG108-15 neuronal cells with the highest metabolic activity were the ones cultured on NH_2^+ with soluble NGF plus BDNF at 1 pg/mL. The lowest metabolic activity was detected for the neuronal cells seeded on NH_2^+. The metabolic activity of the neuronal cells was higher when seeded on bioactive surfaces where NGF plus BDNF were present in comparison to bioactive surfaces without NGF plus BDNF. However, no significant difference was found between the control and test groups, as shown in Figure 51.

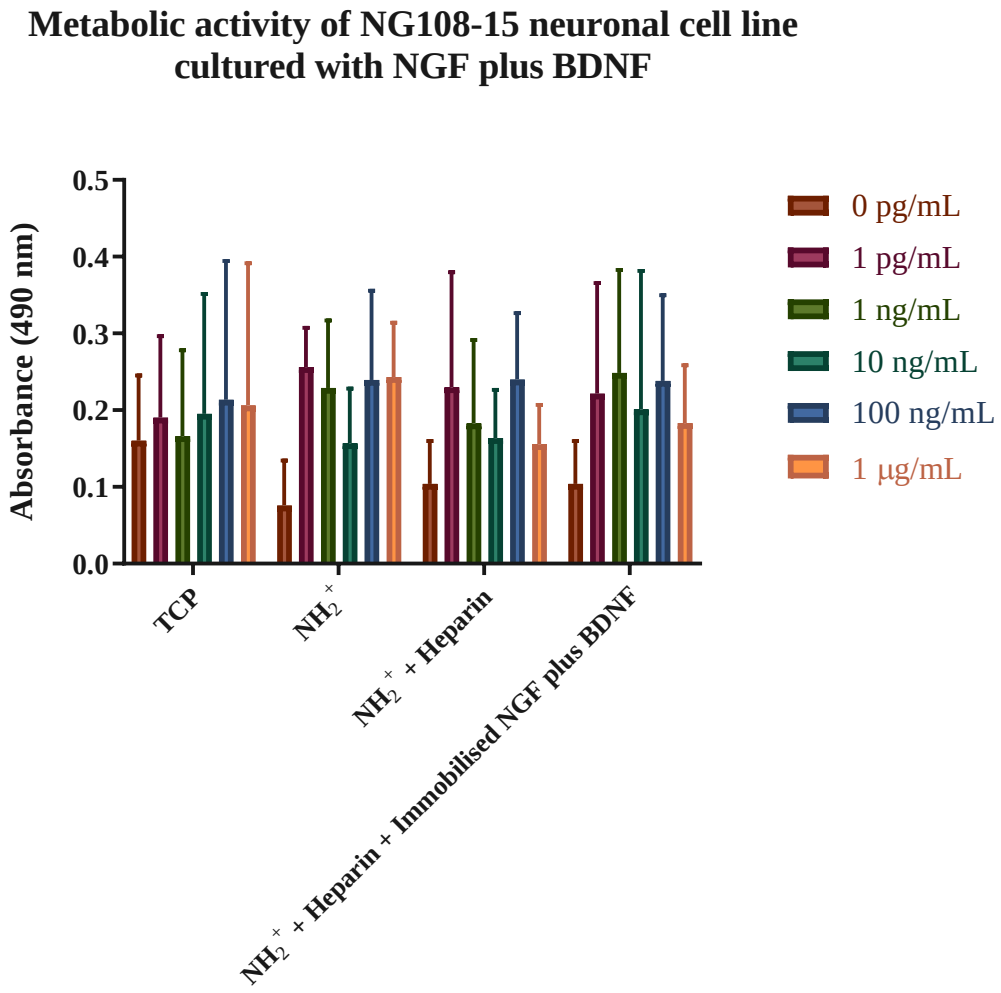

Figure 51. Metabolic activity of NG108-15 neuronal cells, measured with MTS assay at day 7, cultured on different bioactive surfaces with NGF plus BDNF at different concentrations. NGF plus BDNF were present in culture medium on TCP, NH_2^+ and NH_2^+ + Heparin (controls). NGF plus BDNF were immobilised on NH_2^+ + Heparin (test). Two-way ANOVA statistical analysis was performed with Tukey procedure of multiple comparisons (*$p<0.05$). Mean ± SD. N=3, n=3.

Figure 52, Figure 53, Figure 54, Figure 55 show NG108-15 neuronal cells cultured on different bioactive surfaces (TCP, NH_2^+, NH_2^+ + Heparin, and NH_2^+ + Heparin + Immobilised NGF plus BDNF respectively) at the various concentrations of NGF plus BDNF. Developed neurites can be seen in all the images, with some of them highlighted with a yellow brace. DAPI was used to stain nuclei; phalloidin TRITC was used to stain the f-actin filaments of the cytoskeleton of the neuron, which includes the neurite. Regardless of the bioactive surface or concentration used of NGF plus BDNF, all conditions developed neurites. These images are representative of average neurite length.

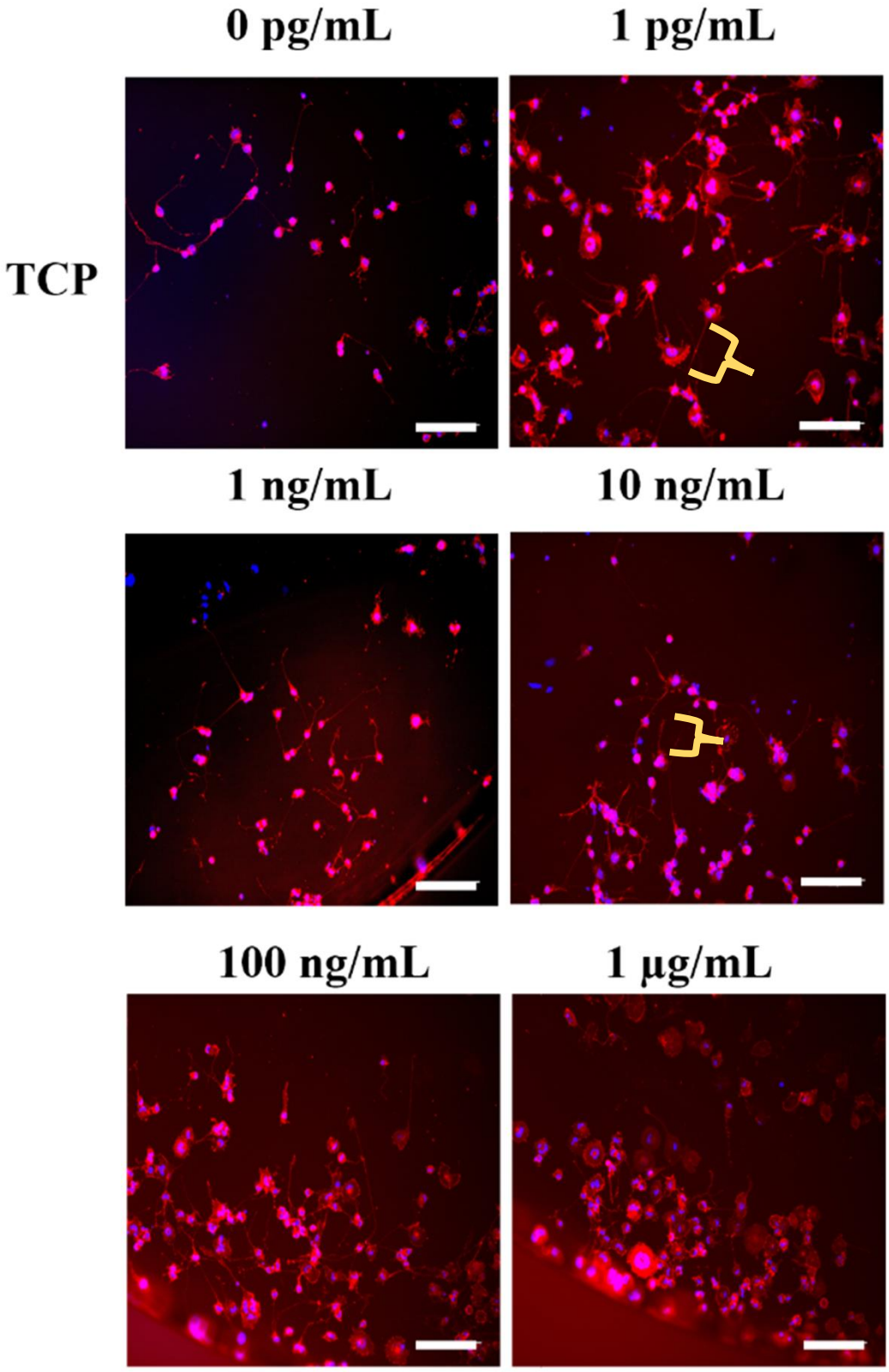

Figure 52. Epifluorescence images of NG108-15 neuronal cells cultured onto TCP with different concentrations of NGF plus BDNF. F-actin filaments are stained in red (phalloidin TRITC)., nuclei are stained in blue (DAPI). Scale bar = 200 µm.

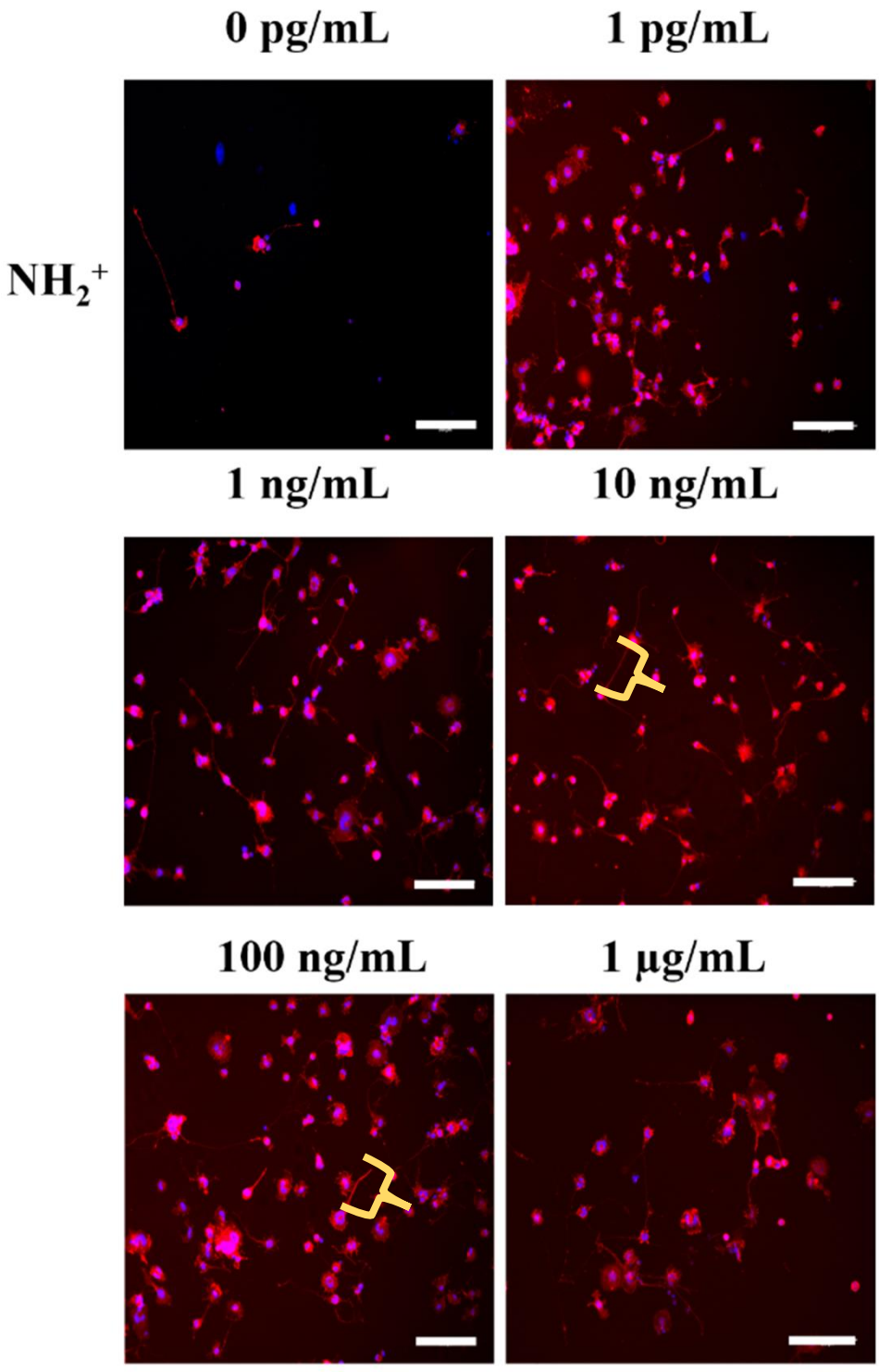

Figure 53. Epifluorescence images of NG108-15 neuronal cells cultured onto NH_2^+ with different concentrations of NGF plus BDNF. F-actin filaments are stained in red (phalloidin TRITC)., nuclei are stained in blue (DAPI). Scale bar = 200 µm.

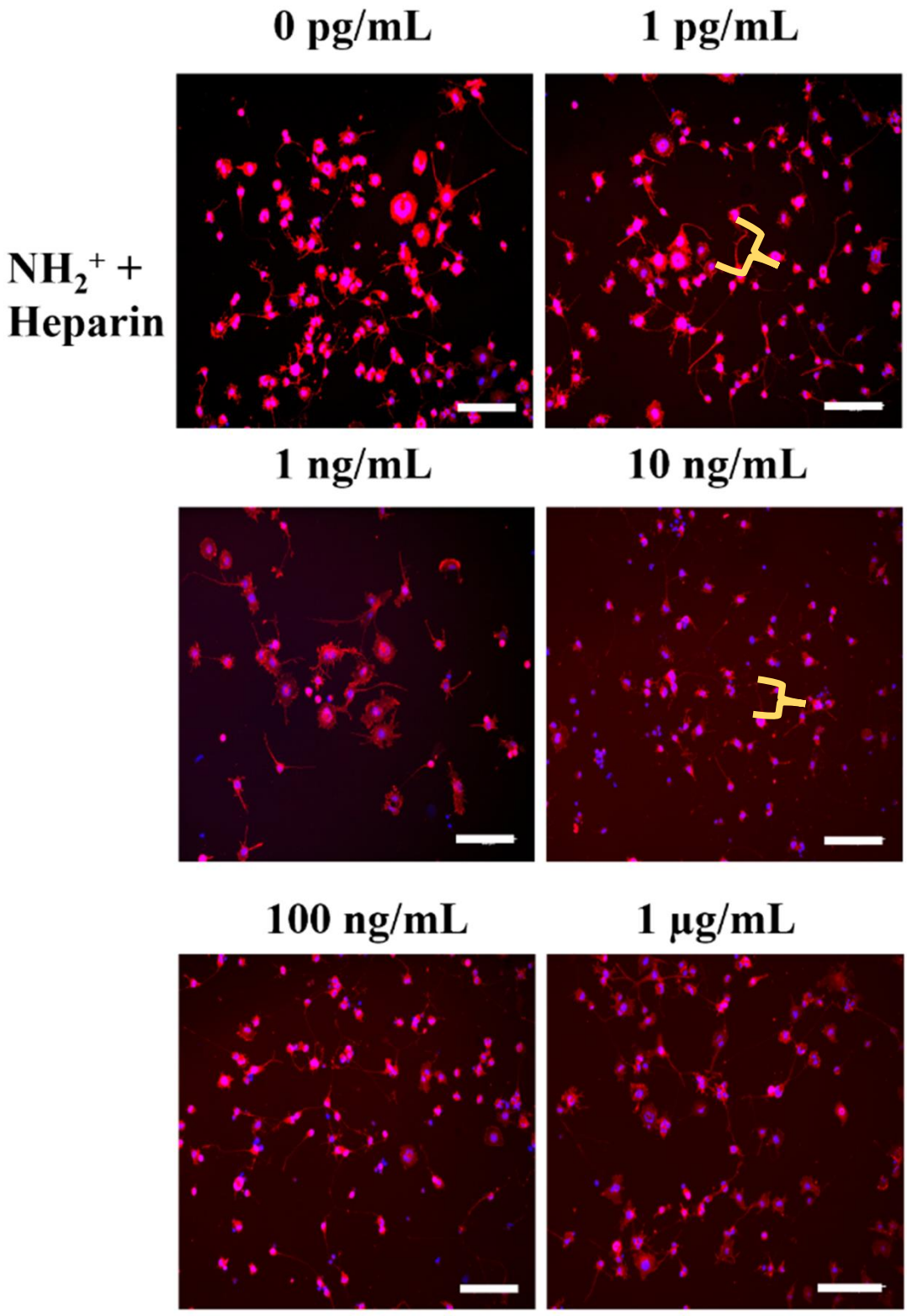

Figure 54. Epifluorescence images of NG108-15 neuronal cells cultured onto NH_2^+ + Heparin with different concentrations of NGF plus BDNF. F-actin filaments are stained in red (phalloidin TRITC)., nuclei are stained in blue (DAPI). Scale bar = 200 µm.

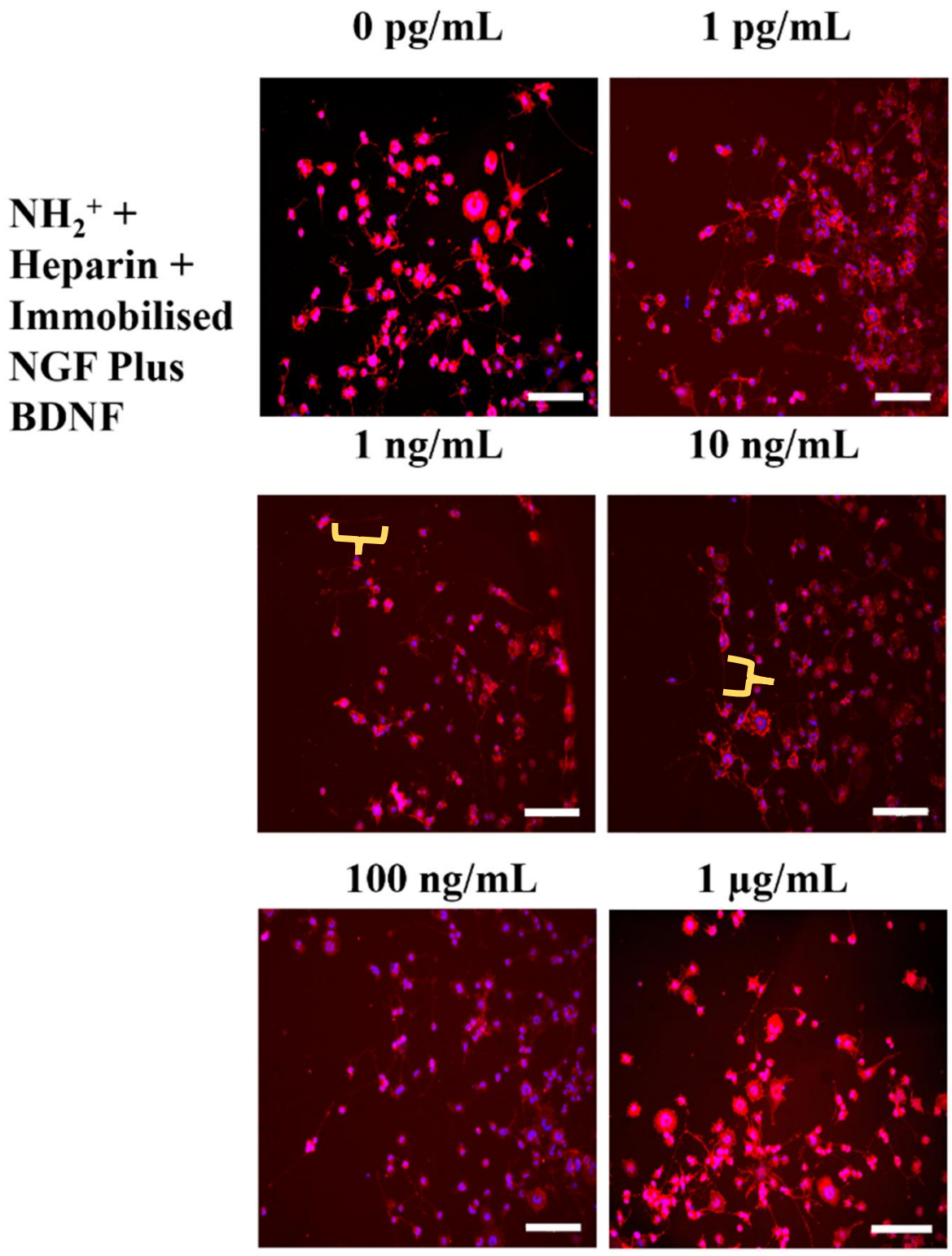

Figure 55. Epifluorescence images of NG108-15 neuronal cells cultured onto NH_2^+ + Heparin + Immobilised NGF plus BDNF with different concentrations of NGF plus BDNF. F-actin filaments are stained in red (phalloidin TRITC)., nuclei are stained in blue (DAPI). Scale bar = 200 µm.

The average neurite length of NG108-15 neuronal cells was calculated from NG108-15 neuronal cells cultured on TCP, NH_2^+, NH_2^+ + Heparin, and NH_2^+ + Heparin + Immobilised NGF plus BDNF. The longest average neurite length, 182 ± 55 µm, was obtained from NG108-15 cells cultured on NH_2^+ + Heparin + Immobilised NGF plus BDNF at a concentration of 1 µg/mL. The shortest average neurite length was 68 ± 62 µm, which was measured and calculated from NG108-15 neuronal cells cultured on NH_2^+ with NGF plus BDNF in solution at a concentration of 1 ng/mL. Interestingly, the average neurite length of NG108-15 neuronal cells increased as the bioactive surface was modified, while seeded with NGF plus BDNF at a concentration of 1 µg/mL: from 143 ± 32 µm (TCP), 153 ± 81 µm (NH_2^+), 177 ± 109 µm (NH_2^+ + Heparin), to 182 ± 55 µm (NH_2^+ + Heparin + Immobilised NGF plus BDNF). However, when the neuronal cells were cultured with NGF plus BDNF at 1 pg/mL, the average neurite length was slightly different when compared to the average neurite length of neuronal cells cultured with NGF plus BDNF at 1 µg/mL: 156 ± 131 µm (TCP), 169 ± 96 µm (NH_2^+), 130 ± 53 µm (NH_2^+ + Heparin), and 178 ± 64 µm (NH_2^+ + Heparin + Immobilised NGF plus BDNF). Nevertheless, there was no significant difference in average neurite length among all control and test groups, as shown in Figure 56.

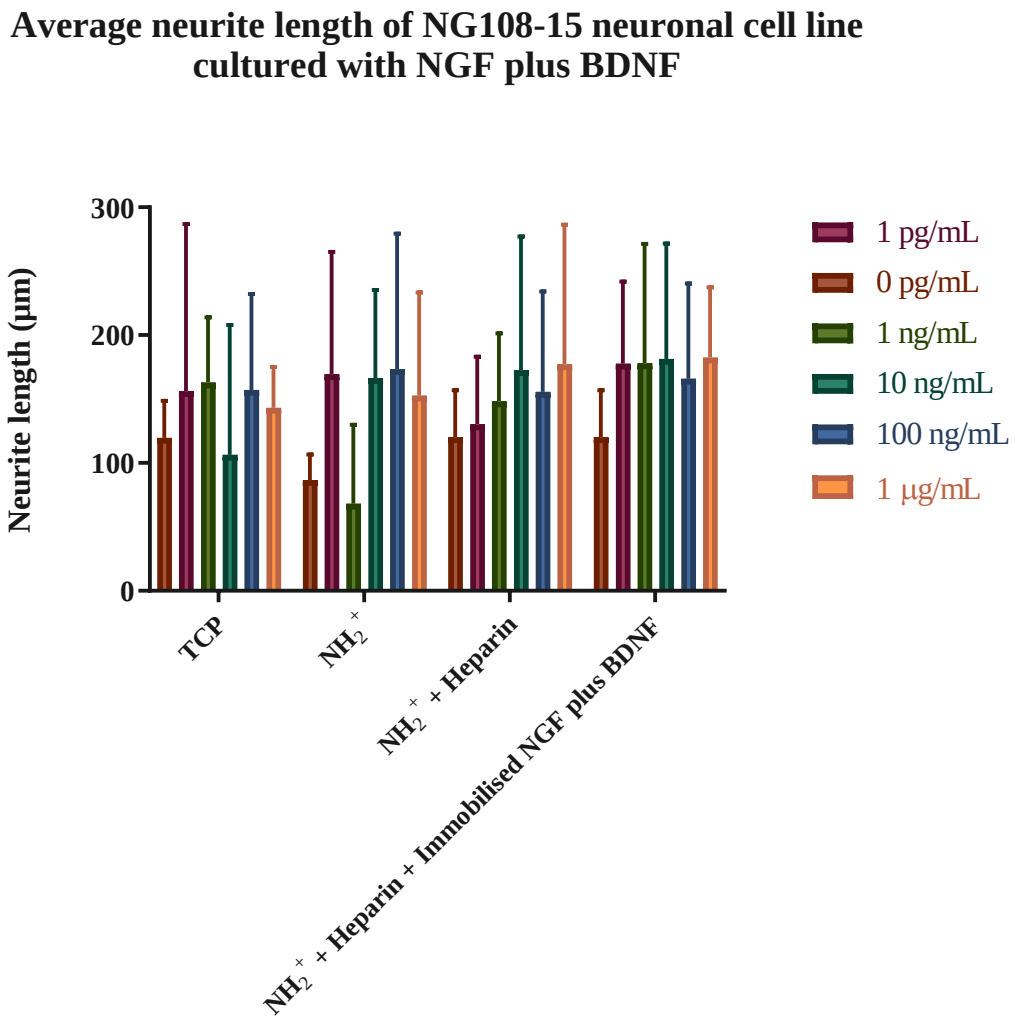

Figure 56. Average neurite length of NG108-15 neuronal cells when cultured on TCP, NH_2^+, NH_2^+ + Heparin (controls), and NH_2^+ + Heparin + Immobilised NGF plus BDNF (test). NGF plus BDNF were added to the bioactive surfaces at different concentrations. Two-way ANOVA statistical analysis was performed with Tukey procedure of multiple comparisons (*$p<0.05$). Mean ± SD. N=3, n=3.

The average maximum neurite length of NG108-15 neuronal cells was calculated from NG108-15 neuronal cells seeded on TCP, NH_2^+, NH_2^+ + Heparin, and NH_2^+ + Heparin + Immobilised NGF plus BDNF. The longest average maximum neurite length was 525 ± 118 µm for NG108-15 neuronal cells seeded on NH_2^+ with NGF plus BDNF in solution at a concentration of 10 ng/mL. The shortest average maximum neurite length was 160 ± 141 µm for NG108-15 neuronal cells cultured on NH_2^+ with NGF plus BDNF in solution at a concentration of 1 ng/mL. When NG108-15 neuronal cells were cultured on NH_2^+ + Heparin + Immobilised NGF plus BDNF, the average maximum neurite length increased as the concentration of NGF plus BDNF increased, until a plateau was reached and then, the average maximum neurite length decreased slightly, as seen in Figure 57: 276 ± 99 µm (0 pg/mL), 368 ± 116 µm (1 pg/mL), 420 ± 213 µm (1 ng/mL), 476 ± 144 µm (10 ng/mL), 475 ± 189 µm (100 ng/mL), and 457 ± 210 µm (1 µg/mL). Nevertheless, there was no significant difference in average maximum neurite length among all control and test groups.

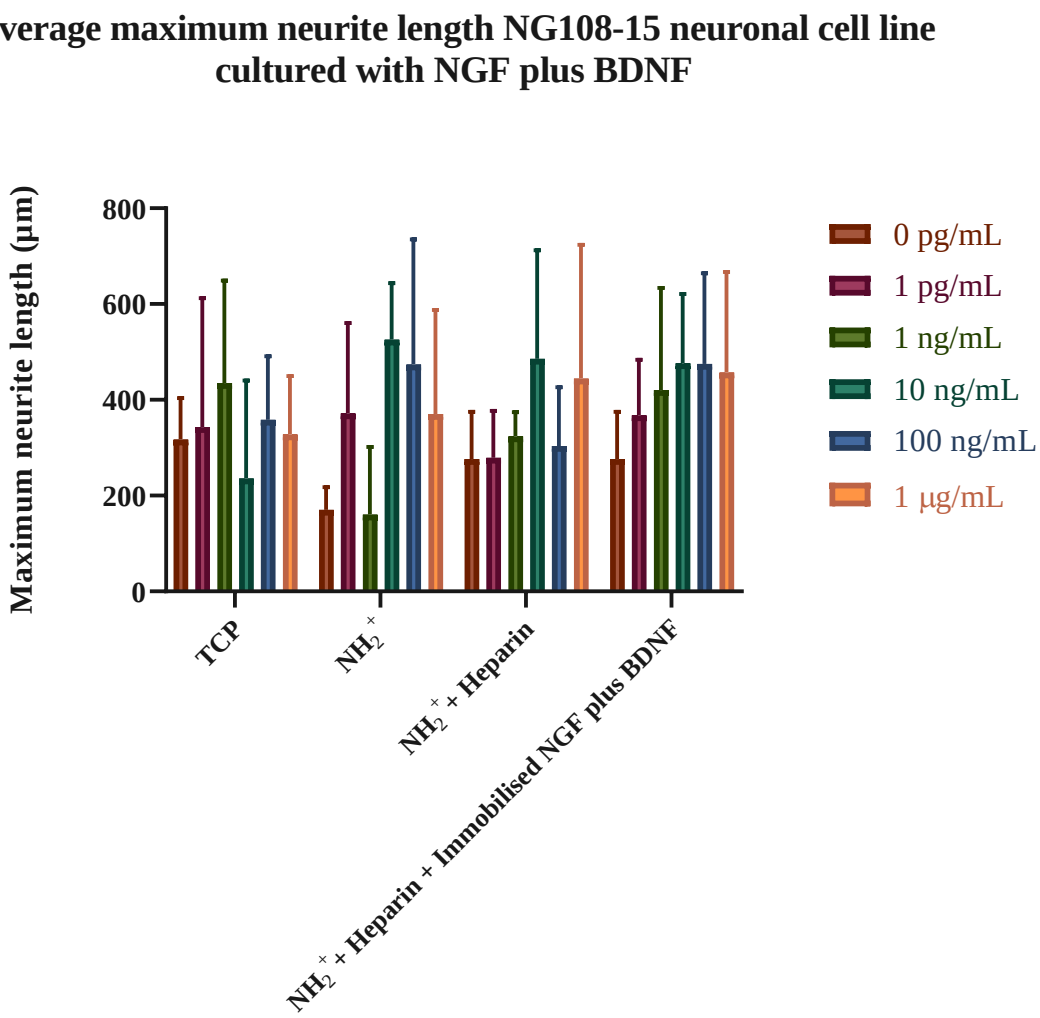

Figure 57. Average maximum neurite length of NG108-15 neuronal cells when cultured on TCP, NH_2^+, NH_2^+ + Heparin (controls), and NH_2^+ + Heparin + Immobilised NGF plus BDNF (test). NGF plus BDNF were added to the bioactive surfaces at different concentrations. Two-way ANOVA statistical analysis was performed with Tukey procedure of multiple comparisons (*$p<0.05$). Mean ± SD. N=3, n=3.

The percentage of neurons bearing neurites of NG108-15 neuronal cells was calculated from NG108-15 neuronal cells cultured on TCP, NH_2^+, NH_2^+ + Heparin, and NH_2^+ + Heparin + Immobilised NGF plus BDNF. The highest percentage was 42 ± 4% for NG108-15 neuronal cells cultured on NH_2^+ + Heparin with NGF plus BDNF in solution at a concentration of 10 ng/mL. The lowest percentage of neurons bearing neurites was 19 ± 17% for neuronal cells cultured on TCP with NGF plus BDNF in solution at a concentration of 10 ng/mL. As shown in Figure 58, there was no significant difference among the control and test groups.

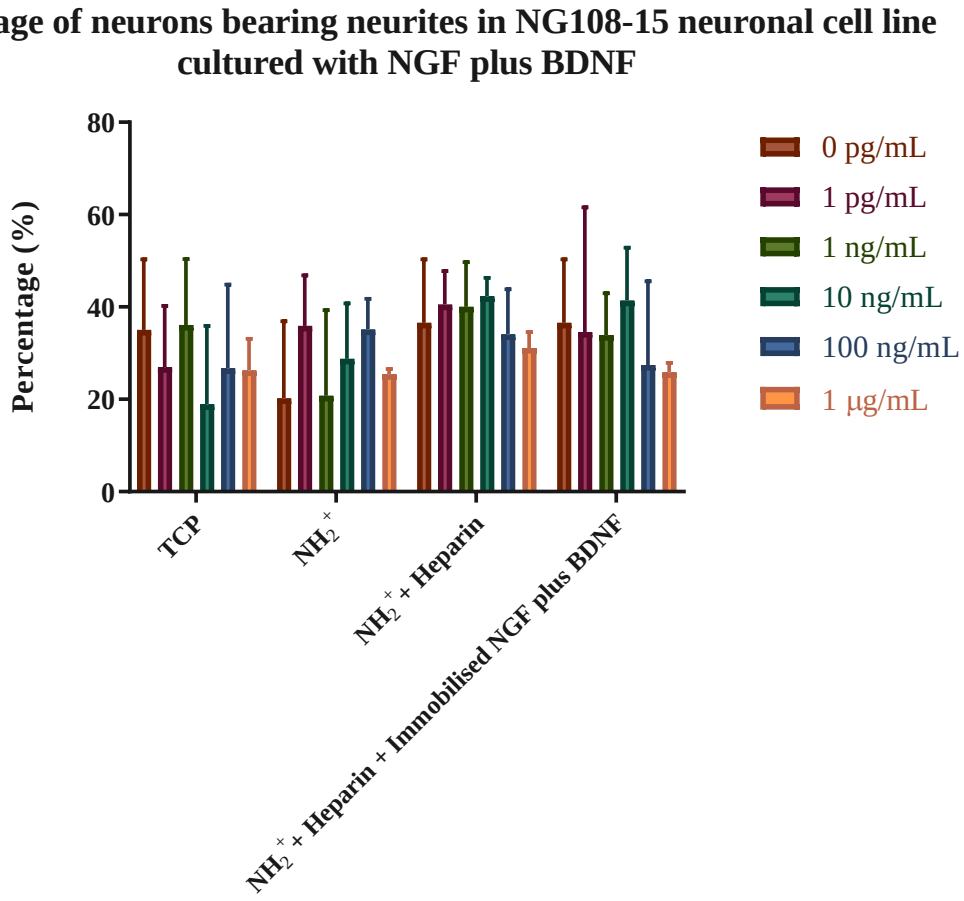

Figure 58. Percentage of neurons bearing neurites of NG108-15 neuronal cells when cultured on TCP, NH_2^+, NH_2^+ + Heparin (controls), and NH_2^+ + Heparin + Immobilised NGF plus BDNF (test). NGF plus BDNF were added to the bioactive surfaces at different concentrations. Two-way ANOVA statistical analysis was performed with Tukey procedure of multiple comparisons (*$p<0.05$). Mean ± SD. N=3, n=3.

6.4.2 Effects of bioactive surfaces on PC12 adh neuronal cell line cultures

6.4.2.1 Effects of Nerve Growth Factor

Metabolic activity was also evaluated for PC12 adh neuronal cells cultured on TCP, NH_2^+, NH_2^+ + Heparin, and NH_2^+ + Heparin + Immobilised NGF. It was important to evaluate how the neuronal cells responded when cultured on the different surfaces with NGF at different concentrations. When PC12 adh neuronal cells were cultured on NH_2^+ + Heparin + Immobilised NGF at 1 µg/mL, the metabolic activity was significantly higher in comparison to the metabolic activity of the PC12 adh neuronal cells seeded on TCP control without NGF. Moreover, the metabolic activity was also significantly higher for neuronal cells seeded on NH_2^+ + Heparin with NGF in solution at 1 µg/mL and on NH_2^+ with NGF in solution at 1 µg/mL in comparison to TCP control without NGF. When PC12 adh neuronal cells were cultured on TCP with NGF, the metabolic activity was slightly lower in comparison with TCP with no NGF, although not statistically different. However, when the neuronal cells were seeded on TCP with NGF in solution at a concentration of 1 µg/mL, as the metabolic activity was higher.

In addition, as shown in Figure 59 when PC12 adh neuronal cells were cultured on NH_2^+ + Heparin, the metabolic activity decreased slightly as the concentration of NGF increased, except for the metabolic activity of the neuronal cells seeded with NGF at 1 µg/mL, which was higher. Furthermore, the metabolic activity of the neuronal cells cultured on NH_2^+ + Heparin + Immobilised NGF was similar, except for the metabolic activity of PC12 adh neuronal cells seeded on NH_2^+ + Heparin + Immobilised NGF at 100 ng/mL and 1 µg/mL, which were lower and higher respectively.

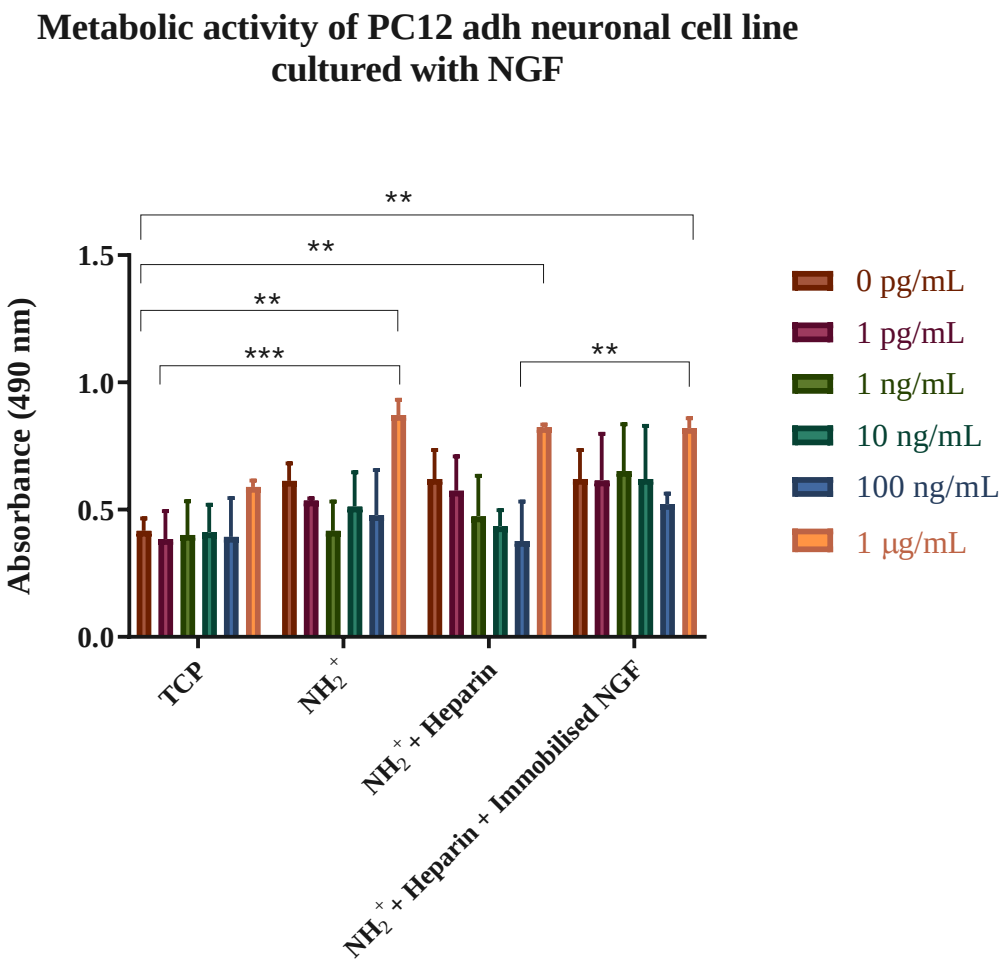

Figure 59. Metabolic activity of PC12 adh neuronal cells, measured with MTS assay at day 5, cultured on different bioactive surfaces with NGF at different concentrations. NGF was present in culture medium in TCP, NH_2^+ and NH_2^+ + Heparin (controls). NGF was immobilised on NH_2^+ + Heparin (test). Two-way ANOVA statistical analysis was performed with Tukey procedure of multiple comparisons *p <0.05, **p<0.01, *** p<0.001, ****p<0.0001 Mean ± SD. N=3, n=3.

Figure 60, Figure 61, Figure 62, Figure 63 show PC12 adh neuronal cells cultured on different bioactive surfaces (TCP, NH_2^+, NH_2^+ + Heparin, and NH_2^+ + Heparin + Immobilised NGF respectively) at different concentrations of NGF. Developed neurites can be seen in images taken from when the cells were cultured with NGF, some of the neurites are highlighted with a yellow brace. DAPI was used to stain nuclei; phalloidin TRITC was used to stain the f-actin filaments of the cytoskeleton of the neuron, which includes the neurite. Increased number of neurites can be observed when PC12 adh neuronal cells were cultured on NH_2^+ + Heparin + Immobilised NGF at 1 µg/mL. Nevertheless, larger neurites developed when cells were seeded on NH_2^+ + Heparin + Immobilised NGF at 1 pg/mL and on NH_2^+ + Heparin + Immobilised NGF at 1 µg/mL. These images are representative of average neurite length.

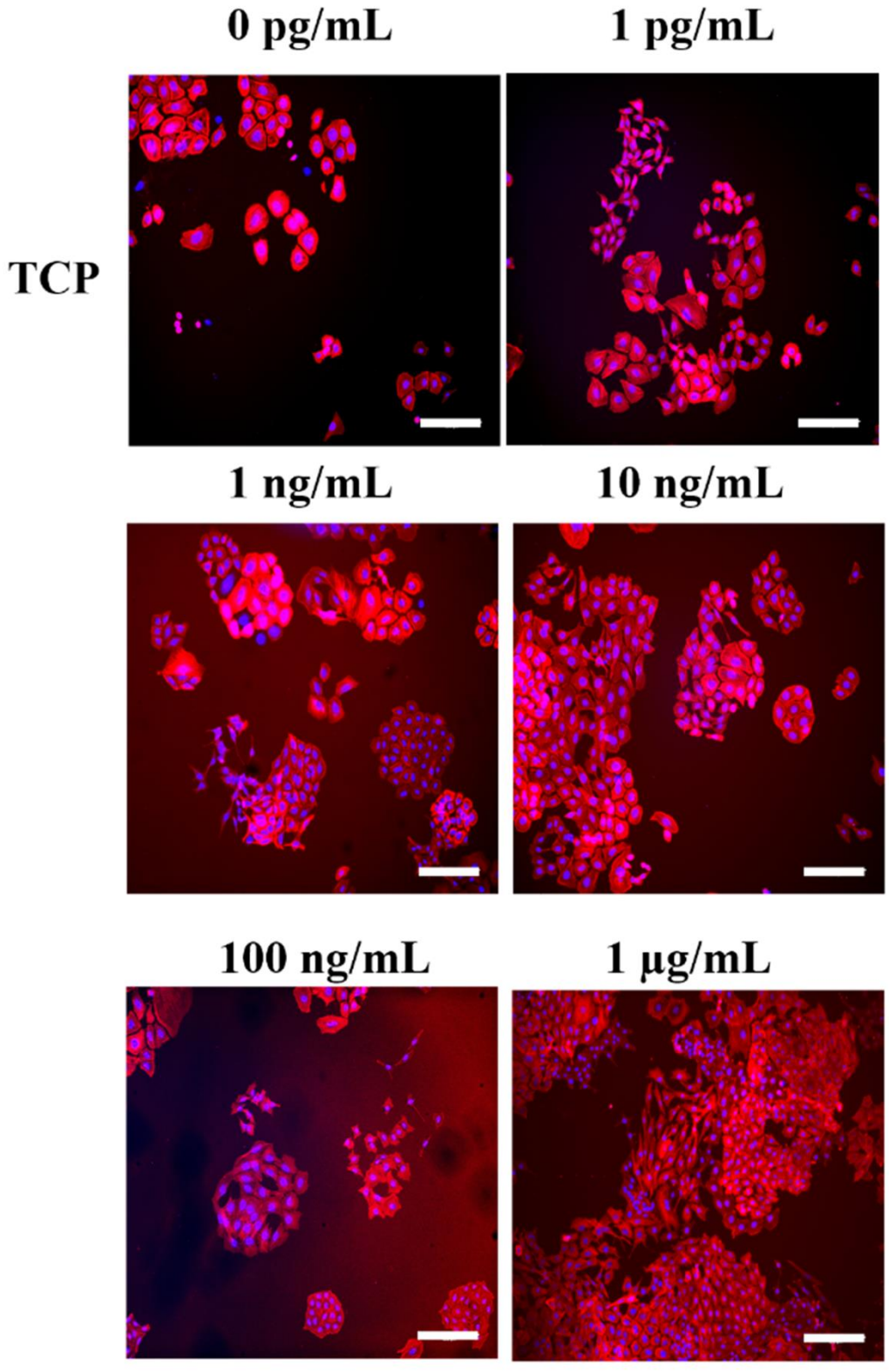

Figure 60. Epifluorescence images of PC12 adh neuronal cells cultured TCP with different concentrations of NGF. F-actin filaments are stained in red (phalloidin TRITC)., nuclei are stained in blue (DAPI). Scale bar = 200 µm.

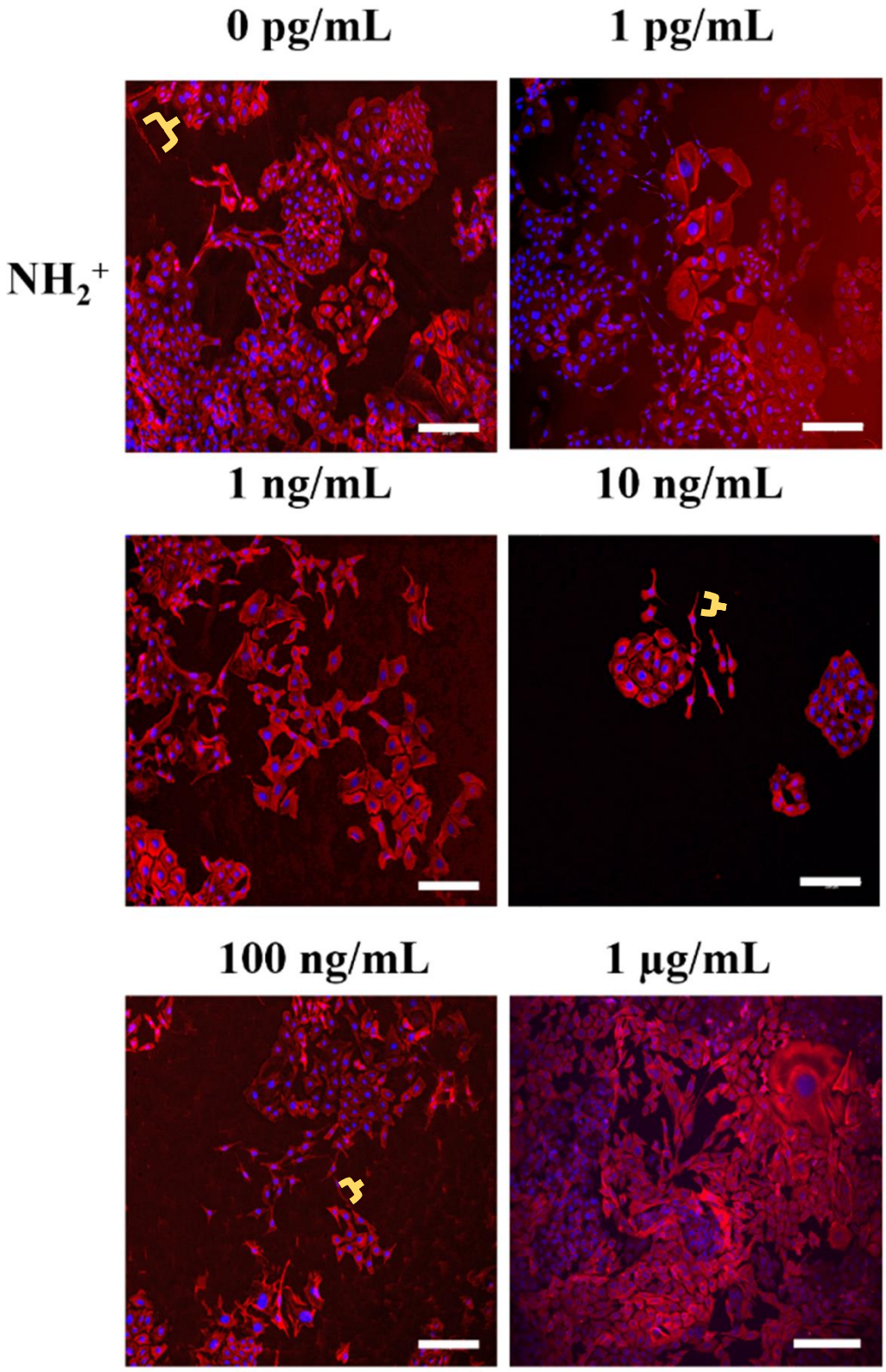

Figure 61. Epifluorescence images of PC12 adh neuronal cells cultured onto NH_2^+ with different concentrations of NGF. F-actin filaments are stained in red (phalloidin TRITC)., nuclei are stained in blue (DAPI). Scale bar = 200 µm.

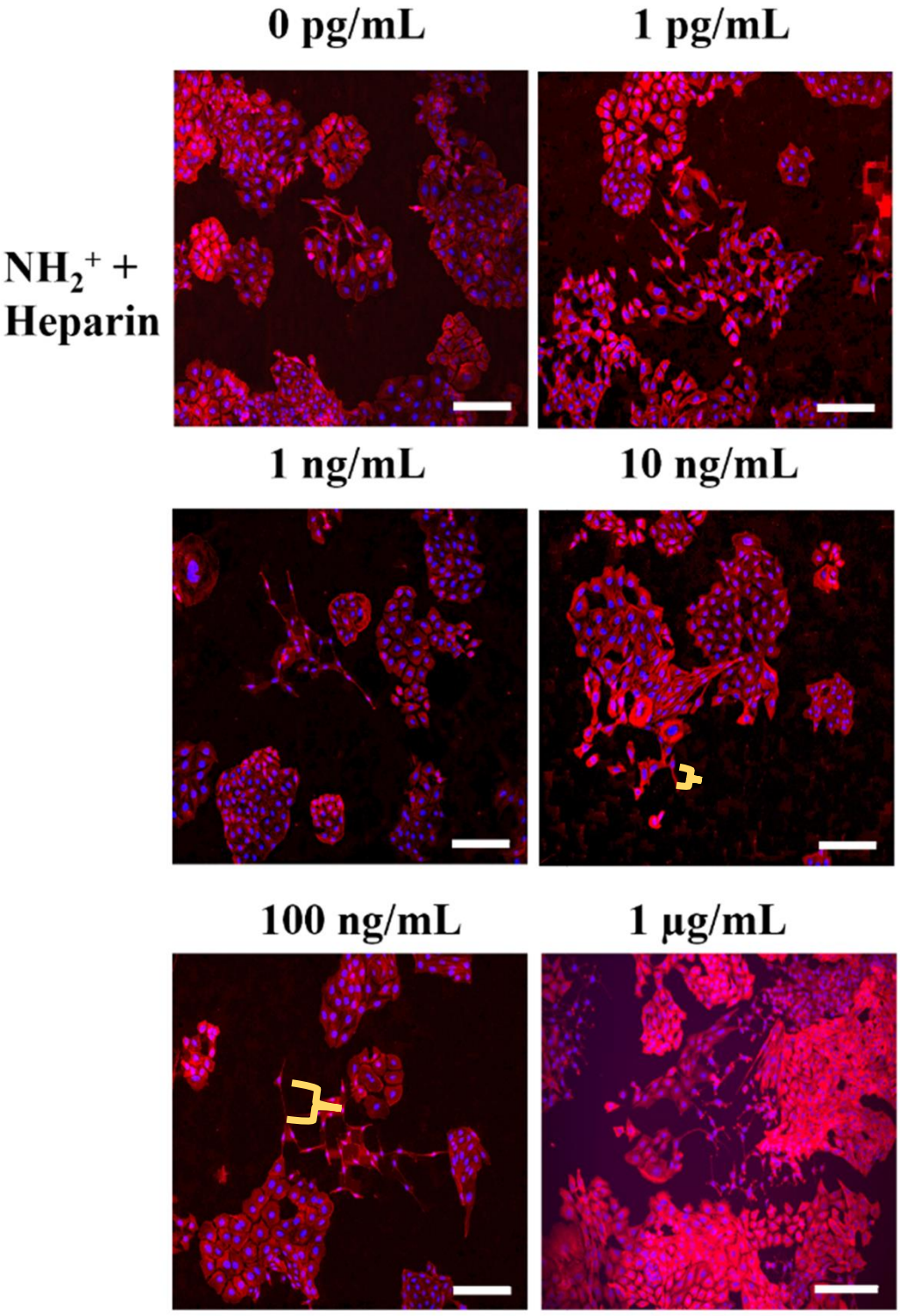

Figure 62. Epifluorescence images of PC12 adh neuronal cells cultured onto NH_2^+ + Heparin with different concentrations of NGF. F-actin filaments are stained in red (phalloidin TRITC)., nuclei are stained in blue (DAPI). Scale bar = 200 µm.

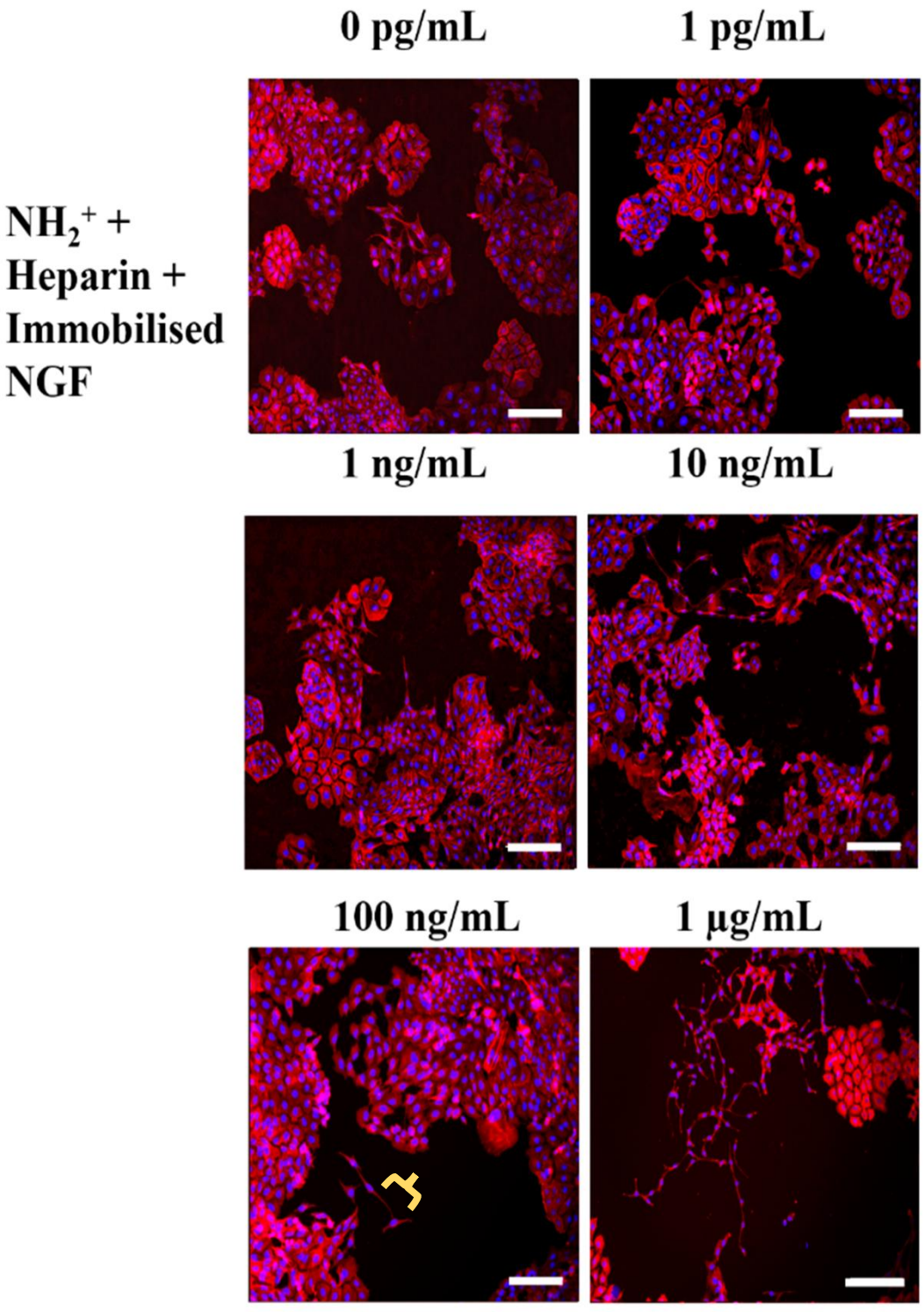

Figure 63. Epifluorescence images of PC12 adh neuronal cells cultured onto NH_2^+ + Heparin + Immobilised NGF with different concentrations of NGF. F-actin filaments are stained in red (phalloidin TRITC)., nuclei are stained in blue (DAPI). Scale bar = 200 µm.

The average neurite length of PC12 adh neuronal cells was calculated from images taken of PC12 adh neuronal cells cultured on TCP, NH_2^+, NH_2^+ + Heparin, and NH_2^+ + Heparin + Immobilised NGF. The longest average neurite length was 56 ± 20 µm for PC12 adh neuronal cells seeded on NH_2^+ + Heparin + Immobilised NGF at a concentration of 1 pg/mL. The shortest average neurite length was 23 ± 17 µm for neuronal cells cultured on TCP.

When PC12 adh neuronal cells were cultured on NH_2^+ with NGF in solution in culture medium, the average neurite length was significantly higher when compared to the average neurite length of neuronal cells seeded on TCP. Moreover, the average neurite length of PC12 adh cells cultured on NH_2^+ + Heparin + Immobilised NGF at 1 pg/mL and 10 ng/mL were significantly higher compared to the average neurite length of neuronal cells cultured on TCP and NH_2^+ + Heparin without NGF. In addition, even though the average neurite lengths of PC12 adh neuronal cells cultured on the NH_2^+ + Heparin bioactive surface did not show significant differences among the NGF concentrations, as seen in Figure 64, the average neurite length of neuronal cells seeded with NGF in solution at 1 pg/mL was 45 ± 6 µm, which was the largest neurite developed within this bioactive surface group.

Interestingly, PC12 adh neuronal cells cultured on NH_2^+ + Heparin + Immobilised NGF at 1 pg/mL showed a neurite outgrowth of 56 ± 20 µm, a length similar to the average neurite length developed by neuronal cells seeded on NH_2^+ + Heparin + Immobilised NGF at 10 ng/mL (55 ± 21 µm). These results suggested that a low immobilised concentration of NGF (1 pg/mL) stimulated a similar neurite outgrowth response as when a higher immobilised concentration of NGF (10 ng/mL) was used.

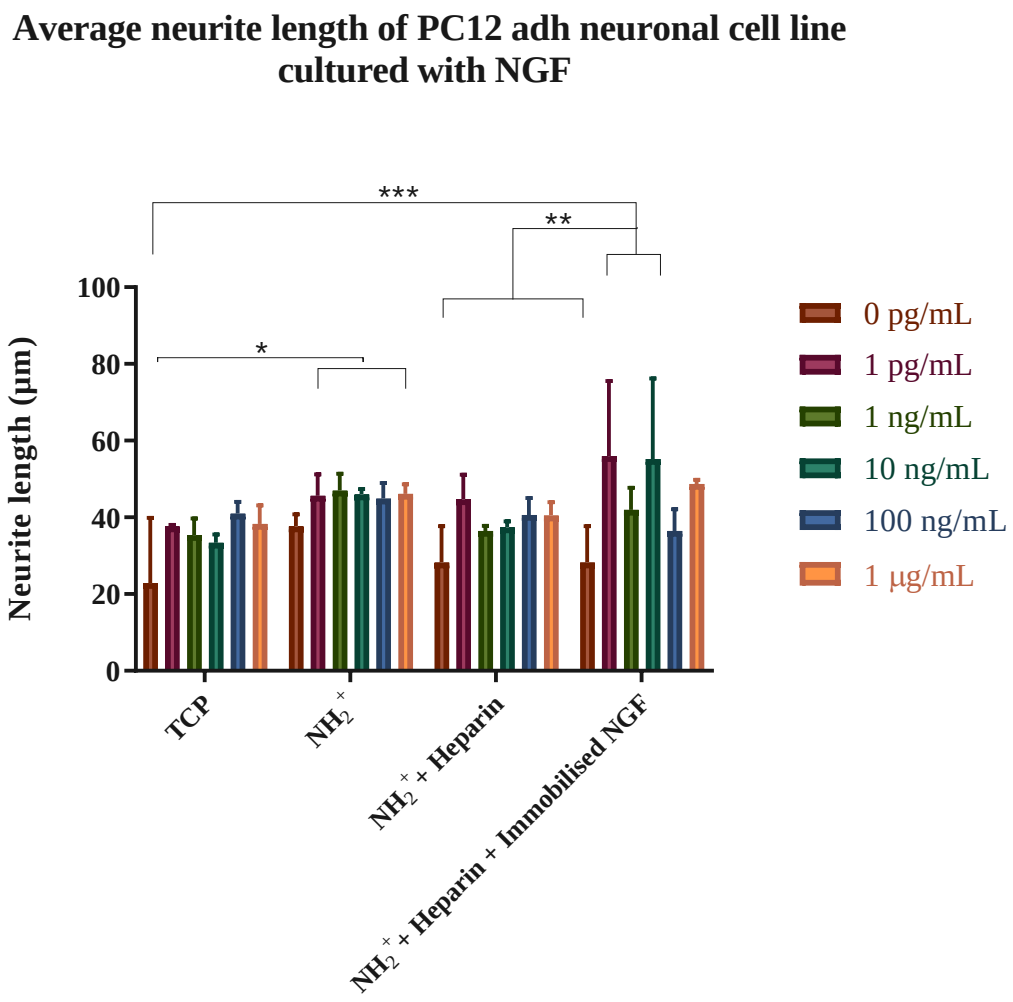

Figure 64. Average neurite length of PC12 adh neuronal cells when cultured on TCP, NH_2^+, NH_2^+ + Heparin (controls), and NH_2^+ + Heparin + Immobilised NGF (test). NGF was added to the bioactive surfaces at different concentrations. Two-way ANOVA statistical analysis was performed with Tukey procedure of multiple comparisons * $p < 0.05$, **$p<0.01$, *** $p< 0.001$, ***$p<0.0001$. Mean ± SD. N=3, n=3.

The average maximum neurite length of PC12 adh neuronal cells was measured and calculated from PC12 adh neuronal cells cultured on TCP, NH_2^+, NH_2^+ + Heparin, and NH_2^+ + Heparin + Immobilised NGF. The longest average maximum neurite length was 124 ± 28 µm for PC12 adh neuronal cells cultured on NH_2^+ + Heparin + Immobilised NGF at a concentration of 1 µg/mL. The shortest was 35 ± 25 µm for neuronal cells cultured on TCP, as shown in Figure 65. There was a significant difference in the average maximum neurite length among neuronal cells cultured on TCP in comparison to neuronal cells seeded on NH_2^+ with soluble NGF at a concentration of 1 µg/mL and NH_2^+ + Heparin + Immobilised NGF at 1 µg/mL. PC12 adh neuronal cells cultured on NH_2^+ with soluble NGF at 1 µg/mL and NH_2^+ + Heparin with soluble NGF at 1 µg/mL developed significantly larger maximum neurite length in comparison to their respective controls (NH_2^+ and NH_2^+ + Heparin respectively).

Moreover, PC12 adh neuronal cells seeded on NH_2^+ + Heparin + Immobilised NGF at 1 µg/mL had a significantly longer average maximum neurite length in comparison to NH_2^+ + Heparin, NH_2^+ + Heparin + Immobilised NGF at 10 ng/mL and NH_2^+ + Heparin + Immobilised NGF at 100 ng/mL. Furthermore, neuronal cells seeded on NH_2^+ + Heparin + Immobilised NGF at 1 pg/mL, developed significantly larger maximum neurite length in comparison to NH_2^+ + Heparin. Interestingly, the average maximum neurite length of PC12 adh neuronal cells seeded on NH_2^+ + Heparin + Immobilised NGF at 1 pg/mL was 112 ± 36 µm, whereas the average maximum neurite length of the neuronal cells when cultured on NH_2^+ + Heparin + Immobilised NGF at 1 µg/mL, and on NH_2^+ + Heparin with soluble NGF at 1 µg/mL was 123 ± 28 µm and 112 ± 49 µm respectively. These results suggest that by immobilising a low concentration of NGF onto the bioactive surface, the maximum neurite outgrowth could be similar to that stimulated by soluble NGF at 1 µg/mL. Furthermore, as there was no significant difference in average maximum neurite length between NH_2^+ + Heparin + Immobilised NGF at 1 pg/mL and NH_2^+ + Heparin + Immobilised NGF at 1 µg/mL, a similar result in average maximum neurite length could be expected, which supports the use of relatively low concentrations of immobilised NGF to encourage maximum neurite growth.

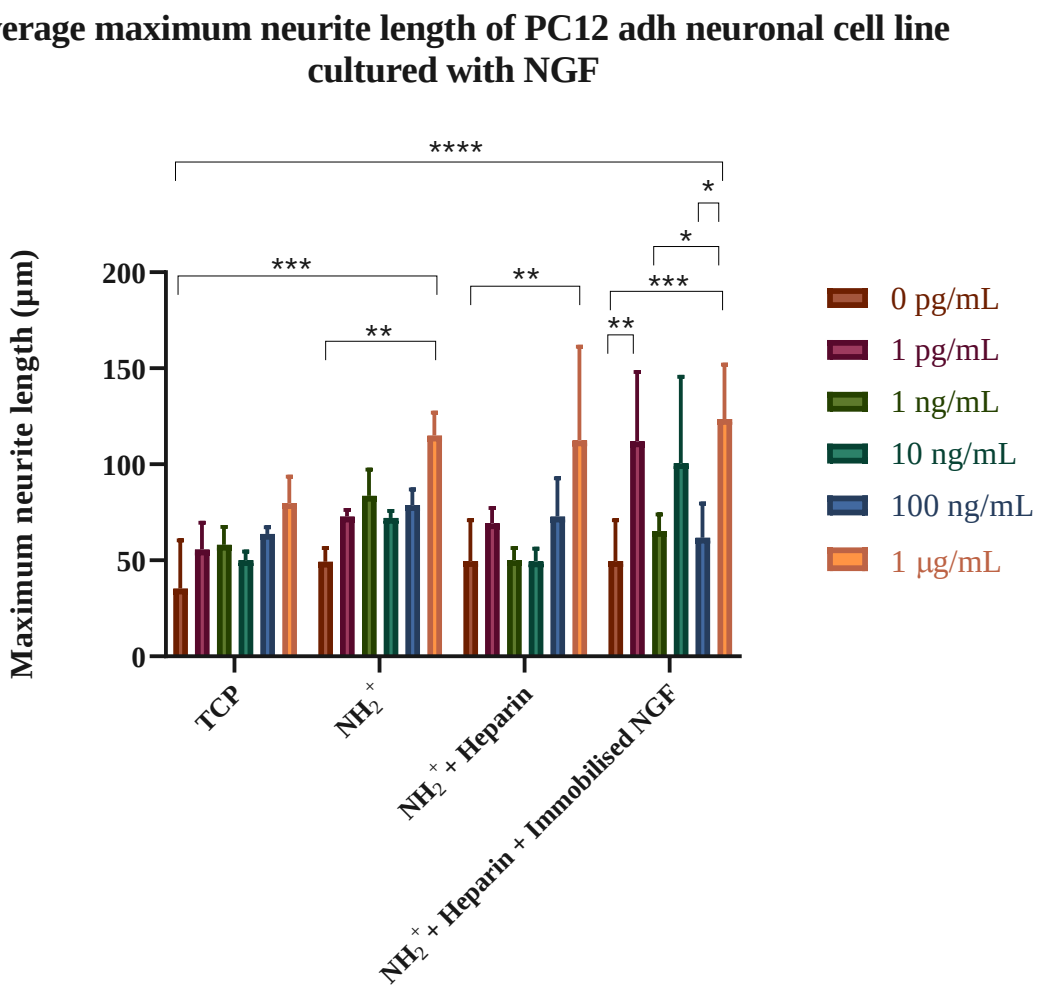

Figure 65. Average maximum neurite length of PC12 adh neuronal cells when cultured on TCP, NH_2^+, NH_2^+ + Heparin (controls), and NH_2^+ + Heparin + Immobilised NGF (test). NGF was added to the bioactive surfaces at different concentrations. Two-way ANOVA statistical analysis was performed with Tukey procedure of multiple comparisons *p< 0.05, **p<0.01, ***p<0.001, **** p<0.0001. Mean ± SD. N=3, n=3.

Percentage of neurons bearing neurites of PC12 adh neuronal cells was calculated from PC12 adh neuronal cells seeded on TCP, NH_2^+, NH_2^+ + Heparin, and NH_2^+ + Heparin + Immobilised NGF. The highest percentage of neurons bearing neurites was 8 ± 2% for PC12 neuronal cells cultured on NH_2^+ + Heparin + Immobilised NGF at a concentration of 1 µg/mL. The lowest percentage was 0.5 ± 0.4% for neuronal cells seeded on TCP. The percentage of neurons bearing neurites was significantly higher when PC12 adh cells were cultured on NH_2^+ with soluble NGF at 10 ng/mL in comparison to when they were seeded on TCP. As seen in Figure 66, even though for some groups there were no significant differences, the percentages of neurons bearing neurites was higher for neuronal cells cultured with NGF, either immobilised or in solution, in comparison to when they were seeded with no neurotrophin. For PC12 adh neuronal cells, the percentage of neurons bearing neurites was significantly higher when cultured on NH_2^+ + Heparin + Immobilised NGF at 1 µg/mL in comparison to when they were seeded on TCP (***p = 0.0008), NH_2^+ (**p = 0.006), NH_2^+ with NGF in solution at 1pg/mL (*p = 0.04), NH_2^+ + Heparin (**p = 0.0015), NH_2^+ + Heparin + Immobilised NGF at 1 pg/mL (**p = 0.0021), NH_2^+ + Heparin + Immobilised NGF at 10 ng/mL and NH_2^+ + Heparin + Immobilised NGF at 100 ng/mL (*p = 0.04 and *p = 0.028, respectively). These results suggested that the immobilisation of NGF at 1 µg/mL stimulated the development of more neurites in comparison to control and test groups.

Percentage of neurons bearing neurites in PC12 adh neuronal cell line cultured with NGF

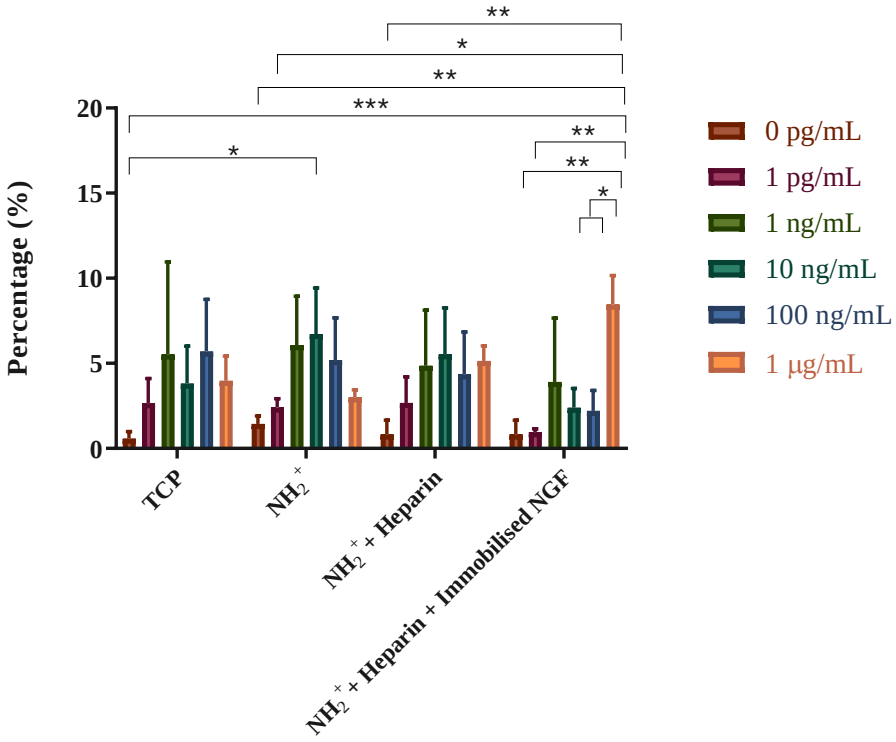

Figure 66. Percentage of neurons bearing neurites of PC12 adh neuronal cells when cultured on TCP, NH_2^+, NH_2^+ + Heparin (controls), and NH_2^+ + Heparin + Immobilised NGF (test). NGF was added to the bioactive surfaces at different concentrations. Two-way ANOVA statistical analysis was performed with Tukey procedure of multiple comparisons *p< 0.05, **p<0.01, ***p<0.001, ****p<0.0001. Mean ± SD. N=3, n=3.

6.4.2.2 Effects of Brain Derived Neurotrophic Factor

Metabolic activity was also evaluated for PC12 adh neuronal cells cultured on TCP, NH_2^+, NH_2^+ + Heparin, and NH_2^+ + Heparin + Immobilised BDNF. It was important to evaluate how the neuronal cells responded when cultured on the different surfaces with BDNF at different concentrations, either in solution or immobilised. As shown in Figure 67, after 5 days of culture, the metabolic activity of tPC12 adh neuronal cells was decreased on all surfaces when cultured with BDNF at a concentration of 1 µg/mL, both in solution or immobilised.

The metabolic activity of PC12 adh neuronal cells was relatively lower when they were cultured on TCP than when they were seeded on NH_2^+, NH_2^+ + Heparin, and NH_2^+ + Heparin + Immobilised BDNF. When PC12 neuronal cells were cultured on NH_2^+ with soluble BDNF at a concentration of 100 ng/mL, the metabolic activity was significantly higher when compared to neuronal cells seeded on NH_2^+ with BDNF in solution at a concentration of 1 µg/mL and TCP with BDNF in solution at 1 µg/mL. Moreover, when PC12 neuronal cells were cultured on NH_2^+ + Heparin + Immobilised BDNF at 1 pg/mL, the metabolic activity was significantly higher in comparison to when the neuronal cells were seeded on TCP, TCP with BDNF at 1 pg/mL, TCP with BDNF at 1 ng/mL, TCP with BDNF at 10 ng/mL and NH_2^+ + Heparin + Immobilised BDNF at 1 µg/mL.

In addition, the metabolic activity was significantly higher for PC12 adh neuronal cells when cultured on NH_2^+ + Heparin + Immobilised BDNF at 1 ng/mL, NH_2^+ + Heparin + Immobilised BDNF at 10 ng/mL and NH_2^+ + Heparin + Immobilised BDNF at 100 ng/mL in comparison to when they were seeded on NH_2^+ + Heparin + Immobilised BDNF at 1 µg/mL. Furthermore, when PC12 adh neuronal cells were seeded on NH_2^+ + Heparin + Immobilised BDNF at a concentration from 1 pg/mL to 100 ng/mL, the metabolic activity was significantly higher in comparison when the neuronal cells were seeded on TCP with BDNF in solution at 1 µg/mL.

Overall, these results suggested that the concentration of BDNF of 1 ug/mL was too high for PC12 adh neuronal cells to continue to be highly active after 5 days in culture. Nevertheless, they were still metabolically active. Furthermore, it did not indicate that

the bioactive surface or the BDNF were cytotoxic. Moreover, when BDNF at 1 pg/mL was immobilised, the metabolic activity of the cells increased significantly after 5 days in culture.

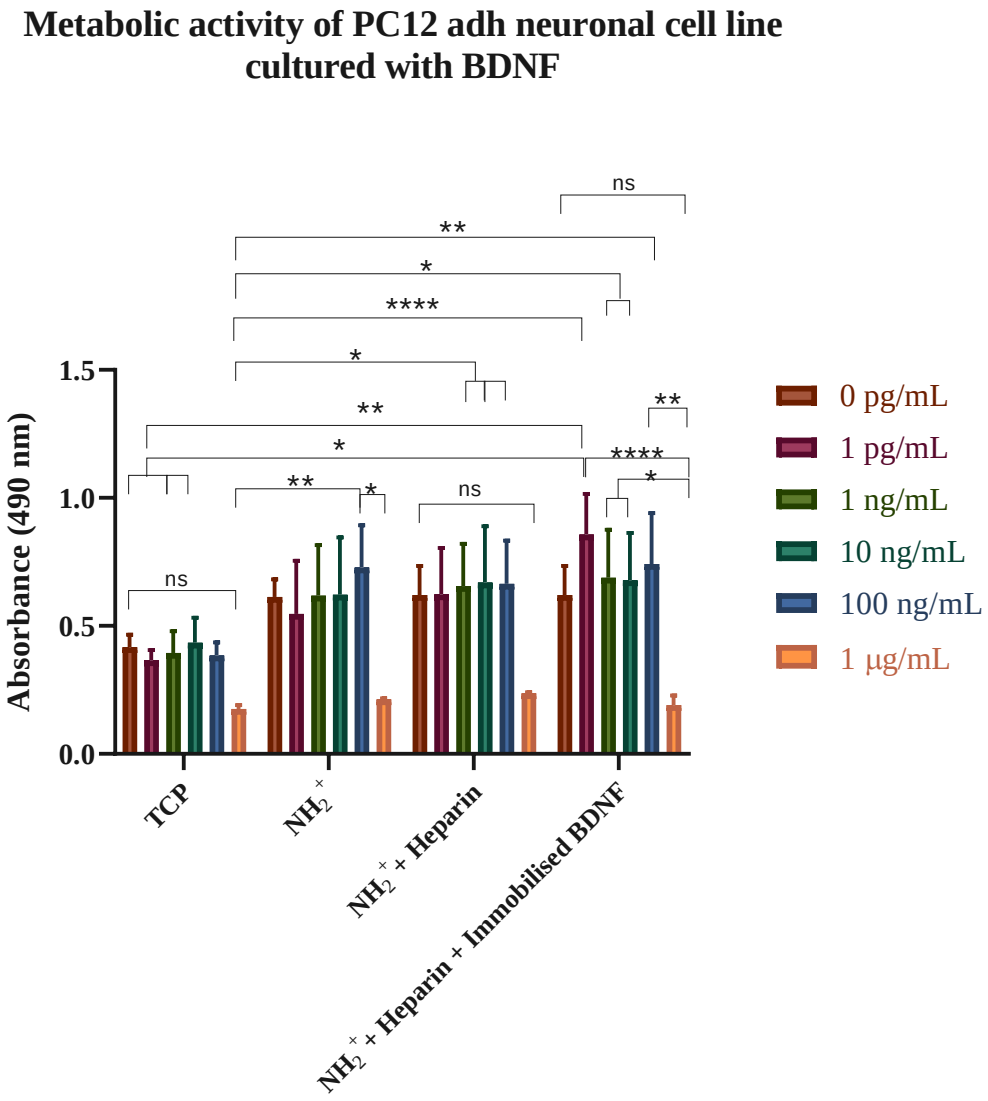

Figure 67. Metabolic activity of PC12 adh neuronal cells cultured on different bioactive surfaces with BDNF at different concentrations. Metabolic activity was measured at day 5, with MTS assay. BDNF was present in culture medium in TCP, NH_2^+ and NH_2^+ + Heparin (controls). BDNF was immobilised on NH_2^+ + Heparin (test). Two-way ANOVA statistical analysis was performed with Tukey procedure of multiple comparisons *p< 0.05, **p<0.01, ***p< 0.001, ****p<0.0001. Mean ± SD. N=3, n=3.

Figure 68, Figure 69, Figure 70, Figure 71 show PC12 adh neuronal cells cultured on different bioactive surfaces (TCP, NH_2^+, NH_2^+ + Heparin, and NH_2^+ + Heparin + Immobilised BDNF respectively) at different concentrations of BDNF. Developed neurites can be seen in images taken from when the cells were cultured with BDNF, with some of them highlighted with a yellow brace. DAPI was used to stain nuclei; phalloidin TRITC was used to stain the f-actin filaments of the cytoskeleton of the neuron, which includes the neurite. A high number of neurites developed when PC12 adh neuronal cells were seeded with BDNF at 1 µg/mL. However, when neuronal cells were seeded on NH_2^+ + Heparin + Immobilised BDNF at 1 pg/mL longer neurites were developed. These images are representative of average neurite length.

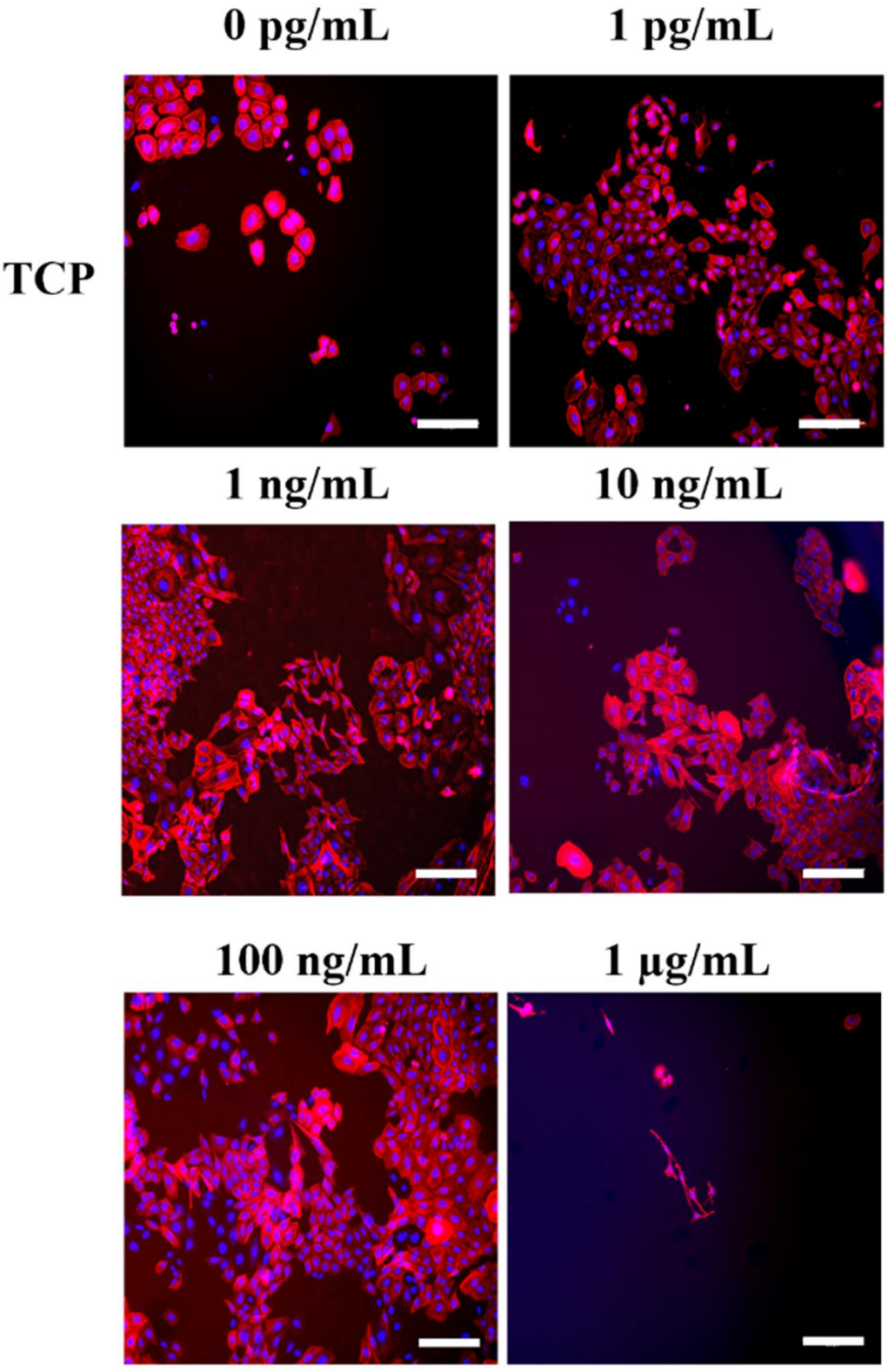

Figure 68. Epifluorescence images of PC12 adh neuronal cells cultured onto TCP with different concentrations of BDNF. F-actin filaments are stained in red (phalloidin TRITC)., nuclei are stained in blue (DAPI). Scale bar = 200 µm.

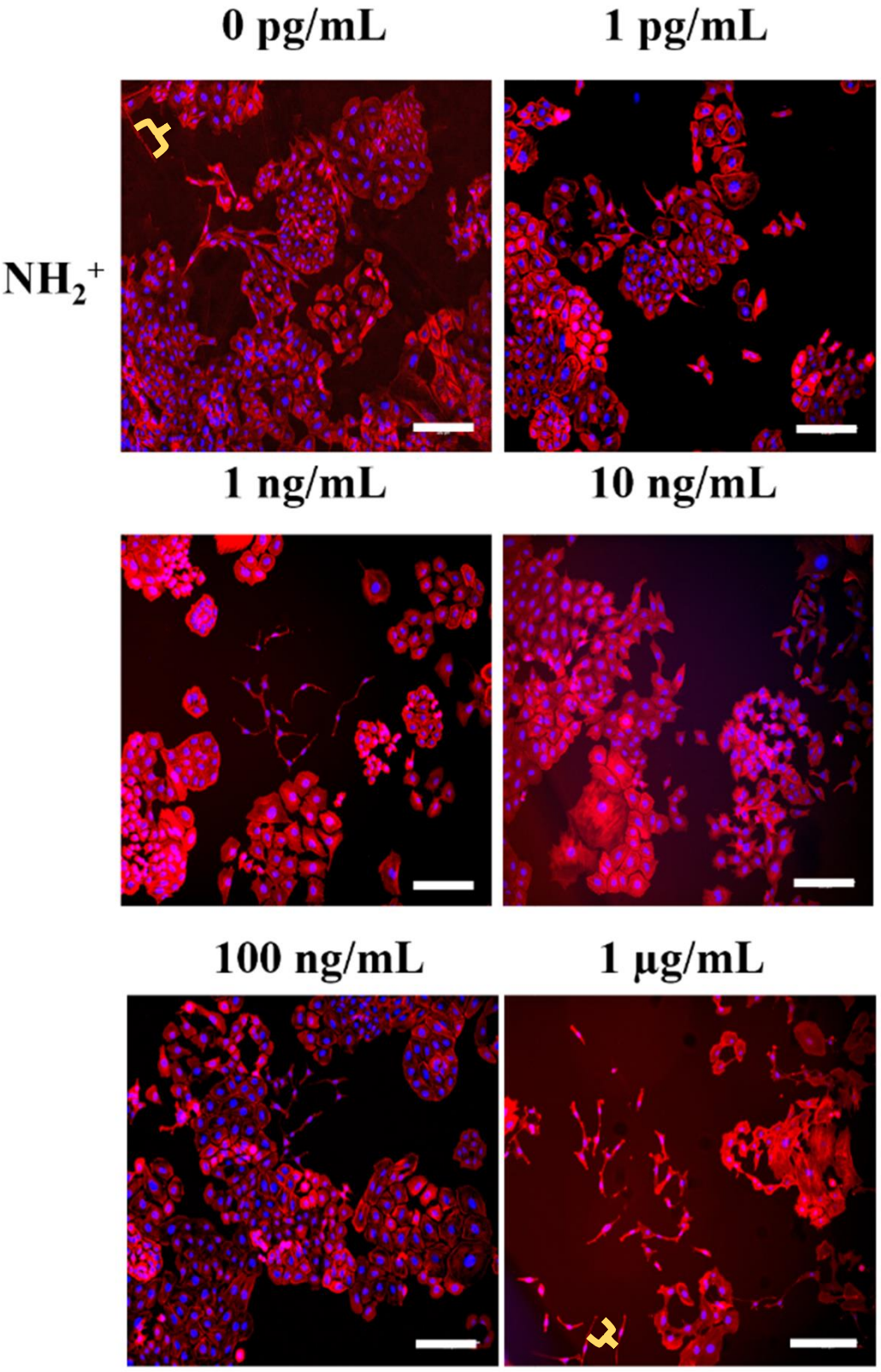

Figure 69. Epifluorescence images of PC12 adh neuronal cells cultured onto NH_2^+ with different concentrations of BDNF. F-actin filaments are stained in red (phalloidin TRITC)., nuclei are stained in blue (DAPI). Scale bar = 200 µm.

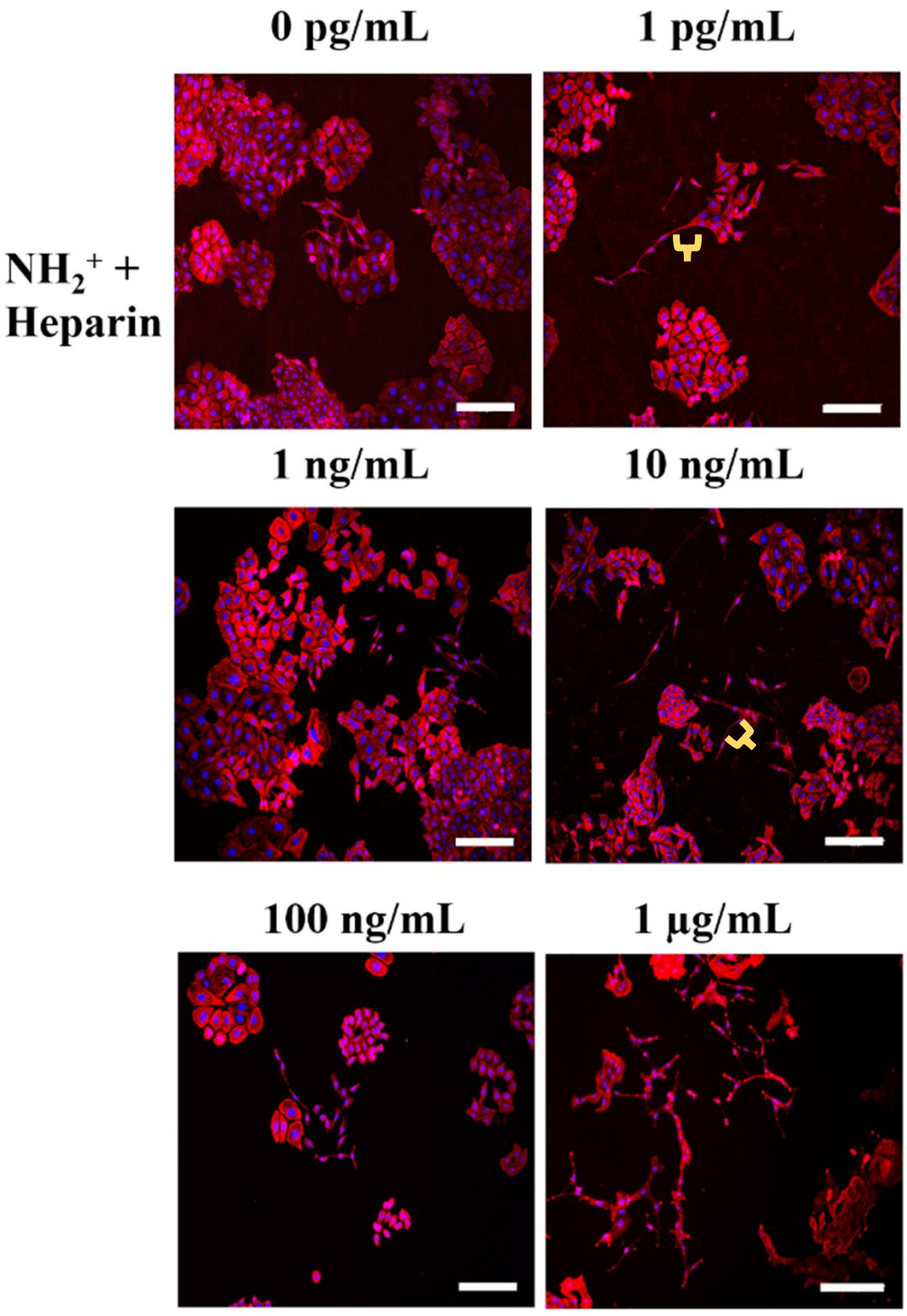

Figure 70. Epifluorescence images of PC12 adh neuronal cells cultured onto NH_2^+ + Heparin with different concentrations of BDNF. F-actin filaments are stained in red (phalloidin TRITC)., nuclei are stained in blue (DAPI). Scale bar = 200 µm.

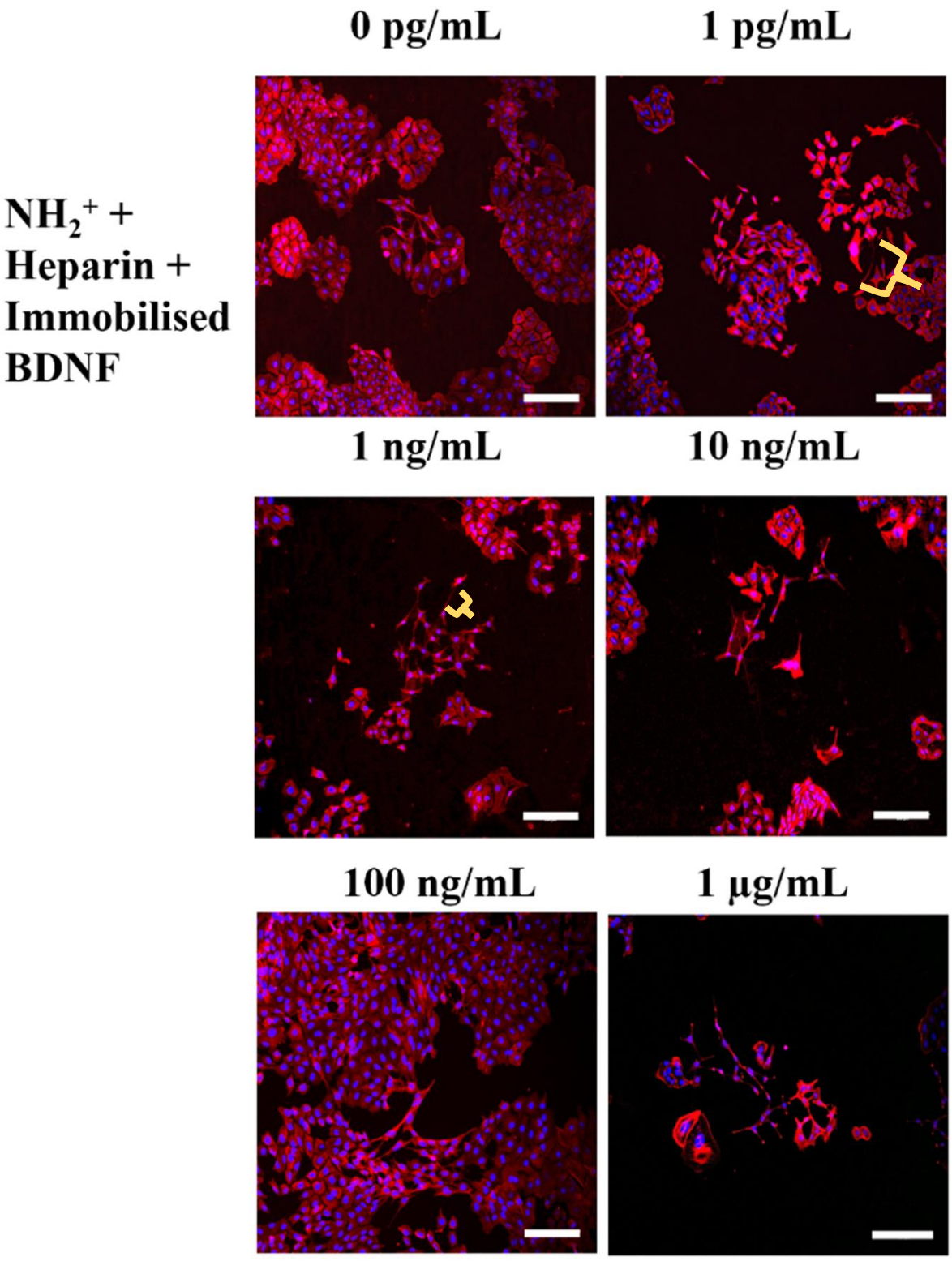

Figure 71. Epifluorescence images of PC12 adh neuronal cells cultured onto NH_2^+ + Heparin + Immobilised BDNF with different concentrations of BDNF. F-actin filaments are stained in red (phalloidin TRITC)., nuclei are stained in blue (DAPI). Scale bar = 200 µm.

The average neurite length of PC12 adh neuronal cells was calculated from PC12 adh neuronal cells seeded on TCP, NH_2^+, NH_2^+ + Heparin, and NH_2^+ + Heparin + Immobilised BDNF. The longest average neurite length was 61 ± 21 µm for PC12 adh neuronal cells cultured on NH_2^+ + Heparin + Immobilised BDNF at a concentration of 100 ng/mL, as seen in Figure 72. The shortest average neurite length was 23 ± 17 µm for neuronal cell seeded on TCP. Interestingly, the delivery of BDNF by immobilisation on the bioactive surface stimulated significant neurite outgrowth, either by immobilising 1 pg/mL (56 ± 16 µm) or immobilising 100 ng/mL (61 ± 21 µm). The presence of this neurotrophin in solution with the bioactive surface or TCP did not encourage any significant neurite growth. Moreover, the immobilisation of BDNF at 1 ng/mL, 10 ng/mL or 1 µg/mL, did not reveal any significant difference in neurite outgrowth.

Furthermore, even though the average neurite length was longer for neuronal cells seeded on NH_2^+ + Heparin + Immobilised BDNF at 100 ng/mL than in NH_2^+ + Heparin + Immobilised BDNF at 1 pg/mL, no significant difference was found between these two groups. These results suggested that using a relatively low concentration of immobilised BDNF, such as 1 pg/mL, encouraged neurite outgrowth similarly to the stimuli of using immobilised BDNF at 100 ng/mL.

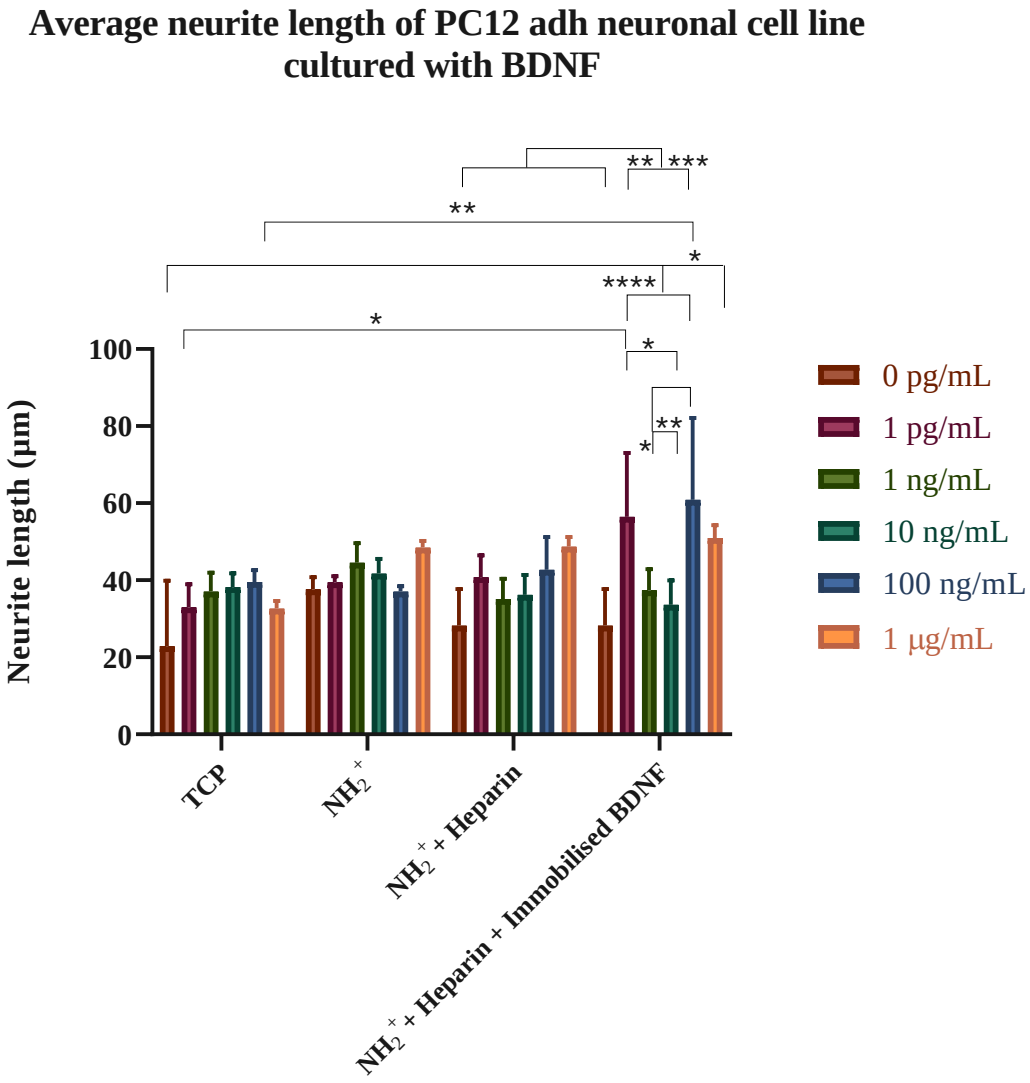

Figure 72. Average neurite length of PC12 adh neuronal cells when cultured, after 5 days, on TCP, NH_2^+, NH_2^+ + Heparin (controls), and NH_2^+ + Heparin + Immobilised BDNF (test). BDNF was added to the bioactive surfaces at different concentrations. Two-way ANOVA statistical analysis was performed with Tukey procedure of multiple comparisons *p< 0.05, **p<0.01, ***p< 0.001, ****p<0.0001. Mean ± SD. N=3, n=3.

The average maximum neurite length of PC12 adh neuronal cells was calculated from PC12 adh neuronal cells seeded on TCP, NH_2^+, NH_2^+ + Heparin, and NH_2^+ + Heparin + Immobilised BDNF. The largest average maximum neurite length was 144 ± 29 µm for PC12 adh neuronal cells cultured on NH_2^+ + Heparin + Immobilised BDNF at a concentration of 1 pg/mL. The shortest average maximum neurite length was 35 ± 25 µm for PC12 adh neuronal cells seeded on TCP. As shown in Figure 73, when neuronal cells were cultured either on NH_2^+ with BDNF in solution at a concentration of 1 µg/mL or NH_2^+ + Heparin with BDNF at 1 µg/mL, the average maximum neurite length was significantly different from the average maximum neurite lengths of neuronal cells cultured on TCP, NH_2^+ and NH_2^+ + Heparin.

These results suggested that the bioactive surfaces, NH_2^+ and NH_2^+ + Heparin, with BDNF in solution at 1µg/mL encouraged maximum neurite outgrowth. Nevertheless, interestingly, bioactive surface NH_2^+ + Heparin + Immobilised BDNF at 1 pg/mL stimulated the largest maximum neurite length, measured as 144 ± 29 µm. This value was not significantly different from the average maximum neurite length developed from the stimulation of NH_2^+ with soluble BDNF at 1 µg/mL, NH_2^+ + Heparin with soluble BDNF at 1 µg/mL, and NH_2^+ + Heparin + Immobilised BDNF at 1 µg/mL, which suggested that immobilisation of BDNF at 1 pg/mL encouraged the average maximum neurite outgrowth similarly to when BDNF was in solution at a higher concentration. Therefore, immobilisation of a relatively low concentration of BDNF on the bioactive surface stimulated a similar response in PC12 adh neuronal cells, compared to when the neurotrophin was delivered in solution at a higher concentration.

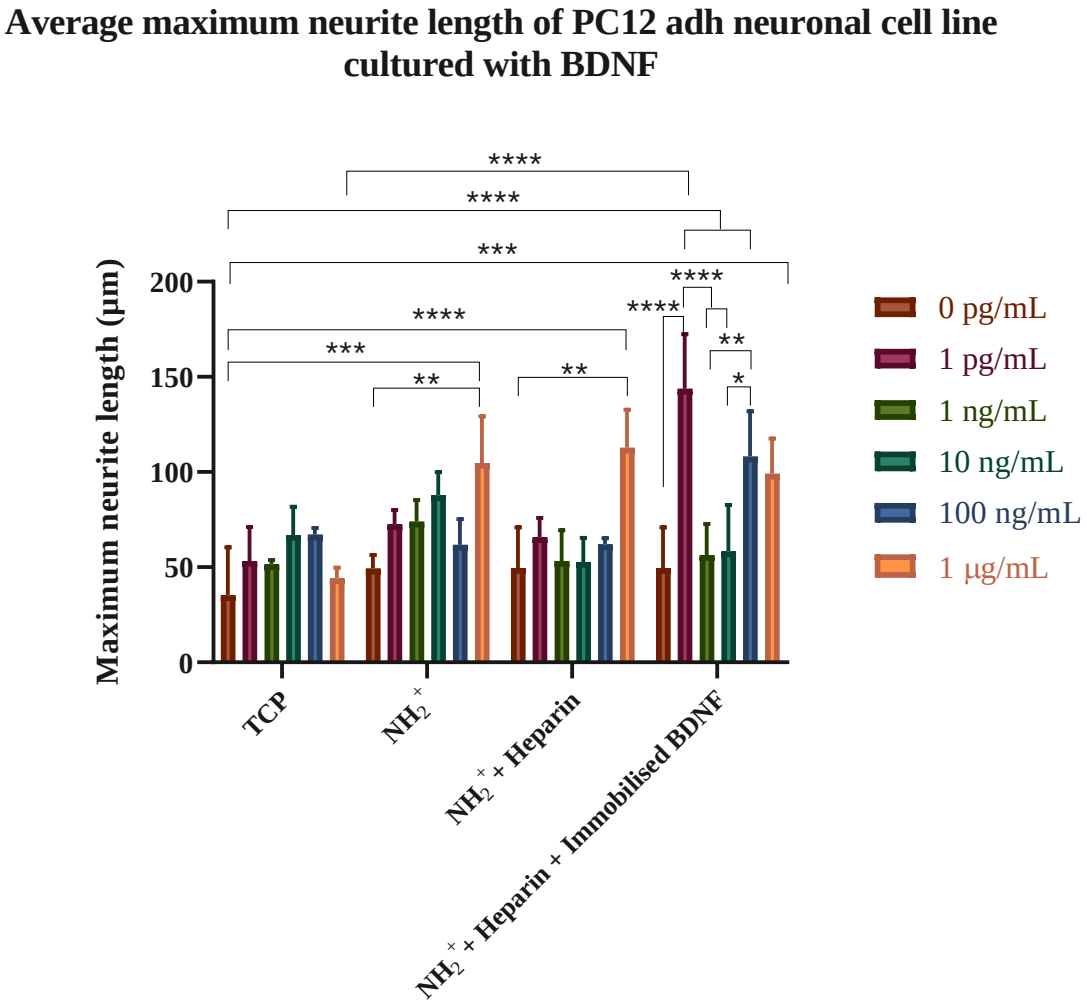

Figure 73. Average maximum neurite length of PC12 adh neuronal cells when cultured on TCP, NH_2^+, NH_2^+ + Heparin (controls), and NH_2^+ + Heparin + Immobilised BDNF (test). BDNF was added to the bioactive surfaces at different concentrations. Two-way ANOVA statistical analysis was performed with Tukey procedure of multiple comparisons *p< 0.05, **p<0.01, ***p< 0.001, ****p<0.0001. Mean ± SD. N=3, n=3.

The percentage of neurons bearing neurites of PC12 adh neuronal cells was calculated from PC12 adh neuronal cells cultured on TCP, NH_2^+, NH_2^+ + Heparin, and NH_2^+ + Heparin + Immobilised BDNF. Disregarding the surface where the neuronal cells were cultured, the concentration of BDNF that encouraged the highest percentage of neurons bearing neurites was 1 µg/mL. The percentages were 10 ± 6% (TCP), 14 ± 2% (NH_2^+), 13 ± 0.4% (NH_2^+ + Heparin), and 14 ± 3% (NH_2^+ + Heparin + Immobilised BDNF). All these groups were significantly different from other surfaces using BDNF at a concentration below 1 µg/mL, as observed in Figure 74. These results suggested that using BDNF at a concentration of 1 µg/mL encouraged the development of neurites.

Percentage of neurons bearing neurites in PC12 adh neuronal cell line cultured with BDNF

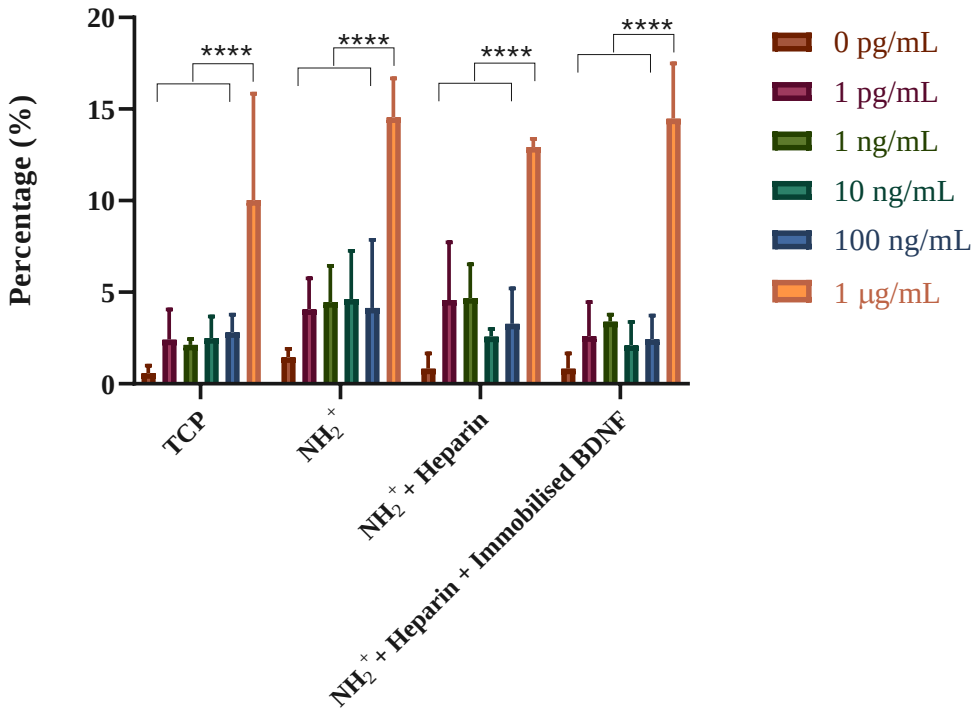

Figure 74. Percentage of neurons bearing neurites of PC12 adh neuronal cells when cultured on TCP, NH_2^+, NH_2^+ + Heparin (controls), and NH_2^+ + Heparin + Immobilised BDNF (test). BDNF was added to the bioactive surfaces at different concentrations. Two-way ANOVA statistical analysis was performed with Tukey procedure of multiple comparisons *p< 0.05, **p<0.01, ***p< 0.001, ****p<0.0001. Mean ± SD. N=3, n=3.

6.4.2.3 Effects of Nerve Growth Factor plus Brain Derived Neurotrophic Factor

MTS assay was used to assess the metabolic activity of PC12 adh neuronal cells cultured on TCP, NH_2^+, NH_2^+ + Heparin, and NH_2^+ + Heparin + Immobilised NGF plus BDNF. It was important to evaluate how the neuronal cells responded when cultured on the different bioactive surfaces with NGF plus BDNF at different concentrations, either in solution or immobilised. The metabolic activity of PC12 adh neuronal cells when cultured on NH_2^+ + Heparin with soluble BDNF at 1 µg/mL, and on NH_2^+ + Heparin + Immobilised NGF plus BDNF at a concentration of 1 µg/mL was significantly higher compared to TCP. Moreover, the metabolic activity of the neuronal cells was significantly higher when seeded on NH_2^+ + Heparin with soluble BDNF at 1 µg/mL compared to when cultured on TCP with BDNF at 1 pg/mL and TCP with BDNF at 100 ng/mL, as shown in Figure 75. These results suggested that when NGF and BDNF were used together, the metabolic activity of PC12 adh neuronal cells increased, even though for some conditions the increase was slight, and no significant differences were found.

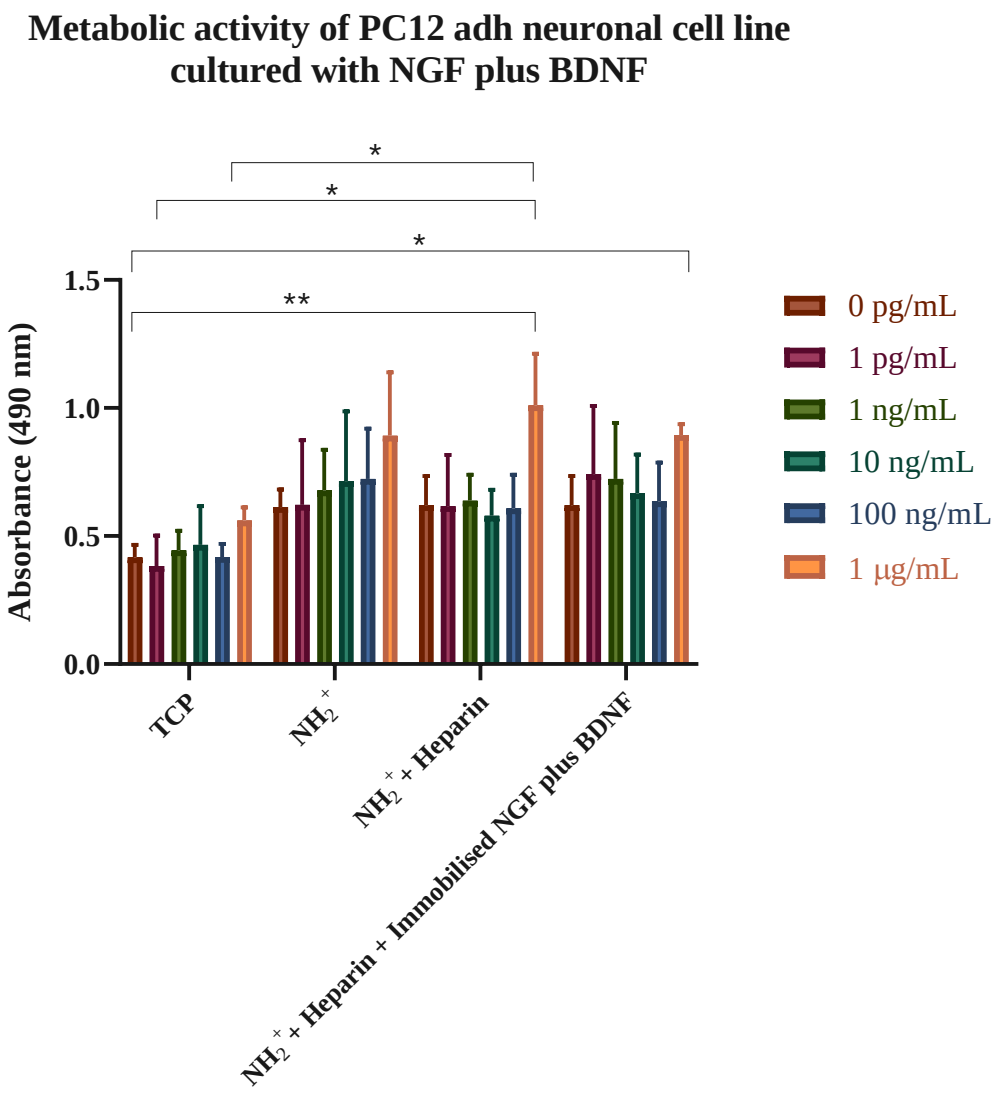

Figure 75. Metabolic activity of PC12 adh neuronal cells, measured with MTS assay at day 5, cultured on different bioactive surfaces with NGF plus BDNF at different concentrations. NGF plus BDNF were present in culture medium in TCP, NH_2^+ and NH_2^+ + Heparin (controls). NGF plus BDNF was immobilised on NH_2^+ + Heparin (test). Two-way ANOVA statistical analysis was performed with Tukey procedure of multiple comparisons *p < 0.05, **p<0.01, ***p< 0.001, ****p<0.0001. Mean ± SD. N=3, n=3.

Figure 76, Figure 77, Figure 78, Figure 79 show PC12 adh neuronal cells cultured on different bioactive surfaces (TCP, NH_2^+, NH_2^+ + Heparin, and NH_2^+ + Heparin + Immobilised NGF respectively) at different concentrations of NGF plus BDNF. Developed neurites can be seen in images taken from when the cells were cultured with NGF plus BDNF, some of them are highlighted with a yellow brace. DAPI was used to stain nuclei; phalloidin TRITC was used to stain the f-actin filaments of the cytoskeleton of the neuron, which includes the neurite. Neurite outgrowth was significantly increased when PC12 adh neuronal cells were seeded on bioactive surfaces immobilised with NGF plus BDNF at 1 ng/mL and 1 µg/mL. Moreover, more neurites developed when PC12 adh neuronal cells were cultured with NGF plus BDNF in solution in culture medium at 1 µg/mL. These images are representative of average neurite length.

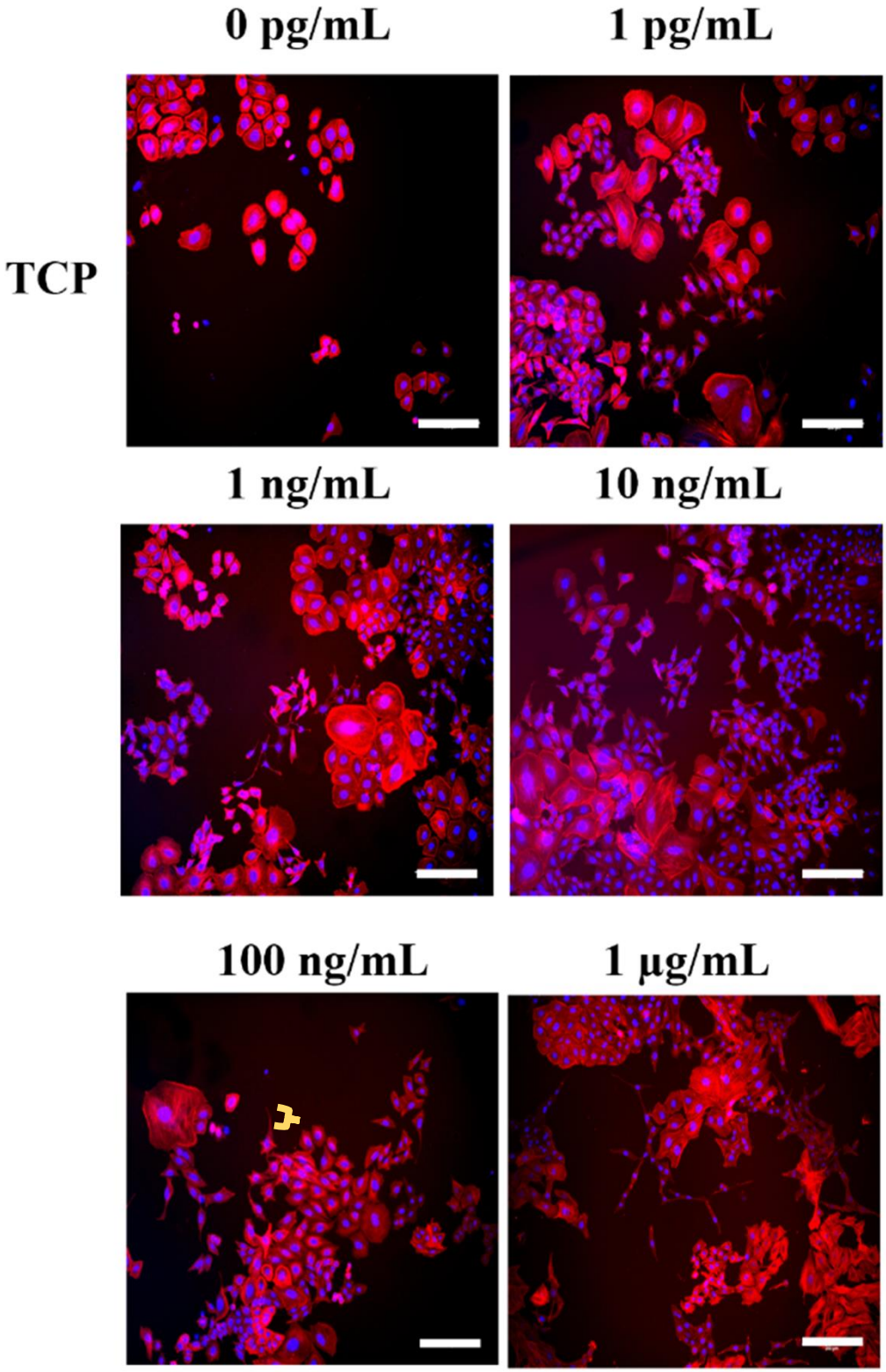

Figure 76. Epifluorescence images of PC12 adh neuronal cells cultured onto TCP with different concentrations of NGF plus BDNF. F-actin filaments are stained in red (phalloidin TRITC)., nuclei are stained in blue (DAPI). Scale bar = 200 µm.

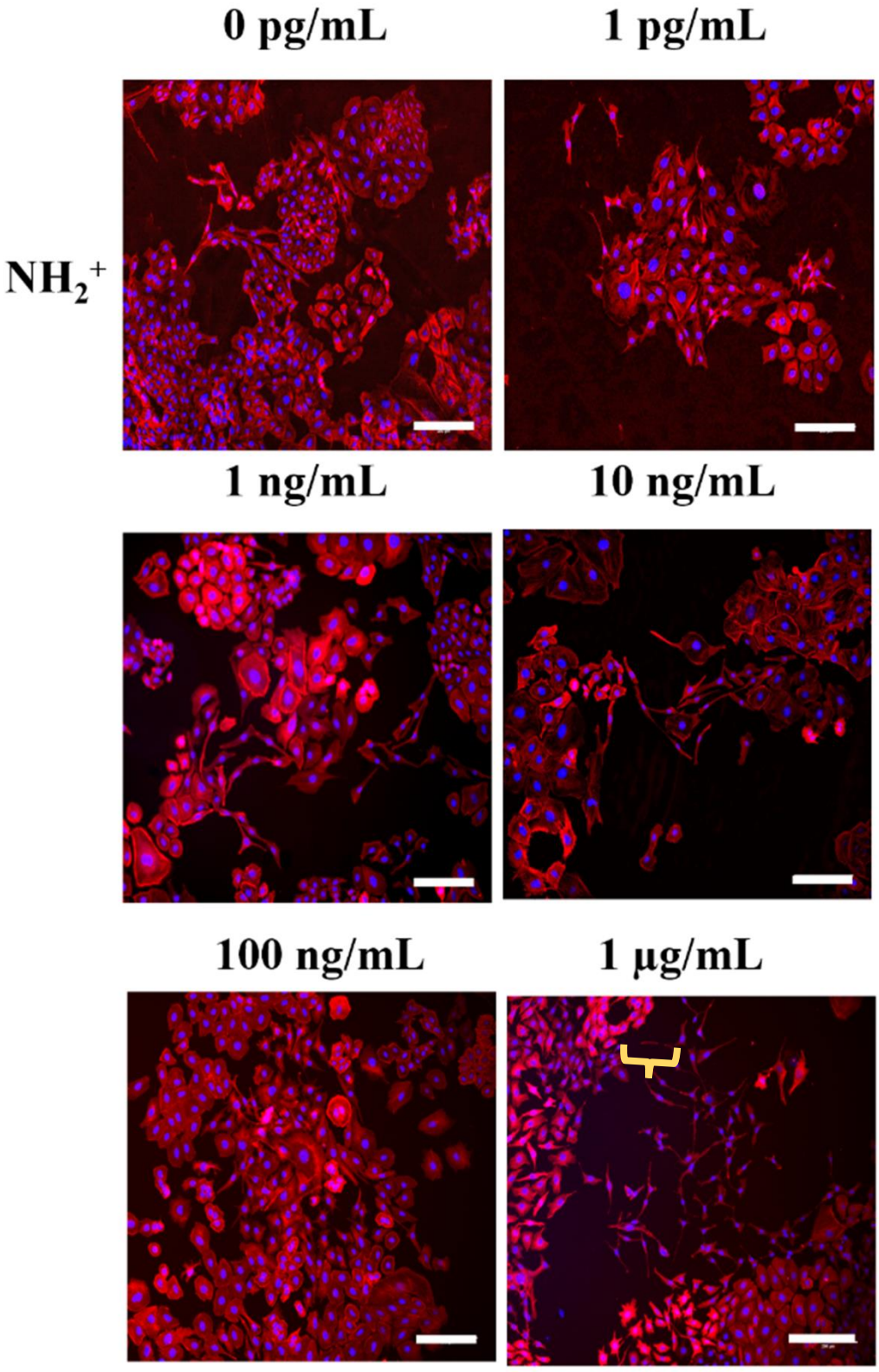

Figure 77. Epifluorescence images of PC12 adh neuronal cells cultured onto NH_2^+ with different concentrations of NGF plus BDNF. F-actin filaments are stained in red (phalloidin TRITC)., nuclei are stained in blue (DAPI). Scale bar = 200 µm.

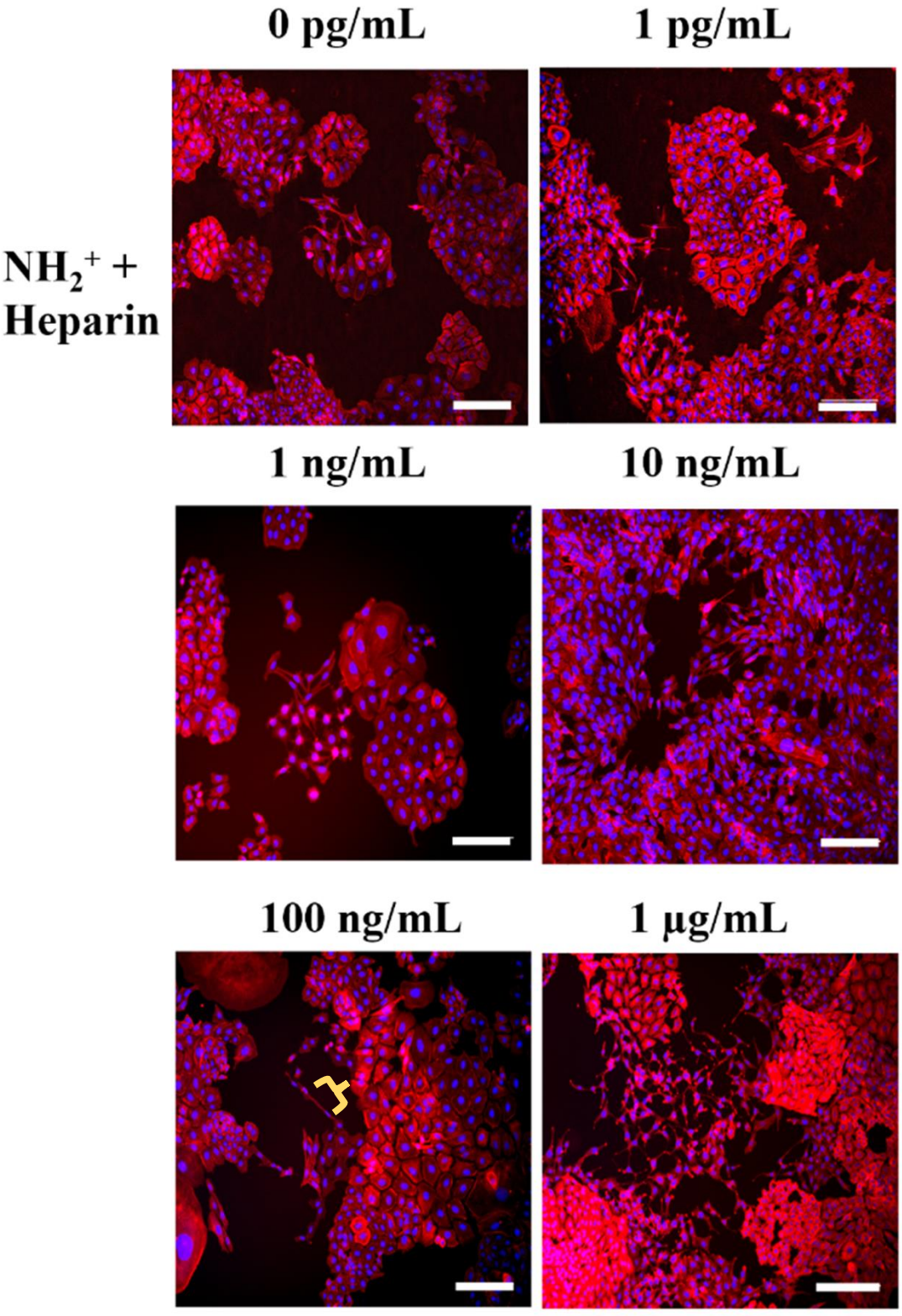

Figure 78. Epifluorescence images of PC12 adh neuronal cells cultured onto NH_2^+ + Heparin with different concentrations of NGF plus BDNF. F-actin filaments are stained in red (phalloidin TRITC)., nuclei are stained in blue (DAPI). Scale bar = 200 µm.

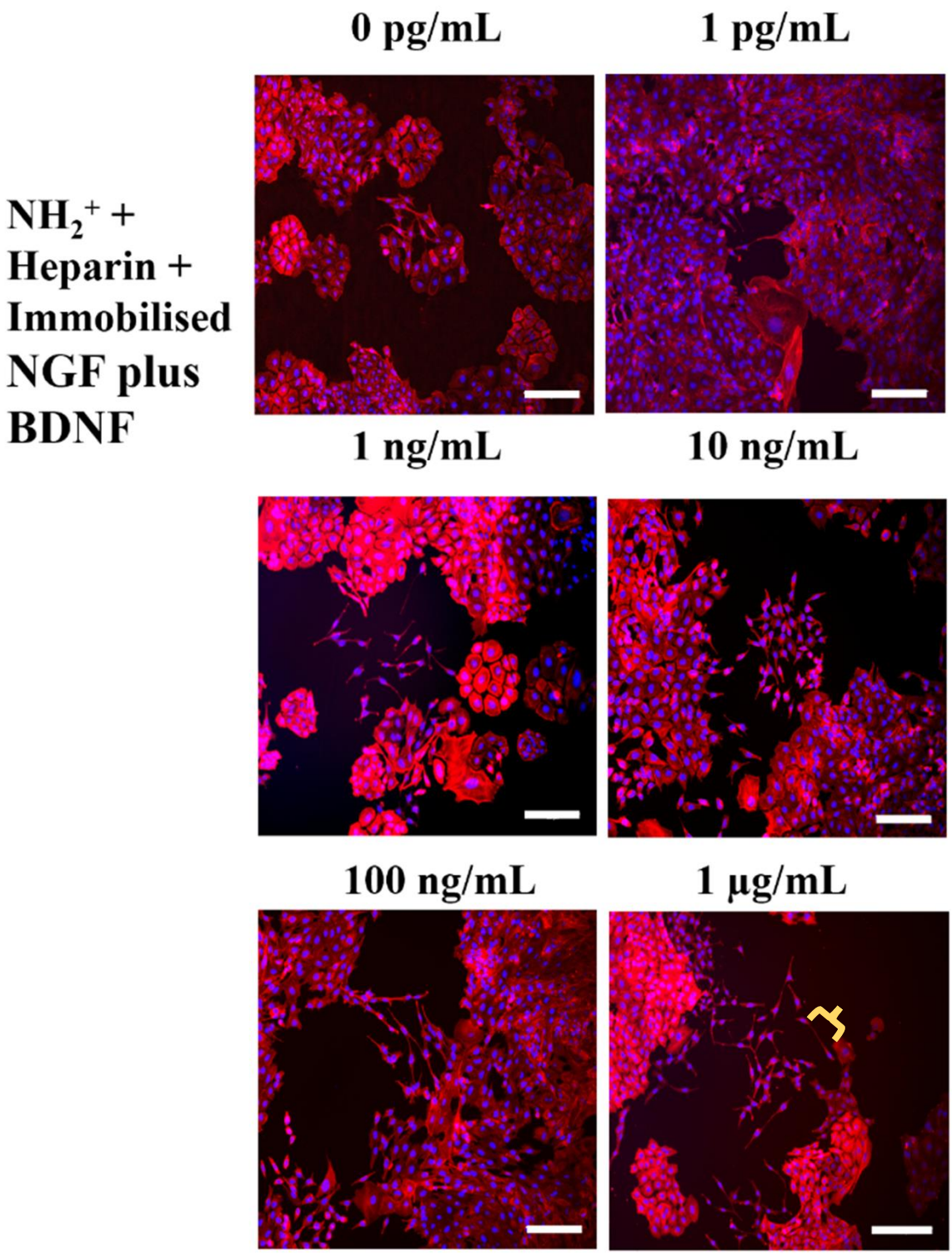

Figure 79. Epifluorescence images of PC12 adh neuronal cells cultured onto NH_2^+ + Heparin + Immobilised NGF plus BDNF with different concentrations of NGF plus BDNF. F-actin filaments are stained in red (phalloidin TRITC)., nuclei are stained in blue (DAPI). Scale bar = 200 µm.

Average neurite length of PC12 adh neuronal cells was calculated from PC12 adh neuronal cells cultured on TCP, NH_2^+, NH_2^+ + Heparin, and NH_2^+ + Heparin + Immobilised NGF plus BDNF. The longest average neurite length was 58 ± 9 µm for PC12 neuronal cells seeded on NH_2^+ with soluble NGF plus BDNF at a concentration of 1 µg/mL. The shortest average neurite length was 23 ± 17 µm for neuronal cells cultured on TCP.

The average neurite length of PC12 adh neuronal cells seeded on TCP was significantly shorter than those from the neuronal cells seeded on NH_2^+ with soluble NGF plus BDNF at 1 pg/mL, 1 ng/mL, 10 ng/mL, and 1 µg/mL, as shown in Figure 80. Furthermore, the averaged neurite length of TCP was also significantly shorter in comparison to NH_2^+ + Heparin with soluble NGF plus BDNF at 10 ng/mL, 100 ng/mL and 1 µg/mL. In addition, the average neurite length of neuronal cells cultured on TCP was significantly shorter than the average neurite length of neuronal cells seeded on NH_2^+ + Heparin + Immobilised NGF plus BDNF at 1 pg/mL, 1 ng/mL, 10 ng/mL, and 1 µg/mL.

Moreover, the average neurite length of PC12 adh neuronal cells was significantly longer when seeded on NH_2^+ + Heparin + Immobilised NGF plus BDNF at 1 ng/mL in comparison to the average neurite length of neuronal cells cultured on NH_2^+ + Heparin. Nevertheless, even though the average neurite length of PC12 adh neuronal cells was longer when seeded on NH_2^+ with soluble NGF plus BDNF at 1 µg/mL (58 ± 9 µm) in comparison to when they were cultured on NH_2^+ + Heparin + Immobilised NGF plus BDNF at 1 ng/mL (49 ± 9 µm) and NH_2^+ + Heparin + Immobilised NGF plus BDNF at 1 µg/mL (49 ± 2 µm), the difference was not significant.

These results suggested that immobilising NGF plus BDNF encouraged the growth of longer neurites in comparison to TCP control. Moreover, the immobilisation of NGF plus BDNF at 1 ng/mL and 1 µg/mL stimulated neurite outgrowth with similar length to when NGF plus BDNF was delivered in solution at 1 µg/mL in NH_2^+ surface. Furthermore, it is important to highlight that the immobilisation of NGF plus BDNF at a relative low concentration of 1 ng/mL encouraged the growth of neurites as long

as the ones stimulated by NH_2^+ with soluble NGF plus BDNF at 1 µg/mL and NH_2^+ + Heparin + Immobilised NGF plus BDNF at 1 µg/mL.

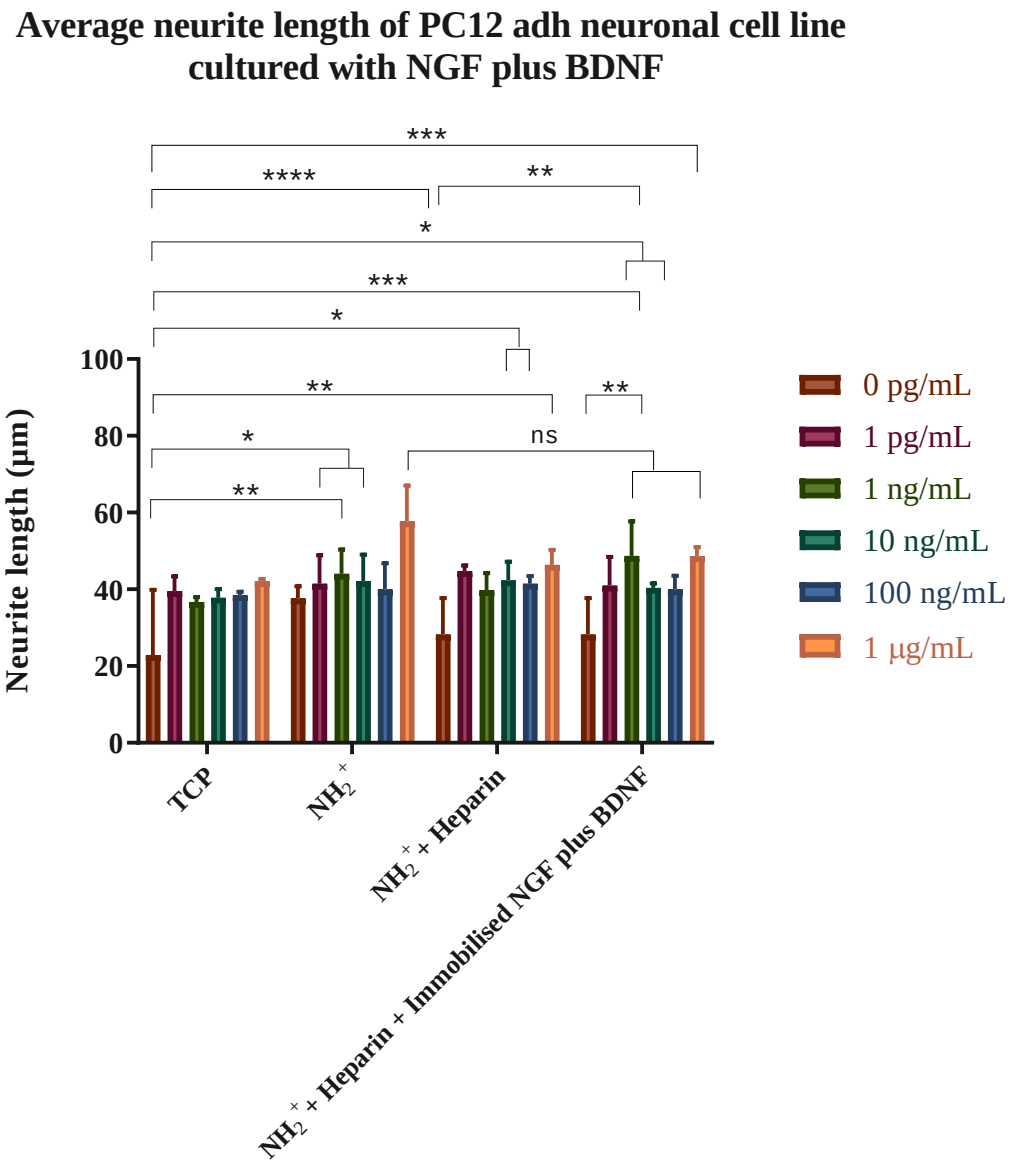

Figure 80. Average neurite length of PC12 adh neuronal cells when cultured on TCP, NH_2^+, NH_2^+ + Heparin (controls), and NH_2^+ + Heparin + Immobilised NGF plus BDNF (test). NGF plus BDNF were added to the bioactive surfaces at different concentrations. Two-way ANOVA statistical analysis was performed with Tukey procedure of multiple comparisons *p < 0.05, **p<0.01, ***p< 0.001, ****p<0.0001. Mean ± SD. N=3, n=3.

The average maximum neurite length of PC12 adh neuronal cells was calculated from PC12 adh neuronal cells seeded on TCP, NH_2^+, NH_2^+ + Heparin, and NH_2^+ + Heparin + Immobilised NGF plus BDNF. The largest average maximum neurite length was 119 ± 26 µm for PC12 adh neuronal cells cultured on NH_2^+ with NGF plus BDNF in solution at a concentration of 1 µg/mL, as seen in Figure 81. Additionally, the shortest maximum neurite length was 35 ± 25 µm for neuronal cells seeded on TCP. The average maximum neurite length was significantly higher for PC12 neuronal cells when they were cultured on NH_2^+ + Heparin + Immobilised NGF plus BDNF at 1 pg/mL (91 ± 30), NH_2^+ + Heparin + Immobilised NGF plus BDNF at 1 ng/mL (110 ± 36 µm) and NH_2^+ + Heparin + Immobilised NGF plus BDNF at 1 µg/mL (110 ± 20 µm) in comparison to when they were cultured on TCP.

Furthermore, the average maximum neurite length of PC12 adh neuronal cells was significantly higher when cultured on NH_2^+ with NGF plus BDNF in solution at 1 µg/mL in comparison when they were cultured on TCP, NH_2^+ (49 ± 7 µm) and NH_2^+ + Heparin (50 ± 21 µm). Additionally, the average maximum neurite length of PC12 adh neuronal cells was significantly higher when cultured on NH_2^+ + Heparin + Immobilised NGF plus BDNF at 1 ng/mL and NH_2^+ + Heparin + Immobilised NGF plus BDNF at 1 µg/mL in comparison to NH_2^+ + Heparin.

Moreover, even though that the average value of the maximum neurite length was higher for PC12 adh neuronal cells seeded on NH_2^+ with NGF plus BDNF in solution at 1 µg/mL than in NH_2^+ + Heparin + Immobilised NGF plus BDNF at 1 ng/mL and NH_2^+ + Heparin + Immobilised NGF plus BDNF at 1 µg/mL, there was no significant difference between them. These results indicated that the delivery of NGF plus BDNF by immobilisation on the bioactive surface was an appropriate platform to encourage neurite outgrowth using a low concentration of growth factors as it stimulated the maximum growth of neurite similarly to when NGF plus BDNF were in solution.

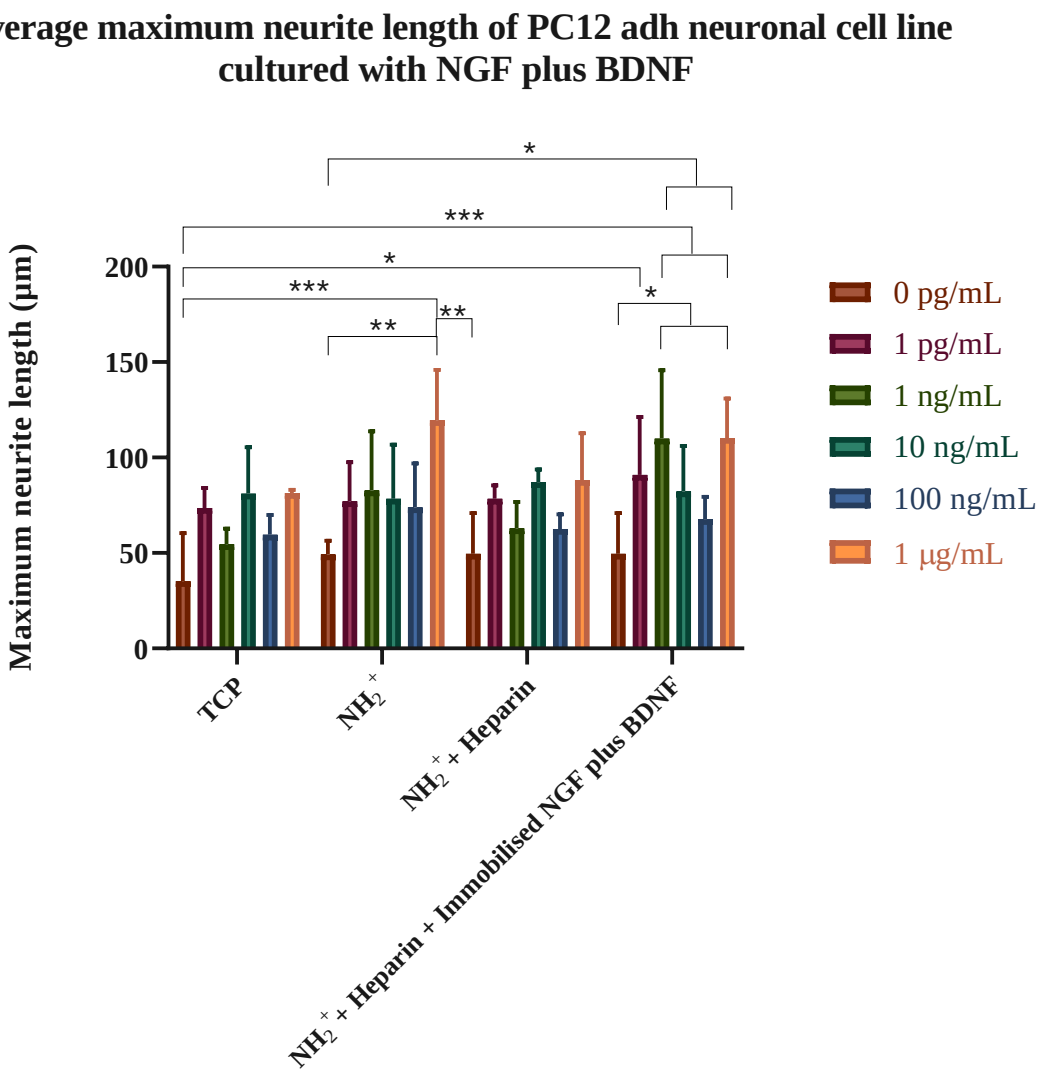

Figure 81. Average maximum neurite length of PC12 adh neuronal cells when cultured on TCP, NH_2^+, NH_2^+ + Heparin (controls), and NH_2^+ + Heparin + Immobilised NGF plus BDNF (test). NGF plus BDNF were added to the bioactive surfaces at different concentrations. Two-way ANOVA statistical analysis was performed with Tukey procedure of multiple comparisons *p < 0.05, **p<0.01, ***p< 0.001, ****p<0.0001. Mean ± SD. N=3, n=3.

The percentage of neurons bearing neurites of PC12 adh neuronal cells was calculated from PC12 adh neuronal cells cultured on TCP, NH_2^+, NH_2^+ + Heparin, and NH_2^+ + Heparin + Immobilised NGF plus BDNF. The highest percentage of neurons bearing neurites was 7.5 ± 2% for PC12 adh neuronal cells seeded on NH_2^+ + Heparin + Immobilised NGF plus BDNF at a concentration of 1 µg/mL. The lowest percentage of neurons bearing neurites was 0.6 ± 0.4% for neuronal cells cultured on TCP.

The percentage of neurons bearing neurites was significantly higher for PC12 adh neuronal cells when cultured on TCP with NGF plus BDNF in solution at a concentration of 1 µg/mL, NH_2^+ with NGF plus BDNF in solution at concentration of 1 ng/mL and 1 µg/mL, and NH_2^+ + Heparin + Immobilised NGF plus BDNF at 1 ng/mL and 10 ng/mL in comparison to when the neuronal cells were seeded on TCP, as shown in Figure 82. Additionally, the percentage of neurons bearing neurites was significantly higher for those neuronal cells cultured on NH_2^+ with NGF plus BDNF in solution at 1 ng/mL and 1 µg/mL, and NH_2^+ + Heparin + Immobilised NGF plus BDNF at 1 ng/mL, 10 ng/mL and 1 µg/mL in comparison to neuronal cells seeded on NH_2^+.

Furthermore, the percentage of neurons bearing neurites was significantly lower for PC12 adh neuronal cells when cultured on NH_2^+ + Heparin compared to when the neuronal cells were seeded on NH_2^+ + Heparin with NGF plus BDNF in solution at 1 µg/mL, NH_2^+ + Heparin + Immobilised NGF plus BDNF at 1 ng/mL, 10 ng/mL and 1 µg/mL. Moreover, even though the percentage of neurons bearing neurites of PC12 adh neuronal cells seeded on NH_2^+ + Heparin + Immobilised NGF plus BDNF at 1 ng/mL was lower (6.4 ± 1.3%) in comparison to neuronal cells cultured on NH_2^+ + Heparin + Immobilised NGF plus BDNF at 1 µg/mL (7.5 ± 2%), there was no significant difference between these two values.

Therefore, these results suggested that with a low immobilised concentration of NGF plus BDNF (1 ng/mL), the percentage of neurons bearing neurites was similar to the percentage of neurons bearing neurites from neuronal cells seeded at higher immobilised concentrations of NGF plus BDNF and with NGF plus BDNF at 1 µg/mL in solution.

Percentage of neurons bearing neurites in PC12 adh neuronal cell line cultured with NGF plus BDNF

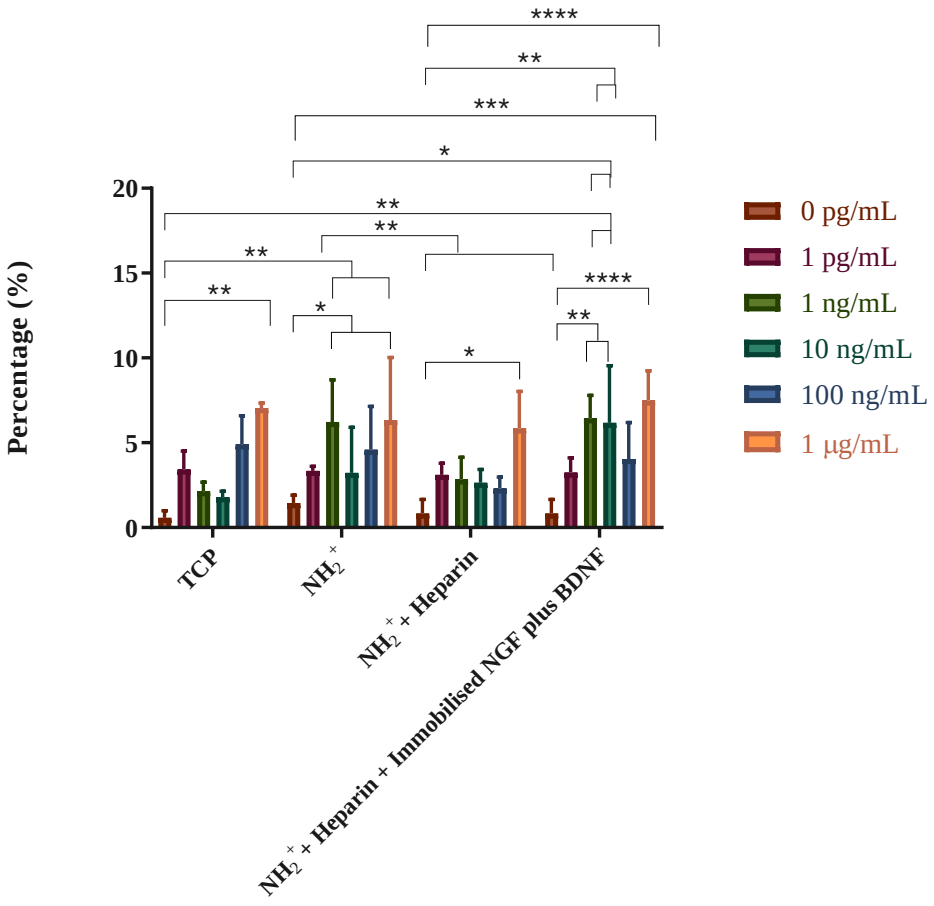

Figure 82. Percentage of neurons bearing neurites of PC12 adh neuronal cells when cultured on TCP, NH_2^+, NH_2^+ + Heparin (controls), and NH_2^+ + Heparin + Immobilised NGF plus BDNF (test). NGF plus BDNF were added to the bioactive surfaces at different concentrations. Two-way ANOVA statistical analysis was performed with Tukey procedure of multiple comparisons *p < 0.05, **p<0.01, ***p< 0.001, ****p<0.0001. Mean ± SD. N=3, n=3.

6.5 Discussion

Metabolic activity, average neurite length, maximum neurite length and percentage of neurons bearing neurites were studied for NG108-15 neuronal cells and PC12 adh neuronal cells in response to when they were cultured on TCP, NH_2^+, NH_2^+ + Heparin, and NH_2^+ + Heparin + Immobilised NGF or BDNF or NGF plus BDNF.

Firstly, the effect of the bioactive surface on NG108-15 neuronal cells was assessed. Metabolic activity was evaluated to study the biocompatibility of the bioactive surface. The assessment of metabolic activity of cells is a standard procedure used *in vitro* to study the biocompatibility of biomaterials. An increase in metabolic activity was taken to mean that cells were not adversely affected by the biomaterials, or in this case the bioactive surface.

The metabolic activity response of NG108-15 neuronal cells when seeded on bioactive surfaces was not significantly different from when the neuronal cells were cultured on TCP, NH_2^+, or NH_2^+ + Heparin with soluble NGF, BDNF, NGF plus BDNF at different concentrations. Moreover, there was no significant difference between the metabolic activity when the neuronal cells were seeded on NH_2^+ + Heparin + Immobilised NGF, BDNF or NGF plus BDNF at different concentrations in comparison to controls. These results suggest that neither the bioactive surface nor the concentrations of the growth factors affected the metabolic activity of the neuronal cells, hence, the bioactive surface is biocompatible.

The average neurite length of NG108-15 neuronal cells when cultured on TCP, NH_2^+, or NH_2^+ + Heparin with soluble growth factors was not significantly different from when they were cultured on NH_2^+ + Heparin + Immobilised NGF, BDNF or NGF plus BDNF. Moreover, for average maximum neurite length, even though neurite length from when the neuronal cells were cultured with NGF plus BDNF were slightly higher, there was no significant difference between these neurite length values. In addition, the percentage of neurons bearing neurites from NG108-15 neuronal cells when seeded on control and test surfaces at different concentrations of NGF, BDNF or NGF plus BDNF were not significantly different from each other.

Therefore, according to these results, the bioactive surfaces NH_2^+ + Heparin + Immobilised NGF, BDNF or NGF plus BDNF are not cytotoxic *in vitro*, however, these bioactive surfaces did not stimulate the growth of longer neurites or more neurites in comparison to control surfaces. Research has previously been conducted using NG108-15 neuronal cells to assess neurite outgrowth and material biocompatibility. For example, Hopper et al. [253] functionalised nanodiamond with amine functional groups. This study assessed cell viability and percentage of NG108-15 cells bearing neurites in order to demonstrate that this coating had the potential to be used for future treatments for peripheral nerve regeneration. This study found that NG108 adhered on glass (negative control), but no neurites were developed. When the cells were cultured on poly-L-lysine (PLL, positive control), neurite formation was observed. In addition, NG108-15 cells cultured on amine functionalised nanodiamond formed long neurites, similarly to when they were seeded on PLL. The percentage of neurons bearing neurites was high (ca. 90%), when cells were cultured on PLL or amine functionalised nanodiamond, in comparison to glass (ca. 20%). Neurite outgrowth was longer (150 µm), in both PLL and amine functionalised nanodiamond in comparison to glass controls. Viability tests showed that cell proliferation was not significantly different between amine functionalised nanodiamond and PLL.

In addition, Armstrong et al. [50] assessed the effect of collagen, fibronectin, laminin and Schwann cells on neurite outgrowth. Neurite length was longer when NG108-15 neuronal cells were seeded in contact with Schwann cells than on collagen, fibronectin or laminin. The authors suggested that neurotrophins released from Schwann cells encouraged the initiation of neurite outgrowth, and that the contact of the neurons with Schwann cells promoted further neurite growth. The percentage of neurons bearing neurites was 77% and 69% when NG108-15 neuronal cells were cultured in contact with Schwann cells with laminin and fibronectin, respectively. The authors suggested that the interaction between Schwann cells and fibronectin, laminin and collagen encouraged the release of neurotrophins, such as NGF, BDNF or CNTF. However, this release was not characterised. Moreover, when NG108-15 neuronal cells were seeded with fibronectin, laminin or collagen alone, there was no significant difference in neurite length or percentage of neurons bearing neurites.

Schuh et al. [297] designed and engineered a neural tissue, composed of a blend of 90% collagen and 10% fibrin, to encourage peripheral nerve repair. This engineered neural tissue, which also included Schwann cells, encouraged average neurite outgrowth of 180.6 ± 76.5 μm on NG108-15 neuronal cells [297]. In comparison to the results presented in this thesis, regarding NG108-15 neuronal cells, the average neurite length when seeded with NGF or NGF plus BDNF fitted within the average neurite length range reported by Schuh et al. Moreover, when the NG108-15 neuronal cells were seeded with immobilised BDNF at low concentrations (1 pg/ml and 1 ng/mL), neurite lengths also fitted within the average neurite length range reported by Schuh et al. These results suggest that a low immobilised concentration of BDNF or by using NGF or NGF in combination with BDNF stimulated a similar neurite outgrowth in NG108-15 neuronal cells than when cultured with collagen, fibrin and Schwann cells [297].

Additionally, Melissinaki et al. [298] fabricated a polylactide-based 3D scaffold and studied its biocompatibility as a neuronal scaffold. MTT assay and DNA quantification assay were performed to evaluate NG108-15 neuronal cell viability and when on these scaffolds. DNA quantification revealed that NG108-15 neuronal cells proliferated similarly on the 3D scaffold and on glass after 72 hours. Moreover, MTT assay showed that, after 72 hours, metabolic activity of NG108-15 neuronal cells was not significantly different when cultured on the 3D scaffold than when cultured on glass. However, after 120 hours, the metabolic activity of the neuronal cells when cultured on the 3D scaffold was significantly higher compared to when they were cultured on glass [298]. These results suggested that the polylactide-based 3D scaffold was biocompatible to use for neuronal tissue engineering.

Most of the research that has been performed using NG108-15 neuronal cells was to assess the biocompatibility of a material, or neurite outgrowth/percentage of neurons bearing neurites as a response to extracellular matrix molecules or Schwann cells being present in a scaffold. Little has been investigated regarding the response of NG108-15 neuronal cells to scaffolds, or other delivery systems that supply growth factors. The research by Lai et al., [299] evaluated the effect of *H. erinaceus* aqueous extract on the percentage of neurons bearing neurites of NG108-15 neuronal cells. As

the extract contained neuroactive molecules that encouraged neurite outgrowth, comparison to NGF was logical. When *H. erinaceus* aqueous extract was combined with NGF (1 µg/mL and 10 ng/mL respectively) the percentage of neurons bearing neurites increased up to 60.6% [299]. When NGF, at 10 ng/mL, or *H. erinaceus* aqueous extract, at 1 µg/mL, were cultured alone with NG108-15 neuronal cells, the percentage of neurons bearing neurites was 33.3% and 34.5% respectively [299]. These results suggested that the highest percentage of neurons bearing neurites was enhanced when both *H. erinaceus* aqueous extract and NGF were present in culture. Nevertheless, when the concentration of *H. erinaceus* aqueous extract increased, the percentage of neurons bearing neurites decreased. This was attributed to the fact that *H. erinaceus* increased extracellular NGF levels, which inhibited neurite outgrowth in NG108-15 neuronal cells [299].

However, to the best knowledge of this author, NG108-15 neuronal cells are not widely used to assess the effects of neurotrophins, such as NGF or BDNF, on neurite outgrowth or neurons bearing neurites. NG108-15 neuronal cells are primarily used to study ion channels and receptors, such as opioid receptors [300], [301]. Moreover, they have been used to evaluate biocompatibility [253], [297], [298]. Nevertheless, PC12 neuronal cells have been used extensively to study the effects of neurotrophins, as these neuronal cells are a well-characterised model to study neuronal differentiation in the presence of neurotrophins. For example, NGF encourages differentiation of PC12 neuronal cells to the mature, sympathetic neuronal phenotype [300], [302], [303]. In addition, the BDNF-TrkB pathway has been studied for its neuroprotective role in PC12 neuronal cells [304], [305].

Therefore, PC12 adh neuronal cells were used to evaluate the effects of NGF and BDNF when immobilised on bioactive surfaces on metabolic activity, neurite length, percentage of neurons bearing neurites and maximum neurite length. The results obtained were very interesting, as they showed that immobilised NGF or BDNF increased the neurite length at lower concentrations compared to when these neurotrophins were in solution in culture medium. The neurite length was also not affected significantly by the concentration of immobilised NGF or BDNF. Moreover, when NGF and BDNF were co-immobilised at a low concentration, the percentage of

neurons bearing neurites was comparable to when the neuronal cells were seeded with the neurotrophins in solution in culture medium. Additionally, when BDNF was present in culture, either in solution or immobilised, at 1 µg/mL, the number of developed neurites was higher in comparison to other groups, even though results from MTS assay showed low metabolic activity at day 5.

Research has been conducted to design a more suitable delivery system for neurotrophins, to achieve an optimised effect. Hu et al. encapsulated 8 µg of NGF in PCL nanofibers and evaluated cytotoxicity, using MTS assay, and neurite length [64]. Their results suggested that the incorporation of NGF did not negatively affect the metabolic activity of PC12 cells [64]. Moreover, the averaged neurite length and maximum neurite length of PC12 neuronal cells were of 17.86 ± 10.39 µm and 41.67 µm, respectively, when cells were cultured on randomly oriented PCL fibers. When PC12 cells were seeded on aligned fibers, the averaged neurite length and maximum neurite length were 30.33 ± 17.92 µm and 70.17 µm [64]. In comparison, the results in this thesis showed that when NGF was immobilised on the bioactive surface at 1 pg/mL and 1 µg/mL, the average neurite length and the maximum neurite length was 56 ± 20 µm and 124 ± 28 µm, respectively. These results suggested that when using a lower concentration of NGF, below 8 µg, a better outcome regarding average neurite length and maximum neurite length can be achieved.

Also, Gomez and Schmidt immobilised 2 µg of NGF on polypyrrole and evaluated its effects regarding neurite length and percentage of neurons bearing neurites on PC12 neuronal cells [227]. After 2 days in cell culture, neurite outgrowth was 16.8 µm and the percentage of neurons bearing neurites was 6%. After 10 days, neurite outgrowth was 42.2 µm, and 9% of PC12 neuronal cells expressed neurites [227]. In comparison, the results in this thesis showed that when NGF was immobilised at 1 pg/mL, neurite outgrowth of PC12 adh neuronal cells was 56 µm after 5 days in culture. However, the percentage of neurons bearing neurites was lower (1%). Moreover, when NGF was immobilised at 1 µg/mL, the percentage of neurons bearing neurites was 8%. The results from Gomez and Schmidt might not have encouraged longer neurite outgrowth because NGF was immobilised using photochemical techniques, suggesting that NGF might have lost bioactivity during the process [227], [258]. Hence, immobilising NGF

by electrostatic means might be an effective approach to stimulate the growth of longer neurites.

Furthermore, Bhang et al. evaluated the percentage of neurons bearing neurites of PC12 neuronal cells when 5, 10 and 100 ng of NGF were immobilised on a heparin-allylamine surface [292]. It is important to highlight that heparin was covalently immobilised to allylamine, then, NGF was immobilised to heparin by electrostatic interactions [292]. The study showed that when 100 ng of NGF were added daily into cell culture, 37% of PC12 neuronal cells developed neurites. Similarly, when 10 ng of NGF were immobilised, the percentage of neurons bearing neurites was also 37% [292]. Moreover, Bhang et al., immobilised 10 ng of NGF per sample (113 mm^2) which might explain the high percentage of neurons bearing neurites [292]. Even though the percentage of neurons bearing neurites was higher in their study, in comparison to the 8% of neurons bearing neurites in this thesis, it is not clear if the immobilisation technique of Bhang et al. encourages the growth of longer neurites, as this was not assessed. Nevertheless, the study performed by Bhang et al., supports the use of small amounts of NGF to encourage PC12 neuronal cells to develop neurites.

A study performed by Achyuta et al. covalently immobilised laminin and NGF (1 µg/mL and 5 µg/mL) on glass coverslips to promote neurite outgrowth on PC12 neuronal cells [229]. The average neurite length was 20 µm and 45 µm for immobilised NGF at 0.25 ng/mm^2 (original load of 1 µg/mL) and 1.5 ng/mm^2 (5 µg/mL) respectively [229]. It is interesting to notice that, from the original loads, just a small amount of growth factor remained on the surface. This suggested that covalently immobilising laminin and NGF might be affecting the bioactivity of both proteins. Comparing these results from Achyuta et al. to the ones obtained in this thesis chapter, the hypothesis that using less quantities of growth factors will stimulate the growth of longer neurites is supported.

Research using BDNF to evaluate neurite length or developed neurites in PC12 neuronal cells is not extensive. However, one study by Iwasaki et al. [306] evaluated the morphology of PC12 neuronal cells when cultured with 100 ng/mL of NGF or 100 ng/mL of BDNF. Iwasaki et al. found that BDNF encouraged the growth of longer

and thicker neurites compared to NGF [306]. The authors suggested that the low affinity NGF receptor, p75LNGFR, might have decreased the activity of TrkA receptor, as p75LNGFR is known to affect the activity of TrkA [306]. The results presented in this thesis showed that at an immobilised concentration of 1 pg/mL, NGF and BDNF encouraged neurite outgrowth similarly (56 ± 20 µm and 56 ± 16 µm respectively). However, regarding maximum neurite length, 1 pg/mL of immobilised BDNF encouraged the growth of longer neurites (144 ± 29 µm) compared to 1 pg/mL of immobilised NGF (124 ± 28 µm). These results agree to a certain extent with Iwasaki et al. because BDNF promoted longer maximum neurite length. Nevertheless, at a lower concentration, both NGF and BDNF stimulated almost the same neurite length. This might suggest that an equilibrium was reached regarding the activation of p75LNGFR and TrkA, where the ERK 1/2 pathway was activated by TrkA, which stimulates neurite growth in PC12 neuronal cells [307].

Furthermore, Bierlein De la Rosa et al. evaluated how BDNF secreted from mesenchymal stem cells affected neurite outgrowth in PC12 neuronal cells [84]. When 39.9 ± 6.3 ng/mL of BDNF were added per day to the cell culture, neurite length at day 8 was 41.6 ± 6 µm. Moreover, when 102.3 ± 30.4 ng/mL were added daily for 20 days, neurite outgrowth in PC12 neuronal cells was 54.3 ± 7.3 µm [84]. In comparison, results in this thesis chapter showed that when 100 ng/mL of BDNF were added in solution in culture medium, neurite outgrowth was, at day 5, 38.2 ± 3.6µm. However, when BDNF at 100 ng/mL was immobilised on the bioactive surface, neurite length was 61 ± 21 µm, at day 5. Hence, the immobilisation of 100 ng/mL of BDNF supported the growth of longer neurites, in lesser time.

In addition, Naka et al. coated nanoscale magnetic beads with 10 µg/mL of NGF, BDNF or NGF and BDNF, and evaluated neurite outgrowth from PC12 neuronal cells [262]. Their findings showed that magnetic beads coated with NGF encouraged neurite outgrowth whereas magnetic beads coated with BDNF did not [262]. Nevertheless, neurite outgrowth was seen on PC12 neuronal cells when cultured with magnetic beads coated with both NGF and BDNF. However, neurite growth was not as great as when only NGF was used [262]. Naka et al. argued that BDNF had no effect on PC12 neuronal cells because these cells do not have TrkB receptor [262].

Nonetheless, Iwasaki et al. stimulated neurite outgrowth in PC12 neuronal cells using BDNF [306]. They also found that the strength of TrkB stimulation was not significantly different from the strength of TrkA stimulation [306]. Moreover, the results in this thesis also showed that PC12 neuronal cells developed neurites when cultured with BDNF. One reason why the results from Naka et al. did not show neurite outgrowth when PC12 neuronal cells were cultured with BDNF might be related with the concentration of BDNF used. The concentration of BDNF might be too high (10 µg/mL), so instead of encouraging neurite outgrowth, it might have inhibited neurite formation signaling [89], [308]. Furthermore, the results of this thesis also showed that, when PC12 neuronal cells were seeded with both NGF and BDNF, neurite development was observed. However, an additive effect was not achieved as the average neurite length was 58 ± 9 µm and maximum neurite length was 119 ± 26 µm for when 1 µg/mL of NGF plus BDNF was in solution with culture medium. Even though there was no significant difference among the before mentioned values of average neurite length and maximum neurite length and the ones developed from immobilised 1 ng/mL and 1 µg/mL NGF plus BDNF surfaces, average neurite length and maximum neurite length were similar in comparison to when NGF or BDNF were immobilised alone.

Growth factors, such as NGF and BDNF, bind to specific membrane receptors tyrosine kinase (Trk) [309]. NGF binds to TrkA [132], [227] and BDNF to TrkB [132], [137]. Moreover, both neurotrophins bind to $p75^{NTR}$ transmembrane receptor [132], [134], [137], [138]. When a neurotrophin binds to its receptor, intrinsic tyrosine kinase activities, such as survival and differentiation, are activated [134], [138], [309]. The subunits of the receptor autophosphorylate residues, enabling the formation of a signal-generating complex. The neurotrophin-receptor complex promotes the internalization of the active receptor into vesicles [27]. These neurotrophin-receptor complexes activate the phosphotidyl-inositol-3 kinase (PI3K) and mitogen activated protein kinase/ extracellular receptor kinase (MAPK/ERK) pathways, which stimulate neurite outgrowth and neurite survival [131], [137], [138], [158], [310].

Gomez and Schmidt stated that not all neurotrophin-receptor complexes need to be internalised to activate signaling pathways [227]. Non-internalised neurotrophin-

receptor complexes also initiate phosphorylation of tyrosines, activating the PI3K pathway and hence, stimulating cell survival and neurite extension [227]. This suggests that neurite formation could be encouraged by neurotrophins while these are being immobilised onto a surface. If the neurotrophins are immobilised on a surface and at the same time are bound to their Trk receptor, the PI3K pathway would be activated, forming neurites and stimulating survival.

Nevertheless, the exact dose at which the growth factors need to be administered, including its frequency, is unknown [217]. This dose would depend on how the neurotrophins are delivered. Also, this dose needs to continuously activate the PI3K and MAPK/ERK pathways to stimulate neurite outgrowth and survival, without activating any pathway that would lead to inhibitory activities or apoptosis [77], [134], [158], [310]. The work in this thesis showed that adding or immobilising 1 pg/mL, 1 ng/mL, 10 ng/mL, 100 ng/mL or 1 µg/mL of NGF or BDNF enhanced neurite development, but it did not lead to cell death. Furthermore, the immobilisation of NGF, BDNF or NGF plus BDNF on a NH_2^+ + Heparin surface was not cytotoxic and the bioactivity of NGF and BDNF was maintained. More importantly, the work in this thesis has revealed that immobilising relatively low concentrations of NGF or BDNF on a NH_2^+ + Heparin surface encouraged the growth of larger neurites in PC12 adh neuronal cells.

6.6 Conclusion

This chapter evaluated how the bioactive surface NH_2^+ + Heparin + Immobilised NGF, NH_2^+ + Heparin + Immobilised BDNF and NH_2^+ + Heparin + Immobilised NGF plus BDNF affected metabolic activity, neurite length and percentage of neurons bearing neurites of NG108-15 neuronal cells and PC12 adh neuronal cells.

Even though metabolic activity, average neurite length, average maximum neurite length and percentage of neurons bearing neurites of NG108-15 neuronal cells showed no significant differences, it can be concluded that the bioactive surface NH_2^+ + Heparin + Immobilised NGF, BDNF or NGF plus BDNF was not cytotoxic.

PC12 adh neuronal cells were used to measure neurite length, and to calculate the percentage of neurons bearing neurites as these cells are widely used to evaluate neurite formation when they are cultured with NGF. The results in this chapter revealed that by immobilising relatively low concentrations of NGF (1 pg/mL), longer neurites were developed in comparison to when NGF was in solution with culture medium. Furthermore, the average neurite length was longer as well.

When BDNF was immobilised at 100 ng/mL, neurite length was longer in comparison to when BDNF was in solution in culture medium. However, when BDNF was immobilised at a lower concentration (1 pg/mL), the average neurite length was not significantly different for the neurite length developed when PC12 adh neuronal cells were seeded with immobilised BDNF at 100 ng/mL. Furthermore, BDNF immobilised at 1 pg/mL developed the average maximum neurite length. These results also suggested that by immobilising a low concentration of neurotrophin, longer neurites can be developed. Moreover, when NGF and BDNF were co-immobilised, the effect was not cumulative as neurites did not grow any longer in comparison to when NGF and BDNF were immobilised alone. Nevertheless, the results showed that at lower concentrations, similar lengths can be achieved to when the neurotrophins were immobilised alone.

In summary, the results in this chapter support the immobilisation of NGF and BDNF at relatively low concentrations as they encouraged the growth of longer neurites in PC12 adh neuronal cells. It will be interesting to investigate if the effects are similar to when the NH_2^+ + Heparin + Immobilised NGF, BDNF or NGF plus BDNF bioactive surface are cultured with dorsal root ganglia. Moreover, it will be interesting to study how the bioactive surface affects primary Schwann cells.

Chapter 7 Effects of bioactive surface on dorsal root ganglia and primary Schwann cells

The following experimental chapter has been partially taken from Sandoval-Castellanos et al., (2020) [203] which was published as an open access article under the terms of the Creative Commons Attribution License, allowing the use, distribution and reproduction of the material provided that it is properly cited.

7.1 Introduction

In chapter 5 and 6 of this thesis, the fabrication, characterisation and biological response, of NG108-15 neuronal cells and PC12 adh neuronal cells, to the bioactive surfaces NH_2^+ + Heparin + Immobilised NGF, NH_2^+ + Heparin + Immobilised BDNF and NH_2^+ + Heparin + Immobilised NGF plus BDNF was investigated.

In this chapter, the effect of the bioactive surfaces was evaluated using chick embryo dorsal root ganglia (DRG) and primary chick embryo Schwann cells. As the use of DRG and primary cells are biologically relevant, it was a logical next step to evaluate the effect on neurite development of DRG and Schwann cell migration from the bioactive surfaces.

Growth factors, which stimulate and regulate growth and survival [264], have been used in research to evaluate their effects on primary cells and tissue. For example, blood vessel formation was encouraged in a chick chorionic allantoic membrane by a scaffold which had immobilised vascular endothelial growth factor (VEGF) [267]. Moreover, nerve growth factor (NGF), brain derived neurotrophic factor (BDNF) and glial cell-derived neurotrophic factor (GDNF), which encourage neurite growth in DRG [61], [84], [264], are being used in different delivery systems to assess their effects in DRG neurite outgrowth. For example, Matsumoto et al. functionalised nanotubes with NGF and BDNF and found that both NGF-nanotubes and BDNF-nanotubes stimulated neurite outgrowth in chick embryo DRG neurons [264].

Furthermore, Madduri et al. studied the release of GDNF (80 ng) or GDNF with NGF (40 ng each) from a collagen nerve conduit and evaluated neurite development in chick embryo DRG [75]. They observed that when using GDNF, only neurite outgrowth was observed. In contrast, when GDNF and NGF were used together, neurite outgrowth and branching was observed [75]. In addition, Naka et al. used 10 µg/mL of either NGF or BDNF to coat nanoscale magnetic beads to promote neurite development in neurons from chick embryo DRG [262]. After 2 days in culture, NGF-magnetic beads and BDNF-magnetic beads encouraged ca. 550 neurons with neurites and ca. 200 neurons with neurites, respectively [262].

Sakiyama-Elbert and Hubbell showed that the release of NGF from a heparin-fibrin matrix encouraged nerve regeneration *in vivo* [157]. However, the authors highlighted and recognised that it was difficult to maintain neurotrophin release over a long time during nerve repair, and that a delivery system that provides a slow and maintained release of growth factors over long periods would be more effective to aid nerve repair [157]. Moreover, this delivery system needs to supply the appropriate neurotrophin dose, as low levels of neurotrophins might not encourage any action, whereas high levels may impede regeneration [158], [217]. Moreover, a localised and sustained delivery of neurotrophins at the injury site may improve regeneration [129], [130]. In addition, as there are no studies that give information about the optimal dose of neurotrophins over long periods [217], it is important to test not only one, but various concentrations of growth factors to elucidate which concentration, used within a delivery system, encourages the best biological response.

Even though one of the main objectives in this thesis is to assess neurite outgrowth, evaluating the effects of the bioactive surface on Schwann cell migration is also important, as Schwann cells migration assists neurite outgrowth during nerve repair [12], [311]. Moreover, Schwann cells remyelinate neurons after regeneration [312], [313]. Hence, an improvement in Schwann cell migration could enhance nerve repair and regeneration [4].

Schwann cell migration has been studied before. Ren et al. fabricated a gradient of poly(3-dimethyl-methacryloyloxyethylammonium propane sulfonate) (PDMAPS)

and KHIFSDDSSE peptide (KHI) to stimulate Schwann cell migration [314]. This research showed that Schwann cell migration was improved and that this migration was directed toward the region with higher KHI peptide density and lower PDMAPS density [314].

Moreover, growth factors, specifically neurotrophins, such as NGF, BDNF, glial cell-derived neurotrophic factor (GDNF), neurotrophin-3 (NT-3) and ciliary neurotrophic factor (CNTF) have been studied in regard to Schwann cell migration, where some contradictory data has been obtained [313], [315]–[318].

Therefore, supported by the data obtained in Chapter 6, it was hypothesized, that bioactive surfaces NH_2^+ + Heparin + Immobilised NGF, NH_2^+ + Heparin + Immobilised BDNF and NH_2^+ + Heparin + Immobilised NGF plus BDNF would encourage neurite outgrowth from DRG. Moreover, it was also hypothesized that primary Schwann cell migration would be affected positively by bioactive surfaces NH_2^+ + Heparin + Immobilised NGF and NH_2^+ + Heparin + Immobilised BDNF.

7.2 Aims and objectives

The bioactive surface was prepared on flat surface tissue culture plastic (TCP).

The aims of this chapter were to:

1. Evaluate the effects of bioactive surface immobilised with NGF on dorsal root ganglia primary cells.
2. Study the effects of bioactive surface immobilised with BDNF on dorsal root ganglia primary cells.
3. Assess the effects of bioactive surface immobilised with NGF plus BDNF on dorsal root ganglia primary cells.
4. Evaluate the migration profile of chick embryo primary Schwann cells when cultured on bioactive surface immobilised with NGF or BDNF.

The objectives of this chapter were to:

1. Calculate the average neurite length of dorsal root ganglia primary cells when cultured on bioactive surface immobilised with NGF, BDNF or NGF plus BNDF.
2. Obtain the maximum average neurite length of dorsal root ganglia primary cells when cultured on bioactive surface immobilised with NGF, BDNF or NGF plus BNDF.
3. Quantify the number of developed neurites from dorsal root ganglia primary cells when cultured on bioactive surface immobilised with NGF, BDNF or NGF plus BNDF.
4. Assess the migration profile of chick embryo primary Schwann cells when cultured on bioactive surface immobilised with NGF or BDNF.

7.3 Materials and Methods

7.3.1 Fabrication of the bioactive surface

Fabrication of the bioactive surface was done by following the protocol described in Chapter 4, sections 4.1.1.1 and 4.1.1.2, using a commercially available 96 well-plate pre-coated with amine groups NH_2^+. Briefly, heparin solution was passively conjugated on the TCP + NH_2^+. Then, NGF, BDNF or NGF plus BDNF, at different concentrations, were immobilised by electrostatic interactions onto the TCP + NH_2^++ Heparin bioactive surface.

7.3.2 Dorsal root ganglia primary cell culture

7.3.2.1 Dorsal root ganglia dissection from chick embryos

The complete methodology to dissect dorsal root ganglia (DRG) from chick embryos is described in Chapter 4, section 4.3.1. Briefly, chick embryos were incubated until embryonic development day 12 (EDD12). The head and organs of the chick embryo were removed. Then, using a dissecting microscope and surgical tweezers, the DRG were dissected from the chick embryo and then placed in a petri dish with phosphate buffered saline (PBS) with 10% v/v penicillin/streptomycin (P/S). DRG were seeded with a density of one DRG per well on the bioactive surface. Culture medium with NGF, BDNF or NGF plus BDNF was used as described in Table 13. DRG were cultured for 7 days at 37℃ and 5% CO_2. Three independent tests were performed. Each bioactive surface was tested in triplicate.

Table 13. The following surfaces were prepared, and NGF and BDNF delivered method are described herein. NGF, BDNF and NGF plus BDNF solutions for immobilisation were prepared in sterile PBS.

Surface	**Growth factor delivery method**	**NGF**	**BDNF**	**NGF plus BDNF**
TCP	In solution with culture medium	0 pg/mL	0 pg/mL	0 pg/mL
		1 µg/mL	1 µg/mL	1 µg/mL
$TCP+NH_2^+$	In solution with culture medium	0 pg/mL	0 pg/mL	0 pg/mL
		1 µg/mL	1 µg/mL	1 µg/mL
$TCP+NH_2^+$+Heparin	In solution with culture medium	0 pg/mL	0 pg/mL	0 pg/mL
		1 µg/mL	1 µg/mL	1 µg/mL
$TCP+NH_2^+$+Heparin	Immobilised on surface	0 pg/mL	0 pg/mL	0 pg/mL
		1 pg/mL	1 pg/mL	1 pg/mL
		1 ng/mL	1 ng/mL	1 ng/mL
		10 ng/mL	10 ng/mL	10 ng/mL
		100 ng/mL	100 ng/mL	100 ng/mL
		1 µg/mL	1 µg/mL	1 µg/mL

7.3.2.2 Fixing and immunolabeling of DRG

Immunolabelling was performed as described in Chapter 4, section 4.3.4. Briefly, cultured medium was discarded, and 3.7% formaldehyde (FA) was added to each sample, which later was incubated for 30 minutes at room temperature. Then, FA was discarded and 0.1% Triton X-100 with 3% bovine serum albumin v/v (BSA) solution was added and incubated for 1 hour at room temperature. This solution was discarded and a primary antibody (anti β-III tubulin to identify neurites) in 1% BSA solution was added to the samples and incubated overnight at 4℃. After, this solution was discarded and the secondary antibody (goat IgG, Alexa Fluor 488) in 1% BSA solution was added and incubated for 3 hours at room temperature. The solution was then discarded and the DAPI solution in PBS was added and incubated for 30 minutes at room temperature. Finally, DAPI solution was discarded, samples washed one time with PBS and stored at 4℃ with PBS. Controls of secondary antibodies were also done.

7.3.2.3 Epifluorescence microscopy and neurite length analysis

DRG images were obtained as described in Chapter 4, section 4.3.5, using an inverted Olympus IX73 epifluorescence microscope and Micro-Manager 1.4.22 software.

Neurites were measured from the DRG body to the tip of the neurite. One image was taken per well. Three images were taken per condition, and 10-15 neurites were measured to determine the average neurite length and number of neurites. Background was subtracted (20-30 pixels) to enhance intensity and contrast.

7.3.3 Primary Schwann cells migration assay

7.3.3.1 Primary Schwann cell isolation from chick embryo

Schwann cell isolation from chick embryo EDD 12 was adapted from Kaewkhaw et al. [220]. This method was described in Chapter 4, section 4.3.2. Briefly, DRG were placed in 10 mL trypsin/EDTA and incubated at 37℃ and 5% CO_2 for 15 minutes. Then, the cell solution was centrifuged for 6 minutes at 1600 rpm. The supernatant was discarded, and the pellet resuspended in 2 mL of Schwann cell isolation medium. Then, 1 mL was transferred to a T-75 culture flask with 13 mL of Schwann cell isolation medium. The cells were incubated at 37℃ and 5% CO_2. After 24 hours, culture medium change was performed, where 50% of the Schwann cell isolation medium was replaced with cell culture medium (as described in Chapter 4). Schwann cells were incubated at 37℃ and 5% CO_2 until confluency was reached.

7.3.3.2 Primary Schwann cell migration assay

Schwann cell migration assay was performed as described in Chapter 4, section 4.3.3. Briefly, stoppers were placed on the bioactive surface and then 10,000 Schwann cells were seeded on them with culture medium and incubated at 37 ℃ and 5% CO_2. After 24 hours, the stoppers were removed, and an image was taken of the free area with no Schwann cells using an inverted Olympus IX73 epifluorescence microscope and Micro-Manager 1.4.22 software (University of California, USA). As a positive control, Tumor Necrosis Factor-α (TNF-α) was used at a concentration of 300 U/mL. This was added after images of day 0 were taken.

Image J 1.52a software (National Institutes of Health, USA) [218] was used to measure cell-free area at day 0, 1, 2, 5 and 7. The value on day 0 was set as 0%, and then, decrements in the cell-free area were calculated as a percentage of Schwann cell migration.

7.3.4 Statistical analysis

ANOVA with Tukey multiple comparison test was performed to analyze statistical differences among the different conditions using GraphPad Prism 8.2.0 software. A p value of < 0.05 was used to indicate significant differences among the data.

7.4 Results

7.4.1 Effects of bioactive surfaces in Dorsal Root Ganglia primary cells cultures

DRG were cultured on bioactive surfaces for 7 days. Then, they were immunolabeled so neurite length, maximum average neurite length and number of neurites could be quantified. Controls of secondary antibodies were done, showing no fluorescence signal (refer to Figure 134 in appendix)

Figure 83 shows neurite development from DRG seeded on control surfaces TCP, NH_2^+ and NH_2^+ + Heparin, with and without NGF, BDNF and NGF plus BDNF in solution in cell culture medium at a concentration of 1 µg/mL. Immunolabelling was performed for β-III tubulin (green). Nuclei were stained with DAPI (blue). From Figure 84, neurite development can be observed from DRG seeded on bioactive surface NH_2^+ + Heparin + Immobilised NGF, NH_2^+ + Heparin + Immobilised BDNF and NH_2^+ + Heparin + Immobilised NGF plus BDNF. Neurotrophins were immobilised at concentrations of 1 pg/mL, 1 ng/mL, 10 ng/mL, 100 ng/mL, and 1 µg/mL. Immunolabelling was performed for β-III tubulin (green). Nuclei was stained with DAPI (blue). Please note that the images represent average neurite length.

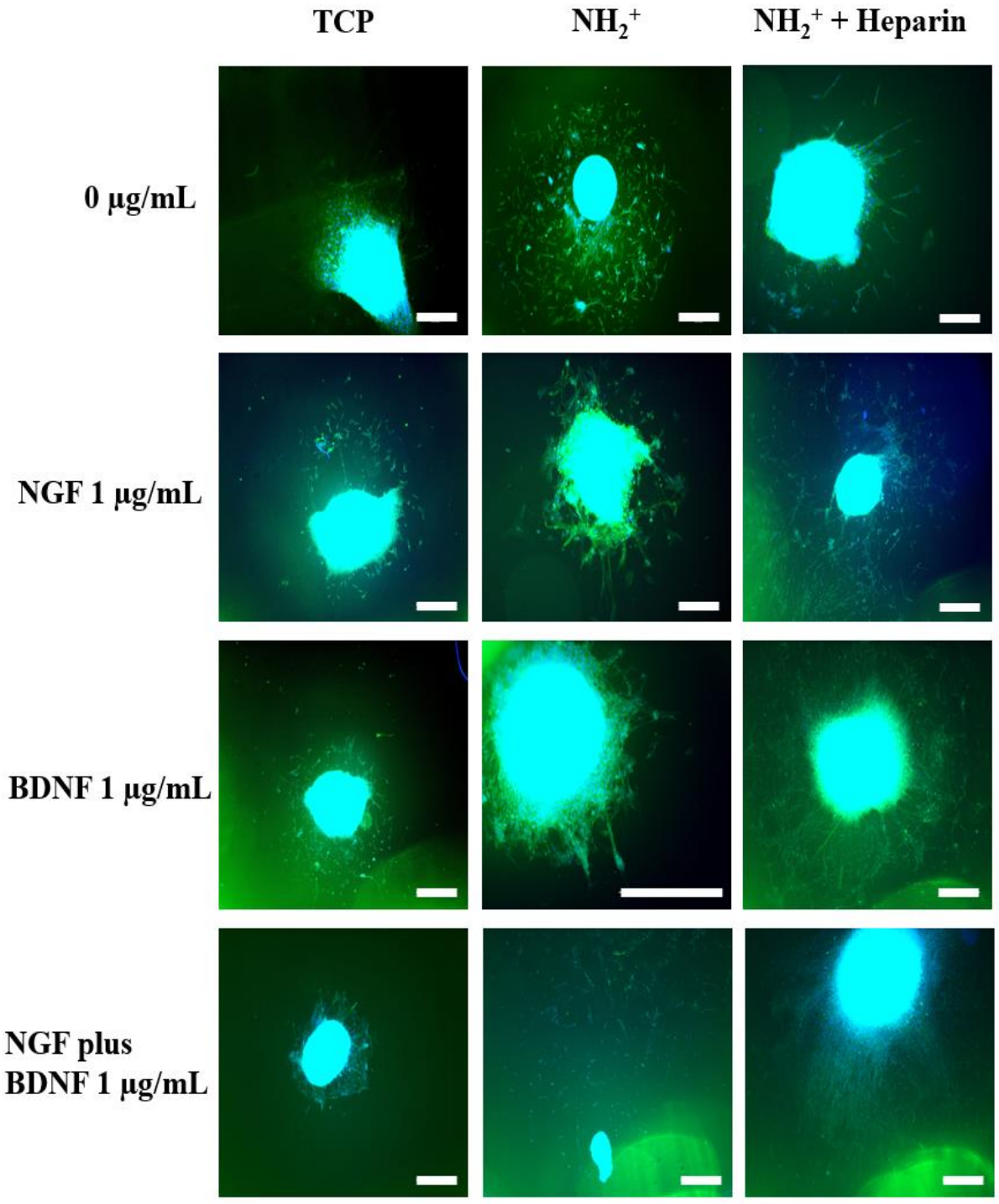

Figure 83. DRG seeded on control bioactive surfaces, where NGF, BDNF or NGF plus BDNF were in solution with culture medium at a concentration of 1 µg/mL. Nuclei stained in blue (DAPI); β-III tubulin protein in neurites stained in green. Scale bar = 500 µm.

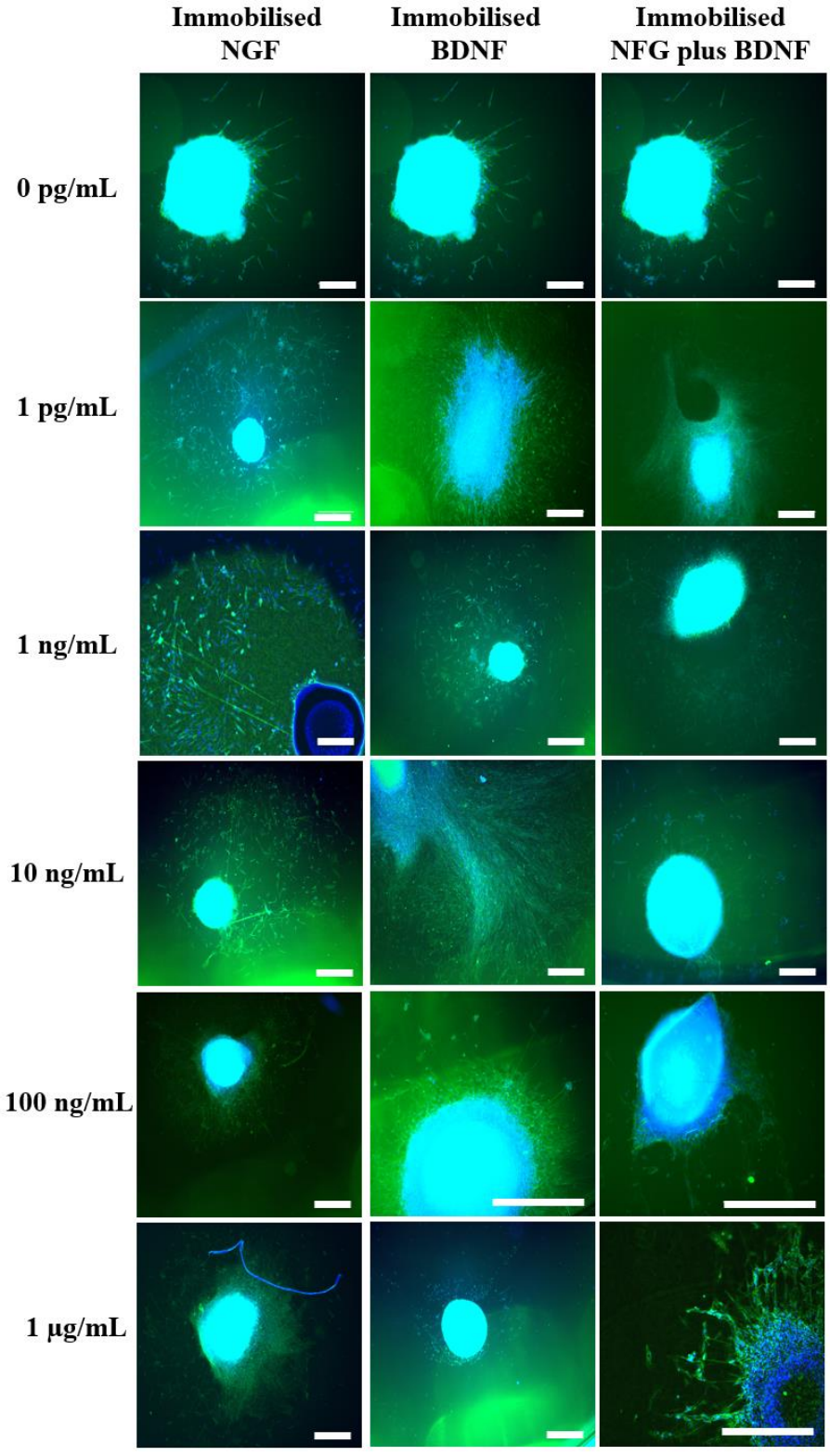

Figure 84. DRG seeded on bioactive surfaces with immobilised NGF, BDNF or NGF plus BDNF at concentrations of 1 pg/mL, 1 ng/mL, 10 ng/mL, 100 ng/mL and 1 µg/mL. Nuclei stained in blue (DAPI); β-III tubulin protein in neurites stained in green. Scale bar = 500 µm.

7.4.1.1 Effect of Nerve Growth factor

Neurite outgrowth of DRG was measured and averaged to obtain average neurite length of DRG cultured on TCP, NH_2^+, NH_2^+ + Heparin, and NH_2^+ + Heparin + Immobilised NGF (immobilised NGF). The largest neurite length was 1075 ± 165 µm for DRGs seeded on immobilised NGF at 1 ng/mL. The shortest neurite length was 44 ± 44 µm for DRGs cultured on TCP. Neurite outgrowth from DRGs cultured on immobilised NGF at 1 ng/mL was significantly longer in comparison to neurite length developed by DRGs when seeded on any other bioactive surface, as observed in Figure 85.

Additionally, it is important to notice that the response of the DRG, regarding neurite length, was related to the immobilised concentration of NGF on the surface: neurite outgrowth increased from 1 pg/mL (159 ± 116 µm) to a maximum length with 1 ng/mL (1075 ± 165 µm), and then neurite outgrowth started to decrease, from 10 ng/mL to 1 µg/mL (377 ± 0 µm, 353 ± 131 µm, 308 ± 112 µm respectively). Even though DRGs seeded on NH_2^+ + Heparin with NGF 1 µg/mL in solution developed neurites of 267 ± 105 µm in length, there was no significant difference from when the DRGs were cultured on immobilised NGF at 1 pg/mL.

These results suggested that the delivery of NGF as an immobilised molecule, encouraged the growth of larger neurites, in comparison to control groups. Moreover, NH_2^+ + Heparin + Immobilised NGF 1 ng/mL stimulated the growth of the longest neurites, indicating that using a relatively low concentration of NGF, long neurite outgrowth was achieved.

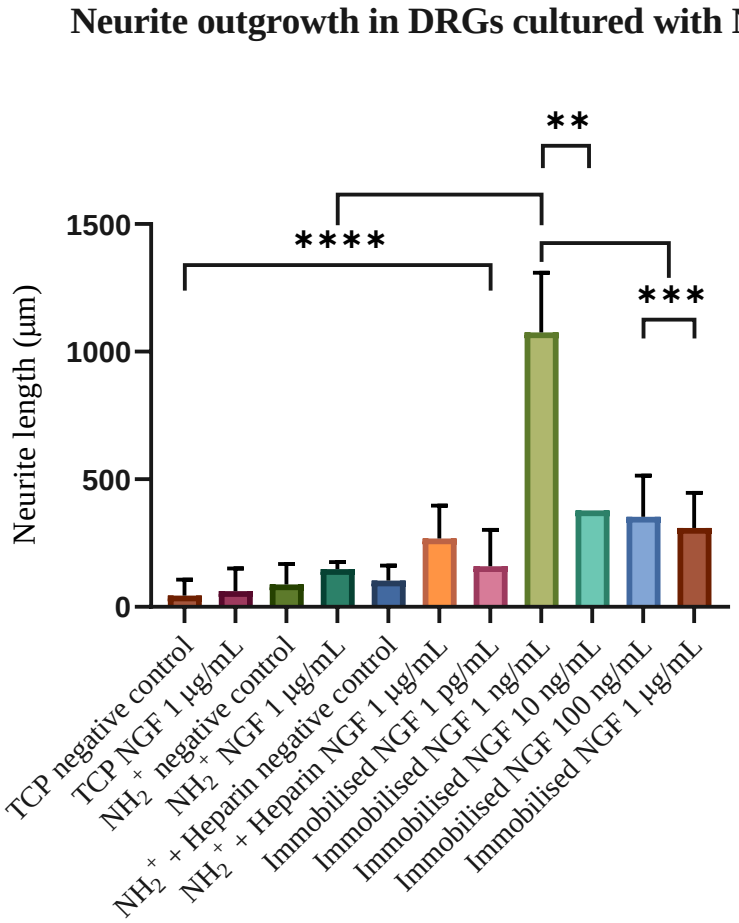

Figure 85. Average neurite length of dorsal root ganglia when cultured on TCP, NH_2^+, NH_2^+ + Heparin, and NH_2^+ + Heparin + Immobilised NGF. NGF was added to the bioactive surfaces at different concentrations. One-way ANOVA statistical analysis was performed with Tukey procedure of multiple comparisons *p< 0.05, **p<0.01, ***p< 0.001, ****p<0.0001. Mean ± SD. N=3, n=3.

Average maximum neurite outgrowth of DRG was measured and averaged to obtain average maximum neurite length of DRG cultured on TCP, NH_2^+, NH_2^+ + Heparin, and NH_2^+ + Heparin + Immobilised NGF (immobilised NGF). The shortest maximum neurite length was 53 ± 75 µm for DRG cultured on TCP. The largest maximum neurite length was 1357 ± 361 µm for DRG seeded on immobilised NGF at 1 ng/mL. A tendency is observed when the concentration of immobilised NGF was increased: for DRG with immobilised NGF at 1 pg/mL, the maximum neurite length was 338 ± 65 µm; then, the maximum neurite length reached the maximum neurite length (1357 ± 361 µm) when DRG were cultured on immobilised NGF 1 ng/mL. Then, when DRG were seeded on immobilised 10 ng/mL, 100 ng/mL and 1 µg/mL, maximum neurite length decreased as the concentration of NGF increased, from 843 ± 0 µm, 535 ± 246 µm to 468 ± 166 µm, respectively.

In addition, as control surfaces changed, from TCP, NH_2^+ to NH_2^+ + Heparin, and the addition of NGF in solution at a concentration of 1 µg/mL increased the maximum neurite length as well, as seen in Figure 86. However, when the DRG were seeded on immobilised NGF 1 ng/mL, the stimuli received from the bioactive surface encouraged the outgrowth of the largest neurite, significantly larger when compared to neurite growth from any other bioactive surface, indicating the significant potential of this bioactive surface to develop larger neurites.

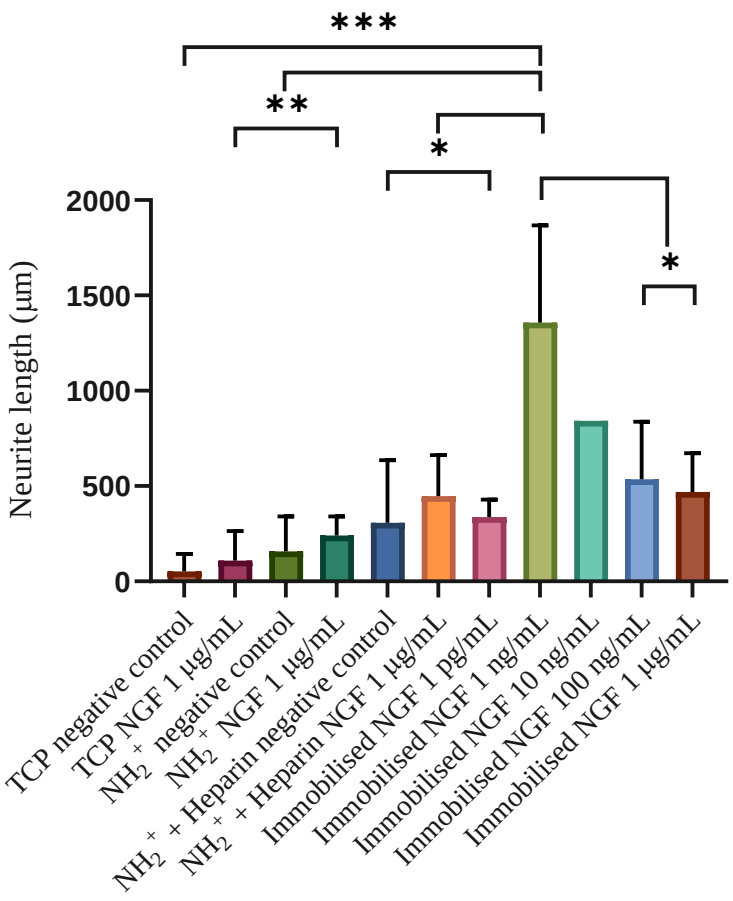

Figure 86. Average maximum neurite length of dorsal root ganglia when cultured on TCP, NH_2^+, NH_2^+ + Heparin, and NH_2^+ + Heparin + Immobilised NGF. NGF was added to the bioactive surfaces at different concentrations. One-way ANOVA statistical analysis was performed with Tukey procedure of multiple comparisons *p< 0.05, **p<0.01, ***p< 0.001, ****p<0.0001. Mean ± SD. N=3, n=3.

Number of neurite outgrowth by DRG was measured and averaged to obtain average number of neurites developed by DRGs cultured on TCP, NH_2^+, NH_2^+ + Heparin, and NH_2^+ + Heparin + Immobilised NGF (immobilised NGF). The lowest number of neurites developed was 2 ± 2, for neurites that grew on TCP (Figure 87). The highest number of neurites was 11 ± 4, for DRG cultured on immobilised NGF 1 ng/mL. However, this number was not significantly different in comparison to the number of neurites developed on other surfaces.

For DRG cultured on NH_2^+ + Heparin + NGF in solution at 1 µg/mL, the number of neurites developed was 10 ± 4, which was not significantly different from the number of developed neurites from DRGs cultures on NH_2^+ + Heparin, and NH_2^+ + Heparin + Immobilised NGF. Nevertheless, from Figure 87, it is noticeable that the number of neurites increased as the surface was modified with the addition of NH_2^+, heparin and NGF.

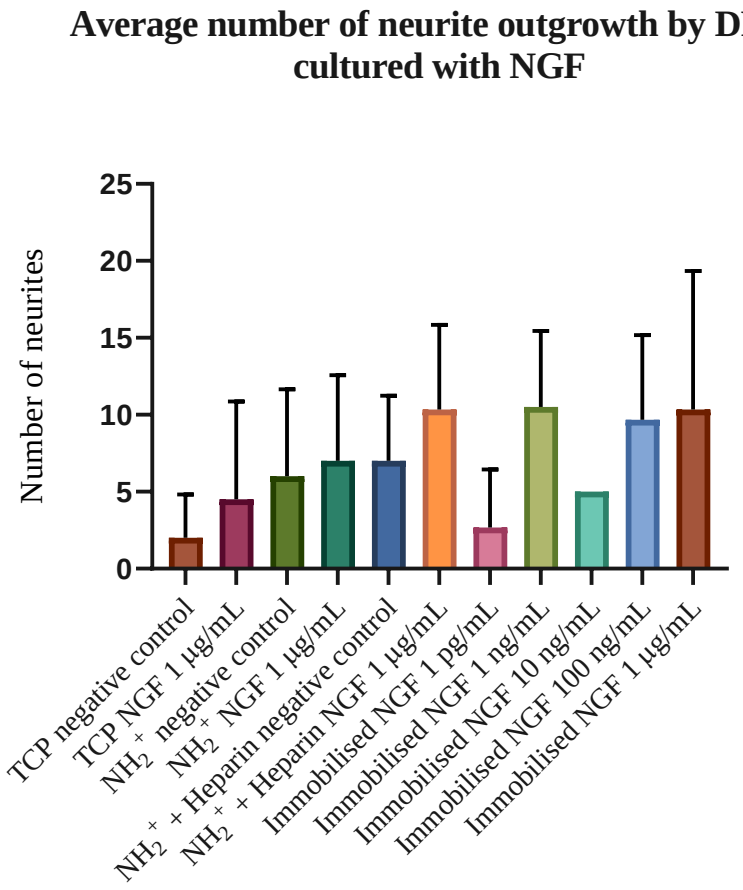

Figure 87. Averaged number of neurites outgrowth by dorsal root ganglia when cultured on TCP, NH_2^+, NH_2^+ + Heparin, and NH_2^+ + Heparin + Immobilised NGF. NGF was added to the bioactive surfaces at different concentrations. One-way ANOVA statistical analysis was performed with Tukey procedure of multiple comparisons *p< 0.05, **p<0.01, ***p< 0.001, ****p<0.0001. Mean ± SD. N=3, n=3.

7.4.1.2 Effects of Brain Derived Neurotrophic Factor

Neurite outgrowth of DRG was measured and averaged to obtain average neurite length of DRGs cultured on TCP, NH_2^+, NH_2^+ + Heparin, and NH_2^+ + Heparin + Immobilised BDNF (immobilised BDNF). The largest neurite length was 310 ± 68 µm for DRG cultured on immobilised BDNF at 1 ng/mL. The shortest neurite length was 44 ± 44 µm for DRGs cultured on TCP. Even though there were no significant differences in neurite length among all groups, it can be observed in Figure 88 that neurite length increased from when DRG were seeded on immobilised BDNF at 1 pg/mL (129 ± 23 µm) to when DRGs were cultured on immobilised BDNF at 1 ng/mL (310 ± 68 µm). After that, neurite length decreased as concentration of immobilised BDNF increased: from 268 ± 41 µm to 112 ± 7 µm.

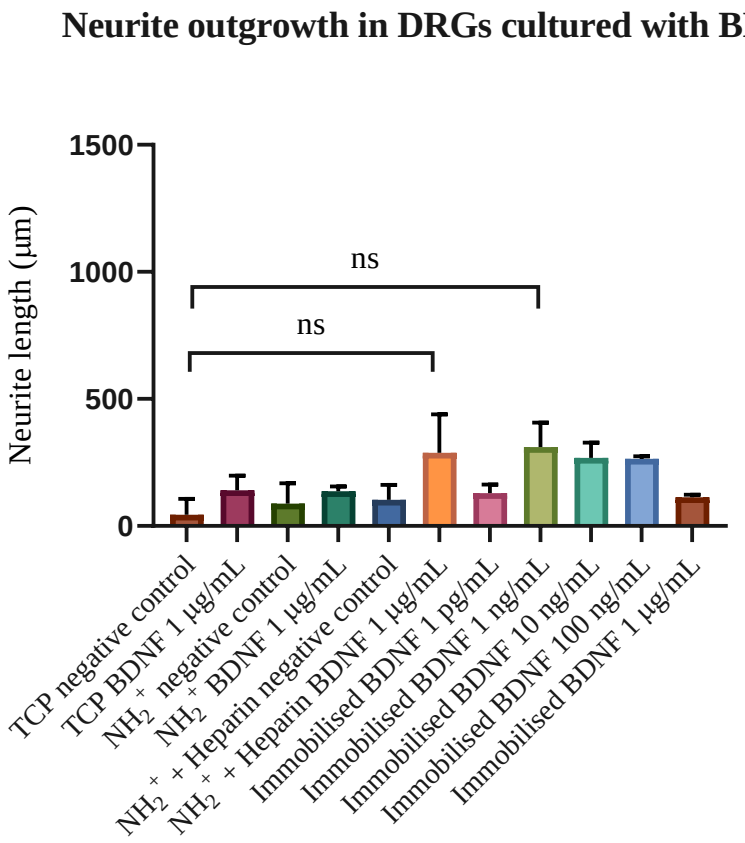

Figure 88. Average neurite length of *d*orsal *r*oot *g*anglia when cultured on TCP, NH_2^+, NH_2^+ + Heparin, and NH_2^+ + Heparin + Immobilised BDNF. BDNF was added to the bioactive surfaces at different concentrations. One-way ANOVA statistical analysis was performed with Tukey procedure of multiple comparisons *p< 0.05, **p<0.01, ***p< 0.001, ****p<0.0001. Mean ± SD. N=3, n=3.

Maximum neurite outgrowth of DRG was measured and averaged to obtain average maximum neurite length of DRG cultured on TCP, NH_2^+, NH_2^+ + Heparin, and NH_2^+ + Heparin + Immobilised BDNF (immobilised BDNF). The longest maximum neurite length was 557 ± 136 µm for DRGs cultured on immobilised BDNF at 1 ng/mL. The shortest maximum neurite length was 53 ± 75 µm for DRG cultured on TCP.

Even though the maximum neurite length was not significantly different among conditions, as seen in Figure 89, the maximum neurite length increased from 137 ± 32 µm (immobilised BDNF 1 pg/mL) to 557 ± 136 µm (immobilised BDNF 1 ng/mL). Then, the maximum neurite length started to decrease as immobilised concentration of BDNF increased: from 526 ± 255 µm, 458 ± 20 µm to 187 ± 12 µm (immobilised BDNF 10 ng/mL, 100 ng/mL and 1 µg/mL respectively. Moreover, maximum neurite length developed from control groups increased with surface modification and with the addition of BDNF at 1 µg/mL in solution.

In addition, although maximum neurite length was not significantly different among control and test groups, the maximum neurite length developed when DRG were cultured on immobilised BDNF 1 ng/mL was longer in comparison to maximum neurite length developed from NH_2^+ + Heparin with BDNF 1 µg/mL in solution (492 ± 130 µm).

Averaged maximum neurite length of DRGs cultured with BDNF

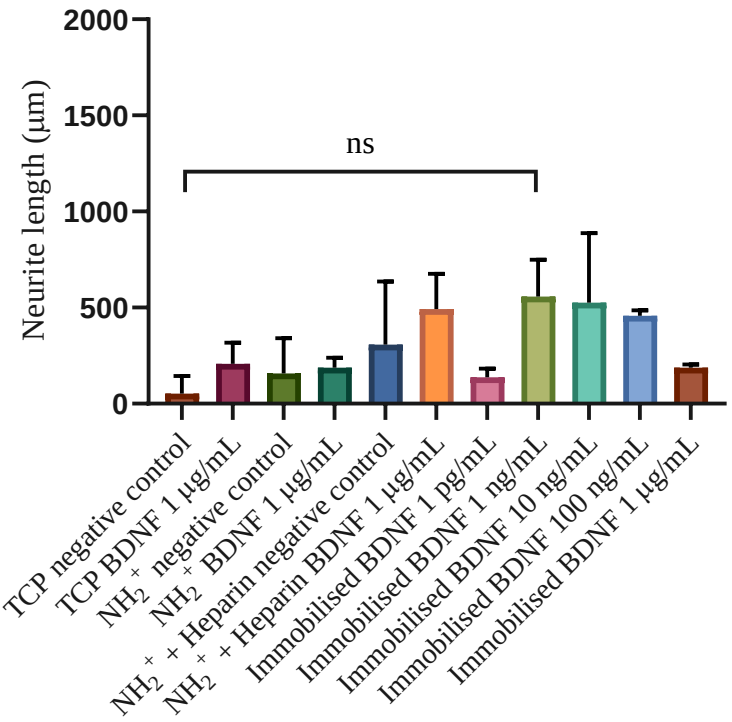

Figure 89. Average maximum neurite length of *d*orsal *r*oot *g*anglia when cultured on TCP, NH_2^+, NH_2^+ + Heparin, and NH_2^+ + Heparin + Immobilised BDNF. BDNF was added to the bioactive surfaces at different concentrations. One-way ANOVA statistical analysis was performed with Tukey procedure of multiple comparisons *p< 0.05, **p<0.01, ***p< 0.001, ****p<0.0001. Mean ± SD. N=3, n=3.

Number of neurite outgrowth by DRG was measured and averaged to obtain average number of neurites developed by DRG cultured on TCP, NH_2^+, NH_2^+ + Heparin, and NH_2^+ + Heparin + Immobilised BDNF (immobilised BDNF). The highest number of neurites developed was 11 ± 2 for DRG seeded on NH_2^+ + Heparin with BDNF in solution at 1 µg/mL. The lowest number of developed neurites was 2 ± 2 and 2 ± 1 for DRG seeded on TCP and immobilised BDNF at 1 pg/mL respectively. Additionally, when DRG were cultured on immobilised BDNF at 1 ng/mL, the average number of neurites developed was 10 ± 7. This could suggest that this bioactive surface encouraged the outgrowth of a maximum of 17 neurites. However, the standard

deviation was, as seen in Figure 90, led to a non-significant difference among this bioactive surface and other control and test groups.

Although there were no significant differences among control and test groups, when BDNF was immobilised at 1 pg/mL and 1 µg/mL, the number of developed neurites was low (2 ± 1 and 4 ±1 respectively), suggesting that a low and a high concentration of BDNF may not encourage the formation of neurites, either by no activation or over activation of neurite formation pathways.

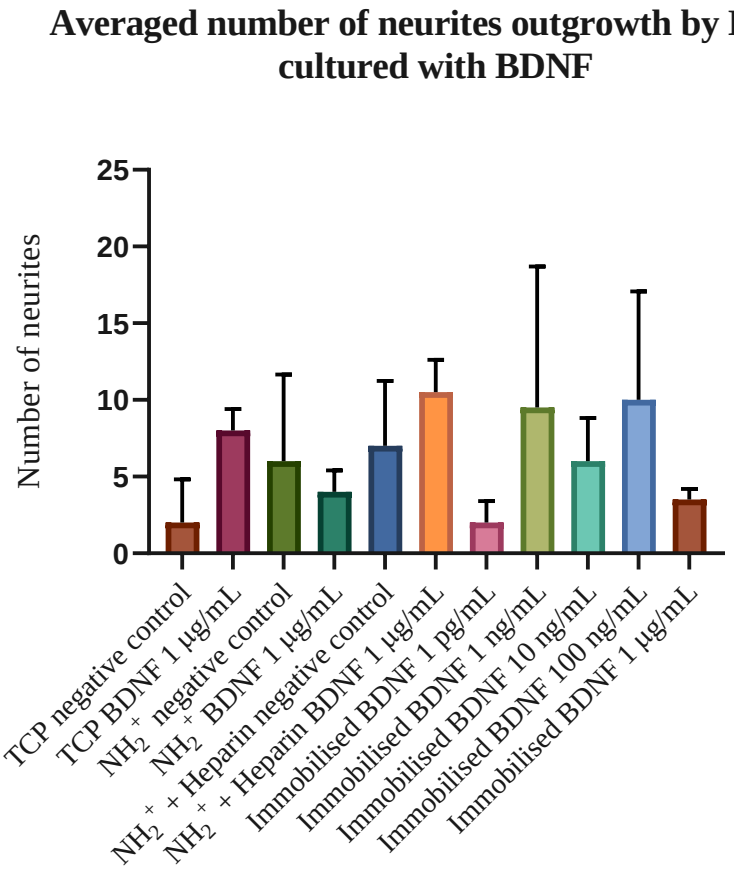

Figure 90. Averaged number of neurites outgrowth by *d*orsal *r*oot *g*anglia when cultured on TCP, NH_2^+, NH_2^+ + Heparin, and NH_2^+ + Heparin + Immobilised BDNF. BDNF was added to the bioactive surfaces at different concentrations. One-way ANOVA statistical analysis was performed with Tukey procedure of multiple comparisons *p< 0.05, **p<0.01, ***p< 0.001, ****p<0.0001. Mean ± SD. N=3, n=3.

7.4.1.3 Effects of Nerve Growth Factor plus Brain Derived Neurotrophic Factor

Neurite outgrowth of DRG was measured and averaged to obtain average neurite length of DRGs cultured on TCP, NH_2^+, NH_2^+ + Heparin, and NH_2^+ + Heparin + Immobilised NGF plus BDNF (immobilised NGF plus BDNF). The largest neurite length was 502 ± 141 µm for DRGs cultured on immobilised NGF plus BDNF at 100 ng/mL. The shortest neurite was 44 ± 44 µm when DRG were cultured on TCP control. Furthermore, NH_2^+ with NGF plus BDNF in solution at 1 µg/mL did not encourage the growth of any neurite.

Interestingly, as observed in Figure 91, neurite outgrowth was low in control groups. However, when the neurotrophins were immobilised on the surface, neurite outgrowth was encouraged further, even though neurite length for DRG cultured on immobilised NGF plus BDNF at 10 ng/mL and 1 µg/mL was 138 ± 36 µm and 188 ± 2 µm, respectively. Moreover, there was no significant difference between neurite length developed from DRG cultured on immobilised NGF plus BDNF 1 ng/mL and immobilised NGF plus BDNF at 100 ng/mL, suggesting that by immobilising both neurotrophins at a relative low concentration (1ng/mL), it may encourage the outgrowth of neurites that are of similar length than the ones developed by a higher concentration (100 ng/mL) of co-immobilised neurotrophins.

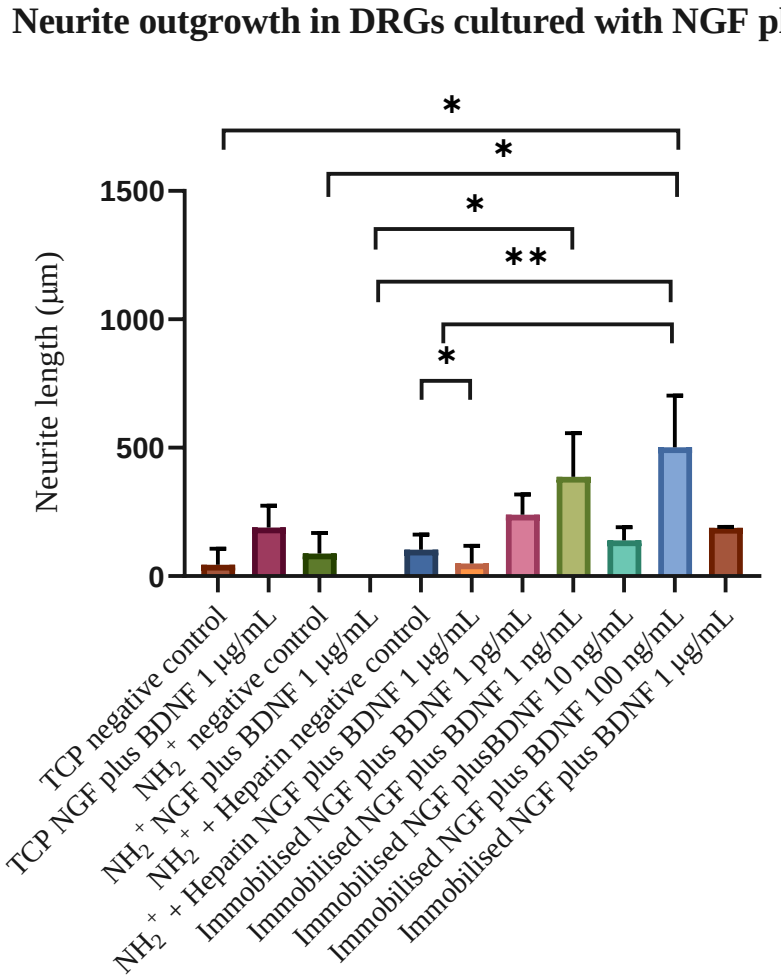

Figure 91. Average neurite length of *d*orsal *r*oot *g*anglia when cultured on TCP, NH_2^+, NH_2^+ + Heparin, and NH_2^+ + Heparin + Immobilised NGF plus BDNF. NGF plus BDNF were added to the bioactive surfaces at different concentrations. One-way ANOVA statistical analysis was performed with Tukey procedure of multiple comparisons *p< 0.05, **p<0.01, ***p< 0.001, ****p<0.0001. Mean ± SD. N=3, n=3.

Maximum neurite outgrowth of DRG was measured and averaged to obtain average maximum neurite length of DRG cultured on TCP, NH_2^+, NH_2^+ + Heparin, and NH_2^+ + Heparin + Immobilised NGF plus BDNF (immobilised NGF plus BDNF). The largest maximum neurite length was 702 ± 104 µm for DRG cultures on immobilised NGF plus BDNF at 100 ng/mL. The shortest maximum neurite length was 0 ± 0 µm and 53 ± 75 µm for DRG cultured on NH_2^+ with NGF plus BDNF in solution at 1 µg/mL and TCP respectively.

Moreover, maximum neurite length increased as the immobilised concentration of NGF plus BDNF increased (as seen in Figure 92), reaching the highest point with immobilised NGF plus BDNF at 100 ng/mL. Then, maximum neurite length decreased from 702 µm to 313 µm (immobilised NGF plus BDNF at 1 µg/mL)

Although maximum neurite length was achieved for DRG cultured on immobilised NGF plus BDNF at 100 ng/mL, there was no significant difference among this and the maximum neurite length developed by immobilised NGF plus BDNF at 1 pg/mL and immobilised NGF plus BDNF at 1 ng/mL (335 ± 148 µm and 460 ± 193 µm, respectively). These results suggest that bioactive surface immobilised with relative low concentrations of NGF plus BDNF at 1 pg/mL and NGF plus BDNF at 1 ng/mL have the potential to encourage a maximum neurite length as long as the one developed by DRG cultured on immobilised NGF plus BDNF at 100 ng/mL.

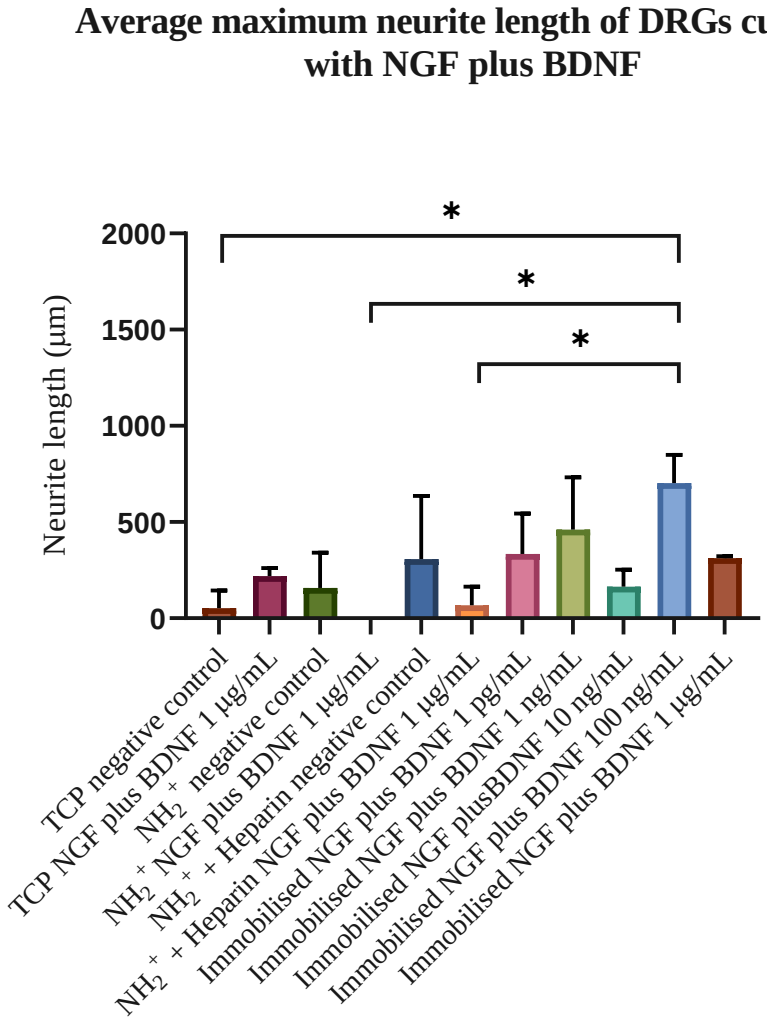

Figure 92. Average maximum neurite length of *d*orsal *r*oot *g*anglia when cultured on TCP, NH_2^+, NH_2^+ + Heparin, and NH_2^+ + Heparin + Immobilised NGF plus BDNF. NGF plus BDNF were added to the bioactive surfaces at different concentrations. One-way ANOVA statistical analysis was performed with Tukey procedure of multiple comparisons *p< 0.05, **p<0.01, ***p< 0.001, ****p<0.0001. Mean ± SD. N=3, n=3.

Number of neurite outgrowth by DRG was measured and averaged to obtain average number of neurites developed by DRG cultured on TCP, NH_2^+, NH_2^+ + Heparin, and NH_2^+ + Heparin + Immobilised NGF plus BDNF (immobilised NGF plus BDNF). The largest number of neurites was 10 ± 2, obtained from DRG cultured on immobilised NGF plus BDNF at 1 µg/mL. The smallest number of neurites was 0 and 2, from DRGs seeded on NH_2^+ with NGF plus BDNF at 1 µg/mL in solution and immobilised NGF plus BDNF at 1 pg/mL.

As observed in Figure 93, the number of neurites increased as the concentration of immobilised NGF plus BDNF increased. However, surface NH_2^+ + Heparin encouraged the growth of 7 ± 3 neurites. Although there was no significant difference among control and test groups, the NH_2^+ + Heparin surface promoted the growth of as many neurites as the immobilised NGF plus BDNF 100 ng/mL surface (8 ± 2). However, immobilised NGF plus BDNF at 100 ng/mL encouraged the growth of longer neurites.

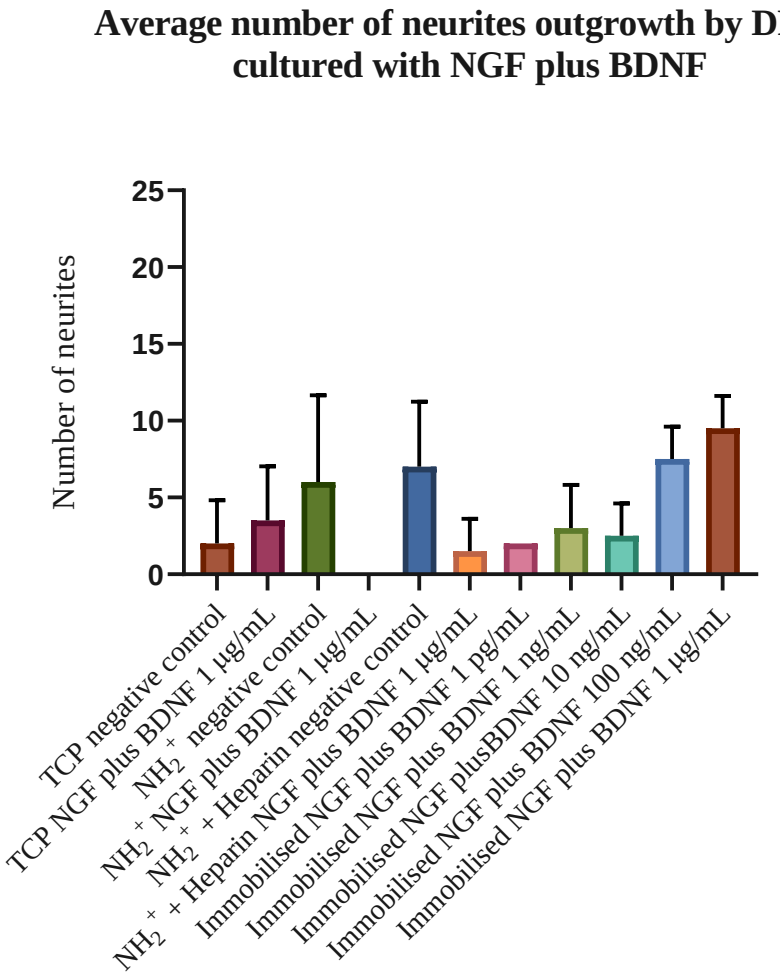

Figure 93. Averaged number of neurites outgrowth by *d*orsal *r*oot *g*anglia when cultured on TCP, NH_2^+, NH_2^+ + Heparin, and NH_2^+ + Heparin + Immobilised NGF plus BDNF. NGF plus BDNF were added to the bioactive surfaces at different concentrations. One-way ANOVA statistical analysis was performed with Tukey procedure of multiple comparisons *p< 0.05, **p<0.01, ***p< 0.001, ****p<0.0001. Mean ± SD. N=3, n=3.

7.4.2 Effects of bioactive surfaces in migration profile of primary Schwann cells

Firstly, the purity of Schwann cells was verified, as the protocol followed from Kaewkhaw et al. [220] was used to purify Schwann cells from adult rat sciatic nerve. Schwann cells were immunolabeled against S100-β, and nuclei were stained with DAPI following the protocol described in Chapter 4, section 4.3.4. Images were taken as described in Chapter 4, section 4.3.5.

Schwann cell purity based on S100-β positive immunolabeling, at passage 3 (Figure 94), was 99.8 ± 0.24%. This percentage of purity was calculated by counting the number of cells that stained positive for S100-β, then multiplying this number by 100, and dividing this value by the total number of cells. Kaewkhaw et al. showed that by passage 2, Schwann cell purity was 98.3 ± 0.3% [220]. Moreover, this increased to 99.9 ± 0.6% (passage 7) [220]. These findings support the idea that the cells isolated from chick embryo DRG, using Kaewkhaw et al. protocol, were Schwann cells.

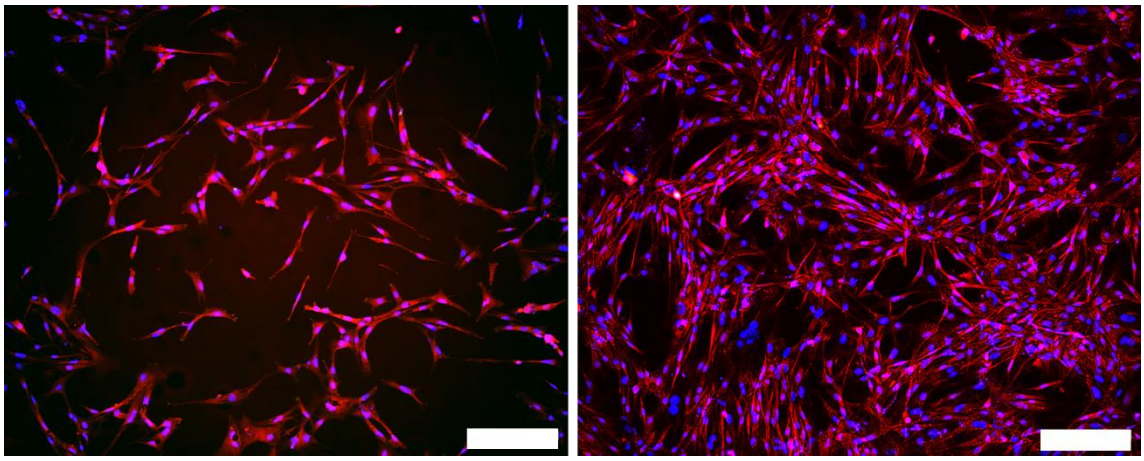

Figure 94. Schwann cell purity based on S100-β positive immunolabeling (red). Nuclei were stained with DAPI (blue). Scale bar = 200 µm

After confirming that the cells isolated from chick embryo DRG were Schwann cells, a migration assay was conducted to evaluate if the bioactive surface affected the migration profile of Schwann cells. Stoppers were used to create an area free of cells, which on day 0 were removed so Schwann cells could migrate to the free space. On days 1, 2, 5 and 7, the free area was measured, and a percentage calculated which represented the area to which Schwann cells migrated on that day.

As seen in Figure 95, bioactive surfaces immobilised with NGF did not show any significant difference in the percentage of area covered by Schwann cells after 7 days in culture. Neither bioactive surfaces, with or without NGF in solution, showed any significant difference regarding Schwann cell migration. However, Schwann cells cultured with TNF-α 300 U/mL revealed that 98 ± 1.7% of the original cell-free area was covered by Schwann cells within 7 days in culture. It is important to highlight that the standard deviation of this condition was small, showing that Schwann cells responded to the stimuli of TNF-α homogeneously. In contrast, Schwann cells cultured on the bioactive surfaces, with or without NGF, showed a heterogeneous response.

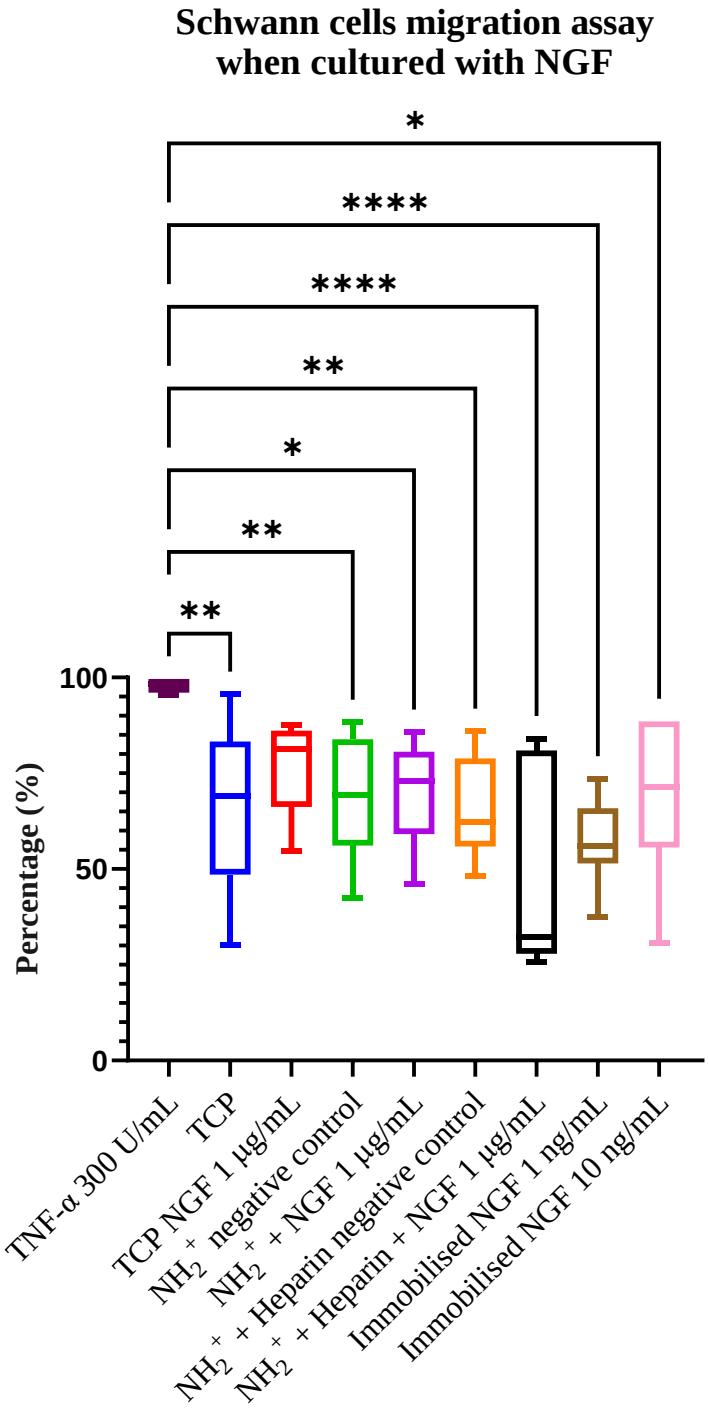

Figure 95. Migration assay of Schwann cells represented as a percentage of cell-free area covered by Schwann cells after 7 days in culture on bioactive surfaces with NGF. Immobilised NGF 1 ng/mL and 10 ng/mL were chosen as they had a better performance in neurite growth in PC12 adh neuronal cells. One-way ANOVA statistical analysis was performed with Tukey procedure of multiple comparisons *p< 0.05, **p<0.01, ***p< 0.001, ****p<0.0001. Mean ± SD. N=3, n=3.

Similarly, the percentage of migration of Schwann cells when cultured on bioactive surfaces immobilised with BDNF did not show any significant difference, as seen in Figure 96. Comparably to the results obtained from Schwann cells cultured with NGF, the response of Schwann cells when cultured with BDNF were not significantly different either. Nevertheless, significant differences were found for the percentage of migration of Schwann cells when cultured with TNF-α.

These results suggested that bioactive surface and bioactive surface with immobilised NGF or BDNF did not encourage Schwann cells to migrate rapidly nor homogeneously.

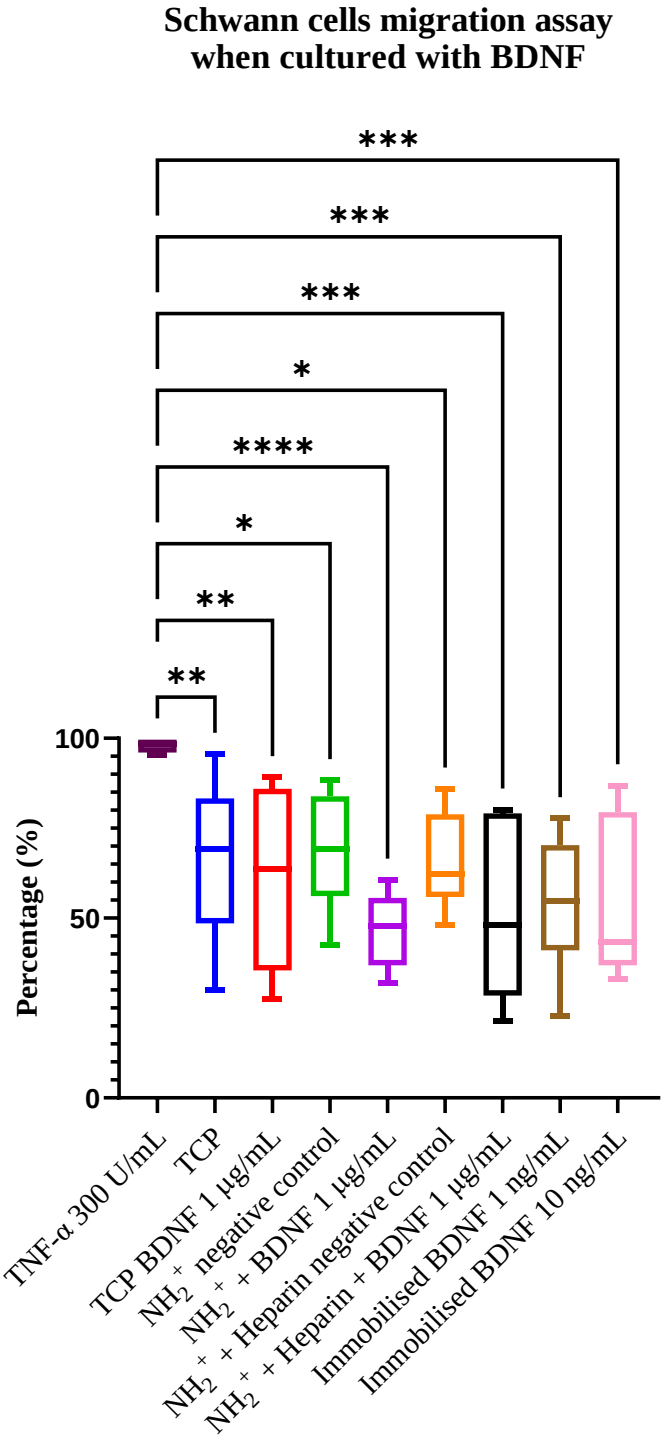

Figure 96. Migration assay of Schwann cells represented as a percentage of cell-free area covered by Schwann cells after 7 days in culture on bioactive surfaces with BDNF. Immobilised BDNF 1 ng/mL and 10 ng/mL were chosen as they had a better performance in neurite growth. One-way ANOVA statistical analysis was performed with Tukey procedure of multiple comparisons *p< 0.05, **p<0.01, ***p< 0.001, ****p<0.0001. Mean ± SD. N=3, n=3.

Migration of Schwann cells on days 0, 1, 2, 5 and 7, on the different surfaces TCP (

Figure 97), NH_2^+ (Figure 98), and NH_2^+ + Heparin (Figure 99), with and without NGF or BDNF at a concentration of 1 μg/mL in solution in cell culture media are shown. Furthermore, images can be seen of Schwann cells seeded on NH_2^+ + Heparin + Immobilised NGF and NH_2^+ + Heparin + Immobilised BDNF (Figure 100). NGF and BDNF were immobilised at 1 ng/mL and 10 ng/mL. Also, TNF-α at 300 U/mL in solution in cell culture medium was used as a positive control.

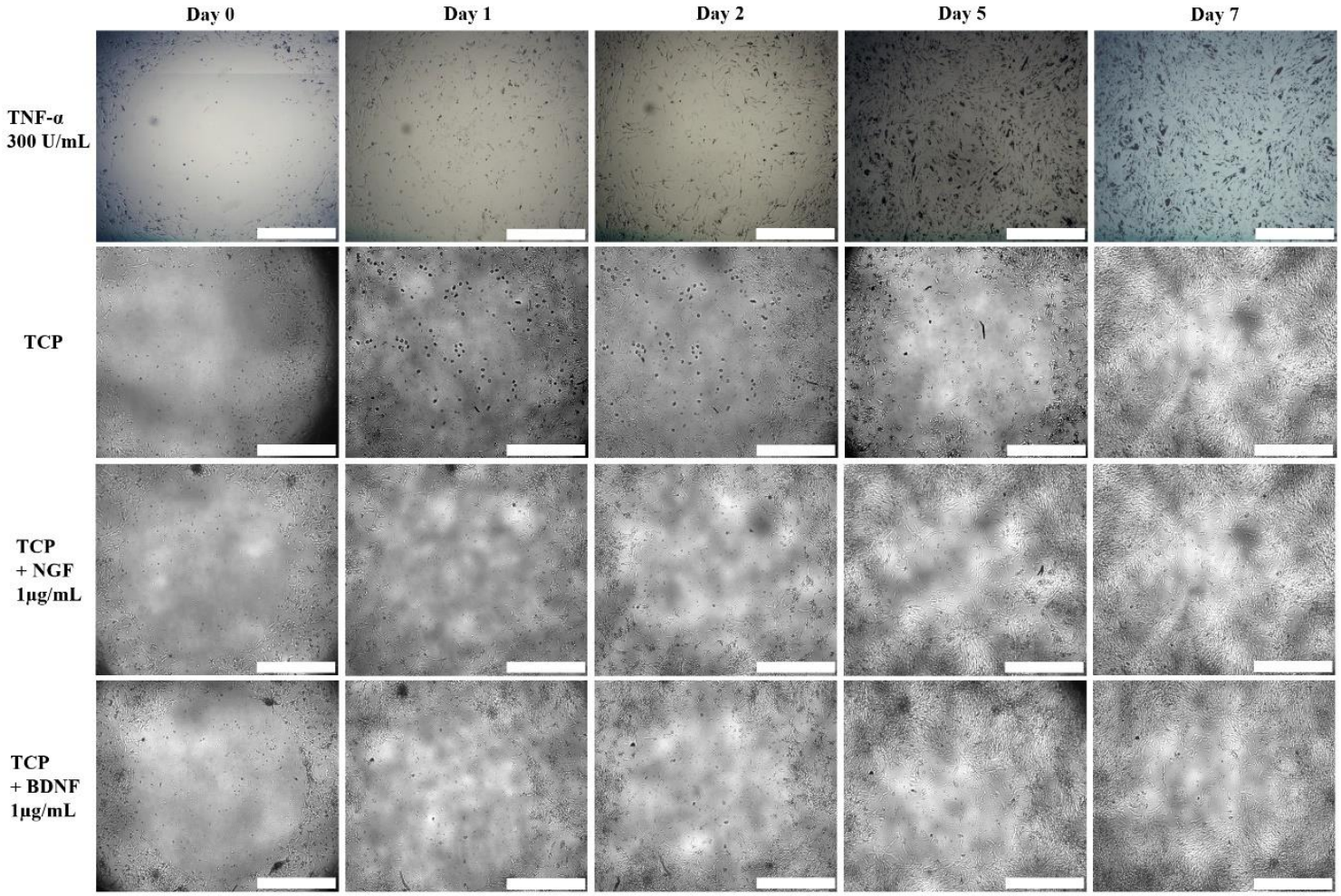

Figure 97. Migration assay when Schwann cells were seeded on TCP with and without NGF or BDNF in solution. Schwann cells migrated towards the cell-free area left by the stoppers. Scale bar = 1 mm. N=3, n=3.

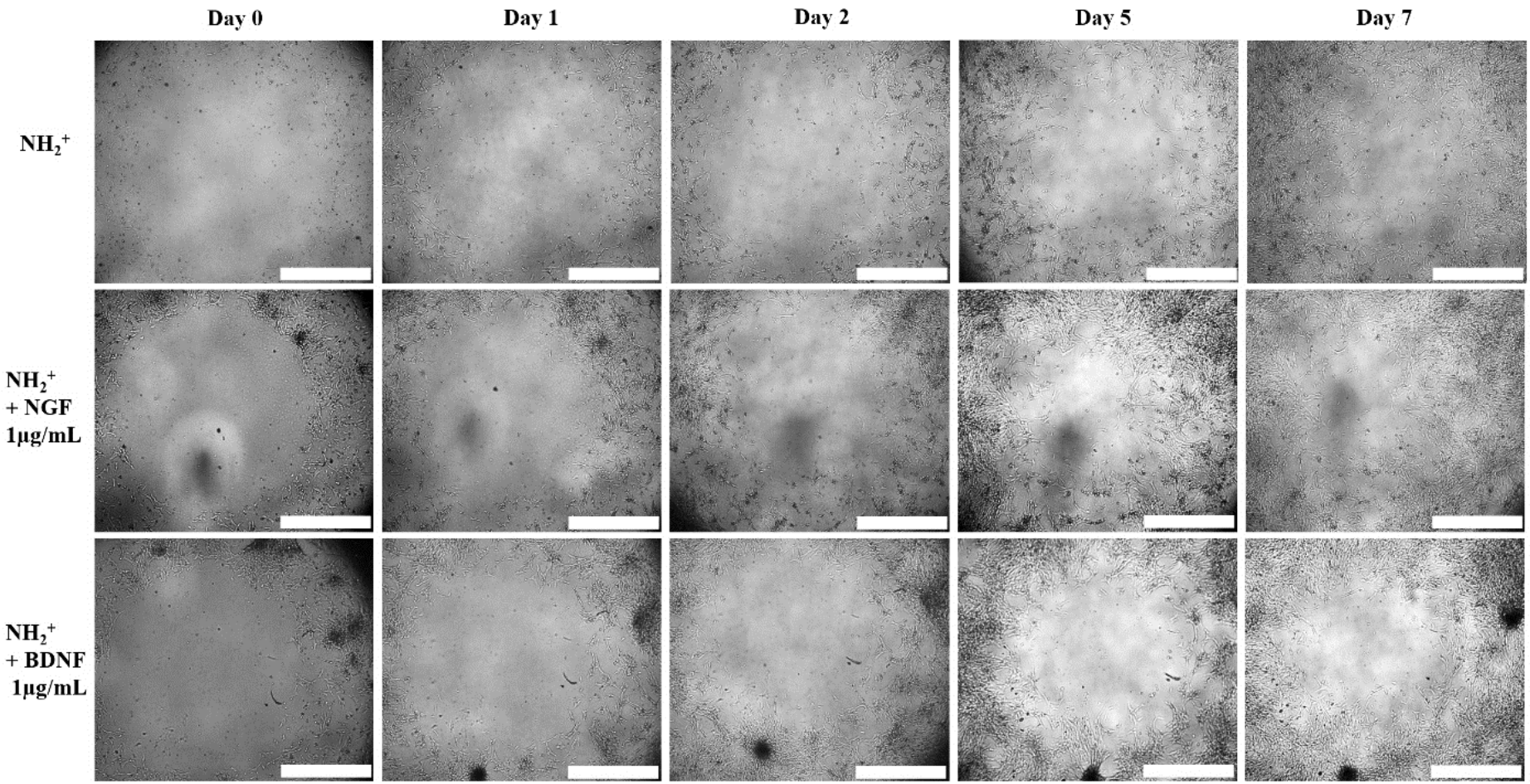

Figure 98. Migration assay when Schwann cells were seeded on NH_2^+ surface with and without NGF or BDNF in solution. Schwann cells migrated towards the free area left by the stoppers. Scale bar = 1 mm. N=3, n=3.

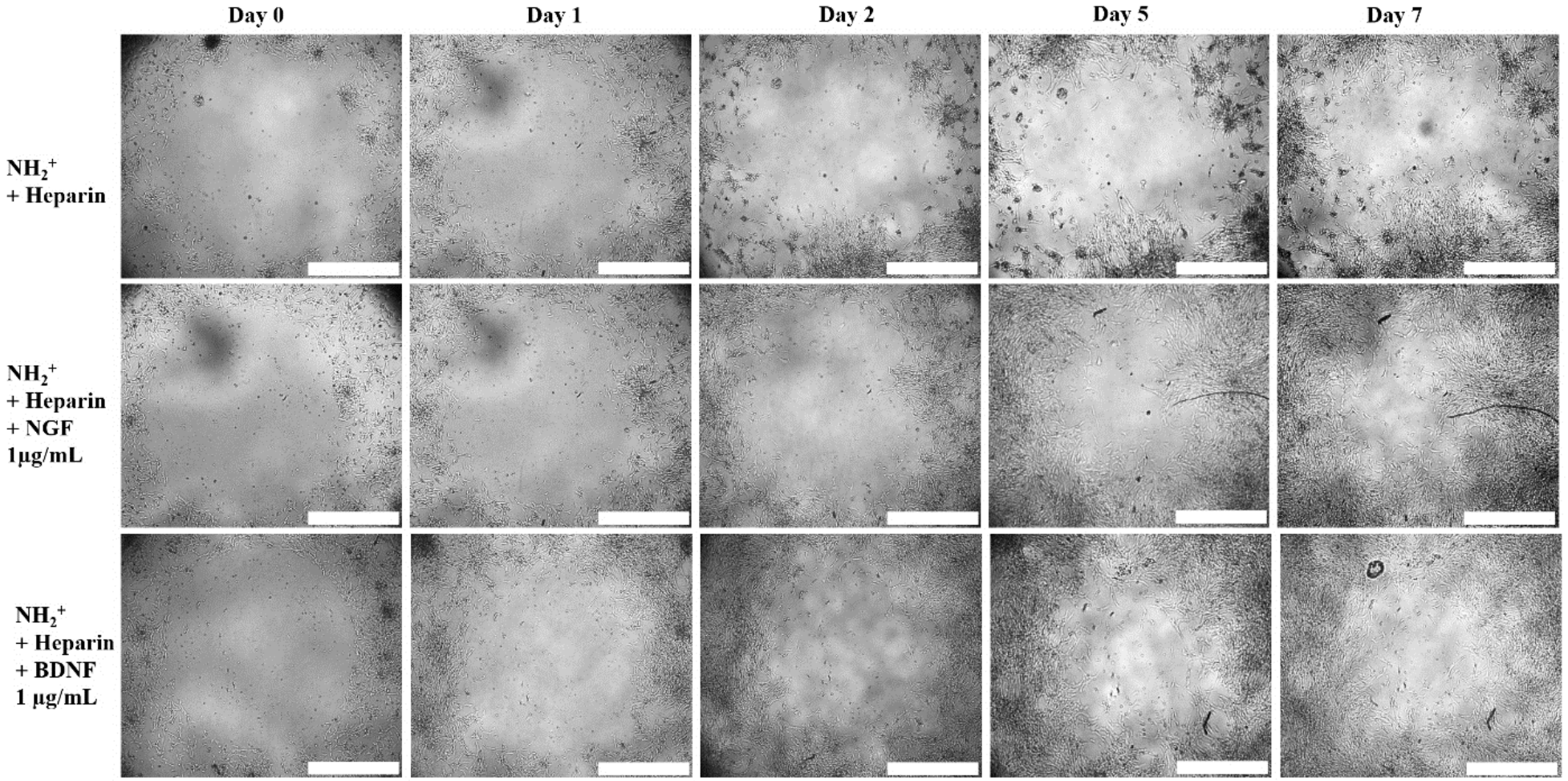

Figure 99. Migration assay when Schwann cells were seeded on NH_2^+ + Heparin surface with and without NGF or BDNF in solution. Schwann cells migrated towards the free area left by the stoppers. Scale bar = 1 mm. N=3, n=3.

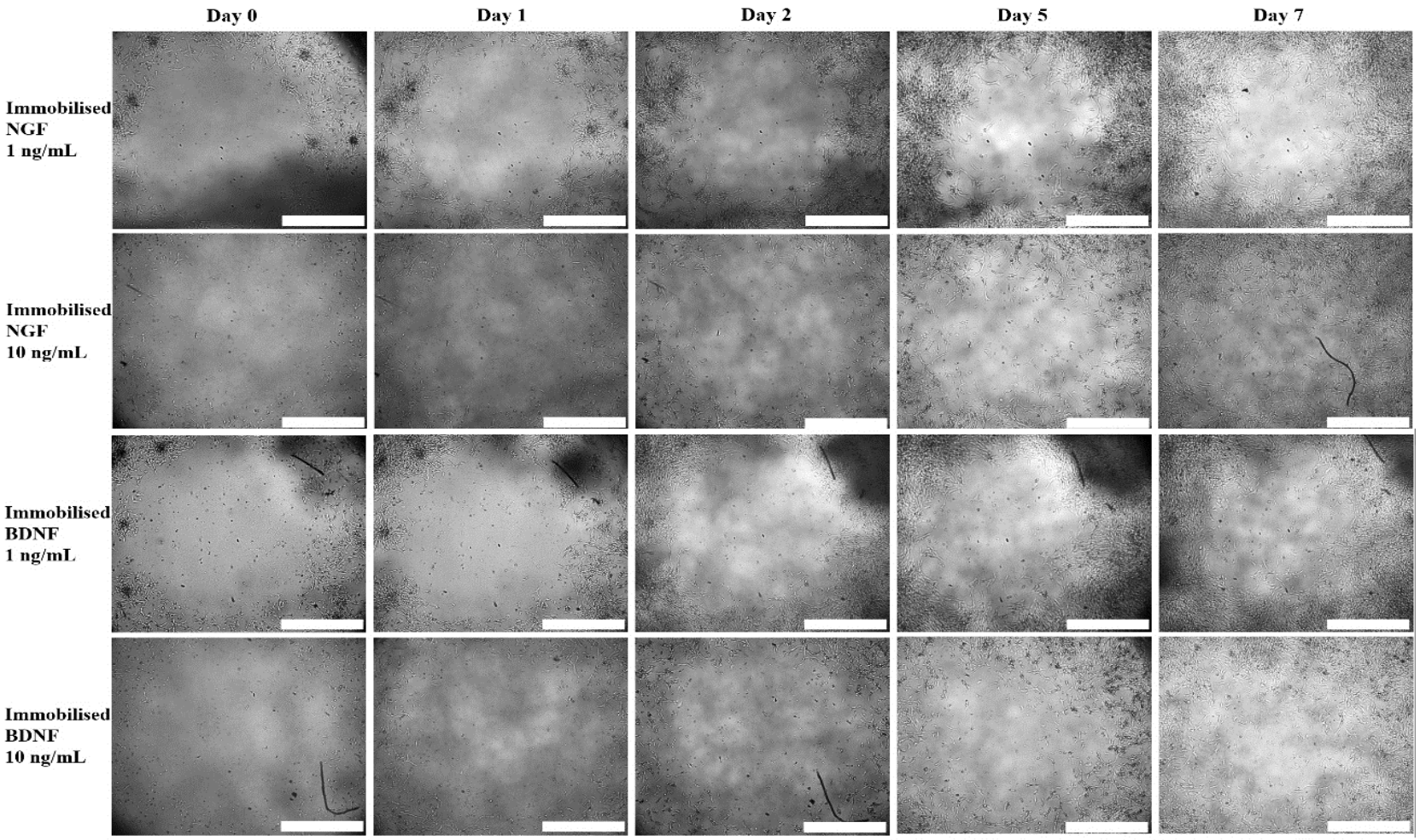

Figure 100. Migration assay when Schwann cells were seeded on bioactive surface with immobilised NGF or BDNF. Schwann cells migrated towards the free area left by the stoppers. Scale bar = 1 mm. N=3, n=3.

7.5 Discussion

Average neurite length, average maximum neurite length, and number of neurites developed by DRG cultured on bioactive surfaces NH_2^+, NH_2^+ + Heparin, and NH_2^+ + Heparin + Immobilised NGF or BDNF or NGF plus BDNF were evaluated. Neurites were grown and developed successfully when cultured on bioactive surfaces with immobilised growth factors. The longest average neurite length was 1075 ± 165 µm for DRG seeded on NH_2^+ + Heparin + Immobilised NGF at 1 ng/mL. Furthermore, under the same condition, average maximum neurite length was 1357 ± 361 µm, and the largest number of neurites was 11 ± 4 (as seen in Figure 84).

Nevertheless, immobilised BDNF also encouraged neurite development and outgrowth, although not to a great extent as when compared to DRG were seeded on surfaces immobilised NGF. Longest neurite length and maximum neurite length were 310 ± 68 µm and 557 ± 136 µm, respectively, for DRGs cultured on surfaces immobilised with BDNF at 1 ng/mL. Moreover, the largest number of neurites was 11 ± 2 for DRG seeded on NH_2^+ + Heparin with BDNF in solution at 1 µg/mL.

It was hypothesised that when NGF and BDNF were co-immobilised on the NH_2^+ + Heparin bioactive surface, their effects on neurite length, maximum neurite length and number of neurites would be cumulative. However, this was not the case. Longest neurite length and longest maximum neurite length were 502 ± 141 µm and 702 ± 104 µm, respectively, when DRG were cultured on surfaces immobilised with NGF plus BDNF at 100 ng/mL. The largest number of neurites was 10 ± 2 observed when DRG were seeded on surfaces immobilised with NGF plus BDNF at 1 µg/mL.

A better response was observed when NGF was immobilised alone on the bioactive surface, but not for BDNF. The co-immobilisation of NGF and BDNF promoted the growth of neurites longer than those grown with BDNF alone, but shorter than those grown with NGF alone. Furthermore, the concentration of co-immobilised NGF and BDNF was 100 ng/mL, 100 times more than when DRG were cultured with NGF or BDNF alone.

The use of DRG to evaluate the effects of the bioactive surface NH_2^+ + Heparin + Immobilised NGF, NH_2^+ + Heparin + Immobilised BDNF and NH_2^+ + Heparin + Immobilised NGF plus BDNF is biologically relevant. DRG are a representative model of the complexity of the nervous system as they are composed of neurons, Schwann cells and supportive cells such as fibroblasts. The use of DRG as a model for peripheral nerve injury mimics similar neurite outgrowth and Schwann cell migration during nerve repair as occurs *in vivo*. Therefore, these results are encouraging, as they demonstrated that by using a relative low concentration of immobilised NGF (1 ng/mL), a higher response from DRG was obtained in comparison to immobilised BDNF, immobilised NGF plus BDNF and control groups.

Researchers have previously evaluated NGF, BDNF, and GDNF in conjunction with nerve guide conduits and scaffolds, and investigated neurite expression [75], [158], [227], [229], [291], [319]. In these studies, neurotrophins were added to the biomaterial's surface using different approaches. The concentration of neurotrophins employed was higher than those used in this thesis. Gomez and Schmidt [227] immobilised 1 ng/mm^2 of NGF on polypyrrole using a photochemical technique. Average neurite length developed by rat DRG was 20 µm after 2 days in culture [227]. Tang et al. [291] fabricated a gradient of immobilised NGF on poly(ε-caprolactone)-poly(L-lactic)acid. The release of NGF within 7 days was 3.6 to 11.35 ng/mL, and neurite length of DRG after 3 days in culture differed according to gradient zone: from 600 to 1,500 µm [291]. In contrast, bioactive surfaces produced herein were used as a platform to deliver immobilised growth factors after 7 days release, using less than 1 ng/mL. The longest average neurite length of 1,075 µm was developed when bioactive surfaces were immobilised with 1 ng/mL of NGF. This indicates that the delivery of neurotrophins is more efficient when using neurotrophins at less than 1 ng/mL for encouraging the growth of neurites greater than 1,000 µm in length *in vitro*.

Furthermore, Matsumoto et al. functionalized amino nanotubes with NGF or BDNF [264]. NGF and BDNF (at a concentration of 10 ng/mL) were covalently immobilised to the amino nanotubes using 1-ethyl-3-(3-dimethylaminopropyl) carbodiimide hydrochloride (EDC) reagent [264]. The NGF-nanotubes and BDNF-nanotubes

stimulated neurite development from chick DRG similarly to when NGF or BDNF were in solution in culture medium at a concentration of 10 ng/mL [264]. Interestingly, when 0.5 to 20 µL of NGF-nanotubes were added to the culture medium, they achieved a dose-response similar to when NGF was in solution in the culture medium. Nevertheless, when adding more than 20 µL of NGF-nanotubes, the number of neurites decreased. The authors suggested that NGF receptors were downregulated in the presence of a high concentration of NGF [264]. In contrast, when 2 µL of BDNF-nanotubes (2 ng of neurotrophin) were added to DRG culture, the highest number of neurites was achieved [264]. The loading concentration of neurotrophins was higher than the ones used in this thesis. Moreover, it is difficult to determine at which volume of NGF-nanotube more neurites were developed. This data may or may not be similar to the response of immobilised NGF at 1 ng/mL shown in this thesis. However, it might be that BDNF-nanotubes stimulated a greater response in comparison to immobilised BDNF regarding the number of developed neurites.

Fine et al. created polymer rods, within a guidance channel, for releasing NGF or GDNF [61]. This rod was fabricated with 760 mg of ethylene-vinyl acetate (EVA), 7.6 mL of methylene chloride, 230 mg BSA and 10 mg of either NGF or GDNF dissolved in 7.6 mL of water (final concentration of 1.3 mg/mL) [61]. Polymer rods were cultured with DRG for 30 minutes and then retrieved. Subsequently, DRG were cultured for a total of 6 days. For DRG cultured with NGF-rods, neurite outgrowth was 1817 ± 55 µm; similarly, when cultured with GDNF-rods, neurite outgrowth was 1124 ± 88 µm [61]. The concentration of either NGF or GNDF in each rod was 1.3 mg/mL [61]. As the authors did not characterised the release of NGF or GDNF, it is unknown how much neurotrophin was released to the culture medium with the DRG. However, neurite length achieved using these rods was very close to neurite outgrowth using a low concentration of immobilised NGF in this thesis (1 ng/mL, average neurite length 1075 ±165 µm; average maximum neurite length 1357 ± 361 µm). This suggests that by using low concentrations of immobilised NGF, specifically 1 ng/mL, a similar response regarding neurite length is obtained when compared with the use of 1.3 mg/mL of NGF.

Additionally, Sakiyama-Elbert and Hubbell immobilised 100 ng/mL of NGF, BDNF or neurotrophin-3 (NT-3) into a fibrin-based cell ingrowth matrix, which contained heparin [157]. This study showed that this delivery system improved neurite extension of chick embryo DRG up to 50, 75 and 100% when DRG were seeded on NT-3, NGF and BDNF fibrin matrices, respectively [157]. Moreover, the authors also tested the effect of 50 and 250 ng/mL of immobilised NGF into the fibrin matrix. They found that neurite length response was biphasic, where significant neurite extension was achieved at 100 ng/mL [157]. This finding was attributed to the saturation of TrkA receptors [157]. Nevertheless, they did not state the neurite length developed from the 3 different amounts of immobilised NGF. Although a biphasic dose response was observed, where the optimal dose encouraged the growth of the longest neurites; doses greater than the optimal dose did not stimulate neurite outgrowth [157]. These findings support the results in this thesis, where NGF and BDNF encourage neurite outgrowth, and where a biphasic dose response was obtained from both immobilised NGF and immobilised BDNF. Moreover, the optimal dose of immobilised NGF and BDNF in this thesis was 1 ng/mL, suggesting that the bioactive surface NH_2^+ + Heparin + Immobilised NGF and NH_2^+ + Heparin + Immobilised BDNF at 1 ng/mL, a relative low concentration, promotes the growth of long neurites, which may be comparable to the ones stimulated by 100 ng/mL of NGF used by Sakiyama-Elbert and Hubbell.

NGF and BDNF stimulate neurite expression and outgrowth. However, their effects may differ depending if the neurons are sensory or motor neurons. Santos et al. characterised the effect of 5, 10, 50 and 100 ng/mL of NGF, BDNF, GDNF, neurotrophin-3 (NT-3) and 25, 50, 250 and 500 ng/mL of fibroblast growth factor-2 (FGF-2) in DRG and in organotypic culture of spinal cord *in vitro* [158]. Results showed that GDNF and FGF-2 stimulated sensory and motor neurite growth at all concentrations. However, concentrations of 50 and 100 ng/mL promoted longer neurites [158]. NGF and NT-3 enhanced sensory neurite outgrowth, with the largest neurite outgrowth obtained at 50 ng/mL. Moreover, 50 ng/mL of BDNF promoted the development of longer neurites in motor neurons. Furthermore, 5 and 10 ng/mL of BDNF slightly encouraged the growth of longer neurites, whereas 100 ng/mL did not stimulate neurite outgrowth [158]. Thereafter, NGF, BDNF and NT-3 were added into

a collagen matrix inside a silicon tube to aid sciatic nerve repair [158]. This experiment showed that high concentrations of BDNF stimulated neurite outgrowth in motor neurons, whereas NGF and NT-3 had no effect [158]. This adds to the findings in this thesis, that even though both NGF and BDNF stimulated neurite outgrowth, immobilised NGF encouraged the growth of longer neurites in comparison to neurites developed from immobilised BDNF.

Moreover, Yang et al. encapsulated NGF within poly(lactide-co-glycolide) (PLG) nerve conduits (single and multi-lumen) and evaluated neurite outgrowth in DRG [129]. These conduits were fabricated by assembly and fusion of microspheres [129]. NGF was either mixed with the microsphere or it was encapsulated inside the microspheres [129]. The concentration of NGF released from the PLG conduit was 14 ng/mL at 1 day, 7 days and 14 days, although, the authors failed to mention the initial load of NGF [129]. At day 7 and at day 14, average neurite length was ca. 350 µm and ca. 450 µm, respectively, for encapsulated NGF, in a single lumen conduit [129]. When NGF was mixed with the microspheres, in a single lumen conduit, average neurite length at day 7 and day 14 were similar, ca. 450 µm [129]. Furthermore, when NGF was encapsulated in a multi-lumen conduit, the average neurite length was ca. 400 µm on both day 7 and day 14 [129]. Even though no significant difference was obtained among the control and test groups, the authors suggested that the minimal difference among them was related to diffusion of NGF through the material [129]. Comparably, the results in this thesis showed that by immobilising relatively low concentration of BDNF (1 ng/mL), similar neurite length was achieved. Moreover, when immobilising relatively low concentrations of NGF (1 ng/mL), longer neurite length was developed. Furthermore, when co-immobilising NGF plus BDNF at 100 ng/mL, neurite outgrowth was similar to the values reported by Yang et al. when they delivered 14 ng/mL. This suggested that the effect of co-immobilising NGF and BDNF was not cumulative and, it needed a higher concentration of growth factor to achieve a similar neurite length for when 14 ng/mL was delivered.

Furthermore, research has been performed to evaluate higher concentrations of growth factors. For example, Pearson et al. evaluated neurite outgrowth of rat DRG using

glass micro-conduit filled with collagen hydrogel solution and 100 ng/mL of NGF [130]. At day 6, average neurite length was ca. 1000 µm, and average maximum neurite length was ca. 2700 µm [130]. At day 13, average neurite length was ca. 1500 µm, and average maximum neurite length was ca. 3300 µm [130]. Nevertheless, the authors stated that, after 7 days, NGF from the conduit was not able to stimulate neurite outgrowth, hence, NGF had to be added to the culture medium (concentration not specified) [130]. The results from this thesis demonstrate that by immobilising NGF at 1 ng/mL onto the bioactive surface NH_2^+ + Heparin, a greater response could be obtained regarding average neurite length as when 100 ng/mL of NGF was used in a collagen hydrogel. Even though Pearson et al. encouraged an average maximum neurite length of 2700 µm, which is longer than the one developed in this thesis (1357 ± 361 µm), it can be seen that their results were highly variable, as their average neurite length was 1000 µm. This would suggest that the delivery system of Pearson et al. might not be optimal, whereas the delivery system developed in this thesis NH_2^+ + Heparin + immobilised NGF 1 ng/mL would be more appropriate because it does not encouraged variability (average neurite length of 1075 ± 165 µm and average maximum neurite length of 1357 ± 361 µm).

Studies have also been performed to evaluate the effect of neurite outgrowth while delivering 2 or 3 neurotrophins at the same time. For example, Deister and Schmidt evaluated average neurite length of rat DRG when NGF, GDNF and ciliary neurotrophic factor (CNTF) were in solution at 50, 10 and 10 ng/mL respectively [285]. When the 3 growth factors were present in solution in culture medium with DRG, the largest neurite length was 2031 ± 97 µm compared to 916 ± 64 µm for DRG with no growth factors [285]. The authors stated that the concentrations used of each growth factor were optimised individually, and that the concentrations that individually encouraged longer neurites were used in combination with the other growth factors [285]. Nevertheless, the authors did not describe how these concentrations performed individually, they only mentioned that those were the optimal values. Hence, a direct comparison of cumulative effect is difficult to do. However, neurite outgrowth was longer than the one presented in this thesis, suggesting that a combination of growth factors may encourage more neurite growth.

In addition, Kim et al. immobilised NGF and basic fibroblast growth factor (bFGF) on PCL/Pluronic F127 microspheres using heparin [320]. The co-immobilisation of NGF and bFGF on the microspheres encouraged more neurite development from muscle-derived stem cells than microspheres immobilised with either NGF or bFGF alone [320]. The authors explained that the co-immobilisation of NGF and bFGF worked better due to a) the sustained release of growth factors, b) their suitable stimulation of cell migration, proliferation and survival, and c) cumulative effect of NGF and bFGF [320].

The research from Deister and Schmidt [285], and Kim et al. [320] suggest that the optimal concentration of growth factors may be different when used individually as when used in combination depending on which growth factors are being used. Moreover, if the concentrations are well defined, a cumulative effect might be observed. In this thesis, NGF was used as it stimulates neurite outgrowth in DRG. BDNF was also used in this thesis as it aids nerve regeneration by promoting survival in neurite extension of DRG [84].

After a biomaterial is implanted inside the body, water molecules start interacting with the surface of the biomaterial, creating an intimate layer [91]. Then, proteins are absorbed onto the surface of the biomaterial, and adherent cells expressing integrins arrive at the surface and start interacting with the protein layer [91]. Afterwards, cells adhere, migrate, and differentiate, which takes place from a few hours to a few days after the biomaterial is implanted [91]. As bioactive surfaces with immobilised NGF at 1 ng/mL did not exhibit any neurotrophin release between 1 and 48 hours (see Chapter 5 in this thesis), such a delivery platform would allow time for neuronal cells to adhere to a functionalized surface of a regenerating guidance scaffold before receiving stimuli from NGF at the surface to promote growth. Chick embryo DRG were seeded on bioactive surfaces containing immobilised growth factors. DRG were used because they are easy to access and are comparable with other model animal systems regarding neurite outgrowth and regeneration [321]–[323].

Bioactive surfaces with immobilised NGF at 1 ng/mL promoted the longest growth of neurite in all groups, which was 18 times higher than negative TCP control. DRG

response on bioactive surfaces immobilised with BDNF showed a similar response, compared to immobilised NGF surfaces, with immobilised 1 ng/mL of BDNF supporting the longest neurite. Bioactive surfaces immobilised with NGF plus BDNF at 100 ng/mL encouraged the growth of neurites significantly longer than those on negative control TCP or TCP with NGF at 1 µg/mL in solution in culture medium. The difference in response of neurite outgrowth can be hypothesised as the activation of second messenger pathways, following neurotrophin binding to expressed cell membrane receptors. NGF and BDNF bind to tyrosine kinase receptors (Trk), specifically TrkA and TrkB respectively [158], [287], [309]. The NGF-TrkA complex is internalised at the neurite growth cone and transported to the neuron's body, stimulating actin and microtubule polymerization, organelle recruitment and calcium influx [319]. When the NGF-TrkA complex is not internalized, the phosphatidylinositol 3-kinase and Akt/protein kinase B (PI3k/Akt) pathway is activated, regulating neurite outgrowth and cell survival [227], [287], [291].

When BDNF binds to its specific receptor, TrkB, the PI3K/Akt pathway is also activated and microtubules rearranged to promote lamellipodial formation and filopodial elongation [137]. Therefore, Trk receptors trigger signaling pathways that stimulate neurite outgrowth in sensory and motor neurons. In DRG, TrkA and TrkB receptors are expressed in the cell membrane. The density of TrkA receptors is higher in comparison to TrkB receptors [324]. However, after nerve injury, the expression of TrkB receptors is upregulated [158]. Therefore, both NGF and BDNF are essential to encourage neurite outgrowth and to inhibit cell death.

The data in this chapter, regarding neurite outgrowth from DRG, would suggest that the expression of TrkB receptors is low, as neurite outgrowth from immobilised BDNF bioactive surfaces was similar to immobilised NGF bioactive surfaces. When NGF and BDNF were co-immobilised, neurite outgrowth was not cumulative. This response might be related to the amount of BDNF released from the bioactive surface, because low doses of BDNF stimulate the upregulation of TrkB receptors, significantly improving the effect of BDNF. In comparison, high doses of BDNF would downregulate the expression of TrkB receptors. Furthermore, high doses of BDNF would impede neurite outgrowth [158], whereas low doses of BDNF promote neurite

elongation in DRG. Hence, when BDNF is delivered with NGF, an equilibrium should be achieved.

So far, the work in this thesis has reported the fabrication, physico-chemical properties and the biological response, regarding neurite development, of bioactive surfaces NH_2^+ + Heparin with immobilised NGF, BDNF and NGF plus BDNF, using commercially available amine coated plates and heparin. However, Schwann cell response to this bioactive surface had not yet been characterised. As Schwann cells migrate and form bands of Bünger to aid nerve regeneration after peripheral nerve injury [86], it was hypothesised that bioactive surfaces with immobilised NGF or immobilised BDNF would enhance Schwann cell migration.

Bioactive surfaces with immobilised NGF at 1 and 10 ng/mL, and bioactive surfaces with immobilised BDNF at 1 and 10 ng/mL were fabricated and used to assess Schwann cell migration. The results in this thesis showed that neither immobilised NGF nor immobilised BDNF stimulated significantly Schwann cell migration among test groups, even though Schwann cells showed an elongated bipolar morphology, suggesting a migratory state [253]. However, when Schwann cells were cultured with tumor necrosis factor-alpha (TNF-α), significant migration was seen. TNF-α was used as a positive control because, after nerve injury, Schwann cells express TNF-α, a pro-inflammatory cytokine [11], [15], [325], [326]. TNF-α encourages macrophage migration to the site of injury. Moreover, TNF-α encourages glial activation, survival, proliferation, migration and differentiation, especially from Schwann cells [312], [326], [327].

Research has been done to study if Schwann cells migrate in the presence of different growth factors. Maniwa et al. studied the effects of NGF, BDNF and NT-3 on migration of Schwann cells *in vitro* [316]. NGF, BDNF and NT-3 were prepared at concentrations of 0.1, 1, 10 and 100 ng/mL. Migration of cells cultured with each growth factor was evaluated for 1 hour [316]. NGF, at a concentration of 10 ng/mL, encouraged and accelerated Schwann cell migration, whereas 1 ng/mL of NT-3 slightly stimulated Schwann cell migration. Nevertheless, BDNF did not promote Schwann cell migration significantly [316]. The authors suggested that the difference

between NT-3 and NGF as neurotrophins that encourage migration might be due to the different distribution of receptors on the cell [316].

The study from Maniwa et al. supports the findings from Min et al. who showed that NGF and GDNF encourage Schwann cell migration whereas BDNF did not [86]. Furthermore, Cornejo et al. studied the effect of neuregulin β-1 (NRG1), GDNF, epidermal growth factor (EGF) and NGF, at a concentration of 200 ng/mL, on Schwann cell (precursor line) migration [328]. The authors wanted to determine if GDF, EGF, NRG1 and NGF were chemokinetic or chemoattractant growth factors for a Schwann cell precursor line [328]. Cornejo et al showed that GDNF, and NRG1 were chemoattractant and chemokinetic growth factors whereas NGF was only a chemokinetic growth factor [328]. The data obtained from EGF was inconclusive [328]. The results from this thesis showed that bioactive surfaces with and without immobilised NGF or BDNF and with or without neurotrophins in solution did not significantly encourage Schwann cell migration. It is interesting to see that studies have indicated that NGF stimulates significantly Schwann cell mobility. However, the work in this thesis did not reflect that. Nevertheless, the results obtained from BDNF were consistent with what other research shows.

In addition, Anton et al. found that 10 ng/mL of NGF encouraged Schwann cell migration through activation of low affinity $p75^{NRT}$ receptor [329]. After 72 hours in culture, Schwann cells migrated more than 350 μm [329]. Moreover, Cao et al. found that Schwann cells migrated over an olfactory ensheathing cell monolayer due to secreted NGF [330]. Unfortunately, concentration of NGF was not specified [330]. Additionally, Yamauchi et al. observed that NT-3 (10 ng/mL), by binding to TrkC, encouraged Schwann cell migration by activation of the Rho GTPases and c-Jun N-terminal kinase signalling pathways [318]. But, Schwann cell migration was not stimulated by NGF nor BDNF [318]. Yamauchi et al. also established that BDNF (100 ng/mL), by binding with the $p75^{NRT}$ receptor, inhibited Schwann cell migration [313]. They showed that BDNF impeded Schwann cell migration by activating the RhoA signalling pathway [313].

This data appears contradictory because other studies had demonstrated that BDNF stimulated Schwann cell migration. For example, Yi et al. and Hou et al. affirmed that BDNF stimulated Schwann cell migration [317], [331]. Moreover, Singh et al. studied how 10, 100 and 200 ng/mL of BDNF, EGF, stromal cell-derived factor (SDF-1), GDNF and CNTF encouraged non-myelinating Schwann cells to migrate [311]. Non-myelinating Schwann cells were seeded on a Boyden chamber, and left overnight at 37°C and 5% CO_2 and then cells that migrated towards the lower chamber, where the growth factors in cultured medium were, were counted [311]. Their results showed that non-myelinating Schwann cells migrated in the presence of BDNF (200 ng/mL) up to 10 fold in comparison to the control [311]. Moreover, BDNF at 100 ng/mL also greatly stimulated non-myelinating Schwann cells [311]. EGF, SDF-1, GDNF and CNTF also promoted non-myelinating Schwann cell migration, however, the migration response was not as great as the migration response obtained from BDNF.

Research has shown that there is a very complex mechanism behind Schwann cell migration, that might involve the coordinated expression and action of different neurotrophins, cytokines and cells. Up to a certain extent, the work from other authors might explain why BDNF did not encourage Schwann cell migration in this thesis. One main reason could be that the concentrations of BDNF used in this thesis were low, 1 ng/mL and 10 ng/mL, in comparison to the concentrations used in other studies, 50-200 ng/mL [311], [317], [331]. Nevertheless, there are other studies that showed that BDNF at 100 ng/mL did not stimulate Schwann cell migration [313]. This suggests that there might be other factors to consider. After peripheral nerve injury, Schwann cells produce NGF, BDNF, NT-3 and neurotrophin-4/5 (NT-4/5). These neurotrophins modulate neurons and Schwann cells phenotype [317], [330]. However, NGF synthesis increases rapidly whereas the production of BDNF increases slowly [316]. This may suggest that NGF might be first to act on Schwann cell migration with BDNF stimulating migration afterwards [316]. Although NGF and BDNF bind to TrkA and TrkB receptors respectively, they also bind to $p75^{NRT}$ receptor. Hence, how these neurotrophins distribute themselves to stimulate different actions between growing neurites and Schwann cells is not clear [86], [315].

Schwann cells migrate after nerve injury and form band of Bünger to guide regenerating neurites [316], [318]. Schwann cell migration is stimulated and regulated by the Rho GTPases Rac1 and Cdc42 signalling pathway [313]. When this pathway is activated, through the $p75^{NTR}$ receptor, the cytoskeleton is reorganized, encouraging not only morphological changes but also migration [313], [328]. Moreover, as Schwann cells continue to migrate, they express high levels of $p75^{NTR}$ receptors, thus, migration is encouraged even more [329]. By activation of $p75^{NTR}$ receptors, Schwann cells migrate. Both NGF and BDNF bind to $p75^{NTR}$ receptor, however, it is not clear how an equilibrium between active and non-active $p75^{NTR}$ receptors should be achieved to encourage Schwann cell migration. More research needs to be done to elucidate this.

7.6 Conclusion

In this chapter, average neurite length, average maximum neurite length and number of neurites developed from primary chick embryo DRG were assessed. DRG were seeded on bioactive surface NH_2^+ + Heparin + Immobilised NGF, NH_2^+ + Heparin + Immobilised BDNF and NH_2^+ + Heparin + Immobilised NGF plus BDNF. Results showed that longest average neurite length and average maximum neurite length were achieved when DRG were cultured on NH_2^+ + Heparin + Immobilised NGF at 1 ng/mL. Moreover, a dose response curve was obtained, where the longest neurites were obtained at NGF 1ng/mL and then, neurite length decreased as immobilised NGF increased. Furthermore, DRG response when seeded on immobilised BDNF showed a similar trend to immobilised NGF, nevertheless, the response was not as significant. In addition, a cumulative effect was not observed when DRG were cultured on bioactive surfaces with immobilised NGF plus BDNF.

Also, Schwann cell migration was studied when primary chick embryo Schwann cells were cultured on bioactive surfaces NH_2^+ + Heparin + Immobilised NGF and NH_2^+ + Heparin + Immobilised BDNF. No significant response was observed from test groups, suggesting that other factors should be considered.

In summary, bioactive surfaces encouraged significant neurite outgrowth from DRG, specially, NH_2^+ + Heparin + Immobilised NGF at 1 ng/mL. This supports the hypothesis that by using the bioactive surface with a relatively low concentration of NGF, neurite outgrowth was significantly obtained.

The system reported herein is relatively simple to fabricate and scalable for direct applications. Up to this point in this thesis, bioactive surfaces were fabricated using commercially available NH_2^+ coated culture plates. In the next chapter, plasma deposition will be used to add NH_2^+ to polycaprolactone electrospun fibers. Moreover, DRG will be seeded on these scaffolds and their response evaluated.

Chapter 8 Scalability of the bioactive surface: adding the bioactive surface to polycaprolactone electrospun scaffolds and its effect on neurite outgrowth

8.1 Introduction

Peripheral nerve injury affects 2.8% of trauma patients [332], and the current treatment is the use of autografts [155]. However, the limitations of using autografts are donor site morbidity, size mismatch, and the need of at least two surgeries [155]. The use of hollow tubes called nerve guide conduits (NGCs) has been studied as an alternative to aid nerve repair [14], [16], [105]. Nevertheless, NGCs do not support sufficient nerve regeneration in gaps longer than 20 mm [2], [14], [63]. Therefore, the addition of topographical and chemical cues to the NGCs has been studied to improve their performance and, hence, nerve repair.

Research using gradients, aligned multichannels, and aligned electrospun scaffolds have demonstrated that an oriented cue can enhance neurite outgrowth as well as Schwann cell migration [104], [314], [333]–[335]. For example, Hurtado et al. showed that aligned nanofibers stimulated neurite regrowth in a spinal cord injury model [336]. Furthermore, Kim et al. reported that aligned fibers encouraged neurite growth in a 17 mm sciatic injury [337]. In addition, studies had stated that the use of aligned electrospun scaffolds would be more beneficial to use as these might resemble the extracellular matrix (ECM) [333], [336]. Therefore, if Schwann cells are stimulated to migrate [12], [316], these cells and the aligned electrospun scaffold would create a regenerative environment to aid nerve repair [104], [338]. Although studies using aligned fibrous scaffold have stimulated neurite outgrowth, the level of nerve regeneration produced is still not sufficient, as the critical nerve gap in humans is 4 cm, and in rats is 1.5 cm [105], [107], [339], An interesting route to further enable

nerve repair is to include chemical cues in the NGCs to provide a long term permissive environment [87], [334].

Nerve growth factor (NGF) and brain derived neurotrophic factor (BDNF) are known to encourage neurite outgrowth and Schwann cell migration after nerve injury [61], [133], [158], [264], [285], [317], [338]. Nevertheless, their use in the clinic, and in different approaches, is limited by their half-life, loss of their biological activity and that they might not reach the injury site [73], [76], [282]. Hence, research has been conducted to design and fabricate systems for the delivery of growth factors, which would protect growth factors from degradation and denaturation [217]. Growth factors can be incorporated onto electrospun scaffolds by covalent binding, electrostatic interactions, coatings, encapsulation and addition of microspheres, emulsion and coaxial electrospinning [76], [164]. With the exception of surface functionalisation via either covalent binding or electrostatic interactions, all the aforementioned techniques compromise the integrity and functionality of the growth factors due to their use of organic solvents [79]. The effectivity of covalent binding of growth factors has been demonstrated before, for example, Guex et al. covalently immobilised vascular endothelial growth factor (VEGF) onto an oxygen plasma treated scaffold and promoted endothelial cell proliferation [165]. Nevertheless, covalent binding might result in the loss of bioactivity or denaturation of the growth factor [182], [228], [340].

A second approach is to use electrostatic interactions to bind growth factors. Indeed, heparin has been used to immobilise growth factors by electrostatic interactions [182], [212]. For example, Robinson et al. bound osteoprotogerin or tissue inhibitor of metalloproteinases 3 to heparin and studied their release [212]. Heparin is highly negatively charged, so to bind heparin to a surface by electrostatic interactions, this surface needs to have a positive charge. Plasma treatment and deposition is commonly used to add charged functional groups to a surface, changing the properties of the surface [61], [212], [341]. For example, air and oxygen plasma treatment are used to make polymeric surfaces hydrophilic [341], and typically render these surfaces negatively charged [342]. To produce positively charged surfaces, amine based plasma deposition can be used, for example, by using allylamine to add positively changed amine NH_2^+ functional groups to a surface [61], [212], [239]. Hence, the surfaces

functionalised by plasma-deposited NH_2^+ groups bind heparin, which consequently binds growth factors such as NGF, BDNF or a mixture of NGF and BDNF.

Chapter 5 of this thesis showed how a bioactive surface, which was used as a delivery system of growth factors, was fabricated by using electrostatic interactions. Furthermore, chapter 6 and 7 demonstrated that bioactive surfaces composed of NH_2^+ + Heparin + Immobilised NGF, NH_2^+ + Heparin + Immobilised BDNF, and NH_2^+ + Heparin + Immobilised NGF plus BDNF encouraged neurite outgrowth on 2-dimensional (2D) surfaces.

In this chapter, it was important to translate this bioactive surface to a 3-dimensional (3D) scaffold, as it would further encourage and enhance neurite outgrowth in comparison to 2D [91]. Moreover, it was critical to design and scale up this bioactive surface so it could be easily translated into clinical use.

Therefore, electrospinning was used to fabricate polycaprolactone (PCL) fibrous scaffolds. Then, NH_2^+ functional groups were added to the scaffold by plasma deposition. Thereafter, heparin was added by passive conjugation. Finally, NGF, BDNF or a combination of NGF plus BDNF were immobilised. Hence, PCL + NH_2^+ + Heparin + Immobilised NGF scaffolds, PCL + NH_2^+ + Heparin + Immobilised BDNF scaffolds, and PCL + NH_2^+ + Heparin + Immobilised NGF plus BDNF scaffolds were fabricated. The bioactive surfaces were characterised by XPS and ELISA to confirm the incorporation of NH_2^+, heparin and growth factors. Moreover, to study the potential of the bioactive surface on the PCL electrospun scaffolds, chick embryo dorsal root ganglia (DRG) were seeded on the scaffolds, and neurite outgrowth and Schwann cell migration were assessed.

8.2 Aims and objectives

The aims of this chapter were:

1. Fabrication and characterisation of the bioactive surface NH_2^+ + Heparin + immobilised NGF/BDNF/NGF plus BDNF when this was added onto polycaprolactone (PCL) electrospun scaffolds.
2. Evaluate the effects of the bioactive surface NH_2^+ + Heparin + immobilised NGF, when added onto PCL electrospun scaffolds, on DRG neurite outgrowth and primary Schwann cell migration.
3. Assess the effects of the bioactive surface NH_2^+ + Heparin + immobilised BDNF, when added onto PCL electrospun scaffolds, on DRG neurite outgrowth and primary Schwann cell migration.
4. Study the effects of the bioactive surface NH_2^+ + Heparin + immobilised with NGF plus BDNF, when added onto PCL electrospun scaffolds, on DRG neurite outgrowth and primary Schwann cell migration.

The objectives of this chapter were:

1. Determine the fibre diameter and alignment of PCL electrospun scaffolds.
2. Add NH_2^+ onto PCL electrospun scaffolds by plasma deposition.
3. Evaluate the physical changes of PCL electrospun fibres before and after plasma treatment.
4. Characterise the NH_2^+ bioactive surface and NH_2^+ + Heparin bioactive surface on the PCL electrospun scaffolds.
5. Calculate the average neurite length of DRG when cultured on PCL electrospun scaffolds with bioactive surface NH_2^+ + Heparin immobilised with NGF, BDNF or NGF plus BNDF.
6. Quantify the average maximum neurite length of DRG when cultured on PCL electrospun scaffolds with bioactive surface NH_2^+ + Heparin immobilised with NGF, BDNF or NGF plus BNDF.

7. Determine the migration length of Schwann cells when cultured on PCL electrospun scaffolds with bioactive surface NH_2^+ + Heparin immobilised with NGF, BDNF or NGF plus BNDF.

8.3 Materials and Methods

8.3.1 Fabrication of polycaprolactone electrospun scaffolds

Fabrication of polycaprolactone (PCL) electrospun scaffolds was performed following the protocol described in Chapter 4, Section 4.4.1. Briefly, a 20% w/v solution of PCL was used for electrospinning. A flow rate of 6 mL/hr, voltage of 16-18 kV, distance of 20 cm, and speed of collector of 2,000 rpm were set to obtain an aligned electrospun PCL scaffold.

8.3.2 Fabrication of PCL spin-coated films

Fabrication of PCL spin-coated films was achieved by following the protocol described in Chapter 4, section 4.4.2. Briefly, a 10% w/v solution of PCL was prepared and loaded on a glass coverslip. The spin-coater was set to spin at 3000 rpm for 35 sec. After the spin time, the PCL film with the coverslip was retrieved.

8.3.3 Adding amine functional groups NH_2^+, heparin and growth factors to PCL electrospun scaffolds, PCL films, and TCP well plates

Plasma deposition was used to clean and add amine functional groups NH_2^+ on PCL electrospun scaffolds, PCL films and TCP culture plates. Allylamine was the monomer used to obtain the NH_2^+ groups. The detailed protocol is described in Chapter 4, section 4.4.3. Nevertheless, the protocol is briefly described in the following subsections.

8.3.3.1 Air plasma cleaning protocol

Air plasma cleaning was performed to clean the glass vessel and the PCL electrospun scaffold and PCL films from any contamination. The cleaning of the glass vessel was done before the cleaning of the PCL electrospun scaffolds.

Firstly, the cold trap (Figure 101.B) was filled with liquid nitrogen. The vacuum pump was turned on (Figure 101.A) to evacuate the plasma rig glass vessel (Figure 101.G) to $7x10^{-2}$ mBar. The equalisation valve (Figure 101.I) was open and adjusted to reach a steady pressure of $1.8x10^{-1}$ mBar. The radio frequency generator (RF generator, Figure 101.F) was turned on and the output power adjusted to 50 W. The air plasma deposition process was left for 30 minutes (Figure 102.A). Then, the RF generator was

turned off. The equalization valve and the isolation valve (Figure 101.C) were closed, and the vacuum pump turned off.

Then, the lid was opened and the PCL electrospun scaffolds or PCL films were placed inside the plasma rig glass vessel. The air plasma cleaning protocol was performed once to clean the PCL electrospun scaffolds or PCL films from any chemical contamination. After this, the allylamine plasma deposition was performed.

8.3.3.2 Allylamine plasma deposition to add NH_2^+ onto PCL electrospun scaffolds, PCL films and TCP well plates

The cold trap was refilled with liquid nitrogen. Then, with the PCL electrospun scaffolds, PCL films or TCP well plates inside the glass vessel and the isolation valve open, the vacuum pump was turned on to evacuate the glass vessel. The monomer flask (Figure 101.J), was attached to the equalisation valve. Then, the equalisation valve was open and adjusted to reach a steady pressure of $2.2x10^{-2}$ mBar. Then, the RF generator was turned on and the output power adjusted to 10 W. The allylamine plasma polymerisation process was left for 10 minutes (Figure 102.B). Then, the RF generator was turned off. The equalization valve and the isolation valve were closed, and the vacuum pump turned off. The atmospheric valve was opened, and the monomer flask was detached from the equalisation valve. Then, the samples were retrieved (PCL + NH_2^+ scaffolds, PCL + NH_2^+ films or TCP + NH_2^+ well plates).

8.3.3.3 Air plasma deposition onto PCL electrospun scaffolds

Air plasma deposition on PCL electrospun scaffolds was performed to add hydroxyl functional groups onto the surface of PCL electrospun scaffolds. These scaffolds were later used as a positive control.

Similarly, to allylamine plasma deposition (Section 8.3.3.2), the cold trap was filled with liquid nitrogen. The glass vessel was evacuated to $7x10^{-2}$ mBar. Then, the equalisation valve was opened and adjusted to reach a steady pressure of $1.8x10^{-1}$ mBar. The RF generator was turned on and the output power adjusted to 25 W. The air plasma deposition was left for 2 minutes. Then, the RF generator was turned off. The equalization valve and the isolation valve were closed, and the vacuum

pump turned off. The atmospheric valve was opened. The lid was opened, and the PCL Air scaffolds were removed.

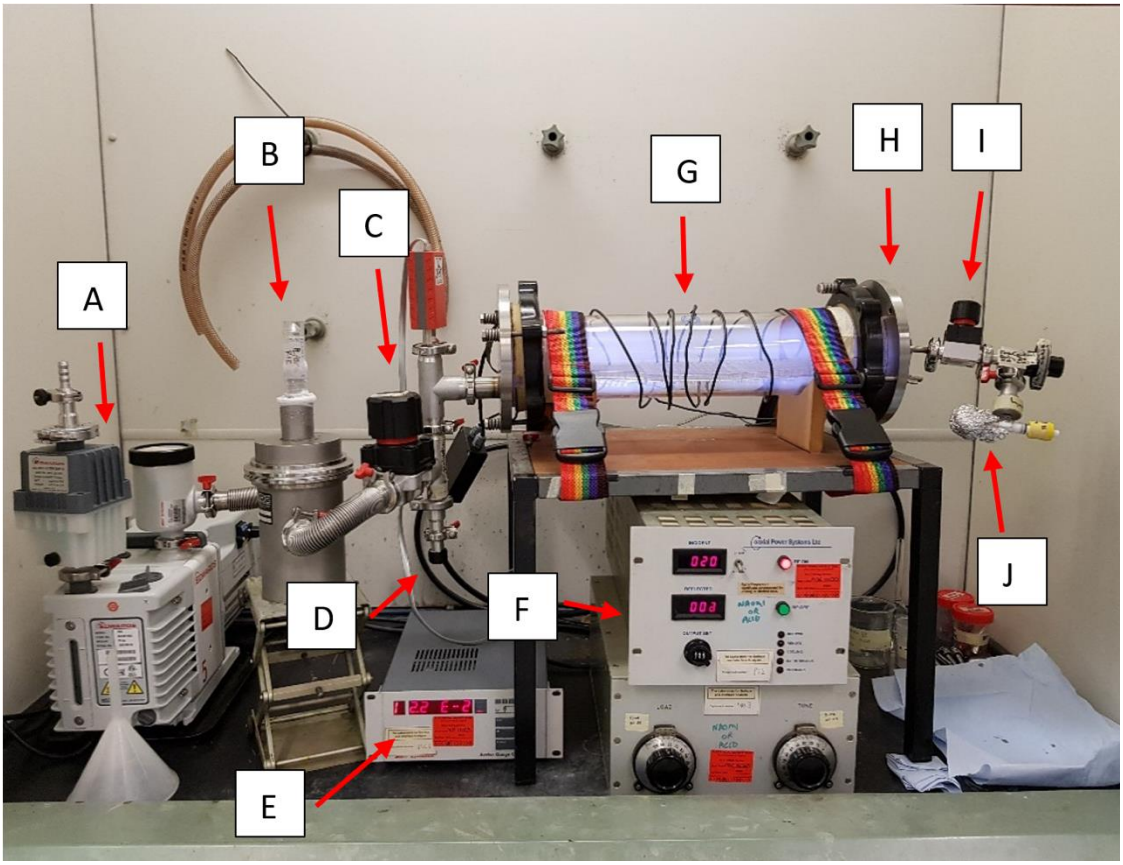

Figure 101. Plasma rig. The components are A) vacuum pump, B) cold trap, C) isolation valve, D) atmospheric valve, E) pressure monitor, F) radiofrequency generator, G) plasma rig chamber, H) lid of the chamber, I) equalisation valve, J) monomer flask.

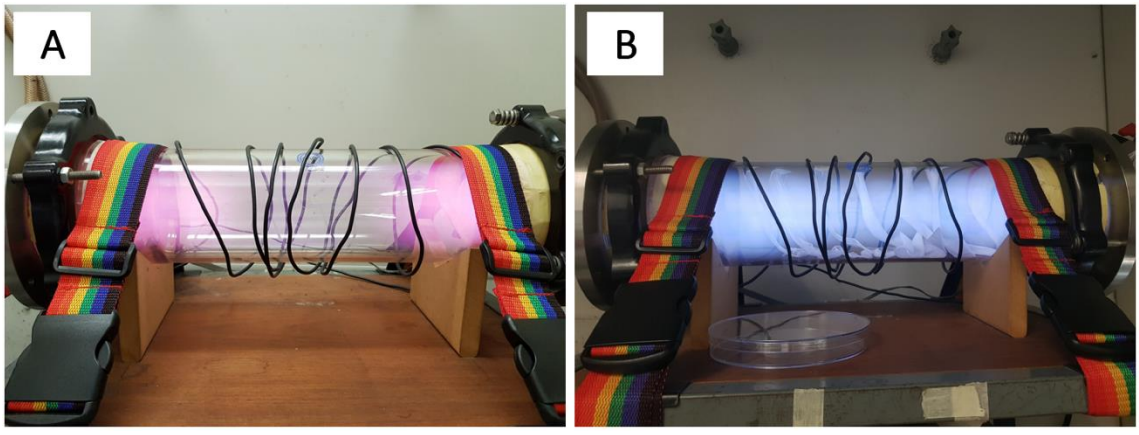

Figure 102. Difference in colour as seen in the plasma rig glass vessel during A) air plasma cleaning/deposition and B) allylamine plasma deposition.

8.3.3.4 Heparin conjugation

Protocol described in Chapter 4, Section 4.4.3.3 was followed. Briefly, heparin solution was added to PCL electrospun scaffolds, PCL films and TCP well plates with amine groups (PCL + NH_2^+ scaffolds, PCL + NH_2^+ films, TCP + NH_2^+) and left overnight at room temperature. Then, the heparin solution was discarded, and the surfaces washed one time with PBS.

PCL films, PCL Air films, PCL + NH_2^+ films and PCL + NH_2^++ Heparin films were used for XPS analysis. Moreover, PCL films + NH_2^++ Heparin were used to quantify bound heparin by toluidine blue assay as described in Section 8.3.8 of this chapter.

TCP, TCP + NH_2^+ and TCP + NH_2^+ + Heparin were used for a storage study described in section 4.4.7 of Chapter 4.

PCL + NH_2^+ scaffolds and PCL + NH_2^++ Heparin scaffolds were used for crystal violet assay. Moreover, they were used for immobilisation of NGF, BDNF or NGF plus BDNF as described in Section 4.4.3.3 of Chapter 4.

8.3.3.5 Immobilisation of NGF, BDNF or NGF plus BDNF onto PCL + NH_2^++ Heparin scaffolds, and TCP + NH_2^+ + Heparin scaffolds

After heparin conjugation, NGF, BDNF and NGF plus BDNF were immobilised to PCL + NH_2^+ scaffolds and PCL + NH_2^++ Heparin scaffolds. NGF plus BDNF were immobilised at a concentration of 1 ng/mL and 100 ng/mL only. NGF or BDNF was immobilised on TCP well plates at 1 ng/mL only. The immobilisation process followed the one described in section 4.1.1.2 of chapter 4. Briefly, NGF or BDNF solutions of concentrations of 1 pg/mL, 1 ng/mL, 10 ng/mL, 100 ng/mL, and 1 µg/mL were prepared and added to the samples. The samples were incubated for 5 hours at room temperature. Then, scaffolds were washed one time with PBS.

PCL electrospun scaffolds, PCL Air scaffolds, PCL + NH_2^+ scaffolds, PCL + NH_2^+ + Heparin scaffolds, PCL + NH_2^+ + Heparin + immobilised NGF/BDNF and were used to analyse neurite growth and Schwann cell migration from a seeded DRG.

TCP + NH_2^+ + Heparin + immobilised NGF/BDNF were used for a 21 day release profile, described in Section 4.4.8 of Chapter 4.

8.3.4 Scanning Electron Microscopy analysis of PCL electrospun scaffolds

Scanning Electron Microscopy (SEM) was performed to obtain images of the PCL electrospun scaffold to measure fibre diameter and alignment. The methodologies used are described in Chapter 4, Sections 4.4.4 and 4.4.5.

Briefly, samples were gold coated before imaging with a field emission SEM. The voltage used was 10 kV and a spot size of 3.5 nm.

Image J 1.52a software was used to measure diameter and alignment of the fibres within the PCL electrospun scaffold [218]. To determine the averaged diameter of the fibres, the straight tool of Image J was used. A straight line was drawn across the fibre, and then the diameter measured using the scale bar of the SEM image. To determine if the PCL electrospun scaffold was aligned, the angular difference between the PCL fibres was measured. Similarly, to the procedure on how to determine the diameter of the fibre, the straight tool of Image J was used. A straight line was drawn along the PCL fibre, and the angle taken from the measurements panel. A 0° zero was defined to calculate the angular difference between the fibres.

Furthermore, a width/length ratio of the pores present on the PCL electrospun scaffolds was measured to identify any changes in pore morphology before and after plasma treatment. Using the straight tool in Image J, the width, and the length of 40 pores were measured. Then, the width was divided by the length to calculate the ratio.

8.3.5 X-ray Photoelectron Spectroscopy analysis of PCL films

X-ray Photoelectron Spectroscopy (XPS) analysis was performed at the Sheffield Surface Analysis Centre. Samples were analysed as described in Chapter 4, Section 4.4.6. Briefly, samples were interrogated to determine surface elemental composition, carbon scans (C 1s), oxygen scans (O 1s), nitrogen scans (N 1s), and sulphur scans (S 2p). Two points per sample were analysed. Data was processed and analysed using CasaXPS software (version 2.3.19 PR 1.0, Casa Software Ltd).

8.3.6 Storage of bioactive surfaces at different temperatures

Polystyrene (PS), TCP, TCP + NH_2^+ and TCP + NH_2^++ Heparin were stored at 4°C, room temperature (ca. 21°C) and 37°C for 24 hours, 1 month and 3 months. After

storage periods, any changes in surface wettability were evaluated by water contact angle, as described in Section 4.1.2.1 of Chapter 4.

8.3.7 Release profile of NGF or BDNF from bioactive surface for 21 days

TCP + NH_2^++ Heparin + immobilised NGF at 1 ng/mL and TCP + NH_2^++ Heparin + immobilised BDNF at 1 ng/mL were used to observe how much NGF or BDNF was released within 21 days.

After immobilisation of NGF or BDNF, bioactive surfaces were incubated at 37℃, with 1 mL of PBS for 21 days. Samples were taken at 1 hour, 24 hours, 48 hours, 168 hours (7 days), 240 hours (10 days), 336 hours (14 days), 408 hours (17 days), and 504 hours (21 days) and stored at -20℃ for later quantification by ELISA. ELISA was performed as described in Section 4.1.2.3 of Chapter 4.

8.3.8 Toluidine blue assay

To quantify the amount of heparin bound to PCL + NH_2^++ Heparin films, toluidine blue (TBO) assay was performed. Firstly, a TBO working solution was prepared with 0.04% wt TBO powder (Toluidine blue O, Sigma-Aldrich, United Kingdom) in 0.01 M hydrochloric acid (HCL, Fisher Scientific, United Kingdom) / 0.2% wt sodium chloride (NaCl). Then, samples were incubated with 2 mL of TBO working solution for 4 hours at 37℃. After, samples were rinsed 3 times with dH_2O. Then, 2 mL of an 80% ethanol (Fisher Scientific, United Kingdom) / 0.1 M sodium hydroxide (NaOH) solution was added to elute the heparin-TBO complex. After, 150 µL of eluted solution was added to a 96-well plate (in triplicate), and the absorbance was read at 530 nm using a Bio-Tek ELx 800 absorbance microplate reader and KC junior software 1.41.8 (Bio-Tek Instruments, USA).

For the calibration curve, solutions of known concentrations of heparin were prepared in dH_2O. Then, 2 mL of TBO working solution was added and the solutions were incubated for 4 hours at 37℃. Then, the samples were centrifuged for 10 minutes at 3500 rpm. The supernatant was removed, and the pellet was rinsed 2 times with

0.01 M HCl / 0.2% wt NaCl. After, 2 mL of 80% ethanol / 0.1 M NaOH was added to dissolve the precipitate. The absorbance was read at 530 nm.

8.3.9 Evaluation of bioactive surface on PCL electrospun scaffold on cancerous cell line and primary cells

8.3.9.1 Crystal violet adhesion assay

PCL scaffolds, PCL Air scaffolds, PCL + NH_2^+ scaffolds and PCL + NH_2^++ Heparin scaffolds were tested to evaluate if NG108-15 neuronal cells adhered to them. The detailed protocol was described in Chapter 4, Section 4.5.1. Briefly, NG108-15 neuronal cells were seeded on each scaffold with culture medium. The samples were incubated for 3 days at 37°C and 5% CO_2. Then, the samples were fixed with 3.7% formaldehyde (FA). A 0.2% crystal violet solution was added to each sample and incubated for 10 minutes at room temperature. Then, the samples were rinsed one time with PBS. After, a 10% acetic acid solution was added to each sample and used to elute the stain. The elute product was transferred to a 96-well plate and the absorbance read at 630 nm using a Bio-Tek ELx 800 absorbance microplate reader and KC junior software 1.41.8.

8.3.9.2 Dorsal root ganglia seeding on PCL electrospun scaffolds

Dorsal root ganglia (DRG) were isolated as described in Chapter 4, Section 4.3.1. Briefly, DRGs were seeded at a density of one DRG per PCL scaffold, PCL Air scaffold, PCL + NH_2^+ scaffold, and PCL + NH_2^++ Heparin scaffold. Then, culture medium and NGF, BDNF or NGF plus BDNF was added as described in Table 14. For the bioactive surface PCL + NH_2^++ Heparin with immobilised NGF, BDNF or NGF plus BDNF, one DRG per scaffold was seeded and culture medium with no growth factors was added. The DRG were cultured for 7 days at 37°C and 5% CO_2. Three independent tests were performed. Each condition was tested in triplicate.

Table 14. Summary of the different bioactive surfaces that were prepared, highlighting the delivery method of growth factor of each surface. NGF, BDNF and NGF plus BDNF solutions for immobilisation were prepared in sterile PBS.

Surface	**Growth factor delivery method**	**NGF**	**BDNF**	**NGF plus BDNF**
Electrospun PCL scaffold (PCL)	In solution with culture medium	0 pg/mL	0 pg/mL	0 pg/mL
		1 µg/mL	1 µg/mL	1 µg/mL
Air plasma electrospun PCL scaffolds	In solution with culture medium	0 pg/mL	0 pg/mL	0 pg/mL
		1 µg/mL	1 µg/mL	1 µg/mL
PCL + NH_2^+	In solution with culture medium	0 pg/mL	0 pg/mL	0 pg/mL
		1 µg/mL	1 µg/mL	1 µg/mL
PCL + NH_2^++ Heparin	In solution with culture medium	0 pg/mL	0 pg/mL	0 pg/mL
		1 µg/mL	1 µg/mL	1 µg/mL
PCL + NH_2^++ Heparin	Immobilised on surface	0 pg/mL	0 pg/mL	0 pg/mL
		1 pg/mL	1 pg/mL	1 ng/mL
		1 ng/mL	1 ng/mL	100 ng/mL
		10 ng/mL	10 ng/mL	--
		100 ng/mL	100 ng/mL	--
		1 µg/mL	1 µg/mL	--

8.3.9.3 Fixing and immunolabelling of DRG

Immunolabelling was performed for β-III tubulin protein, to identify neurons and measure neurite outgrowth and S100-β protein to identify Schwann cells. This was performed following the protocol described in Section 4.3.4 of Chapter 4. Briefly, the samples were fixed using 3.7% FA. Then, 0.1% Triton X-100 with 3% BSA solution was added to the samples and incubated for 1 hour at room temperature. Primary antibodies (anti-β-III tubulin and anti-S100-β) in 1% BSA solution were added to the samples and incubated overnight at 4℃ (Table 15). Then, the solution was discarded and secondary antibodies in 1% BSA solution were added and incubated for 3 hours at 4℃. The samples were rinsed one time with PBS and then stored at 4℃ with PBS.

Table 15. Primary (1°) and secondary (2°) antibodies used for immunolabeling of DRG, for β-III tubulin protein, and Schwann cells S100-β.

Structure	**1° antibody**	**Dilution factor of 1° antibody**	**2° antibody**	**Dilution factor of 2° antibody**
β-III tubulin protein (neurons and neurites)	Mouse Anti-β-III tubulin (Abcam, United Kingdom)	1:1000	Alexa Fluor 488 goat anti-mouse (Life technologies, USA)	1:400
S100-β protein (Schwann cells)	Rabbit Anti-S100-β (Dako, USA)	1:400	Alexa Fluor 546 goat anti-rabbit (Life technologies, USA)	1:400

8.3.9.4 Lightsheet microscopy

Lightsheet microscopy was used to obtain images of the DRG seeded on PCL + NH_2^++ Heparin+ Immobilised NGF scaffolds, PCL + NH_2^++ Heparin+ Immobilised BDNF scaffolds, and PCL + NH_2^++ Heparin+ Immobilised NGF plus BDNF scaffolds. The protocol to perform this was described in Chapter 4, Section 4.5.4. Briefly, Z.1 lightsheet microscope and ZEN imaging software were used to obtain the images. Samples were mounted in 1% agarose solution inside glass capillaries. A plunger with Teflon tip was used to insert the sample inside the glass capillaries. Then, capillaries were mounted inside a sample holder and placed inside the sample chamber. Samples were localised and positioned in front of the objective. Alexa Fluor-488 and Alexa Fluor-546 were imaged using excitation and emission wavelengths of λ_{ex} = 488 nm / λ_{em} = 550 nm (short band filter), and λ_{ex} = 561 nm / λ_{em} = 545-590 nm (band pass filter) respectively. For each sample, various fields of view (longitudinally) were taken to capture all neurite outgrowth and Schwann cell migration. Each field of view was imaged in z-stack.

The z-stack was combined to maximum projection intensity using ZEN lite software (Carl Zeiss, Germany). Then, the maximum projection intensity images were put together using the stitching tool in Image J [221]. Neurites were measured from the DRG body to the tip of the neurite. Schwann cells were measured from the DRG. Two images were taken per sample (upper and lower DRG, see Chapter 4, Section 4.5.4). Three independent tests were performed. Each condition was tested in triplicate.

8.3.10 Statistical analysis

Analysis of variance (ANOVA) with Tukey multiple comparison test was performed to analyse statistical difference among the different conditions using GraphPad Prism 8.2.0 software (USA). A p value of < 0.05 was used to indicate if differences in data were significant.

8.4 Results

8.4.1 Determination of fibre diameter and alignment of PCL electrospun scaffolds

After electrospinning, an aligned scaffold (Figure 103) was obtained (according to the parameters described earlier in section 8.3.1 of this chapter). Scanning Electron Microscopy (SEM) analysis was performed, as described in Section 8.3.4 of this Chapter, to measure the diameter of the PCL fibres, and to see if the fibres of the PCL electrospun scaffold were aligned.

Figure 103. PCL electrospun scaffold after the electrospinning process. The scaffold was collected on aluminium foil. Scale bar = 1 cm.

An appropriate fibre diameter is important to achieve to further encourage neurite outgrowth. In Figure 104.A and Figure 104.B the PCL fibres are highlighted at magnifications of 6,000x and 10,000x, respectively. The average diameter of the PCL fibres in the electrospun scaffold was 8 ± 0.7 µm, as seen in the graph in Figure 104.C.

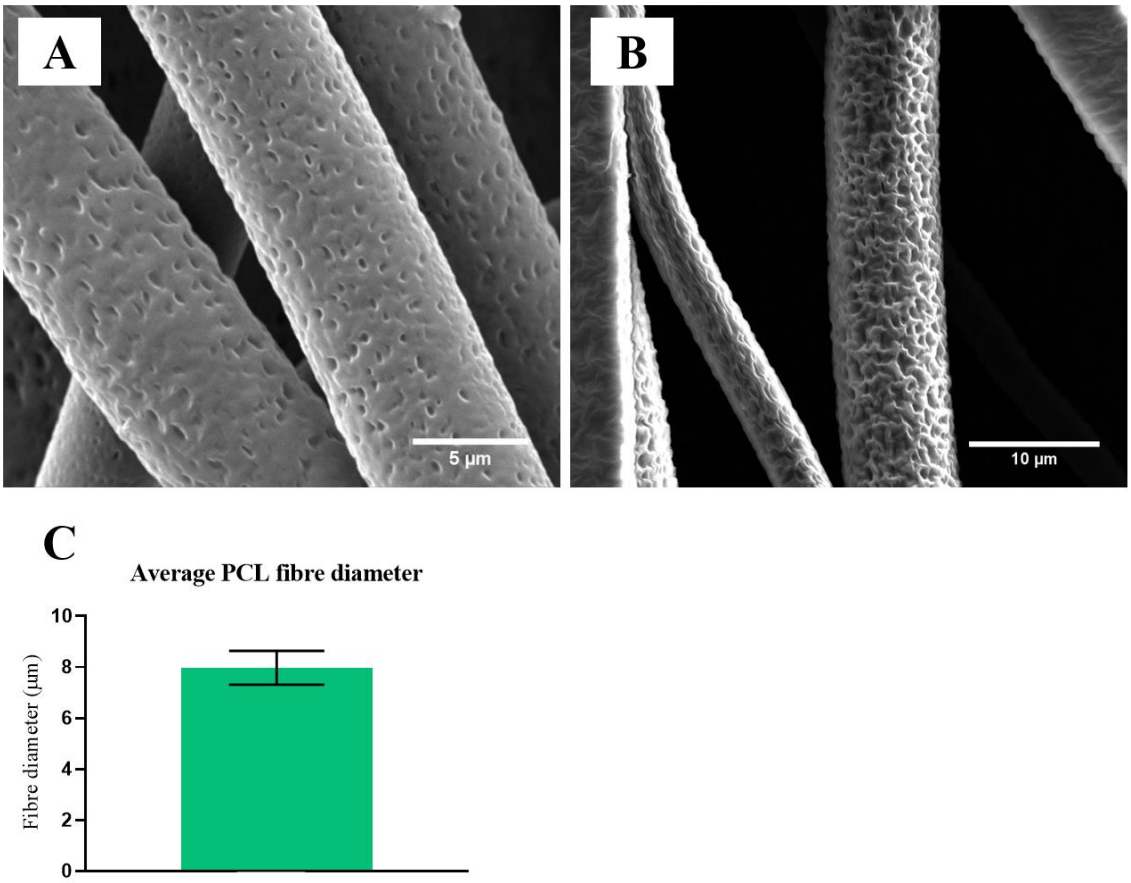

Figure 104. PCL electrospun scaffold. A) PCL fibre from the electrospun scaffold observed at a magnification of 6,000x B). PCL fibre from the electrospun scaffold observed at a magnification of 10,000x. C) Average PCL fibre diameter of 8 ± 0.7 µm. Mean ± SD. N=3, n=10.

An aligned scaffold will provide physical cues to neurites to orientate and grow in one direction. Figure 105.A shows an SEM image, at 94x magnification highlighting the alignment of the PCL electrospun scaffold. However, a deeper analysis was performed to investigate whether fibres in the PCL electrospun scaffold were truly aligned. Three tests were run independently, two PCL electrospun scaffolds chosen as samples to image. Three images were taken, and 10 PCL fibres (per image) were used to determine the angular difference between them. Using the straight tool in Image J, a straight line was drawn along the PCL fibre. Then, the angle was taken from the measurements panel. The measurements were averaged. The angular difference of the PCL fibres was 1.5°, as shown in Figure 105.B.

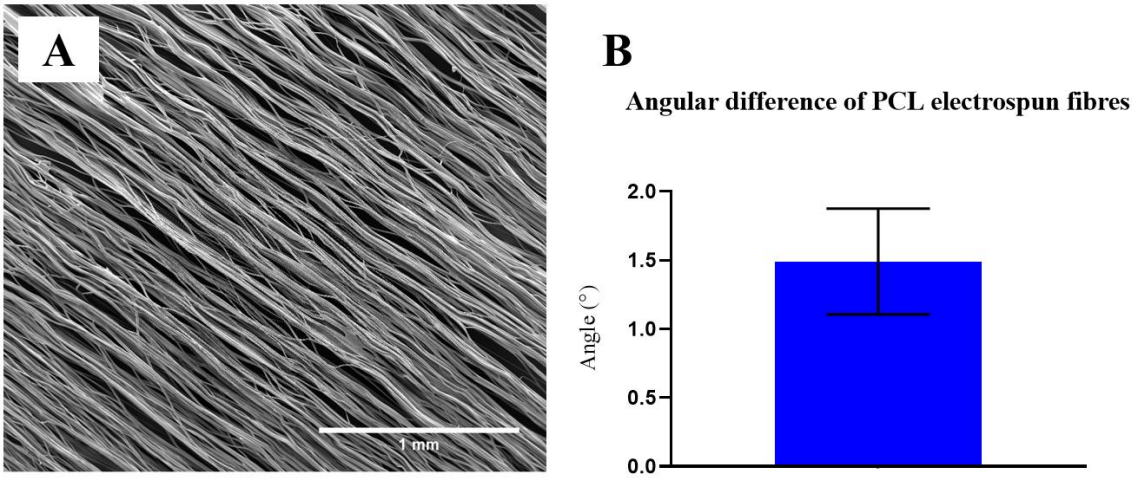

Figure 105. Align PCL electrospun scaffold. A) Aligned PCL electrospun scaffold (magnification of 94x). B) Angular difference of PCL electrospun fibres was 1.5° ± 0.38. Mean ± SD. N=3, n=10.

8.4.2 Evaluation of physical changes on PCL electrospun scaffolds before and after plasma treatment

The fibre diameter and pore width/length ratio of the non-treated PCL scaffold were measured and compared to the plasma treated scaffolds, either after air plasma treatment or allylamine plasma treatment or deposition. This was mainly to identify if PCL fibres had undergone significant changes after plasma deposition. Figure 106 presents representative SEM figures of the fibres before and after treatment. The PCL fibres showed a wavy surface micro-texture both before and after surface treatment, at a 0.5 to 1 µm length scale. This texture is likely due to solvent evaporation during the electrospinning process [108], [343]. Additionally, the diameter of PCL fibres (Figure 106.A), PCL air plasma treated fibres (Figure 106.B) and PCL NH_2^+ fibres (Figure 106.C) were measured to be 8 ± 0.7 µm, 7.7 ± 0.9 µm and 8.1 ± 0.9 µm, respectively. There was no significant difference between these values, as shown in Figure 106.D.

Furthermore, after obtaining SEM images from PCL fibres, PCL Air fibres and PCL NH_2^+ fibres, it was observed that the pore morphology was different among the

samples, more evidently in PCL NH_2^+ fibres, as shown in Figure 106.A, Figure 106.B and Figure 106.C. The width and the length of the pores was measured, and a ratio calculated. If this ratio was closer to 1, it meant that the pore shape was similar to a perfect circle. The pore ratio of PCL fibres, PCL Air fibres and PCL NH_2^+ fibres was 0.3 ± 0.1, 0.4 ± 0.1, and 0.6 ± 0.2, respectively. As observed in Figure 106.E, significant differences existed among the samples, suggesting that, even though plasma treatment did not affect fibre diameter, it indeed changed the pore morphology. This change in pore morphology may indicate a difference in roughness among the different surfaces.

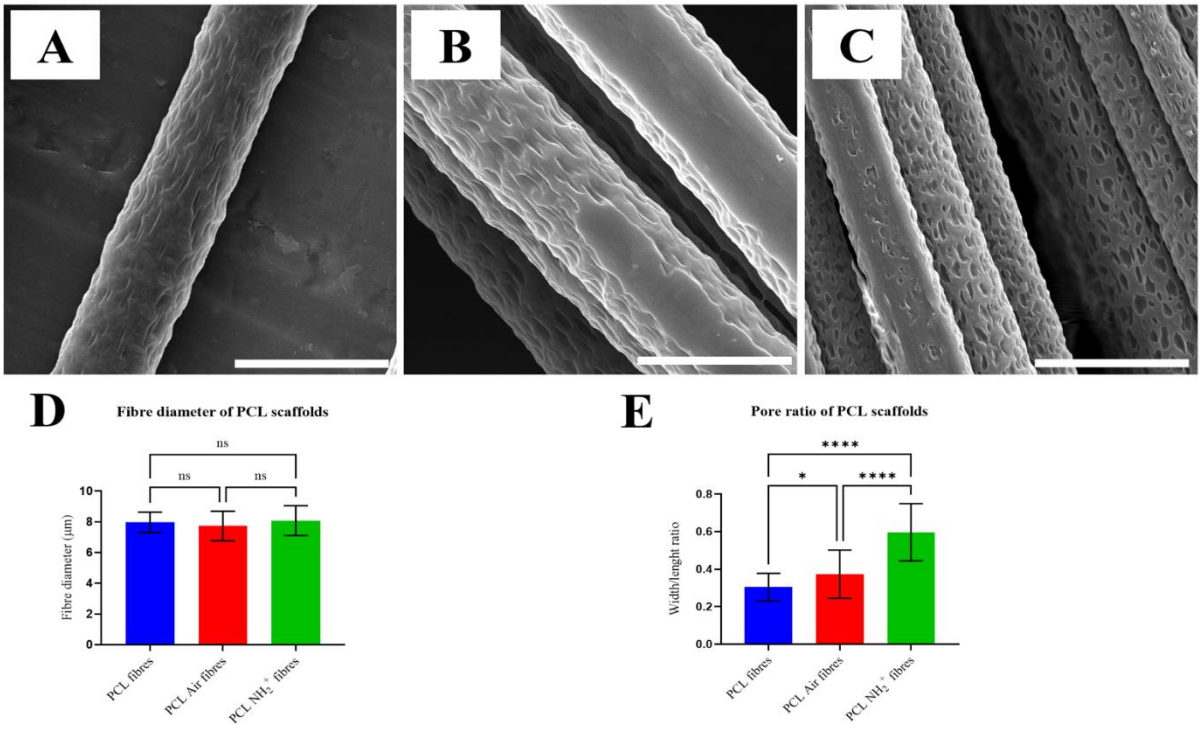

Figure 106. Physical changes in PCL electrospun fibres after plasma treatment. A) PCL fibre; B) PCL fibre after air plasma treatment; C) PCL fibre after allylamine plasma treatment; D) bar graph showing fibre diameter of PCL fibres, which were no significant different from each other; E) histogram of width/length ratio of pores of PCL fibres before and after plasma treatment. Significant difference was found using One-way ANOVA * $p < 0.05$, **** $p < 0.0001$. Mean ± SD. n=40. Scale bar = 10 µm.

8.4.3 Characterisation of NH2+ bioactive surface and NH2+ + Heparin bioactive surface on PCL electrospun fibres, PCL films or TCP well-plates

X-ray Photoelectron Spectroscopy (XPS) analysis, contact angle, ELISA and crystal violet protocols were performed to characterise the bioactive surface at different conditions.

8.4.3.1 XPS analysis of bioactive surface on PCL films

XPS analysis was performed to confirm the presence of amine NH_2^+ functional groups and heparin (through sulphur detection) in PCL films. Table 16 shows the percentage of atomic concentration of PCL film, PCL Air film, PCL NH_2^+ film and PCL NH_2^+ + Heparin film. It can be observed that PCL film had silicon contamination, which was higher in comparison to PCL Air film, PCL NH_2^+ film and PCL NH_2^+ + Heparin film. Furthermore, survey scans of the samples showed that nitrogen was introduced after allylamine plasma treatment and that sulphur was detected in PCL NH_2^+ + Heparin film, confirming the successful adsorption of heparin on this film (Figure 107.C and Figure 107.D respectively).

Table 16. Percentage of atomic concentration of PCL film, PCL Air film, PCL NH_2^+ film and PCL NH_2^++ Heparin film obtained from XPS analysis survey scans.

Sample	**Survey scan: percentage atomic concentration %**				
	O	N	C	S	Si
PCL film	23.4 ± 0.7	0 ± 0	70.2 ± 2.4	0 ± 0	5.0 ± 4.4
PCL Air film	26.9 ± 0.4	0 ± 0	72.4 ± 0.4	0 ± 0	0.8 ± 0
PCL NH_2^+ film	23.1 ± 2.7	21.2 ± 11.7	54.2 ± 8.3	0 ± 0	1.9 ± 0.9
PCL NH_2^+ + Heparin film	26.0 ± 1.2	7.5 ± 1.1	64.7 ± 2.0	0.2 ± 0	1.7 ± 0.8

PCL is a polymer with a chemical formula of $C_6H_{10}O_2$. The peaks for this chemical structure are shown on Figure 107.A, where oxygen and carbon peaks are observed at 532 eV and 285 eV. Furthermore, PCL Air film showed these peaks as well, Figure 107.B, with a small increment in oxygen content, from 23.4 to 26.9%. After allylamine plasma treatment, a nitrogen peak at 400 eV was expected to appear on the PCL NH_2^+ film, which XPS analysis confirmed (Figure 107.C). In addition, a sulphur peak was detected at 168 eV in the PCL NH_2^+ + Heparin film, Figure 107.D, confirming the presence of heparin on the film.

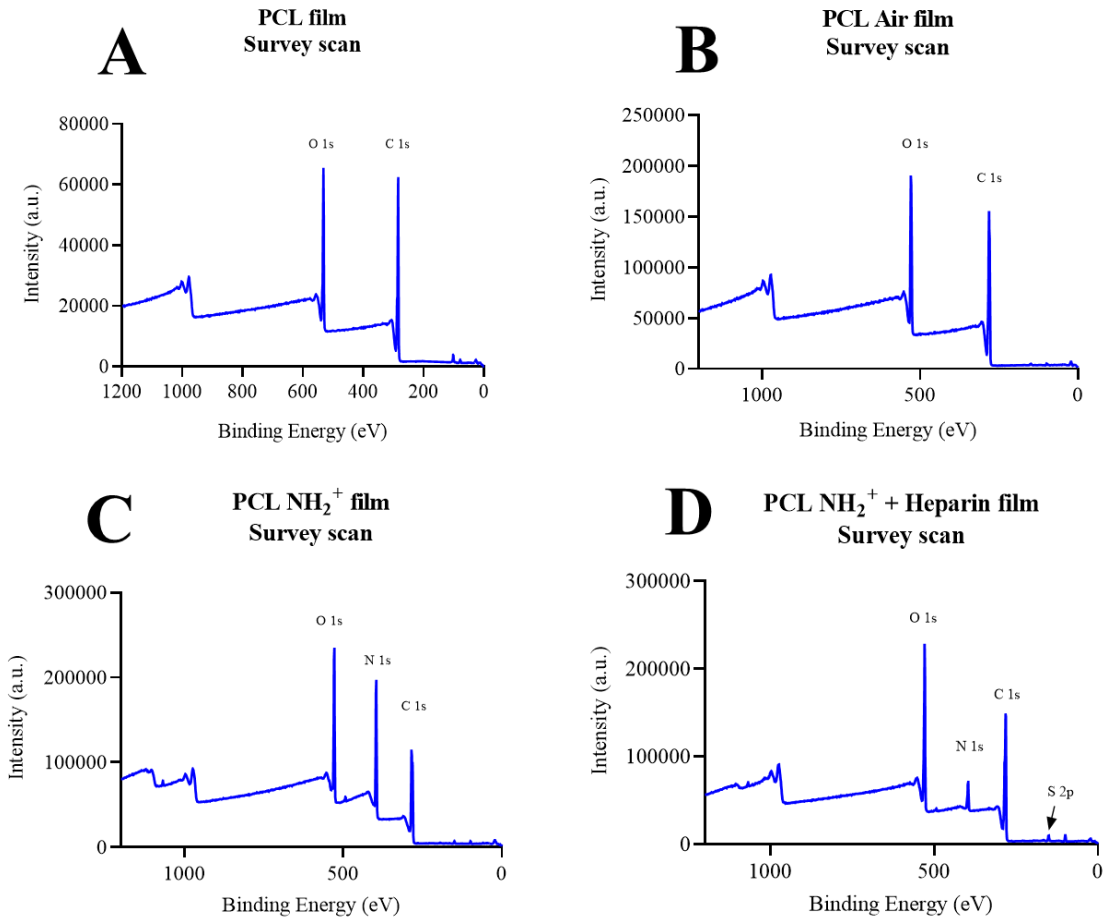

Figure 107. XPS survey scans of A) PCL film; B) PCL Air film; C) PCL NH_2^+ film; D) PCL NH_2^+ + Heparin film. Carbon was detected at 285 eV, oxygen at 532 eV, nitrogen at 400 eV and sulphur at 168 eV. N=3, n=3.

The C 1s high resolution scan of PCL film, PCL Air film, PCL NH_2^+ film and PCL NH_2^+ + Heparin film are shown in Figure 108. The characteristic peaks of PCL film, Figure 108.A, that were identified were 66% C-C/C-H at 258 eV, 17% C-O at 286.5 eV, and 17% O-C=O at 289 eV. These peaks are consistent with the ones found in the literature [344], [345]. These peaks were also identified for PCL Air films. However, a new peak at 288 eV attributed to C-C=O was also identified (Figure 108.B). This new peak of C-C=O reveals that oxygen was added to the surface of the PCL film. Moreover, this suggestion is supported by the increase of C-O, from 17% in PCL film to 23% in PCL Air film; and the decrease of C-C from 66% in PCL film to 38% in PCL Air film. This data was supported by Jacobs et al. and Recek et al. [345], [346].

The C 1s of PCL NH_2^+ film, Figure 108.C, revealed that C-C increased from 38% to 42% in comparison to PCL Air film. Furthermore, C-C=O and O-C=O also increased, from 18% to 26%, and 14% to 20% respectively in comparison to PCL Air film. However, C-O/C-N decreased from 23% to 18% in comparison to PCL Air film. This might suggest the incorporation of allylamine into the film, by the increase of C-C. Moreover, it may also indicate that the allylamine surface was oxidised.

In addition, the C 1s of PCL NH_2^+ + Heparin film revealed that C-C increased from 42% to 59% in comparison to PCL NH_2^+ film, as observed in Figure 108.D. This might suggest that heparin was incorporated onto the film as the carbon content was increased. Furthermore, C-C=O and O-C=O decreased, from 26% to 8%, and 20% to 15% respectively, in comparison to PCL NH_2^+ film.

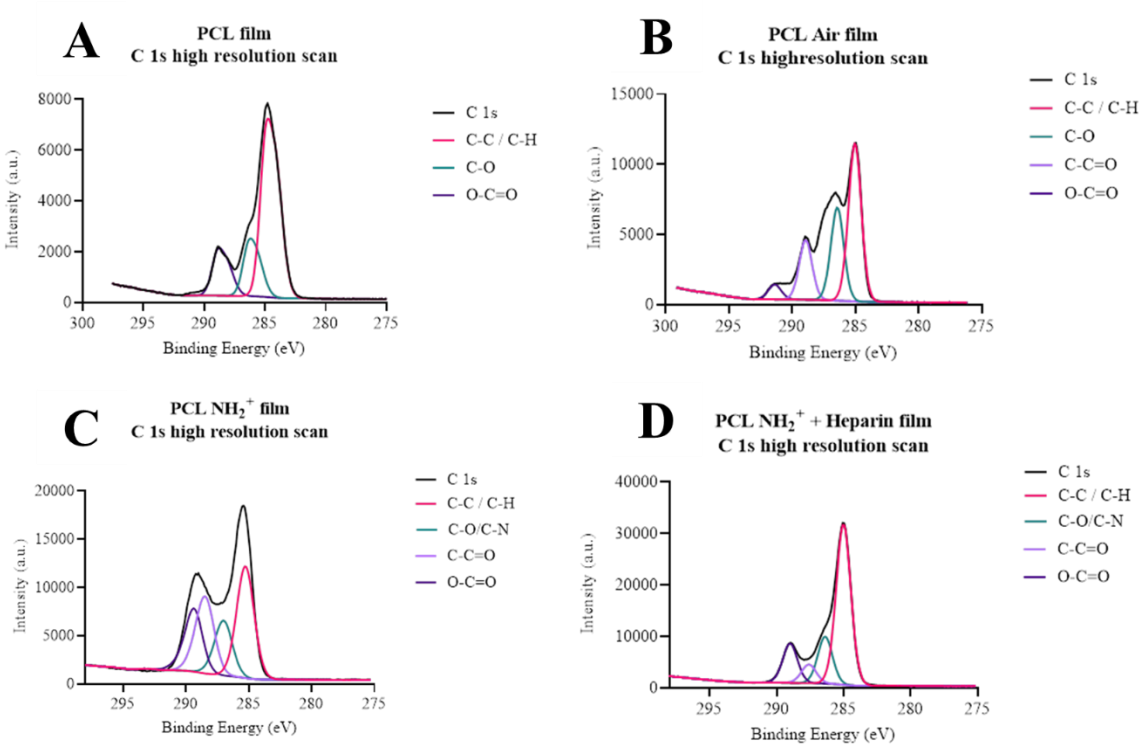

Figure 108. C 1s high resolution scans of A) PCL film; B) PCL Air film; C) PCL NH_2^+ film; D) PCL NH_2^+ + Heparin film. N=3, n=3.

Figure 109 shows the O 1s high resolution scans of PCL film, PCL Air film, PCL NH_2^+ film and PCL NH_2^+ + Heparin film. For PCL film, C=O at 532.3 eV and C-O at 533.7 eV were revealed, as seen in Figure 109.A. These components are consistent with the ones found in the literature [344], [347]. Furthermore, for PCL Air films, an increase at 533.7 eV was observed (Figure 109.B), suggesting that oxygen was further added into the film as C-O.

In addition, the O 1s scan of PCL NH_2^+ film, Figure 109.C, revealed an increased C=O peak, consistent with the increased C-C=O in the C 1s scan. This may also suggest the oxidation of allylamine on the film. Moreover, the O 1s scan of PCL NH_2^+ + Heparin film showed peaks of C=O and C-O, Figure 109.D, where C-O was increased, from 24% to 31% in comparison to PCL NH_2^+ film. This may also support the addition of heparin onto the film [250].

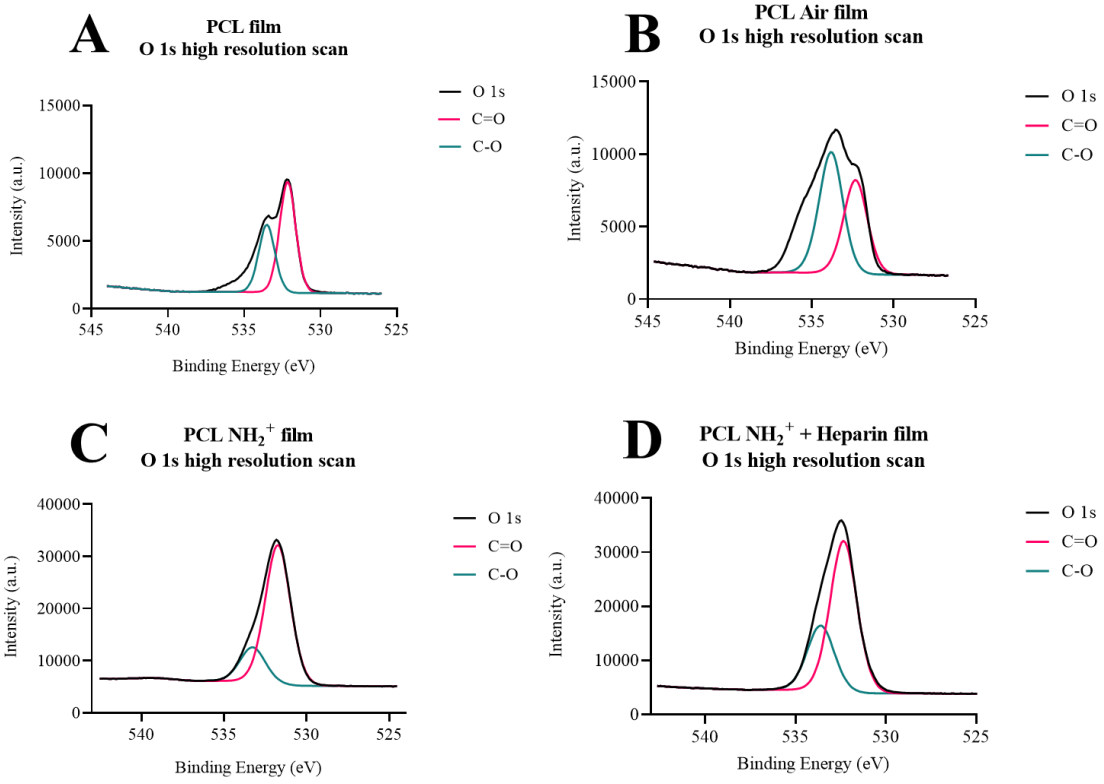

Figure 109. O 1s high resolution scans of A) PCL film; B) PCL Air film; C) PCL NH_2^+ film; D) PCL NH_2^+ + Heparin film. N=3, n=3.

N 1s high resolution scans of PCL NH_2^+ film and PCL NH_2^+ + Heparin film, shown in Figure 110.A and Figure 110.B respectively, revealed that nitrogen was incorporated into the films. Moreover, two peaks were identified, one at 399 eV, indicating C-N, and a peak at 401 eV, which was attributed to NH_2^+ [246]. However, overall nitrogen content decreased from 21.2% to 7.5%, after heparin attachment, this could indicate that nitrogen might have been lost after the incubation step of heparin or after rinsing step [241]. [241]. On the other hand, the drop in percentage of nitrogen content can also be attributed to strong binding of heparin to the plasma polymerised allylamine coating. Heparin (with atomic formula $C_{12}H_{19}NO_{20}S_3$) contains only 3 at. % N (excluding H), and a concentration of heparin within the analysis depth of XPS (typically 10 nm) decrease the nitrogen content.

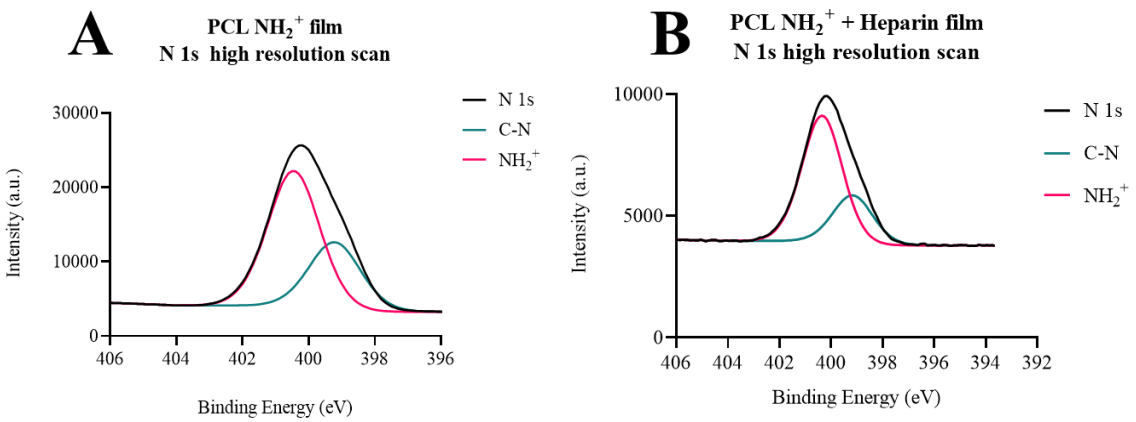

Figure 110. N 1s high resolution scans of A) PCL NH_2^+ film; B) PCL NH_2^+ + Heparin film. The peak at 399 eV was attributed *to* C-N. The peak at 401 eV was attributed to NH_2^+. N=3, n=3.

Additionally, S 2p high resolution scan of PCL NH_2^+ + Heparin film is seen in Figure 111. Two peaks were identified, which were consistent with sulphur present in heparin (OSO_3 and NSO_3) [234], [251], [252]. These two peaks correspond to the spin orbit split of S 2p, S $2p^{3/2}$ (168.2 eV) and S $2p^{1/2}$ (169.3 eV). Interestingly, the amount of sulphur detected by the survey scan was 0.2 at. %, this confirms the electrostatic binding of heparin to the surface. The amount of sulphur on the surface is in line with our previously reported surface concentration of allylamine-heparin coating in tissue culture plastic [203]. Additionally, this is also in line with the figure reported of 0.5 at. % S on the surface by layer-by-layer deposition of polyethylene-heparin on a polylactic acid surface [267]. Hence, heparin was adsorbed successfully to the PCL NH_2^+ + Heparin film.

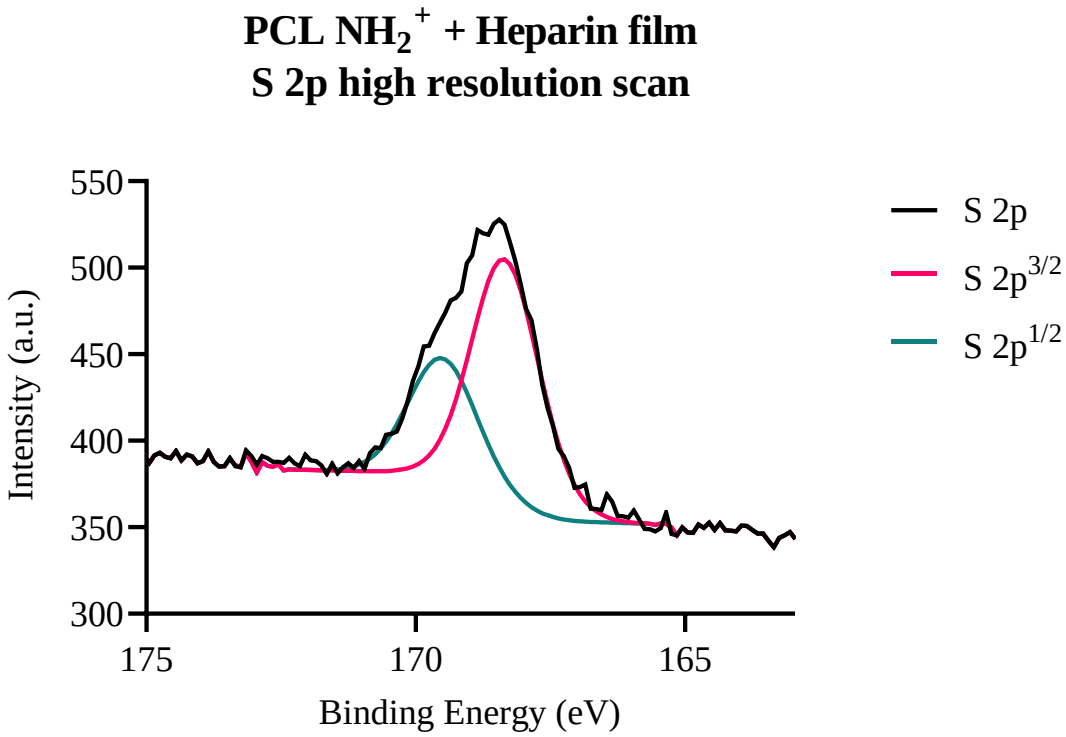

Figure 111. S 2p high resolution scan of PCL NH_2^+ + Heparin film. The S 2p peak shows a doublet in a 2:1 proportion of S $2p^{3/2}$ and S $2p^{1/2}$ (66.6% and 33.3% respectively) corresponding to sulphur present in heparin. N=3, n=3.

8.4.3.2 Storage of bioactive surface

PS, TCP, TCP + NH_2^+ and TCP + NH_2^++ Heparin were stored at 4°C, 21°C and 37°C for 24 hours, 1 month and 3 months. After storage periods, any changes in surface wettability were evaluated by water contact angle. The aim of this evaluation was to find if the bioactive surfaces had the potential to be stored, and what the ideal condition would be.

Firstly, a 24 hours control was performed to evaluate any immediate changes in water contact angle due to temperature exposure. Contact angle analysis revealed no significant change in wettability in the surfaces after exposing them to 4°C, 21°C and 37°C for 24 hours, as seen in Figure 112.

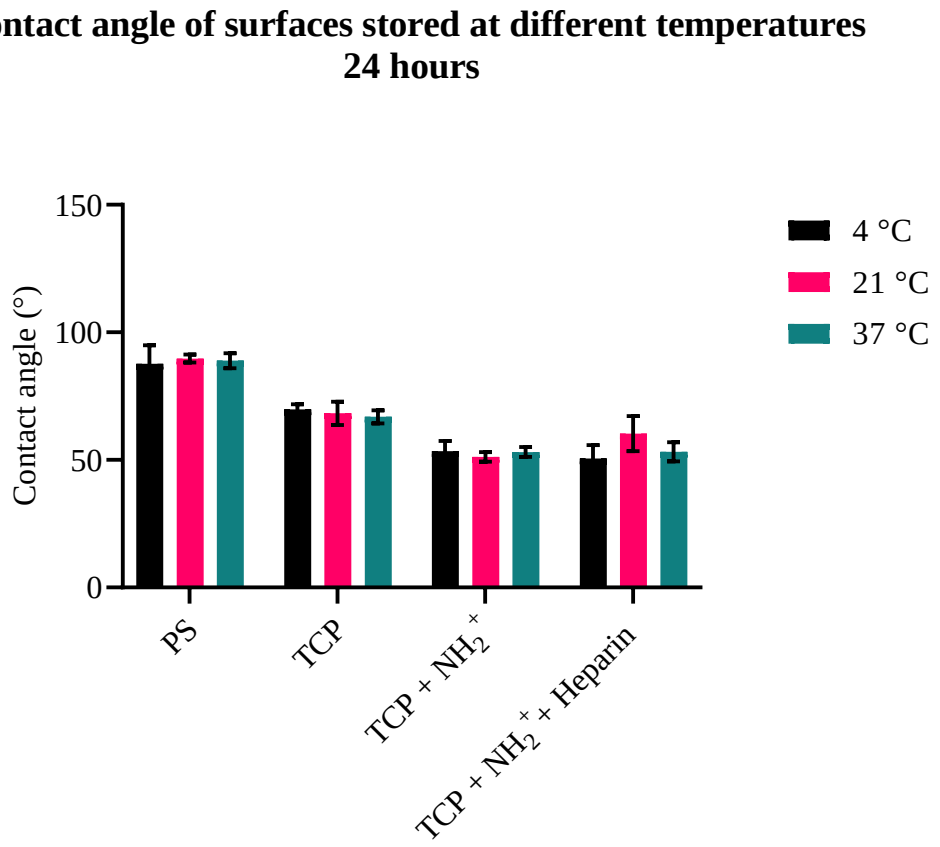

Figure 112. Contact angle of PS, TCP, TCP + NH_2^+ and TCP + NH_2^+ + Heparin after being incubated for 24 hours at 4°C, 21°C and 37°C. Two-way ANOVA was performed to analyse any significant difference among test and control groups. Mean ± SD. N=2, n=4.

The bioactive surfaces were incubated for 1 month at 4°C, 21°C and 37°C. Slight changes were obtained from water contact angle, after being exposed to different temperatures, as seen in Figure 113. However, no significant difference was found in the contact angle of the bioactive surfaces among the 3 temperatures.

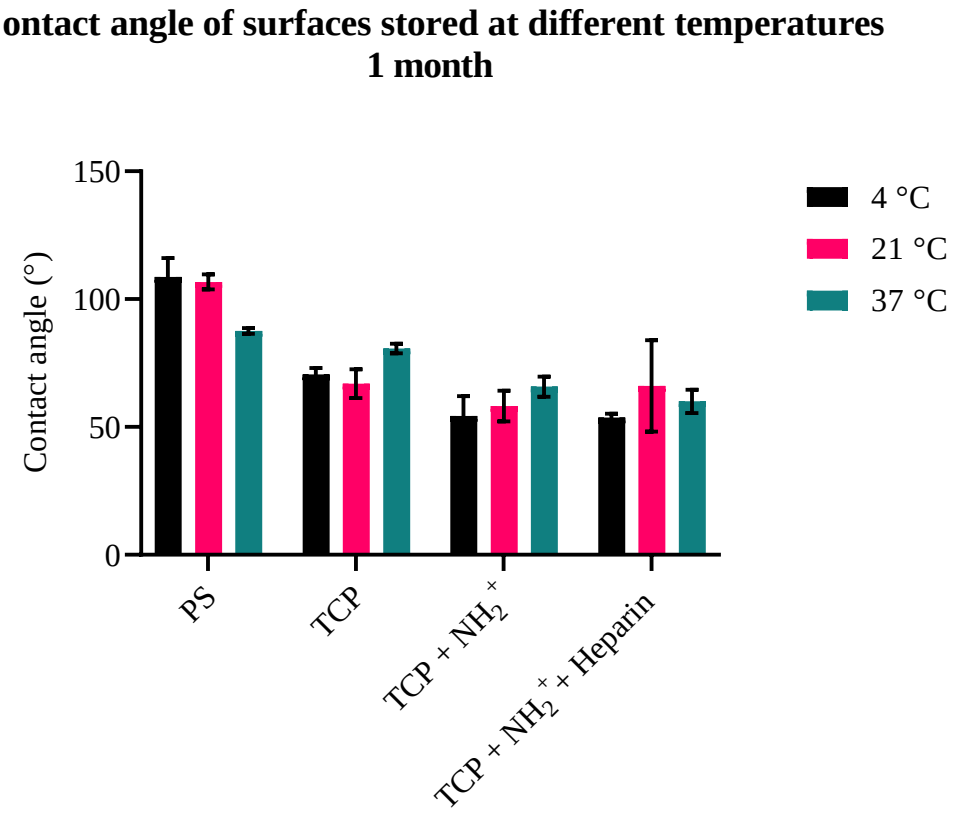

Figure 113. Contact angle of PS, TCP, TCP + NH2+ and TCP + NH2+ + Heparin after being incubated for 1 month at 4°C, 21°C and 37°C. Two-way ANOVA was performed to analyse any significant difference among test and control groups. Mean ± SD. N=2, n=4.

After 3 months of incubation at 4°C, 21°C and 37°C, the contact angle of the bioactive surface showed no significant difference in PS and TCP conditions. Moreover, the contact angle of TCP + NH_2^+ did not reveal any changes in wettability when incubated at 4°C, 21°C and 37°C. However, contact angle results from TCP + NH_2^++ Heparin showed that hydrophobicity changed regarding incubation temperature. When TCP + NH_2^++ Heparin was incubated at 4°C, Figure 114, its contact angles was 35°, which was significantly different from when TCP + NH_2^++ Heparin was incubated at 21°C and 37°C, contact angle of 55° and 63° respectively.

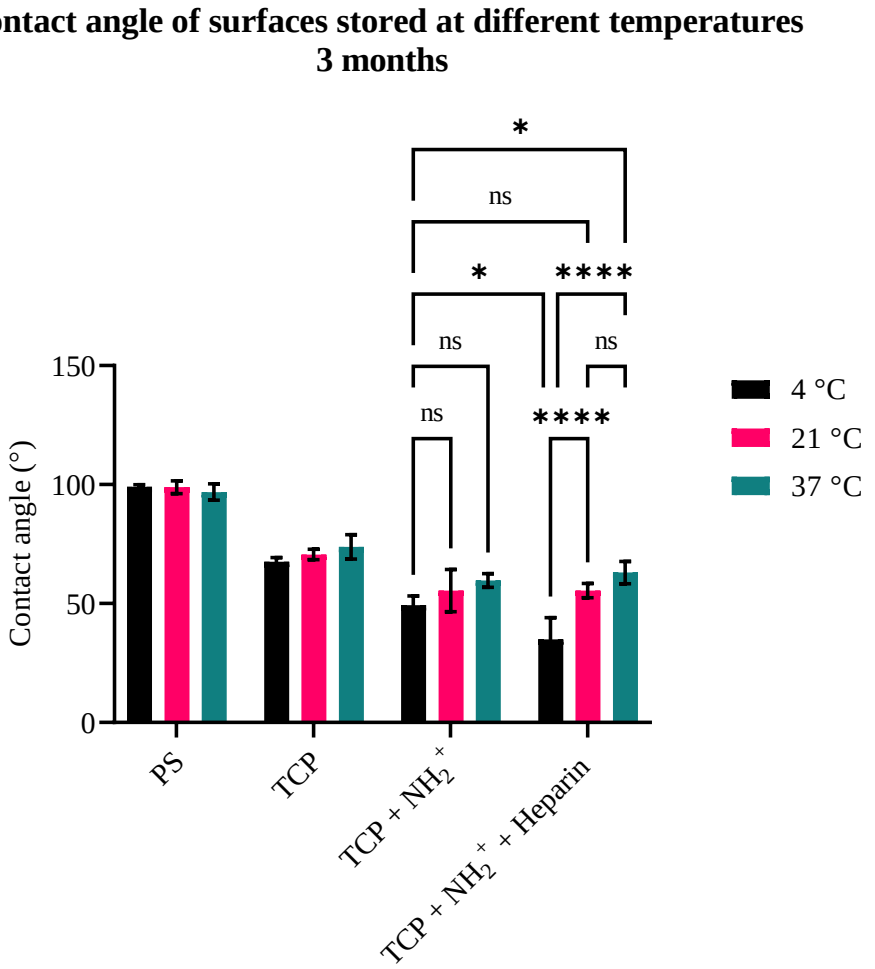

Figure 114. Contact angle of PS, TCP, TCP + NH_2^+ and TCP + NH_2^+ + Heparin after being incubated for 3 months at 4°C, 21°C and 37°C. Two-way ANOVA was performed to analyse any significant difference among test and control groups. * $p < 0.05$, ** $p < 0.01$, * $p < 0.001$, * $p < 0.0001$. Mean ± SD. N=2, n=4.

A separate statistical comparison of bioactive surface TCP + NH_2^++ Heparin was performed to determine any significant changes within the surface, at different time points. This analysis, as shown in Figure 115, showed significant differences when TCP + NH_2^++ Heparin surface was incubated at 4℃, for 24 hours, 1 month and 3 months, where a low average contact angle of 35° was registered when the surface was incubated for 3 months. Furthermore, when the TCP + NH_2^++ Heparin was incubated at 37℃, a slightly increased contact angle was found, which, even though it was not significant, would suggest some level of degradation of the bioactive surface.

It is interesting to notice that contact angle decreased from 51° and 54° (24 hours and 1 month respectively) to 35°. This could be because, either the surface gained environmental moisture and heparin was not lost while being at 4℃ for 3 months or just because of environmental moisture. To investigate further, XPS analysis was performed.

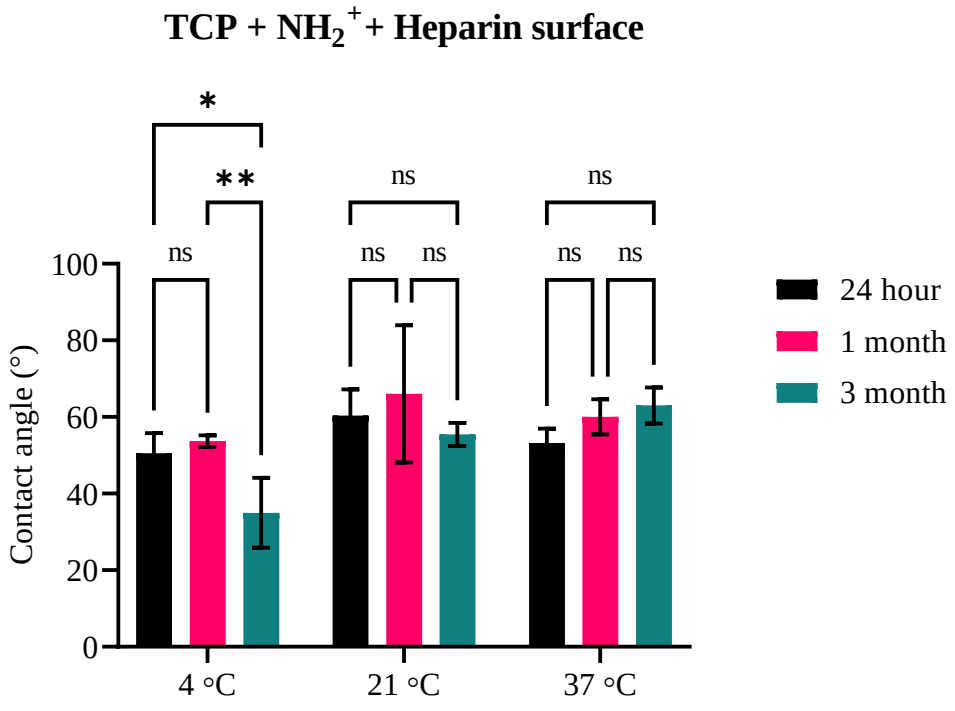

Figure 115. Contact angle TCP + NH_2^+ + Heparin after being incubated for 24 hours, 1 month and 3 months at 4℃, 21℃ and 37℃. Two-way ANOVA was performed to analyse any significant difference within the surface at different time points. * $p < 0.05$, ** $p < 0.01$. Mean ± SD. N=2, n=4.

XPS analysis revealed that heparin was present on NH_2^++ Heparin after being incubated for 3 months at 4℃, 21℃ and 37℃ (Table 17). Nevertheless, S 2p scans showed 4 peaks (168 eV, 169 eV, 164 eV and 165 eV), instead of the characteristic 2 peaks of sulphur (168 eV and 169 eV), for NH_2^++ Heparin incubated at 37℃. This information suggested that either the conformation of heparin changed (which may not bind NGF or BDNF), or some contaminant populated the bioactive surface while being incubated at 37℃ for 3 months. Overall, 4℃ and 21℃ could be ideal storage temperatures for the bioactive surface NH_2^++ Heparin.

Table 17.Percentage of atomic concentration of NH_2^++ Heparin, stored at 4℃, 21℃ and 37℃ for 3 months from XPS analysis survey scans. Mean ± SD. N=1, n=2.

Sample	**Survey scan: percentage atomic concentration %**				
	O	N	C	S	Si
NH_2^++ Heparin 4℃	24.0 ± 0.7	5.6 ± 0.2	69.7 ± 0.5	0.1 ± 0	0.5 ± 0.1
NH_2^++ Heparin 21℃	23.6 ± 0.1	3.8 ± 0.2	72.1 ± 0.1	0.1 ± 0	0.3 ± 0.1
NH_2^++ Heparin 37℃	23.6 ± 0.3	6.1 ± 0.1	68.9 ± 0.6	0.3 ± 0	1.1 ± 0.2

8.4.3.3 Release profile of NGF or BDNF from bioactive surface for 21 days

TCP + NH_2^+ + Heparin + Immobilised NGF 1 ng/mL and TCP + NH_2^+ + Heparin + Immobilised BDNF 1 ng/mL were used to evaluate, using ELISA, the release of NGF and BDNF, respectively, for 21 days. NGF at 1 ng/mL was added to TCP + NH_2^+ surface, to study how, without heparin, the release of NGF would be. The same was done for BDNF. Incubation temperature was 37°C.

NGF was released from TCP + NH_2^+ + Heparin + Immobilised NGF 1 ng/mL surface for 21 days, where a stable release can be seen in Figure 116. NGF was released from

TCP + NH_2^+ surface at 1 h, 24 h, 48 h and 168 h. After the 168 h time point, no release of NGF was observed. Furthermore, from the control, active NGF was not detected at and after 48 h. Quantities of NGF detected at the different time points can be found in Table 18.

These results suggested that TCP + NH_2^+ + Heparin + Immobilised NGF 1 ng/mL can maintain a stable release of NGF for 21 days, whereas TCP + NH_2^+ surface would only release NGF for 7 days. The difference between these two surfaces was the presence of heparin. This indicates that the immobilisation strategy via binding of NGF to heparin allows for a sustained release of active neurotrophins over an extended time period.

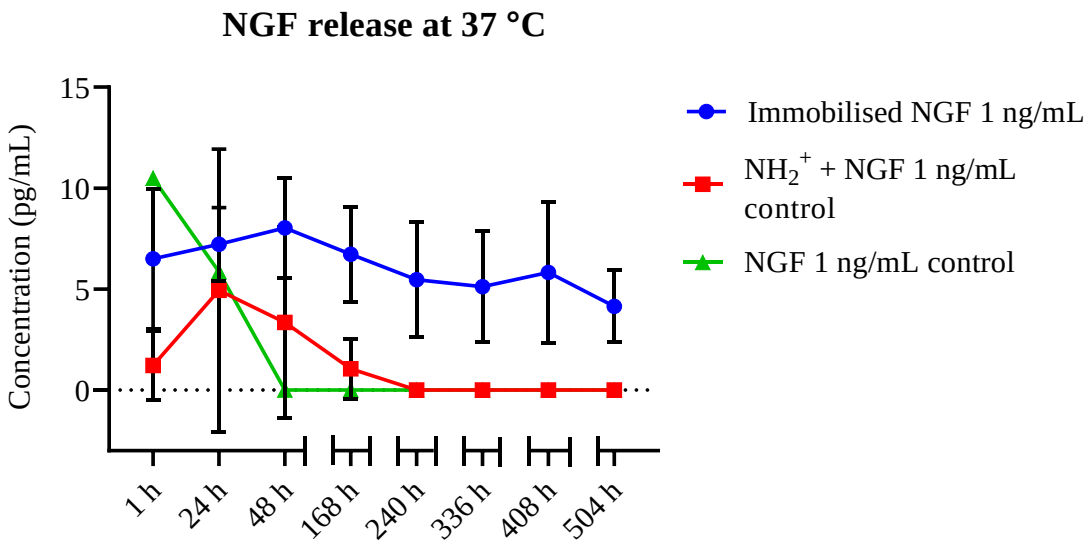

Figure 116. NGF release from TCP + NH_2^++ Heparin + Immobilised NGF 1 ng/mL (blue circles), and TCP + NH_2^+ (red squares) at different time points, from 1 h to 504 h (21 days). NGF at 1 ng/mL in solution was used as a control (green triangles). Mean ± SD. N=2, n=4.

Table 18. NGF released from TCP + NH_2^+ + Heparin + Immobilised NGF 1 ng/mL, TCP + NH_2^+ surface and NGF 1 ng/mL control at different time points, for 21 days (504 h). Mean ± SD. N=2, n=4.

	TCP + NH_2^+ + Heparin + Immobilised NGF 1 ng/mL	TCP + NH_2^+ + NGF 1 ng/mL	NGF 1 ng/mL control
1 h	6.5 ± 3.5 pg/mL	1.2 ± 1.7 pg/mL	10.5 ± 0 pg/mL
24 h	7.2 ± 1.8 pg/mL	4.9 ± 6.9 pg/mL	5.9 ± 0 pg/mL
48 h	8.0 ± 2.5 pg/mL	3.3 ± 4.7 pg/mL	0 ± 0 pg/mL
168 h	6.7 ± 2.4 pg/mL	1.1 ± 1.5 pg/mL	0 ± 0 pg/mL
240 h	5.5 ± 2.8 pg/mL	0 ± 0 pg/mL	0 ± 0 pg/mL
336 h	5.1 ± 2.7 pg/mL	0 ± 0 pg/mL	0 ± 0 pg/mL
408 h	5.8 ± 3.5 pg/mL	0 ± 0 pg/mL	0 ± 0 pg/mL
504 h	4.1 ± 1.8 pg/mL	0 ± 0 pg/mL	0 ± 0 pg/mL

BDNF was released from TCP + NH_2^+ + Heparin + Immobilised BDNF 1 ng/mL surface for 21 days, where a stable release can be seen in Figure 117. BDNF was released from TCP + NH_2^+ surface at 1 h, 24 h and 48 h. After the 48 h time point, no release of BDNF was observed. Furthermore, from the control, active BDNF was not detected at and after 168 h. Quantities of BDNF detected at the different time points can be found in Table 19.

These results suggested that TCP + NH_2^+ + Heparin + Immobilised BDNF 1 ng/mL could maintain a stable release of BDNF for 21 days, whereas TCP + NH_2^+ surface would only release BDNF for 2 days. The difference between these two surfaces was the presence of heparin. This indicates that the immobilisation strategy via binding of BDNF to heparin allows for a sustained release of active neurotrophins over an extended time period.

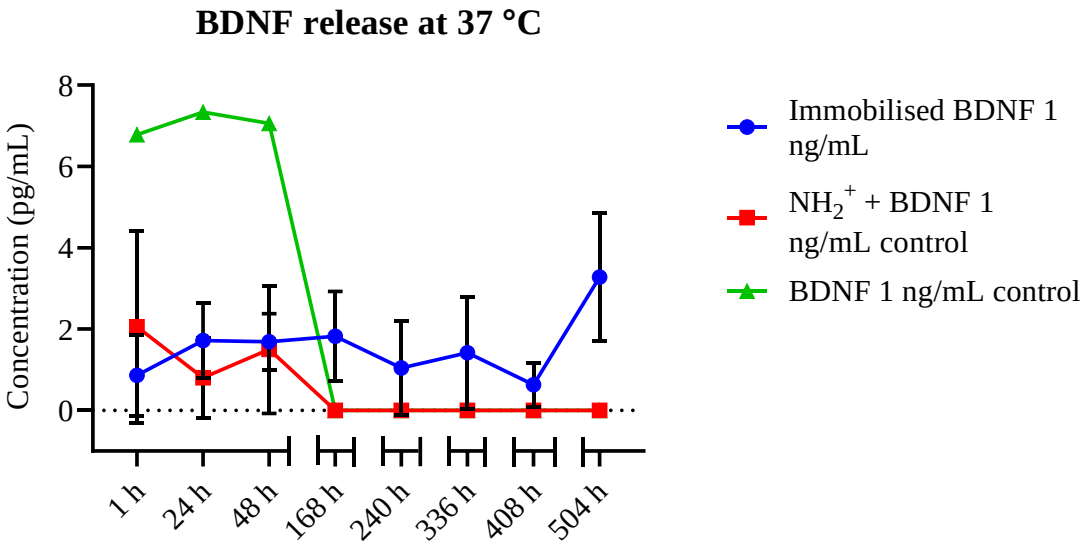

Figure 117. BDNF release from TCP + NH_2^++ Heparin + Immobilised BDNF 1 ng/mL (blue circles), and TCP + NH_2^+ (red squares) at different time points, from 1 h to 504 h (21 days). BDNF at 1 ng/mL in solution was used as a control (green triangles). Mean ± SD. N=2, n=4.

Table 19. BDNF released from TCP + NH_2^+ + Heparin + Immobilised BDNF 1 ng/mL, TCP + NH_2^+ surface and BDNF 1 ng/mL control at different time points, for 21 days (504 h). Mean ± SD. N=2, n=4.

	TCP + NH_2^+ + Heparin + Immobilised BDNF 1 ng/mL	TCP + NH_2^+ + BDNF 1 ng/mL	BDNF 1 ng/mL control
1 h	0.9 ± 0.9 pg/mL	2.1 ± 2.4 pg/mL	6.8 ± 0 pg/mL
24 h	1.7 ± 0.9 pg/mL	0.8 ± 0.9 pg/mL	7.3 ± 0 pg/mL
48 h	1.7 ± 0.7 pg/mL	1.5 ± 1.6 pg/mL	7.1 ± 0 pg/mL
168 h	1.8 ± 1.1 pg/mL	0 ± 0 pg/mL	0 ± 0 pg/mL
240 h	1.0 ± 1.1 pg/mL	0 ± 0 pg/mL	0 ± 0 pg/mL
336 h	1.4 ± 1.4 pg/mL	0 ± 0 pg/mL	0 ± 0 pg/mL
408 h	0.6 ± 0.5 pg/mL	0 ± 0 pg/mL	0 ± 0 pg/mL
504 h	3.2 ± 1.6 pg/mL	0 ± 0 pg/mL	0 ± 0 pg/mL

8.4.3.4 Crystal violet adhesion assay

PCL scaffolds, PCL Air scaffolds, PCL + NH_2^+ scaffolds and PCL + NH_2^++ Heparin scaffolds were used to assess cell adhesion by crystal violet assay, as observed in Figure 118. Assuming that all the NG108-15 neuronal cells adhere to TCP (100%), the adhesion of PCL scaffolds decreased by 18%, however, it was not significantly different with respect to TCP.

Furthermore, PCL Air scaffolds increased their adhesion properties by 47% in comparison to TCP. This may be due to the incorporation of oxygen in the scaffold, which would increase its wettability, and hence, increase cell adhesion [346]. Moreover, PCL + NH_2^+ scaffolds and PCL + NH_2^++ Heparin scaffolds had an increased percentage of cell adhesion, 76% and 121% respectively, in comparison to TCP. Both scaffolds had been previously modified with functional groups, which would increase the hydrophilicity of the scaffold, enabling cells to better adhere onto the surfaces. In addition, as the fibres of the scaffold have pores, which changed after

plasma treatment, it might be a combined effect as to why cell adhesion highly increased in comparison to TCP and even PCL scaffolds.

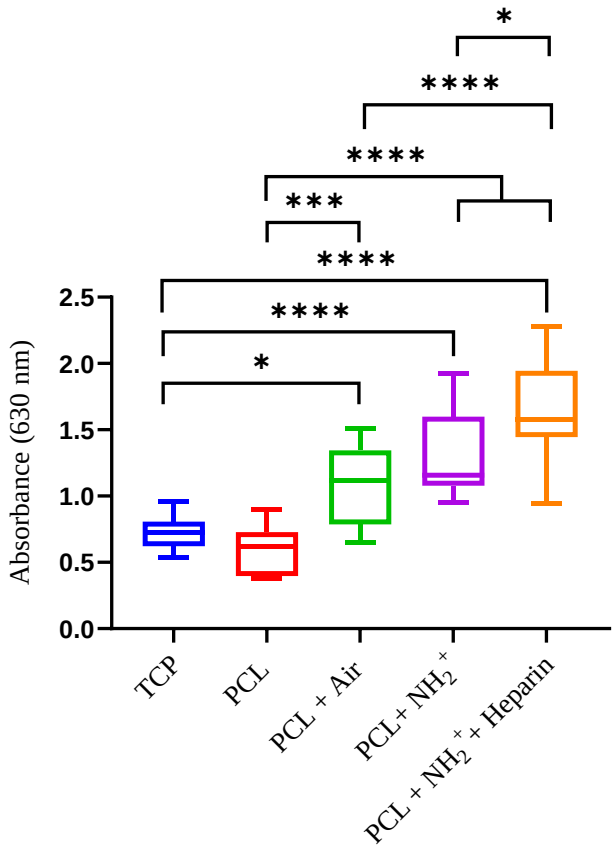

Figure 118. Crystal Violet assay to evaluate NG108-15 neuronal cell adhesion to bioactive surface on electrospun PCL scaffold. One-way ANOVA with Tukey's multiple comparison test. *p< 0.05, **p<0.01, ***p<0.001, ****p<0.0001. Mean ± SD. N=3, n=3.

8.4.3.5 Heparin quantification: TBO assay

Heparin was quantified by TBO assay. PCL + NH_2^++ Heparin films were incubated with TBO working solution and the TBO-heparin complex was eluted with ethanol / NaOH solution. Then this eluted solution was read at an absorbance of 530 nm. TBO assay revealed that 1.2 ± 0.5 µg of heparin were adsorbed in 1 cm^2 of the film.

8.4.4 Effects of bioactive surfaces on PCL electrospun scaffolds on primary cells

DRG were cultured on PCL scaffolds, PCL Air scaffolds, PCL + NH_2^+ scaffolds, PCL + NH_2^++ Heparin scaffolds and PCL + NH_2^++ Heparin + Immobilised NGF/BDNF scaffolds for 7 days. Then, they were immunolabeled against β-III tubulin and S100, so the average neurite length, average maximum neurite length and Schwann cell migration length could be quantified. Controls of secondary antibodies were done, showing no fluorescence signal (refer to Figure 135 in appendix).

The following figures show representative light-sheet images of DRG grown on PCL, PCL Air, PCL + NH_2^+, PCL + NH_2^++ Heparin, with and without NGF, BDNF, NGF plus BDNF in solution in culture medium; PCL + NH_2^+ + Heparin + Immobilised NGF, PCL + NH_2^+ + Heparin + Immobilised BDNF and PCL + NH_2^+ + Heparin + Immobilised NGF plus BDNF. Neurites were stained against β-III tubulin (green), and Schwann cells were stained against S100β (red). Growing neurites are usually accompanied by migrating Schwann cells, hence, co-localisation of both β-III tubulin and S100β was expected. This co-localisation is observed in yellow. Control surfaces are shown in Figure 119. NGF surfaces are shown in Figure 120. BDNF surfaces are shown in Figure 121. And NGF plus BDNF surfaces are shown in Figure 122.

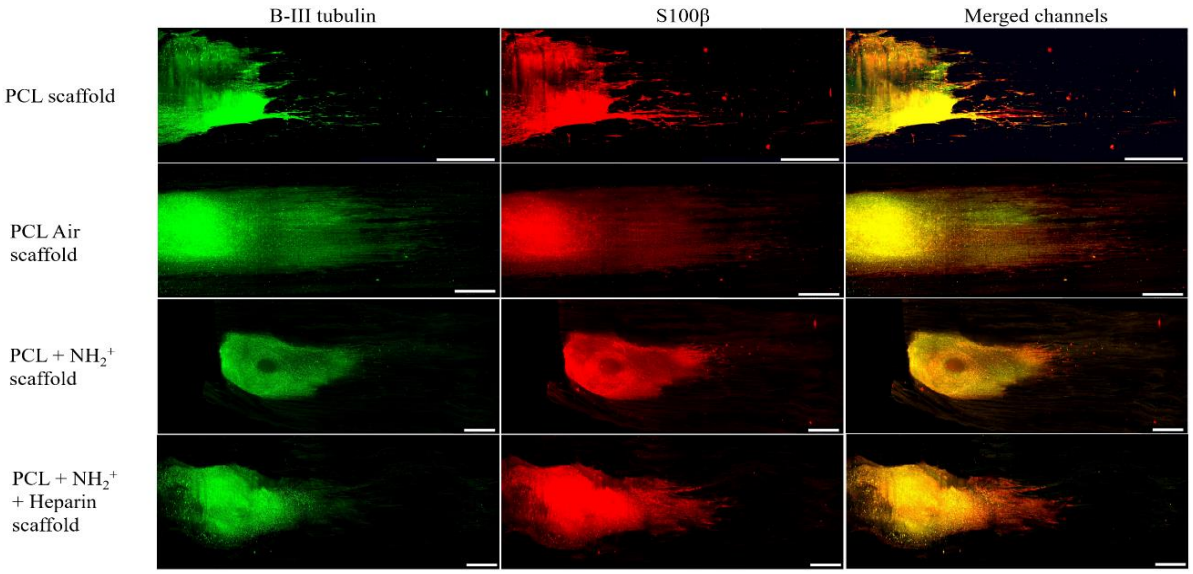

Figure 119. DRG seeded onto PCL control surfaces: PCL scaffold, PCL Air scaffold, PCL + NH_2^+ scaffold and PCL + NH_2^+ + Heparin scaffold. β-III tubulin protein in neurites stained in green. S100β of Schwann cells stained in red. Merged channels are yellow, representing the co-localisation of growing neurites and Schwann cells. Scale bar = 500 µm.

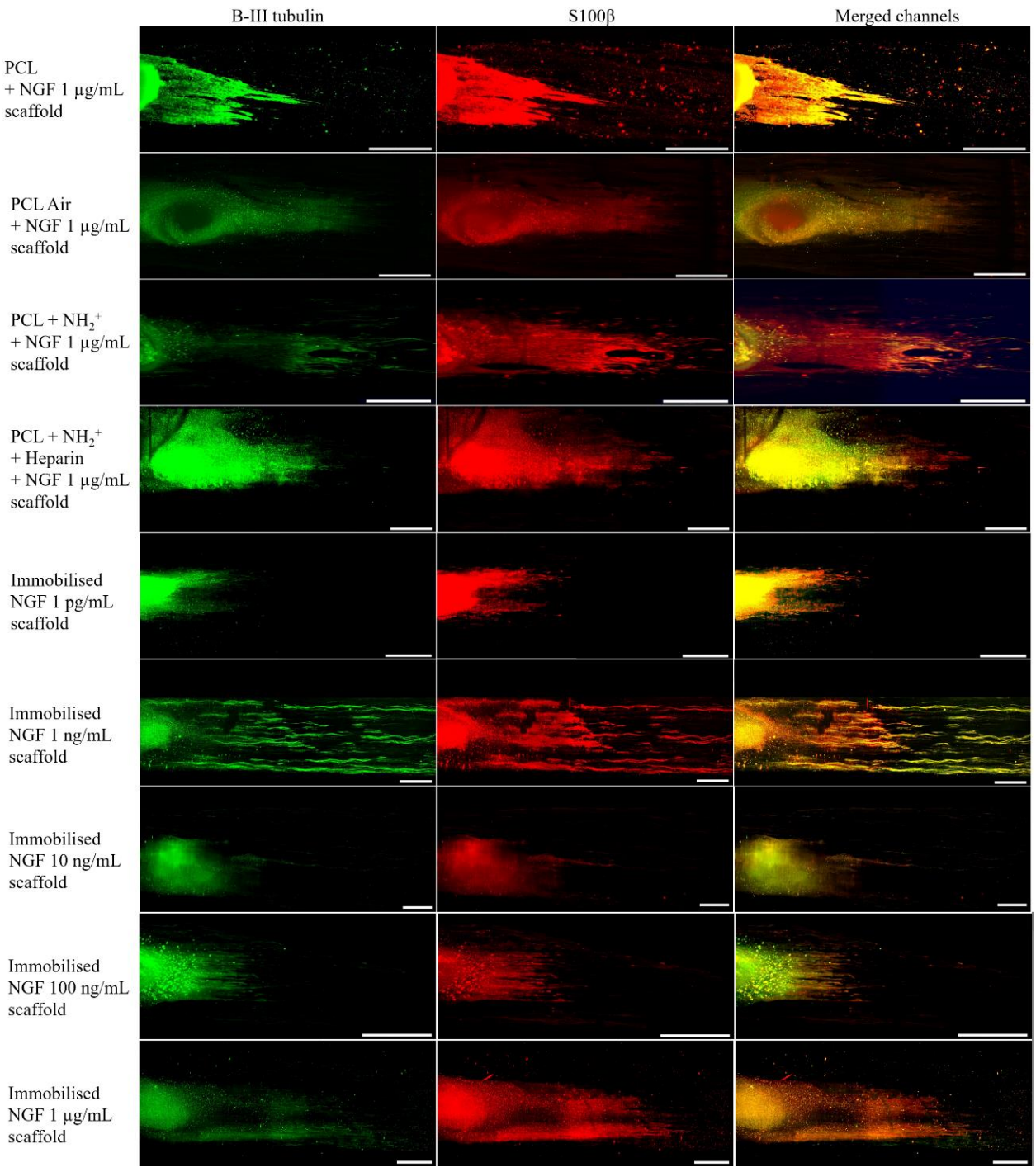

Figure 120. DRG seeded on control PCL bioactive surfaces: PCL scaffold, PCL Air scaffold, PCL + NH_2^+ scaffold and PCL + NH_2^+ + Heparin scaffold, where NGF was in solution with culture medium at a concentration of 1 µg/mL. Also, DRG seeded on bioactive surfaces PCL + NH_2^+ + Heparin + immobilised NGF at concentrations of 1 pg/mL, 1 ng/mL, 10 ng/mL, 100 ng/mL and 1 µg/mL β-III tubulin protein in neurites stained in green. S100β of Schwann cells stained in red. Merged channels are yellow, representing the co-localisation of growing neurites and Schwann cells. Scale bar = 500 µm.

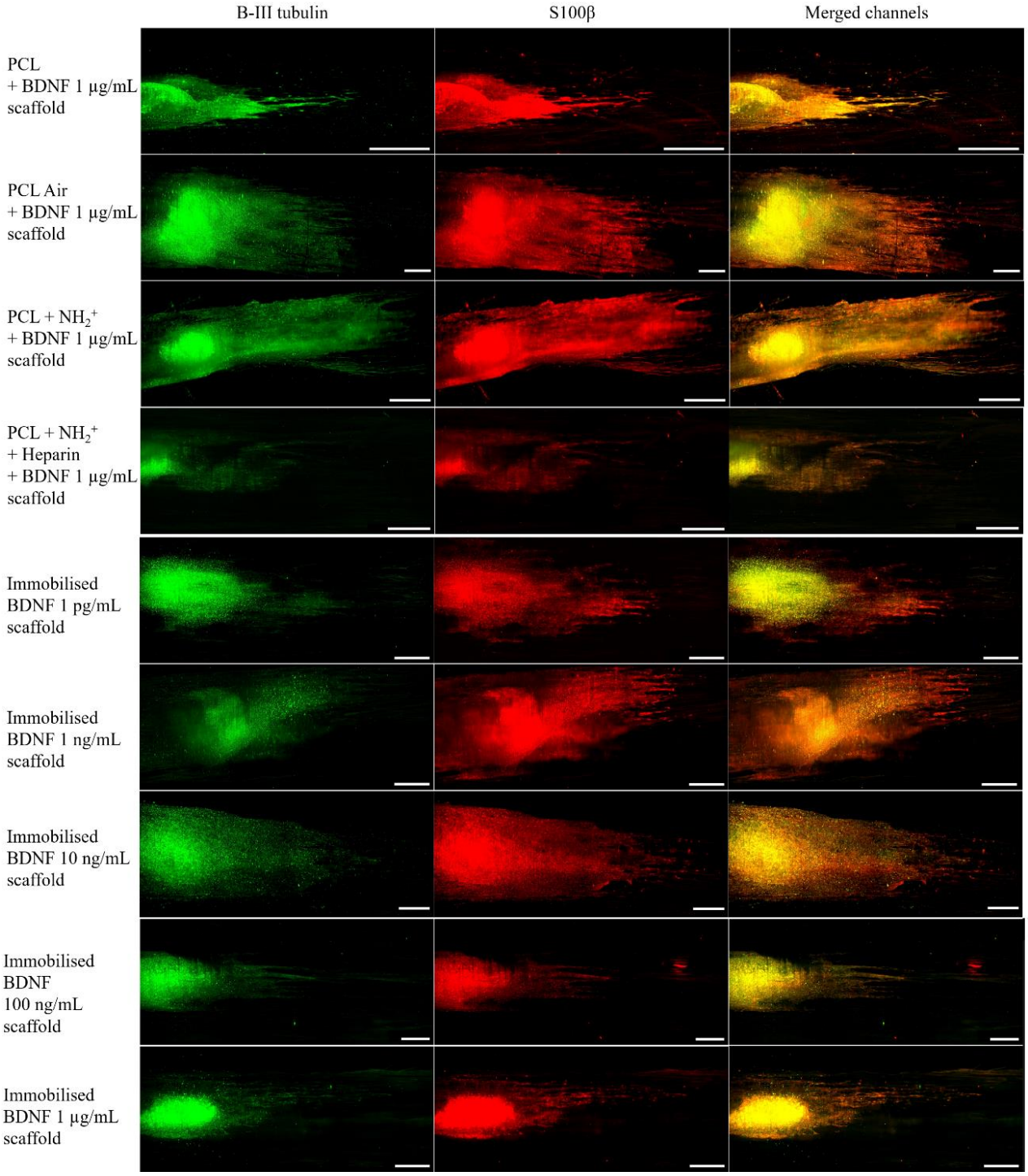

Figure 121. DRG seeded on control PCL bioactive surfaces: PCL scaffold, PCL Air scaffold, PCL + NH_2^+ scaffold and PCL + NH_2^+ + Heparin scaffold, where BDNF was in solution with culture medium at a concentration of 1 µg/mL. Also, DRG seeded on bioactive surfaces PCL + NH_2^+ + Heparin + immobilised BDNF at concentrations of 1 pg/mL, 1 ng/mL, 10 ng/mL, 100 ng/mL and 1 µg/mL β-III tubulin protein in neurites stained in green. S100β of Schwann cells stained in red. Merged channels are yellow representing the co-localisation of growing neurites and Schwann cells. Scale bar = 500 µm.

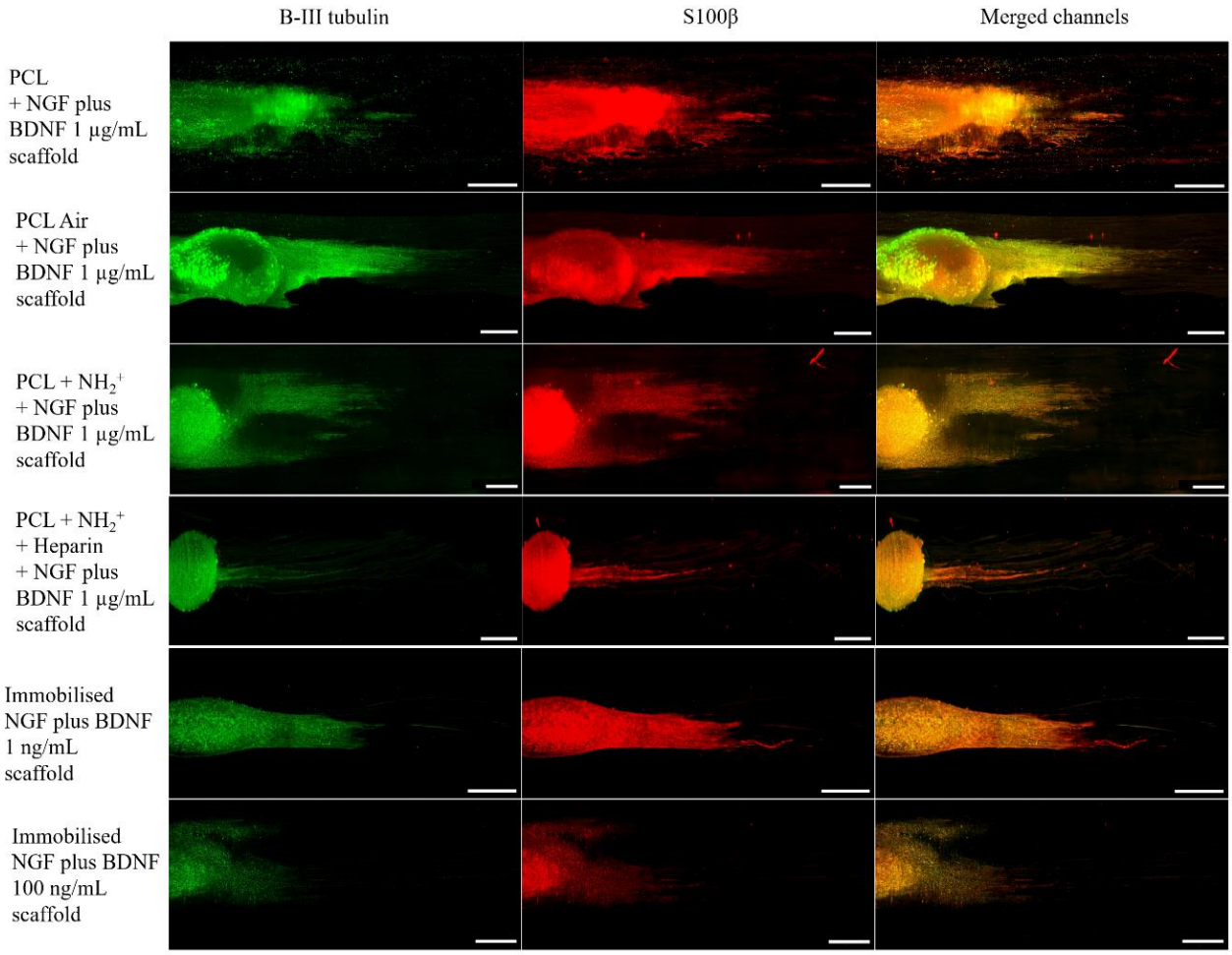

Figure 122. DRG seeded on control PCL bioactive surfaces: PCL scaffold, PCL Air scaffold, PCL + NH_2^+ scaffold and PCL + NH_2^+ + Heparin scaffold, where NGF plus BDNF were in solution with culture medium at a concentration of 1 µg/mL. Also, DRG seeded on bioactive surfaces PCL + NH_2^+ + Heparin + immobilised NGF plus BDNF at concentrations of 1 ng/mL and 100 ng/mL. β-III tubulin protein in neurites stained in green. S100β of Schwann cells stained in red. Merged channels are yellow representing the co-localisation of growing neurites and Schwann cells. Scale bar = 500 µm.

8.4.4.1 Effects in neurite outgrowth of Dorsal Root Ganglia

8.4.4.1.1 Effects of Nerve Growth Factor

Neurite outgrowth of DRG was measured and averaged to obtain average neurite length of DRG cultured on PCL scaffolds, PCL Air scaffolds, PCL + NH_2^+ scaffolds, PCL + NH_2^++ Heparin scaffolds and PCL + NH_2^++ Heparin + Immobilised NGF scaffolds (immobilised NGF). The longest average neurite length was 3041 ± 843 µm for DRG seeded on immobilised NGF at 1 ng/mL. The shortest average neurite length was 226 ± 177 µm for DRG cultured on PCL scaffolds. Average neurite outgrowth of DRG seeded on immobilised NGF 1 ng/mL was significantly longer in comparison to average neurite length developed by DRG when cultured on any other scaffold, as observed in Figure 123.

In addition, the immobilisation of 1 pg/mL, 10 ng/mL, 100 ng/mL and 1 µg/mL did not stimulate the growth of larger neurites in comparison to PCL Air scaffolds, PCL + NH_2^+ scaffolds, PCL + NH_2^++ Heparin scaffolds, with and without NGF in solution in culture medium. Nevertheless, neurite outgrowth was longer in comparison to PCL scaffolds, with and without NGF in solution in culture medium.

These results suggested that the delivery of NGF at a relative low concentration of 1 ng/mL as an immobilised neurotrophin from PCL + NH_2^++ Heparin + Immobilised NGF scaffolds, encouraged the growth of longer neurites, in comparison to the other control and test scaffolds. This delivery system, using NGF at 1 ng/mL would be an appropriate candidate for further studies regarding nerve repair.

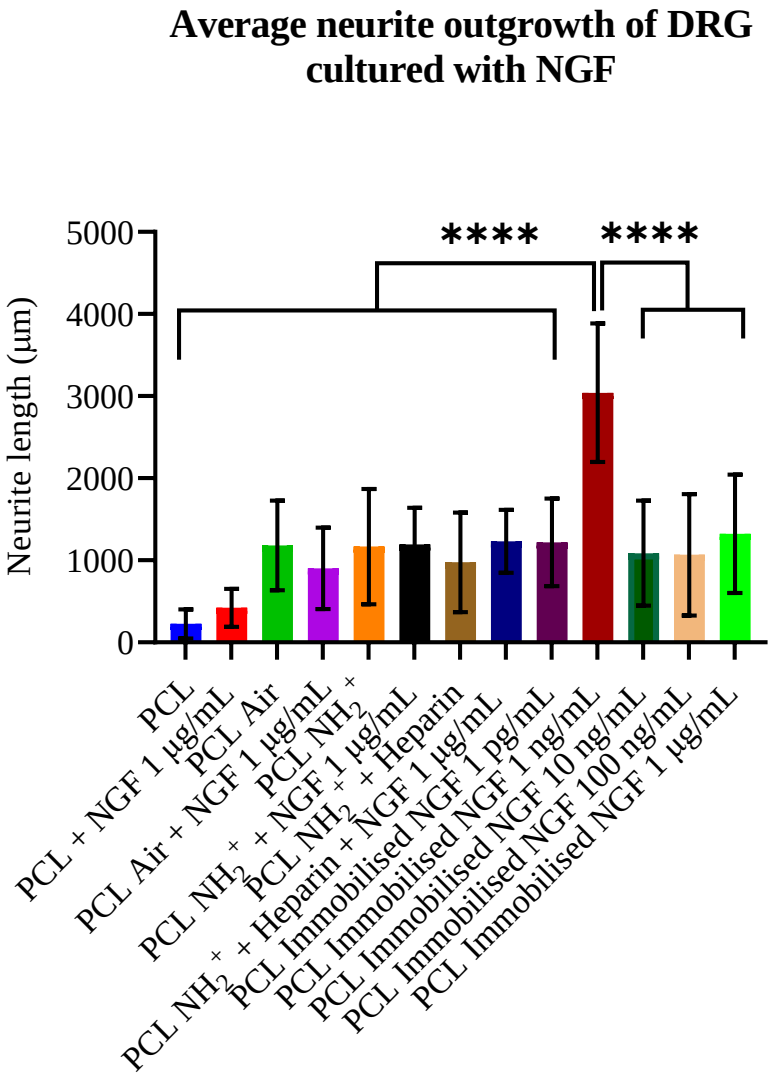

Figure 123. Average neurite length of *d*orsal *r*oot *g*anglia when cultured on PCL scaffolds, PCL Air scaffolds, PCL + NH_2^+ scaffolds, PCL + NH_2^++ Heparin scaffolds and PCL + NH_2^++ Heparin + Immobilised NGF for 7 days. NGF was immobilised on the bioactive surfaces at 1 pg/mL, 1 ng/mL, 10 ng/mL, 100 ng/mL, and 1 µg/mL. NGF was added in solution at 1 µg/mL with control surfaces. One-way ANOVA statistical analysis was performed with Tukey procedure of multiple comparisons **** $p < 0.0001$. Mean ± SD. N=3, n=3.

Average maximum neurite outgrowth of DRG was measured and averaged to obtain average maximum neurite length of DRG seeded on PCL scaffolds, PCL Air scaffolds, PCL + NH_2^+ scaffolds, PCL + NH_2^++ Heparin scaffolds and PCL + NH_2^++ Heparin + Immobilised NGF scaffolds (immobilised NGF). The shortest average maximum neurite length was 731 ± 179 µm for DRG cultured on PCL scaffolds. The longest average maximum neurite length was 3869 ± 1092 µm for DRG seeded on immobilised NGF at 1 ng/mL.

As observed in Figure 124, immobilised NGF 1 ng/mL was significantly different from PCL scaffold, PCL scaffold with NGF 1µg/mL in solution, PCL Air scaffold with NGF 1µg/mL in solution, PCL + NH_2^+ scaffold with NGF 1µg/mL in solution, PCL + NH_2^++ Heparin scaffold with NGF 1µg/mL in solution, immobilised 1 pg/mL, immobilised 10 ng/mL and immobilised 100 ng/mL. Even though immobilised NGF 1 ng/mL was not significantly different from PCL Air scaffold, PCL + NH_2^+ scaffold, PCL + NH_2^++ Heparin scaffold and immobilised NGF 1 µg/mL, the average maximum neurite length of these groups, 2367 ± 30 µm, 2566 ± 20 µm, 2817 ± 218 µm and 2193 ± 806 µm, respectively, was lower than immobilised NGF 1 ng/mL.

These results suggested that immobilised NGF 1 ng/mL may have the potential to stimulate the growth of longer neurites using this bioactive surface on PCL electrospun scaffolds.

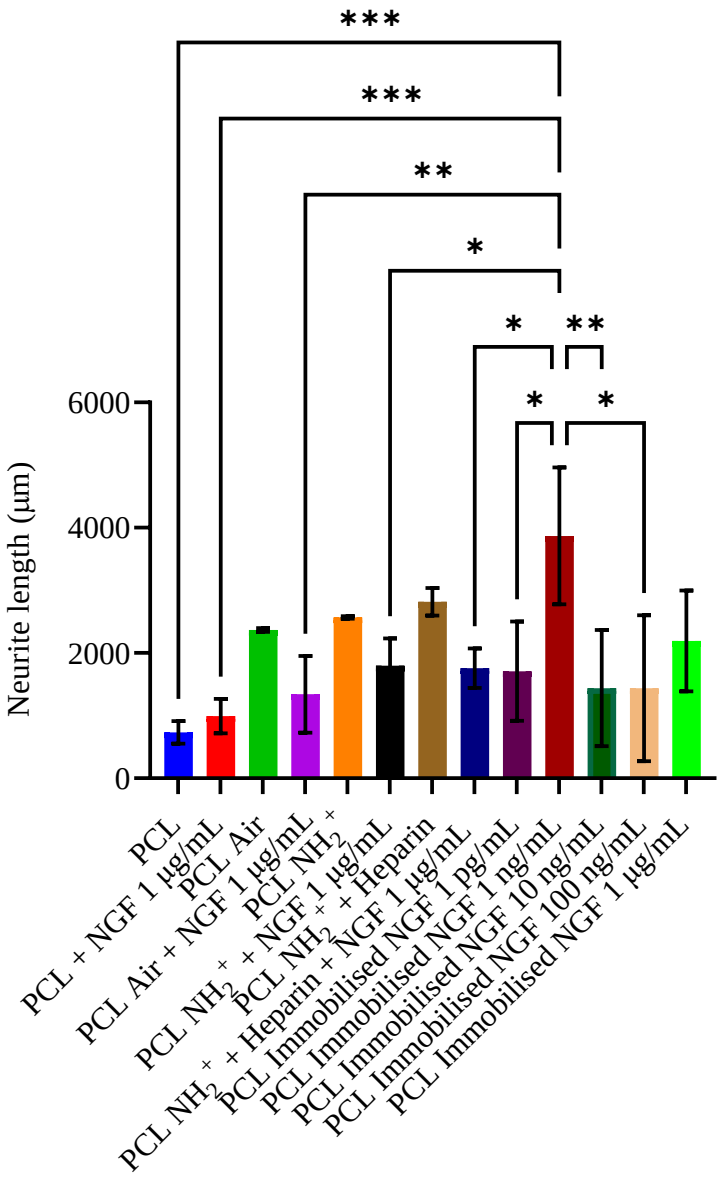

Figure 124. Average maximum neurite length of *d*orsal *r*oot *g*anglia when cultured on PCL scaffolds, PCL Air scaffolds, PCL + NH_2^+ scaffolds, PCL + NH_2^++ Heparin scaffolds and PCL + NH_2^++ Heparin + Immobilised NGF for 7 days. NGF was immobilised on the bioactive surfaces at 1 pg/mL, 1 ng/mL, 10 ng/mL, 100 ng/mL, and 1 µg/mL. NGF was added in solution at 1 µg/mL with control surfaces. One-way ANOVA statistical analysis was performed with Tukey procedure of multiple comparisons * $p < 0.05$, ** $p < 0.01$, *** $p < 0.001$. Mean ± SD. N=3, n=3.

8.4.4.1.2 Effects of Brain Derived Neurotrophic Factor

Neurite outgrowth of DRG was measured and averaged to obtain average neurite length of DRG cultured on PCL scaffolds, PCL Air scaffolds, PCL + NH_2^+ scaffolds, PCL + NH_2^++ Heparin scaffolds and PCL + NH_2^++ Heparin + Immobilised BDNF scaffolds (immobilised BDNF). The longest average neurite length was 1536 ± 762 µm for when DRG were cultured on immobilised BDNF 1 ng/mL. The shortest average neurite length was 226 ± 177 µm for DRG culture on PCL scaffolds.

Moreover, as seen in Figure 125, immobilised BDNF at 1 ng/mL encouraged the growth of neurites significantly different in comparison to PCL scaffold, PCL scaffold with BDNF 1µg/mL in solution, PCL Air scaffold, PCL + NH_2^++ Heparin scaffold, PCL + NH_2^++ Heparin scaffold with BDNF 1µg/mL in solution, immobilised 1 pg/mL and immobilised 100 ng/mL. Nevertheless, immobilised BDNF 1 ng/mL was not significantly different from either immobilised BDNF 10 ng/mL and immobilised BDNF 1 µg/mL. In addition, immobilised BDNF 1 ng/mL was not significant different from PCL Air scaffold with BDNF 1 µg/mL in solution nor PCL + NH_2^++ Heparin scaffold with BDNF 1 µg/mL in solution. These results suggest that with a relative low concentration of immobilised BDNF at 1 ng/mL, longer neurites could be developed in similar length as when BDNF at 1 µg/mL in solution was used in culture medium, which would make the delivery system of immobilised BDNF at 1 ng/mL an adequate candidate for further studies regarding nerve repair.

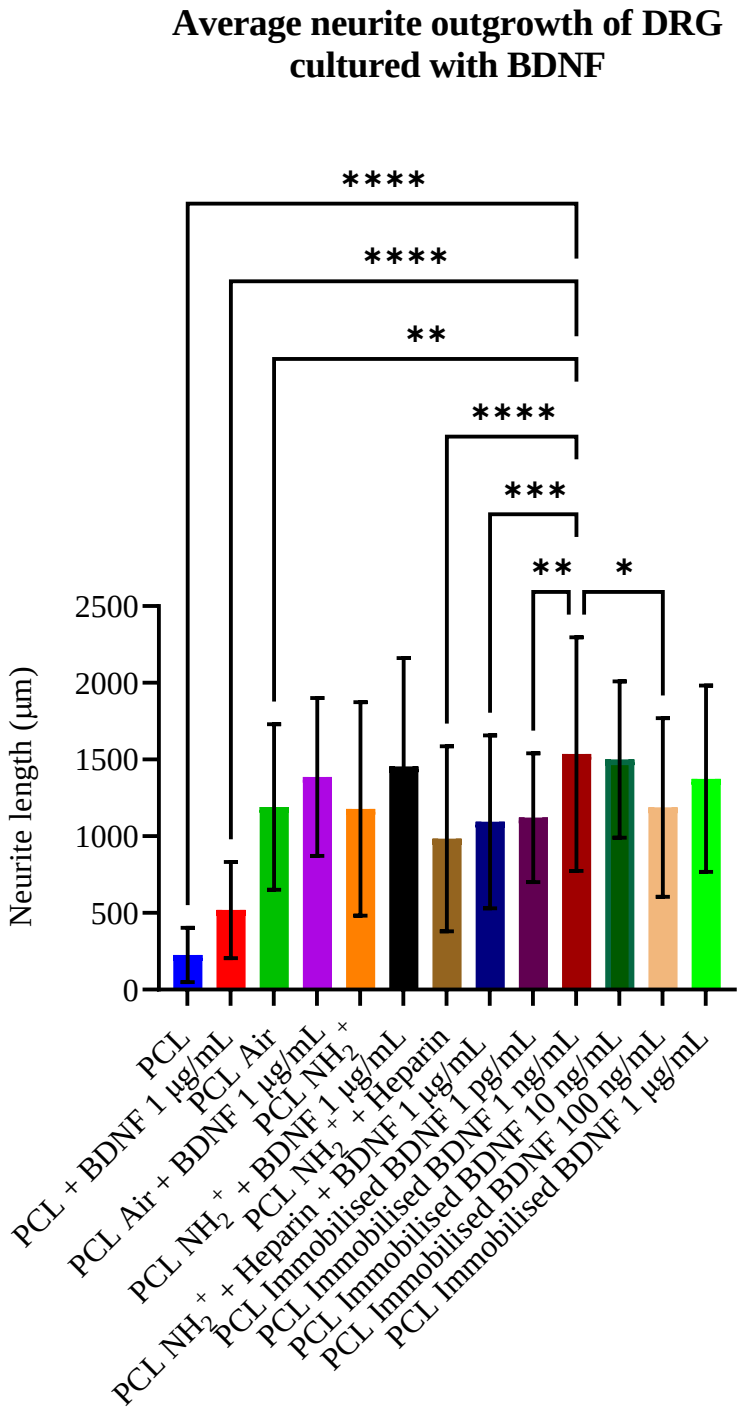

Figure 125. Average neurite length of *d*orsal *r*oot *g*anglia when cultured on PCL scaffolds, PCL Air scaffolds, PCL + NH_2^+ scaffolds, PCL + NH_2^++ Heparin scaffolds and PCL + NH_2^++ Heparin + Immobilised BDNF for 7 days. BDNF was immobilised on the bioactive surfaces at 1 pg/mL, 1 ng/mL, 10 ng/mL, 100 ng/mL, and 1 µg/mL. BDNF was added in solution at 1 µg/mL with control surfaces. One-way ANOVA statistical analysis was performed with Tukey procedure of multiple comparisons * $p < 0.05$, ** $p < 0.01$, *** $p < 0.001$, **** $p < 0.0001$. Mean ± SD. N=3, n=3.

Average maximum neurite outgrowth of DRG was measured and averaged to obtain average maximum neurite length of DRG seeded on PCL scaffolds, PCL Air scaffolds, PCL + NH_2^+ scaffolds, PCL + NH_2^++ Heparin scaffolds and PCL + NH_2^++ Heparin + Immobilised BDNF scaffolds (immobilised BDNF). The shortest average maximum neurite length was 731 ± 179 µm for DRG cultured on PCL scaffolds. The longest average maximum neurite length was 2817 ± 218 µm for DRG seeded on PCL + NH_2^++ Heparin scaffolds.

Even though PCL + NH_2^++ Heparin scaffolds developed neurites significantly larger in comparison to PCL scaffold and PCL scaffolds with BDNF at 1 µg/mL, they did not have any significant difference in comparison to the other groups, as observed in Figure 126. Immobilised BDNF at 1 ng/mL encouraged the growth on maximum neurite length of 2498 ± 1130 µm, which would suggest that by using immobilised BNDF 1 ng/mL surface, the potential of stimulating the growth of longer neurites exists.

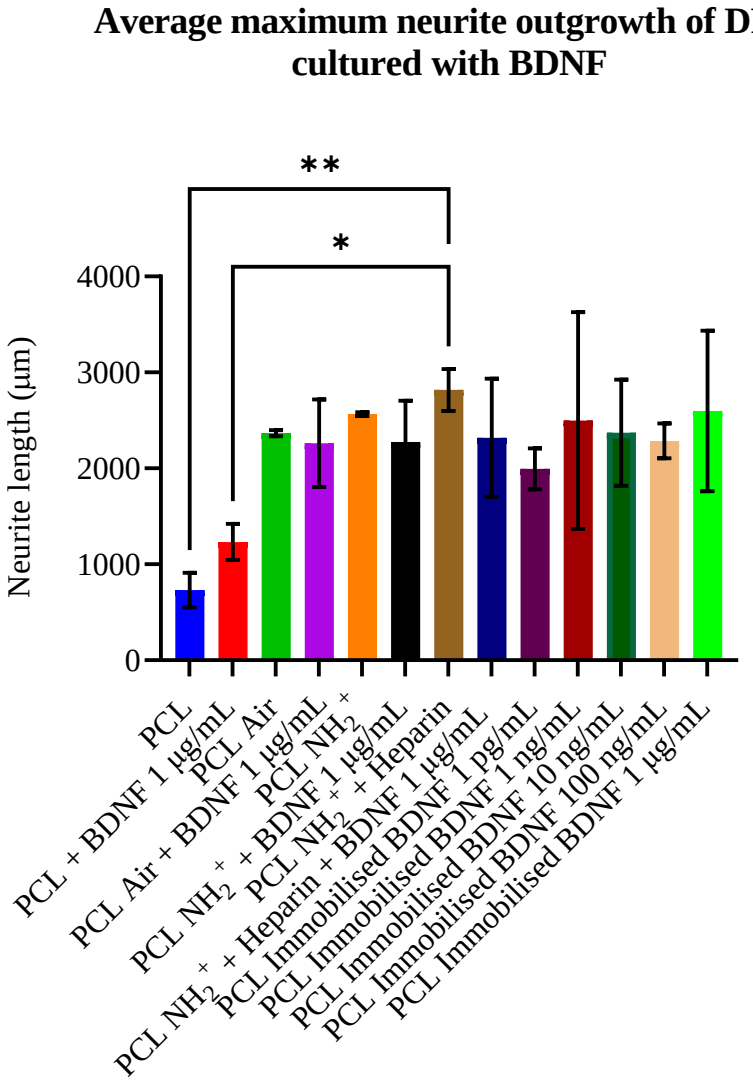

Figure 126. Average maximum neurite length of *d*orsal *r*oot *g*anglia when cultured on PCL scaffolds, PCL Air scaffolds, PCL + NH_2^+ scaffolds, PCL + NH_2^++ Heparin scaffolds and PCL + NH_2^++ Heparin + Immobilised BDNF for 7 days. BDNF was immobilised on the bioactive surfaces at 1 pg/mL, 1 ng/mL, 10 ng/mL, 100 ng/mL, and 1 µg/mL. BDNF was added in solution at 1 µg/mL with control surfaces. One-way ANOVA statistical analysis was performed with Tukey procedure of multiple comparisons * $p < 0.05$, ** $p < 0.01$. Mean ± SD. N=3, n=3.

8.4.4.1.3 Effect of Nerve Growth Factor plus Brain Derived Neurotrophic Factor

Neurite outgrowth of DRG was measured and averaged to obtain average neurite length of DRG cultured on PCL scaffolds, PCL Air scaffolds, PCL + NH_2^+ scaffolds, PCL + NH_2^++ Heparin scaffolds and PCL + NH_2^++ Heparin + Immobilised NGF plus BDNF scaffolds (immobilised NGF plus BDNF). The longest average neurite length was 1816 ± 583 µm when DRG were cultured on PCL Air scaffold with NGF plus BDNF in solution in culture medium. The shortest average neurite length was 226 ± 177 µm when DRG were cultured on PCL scaffolds.

PCL Air scaffolds with NGF plus BDNF in solution in culture medium developed neurites significantly longer, as seen in Figure 127, in comparison to PCL scaffold, PCL scaffold with NGF plus BDNF at 1 µg/mL in solution, PCL Air scaffold, PCL + NH_2^+ scaffold, PCL + NH_2^++ Heparin scaffold, PCL + NH_2^++ Heparin scaffold with NGF plus BDNF at 1 µg/mL in solution, and most importantly, immobilised NGF plus BDNF 1 ng/mL and immobilised NGF plus BDNF 100 ng/mL. These results might indicate that immobilisation of both NGF and BDNF would not encourage the growth of longer neurites.

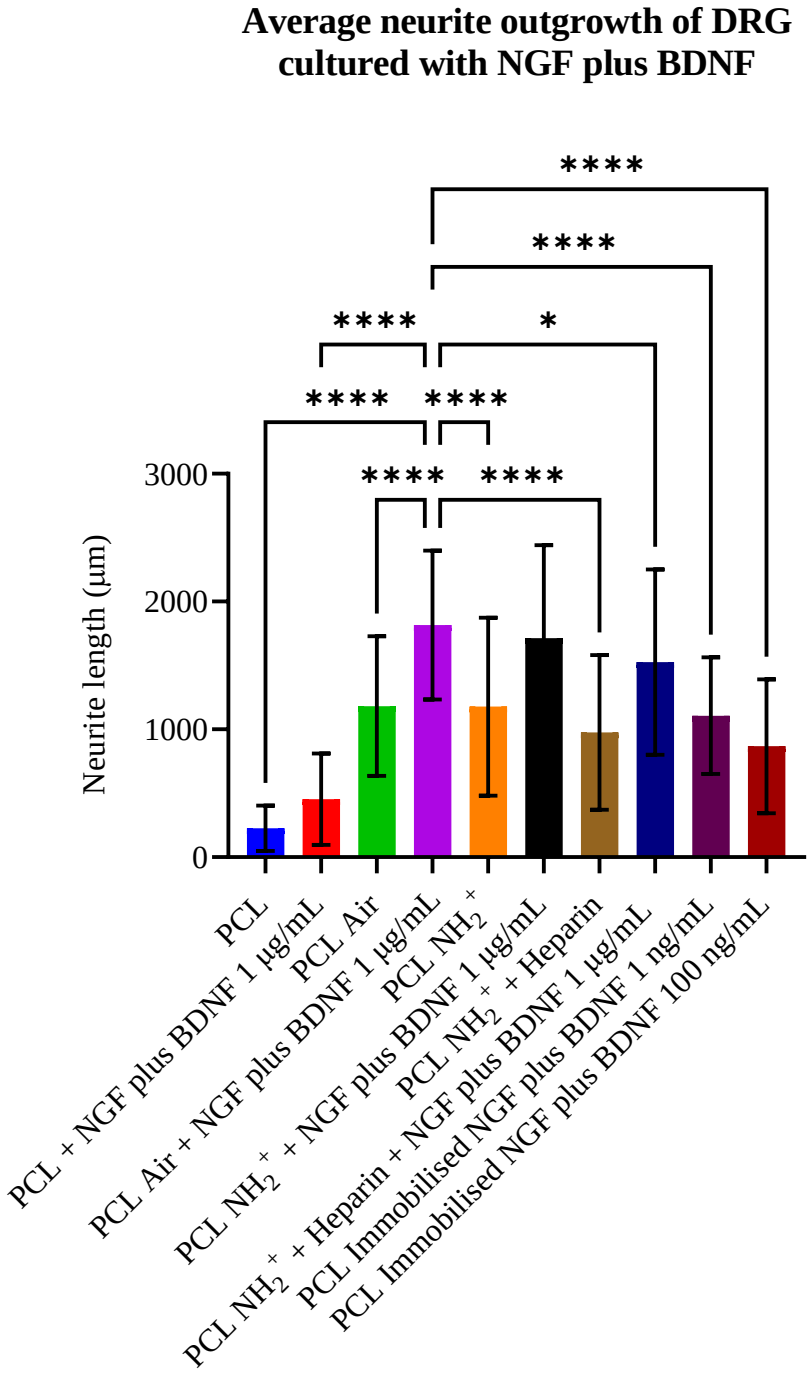

Figure 127. Average neurite length of *d*orsal *r*oot *g*anglia when cultured on PCL scaffolds, PCL Air scaffolds, PCL + NH_2^+ scaffolds, PCL + NH_2^++ Heparin scaffolds and PCL + NH_2^++ Heparin + Immobilised NGF plus BDNF for 7 days. NGF plus BDNF were immobilised on the bioactive surfaces at 1 ng/mL and 100 ng/mL. NGF plus BDNF were added in solution at 1 µg/mL with control surfaces. One-way ANOVA statistical analysis was performed with Tukey procedure of multiple comparisons * $p < 0.05$, ** $p < 0.01$, *** $p < 0.001$, **** $p < 0.0001$. Mean ± SD. N=3, n=3.

Average maximum neurite outgrowth of DRG was measured and averaged to obtain average maximum neurite length of DRG seeded on PCL scaffolds, PCL Air scaffolds, PCL + NH_2^+ scaffolds, PCL + NH_2^++ Heparin scaffolds and PCL + NH_2^++ Heparin + Immobilised NGF plus BDNF scaffolds (immobilised NGF plus BDNF). The shortest average maximum neurite length was 731 ± 179 µm for DRG cultured on PCL scaffolds. The longest average maximum neurite length was 2861 ± 43 µm for DRG seeded on PCL Air scaffolds with NGF plus BDNF at 1 µg/mL in solution in culture medium.

PCL Air scaffolds with NGF plus BDNF at 1 µg/mL in solution encouraged the growth of longer neurites, which length were significantly different to the ones developed from PCL scaffolds, PCL scaffolds with NGF plus BDNF at 1 µg/mL in solution and immobilised NGF plus BDNF 100 ng/mL, as observed in Figure 128. However, even though average maximum neurite length of PCL Air scaffolds with NGF plus BDNF at 1 µg/mL in solution was not significantly different from immobilised NGF plus BDNF 1 ng/mL, the average maximum neurite length of the latter was 1826 ± 360 µm, which was almost 1000 µm shorter. Hence, immobilised NGF plus BDNF 1 ng/mL would not be an appropriate delivery system to use to encourage neurite outgrowth.

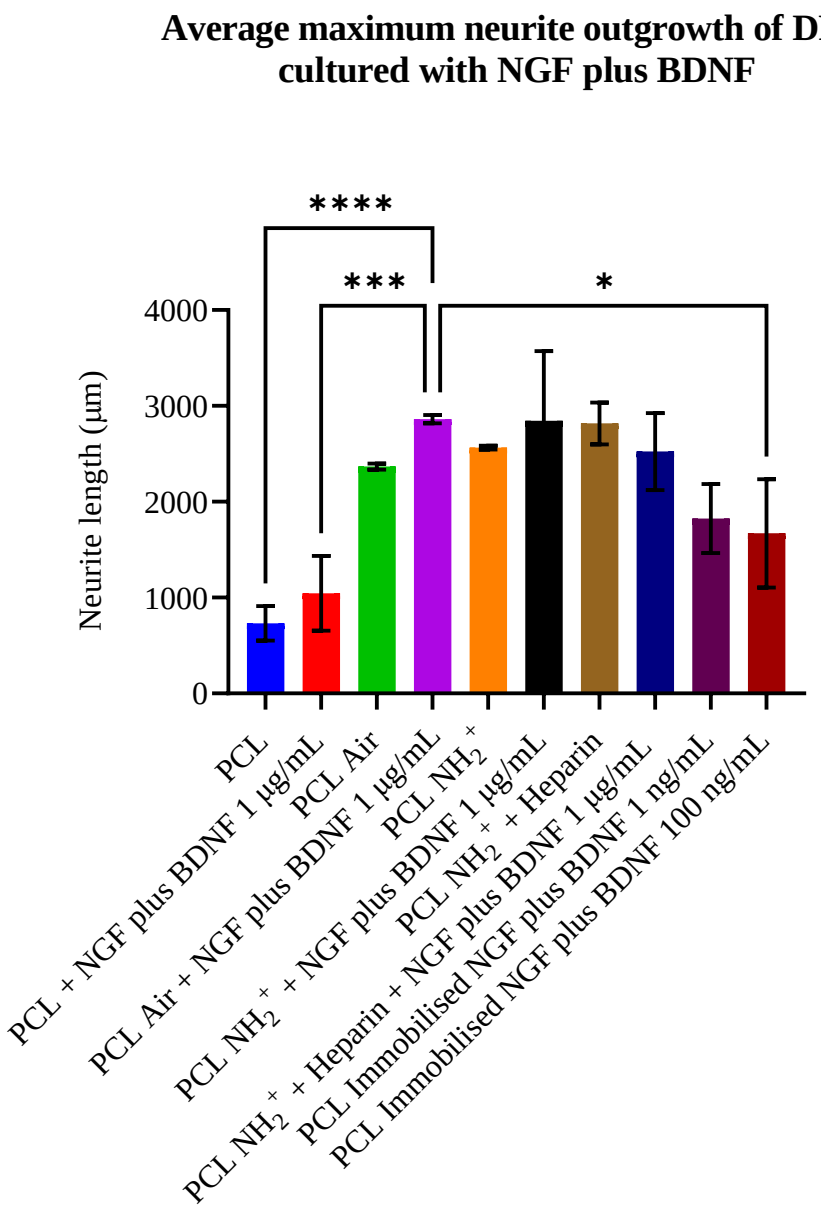

Figure 128. Average maximum neurite length of *d*orsal *r*oot *g*anglia when cultured on PCL scaffolds, PCL Air scaffolds, PCL + NH_2^+ scaffolds, PCL + NH_2^++ Heparin scaffolds and PCL + NH_2^++ Heparin + Immobilised NGF plus BDNF for 7 days. NGF plus BDNF were immobilised on the bioactive surfaces at 1 ng/mL and 100 ng/mL. NGF plus BDNF were added in solution at 1 µg/mL with control surfaces. One-way ANOVA statistical analysis was performed with Tukey procedure of multiple comparisons * $p < 0.05$, *** $p < 0.001$. Mean ± SD. N=3, n=3.

8.4.4.2 Effect in migration length of Schwann cells

8.4.4.2.1 Effects of Nerve Growth Factor

Migration length of Schwann cells from DRG was measured for DRG cultured on PCL scaffolds, PCL Air scaffolds, PCL + NH_2^+ scaffolds, PCL + NH_2^++ Heparin scaffolds and PCL + NH_2^++ Heparin + Immobilised NGF scaffolds (immobilised NGF). The longest migration length of Schwann cells was 2718 ± 911 µm when DRG were seeded on immobilised NGF at 1 ng/mL. The shortest migration length of Schwann cells was 270 ± 185 µm when DRG were cultured on PCL scaffolds.

Moreover, the migration length of Schwann cells when they were cultured on immobilised NGF at 1 ng/mL was significantly longer in comparison to other control and test groups, as seen in Figure 129. These results showed that Schwann cells migrate farther when cultured on immobilised NGF 1 ng/mL, which would suggest this would aid the growth of longer neurites.

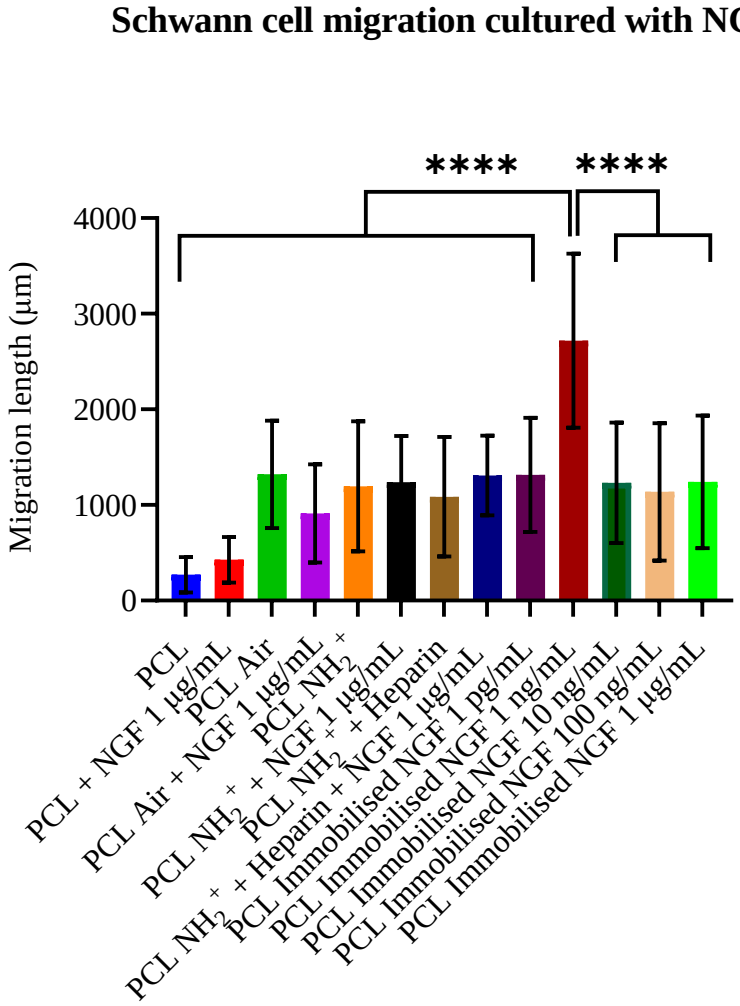

Figure 129. Schwann cell migration when cultured on PCL scaffolds, PCL Air scaffolds, PCL + NH_2^+ scaffolds, PCL + NH_2^++ Heparin scaffolds and PCL + NH_2^++ Heparin + Immobilised NGF for 7 days. NGF was immobilised on the bioactive surfaces at 1 pg/mL, 1 ng/mL, 10 ng/mL, 100 ng/mL, and 1 µg/mL. NGF was added in solution at 1 µg/mL with control surfaces. One-way ANOVA statistical analysis was performed with Tukey procedure of multiple comparisons **** $p < 0.0001$. Mean ± SD. N=3, n=3.

8.4.4.2.2 Effects of Brain Derived Neurotrophic Factor

Migration length of Schwann cells from DRG was measured for DRG cultured on PCL scaffolds, PCL Air scaffolds, PCL + NH_2^+ scaffolds, PCL + NH_2^++ Heparin scaffolds and PCL + NH_2^++ Heparin + Immobilised BDNF scaffolds (immobilised BDNF). The longest migration length of Schwann cells was 1614 ± 543 µm when DRG were seeded on immobilised BDNF at 10 ng/mL. The shortest migration length of Schwann cells was 270 ± 185 µm when DRG were cultured on PCL scaffolds.

Migration length of Schwann cells cultured on immobilised BDNF at 10 ng/mL was not significantly different from migration length of Schwann cells cultured on PCL Air scaffolds with BDNF 1 µg/mL in solution, PCL + NH_2^+ scaffolds with BDNF 1 µg/mL in solution, immobilised BDNF 1 pg/mL, immobilised BDNF 1 ng/mL, immobilised BDNF 100 ng/mL and immobilised BDNF 1 µg/mL, as observed in Figure 130. Nevertheless, it is important to notice that with a low concentration of immobilised BDNF, in this case 10 ng/mL, Schwann cells were stimulated to migrate as further as when BDNF was at a concentration of 1 µg/mL in solution in culture media. Furthermore, immobilised BDNF at 1 ng/mL encouraged Schwann cells to migrate 1571 ± 828 µm, which was not significantly different from migration length of Schwann cells from immobilised 10 ng/mL (1614 ± 543 µm).

These results showed that with a relatively low concentration of BDNF, Schwann cells migrated farther, which would suggest further support during nerve repair, as these conditions encouraged the growth of longer neurites.

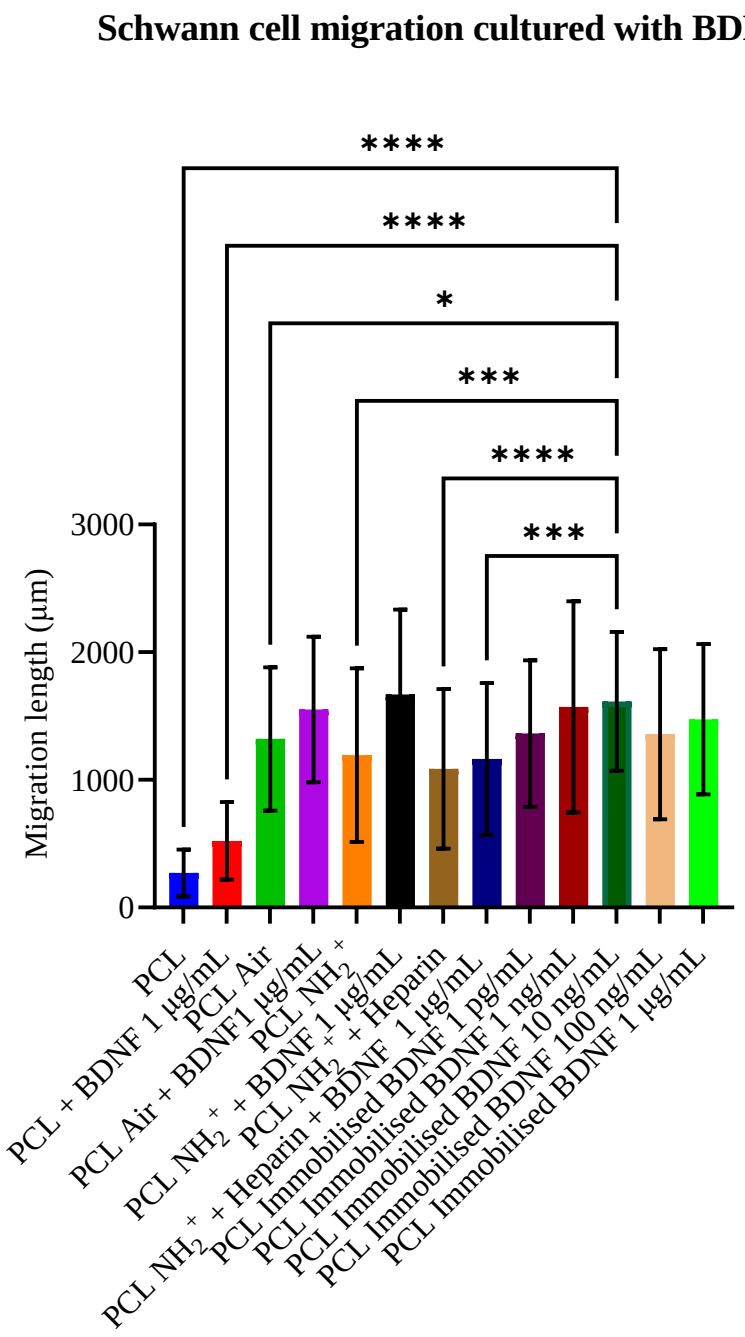

Figure 130. Schwann cell migration when cultured on PCL scaffolds, PCL Air scaffolds, PCL + NH_2^+ scaffolds, PCL + NH_2^++ Heparin scaffolds and PCL + NH_2^++ Heparin + Immobilised BDNF for 7 days. BDNF was immobilised on the bioactive surfaces at 1 pg/mL, 1 ng/mL, 10 ng/mL, 100 ng/mL, and 1 µg/mL. BDNF was added in solution at 1 µg/mL with control surfaces. One-way ANOVA statistical analysis was performed with Tukey procedure of multiple comparisons * $p < 0.05$, ** $p < 0.01$, *** $p < 0.001$, **** $p < 0.0001$. Mean ± SD. N=3, n=3.

8.4.4.2.3 Effect of Nerve Growth Factor plus Brain Derived Neurotrophic Factor

Migration length of Schwann cells from DRG was measured for DRG cultured on PCL scaffolds, PCL Air scaffolds, PCL + NH_2^+ scaffolds, PCL + NH_2^++ Heparin scaffolds and PCL + NH_2^++ Heparin + Immobilised NGF plus BDNF scaffolds (immobilised NGF plus BDNF). The longest migration length of Schwann cells was 1974 ± 708 µm when DRG were seeded on PCL Air scaffolds with NGF plus BDNF at 1 µg/mL in solution in culture medium. The shortest migration length of Schwann cells was 270 ± 185 µm when DRG were cultured on PCL scaffolds.

Figure 131 shows a bar chart of Schwann cell migration length, where PCL Air scaffolds with NGF plus BDNF at 1 µg/mL in solution encouraged a migration length significantly further in comparison to PCL scaffolds, PCL scaffolds with NGF plus BDNF at 1 µg/mL in solution, PCL Air scaffolds, PCL + NH_2^+ scaffolds, PCL + NH_2^++ Heparin scaffolds, PCL + NH_2^++ Heparin scaffolds with NGF plus BDNF at 1 µg/mL in solution, immobilised NGF plus BDNF at 1 ng/mL and immobilised NGF plus BDNF at 100 ng/mL. These results showed that immobilised NGF plus BDNF surfaces did not stimulate Schwann cells to migrate further in comparison to Schwann cell migration length from scaffold control PCL Air scaffolds with NGF plus BDNF at 1 µg/mL in solution. This suggested that NGF co-immobilised with BDNF may not encourage sufficient neurite outgrowth to promote nerve repair.

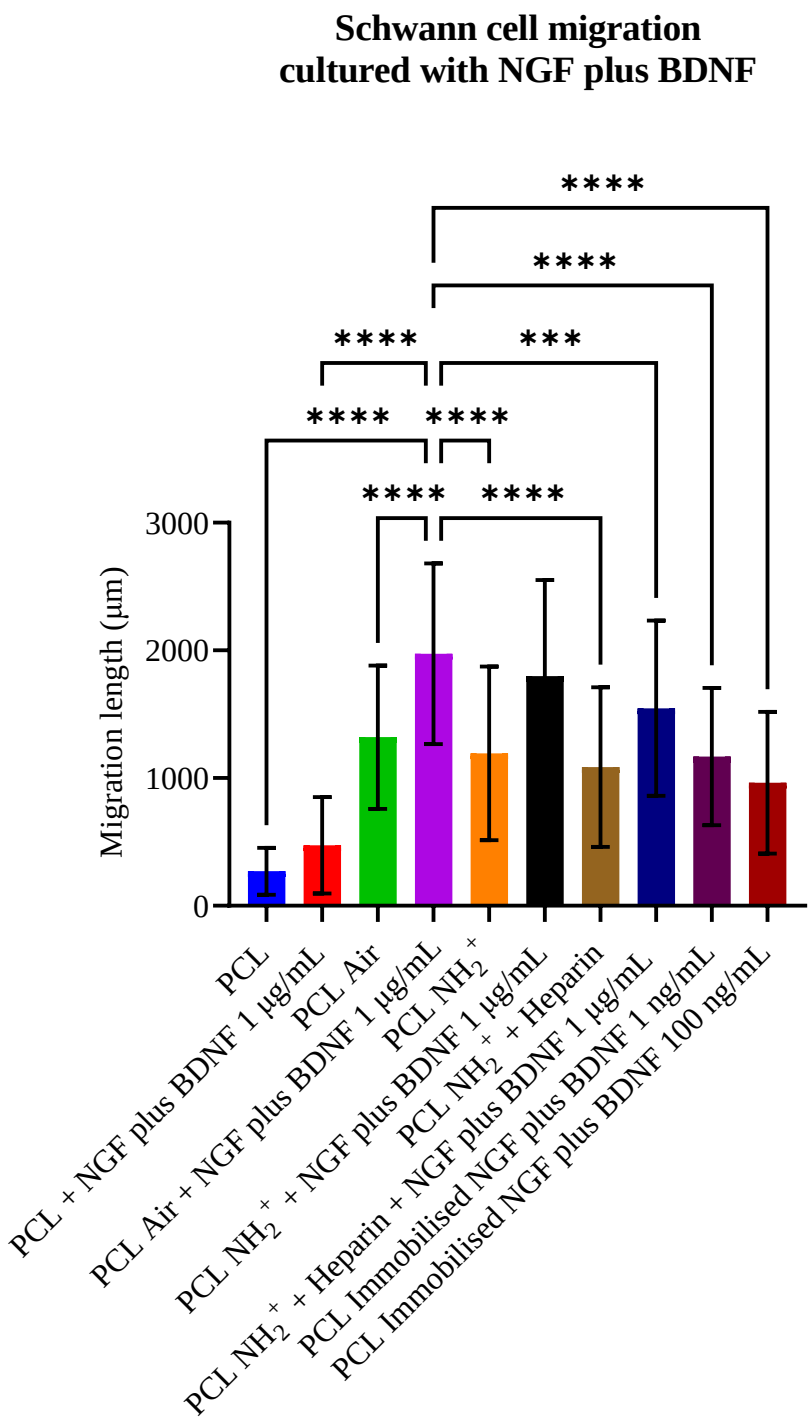

Figure 131. Schwann cell migration when cultured on PCL scaffolds, PCL Air scaffolds, PCL + NH_2^+ scaffolds, PCL + NH_2^++ Heparin scaffolds and PCL + NH_2^++ Heparin + Immobilised NGF plus BDNF for 7 days. NGF plus BDNF was immobilised on the bioactive surfaces at 1 ng/mL, and 100 ng/mL. NGF plus BDNF was added in solution at 1 µg/mL with control surfaces. One-way ANOVA statistical analysis was performed with Tukey procedure of multiple comparisons *** $p < 0.001$, **** $p < 0.0001$. Mean ± SD. N=3, n=3.

8.5 Discussion

Bioactive surfaces for the delivery of NGF, BDNF or NGF plus BDNF were successfully fabricated on PCL scaffolds. PCL fibrous scaffolds were fabricated by electrospinning, and fibre diameter and alignment were measured using SEM. NH_2^+ functional groups were added by plasma deposition onto the PCL electrospun scaffold. Furthermore, NGF and BDNF were successfully immobilised onto the surface via binding to the electrostatically immobilised heparin. The addition of NH_2^+ and heparin was confirmed by XPS. Moreover, the addition of NGF or BDNF was confirmed by ELISA. Culture of primary chick embryo DRG was used to assess the effects of the bioactive scaffolds.

The diameter of PCL fibres and pore ratio were measured before and after plasma deposition, revealing that, even though fibre diameter was not significantly different, pore morphology was significantly different. In addition, crystal violet assay was performed to observe if the quantity of adhered NG108-15 neuronal cells onto the bioactive surfaces was different. Interestingly, it was found that adhesion of NG108-15 neuronal cells increased when PCL scaffolds were plasma treated. Moreover, the adhesion of NG108-15 neuronal cells increased when heparin was added to the surface.

Differences in wettability were characterised by contact angle, when the bioactive surface was stored for 24 hours, 1 month and 3 months at 4°C, 21°C and 37°C. The results showed that, for the NH_2^+ + Heparin, contact angle changed during the storage period when this bioactive surface was incubated at 4°C. Furthermore, XPS analysis showed that heparin was present on the bioactive surfaces when incubated at 4°C and 21°C after 3 months of storage. Even though heparin was also present on the bioactive surface when incubated at 37°C, S 2p scan revealed 4 peaks instead of 2, suggesting that the conformation of heparin might have changed. Therefore, it is unknown if NGF or BDNF would bind to the bioactive surface after being stored at 37°C.

Average neurite length, average maximum neurite length, and migration length of Schwann cells were evaluated when DRG were cultured on bioactive surfaces PCL NH_2^+ scaffold, PCL NH_2^+ + Heparin scaffold, PCL NH_2^+ + Heparin + Immobilised

NGF scaffold, PCL NH_2^+ + Heparin + Immobilised BDNF scaffold and, PCL NH_2^+ + Heparin + Immobilised NGF plus BDNF scaffold. Neurites were grown and developed successfully when cultured on bioactive surfaces with immobilised growth factors. The longest average neurite length was 3041 ± 843 µm when DRG were seeded on PCL NH_2^+ + Heparin + Immobilised NGF 1ng/mL scaffold. Furthermore, longest average maximum neurite length and longest migration length of Schwann cells were 3869 ± 1092 µm and 2718 ± 911 µm for DRG cultured on PCL NH_2^+ + Heparin + Immobilised NGF 1ng/mL scaffold.

PCL NH_2^+ + Heparin + Immobilised BDNF scaffold also encouraged neurite outgrowth and Schwann cell migration, but the response was lower as when DRG were cultured on immobilised NGF scaffolds. Longest average neurite length and longest average maximum neurite lengths were 1536 ± 762 µm and 2817 ± 218 µm when DRG were seeded on PCL NH_2^+ + Heparin + Immobilised BDNF 1 ng/mL scaffold and PCL NH_2^+ + Heparin scaffold with BDNF 1 µg/mL in solution in culture medium, respectively. The longest Schwann cell migration length was 1614 ± 543 µm when DRG were cultured on PCL NH_2^+ + Heparin + Immobilised BDNF 10 ng/mL scaffold.

It was concluded, from Chapter 7 of this thesis, that the co-immobilisation of NGF and BDNF did not result in a cumulative effect. Nevertheless, NGF and BDNF were co-immobilised at 1 ng/mL and 100 ng/mL to see if, by adding this surface to PCL fibres, the outcome could be improved. Longest average neurite length and longest average maximum neurite length were 1816 ± 583 µm and 2861 ± 43 µm respectively, for DRG cultured on PCL Air with NGF plus BDNF at a concentration of 1 µg/mL in solution in culture medium. Furthermore, Schwann cells migrated 1974 ± 708 µm for DRG cultured on PCL Air with NGF plus BDNF at a concentration of 1 µg/mL in solution in culture medium. These results support the conclusion of chapter 7, which stated that the co-immobilisation of NGF with BDNF would not result in an accumulative effect.

A significantly higher response was observed when NGF was immobilised alone on PCL NH_2^+ + Heparin scaffold, but not for BDNF. The co-immobilisation of NGF and

BDNF promoted the growth of neurites longer than those grown with BDNF alone, but shorter than those grown with NGF alone. Moreover, the relatively low concentration of immobilised NGF of 1 ng/mL encouraged the development of the longest neurite among all control and test groups.

Interestingly, neurite response was improved from when the surface was fabricated on flat surfaces in comparison to when the bioactive surface was on PCL fibres. This may indicate that a topographical cue, in this case PCL micro fibres, plus the bioactive surface NH_2^+ + Heparin + Immobilised NGF or BDNF enhanced neurite length.

Research has been conducted to study how scaffolds with aligned structures can improve neurite outgrowth to aid nerve repair. Daud et al. studied how PCL fibre diameter impacted neurite formation and growth [104]. They found that, among 1, 5 and 8 µm diameter PCL fibres, 8 µm fibres encouraged the development of longer neurites in NG108-15 neuronal cells. Moreover, Schwann cells migrated on these 8 µm PCL fibres [104]. Furthermore, when they cultures DRG on 8 µm PCL fibres for 10 days, neurite growth was 1.6 mm and Schwann cell migration was 1.9 mm [104]. Furthermore, Behbehani et al. compared neuronal orientation when cells were cultured on TCP and on aligned PCL fibres (5 µm diameter) [105]. The authors observed that the orientation of NG108-15 neuronal cells changed, growing, and migrating along the PCL fibre. Moreover, when NG108-15 neuronal cells were cultured on TCP, their attachment and growth were random [105]. In addition, Chwalek et al. evaluated neurite outgrowth of DRG on polylactic acid (PLA) fibres (20.5 ± 1.8 µm diameter), and also observed that neurite outgrowth was oriented along the fibres [334].

Fibre diameter, when used to study neurite outgrowth and Schwann cell migration, ranges from micro to nanometres. However, research has reported that fibre diameter below 200 nm and higher than 30 µm inhibit neurite outgrowth and Schwann cell migration [104], [348], [349]. Moreover, features on the fibres such as grooves and porosity, might also affect cell adhesion, morphology, differentiation, orientation and migration [91]. However, fibre porosity is difficult to optimise, and it has been reported that depending on the materials used for fabrication, cell behaviour could

change [91], [350]. In addition, regarding fibre alignment, it was found that a 5° angular difference still oriented neurite outgrowth and Schwann cell migration [164]. These are desirable characteristics to consider when designing a fibrous scaffold for nerve regeneration, as cells behave differently in a 3D scaffold, in comparison to a 2D environment. Additionally, cells distribute in the whole surface area of the 3D scaffold, depositing extracellular matrix proteins and neurotrophic factors [91], [104].

Daud et al. fabricated PCL electrospun scaffold, 8 µm fibre diameter, and seeded DRG on them to evaluate neurite outgrowth and Schwann cell migration. This study showed that Schwann cells migrated 1.9 mm and that neurite outgrowth was 1.6 mm [104]. Additionally, Bozkurt et al. fabricated a parallel-oriented porous scaffold using collagen and evaluated neurite outgrowth from DRG. This study revealed that, after 21 days in culture, maximum and average neurite outgrowth was 1496 µm, and 756 µm respectively [155]. Moreover, Behbehani et al. fabricated PCL fibres and introduced them (6000-7000 PCL fibres) inside a polyethylene glycol conduit. Neurite outgrowth and Schwann cell migration from DRG seeded on this construct was 2.1 mm, and 2.2 mm respectively, after 21 days in culture [105]. Furthermore, Hurtado et al. fabricated random and aligned poly-L-lactic acid (PLLA) fibres and measured neurite length developed by DRG after 5 days in culture. This study showed that random PLLA fibres encouraged neurite growth of ca. 900 µm and 800 µm (maximum and average neurite length respectively), whereas aligned PLLA fibres promoted neurite growth of ca. 1700 µm and 1500 µm (maximum and average neurite length respectively) [336].

Nevertheless, even if different materials can be used as guidance, and the alignment and fibre diameter and density can be controlled, these features alone are not sufficient to induce rapid cell attachment, which is needed for nerve repair [74], [351], [352]. Therefore, it is important to improve these strategies to encourage the growth of longer neurites.

The surface properties of a material have been modified to change how cells interact with the material. Proteins, such as laminin, fibronectin, collagen, and functional groups, such as hydroxyl, carboxyl and amino have been introduced to enhance cell

adhesion and proliferation [91], [239], [334], [341], [346], [353]. Moreover, these proteins and functional groups have been used to bind proteins and other molecules to encourage cell migration, proliferation and differentiation [130], [182], [212], [239], [333].

For example, a study performed by Chwalek et al. fabricated PLA fibres, of 20.5 µm in diameter, and coated them either with laminin, fibronectin, or collagen I. Then, they seeded DRG and cultured them for 2 days with culture medium supplemented with 100 ng/mL of NGF [334]. Neurite outgrowth was ca. 1500 µm, 1000 µm and 800 µm when DRG were seeded on PLA fibres coated with fibronectin, laminin and collagen I respectively [334]. Moreover, Xie et al. produced PCL fibres and coated them with poly-L lysine and laminin. Thereafter, they cultured DRG on the fibres with 30 ng/mL of NGF in culture medium [333]. Their results showed that PCL fibres coated with poly-L-lysine and laminin stimulated neurite growth of ca. 1-1.5 mm [333]. Furthermore, Armstrong et al. demonstrated that Schwann cell proliferation increased when these cells were cultured on poly-3-hydroxubutyrate (PHB) coated with poly-D-lysine [50]. In addition, Lee et al. grafted amine groups and carboxyl groups onto polyethylene sheets and showed that cell adhesion, proliferation and growth was further stimulated when cells were cultured on the amine surface [239]. Rangappa et al. coated PLLA filaments with laminin and reported that oriented neurite outgrowth was stimulated [353].

Plasma deposition technique is usually used to add functional groups onto surfaces of materials to modify surface properties, such as surface energy and wettability [187], [341]. For example, oxygen containing plasmas can be added to the surface to make it hydrophilic. In contrast, fluorine-containing plasmas are added to the surface to make it hydrophobic [187], [341]. This technique has been used to improve cell adhesion, proliferation, and to add functional groups to further modify the surface of a material. For example, Recek et al. modified PCL electrospun scaffolds with oxygen, ammonia, and sulphur dioxide plasma treatments. Moreover, they also modified polyethylene terephthalate (PET) with oxygen plasma treatment. [341], [346]. These studies showed that cell adhesion and proliferation were improved in surfaces plasma treated with oxygen and ammonia [341], [346].

Furthermore, functional groups have been introduced by plasma deposition on the surface of a material to bind growth factors. Thus, allowing the delivery of the growth factor in a sustained manner to encourage a specific cell response. Bhang et al. plasma treated coverslips firstly with oxygen and then allylamine. Then, covalently bound heparin to the allylamine surface. Finally, NGF was bound to heparin [292]. This NGF-heparin-allylamine-oxygen surface encouraged the development of neurites in PC12 neuronal cells [292]. In addition, Guex et al. functionalised PCL fibrous scaffolds via plasma deposition of carbon dioxide, ethene and argon. Then, vascular endothelial growth factor (VEGF) was covalently immobilised onto the activated PCL scaffold [165]. This study showed that proliferation of endothelial cells was improved when VEGF was immobilised on the surface [165]. Moreover, Shen et al. evaluated that adhesion and proliferation of fibroblast was improved by the immobilisation of basic fibroblast growth factor (bFGF) on carbon dioxide plasma treated poly(lactide-co-glycolide) (PLGA) films [354]. Moreover, Charbonneau et al. functionalised PET with plasma deposition of anhydrous ammonia [355]. Then, chondroitin sulphate was covalently bonded to the amine groups. Thereafter, endothelial growth factor (EGF) was covalently bonded to chondroitin sulphate [355]. Smooth muscle cells were seeded on the functionalised PET scaffold and results showed increased growth of muscle cells as well as apoptosis resistance [355].

The studies described above suggested that surfaces can be modified to obtain a specific cell response, such as adhesion, proliferation, and differentiation. Moreover, the results from Chapters 5, 6 and 7 of this thesis also supported that by modifying a surface, neurite outgrowth can be stimulated and enhanced. Therefore, allylamine plasma deposition was performed to fabricate the bioactive surface NH_2^+ + Heparin + Immobilised NGF/ BDNF/ NGF plus BDNF on PCL electrospun scaffolds, in order to translate this technology for future applications into medical devices to aid nerve repair.

Allylamine monomer was used during plasma deposition to add amine functional groups onto PCL fibres. As amine functional groups, NH_2^+, have a positive charge [212], heparin, a negatively charged molecule, will be bound to amine by electrostatic interactions [212]. This passive binding is advantageous because covalent binding

may modify the functionality of the bonded molecule [182]. Therefore, heparin would not lose its functionality because it will be bound to amine by electrostatic interactions [182]. The successful addition of NH_2^+ and heparin was confirmed with XPS analysis.

A storage study was performed to see if NH_2^+ and heparin would still be present on the surface when this bioactive surface was exposed to 4°C, 21°C and 37°C for 24 hours, 1 month and 3 months. Contact angle revealed that wettability of the NH_2^+ + Heparin changed when stored at 4°C. Moreover, XPS analysis revealed that heparin was present on the surface after it was stored at 4°C, 21°C and 37°C for 3 months. Nevertheless, S 2p scans showed two additional peaks of sulphur when NH_2^+ + Heparin was incubated at 37°C for 3 months. Interestingly, these additional peaks were found at lower binding energies (164 eV and 165 eV), suggesting that heparin was not oxidised. Moreover, this analysis may indicate that the conformation of heparin changed, or that some contaminant populated the bioactive surface. Regardless, this information may suggest that heparin will not bind NGF or BDNF when the surface was stored for 3 months at 37°C. Furthermore, when the NH_2^+ + Heparin surfaces were stored at 4°C and 21°C, the S 2p scans revealed the two characteristic peaks of sulphur, suggesting that heparin was present on the surface with no conformational changes. This may indicate the heparin on this surface could bind NGF and BNDF. Nevertheless, further tests need to be performed to evaluate the biological response of the bioactive surfaces after being stored at 4°C and 21°C.

Even though there are multiple applications that use plasma deposition, only a few studies have attempted to characterise the changes in surface chemical composition after months of storage. For example, Gengenbach studied how surfaces modified with nitrogen containing plasmas were modified by being stored at room temperature within 4 months [356]–[358]. Gengenbach and his colleagues showed that oxygen content increased, by direct contact with air or moisture, and nitrogen content decreased [356]–[358]. This may explain the results obtained from XPS analysis, where nitrogen content decreased in all samples. However, oxygen content remained similar. Further tests need to be done to understand how storage temperatures and time affect the performance (neurotrophin release, average neurite length, Schwann cell migration) of the bioactive surface fabricated in this thesis.

ELISA was performed to confirm the presence of NGF and BDNF on the fabricated NH_2^+ + Heparin scaffold. Moreover, ELISA was also performed to assess the release of NGF and BDNF from the bioactive surface within 21 days. This was important to evaluate as the bioactive surface was fabricated completely in the laboratory and changes on the release of NGF and BDNF were expected. The results from ELISA revealed the presence of NGF and BDNF in the surface. Moreover, it showed that a sustained delivery of both neurotrophins, with no burst released, was achieved. Furthermore, the quantity released from NH_2^+ + Heparin scaffold of NGF and BDNF was different (see Chapter 5, Section 5.5), which is supported by the findings by Robinson et al. who bound osteoprotogerin and tissue inhibitor of metalloproteinases 3 to heparin, and their release was different from each other [212].

The NH_2^+ + Heparin scaffold stabilised and delivered NGF and BDNF for 21 days. When NGF and BDNF were bound to NH_2^+ scaffold, NGF and BDNF release was seen within 7 days and 48 hours respectively. After that, no growth factor release was observed. This could be due to a very low quantity of growth factors bound to the surface by weak interactions, and the degradation of NGF and BDNF because they were not stabilised [281]. These findings are supported by Kim et al. who found that microspheres loaded with heparin bound significantly more bFGF and NGF than microspheres without heparin [320]. Moreover, Johnson et al. also incorporated heparin into hydrogels to stabilise both NGF and BDNF [359]. This suggests that NH_2^+ + Heparin bioactive scaffold is an appropriate delivery system for the release of NGF and BDNF for 21 days, as it can bind higher quantities of growth factor and stabilise them.

The release of growth factors, or other molecules, will depend on how these were incorporated into a delivery system. Moreover, their release will impact the intended biological response. For example, Shen et al. plasma treated PLGA films with carbon dioxide and immobilised 500 ng/mL of bFGF on the surface [354]. Binding efficiency was 66.3%, which meant that of the original 500 ng/mL bFGF amount, 331.5 ng/mL were bound to the surface [354]. The PLGA-bFGF film showed a sustained release of bFGF for 7 days, after a slight burst release [354]. Furthermore, Liu et al. encapsulated NGF in poly(D, L-lactic acid) (PDLLA) nanofibers, and glial-cell derived

neurotrophic factor (GDNF) in PLGA nanofibers by emulsion electrospinning [162]. Encapsulation efficiency was 80.7 ± 1.6% and 86.6 ± 1.0% for GDNF and NGF, respectively (5 µg initial load). Moreover, the release at day 1 was 12.4% and 20.3% for NGF and GDNF, respectively. The release, after 42 days, increased to 26.5% and 62.5% for NGF and GDNF respectively [162]. PLGA degrades faster than PDLLA, therefore, this would explain why GDNF was released faster than NGF [162]. PC12 neuronal cells were cultured with these scaffolds, and neurite length, at day 7, was 59.4 µm and 67.2 µm for NGF-PDLLA scaffolds and GDNF-PLGA scaffolds, respectively [162]. The authors explained that, even though bioactivity of released NGF and GNDF from the scaffolds was maintained, this bioactivity was lower when compared to when NGF and GNDF were added in culture medium, as neurite length was higher in these control groups (68.2 µm and 76 µm, respectively) [162].

Additionally, Madduri et al. crosslinked collagen NGCs by dehydro-thermal treatment. Then, loaded GDNF (80 ng) or GDNF and NGF (40 ng and 40 ng). Afterwards, they coated the NGCs with PLGA [75]. This study revealed that, within 30 days, GDNF and GDNF and NGF were released at 68% and 56% respectively. Furthermore, the control group, which consisted of non-cross-linked collagen, released 78% and 83% of GDNF and GNDF and NGF, respectively [75]. Also, Whitehead et al. electrospun methacrylated hyaluronic acid with PLGA microspheres, which contained NGF (0 to 100 µg/mL) [79]. NGF was incorporated into the PLGA microspheres by a water-oil-water emulsion technique, which consisted of adding NGF to a solution of BSA in PBS and polyvinyl alcohol (PVA). Afterwards, this solution was introduced in a PLGA solution in DCM. Then, the emulsion was added to a PVA solution [79]. For electrospinning of aligned fibres, 30 mg of PLGA microspheres were added per mL of methacrylated hyaluronic acid solution [79]. ELISA revealed that 85% of the initial load of NGF was found in the PLGA microspheres. Furthermore, ELISA test showed that by day 5, 40% to 80% of NGF was released from the microspheres, and, by day 10, 80% to 100% of NGF was released from the microspheres [79].

Moreover, Chang fabricated a porous PCL conduit, to which gelatin was injected and then genipin (0, 0.1, 0.5, 1.0, and 1.5% w/w), after which the conduit was left for 7

days to crosslink [154]. After, the conduit was freeze-dried for 24 hours and then, it was submerged in a solution of 5 µg/mL of NGF for 24 hours [154]. ELISA showed an initial burst release of NGF, nevertheless, after 10 days, the release of NGF was decreased. For the conduits where genipin was injected at 0.1% w/w, a sustained release of between 2 ng/mL and 4 ng/mL was observed from day 10 to day 60. This conduit also exhibited the highest activity in PC12 neuronal cells [154]. Other groups with different genipin concentrations, showed low NGF release, close to zero [154]. Chang explained that this behaviour might be due to the degradation of the treated conduits and quantity of used genipin, highlighting that the conduit that was injected with genipin 1.0% w/w, bound more NGF as its release was not observed after 10 days [154]. This conclusion is misleading, as it suggested that because there was no release of NGF, the delivery system was accomplishing its purpose. However, the PCL conduit where genipin was injected at 0.1% w/w encouraged a higher metabolic activity of PC12 neuronal cells. Moreover, this same conduit stimulated the growth of larger neurites in a rat sciatic model [154]. Therefore, the results suggest that the PCL conduit with genipin 0.1% achieved a better outcome in comparison to other test PCL conduits.

Hsieh et al. immobilised NGF (5 µg/mL) inside of a poly(DL-lactic acid-co-glycolic acid) conduit by genipin (GP) and 1-ethyl-3-(3-dimethylamino-propyl) carbodiimide (EDC) / N-hydroxysuccinimide (NHS)/ 2-morpholinoethane sulfonicacid (MES) system [230]. ELISA revealed an initial burst release during the first 5 days; then, from day 6 to 10, the burst release decreased, until a sustained release was observed from day 10 to 40 [230]. Moreover, Fujimaki et al. immobilised 2.5 µg/mL, 5 µg/mL and 10 µg/mL of bFGF in oriented collagen tubes [360]. ELISA showed that 48.8%, 49.6% and 36.8% of the original load was adsorbed onto the collagen tubes when 2.5 µg/mL, 5 µg/mL and 10 µg/mL were immobilised respectively [360]. These results demonstrated that adding more growth factor to a delivery system may not always increase the amount of immobilised growth factor in the system. Furthermore, Horne et al. immobilised BDNF on PCL nanofibers to enhance proliferation and differentiation of cortical neural stem cells [338]. PCL nanofibers were aminolysed in ethylenediamine. Then, PCL nanofibers were incubated in succinimidyl 4-(N-

maleimidomethyl)-cyclohexane-1-carboxylate (SMCC). Then, the PCL nanofibers were incubated with 10 µg/mL of BDNF for 10 hours at 4°C [338]. ELISA showed that BDNF was bound to the PCL nanofibers [338]. Nevertheless, the amount of BDNF bound to the nanofibers was not quantified and a release study of BDNF from PCL nanofibers was not performed.

Currently, there is not a defined standard release profile of growth factors to obtain a desired cellular response. This cellular response should be evaluated for each delivery system. After this, the delivery system and its response are assessed as a whole to determine if it can be translated to the clinic. For nerve repair, there are two desirable outcomes: encouraging neurite growth and Schwann cell migration. Schwann cells create an environment to stimulate neurite growth and formation. Moreover, neurotrophic factors are produced, by neurite outgrowth and Schwann cell stimulation, to aid both neurite outgrowth and Schwann cell migration [88], [104], [133], [158], [314], [317], [361]. Hence, both neurite outgrowth and Schwann cell migration were assessed herein.

As NGF and BDNF are known to encourage neurite outgrowth in DRG [264], both growth factors were immobilised, alone and in combination, on the bioactive surface NH_2^+ + heparin described in this thesis. This bioactive surface was added to PCL electrospun scaffolds, as the fibres would direct neurite growth and Schwann cell migration. The results in this thesis showed that PCL + NH_2^+ + Heparin + Immobilised NGF 1 ng/mL encouraged the longest average neurite length and furthest Schwan cell migration (3041 ± 843 µm and 2718 ± 911 µm respectively). PCL + NH_2^+ + Heparin + Immobilised BDNF 1 ng/mL also stimulated neurite outgrowth and Schwann cell migration (1536 ± 762 µm, 1571 ± 828 µm respectively), but not as long as the ones encouraged by immobilised NGF. Interestingly, PCL + NH_2^+ + Heparin + Immobilised NGF plus BDNF did not promote comparable neurite outgrowth (1107 ± 456 µm) and Schwann cell migration (1169 ± 538 µm) when compared to immobilised NGF 1 ng/mL and immobilised BDNF 1 ng/mL.

Research has been performed to stimulate neurite outgrowth and Schwann cell migration that could compete with the regeneration capabilities of an autograft. For

example, Deister and Schmidt cultured DRG with NGF, GDNF and ciliary neurotrophic factor (CNTF) at concentrations of 50 ng/mL, 10 ng/mL and 10 ng/mL, respectively, developing an average neurite length of 2031 ± 97 μm [285]. Kim et al. cultured DRG on electrospun poly(acrylonitrile-co-methyl acrylate) fibers for 1 week. NGF at 50 ng/mL was dissolved in culture medium, which was changed every two days [337]. This study showed that neurite outgrowth was ca. 2 mm and Schwann cell migration was ca. 3 mm [337].

The use of growth factors to stimulate Schwann cell migration is controversial, as some studies showed that certain neurotrophins encourage Schwann cell migration whereas others show the opposite response. Maniwa et al. studied the effects of NGF, BDNF and neurotrophin-3 (NT-3) on Schwann cell migration [316]. This study showed that NGF and NT-3 did promote Schwann cell migration, whereas BDNF did not stimulate Schwann cell migration [316]. Cornejo et al, showed that NGF induced Schwann cell motility [328], whereas Anton et al. demonstrated the NGF stimulated Schwann cell migration [329]. Yamauchi et al. studied that NT-3 and BDNF encouraged and inhibited Schwann cell migration, respectively [313], [318]. Nevertheless, Yi et al. inhibited the expression of microRNA-1 to encourage BDNF production, which promoted Schwann cell proliferation and migration [317]. Additionally, Gisbert Roca et al. transfected Schwann cell to increase BDNF production. Then, DRG were co-cultured with transfected Schwann cells on polypyrrole-PLA fibres, showing that neurite length, after 5 days in culture, was ca. 5 mm [362].

These studies demonstrated that neurotrophins were crucial to enhance neurite outgrowth and Schwann cell migration. However, due to the half-life of the growth factors, it is essential to design a system which stabilises and delivers growth factors with the purpose of extending the half-life of growth factors, and hence reducing the amount required, and to maintain a sustained delivery of these during the healing process. Liu et al. fabricated micropatterned channels scaffold with polydimethyl-siloxane (PDMS) [87]. Then, DRG were co-cultured with Schwann cells for 21 days to study neurite outgrowth. Moreover, Liu et al. encapsulated NGF (50 μg/mL) in a collagen gel, which then was incorporated into one of the sides of the PDMS channels.

They also studied neurite outgrowth of DRG when these were cultured for 21 days in the collagen gel-PDMS scaffold [87]. Neurite outgrowth was ca. 2000 - 2500 µm for both DRG seeded with Schwann cells and collagen-loaded NGF [87]. This study showed that both NGF and Schwann cells encouraged the oriented growth of axon bundles, with no significant difference between each other. The results presented in this experimental Chapter, showed a longer neurite outgrowth (3041 µm) using a relatively low concentration of immobilised NGF (1 ng/mL), when DRG were cultured on PCL + NH_2^+ + Heparin + Immobilised NGF 1 ng/mL.

Additionally, Dinis et al. added NGF and/or CNTF (1 µg/mL and 100 ng/mL respectively, in 0.1% BSA) into a 9% silk fibroin in polyethylene oxide to produce electrospun aligned fibres. Then, either primary neurons from DRG, or the whole DRG, were cultured on these scaffolds for 5 days and 12 days, respectively [164]. Neurite length was 192.5 ± 80.3 µm, 78.9 ± 39.5 µm, and 124.4 ± 45.9 µm of primary cells when cultured on NGF, CNTF, and NGF and CNTF silk fibres, respectively [164]. Furthermore, when whole DRG were cultured, for 5 days, on NGF and CNTF silk fibres, neurite outgrowth was of ca. 1000-1500 µm [164]. This study partially supported the findings on this thesis, where the use of two growth factors did not have a cumulative effect in neurite outgrowth. Nevertheless, its effect was better than when one of the growth factors was used, in this case, CNTF alone. However, the results presented in this Chapter showed longer neurite length, in DRG (3041 ± 843 µm), using a relatively lower concentration of immobilised NGF (1 ng/mL).

Whitehead et al. electrospun aligned methacrylated hyaluronic acid with PLGA microspheres, which contained NGF (0 to 100 µg/mL) [79]. NGF was incorporated into the PLGA microspheres by a water-oil-water emulsion technique, which consisted of adding NGF to a solution of BSA in PBS and polyvinyl alcohol (PVA). Afterwards, this solution was introduced in a PLGA solution in DCM. Then, the emulsion was added to a PVA solution [79]. For electrospinning of aligned fibres, 30 mg of PLGA microspheres were added per mL of methacrylated hyaluronic acid solution. Optimisations studies were performed, where 100 µg/mL of encapsulated NGF was further used. Therefore, DRG were seeded on this electrospun scaffold for 5 days [79]. This study revealed that, after 5 days in culture, 40% - 80% of NGF was

released from the microspheres, encouraging neurite outgrowth of ca. 1.5-2 mm [79]. The results presented in this Chapter showed longer neurite length, in DRG (3041 ± 843 µm), using a relatively lower concentration of immobilised NGF (1 ng/mL).

Furthermore, Liu et al. designed a tissue-engineered nerve graft (TENG) with an injectable drug delivery system, which consisted of a chitosan scaffold and a methoxy-poly(ethylene glycol)-b-poly(γ-ethyl-L-glutamate) (mPEG-PELG) hydrogel inside the lumen of the chitosan scaffold, which forms a gel at body temperature [76]. NGF was loaded to the mPEG-PELG hydrogel to a concentration of 1 µg/mL. This NGF-mPEG-PELG hydrogel released 13.87 ng/mL at day 1, and released 1.5 ng/mL of NGF for 28 days [76]. These devices were tested in a rat sciatic nerve model for 14 days. Neurites, neither in the control nor test groups, were able to regenerate across the 10 mm nerve gap. NGF- mPEG-PELG hydrogel scaffold showed neurite outgrowth of 0.72 ± 0.02 mm and intramuscular injection of NGF (2 µg/ kg) showed 0.37 ± 0.02 mm of neurite outgrowth [76].

In contrast, the bioactive surface described in this thesis chapter PCL + NH_2^+ + Heparin + Immobilised NGF 1 ng/mL encouraged 3041 ± 843 µm neurite growth and 2718 ± 911 µm Schwann cell migration from DRG after 7 days in culture. This outcome showed that this bioactive surface used as a delivery system optimised the use of NGF and achieved a greater outcome than the ones reported in current literature. PCL + NH_2^+ + Heparin + Immobilised BDNF also stimulated neurite outgrowth, but its growth was not as long as the neurite outgrowth reached immobilising NGF. Moreover, the results in this chapter showed that PCL + NH_2^+ + Heparin + Immobilised NGF plus BDNF, although it also promoted neurite outgrowth, it might not be the best combination of growth factors to co-immobilise to obtain a significant neurite outgrowth and Schwann cell migration.

NGF and BDNF immobilised alone are promising approaches to encourage neurite growth and Schwann cell migration after injury. The reason why DRG were stimulated significantly by immobilised NGF more than BDNF might be related to the number of high affinity receptors present in the DRG [316], [363]. It is known that in an adult

DRG, 40% to 50% of the receptors are tyrosine kinase receptor (Trk) A, 5% - 30% are TrkB, and 10% - 20% are TrkC [363]. As NGF binds to TrkA and BDNF binds to TrkB, the possibility to stimulate a response with NGF was higher. Moreover, NGF and BDNF also bind to the low affinity receptor $p75^{NTR}$, therefore, NGF and BDNF would be also competing for this receptor, suggesting that an equilibrium of interactions between TrkA and $p75^{NTR}$ or TrkB and $p75^{NTR}$ [363] should be achieved to maximise neurite length and Schwann cell migration. Furthermore, as mentioned before, sensory neurons (DRG) express more TrkA receptors, whereas motor neurons express more TrkB receptors [86], [133]. Hence, PCL + NH_2^+ + Heparin + Immobilised BDNF should be tested with motor neurons or with a model that combines both sensory neurons and motor neurons to study if this bioactive study is able to encourage neurite outgrowth and Schwann cell migration.

In comparison to the results obtained from Chapter 7, adding the bioactive surface NH_2^+ + Heparin + Immobilised NGF/BDNF onto PCL electrospun scaffolds significantly stimulated neurite outgrowth and Schwann cell migration. This might be due to the combination of two elements: 1) topographical cues (PCL electrospun scaffold) as these encourage enhanced neurite outgrowth [337]; and 2) chemical cues (bioactive surface) as it is known that by adjusting the surface properties of the scaffold, cell behaviour, such as adhesion, proliferation and migration, is enhanced [86], [314]. Therefore, combining PCL electrospun scaffold with the bioactive surface NH_2^+ + Heparin + Immobilised NGF/BDNF could create a permissive environment, which would mimic up to a certain extent the ECM, to further improve neurite growth and guidance, as well as Schwann cell migration to aid nerve repair.

8.6 Conclusion

The bioactive surfaces NH_2^+ + Heparin + Immobilised NGF, NH_2^+ + Heparin + Immobilised BDNF and NH_2^+ + Heparin + Immobilised NGF plus BDNF were successfully added onto PCL electrospun scaffolds. XPS analysis confirmed that NH_2^+ and heparin were added to the scaffolds. Moreover, ELISA revealed that NGF and BDNF were immobilised on the surface and that a sustained release of both NGF and BDNF was maintained for 21 days. This was a major step, as the bioactive surfaces were successfully added onto PCL electrospun scaffold, representing a step closer to translating this technology into an NGC for future clinical use.

Furthermore, PCL + NH_2^+ + Heparin + Immobilised NGF scaffolds and PCL + NH_2^+ + Heparin + Immobilised BDNF enhanced neurite outgrowth and Schwann cell migration. However, PCL + NH_2^+ + Heparin + Immobilised NGF plus BDNF showed insufficient neurite outgrowth and Schwann cell migration.

Most importantly, PCL + NH_2^+ + Heparin + Immobilised NGF at 1 ng/mL encouraged the average neurite outgrowth 3041 ± 843 µm, average maximum neurite length 3869 ± 1092 µm, and Schwann cell migration length 2718 ± 911 µm. These outcomes were the highest achieved among control and test groups and, to the best of this author's knowledge, these outcomes have the highest neurite length to NGF ratio found in the literature.

This suggests that by immobilising a relatively low concentration of NGF, 1 ng/mL, onto the bioactive surface NH_2^+ + Heparin on PCL electrospun scaffolds, the growth of longer neurites and the further migration of Schwann cells can be achieved. Therefore, these scaffolds PCL + NH_2^+ + Heparin + Immobilised NGF at 1 ng/mL are a promising approach to improve current NGC to aid nerve repair.

Chapter 9 General discussion

This thesis reported on the fabrication and characterisation of the novel bioactive surfaces NH_2^+ + Heparin + Immobilised NGF, NH_2^+ + Heparin + Immobilised BDNF, and NH_2^+ + Heparin + Immobilised NGF plus BDNF. The biological effects of the surfaces were studied *in vitro* (PC12 adh neuronal cells and NG108-15 neuronal cells), and *ex vivo* (embryonic chick DRG) in terms of neurite outgrowth and Schwann cell migration. The bioactive surfaces were successfully fabricated on commercially available amine-96 well plates (Chapter 5, Chapter 6 and Chapter 7) and on PCL electrospun fibres (Chapter 8). It was found that these bioactive surfaces encouraged neurite outgrowth and Schwann cell migration by the sustained delivery of NGF and BDNF. Furthermore, the bioactive surfaces may have stabilised the growth factors, prolonging their half-lives.

The use of growth factors, specifically neurotrophins, to promote neurite outgrowth has been studied and tested before as a promising approach to enhance nerve regeneration. It has been highlighted that extending the half-life of the neurotrophins, maintaining their bioactivity, and their local and sustained delivery are important strategies to follow to improve neurite outgrowth, Schwann cell migration and, hence, nerve regeneration [163]. Nevertheless, it is unknown what is the optimal quantity to use of neurotrophins, as this would mainly depend on the characteristic of the delivery system.

Covalent binding techniques have been used to incorporate neurotrophins to delivery systems. Nevertheless, the high amount of neurotrophin to use, and their interactions with solvents, makes this approach undesirable as it hinders the bioactivity of the molecule. High quantities of neurotrophins, ranging from 10 mg to 100 ng, have been used with covalent-based delivery systems [61], [227], [258]. Nevertheless, only between 5% and 80% of the initial load was retained in the delivery system [227], [258], because different fabrication methods can modify the structure and decrease the function of the neurotrophin [162], [258]. Furthermore, using high amounts of neurotrophins would increase the cost of the device, and it can cause undesirable

effects, such as excessive branching and neuroma formation [76], [163]. Therefore, fabrication of a delivery system using electrostatic interactions is fundamental.

Strong binding of neurotrophins is possible by electrostatic interactions, as the optimization of repulsive and attractive forces leads to a sustained binding and delivery of neurotrophins [166]. This was demonstrated when NGF and BDNF were immobilised to NH_2^+ + Heparin surfaces and NH_2^+ surfaces. ELISA showed that NGF and BDNF were released from NH_2^+ + Heparin for 21 days, in a sustained manner. In contrast, without heparin, NGF and BDNF were released from the NH_2^+ surfaces within 24 hours and 48 hours. After those time points, no neurotrophins release was observed. These results suggested that firstly, electrostatic forces from NH_2^+ surfaces bound small quantities of the original load of neurotrophins, and released them within 48 hours, whereas NH_2^+ + Heparin surfaces bound a high quantity of the original load of NGF or BDNF, which were then released for 21 days. Therefore, NH_2^+ + Heparin surfaces are a promising bioactive surface to which immobilise NGF and BDNF for their further support during nerve repair.

Most of the research has tested growth factors delivery on neuronal cell lines and reported if there was any effect on neuronal differentiation. After that, the delivery system was directly tested in a rat sciatic nerve injury model. For *in vitro* studies, neurite length is rarely reported, while number of neurites or percentage of neurons bearing neurites are reported. It is difficult to understand why neurite length would not be an important parameter, as the aim of nerve repair, amongst other parameters, is to bridge a long injury gap. Then, it is of no surprise when current research failed to bridge long gaps in *in vivo* studies. Hence, the work in this thesis focuses primarily on measuring neurite length to assess the potential of the bioactive surface to bridge nerve gaps.

Bioactive surfaces NH_2^+ + Heparin + Immobilised NGF, NH_2^+ + Heparin + Immobilised BDNF, NH_2^+ + Heparin + Immobilised NGF plus BDNF were firstly tested using NG108-15 neuronal cells and PC12 adh neuronal cells. Even though neurite outgrowth assessment of NG108-15 neuronal cell did not reveal any significant result, neurite outgrowth evaluation of PC12 adh neuronal cells showed that by using

relatively low concentrations of immobilised NGF, immobilised BDNF, and immobilised NGF plus BDNF, the growth of long neurites was stimulated. Previous research showed that using higher quantities of growth factors does not necessarily mean that the outcome would be longer neurites [64], [229]. Therefore, bioactive surfaces NH_2^+ + Heparin + Immobilised NGF, NH_2^+ + Heparin + Immobilised BDNF, NH_2^+ + Heparin + Immobilised NGF plus BDNF were promising approaches to keep testing.

Bioactive surfaces were then tested using DRG, a more relevant biological model. Neurite outgrowth and Schwann cell migration were evaluated. Schwann cells were isolated from chick embryo DRG. Then, Schwann cells were seeded on the bioactive surfaces, showing no significant differences among the test and control groups. DRG were cultured on the bioactive surfaces for 7 days. Neurite outgrowth assessment revealed that NH_2^+ + heparin + immobilised NGF 1 ng/mL encouraged the growth of the longest neurite (1075 µm) in comparison to other test and control groups. Although NH_2^+ + Heparin + Immobilised BDNF 1 ng/mL stimulated the growth of the longest neurite within its growth factor group, this surface did not promote neurite length similar to the ones developed by NH_2^+ + Heparin + Immobilised NGF 1 ng/mL. Furthermore, NH_2^+ + Heparin + Immobilised NGF plus BDNF did not show an accumulative neurite outgrowth. Nevertheless, neurite outgrowth was longer than immobilised BDNF but shorter than immobilised NGF. Other research has found that using other strategies to deliver neurotrophins also encouraged the growth of long neurites [61], [129], [130], [291], however, they were not as long as the ones promoted by NH_2^+ + Heparin + Immobilised NGF 1 ng/mL within 7 days. This analysis gave confidence to scale up this bioactive surface onto PCL electrospun fibres.

PCL electrospun fibres have shown to support guided neurite outgrowth and Schwann cell migration as they function as a topographical cue [105]. PCL is a biodegradable polyester, with good biocompatibility which has been used for numerous medical applications [108], [214]. Moreover, PCL nanofibers are commercially available for biomedical applications [108]. Therefore, PCL electrospun scaffolds were an ideal candidate to scale up the bioactive surface.

To scale up the bioactive surface, plasma deposition was the technique chosen to add NH_2^+ onto the PCL electrospun scaffolds. Plasma deposition is a solvent free, waste free and fast reaction technique that functionalises a surface without altering the bulk properties of the material [187]. Allylamine plasma deposition was performed to add NH_2^+ on the PCL electrospun scaffolds. Then, heparin was bound by electrostatic interactions to NH_2^+. After, NGF, BDNF and a combination of NGF plus BDNF were immobilised to the surface. Interestingly, pore width/ratio changed significantly after allylamine plasma deposition. Hence, it was hypothesised that surface roughness and the chemical cue (NH_2^+ and heparin) on the PCL fibres would change cell adherence. Crystal violet assay confirmed that significantly more cells adhered to PCL + NH_2^+ and PCL + NH_2^+ + Heparin in comparison to PCL. Therefore, a question was risen, whether the combination in roughness and chemical modification would elicit a different biological response regarding neurite outgrowth and Schwann cell migration.

Additionally, the bioactive surface NH_2^+ + Heparin was stored for 3 months at 4°C, 21°C and 37°C. XPS analysis revealed that heparin was still present at the surface after 3 months, which suggested that this bioactive surface might have a shelf life for future applications. To the best of this author's knowledge there is no research regarding the shelf life of a delivery system and how it may impact its biological effects. It would be interesting to further explore this approach.

Neurite outgrowth and Schwann cell migration were evaluated when DRG were cultured on PCL + NH_2^+ + Heparin + Immobilised NGF, PCL + NH_2^+ + Heparin + Immobilised BDNF and PCL + NH_2^+ + Heparin + Immobilised NGF plus BDNF scaffolds. This study showed that PCL + NH_2^+ + Heparin + Immobilised NGF 1 ng/mL encouraged the growth of the largest neurites (3041 µm) and longest Schwann cell migration (2718 µm). Moreover, PCL + NH_2^+ + Heparin + Immobilised BDNF 1 ng/mL stimulated neurite outgrowth of 1536 µm. Even though this value was not as high as the one from immobilised NGF 1 ng/mL, it was still an improvement because NH_2^+ + Heparin + Immobilised BDNF 1 ng/mL on TCP promoted neurite outgrowth of 310 µm. Therefore, the bioactive surface with immobilised BDNF is a promising candidate for further testing and characterisation using other neuronal cells, such as motor neurons. In addition, PCL + NH_2^+ + Heparin + Immobilised NGF plus BDNF

did not encourage sufficient neurite outgrowth. The reason for this might be that the combination of NGF with BDNF is not adequate, or that the concentrations used need to be different from each other, for example NGF 1 ng/mL and BDNF 10 ng/mL. However, it might be interesting to test this bioactive surface (with immobilised BDNF or immobilised NGF plus BDNF) using motor neurons due to the presence of more TrkB receptors on motor neurons as opposed to DRG sensory neurons. Moreover, a co-culture of sensory and motor neurons will be interesting to use to evaluate the effects of NGF and BDNF delivered simultaneously. Furthermore, these results also suggest that pore width/ratio changes might not have affected neurite outgrowth.

There is a clear advantage when using the delivery system reported in this thesis when analysing the relationship between the amount of NGF loaded and neurite outgrowth. For the PCL + NH_2^+ + Heparin + Immobilised NGF 1 ng/mL scaffold, neurite outgrowth was longer than results reported by other research groups [76], [79], [87], [275]. Hence, by immobilising relatively low concentrations of NGF on the bioactive surface, and by adding this bioactive surface onto PCL electrospun scaffolds, longer neurite outgrowth was achieved.

Therefore, PCL + NH_2^+ + Heparin + Immobilised NGF 1 ng/mL scaffold and PCL + NH_2^+ + Heparin + Immobilised BDNF scaffold are promising approaches to improve the performance of current NGCs to assist nerve repair.

Chapter 10 Conclusion and future work

This thesis aimed to develop a scalable bioactive surface that encouraged neurite outgrowth using NH_2^+, heparin and NGF, BDNF or a combination of NGF plus BDNF; and to identify the optimal concentration of NGF, BDNF or NGF plus BDNF to use to maximise neurite outgrowth. To accomplish these aims, four objectives were defined: (i) to fabricate and characterise the bioactive surface on tissue culture plastic; (ii) to evaluate the effects of the bioactive surface on neurite outgrowth of NG108-15 neuronal cell and PC12 adh neuronal cells; (iii) to evaluate the effects of the bioactive surface on TCP on DRG outgrowth; and (iv) to fabricate and characterise the bioactive surface on PCL electrospun fibres; and to evaluate the effect of the bioactive surface on PCL on DRG outgrowth.

The bioactive surface was firstly fabricated onto commercially available amine (NH_2^+)-coated TCP 96 well plates, where heparin was bound to NH_2^+, then, NGF, BDNF or NGF plus BDNF were immobilised to heparin by electrostatic interactions. XPS analysis and ELISA confirmed the successful fabrication of the bioactive surface, as they detected the presence of heparin, and NGF and BDNF respectively, on the surface. Afterward, NG108-15 neuronal cells and PC12 adh neuronal cells were seeded on the bioactive surfaces. Metabolic assay showed that the surfaces were not cytotoxic to the cells. Moreover, the potential of the bioactive surfaces to encourage neurite outgrowth was confirmed, as PC12 adh neuronal cells developed longer neurites when relatively low concentrations of growth factors were immobilised.

The bioactive surfaces were then evaluated using DRG, as they are more biologically relevant model. Results from this experiment showed that DRG developed long neurites at relatively low concentrations of immobilised NGF or BDNF, suggesting that the use of bioactive surface immobilised with low concentration of NGF or BDNF were suitable candidates to scale up this approach to enhance NGCs.

The bioactive surface was incorporated onto PCL electrospun fibres. Allylamine plasma deposition was the technique used to add NH_2^+ to the surface of the PCL electrospun fibres. Heparin was then bound to NH_2^+ by electrostatic interactions. Furthermore, NGF, BDNF and NGF plus BDNF were immobilised on the surface by binding to heparin. XPS analysis and ELISA confirmed the successful fabrication of the bioactive surface on the PCL electrospun fibres. Furthermore, ELISA revealed the sustained delivery of NGF and BDNF for 21 days from the bioactive surface on the PCL fibres. In addition, XPS analysis confirmed the presence of heparin on the bioactive surface after being stored for 3 months at 4°C and 21°C, suggesting that the bioactive surface has a storage life, which is encouraging for the translation of this bioactive surface to an NGC.

Most importantly, DRG were cultured on the bioactive surface on PCL electrospun fibres. Neurite outgrowth and Schwann cell evaluation revealed that the bioactive surface PCL + NH_2^+ + Heparin + Immobilised NGF 1 ng/mL stimulated the growth of longest neurites, as well as the longest Schwann cell migration length. Moreover, even if bioactive surfaces with immobilised BDNF did not encourage the growth of the longest neurites in this thesis, they are a promising approach to test with motor neurons. Nevertheless, the bioactive surfaces with immobilised NGF plus BDNF need to be investigated further, as these bioactive surfaces did not promote any significant neurite outgrowth.

Future work could explore the use of the bioactive surface NH_2^+ + Heparin + Immobilised NGF 1 ng/mL on PCL electrospun fibres, where these fibres would go inside the lumen of the NGC. This device could be tested on a rat sciatic nerve model and neurite formation, neurite length and myelination could be evaluated at the proximal, middle and distal stump. Furthermore, NH_2^+ + Heparin + Immobilised BDNF on PCL electrospun fibres could be assessed using primary motor neurons, to observe if BDNF promotes significant neurite outgrowth. Also, a mixed model of motor and sensory neurons could be used to better assess the effects of immobilised NGF plus BDNF when delivered simultaneously. Moreover, the addition of other growth factors, such as GDNF and VEGF in combination with NGF, could be studied to assess further neurite outgrowth and angiogenesis. Additionally, the bioactive

surface could be stored for 3 months at 4°C and 21°C, and then, evaluate any significant differences in neurite outgrowth from DRG compared to when the bioactive surface was not stored.

Overall, the work presented in this thesis showed that bioactive surfaces, especially PCL+ NH_2^+ + Heparin + Immobilised NGF 1 ng/mL, encouraged neurite outgrowth on DRG using a relatively low concentration of neurotrophin, making this approach directly applicable and scalable for enhancing the performance of current NGCs.

References

[1] A. Seddighi, A. Nikouei, A. S. Seddighi, A. R. Zali, and S. M. Tabatabaei, "Peripheral Nerve Injury: a Review Article," *Int. Clin. Neurosci. J.*, vol. 3, no. 1, pp. 1–6, 2016, doi: 10.22037/icnj.v3i1.12016.

[2] O. S. Manoukian *et al.*, "Functional polymeric nerve guidance conduits and drug delivery strategies for peripheral nerve repair and regeneration," *J. Control. Release*, vol. 317, pp. 78–95, 2020, doi: 10.1016/j.jconrel.2019.11.021.

[3] I. Allodi, E. Udina, and X. Navarro, "Specificity of peripheral nerve regeneration: Interactions at the axon level," *Prog. Neurobiol.*, vol. 98, no. 1, pp. 16–37, 2012, doi: 10.1016/j.pneurobio.2012.05.005.

[4] G. Wu, X. Li, M. Li, and Z. Zhang, "Long non-coding RNA MALAT1 promotes the proliferation and migration of Schwann cells by elevating BDNF through sponging miR-129-5p," *Exp. Cell Res.*, vol. 390, no. 1, p. 111937, 2020, doi: 10.1016/j.yexcr.2020.111937.

[5] A. Höke *et al.*, "Schwann cells express motor and sensory phenotypes that regulate axon regeneration.," *J. Neurosci.*, vol. 26, no. 38, pp. 9646–9655, 2006.

[6] M. G. Burnett and E. L. Zager, "Pathophysiology of peripheral nerve injury: a brief review," *Neurosurg. Focus*, vol. 16, no. 5, pp. 1–7, 2004.

[7] K. S. Saladin, "The Nervous System I: Nervous Tissue," in *Human Anatomy*, New York: McGraw-Hill, 2014, pp. 349-368.

[8] K. Bhatheja and J. Field, "Schwann cells: Origins and role in axonal maintenance and regeneration," *Int. J. Biochem. Cell Biol.*, vol. 38, no. 12, pp. 1995–1999, 2006, doi: 10.1016/j.biocel.2006.05.007.

[9] A. F. Rosenberg, M. A. Wolman, C. Franzini-Armstrong, and M. Granato, "In Vivo nerve–macrophage interactions following peripheral nerve injury," *J. Neurosci.*, vol. 32, no. 11, pp. 3898–3909, 2012.

[10] C. M. A. P. Schuh, A. M. Sandoval-Castellanos, C. De Gregorio, P. Contreras-Kallens, and J. W. Haycock, “The Role of Schwann Cells in Peripheral Nerve Function, Injury, and Repair,” in *Cell Engineering and Regeneration*, R. H. Gimble J., Marolt Presen D., Oreffo R., Wolbank S., Ed. Switzerland: Springer, Cham, 2020, pp. 215–236.

[11] W. M. Campana, “Schwann cells: Activated peripheral glia and their role in neuropathic pain,” *Brain, Behavior, and Immunity*, vol. 21, no. 5. pp. 522–527, 2007, doi: 10.1016/j.bbi.2006.12.008.

[12] S. Heermann and M. H. Schwab, “Molecular control of Schwann cell migration along peripheral axons: Keep moving!,” *Cell Adhes. Migr.*, vol. 7, no. 1, pp. 18–22, 2013, doi: 10.4161/cam.22123.

[13] K. R. Jessen and R. Mirsky, “The origin and development of glial cells in peripheral nerves,” *Nat. Rev. Neurosci.*, vol. 6, no. 9, pp. 671–682, 2005.

[14] C. J. Pateman *et al.*, “Nerve guides manufactured from photocurable polymers to aid peripheral nerve repair,” *Biomaterials*, vol. 49, pp. 77–89, 2015, doi: 10.1016/j.biomaterials.2015.01.055.

[15] G. Stoll, S. Jander, and R. R. Myers, “Degeneration and regeneration of the peripheral nervous system: From Augustus Waller’s observations to neuroinflammation,” *J. Peripher. Nerv. Syst.*, vol. 7, no. 1, pp. 13–27, 2002, doi: 10.1046/j.1529-8027.2002.02002.x.

[16] M. Caillaud, L. Richard, J. M. Vallat, A. Desmoulière, and F. Billet, “Peripheral nerve regeneration and intraneural revascularization,” *Neural Regen. Res.*, vol. 14, no. 1, pp. 24–33, 2019, doi: 10.4103/1673-5374.243699.

[17] S. K. Lee and S. W. Wolfe, “Peripheral nerve injury and repair,” *JAAOS-Journal Am. Acad. Orthop. Surg.*, vol. 8, no. 4, pp. 243–252, 2000.

[18] G. Lundborg and L. B. Dahlin, “The pathophysiology of nerve compression,” *Hand Clin.*, vol. 8, no. 2, pp. 215–227, 1992.

[19] S. E. Mackinnon, “Pathophysiology of nerve compression,” *Hand Clin.*, vol.

18, no. 2, pp. 231–241, 2002.

[20] J. A. Machado *et al.*, “Stretch-induced nerve injury: a proposed technique for the study of nerve regeneration and evaluation of the influence of gabapentin on this model,” *Brazilian J. Med. Biol. Res.*, vol. 46, pp. 929–935, 2013.

[21] R. M. G. Menorca, T. S. Fussell, and J. C. Elfar, “Peripheral nerve trauma: Mechanisms of injury and recovery.,” *Hand Clin.*, vol. 29, no. 3, pp. 317–330, 2013, doi: 10.1016/j.hcl.2013.04.002.

[22] A. George, C. Kleinschnitz, M. Zelenka, J. Brinkhoff, G. Stoll, and C. Sommer, “Wallerian degeneration after crush or chronic constriction injury of rodent sciatic nerve is associated with a depletion of endoneurial interleukin-10 protein,” *Exp. Neurol.*, vol. 188, no. 1, pp. 187–191, 2004.

[23] J. Haftek, “Stretch injury of peripheral nerve: acute effects of stretching on rabbit nerve,” *J. Bone Joint Surg. Br.*, vol. 52, no. 2, pp. 354–365, 1970.

[24] M. K. Kwan, E. J. Wall, J. Massie, and S. R. Garfin, “Strain, stress and stretch of peripheral nerve rabbit experiments in vitro and in vivo,” *Acta Orthop. Scand.*, vol. 63, no. 3, pp. 267–272, 1992.

[25] P. J. Driscoll, M. A. Glasby, and G. M. Lawson, “An in vivo study of peripheral nerves in continuity: biomechanical and physiological responses to elongation,” *J. Orthop. Res.*, vol. 20, no. 2, pp. 370–375, 2002.

[26] M. J. Teixeira *et al.*, “Neuropathic pain after brachial plexus avulsion-central and peripheral mechanisms,” *BMC Neurol.*, vol. 15, no. 1, pp. 1–9, 2015.

[27] W. S. Jellish and M. Oftadeh, “Peripheral nerve injury in cardiac surgery,” *J. Cardiothorac. Vasc. Anesth.*, vol. 32, no. 1, pp. 495–511, 2018.

[28] B. Radić, P. Radić, and D. Duraković, “Peripheral nerve injury in sports,” *Acta Clin. Croat.*, vol. 57, no. 3., pp. 561–569, 2018.

[29] G. Karahan, H. Kaya, R. S. Eyceyurt, M. A. Erdogan, G. Yigitturk, and O. Erbas, “Dexpanthenol reduces fibrosis and aids repair following nerve laceration and neurorrhaphy,” *Exp. Ther. Med.*, vol. 21, no. 3, p. 1, 2021.

[30] J. R. Costales, M. Socolovsky, J. A. S. Lázaro, and R. Á. García, “Peripheral nerve injuries in the pediatric population: a review of the literature. Part I: traumatic nerve injuries,” *Child’s Nerv. Syst.*, vol. 35, no. 1, pp. 29–35, 2019.

[31] B. Sydney Sunderland, “A Classification Of Peripheral Nerve Injuries Producing Loss Of Function,” *Brain*, vol. 74, no. 4, pp. 491–516, 1951.

[32] A. Beris, I. Gkiatas, I. Gelalis, D. Papadopoulos, and I. Kostas-Agnantis, “Current concepts in peripheral nerve surgery,” *Eur. J. Orthop. Surg. Traumatol.*, vol. 29, no. 2, pp. 263–269, 2019.

[33] N. Kamble, D. Shukla, and D. Bhat, “Peripheral nerve injuries: electrophysiology for the neurosurgeon,” *Neurol. India*, vol. 67, no. 6, p. 1419, 2019.

[34] M. Nadi and R. Midha, “Management of Peripheral Nerve Injuries,” in *Principles of Neurological Surgery*, Fourth Edi., Elsevier Inc., 2018, pp. 832–841.

[35] C. Ide, “Peripheral nerve regeneration,” *Neurosci. Res.*, vol. 25, pp. 101–121, 1996.

[36] L. Conforti, J. Gilley, and M. P. Coleman, “Wallerian degeneration: an emerging axon death pathway linking injury and disease,” *Nat. Rev. Neurosci.*, vol. 15, no. 6, pp. 394–409, 2014.

[37] M. C. Subang and P. M. Richardson, “Influence of injury and cytokines on synthesis of monocyte chemoattractant protein-1 mRNA in peripheral nervous tissue,” *Eur. J. Neurosci.*, vol. 13, no. 3, pp. 521–528, 2001.

[38] A. D. Gaudet, P. G. Popovich, and M. S. Ramer, “Wallerian degeneration: gaining perspective on inflammatory events after peripheral nerve injury,” *J. Neuroinflammation*, vol. 8, no. 1, pp. 1–13, 2011.

[39] W. M. Renno, L. Benov, and K. M. Khan, “Possible role of antioxidative capacity of (-)-epigallocatechin-3-gallate treatment in morphological and neurobehavioral recovery after sciatic nerve crush injury,” *J. Neurosurg. Spine*,

vol. 27, no. 5, pp. 593–613, 2017, doi: 10.3171/2016.10.SPINE16218.

[40] M. Kim *et al.*, “Heme oxygenase 1 in Schwann cells regulates peripheral nerve degeneration against oxidative stress,” *ASN Neuro*, vol. 11, p. 1759091419838949, 2019.

[41] A. S. Dubuisson, C. M. Lapiere, and B. V Nusgens, “Development of a reconstituted nerve in a three-dimensional collagen gel under tension populated with fibroblasts and Schwann cells,” *Restor. Neurol. Neurosci.*, vol. 14, no. 4, pp. 275–284, 1999.

[42] R. J. Reynolds, G. J. Little, M. Lin, and J. W. Heath, “Imaging myelinated nerve fibres by confocal fluorescence microscopy: individual fibres in whole nerve trunks traced through multiple consecutive internodes,” *J. Neurocytol.*, vol. 23, no. 9, pp. 555–564, 1994.

[43] M. Röyttä and C. S. Raine, “Taxol-induced neuropathy: chronic effects of local injection,” *J. Neurocytol.*, vol. 15, no. 4, pp. 483–496, 1986.

[44] N. Mokarram, A. Merchant, V. Mukhatyar, G. Patel, and R. V Bellamkonda, “Effect of modulating macrophage phenotype on peripheral nerve repair,” *Biomaterials*, vol. 33, no. 34, pp. 8793–8801, 2012.

[45] H. W. Müller and P. Minwegen, “Nonresident macrophages in peripheral nerve of rat: effect of silica on migration, myelin phagocytosis, and apolipoprotein E expression during Wallerian degeneration,” *J. Neurosci. Res.*, vol. 18, no. 1, pp. 222–229, 1987.

[46] D. R. Kaplan and F. D. Miller, “Signal transduction by the neutrophin receptors,” *Curr. Opin. Cell Biol.*, vol. 9, no. 2, pp. 213–221, 1997.

[47] D. T. Hess, S. I. Patterson, D. S. Smith, and J. H. P. Skene, “Neuronal growth cone collapse and inhibition of protein fatty acylation by nitric oxide,” *Nature*, vol. 366, no. 6455, pp. 562–565, 1993.

[48] R. P. Bunge, “The role of the Schwann cell in trophic support and regeneration,” *J. Neurol.*, vol. 242, no. 1, pp. S19–S21, 1994.

[49] S. B. Bailey, M. E. Eichler, A. Villadiego, and K. M. Rich, “The influence of fibronectin and laminin during Schwann cell migration and peripheral nerve regeneration through silicon chambers,” *J. Neurocytol.*, vol. 22, no. 3, pp. 176–184, 1993, doi: 10.1007/BF01246356.

[50] S. J. Armstrong, M. Wiberg, G. Terenghi, and P. J. Kingham, “ECM Molecules Mediate Both Schwann Cell Proliferation and Activation to Enhance Neurite Outgrowth,” *Tissue Eng.*, vol. 13, no. 12, pp. 2863–2870, 2007, doi: 10.1089/ten.2007.0055.

[51] M. Lindsay, “Nerve Growth Factors (NGF , BDNF) Enhance Axonal Regeneration but Are not Required for Survival of Adult Sensory Neurons,” *J. Neurosci.*, vol. 8, no. 7, pp. 2394–2405, 1988.

[52] R. Hellweg, G. Raivich, H.-D. Hartung, C. Hock, and G. W. Kreutzberg, “Axonal transport of endogenous nerve growth factor (NGF) and NGF receptor in experimental diabetic neuropathy,” *Exp. Neurol.*, vol. 130, no. 1, pp. 24–30, 1994.

[53] C. R. Jimenez *et al.*, “Proteomics of the injured rat sciatic nerve reveals protein expression dynamics during regeneration,” *Mol. Cell. Proteomics*, vol. 4, no. 2, pp. 120–132, 2005.

[54] J. M. Vallat, M. J. Leboutet, A. Loubet, J. Hugon, and J. J. Moreau, “Effects of glycerol injection into rat sciatic nerve,” *Muscle Nerve Off. J. Am. Assoc. Electrodiagn. Med.*, vol. 11, no. 6, pp. 540–545, 1988.

[55] X. Jiang, S. H. Lim, H. Q. Mao Hai-Quan, and S. Y. Chew, “Current applications and future perspectives of artificial nerve conduits,” *Exp. Neurol.*, vol. 223, no. 1, pp. 86–101, 2010, doi: 10.1016/j.expneurol.2009.09.009.

[56] X. Gu, F. Ding, Y. Yang, and J. Liu, “Construction of tissue engineered nerve grafts and their application in peripheral nerve regeneration,” *Prog. Neurobiol.*, vol. 93, no. 2, pp. 204–230, 2011, doi: 10.1016/j.pneurobio.2010.11.002.

[57] V. Chiono and C. Tonda-Turo, “Trends in the design of nerve guidance

channels in peripheral nerve tissue engineering," *Prog. Neurobiol.*, vol. 131, pp. 87–104, 2015, doi: 10.1016/j.pneurobio.2015.06.001.

[58] S. Catrina, B. Gander, and S. Madduri, "Nerve conduit scaffolds for discrete delivery of two neurotrophic factors," *Eur. J. Pharm. Biopharm.*, vol. 85, no. 1, pp. 139–142, 2013, doi: 10.1016/j.ejpb.2013.03.030.

[59] C. E. Schmidt and J. B. Leach, "NEURAL TISSUE ENGINEERING: Strategies for Repair and Regeneration," *Annu. Rev. Biomed. Eng*, vol. 5, pp. 293–347, 2003, doi: 10.1146/annurev.bioeng.5.011303.120731.

[60] S. Hall, "The response to injury in the peripheral nervous system," *J Bone Jt. Surg [Br]*, vol. 8787, no. 10, pp. 1309–19, 2005, doi: 10.1302/0301-620X.87B10.

[61] E. G. Fine, I. Decosterd, M. Papaloïzos, A. D. Zurn, and P. Aebischer, "GDNF and NGF released by synthetic guidance channels support sciatic nerve regeneration across a long gap," *Eur. J. Neurosci.*, vol. 15, pp. 589–601, 2002, doi: 10.1046/j.1460-9568.2002.01892.x.

[62] J. M. Rovak, P. S. Cederna, V. Macionis, M. S. Urbanchek, J. H. Van Der Meulen, and W. M. Kuzon, "Termino-lateral neurorrhaphy: The functional axonal anatomy," *Microsurg. Off. J. Int. Microsurg. Soc. Eur. Fed. Soc. Microsurg.*, vol. 20, no. 1, pp. 6–14, 2000, doi: 10.1002/(SICI)1098-2752(2000)20:1<6::AID-MICR2>3.0.CO;2-5.

[63] W. Daly, L. Yao, D. Zeugolis, A. Windebank, and A. Pandit, "A biomaterials approach to peripheral nerve regeneration: bridging the peripheral nerve gap and enhancing functional recovery," *J. R. Soc. Interface*, vol. 9, no. 67, pp. 202–221, 2012, doi: 10.1098/rsif.2011.0438.

[64] J. Hu, L. Tian, M. P. Prabhakaran, X. Ding, and S. Ramakrishna, "Fabrication of nerve growth factor encapsulated aligned poly(ε-caprolactone) nanofibers and their assessment as a potential neural tissue engineering scaffold," *Polymers (Basel).*, vol. 8, no. 54, pp. 1–17, 2016, doi: 10.3390/polym8020054.

[65] C. Chen, X. Kong, and I.-S. Lee, “Modification of surface/neuron interfaces for neural cell-type specific responses: a review,” *Biomed. Mater.*, vol. 11, no. 1, p. 014108, 2015, doi: 10.1088/1748-6041/11/1/014108.

[66] L. M. Marquardt and S. E. Sakiyama-Elbert, “Engineering peripheral nerve repair,” *Curr. Opin. Biotechnol.*, vol. 24, no. 5, pp. 887–892, 2013, doi: 10.1016/j.copbio.2013.05.006.

[67] S. H. Hsu *et al.*, “New nerve regeneration strategy combining laminin-coated chitosan conduits and stem cell therapy,” *Acta Biomater.*, vol. 9, no. 5, pp. 6606–6615, 2013, doi: 10.1016/j.actbio.2013.01.025.

[68] Q. Hogan, D. Sapunar, K. Modric-Jednacak, and J. B. McCallum, “Detection of neuropathic pain in a rat model of peripheral nerve injury,” *J. Am. Soc. Anesthesiol.*, vol. 101, no. 2, pp. 476–487, 2004.

[69] E. O. Johnson, A. B. Zoubos, and P. N. Soucacos, “Regeneration and repair of peripheral nerves,” *Inj. Int. J. Care Inj.*, vol. 365, no. 4, pp. S24–S29, 2005, doi: 10.1016/j.injury.2005.10.012.

[70] J. H. A. Bell and J. W. Haycock, “Next Generation Nerve Guides: Materials, Fabrication, Growth Factors, and Cell Delivery,” *Tissue Eng. Part B Rev.*, vol. 18, no. 2, pp. 116–128, 2012, doi: 10.1089/ten.teb.2011.0498.

[71] I. H. Whitworth, R. A. Brown, C. J. Dore, P. Anand, C. J. Green, and G. Terenghi, “Nerve Growth Factor Enhances Nerve Regeneration Through Fibronectin Grafts,” *J. Hand Surg. Am.*, vol. 4, pp. 2–514, 1996.

[72] M. Behbehani, A. Glen, C. S. Taylor, A. Schuhmacher, F. Claeyssens, and J. W. Haycock, “Pre-clinical evaluation of advanced nerve guide conduits using a novel 3D in vitro testing model,” *Int. J. Bioprinting*, vol. 4, no. 1, 2018.

[73] L. A. Pfister, E. Alther, M. Papaloïzos, H. P. Merkle, and B. Gander, “Controlled nerve growth factor release from multi-ply alginate/chitosan-based nerve conduits,” *Eur. J. Pharm. Biopharm.*, vol. 69, no. 2, pp. 563–572, 2008, doi: 10.1016/j.ejpb.2008.01.014.

[74] S. Kehoe, X. F. Zhang, and D. Boyd, “FDA approved guidance conduits and wraps for peripheral nerve injury : A review of materials and efficacy,” *Injury*, vol. 43, no. 5, pp. 553–572, 2012, doi: 10.1016/j.injury.2010.12.030.

[75] S. Madduri, K. Feldman, T. Tervoort, M. Papaloïzos, and B. Gander, “Collagen nerve conduits releasing the neurotrophic factors GDNF and NGF,” *J. Control. Release*, vol. 143, no. 2, pp. 168–174, 2010, doi: 10.1016/j.jconrel.2009.12.017.

[76] Y. Liu, S. Yu, X. Gu, and R. Cao, “Tissue-engineered nerve grafts using a scaffold-independent and injectable drug delivery system : a novel design with translational advantages,” *J. Neural Eng.*, vol. 16, no. 3, p. 036030, 2019, doi: 10.1088/1741-2552/ab17a0.

[77] E. J. Calabrese, “Enhancing and regulating neurite outgrowth,” *Critical Reviews in Toxicology*, vol. 38, no. 4. pp. 391–418, 2008, doi: 10.1080/10408440801981981.

[78] M. D. Sarker, S. Naghieh, A. D. Mcinnes, D. J. Schreyer, and X. Chen, “Regeneration of peripheral nerves by nerve guidance conduits : Influence of design , biopolymers , cells , growth factors , and physical stimuli,” *Prog. Neurobiol.*, vol. 171, pp. 125–150, 2018, doi: 10.1016/j.pneurobio.2018.07.002.

[79] T. J. Whitehead, C. O. C. Avila, and H. G. Sundararaghavan, “Combining growth factor releasing microspheres within aligned nanofibers enhances neurite outgrowth,” *J. Biomed. Mater. Res. - Part A*, vol. 106, no. 1, pp. 17–25, 2018, doi: 10.1002/jbm.a.36204.

[80] K. L. Menzies and L. Jones, “The Impact of Contact Angle on the Biocompatibility of Biomaterials,” *Optom. Vis. Sci.*, vol. 87, no. 6, pp. 387–399, 2010.

[81] M. R. Kreke, A. S. Badami, J. B. Brady, R. Michael Akers, and A. S. Goldstein, “Modulation of protein adsorption and cell adhesion by poly(allylamine hydrochloride) heparin films,” *Biomaterials*, vol. 26, no. 16, pp. 2975–2981, 2005, doi: 10.1016/j.biomaterials.2004.08.013.

[82] M. Sondell, G. Ran Lundborg, and M. Kanje, “Vascular Endothelial Growth Factor Has Neurotrophic Activity and Stimulates Axonal Outgrowth, Enhancing Cell Survival and Schwann Cell Proliferation in the Peripheral Nervous System,” *J. Neurosci.*, vol. 19, no. 14, pp. 5731–5740, 1999.

[83] R. Rietze, H. Valcanis, G. F. Brooker, T. Thomas, A. K. Voss, and P. F. Bartlett, “Purification of a pluripotent neural stem cell from the adult mouse brain,” *Nature*, vol. 412, no. 6848, pp. 736–739, 2001.

[84] M. Bierlein De la Rosa, A. D. Sharma, S. K. Mallapragada, and D. S. Sakaguchi, “Transdifferentiation of brain-derived neurotrophic factor (BDNF)-secreting mesenchymal stem cells significantly enhance BDNF secretion and Schwann cell marker proteins,” *J. Biosci. Bioeng.*, vol. 124, no. 5, pp. 572–582, 2017, doi: 10.1016/j.jbiosc.2017.05.014.

[85] B. Hood, H. B. Levene, and A. D. Levi, “Transplantation of autologous Schwann cells for the repair of segmental peripheral nerve defects,” *Neurosurg. Focus*, vol. 26, no. 2, p. E4, 2009, doi: 10.3171/FOC.2009.26.2.E4.

[86] Q. Min, D. B. Parkinson, and X. P. Dun, “Migrating Schwann cells direct axon regeneration within the peripheral nerve bridge,” *Glia*, vol. 69, no. 2, pp. 235–254, 2021, doi: 10.1002/glia.23892.

[87] C. Liu, J. Kray, and C. Chan, “Schwann Cells Enhance Penetration of Regenerated Axons into Three-Dimensional Microchannels,” *Tissue Eng. Regen. Med.*, vol. 15, no. 3, pp. 351–361, 2018, doi: 10.1007/s13770-018-0115-0.

[88] A. Shakhbazau *et al.*, “Early regenerative effects of NGF-transduced Schwann cells in peripheral nerve repair,” *Mol. Cell. Neurosci.*, vol. 50, no. 1, pp. 103–112, 2012, doi: 10.1016/j.mcn.2012.04.004.

[89] S. Liu *et al.*, “Regulated viral BDNF delivery in combination with Schwann cells promotes axonal regeneration through capillary alginate hydrogels after spinal cord injury,” *Acta Biomater.*, vol. 60, pp. 167–180, 2017, doi: 10.1016/j.actbio.2017.07.024.

[90] A. Faroni, S. A. Mobasseri, P. J. Kingham, and A. J. Reid, “Peripheral nerve regeneration: Experimental strategies and future perspectives,” *Adv. Drug Deliv. Rev.*, vol. 82, pp. 160–167, 2015, doi: 10.1016/j.addr.2014.11.010.

[91] P. Roach, D. Eglin, K. Rohde, and C. C. Perry, “Modern biomaterials: A review - Bulk properties and implications of surface modifications,” *Journal of Materials Science: Materials in Medicine*, vol. 18, no. 7. pp. 1263–1277, 2007, doi: 10.1007/s10856-006-0064-3.

[92] D. Hoffman-Kim, J. A. Mitchel, and R. V. Bellamkonda, “Topography, cell response, and nerve regeneration,” *Annu. Rev. Biomed. Eng.*, vol. 12, no. September, pp. 203–231, 2010, doi: 10.1146/annurev-bioeng-070909-105351.

[93] F. Liu *et al.*, “The Influence of the Surface Topographical Cues of Biomaterials on Nerve Cells in Peripheral Nerve Regeneration: A Review,” *Stem Cells Int.*, vol. 2021, 2021.

[94] E. Ueda and P. A. Levkin, “Micropatterning Hydrophobic Liquid on a Porous Polymer Surface for Long-Term Selective Cell-Repellency,” *Adv. Healthc. Mater.*, vol. 2, no. 11, pp. 1425–1429, 2013.

[95] B. Honig and L. Shapiro, “Adhesion protein structure, molecular affinities, and principles of cell-cell recognition,” *Cell*, vol. 181, no. 3, pp. 520–535, 2020.

[96] J. Field, J. W. Haycock, F. M. Boissonade, and F. Claeyssens, “A Tuneable, Photocurable, Poly(Caprolactone)-Based Resin for Tissue Engineering—Synthesis, Characterisation and Use in Stereolithography,” *Molecules*, vol. 26, no. 5, p. 1199, 2021, doi: 10.3390/molecules26051199.

[97] W. Zhu *et al.*, “Rapid continuous 3D printing of customizable peripheral nerve guidance conduits,” *Mater. Today*, vol. 21, no. 9, pp. 951–959, 2018, doi: 10.1016/j.mattod.2018.04.001.

[98] L. Yao *et al.*, “Effect of functionalized micropatterned PLGA on guided neurite growth,” *Acta Biomater.*, vol. 5, no. 2, pp. 580–588, 2009, doi: 10.1016/j.actbio.2008.09.002.

[99] M. Sun, M. McGowan, P. J. Kingham, G. Terenghi, and S. Downes, “Novel thin-walled nerve conduit with microgrooved surface patterns for enhanced peripheral nerve repair,” *J. Mater. Sci. Mater. Med.*, vol. 21, no. 10, pp. 2765–2774, 2010, doi: 10.1007/s10856-010-4120-7.

[100] A. M. Rajnicek, S. Britland, and C. D. McCaig, “Contact guidance of CNS neurites on grooved quartz: Influence of groove dimensions, neuronal age and cell type,” *J. Cell Sci.*, vol. 110, no. 23, pp. 2905–2913, 1997.

[101] R. Deumens *et al.*, “Repairing injured peripheral nerves: Bridging the gap,” *Prog. Neurobiol.*, vol. 92, no. 3, pp. 245–276, 2010, doi: 10.1016/j.pneurobio.2010.10.002.

[102] C. D. L. Johnson, R. D’Amato, Anthony, and R. J. Gilbert, “Electrospun fibers for drug delivery after spinal cord injury and the effects of drug incorporation on fiber properties,” *Cells Tissues Organs*, vol. 202, no. 1–2, pp. 116–135, 2016, doi: 10.1159/000446621.Electrospun.

[103] R. L. Dahlin, F. K. Kasper, and A. G. Mikos, “Polymeric Nanofibers in Tissue Engineering,” *Tissue Eng. Part B Rev.*, vol. 17, no. 5, pp. 349–364, 2011, doi: 10.1089/ten.teb.2011.0238.

[104] M. F. B. Daud, K. C. Pawar, F. Claeyssens, A. J. Ryan, and J. W. Haycock, “An aligned 3D neuronal-glial co-culture model for peripheral nerve studies,” *Biomaterials*, vol. 33, pp. 5901–5913, 2012, doi: 10.1016/j.biomaterials.2012.05.008.

[105] M. Behbehani, A. Glen, C. S. Taylor, A. Schuhmacher, F. Claeyssens, and J. W. Haycock, “Pre-clinical evaluation of advanced nerve guide conduits using a novel 3D in vitro testing model,” *Int. J. Bioprinting*, vol. 4, no. 1, 2018, doi: 10.18063/IJB.v4i1.123.

[106] W. T. Daly *et al.*, “The effect of intraluminal contact mediated guidance signals on axonal mismatch during peripheral nerve repair,” *Biomaterials*, vol. 33, no. 28, pp. 6660–6671, 2012, doi: 10.1016/j.biomaterials.2012.06.002.

[107] H. B. Wang, M. E. Mullins, J. M. Cregg, C. W. McCarthy, and R. J. Gilbert, “Varying the diameter of aligned electrospun fibers alters neurite outgrowth and Schwann cell migration,” *Acta Biomater.*, vol. 6, no. 8, pp. 2970–2978, 2010, doi: 10.1016/j.actbio.2010.02.020.

[108] J. Xue, T. Wu, Y. Dai, and Y. Xia, “Electrospinning and Electrospun Nano fi bers : Methods , Materials , and Applications,” *Chem. Rev.*, vol. 119, no. 8, pp. 5298–5415, 2019, doi: 10.1021/acs.chemrev.8b00593.

[109] N. Tucker, J. J. Stanger, M. P. Staiger, H. Razzaq, and K. Hofman, “The history of the science and technology of electrospinning from 1600 to 1995,” *J. Eng. Fiber. Fabr.*, vol. 7, no. 3, pp. 63–73, 2012, doi: 10.1177/155892501200702s10.

[110] D. H. Reneker and I. Chun, “Nanometre diameter fibres of polymer, produced by electrospinning,” *Nanotechnology*, vol. 7, no. 3, pp. 216–223, 1996, doi: 10.1088/0957-4484/7/3/009.

[111] S. V. Fridrikh, J. H. Yu, M. P. Brenner, and G. C. Rutledge, “Controlling the Fiber Diameter during Electrospinning,” *Phys. Rev. Lett.*, vol. 90, no. 14, p. 4, 2003, doi: 10.1103/PhysRevLett.90.144502.

[112] A. Haider, S. Haider, and I. K. Kang, “A comprehensive review summarizing the effect of electrospinning parameters and potential applications of nanofibers in biomedical and biotechnology,” *Arab. J. Chem.*, vol. 11, no. 8, pp. 1165–1188, 2018, doi: 10.1016/j.arabjc.2015.11.015.

[113] B. Sundaray, V. Subramanian, T. S. Natarajan, R. Z. Xiang, C. C. Chang, and W. S. Fann, “Electrospinning of continuous aligned polymer fibers,” *Appl. Phys. Lett.*, vol. 84, no. 7, pp. 1222–1224, 2004, doi: 10.1063/1.1647685.

[114] Í. Ortega, A. J. Ryan, P. Deshpande, S. MacNeil, and F. Claeyssens, “Combined microfabrication and electrospinning to produce 3-D architectures for corneal repair,” *Acta Biomater.*, vol. 9, no. 3, pp. 5511–5520, 2013, doi: 10.1016/j.actbio.2012.10.039.

[115] X. Hu, S. Liu, G. Zhou, Y. Huang, Z. Xie, and X. Jing, “Electrospinning of polymeric nanofibers for drug delivery applications,” *J. Control. Release*, vol. 185, no. 1, pp. 12–21, 2014, doi: 10.1016/j.jconrel.2014.04.018.

[116] T. J. Sill and H. A. von Recum, “Electrospinning: Applications in drug delivery and tissue engineering,” *Biomaterials*, vol. 29, no. 13, pp. 1989–2006, 2008, doi: 10.1016/j.biomaterials.2008.01.011.

[117] D. Il Cha, K. W. Kim, G. H. Chu, H. Y. Kim, K. H. Lee, and N. Bhattarai, “Mechanical behaviors and characterization of electrospun polysulfone/polyurethane blend nonwovens,” *Macromol. Res.*, vol. 14, no. 3, pp. 331–337, 2006, doi: 10.1007/BF03219090.

[118] S. De Vrieze, T. Van Camp, A. Nelvig, B. Hagström, P. Westbroek, and K. De Clerck, “The effect of temperature and humidity on electrospinning,” *J. Mater. Sci.*, vol. 44, no. 5, pp. 1357–1362, 2009, doi: 10.1007/s10853-008-3010-6.

[119] S. Agarwal, J. H. Wendorff, and A. Greiner, “Use of electrospinning technique for biomedical applications,” *Polymer (Guildf).*, vol. 49, no. 26, pp. 5603–5621, 2008, doi: 10.1016/j.polymer.2008.09.014.

[120] A. L. Yarin, “Coaxial electrospinning and emulsion electrospinning of core-shell fibers,” *Polym. Adv. Technol.*, vol. 22, no. 3, pp. 310–317, 2011, doi: 10.1002/pat.1781.

[121] W. Ji *et al.*, “Fibrous scaffolds loaded with protein prepared by blend or coaxial electrospinning,” *Acta Biomater.*, vol. 6, no. 11, pp. 4199–4207, 2010, doi: 10.1016/j.actbio.2010.05.025.

[122] E. R. Kenawy *et al.*, “Release of tetracycline hydrochloride from electrospun poly(ethylene-co-vinylacetate), poly(lactic acid), and a blend,” *J. Control. Release*, vol. 81, no. 1, pp. 57–64, 2002.

[123] E. Luong-Van, L. Grøndahl, K. N. Chua, K. W. Leong, V. Nurcombe, and S. M. Cool, “Controlled release of heparin from poly(e-caprolactone) electrospun fibers,” *Biomaterials*, vol. 27, no. 9, pp. 2042–2050, 2006, doi:

10.1016/j.biomaterials.2005.10.028.

[124] D. Kai, M. P. Prabhakaran, G. Jin, L. Tian, and S. Ramakrishna, “Potential of VEGF-encapsulated electrospun nano fibers for in vitro cardiomyogenic differentiation of human mesenchymal stem cells,” *J. Tissue Eng. Regen. Med.*, vol. 11, no. 4, pp. 1002–1010, 2017, doi: 10.1002/term.1999.

[125] S. Y. Chew, J. Wen, E. K. F. Yim, and K. W. Leong, “Sustained Release of Proteins from Electrospun Biodegradable Fibers,” *Biomacromolecules*, vol. 6, no. 4, pp. 2017–2024, 2005.

[126] L. Gritsch, L. Liverani, C. Lovell, and A. R. Boccaccini, “Polycaprolactone Electrospun Fiber Mats Prepared Using Benign Solvents : Blending with Copper (II) -Chitosan Increases the Secretion of Vascular Endothelial Growth Factor in a Bone Marrow Stromal Cell Line,” *Macromol. Biosci.*, vol. 20, no. 3, p. p.1900355, 2020, doi: 10.1002/mabi.201900355.

[127] D. I. Zeugolis *et al.*, “Electro-spinning of pure collagen nano-fibres - Just an expensive way to make gelatin ?,” *Biomaterials*, vol. 29, no. 15, pp. 2293–2305, 2008, doi: 10.1016/j.biomaterials.2008.02.009.

[128] L. A. Pfister, M. Papaloïzos, H. P. Merkle, and B. Gander, “Nerve conduits and growth factor delivery in peripheral nerve repair,” *J. Peripher. Nerv. Syst.*, vol. 12, no. 2, pp. 65–82, 2007, doi: 10.1111/j.1529-8027.2007.00125.x.

[129] Y. Yang *et al.*, “Neurotrophin releasing single and multiple lumen nerve conduits,” *J. Control. Release*, vol. 104, no. 3, pp. 433–446, 2005, doi: 10.1016/j.jconrel.2005.02.022.

[130] R. G. Pearson *et al.*, “Spatial Confinement of Neurite Regrowth from Dorsal Root Ganglia within Nonporous Microconduits,” *TISSUE Eng.*, vol. 9, no. 2, pp. 201–208, 2003, [Online]. Available: www.liebertpub.com.

[131] E. J. Huang and L. F. Reichardt, “NEUROTROPHINS: Roles in Neuronal Development and Function,” *Annu. Rev. Neurosci.*, vol. 24, no. 1, pp. 677–736, 2001.

[132] M. E. Önger, B. Delibaş, A. P. Türkmen, E. Erener, B. Z. Altunkaynak, and S. Kaplan, “The role of growth factors in nerve regeneration,” *Drug Discov. Ther.*, vol. 10, no. 6, pp. 285–291, 2016, doi: 10.5582/ddt.2016.01058.

[133] S. P. Frostick, Q. Yin, and G. J. Kemp, “Schwann cells, neurotrophic factors, and peripheral nerve regeneration,” *Microsurg. Off. J. Int. Microsurg. Soc. Eur. Fed. Soc. Microsurg.*, vol. 18, no. 7, pp. 397–405, 1998, doi: 10.1002/(SICI)1098-2752(1998)18:7<397::AID-MICR2>3.0.CO;2-F.

[134] M. V Sofroniew, C. L. Howe, and W. C. Mobley, “Nerve Growth Factor Signaling, Neuroprotection, And Neural Repair,” *Annu. Rev. Neurosci*, vol. 18, no. 24, pp. 1217–281, 2001.

[135] M. L. Rocco, M. Soligo, L. Manni, and L. Aloe, “Nerve Growth Factor: Early Studies and Recent Clinical Trials,” *Curr. Neuropharmacol.*, vol. 16, no. 10, pp. 1455–1465, 2018, doi: 10.2174/1570159x16666180412092859.

[136] P. Artimo *et al.*, “Nuclei Acids res,” *ExPASy: SIB bioinformatics resource portal*, 2012. https://web.expasy.org/protparam/ (accessed May 29, 2020).

[137] C. E. Mcgregor and A. W. English, “The Role of BDNF in Peripheral Nerve Regeneration : Activity-Dependent Treatments and Val66Met,” *Front. Cell. Neurosci.*, vol. 12, p. 522, 2019, doi: 10.3389/fncel.2018.00522.

[138] H. Zhao *et al.*, “Molecular mechanisms of brain-derived neurotrophic factor in neuro-protection: Recent developments,” *Brain Res.*, vol. 1665, pp. 1–21, 2017, doi: 10.1016/j.brainres.2017.03.029.

[139] S. Bathina and U. N. Das, “Brain-derived neurotrophic factor and its clinical Implications,” *Arch. Med. Sci.*, vol. 11, no. 6, pp. 1164–1178, 2015, doi: 10.5114/aoms.2015.56342.

[140] M. Karimi *et al.*, “Rat Sciatic Nerve Reconstruction Across a 30 mm Defect Bridged by an Oriented Porous PHBV Tube With Schwann Cell as Artificial Nerve Graft,” *ASAIO J.*, vol. 60, no. 2, p. 224, 2014.

[141] T. Numakawa, S. Suzuki, E. Kumamaru, N. Adachi, M. Richards, and H.

Kunugi, “BDNF function and intracellular signaling in neurons,” *Histol. Histopathol.*, vol. 25, pp. 237–258, 2010.

[142] L. Aloe, M. L. Rocco, P. Bianchi, and L. Manni, “Nerve growth factor: From the early discoveries to the potential clinical use,” *J. Transl. Med.*, vol. 10, no. 1, pp. 1–15, 2012, doi: 10.1186/1479-5876-10-239.

[143] R. Li, D. Li, H. Zhang, J. Wang, X. Li, and J. Xiao, “Growth factors-based therapeutic strategies and their underlying signaling mechanisms for peripheral nerve regeneration,” *Acta Pharmacol. Sin.*, vol. 41, no. 10, pp. 1289–1300, 2020, doi: 10.1038/s41401-019-0338-1.

[144] M. V. Chao, “Growth factor signaling: Where is the specificity?,” *Cell*, vol. 68, no. 6, pp. 995–997, 1992.

[145] A. Paoletti, F., de Chiara, C., Kelly, G., Covaceuszach, S., Malerba, F., Yan, R., Lamba, D., Cattaneo, A., Pastore, “Conformational Rigidity within Plasticity Promotes Differential Target Recognition of Nerve Growth Factor,” *Front Mol Biosci*, vol. 3, p. 83, 2016.

[146] E. Y. Robinson, R.C., Radziejewski, C., Spraggon, G., Greenwald, J., Kostura, M.R., Burtnick, L.D., Stuart, D.I., Choe, S., Jones, “The structures of the neurotrophin 4 homodimer and the brain-derived neurotrophic factor/neurotrophin 4 heterodimer reveal a common Trk-binding site,” *Protein Sci*, vol. 8, pp. 2589–2597, 1999.

[147] M. C. Manning, D. K. Chou, B. M. Murphy, R. W. Payne, and D. S. Katayama, “Stability of protein pharmaceuticals: An update,” *Pharm. Res.*, vol. 27, no. 4, pp. 544–575, 2010, doi: 10.1007/s11095-009-0045-6.

[148] M. Sondell, G. Lundborg, and M. Kanje, “Vascular endothelial growth factor stimulates Schwann cell invasion and neovascularization of acellular nerve grafts,” *Brain Res.*, vol. 846, no. 2, pp. 219–228, 1999, [Online]. Available: www.elsevier.comrlocaterbres.

[149] S. Madduri and B. Gander, “Growth factor delivery systems and repair

strategies for damaged peripheral nerves," *J. Control. Release*, vol. 161, no. 2, pp. 274–282, 2012, doi: 10.1016/j.jconrel.2011.11.036.

[150] D. H. Kim, S. M. Richardson-Burns, J. L. Hendricks, C. Sequera, and D. C. Martin, "Effect of immobilized nerve growth factor on conductive polymers: Electrical properties and cellular response," *Adv. Funct. Mater.*, vol. 17, no. 1, pp. 79–86, 2007, doi: 10.1002/adfm.200500594.

[151] A. Piotrowicz and M. S. Shoichet, "Nerve guidance channels as drug delivery vehicles," *Biomaterials*, vol. 27, no. 9, pp. 2018–2027, 2006, doi: 10.1016/j.biomaterials.2005.09.042.

[152] D. S. Utley, S. L. Lewin, E. T. Cheng, A. N. Verity, D. Sierra, and D. J. Terris, "Brain-Derived Neurotrophic Factor and Collagen Tubulization Enhance Functional Recovery After Peripheral Nerve Transection and Repair," *Arch. Otolaryngol. Neck Surg.*, vol. 122, no. 4, pp. 407–413, 1996.

[153] P.-R. Chen, M.-H. Chen, F.-H. Lin, and W.-Y. Su, "Release characteristics and bioactivity of gelatin-tricalcium phosphate membranes covalently immobilized with nerve growth factors," *Biomaterials*, vol. 26, no. 33, pp. 6579–6587, 2005, doi: 10.1016/j.biomaterials.2005.03.037.

[154] C. J. Chang, "Effects of nerve growth factor from genipin-crosslinked gelatin in polycaprolactone conduit on peripheral nerve regeneration - In vitro and in vivo," *J. Biomed. Mater. Res. - Part A*, vol. 91, no. 2, pp. 586–596, 2009, doi: 10.1002/jbm.a.32252.

[155] A. Bozkurt *et al.*, "In Vitro Assessment of Axonal Growth Using Dorsal Root Ganglia Explants in a Novel Three-Dimensional Collagen Matrix," *Tissue Eng.*, vol. 13, no. 12, pp. 2971–2979, 2007, doi: 10.1089/ten.2007.0116.

[156] R. Li *et al.*, "Heparin-Poloxamer Thermosensitive Hydrogel Loaded with bFGF and NGF Enhances Peripheral Nerve Regeneration in Diabetic Rats," *Biomaterials*, vol. 168, pp. 24–37, 2018, doi: 10.1016/j.biomaterials.2018.03.044.

[157] S. E. Sakiyama-Elbert and J. A. Hubbell, “Controlled release of nerve growth factor from a heparin-containing fibrin-based cell ingrowth matrix,” *J. Control. Release*, vol. 69, no. 1, pp. 149–158, 2000, doi: 10.1016/S0168-3659(00)00296-0.

[158] D. Santos, F. Gonzalez-Perez, X. Navarro, and J. Del Valle, “Dose-Dependent Differential Effect of Neurotrophic Factors on in Vitro and in Vivo Regeneration of Motor and Sensory Neurons,” *Neural Plast.*, vol. 2016, pp. 1–13, 2016, doi: 10.1155/2016/4969523.

[159] W. Zhang *et al.*, “A sequential delivery system employing the synergism of EPO and NGF promotes sciatic nerve repair,” *Colloids Surfaces B Biointerfaces*, vol. 159, pp. 327–336, 2017, doi: 10.1016/j.colsurfb.2017.07.088.

[160] H. Yu, J. Liu, J. Ma, and L. Xiang, “Local delivery of controlled released nerve growth factor promotes sciatic nerve regeneration after crush injury,” *Neurosci. Lett.*, vol. 566, pp. 177–181, 2014, doi: 10.1016/j.neulet.2014.02.065.

[161] X. Xu, H. Yu, S. Gao, H. Mao, and K. W. Leong, “Polyphosphoester microspheres for sustained release of biologically active nerve growth factor,” *Biomaterials*, vol. 23, no. 17, pp. 3765–3772, 2002.

[162] C. Liu *et al.*, “Incorporation and release of dual growth factors for nerve tissue engineering using nanofibrous bicomponent scaffolds,” *Biomed. Mater.*, vol. 13, no. 4, pp. 1–17, 2018, doi: 10.1088/1748-605X/aab693.

[163] F. Ma *et al.*, “Use of natural neural scaffolds consisting of engineered vascular endothelial growth factor immobilized on ordered collagen fibers filled in a collagen tube for peripheral nerve regeneration in rats,” *Int. J. Mol. Sci.*, vol. 15, no. 10, pp. 18593–18609, 2014, doi: 10.3390/ijms151018593.

[164] T. M. Dinis *et al.*, “Complementary effects of two growth factors in multifunctionalized silk nanofibers for nerve reconstruction,” *PLoS One*, vol. 9, no. 10, p. e109770, 2014, doi: 10.1371/journal.pone.0109770.

[165] A. G. Guex *et al.*, “Covalent immobilisation of VEGF on plasma-coated electrospun scaffolds for tissue engineering applications,” *Colloids Surfaces B Biointerfaces*, vol. 123, pp. 724–733, 2014, doi: 10.1016/j.colsurfb.2014.10.016.

[166] M. C. Z. Meneghetti *et al.*, “Heparan sulfate and heparin interactions with proteins,” *J. R. Soc. Interface*, vol. 12, no. 110, p. 20150589, 2015, doi: 10.1098/rsif.2015.0589.

[167] B. Casu, A. Naggi, and G. Torri, “Re-visiting the structure of heparin,” *Carbohydr. Res.*, vol. 403, pp. 60–68, 2015, doi: 10.1016/j.carres.2014.06.023.

[168] P. K. Smith, A. K. Mallia, and G. T. Hermanson ’, “Calorimetric Method for the Assay of Heparin Content in Immobilized Heparin Preparations,” *Anal. Biochem.*, vol. 109, pp. 466–473, 1980.

[169] D. Yang, S. Moon, and D.-W. Lee, “Surface Modification of Titanium with BMP-2/GDF-5 by a Heparin Linker and Its Efficacy as a Dental Implant,” *Int. J. Mol. Sci.*, vol. 18, no. 1, p. 229, 2017, doi: 10.3390/ijms18010229.

[170] B. Casu, A. Naggi, and G. Torri, “Heparin-derived heparan sulfate mimics to modulate heparan sulfate-protein interaction in inflammation and cancer,” *Matrix Biol.*, vol. 29, no. 6, pp. 442–452, 2010, doi: 10.1016/j.matbio.2010.04.003.

[171] D. H. Atha, A. K. Gaigalas, and V. Reipa, “Structural analysis of heparin by Raman spectroscopy,” *J. Pharm. Sci.*, vol. 85, no. 1, pp. 52–56, 1996, doi: 10.1021/js950216c.

[172] J. M. Goddard and J. H. Hotchkiss, “Polymer surface modification for the attachment of bioactive compounds,” *Prog. Polym. Sci.*, vol. 32, no. 7, pp. 698–725, 2007, doi: 10.1016/j.progpolymsci.2007.04.002.

[173] B. Mulloy, “The specificity of interactions between proteins and sulfated polysaccharides,” *An. Acad. Bras. Cienc.*, vol. 77, no. 4, pp. 651–664, 2005, doi: 10.1590/S0001-37652005000400007.

[174] K. N. Pandiyaraj, V. Selvarajan, Y. H. Rhee, H. W. Kim, and S. I. Shah, “Glow discharge plasma-induced immobilization of heparin and insulin on polyethylene terephthalate film surfaces enhances anti-thrombogenic properties,” *Mater. Sci. Eng. C*, vol. 29, no. 3, pp. 796–805, 2009, doi: 10.1016/j.msec.2008.07.013.

[175] P. Chiodelli, A. Bugatti, C. Urbinati, and M. Rusnati, “Heparin/heparan sulfate proteoglycans glycomic interactome in angiogenesis: Biological implications and therapeutical use,” *Molecules*, vol. 20, no. 4, pp. 6342–6388, 2015, doi: 10.3390/molecules20046342.

[176] B. M. Loo and M. Salmivirta, “Heparin/heparan sulfate domains in binding and signaling of fibroblast growth factor 8b,” *J. Biol. Chem.*, vol. 277, no. 6, pp. 32616–32623, 2002, doi: 10.1074/jbc.M204961200.

[177] M. D. Wood *et al.*, “Affinity-based release of glial-derived neurotrophic factor from fibrin matrices enhances sciatic nerve regeneration q,” *Acta Biomater.*, vol. 5, no. 4, pp. 959–968, 2009, doi: 10.1016/j.actbio.2008.11.008.

[178] M. D. Wood *et al.*, “Fibrin Matrices With Affinity-Based Delivery Systems and Neurotrophic Factors Promote Functional Nerve Regeneration,” *Biotechnol. Bioeng.*, vol. 106, no. 6, pp. 970–979, 2010, doi: 10.1002/bit.22766.

[179] S. E. Sakiyama-Elbert, “Incorporation of heparin into biomaterials,” *Acta Biomater.*, vol. 10, no. 4, pp. 1581–1587, 2014, doi: 10.1016/j.actbio.2013.08.045.

[180] A. Zhu, M. Zhang, J. Wu, and J. Shen, “Covalent immobilization of chitosan/heparin complex with a photosensitive hetero-bifunctional crosslinking reagent on PLA surface,” *Biomaterials*, vol. 23, pp. 4657–4665, 2002, doi: 10.1016/S0142-9612(02)00215-6.

[181] D. Liao, X. Wang, P. H. Lin, Q. Yao, and C. Chen, “Covalent linkage of heparin provides a stable anti-coagulation surface of decellularized porcine arteries,” *J. Cell. Mol. Med.*, vol. 13, no. 8B, pp. 2736–2743, 2009, doi: 10.1111/j.1582-4934.2008.00589.x.

[182] D. E. Robinson *et al.*, “Surface gradient of functional heparin,” *Adv. Mater.*, vol. 20, no. 6, pp. 1166–1169, 2008, doi: 10.1002/adma.200702586.

[183] M. Fazley Elahi, G. Guan, L. Wang, and M. W. King, “Improved Hemocompatibility of Silk Fibroin Fabric Using Layer- by-Layer Polyelectrolyte Deposition and Heparin Immobilization,” *J. Appl. Polym. Sci*, vol. 131, no. 18, pp. 1–12, 2014, doi: 10.1002/app.40772.

[184] P. T. Hammond, “Building biomedical materials layer-by-layer,” *Mater. Today*, vol. 15, no. 5, pp. 196–206, 2012, doi: 10.1016/S1369-7021(12)70090-1.

[185] J. H. Park, B. S. Kim, Y. C. Yoo, M. S. Khil, and H. Y. Kim, “Enhanced Mechanical Properties of Multilayer Nano-Coated Electrospun Nylon 6 Fibers via a Layer-by-Layer Self-Assembly,” *J. Appl. Polym. Sci.*, vol. 107, no. 4, pp. 2211–2216, 2008, doi: 10.1002/app.27322.

[186] D. Bodas and C. Khan-malek, “Hydrophilization and hydrophobic recovery of PDMS by oxygen plasma and chemical treatment — An SEM investigation,” *Sensors and actuators B:Chemical*, vol. 123, no. 1, pp. 368–373, 2007, doi: 10.1016/j.snb.2006.08.037.

[187] C. M. Chan, T. M. Ko, and H. Hiraoka, “Polymer surface modification by plasmas and photons,” *Surf. Sci. Rep.*, vol. 24, no. 1–2, pp. 1–54, 1996, doi: 10.1016/0167-5729(96)80003-3.

[188] S. Zhang *et al.*, “Selection of micro-fabrication techniques on stainless steel sheet for skin friction,” *Friction*, vol. 4, no. 2, pp. 89–104, 2016, doi: 10.1007/s40544-016-0115-9.

[189] C. Borcia, G. Borcia, and N. Dumitrascu, “Surface treatment of polymers by plasma and uv radiation,” *Journ. Phys.*, vol. 56, no. 11, pp. 224–232, 2011.

[190] S. K. Nemani *et al.*, “Surface Modification of Polymers : Methods and Applications,” *Adv. Mater. Interfaces*, vol. 5, no. 1801247, pp. 1–26, 2018, doi: 10.1002/admi.201801247.

[191] E. Yousif and R. Haddad, “Photodegradation and photostabilization of polymers , especially polystyrene : review,” *Springerplus*, vol. 2, no. 398, pp. 1–32, 2013.

[192] M. Mrksich and G. M. Whitesides, “Using self-assembled monolayers to understand the interactions of man- made surfaces with proteins and cells,” *Annu. Re. Biophys. Biomol. Struct.*, vol. 25, pp. 55–78, 1996.

[193] A. Jedaa *et al.*, “The impact of self-assembled monolayer thickness in hybrid gate dielectrics for organic thin-film transistors,” *Org. Electron.*, vol. 10, no. 8, pp. 1442–1447, 2009, doi: 10.1016/j.orgel.2009.08.006.

[194] A. Ulman, “Formation and Structure of Self-Assembled Monolayers,” *Chem. Rev.*, vol. 96, pp. 1533–1554, 1996.

[195] M. Thomas and K. L. Mittal, “Fundamental Aspects,” in *Atmospheric pressure plasma treatment of polymers : relevance to adhesion*, New Jersey: Scrivener Publishing : Wiley, 2013, pp. 22–30.

[196] P. K. Chu, J. Y. Chen, L. P. Wang, and N. Huang, “Plasma-surface modification of biomaterials,” *Mater. Sci. Eng. R*, vol. 36, no. 5–6, pp. 143–206, 2002.

[197] F. A. V Andre and J. Amouroux, “Plasma polymerization and surface treatment of polymers,” *Pure Appl. Chem*, vol. 64, no. 5, pp. 715–723, 1992.

[198] C. M. Lee, S. W. Yang, S. C. Jung, and B. H. Kim, “Oxygen plasma treatment on 3D-printed chitosan/gelatin/hydroxyapatite scaffolds for bone tissue engineering,” *J. Nanosci. Nanotechnol.*, vol. 17, no. 4, pp. 2747–2750, 2017.

[199] A. Nandakumar *et al.*, “Surface modification of electrospun fibre meshes by oxygen plasma for bone,” *Biofabrication*, vol. 5, no. 1, pp. 1–14, 2012, doi: 10.1088/1758-5082/5/1/015006.

[200] J. L. Holloway, A. M. Lowman, M. R. Vanlandingham, and G. R. Palmese, “Chemical grafting for improved interfacial shear strength in UHMWPE / PVA-hydrogel fiber-based composites used as soft fibrous tissue replacements,” *Compos. Sci. Technol.*, vol. 85, pp. 118–125, 2013, doi:

10.1016/j.compscitech.2013.06.007.

[201] J. M. Ino, P. Chevallier, D. Letourneur, D. Mantovani, and C. Le Visage, “Plasma functionalization of poly(vinyl alcohol) hydrogel for cell adhesion enhancement,” *Biomatter*, vol. 3, no. 4, pp. 1–7, 2013.

[202] X. Liu, Q. Feng, A. Bachhuka, and K. Vasilev, “Surface Modification by Allylamine Plasma Polymerization Promotes Osteogenic Differentiation of Human Adipose-Derived Stem Cells,” *ACS Appl. Mater. interfaces,* vol. 6, no. 12, pp. 9733-9741., 2014.

[203] A. M. Sandoval-Castellanos, F. Claeyssens, and J. W. Haycock, “Biomimetic surface delivery of NGF and BDNF to enhance neurite outgrowth,” *Biotechnol. Bioeng.*, vol. 117, no. 10, pp. 3124–3135, 2020, doi: 10.1002/bit.27466.

[204] X. Zhu, K. S. Chian, M. B. E. Chan-park, and S. T. Lee, “Effect of argon-plasma treatment on proliferation of human-skin – derived fibroblast on chitosan membrane in vitro,” *J. Biomed. Mater. Res. Part A An Off. J. Soc. Biomater. Japanese Soc. Biomater. Aust. Soc. Biomater. Korean Soc. Biomater.*, vol. 73, no. 3, pp. 264–274, 2005, doi: 10.1002/jbm.a.30211.

[205] H. Sook, Y. Hwan, C. Seok, J. Park, and D. Kyun, “Enhanced chondrogenic responses of articular chondrocytes onto porous silk fi broin scaffolds treated with microwave-induced argon plasma,” *Surf. Coat. Technol.*, vol. 202, pp. 5794–5797, 2008, doi: 10.1016/j.surfcoat.2008.06.154.

[206] D. Szmigiel *et al.*, “Fluorine-Based Plasma Treatment of Biocompatible Silicone Elastomer : The Effect of Temperature on Etch Rate and Surface Properties,” *Plasma Process. Polym.*, vol. 5, no. 3, pp. 246–255, 2008, doi: 10.1002/ppap.200700130.

[207] J. R. Piascik, S. D. Wolter, B. R. Stoner, O. Dentistry, N. Carolina, and C. Hill, “Development of a novel surface modification for improved bonding to zirconia,” *Dent. Mater.*, vol. 27, no. 5, pp. e99–e105, 2011, doi: 10.1016/j.dental.2011.01.005.

[208] N. Eswaramoorthy and D. R. McKenzie, “Plasma treatments of dressings for wound healing: a review,” *Biophys. Rev.*, vol. 9, no. 6, pp. 895–917, 2017, doi: 10.1007/s12551-017-0327-x.

[209] Q. Cheng, K. Komvopoulos, and S. Li, “Plasma-assisted heparin conjugation on electrospun poly(L-lactide) fibrous scaffolds,” *J. Biomed. Mater. Res. - Part A*, vol. 102, no. 5, pp. 1408–1414, 2014, doi: 10.1002/jbm.a.34802.

[210] Z. Yang *et al.*, “The covalent immobilization of heparin to pulsed-plasma polymeric allylamine films on 316L stainless steel and the resulting effects on hemocompatibility,” *Biomaterials*, vol. 31, no. 8, pp. 2072–2083, 2010, doi: 10.1016/j.biomaterials.2009.11.091.

[211] D. J. Mahoney *et al.*, “A method for the non-covalent immobilization of heparin to surfaces,” *Anal. Biochem.*, vol. 330, no. 1, pp. 123–129, 2004, doi: 10.1016/j.ab.2004.03.055.

[212] D. E. Robinson, D. J. Buttle, R. D. Short, S. L. McArthur, D. A. Steele, and J. D. Whittle, “Glycosaminoglycan (GAG) binding surfaces for characterizing GAG-protein interactions,” *Biomaterials*, vol. 33, no. 4, pp. 1007–1016, 2012, doi: 10.1016/j.biomaterials.2011.10.042.

[213] D. E. Robinson *et al.*, “Plasma Polymer and Biomolecule Modification of 3D Scaffolds for Tissue Engineering,” *Plasma Process. Polym.*, vol. 13, no. 7, pp. 678–689, 2016, doi: 10.1002/ppap.201500162.

[214] B. Azimi, P. Nourpanah, M. Rabiee, and S. Arbab, “Poly (ε -caprolactone) Fiber : An Overview,” *J. Eng. Fiber. Fabr.*, vol. 9, no. 3, pp. 74–90, 2014, doi: 10.1177/155892501400900309.

[215] J. W. Crawford-Corrie, A., Buttle, D. J., Haycock, “Medical Implant,” WO 2017/017425 A1, 2017.

[216] Q. Yan, Y. Yin, and B. Li, “Use new PLGL-RGD-NGF nerve conduits for promoting peripheral nerve regeneration,” *Biomed. Eng. Online*, vol. 11, no. 36, pp. 1–16, 2012, doi: 10.1186/1475-925X-11-36.

[217] W. Zeng *et al.*, “Incorporation of chitosan microspheres into collagen-chitosan scaffolds for the controlled release of nerve growth factor,” *PLoS One*, vol. 9, no. 7, p. e101300, 2014, doi: 10.1371/journal.pone.0101300.

[218] C. A. Schneider, W. S. Rasband, and K. W. Eliceiri, “NIH Image to ImageJ : 25 years of image analysis,” *Nat. Methods*, vol. 9, no. 7, pp. 671–675, 2012, doi: 10.1038/nmeth.2089.

[219] S. Powell, A. Vinod, and M. L. Lemons, “Isolation and Culture of Dissociated Sensory Neurons From Chick Embryos,” *J. Vis. Exp.*, vol. 91, pp. 1–8, 2014, doi: 10.3791/51991.

[220] R. Kaewkhaw, A. M. Scutt, and J. W. Haycock, “Integrated culture and purification of rat Schwann cells from freshly isolated adult tissue,” *Nat. Protoc.*, vol. 7, no. 11, pp. 1996–2004, 2012, doi: 10.1038/nprot.2012.118.

[221] P. Preibish, Stephan., Saalfeld, Stephan., Tomancak, “Globally optimal stitching of tiled 3D microscopic image acquisitions,” *Bioinformatics*, vol. 25, no. 11, pp. 1463–1465, 2009, doi: 10.1093/bioinformatics/btp184.

[222] D. A. Puleo, R. A. Kissling, and M.-S. Sheu, “A technique to immobilize bioactive proteins, including bone morphogenetic protein-4 (BMP-4), on titanium alloy,” *Biomaterials*, vol. 23, pp. 2079–2087, 2002.

[223] T. Liu *et al.*, “Immobilization of heparin / poly- L -lysine nanoparticles on dopamine-coated surface to create a heparin density gradient for selective direction of platelet and vascular cells behavior,” *Acta Biomater.*, vol. 10, no. 5, pp. 1940–1954, 2014, doi: 10.1016/j.actbio.2013.12.013.

[224] S. Madduri, K. Feldman, T. Tervoort, M. Papaloïzos, and B. Gander, “Collagen nerve conduits releasing the neurotrophic factors GDNF and NGF,” *J. Control. Release*, vol. 143, no. 2, pp. 168–174, 2010, doi: 10.1016/j.jconrel.2009.12.017.

[225] T. M. Dinis *et al.*, “3D multi-channel bi-functionalized silk electrospun conduits for peripheral nerve regeneration,” *J. Mech. Behav. Biomed. Mater.*, vol. 41, pp. 43–55, 2015, doi: 10.1016/j.jmbbm.2014.09.029.

[226] J. Hu, L. Tian, M. P. Prabhakaran, X. Ding, and S. Ramakrishna, “Fabrication of nerve growth factor encapsulated aligned poly(ε-caprolactone) nanofibers and their assessment as a potential neural tissue engineering scaffold,” *Polymers (Basel).*, vol. 8, no. 54, 2016, doi: 10.3390/polym8020054.

[227] N. Gomez and C. E. Schmidt, “Nerve growth factor-immobilized polypyrrole: Bioactive electrically conducting polymer for enhanced neurite extension,” *J. Biomed. Mater. Res. Part A*, vol. 81, no. 1, pp. 135–149, 2007, doi: 10.1002/jbm.a.31047.

[228] M. Hajimiri, S. Shahverdi, G. Kamalinia, and R. Dinarvand, “Growth factor conjugation: Strategies and applications,” *J. Biomed. Mater. Res. - Part A*, vol. 103A, pp. 819–838, 2015, doi: 10.1002/jbm.a.35193.

[229] A. K. H. Achyuta, R. Cieri, K. Unger, and S. K. Murthy, “Synergistic effect of immobilized laminin and nerve growth factor on PC12 neurite outgrowth,” *Biotechnol. Prog.*, vol. 25, no. 1, pp. 227–234, 2009, doi: 10.1002/btpr.58.

[230] S. C. Hsieh *et al.*, “Comparison between two different methods of immobilizing NGF in poly(DL -lactic acid-co-glycolic acid) conduit for peripheral nerve regeneration by EDC/NHS/MES and genipin,” *J. Biomed. Mater. Res. - Part A*, vol. 99 A, no. 4, pp. 576–585, 2011, doi: 10.1002/jbm.a.33157.

[231] J. Y. Lee and C. E. Schmidt, “Amine-functionalized polypyrrole: Inherently cell adhesive conducting polymer,” *J. Biomed. Mater. Res. - Part A*, vol. 103, no. 6, pp. 2126–2132, 2015, doi: 10.1002/jbm.a.35344.

[232] D. Y. Kwok and A. W. Neumann, “Contact angle measurement and contact angle interpretation,” *Adv. Colloid Interface Sci.*, vol. 81, no. 3, pp. 167–249, 1999.

[233] E. L. Decker, B. Frank, Y. Suo, and S. Garoff, “Physics of contact angle measurement,” *Colloids Surfaces A Physicochem. Eng. Asp.*, vol. 156, no. 1–3, pp. 177–189, 1999, [Online]. Available: www.elsevier.nl/locate/colsurfa.

[234] K. D. B. John F. Moulder, Willian F. Stickle, Peter E. Sobol, *Handbook of X-*

ray Photoelectron Spectroscopy. Eden Prairie: Perkin-Elmer Corporation, 1992.

[235] A. Gao, F. Liu, and L. Xue, "Preparation and evaluation of heparin-immobilized poly (lactic acid) (PLA) membrane for hemodialysis," *J. Memb. Sci.*, vol. 452, pp. 390–399, 2014, doi: 10.1016/j.memsci.2013.10.016.

[236] H. J. Steffen, J. Schmidt, and A. Gonzalez-Elipe, "Biocompatible surfaces by immobilization of heparin on diamond-like carbon films deposited on various substrates," *Surf. Interface Anal.*, vol. 29, no. 6, pp. 386–391, 2000, doi: 10.1002/1096-9918(200006)29:6<386::AID-SIA882>3.0.CO;2-0.

[237] S. Wang, Y. Zhang, H. Wang, and Z. Dong, "Preparation, characterization and biocompatibility of electrospinning heparin-modified silk fibroin nanofibers," *Int. J. Biol. Macromol.*, vol. 48, no. 2, pp. 345–353, 2011, doi: 10.1016/j.ijbiomac.2010.12.008.

[238] A. Ogino, S. Noguchi, and M. Nagatsu, "Effect of plasma pretreatment on heparin immobilization on polymer sheet," *J. Photopolym. Sci. Technol.*, vol. 22, no. 4, pp. 461–466, 2009.

[239] J. H. Lee, H. W. Jung, I.-K. Kang, and H. B. Lee, "Cell behaviour on polymer surfaces with different functional groups," *Biomaterials*, vol. 15, no. 9, pp. 705–711, 1994, doi: 10.1016/0142-9612(94)90169-4.

[240] A. J. Beck *et al.*, "Plasma co-polymerisation of two strongly interacting monomers: Acrylic acid and allylamine," *Plasma Process. Polym.*, vol. 2, no. 8, pp. 641–649, 2005, doi: 10.1002/ppap.200500043.

[241] C. Dehili, P. Lee, K. M. Shakesheff, and M. R. Alexander, "Comparison of Primary Rat Hepatocyte Attachment to Collagen and Plasma-Polymerised Allylamine on Glass," *Plasma Process. Polym.*, vol. 3, no. 6–7, pp. 474–484, 2006, doi: 10.1002/ppap.200500169.

[242] P. Di Pietro *et al.*, "Immobilization of Neurotrophin Peptides on Gold Nanoparticles by Direct and Lipid-Mediated Interaction: A New Multipotential

Therapeutic Nanoplatform for CNS Disorders," *ACS Omega*, vol. 2, no. 8, pp. 4071–4079, 2017, doi: 10.1021/acsomega.7b00458.

[243] M. R. Koller, M. A. Palsson, I. Manchel, R. J. Maher, and B. Palsson, "Tissue culture surface characteristics influence the expansion of human bone marrow cells," *Biomaterials*, vol. 19, no. 21, pp. 1963–1972, 1998, doi: 10.1016/S0142-9612(98)00101-X.

[244] S. C. Baker *et al.*, "Characterisation of electrospun polystyrene scaffolds for three-dimensional in vitro biological studies," *Biomaterials*, vol. 27, no. 16, pp. 3136–3146, 2006, doi: 10.1016/j.biomaterials.2006.01.026.

[245] J. S. Stevens, C. R. Seabourne, C. Jaye, D. A. Fischer, A. J. Scott, and S. L. M. Schroeder, "Incisive probing of intermolecular interactions in molecular crystals: Core level spectroscopy combined with density functional theory," *J. Phys. Chem. B*, vol. 118, no. 42, pp. 12121–12129, 2014, doi: 10.1021/jp506983s.

[246] H. Begum, M. S. Ahmed, and S. Jeon, "New Approach for Porous Chitosan-Graphene Matrix Preparation through Enhanced Amidation for Synergic Detection of Dopamine and Uric Acid," *ACS Omega*, vol. 2, no. 6, pp. 3043–3054, 2017, doi: 10.1021/acsomega.7b00331.

[247] I. Kurylo *et al.*, "Characterization of peptide attachment on silicon nanowires by X-ray photoelectron spectroscopy and mass spectrometry," *Analyst*, vol. 142, no. 6, pp. 969–978, 2017, doi: 10.1039/c6an02588a.

[248] H. Chen, Y. Chen, H. Sheardown, and M. A. Brook, "Immobilization of heparin on a silicone surface through a heterobifunctional PEG spacer," *Biomaterials*, vol. 26, no. 35, pp. 7418–7424, 2005, doi: 10.1016/j.biomaterials.2005.05.053.

[249] M. V. Sefton *et al.*, "Does surface chemistry affect thrombogenicity of surface modified polymers?," *J. Biomed. Mater. Res.*, vol. 55, no. 4, pp. 447–459, 2001, doi: 10.1002/1097-4636(20010615)55:4<447::AID-JBM1036>3.0.CO;2-5.

[250] L. P. Zhu, J. Z. Yu, Y. Y. Xu, Z. Y. Xi, and B. K. Zhu, "Surface modification

of PVDF porous membranes via poly(DOPA) coating and heparin immobilization," *Colloids Surfaces B Biointerfaces*, vol. 69, no. 1, pp. 152–155, 2009, doi: 10.1016/j.colsurfb.2008.11.011.

[251] E. M. E. Kristensen, R. Larsson, J. Sánchez, H. Rensmo, U. Gelius, and H. Siegbahn, "Heparin coating durability on artificial heart valves studied by XPS and antithrombin binding capacity," *Colloids Surfaces B Biointerfaces*, vol. 49, no. 1, pp. 1–7, 2006, doi: 10.1016/j.colsurfb.2006.02.007.

[252] E. M. E. Kristensen, H. Rensmo, R. Larsson, and H. Siegbahn, "Characterization of heparin surfaces using photoelectron spectroscopy and quartz crystal microbalance," *Biomaterials*, vol. 24, no. 23, pp. 4153–4159, 2003, doi: 10.1016/S0142-9612(03)00297-7.

[253] A. P. Hopper *et al.*, "Amine functionalized nanodiamond promotes cellular adhesion, proliferation and neurite outgrowth," *Biomed. Mater.*, vol. 9, no. 4, p. 045009, 2014, doi: 10.1088/1748-6041/9/4/045009.

[254] W. Graisuwan *et al.*, "Multilayer film assembled from charged derivatives of chitosan: Physical characteristics and biological responses," *J. Colloid Interface Sci.*, vol. 376, pp. 177–188, 2012, doi: 10.1016/j.jcis.2012.02.039.

[255] X. H. Wang *et al.*, "Covalent immobilization of chitosan and heparin on PLGA surface," *Int. J. Biol. Macromol.*, 2003, doi: 10.1016/S0141-8130(03)00072-2.

[256] I.-K. Kang, O. H. Kwon, Y. M. Lee+, and Y. Kiel, "Preparation and surface characterization of functional group-grafted and heparin-immobilized polyurethanes by plasma glow discharge," *Biomaterials*, vol. 17, no. 8, pp. 841–847, 1996.

[257] M. F. Clark and A. . N. Adams, "Characteristics of the Microplate Method of Enzyme-Linked Immunosorbent Assay for the Detection of Plant Viruses," *J. Gen. Virol.*, vol. 34, no. 3, pp. 475–483, 1977.

[258] T. A. Kapur and M. S. Shoichet, "Chemically-bound nerve growth factor for neural tissue engineering applications," *J. Biomater. Sci. Polym. Ed.*, vol. 14,

no. 4, pp. 383–394, 2003.

[259] M. G. Haugh, M. J. Jaasma, and F. J. O'Brien, "The effect of dehydrothermal treatment on the mechanical and structural properties of collagen-GAG scaffolds," *J. Biomed. Mater. Part A Japanese Soc. Biomater. Aust. Soc. Biomater. Korean Soc. Biomater.*, vol. 89, no. 2, pp. 363–369, 2009.

[260] J.-Y. Lee, S.-M. Kim, M.-J. Kim, and J.-H. Lee, "Controlled release of nerve growth factor from heparin-conjugated fibrin gel within the nerve growth factor-delivering implant," *J. Korean Assoc. Oral Maxillofac. Surg.*, vol. 40, no. 1, pp. 3–10, 2014, doi: 10.5125/jkaoms.2014.40.1.3.

[261] L. Uebersax, M. Mattotti, H. P. Merkle, B. Gander, and L. Meinel, "Silk fibroin matrices for the controlled release of nerve growth factor (NGF)," *Biomaterials*, vol. 28, no. 30, pp. 4449–4460, 2007, doi: 10.1016/j.biomaterials.2007.06.034.

[262] Y. Naka, A. Kitazawa, Y. Akaishi, and N. Shimizu, "Neurite outgrowths of neurons using neurotrophin-coated nanoscale magnetic beads," *J. Biosci. Bioeng.*, vol. 98, no. 5, pp. 348–352, 2004, doi: 10.1016/S1389-1723(04)00294-4.

[263] K. Pal, A. T. Paulson, and D. Rousseau, "Biopolymers in Controlled-Release Delivery Systems," in *Handbook of Biopolymers and Biodegradable Plastics*, S. Ebnesajjad, Ed. William Andrew Publishing, 2013, pp. 329–363.

[264] K. Matsumoto, C. Sato, Y. Naka, A. Kitazawa, R. L. D. Whitby, and N. Shimizu, "Neurite outgrowths of neurons with neurotrophin-coated carbon nanotubes," *J. Biosci. Bioeng.*, vol. 103, no. 3, pp. 216–220, 2007, doi: 10.1263/jbb.103.216.

[265] T. H. Kim, S. H. Oh, D. B. An, J. Y. Lee, and J. H. Lee, "Dual growth factor immobilized microspheres for tissue reinnervation in vitro and preliminary in vivo studies," *J. Biomater. Sci. Polym. Ed.*, vol. 26, no. 5, pp. 322–337, 2015.

[266] S. O. Campbell, Mary, K., Farrel, "Amino acids and peptides," in *Biochemistry*,

6th ed., Belmont: Thomson/Brooks/Cole, 2008, pp. 73–76.

[267] G. Gigliobianco, C. K. Chong, and S. Macneil, “Simple surface coating of electrospun poly-L-lactic acid scaffolds to induce angiogenesis,” *J. Biomater. Appl.*, vol. 30, no. 1, pp. 50–60, 2015, doi: 10.1177/0885328215569891.

[268] C. Satriano *et al.*, “Neurotrophin-mimicking peptides at the biointerface with gold respond to copper ion stimuli,” *Phys. Chem. Chem. Phys.*, vol. 18, no. 44, pp. 30595–30604, 2016, doi: 10.1039/c6cp05476e.

[269] Q. Liu, J. Huang, H. Shao, L. Song, and Y. Zhang, “Dual-factor loaded functional silk fibroin scaffolds for peripheral nerve regeneration with the aid of neovascularization,” *RSC Adv.*, vol. 6, no. 9, pp. 7683–7691, 2016.

[270] G. P. Harper, R. W. Glanville, and H. Thoenen, “The Purification of Nerve Growth Factor from Bovine Seminal Plasma. Biochemical characterization and partial amino acid sequence,” *J. Biol. Chem.*, vol. 257, no. 14, pp. 8541–8548, 1982.

[271] R&D Systems, “Recombinant Rat beta-NGF Protein, CF,” 2020. https://www.rndsystems.com/products/recombinant-rat-beta-ngf-protein-cf_556-ng-cf (accessed May 29, 2020).

[272] R&D Systems, “Recombinant Human BDNF Protein, CF,” 2020. https://www.rndsystems.com/products/recombinant-human-bdnf-protein-cf_248-bd-cf (accessed May 29, 2020).

[273] D. P. Mascotti and T. M. Lohman, “Thermodynamics of Charged Oligopeptide-Heparin Interactions,” *Biochemistry*, vol. 34, no. 9, pp. 2908–2915, 1995, doi: 10.1021/bi00009a022.

[274] C. R. Wittmer *et al.*, “Multifunctionalized electrospun silk fibers promote axon regeneration in the central nervous system,” *Adv. Funct. Mater.*, vol. 21, no. 22, pp. 4232–4242, 2011.

[275] T. M. Dinis, G. Vidal, R. R. Jose, P. Vigneron, and D. Bresson, “Complementary Effects of Two Growth Factors in Multifunctionalized Silk

Nanofibers for Nerve Reconstruction," *PLoS One*, vol. 9, no. 10, p. e109770, 2014.

[276] M. Yamamoto, Y. Ikada, and Y. Tabata, "Controlled release of growth factors based on biodegradation of gelatin hydrogel," *J. Polym. Sci. Polym. Ed.*, vol. 12, no. 1, pp. 77–88, 2001.

[277] K. E. Neet and R. B. Campenot, "Receptor binding , internalization , and retrograde transport of neurotrophic factors," *Cell. Mol. Life Sci.*, vol. 58, pp. 1021–1035, 2001.

[278] C. Wiesmann and A. M. De Vos, "Nerve growth factor : structure and function," *Cell. Mol. Life Sci.*, vol. 58, pp. 748–759, 2001.

[279] R. C. Robinson *et al.*, "The structures of the neurotrophin 4 homodimer and the brain-derived neurotrophic factor 0 neurotrophin 4 heterodimer reveal a common Trk-binding site," *Protein Sci.*, vol. 8, pp. 2589–2597, 1999.

[280] M. Eng *et al.*, "Formulation Development and Primary Degradation Pathways for Recombinant Human Nerve Growth Factor," *Anal. Chem.*, vol. 69, no. 20, pp. 4184–4190, 1997, doi: 10.1021/ac9704016.

[281] X. M. Lam, E. T. Duenas, and J. L. Cleland, "Encapsulation and stabilization of nerve growth factor into poly(lactic-co-glycolic) acid microspheres," *J. Pharm. Sci.*, vol. 90, no. 9, pp. 1356–1365, 2001, doi: 10.1002/jps.1088.

[282] M. F. DeYoung, Linda R., Lam, Xanthe M., Nguyen, Tue H., Powell, "Stabilizing formulation for NGF," 2004.

[283] M. Polyakova, H. Schlögl, J. Sacher, and M. Schmidt-kassow, "Stability of BDNF in Human Samples Stored Up to 6 Months and Correlations of Serum and EDTA-Plasma Concentrations," *Int. J. Mol. Sci.*, vol. 18, no. 6, pp. 1–11, 2017, doi: 10.3390/ijms18061189.

[284] W. J. Callahan, L. O. Narhi, A. A. Kosky, and M. J. Treuheit, "Sodium Chloride Enhances the Storage and Conformational Stability of BDNF and PEG-BDNF," *Pharm. Res.*, vol. 18, no. 3, pp. 261–266, 2001.

[285] C. Deister and C. E. Schmidt, “Optimizing neurotrophic factor combinations for neurite outgrowth,” *J. Neural Eng.*, vol. 3, no. 2, pp. 172–179, 2006, doi: 10.1088/1741-2560/3/2/011.

[286] N. B. Fadia *et al.*, “Long-gap peripheral nerve repair through sustained release of a neurotrophic factor in nonhuman primates,” *Sci. Transl. Med.*, vol. 12, no. 527, 2020, doi: 10.1126/scitranslmed.aav7753.

[287] S. Madduri, M. Papaloïzos, and B. Gander, “Synergistic effect of GDNF and NGF on axonal branching and elongation in vitro,” *Neurosci. Res.*, vol. 65, no. 1, pp. 88–97, 2009, doi: 10.1016/j.neures.2009.06.003.

[288] A. Kishino *et al.*, “Analysis of effects and pharmacokinetics of subcutaneously administered BDNF,” *Neuroreport*, vol. 12, no. 5, pp. 1067–1072, 2001, doi: 10.1097/00001756-200104170-00040.

[289] R. Tria, M. A., Fusco, M., Vantini, G., Mariot, “Pharmacokinetics of Nerve Growth Factor (Ngf) Following Different Routes of Administration to Adult Rats,” *Exp. Neurol.*, vol. 127, pp. 178–183, 1994.

[290] K. Lee, E. A. Silva, and D. J. Mooney, “Growth factor delivery-based tissue engineering: general approaches and a review of recent developments,” *J. R. Soc. Interface*, vol. 8, pp. 153–170, 2011, doi: 10.1098/rsif.2010.0223.

[291] S. Tang, J. Zhu, Y. Xu, A. P. Xiang, M. H. Jiang, and D. Quan, “The effects of gradients of nerve growth factor immobilized PCLA scaffolds on neurite outgrowth invitro and peripheral nerve regeneration in rats,” *Biomaterials*, vol. 34, no. 29, pp. 7086–7096, 2013, doi: 10.1016/j.biomaterials.2013.05.080.

[292] S. H. Bhang *et al.*, “Enhanced nerve growth factor efficiency in neural cell culture by immobilization on the culture substrate,” *Biochem. Biophys. Res. Commun.*, vol. 382, no. 2, pp. 315–320, 2009, doi: 10.1016/j.bbrc.2009.03.016.

[293] G. Chen, Y. Ito, and Y. Imanishi, “Photo-immobilization of epidermal growth factor enhances its mitogenic effect by artificial juxtacrine signaling,” *Biochim. Biophys. Acta - Mol. Cell Res.*, vol. 1358, no. 2, pp. 200–208, 1997, doi:

10.1016/S0167-4889(97)00065-7.

[294] H. H. Oh, H. Lu, N. Kawazoe, and G. Chen, “Differentiation of PC12 cells in three-dimensional collagen sponges with micropatterned nerve growth factor,” *Biotechnol. Prog.*, 2012, doi: 10.1002/btpr.1520.

[295] P. Lequoy, F. Murschel, B. Liberelle, S. Lerouge, and G. De Crescenzo, “Controlled co-immobilization of EGF and VEGF to optimize vascular cell survival,” *Acta Biomater.*, vol. 29, pp. 239–247, 2016, doi: 10.1016/j.actbio.2015.10.026.

[296] M. I. Romero, N. Rangappa, L. Li, E. Lightfoot, M. G. Garry, and G. M. Smith, “Erratum: Extensive sprouting of sensory afferents and hyperalgesia induced by conditional expression of nerve growth factor in the adult spinal cord (Journal of Neuroscience (June 15, 2000) (4435-4445)),” *J. Neurosci.*, vol. 20, no. 22, pp. 4435–4445, 2000.

[297] C. M. A. P. Schuh, A. G. E. Day, H. Redl, and J. Phillips, “An Optimized Collagen-Fibrin Blend Engineered Neural Tissue Promotes Peripheral Nerve Repair,” *Tissue Eng. - Part A*, vol. 24, no. 17–18, pp. 1332–1340, 2018, doi: 10.1089/ten.tea.2017.0457.

[298] V. Melissinaki *et al.*, “Direct laser writing of 3D scaffolds for neural tissue engineering applications,” *Biofabrication*, vol. 3, no. 4, p. 045005, 2011, doi: 10.1088/1758-5082/3/4/045005.

[299] P. L. Lai *et al.*, “Neurotrophic properties of the lion’s mane medicinal mushroom, Hericium erinaceus (Higher Basidiomycetes) from Malaysia,” *Int. J. Med. Mushrooms*, vol. 15, no. 6, pp. 539–554, 2013, doi: 10.1615/IntJMedMushr.v15.i6.30.

[300] D. Rasouly *et al.*, “Staurosporine induces neurite outgrowth in neuronal hybrids (PC12EN) lacking NGF receptors,” *J. Cell. Biochem.*, vol. 62, no. 3, pp. 356–371, 1996, doi: 10.1002/(SICI)1097-4644(199609)62:3<356::AID-JCB6>3.0.CO;2-Q.

[301] A. H. S. Hassan, O. F. X. Almeida, C. Gramsch, and A. Herz, "Immunocytochemical demonstration of opioid receptors in selected rat brain areas and neuroblastoma × glioma hybrid (NG108-15) cells using a monoclonal anti-idiotypic antibody," *Neuroscience*, vol. 32, no. 1, pp. 269–278, 1989, doi: 10.1016/0306-4522(89)90126-7.

[302] G. Guroff, "PC12 cells as a model of neuronal differentiation," in *Cell culture in the neuroscience*, G. Bottenstein, J. E. and Sato, Ed. New York: Plenum Press, 1985, pp. 245–272.

[303] D. G. Drubin, S. C. Feinstein, E. M. Shooter, and M. W. Kirschner, "Nerve Growth Factor-induced Neurite Outgrowth in PC12 Cells Involves the Coordinate Induction of Microtubule Assembly and Assembly-promoting Factors," *J. Cell Biol.*, vol. 101, pp. 1799–1807, 1985.

[304] Q. Wu, J. Song, D. Meng, and Q. Chang, "TPPU, a sEH Inhibitor, Attenuates Corticosterone-Induced PC12 Cell Injury by Modulation of BDNF-TrkB Pathway," *J. Mol. Neurosci.*, vol. 67, no. 3, pp. 364–372, 2019, doi: 10.1007/s12031-018-1230-z.

[305] J.-M. Jiang *et al.*, "BDNF-TrkB Pathway Mediates Neuroprotection of Hydrogen Sulfide against Formaldehyde-Induced Toxicity to PC12 Cells," *PLoS One*, vol. 10, no. 3, p. e0119478, 2015, doi: 10.1371/journal.pone.0119478.

[306] Y. Iwasaki, M. Ishikawa, N. Okada, and S. Koizumi, "Induction of a Distinct Morphology and Signal Transduction in TrkB/PC12 Cells by Nerve Growth Factor and Brain-Derived Neurotrophic Factor," *J. Neurochem.*, vol. 68, no. 3, pp. 927–934, 2002.

[307] Y. S. Kang *et al.*, "Visfatin induces neurite outgrowth in PC12 cells via ERK1/2 signaling pathway," *Neurosci. Lett.*, vol. 504, no. 2, pp. 121–126, Oct. 2011, doi: 10.1016/j.neulet.2011.09.014.

[308] C. Cunha *et al.*, "Neurobiology of Disease Brain-derived neurotrophic factor (BDNF) overexpression in the forebrain results in learning and memory

impairments," *Neurobiol. Dis.*, vol. 33, no. 3, pp. 358–368, 2009, doi: 10.1016/j.nbd.2008.11.004.

[309] Y. Z. Zhang, D. B. Moheban, B. R. Conway, A. Bhattacharyya, and R. A. Segal, "Cell surface Trk receptors mediate NGF-Induced survival while internalized receptors regulate NGF-Induced differentiation," *J. Neurosci.*, vol. 20, no. 15, pp. 5671–5678, 2000.

[310] D. Vaudry, P. J. S. Stork, P. Lazarovici, and L. E. Eiden, "Signaling pathways for PC12 cell differentiation: Making the right connections," *Science (80-.).*, vol. 296, no. 5573, pp. 1648–1649, 2002, doi: 10.1126/science.1071552.

[311] T. Singh, D. Robles, and M. Vazquez, "Neuronal substrates alter the migratory responses of nonmyelinating Schwann cells to controlled brain-derived neurotrophic factor gradients," *J. Tissue Eng. Regen. Med.*, vol. 14, no. 4, pp. 609–621, 2020, doi: 10.1002/term.3025.

[312] X. Tang, Y. Wang, S. Zhou, T. Qian, and X. Gu, "Signaling pathways regulating dose-dependent dual effects of TNF-α on primary cultured Schwann cells," *Mol. Cell. Biochem.*, vol. 378, no. 1–2, pp. 237–246, 2013, doi: 10.1007/s11010-013-1614-x.

[313] J. Yamauchi, J. R. Chan, and E. M. Shooter, "Neurotrophins regulate Schwann cell migration by activating divergent signaling pathways dependent on Rho GTPases," *Proc. Natl. Acad. Sci. U. S. A.*, vol. 101, no. 23, pp. 8774–8779, 2004, doi: 10.1073/pnas.0402795101.

[314] T. Ren, S. Yu, Z. Mao, and C. Gao, "A complementary density gradient of zwitterionic polymer brushes and NCAM peptides for selectively controlling directional migration of Schwann cells," *Biomaterials*, vol. 56, pp. 58–67, 2015, doi: 10.1016/j.biomaterials.2015.03.052.

[315] S. P. Frostick, Q. Yin, and G. J. Kemp, "Schwann cells, neurotrophic factors, and peripheral nerve regeneration," *Microsurgery*, vol. 18, no. 7, pp. 397–405, 1998, doi: 10.1002/(SICI)1098-2752(1998)18:7<397::AID-MICR2>3.0.CO;2-F.

[316] S. Maniwa, A. Iwata, H. Hirata, and M. Ochi, “Effects of neurotrophic factors on chemokinesis of Schwann cells in culture,” *Scand. J. Plast. Reconstr. Surg. Hand Surg.*, vol. 37, no. 1, pp. 14–17, 2003, doi: 10.1080/alp.37.1.14.17.

[317] S. Yi *et al.*, “Regulation of Schwann cell proliferation and migration by MIR-1 targeting brain-derived neurotrophic factor after peripheral nerve injury,” *Sci. Rep.*, vol. 6, no. 1, pp. 1–10, 2016, doi: 10.1038/srep29121.

[318] J. Yamauchi, J. R. Chan, and E. M. Shooter, “Neurotrophin 3 activation of TrkC induces Schwann cell migration through the c-Jun N-terminal kinase pathway,” *Proc. Natl. Acad. Sci.*, vol. 100, no. 24, pp. 14421–14426, 2003, [Online]. Available: www.pnas.orgcgidoi10.1073pnas.2336152100.

[319] T. A. Kapur and M. S. Shoichet, “Immobilized concentration gradients of nerve growth factor guide neurite outgrowth,” *J. Biomed. Mater. Res. - Part A*, vol. 68, no. 2, pp. 235–243, 2004, doi: 10.1002/jbm.a.10168.

[320] T. H. Kim, S. H. Oh, D. B. An, J. Y. Lee, and J. H. Lee, “Dual growth factor-immobilized microspheres for tissue reinnervation: In vitro and preliminary in vivo studies,” *J. Biomater. Sci. Polym. Ed.*, vol. 26, no. 5, pp. 322–337, 2015, doi: 10.1080/09205063.2015.1008882.

[321] T. B. Kuhn, E. T. Stoeckli, M. A. Condrau, F. G. Rathjen, and P. Sonderegger, “Neurite outgrowth on immobilized axonin-1 is mediated by a heterophilic interaction with L1(G4),” *J. Cell Biol.*, vol. 115, no. 4, pp. 1113–1126, 1991, doi: 10.1083/jcb.115.4.1113.

[322] E. T. Stoeckli, T. B. Kuhn, C. O. Duc, M. A. Ruegg, and P. Sonderegger, “The axonally secreted protein axonin-1 is a potent substratum for neurite growth,” *J. Cell Biol.*, vol. 112, no. 3, pp. 449–455, 1991, doi: 10.1083/jcb.112.3.449.

[323] E. T. Stoeckli, P. F. Lemkin, T. B. Kuhm, M. A. Ruegg, M. Heller, and P. Sonderegger, “Identification of proteins secreted from axons of embryonic dorsal-root-ganglia neurons,” *Eur. J. Biochem.*, vol. 180, no. 2, pp. 249–258, 1989, doi: 10.1111/j.1432-1033.1989.tb14640.x.

[324] S. B. McMahon, M. P. Armanini, L. H. Ling, and H. S. Phillips, “Expression and coexpression of Trk receptors in subpopulations of adult primary sensory neurons projecting to identified peripheral targets,” *Neuron*, vol. 12, no. 5, pp. 1161–1171, 1994, doi: 10.1016/0896-6273(94)90323-9.

[325] M. Liefner, H. Siebert, T. Sachse, U. Michel, G. Kollias, and W. Bruck, “The role of TNF-a during Wallerian degeneration,” *J. Neuroimmunol.*, vol. 108, no. 1–2, pp. 147–152, 2000, [Online]. Available: www.elsevier.com/locate/jneuroin.

[326] Y. Qin, C. Cheng, H. Wang, X. Shao, Y. Gao, and A. Shen, “TNF-α as an autocrine mediator and its role in the activation of Schwann cells,” *Neurochem. Res.*, vol. 33, no. 6, pp. 1077–1084, 2008, doi: 10.1007/s11064-007-9552-1.

[327] T. Tao *et al.*, “Tumor necrosis factor-alpha inhibits Schwann cell proliferation by up-regulating Src-suppressed protein kinase C substrate expression,” *J. Neurochem.*, vol. 111, no. 3, pp. 647–655, 2009, doi: 10.1111/j.1471-4159.2009.06346.x.

[328] M. Cornejo *et al.*, “Effect of NRG1, GDNF, EGF and NGF in the migration of a Schwann cell precursor line,” *Neurochem. Res.*, vol. 35, no. 10, pp. 1643–1651, 2010, doi: 10.1007/s11064-010-0225-0.

[329] E. S. Anton, G. Weskampt, L. F. Reichardt, and W. D. Matthew, “Nerve growth factor and its low-affinity receptor promote Schwann cell migration (neurotrophins/peripheral nerve/glial cell/motit),” *Proc. Nati. Acad. Sci. USA*, vol. 91, no. 7, pp. 2795–2799, 1994.

[330] L. Cao *et al.*, “Olfactory ensheathing cells promote migration of Schwann cells by secreted nerve growth factor,” *Glia*, vol. 55, no. 9, pp. 897–904, 2007, doi: 10.1002/glia.20511.

[331] X. Hou, Q. Liang, and Y. Wu, “Transplantation of Schwann cells co-cultured with brain-derived neurotrophic factor for the treatment of experimental autoimmune neuritis,” *J. Neuroimmunol.*, vol. 263, no. 1–2, pp. 83–90, 2013, doi: 10.1016/j.jneuroim.2013.08.004.

[332] O. S. Manoukian, M. R. Arul, S. Rudraiah, and I. Kalajzic, “Aligned microchannel polymer-nanotube composites for peripheral nerve regeneration : Small molecule drug delivery,” *J. Control. Release*, vol. 296, pp. 54–67, 2019, doi: 10.1016/j.jconrel.2019.01.013.

[333] J. Xie, W. Liu, M. R. Macewan, P. C. Bridgman, and Y. Xia, “Neurite outgrowth on electrospun nanofibers with uniaxial alignment: The effects of fiber density, surface coating, and supporting substrate,” *ACS Nano*, vol. 8, no. 2, pp. 1878–1885, 2014, doi: 10.1021/nn406363j.

[334] K. Chwalek, Y. Dening, C. Hinüber, H. Brünig, M. Nitschke, and C. Werner, “Providing the right cues in nerve guidance conduits: Biofunctionalization versus fiber profile to facilitate oriented neuronal outgrowth,” *Mater. Sci. Eng. C*, vol. 61, pp. 466–472, 2016, doi: 10.1016/j.msec.2015.12.059.

[335] V. Guenard, N. Kleitman, T. K. Morrissey, R. P. Bunge, and P. Aebischer, “Syngeneic Schwann cells derived from adult nerves seeded in semipermeable guidance channels enhance peripheral nerve regeneration,” *J. Neurosci.*, vol. 12, no. 9, pp. 3310–3320, 1992.

[336] A. Hurtado *et al.*, “Robust CNS regeneration after complete spinal cord transection using aligned poly-l-lactic acid microfibers,” *Biomaterials*, vol. 32, no. 26, pp. 6068–6079, 2011, doi: 10.1016/j.biomaterials.2011.05.006.

[337] Y. Kim, V. K. Haftel, S. Kumar, and R. V. Bellamkonda, “The role of aligned polymer fiber-based constructs in the bridging of long peripheral nerve gaps,” *Biomaterials*, vol. 29, no. 21, pp. 3117–3127, 2008, doi: 10.1016/j.biomaterials.2008.03.042.

[338] M. K. Horne, D. R. Nisbet, J. S. Forsythe, and C. L. Parish, “Three-Dimensional Nanofibrous Scaffolds Incorporating Immobilized BDNF Promote Proliferation and Differentiation of Cortical Neural Stem Cells,” *Stem Cells Dev.*, vol. 19, no. 6, pp. 843–852, 2010, doi: 10.1089/scd.2009.0158.

[339] H. M. Kaplan, P. Mishra, and J. Kohn, “The overwhelming use of rat models in nerve regeneration research may compromise designs of nerve guidance

conduits for humans," *J. Mater. Sci. Mater. Med.*, vol. 26, no. 8, p. 226, Aug. 2015, doi: 10.1007/s10856-015-5558-4.

[340] S. M. Willerth and S. E. Sakiyama-Elbert, "Approaches to neural tissue engineering using scaffolds for drug delivery," *Adv. Drug Deliv. Rev.*, vol. 59, no. 4–5, pp. 325–338, 2007, doi: 10.1016/j.addr.2007.03.014.

[341] N. Recek *et al.*, "Protein adsorption on various plasma-treated polyethylene terephthalate substrates," *Molecules*, vol. 18, no. 10, pp. 12441–12463, 2013, doi: 10.3390/molecules181012441.

[342] M. Lehocký *et al.*, "Plasma surface modification of polyethylene," *Colloids Surfaces A Physicochem. Eng. Asp.*, vol. 222, no. 1–3, pp. 125–131, 2003, doi: 10.1016/S0927-7757(03)00242-5.

[343] G. Yazgan *et al.*, "Steering surface topographies of electrospun fibers: Understanding the mechanisms," *Sci. Rep.*, vol. 7, no. 1, pp. 1–13, 2017, doi: 10.1038/s41598-017-00181-0.

[344] L. A. Can-Herrera, A. Ávila-Ortega, S. de la Rosa-García, A. I. Oliva, J. V. Cauich-Rodríguez, and J. M. Cervantes-Uc, "Surface modification of electrospun polycaprolactone microfibers by air plasma treatment: Effect of plasma power and treatment time," *Eur. Polym. J.*, vol. 84, pp. 502–513, 2016, doi: 10.1016/j.eurpolymj.2016.09.060.

[345] T. Jacobs, N. De Geyter, R. Morent, T. Desmet, P. Dubruel, and C. Leys, "Plasma treatment of polycaprolactone at medium pressure," *Surf. Coatings Technol.*, vol. 205, no. SUPPL. 2, pp. S543–S547, 2011, doi: 10.1016/j.surfcoat.2011.02.012.

[346] N. Recek *et al.*, "Cell Adhesion on Polycaprolactone Modified by Plasma Treatment," *Int. J. Polym. Sci.*, vol. 2016, 2016, doi: 10.1155/2016/7354396.

[347] N. E. Zander, J. A. Orlicki, A. M. Rawlett, and T. P. Beebe, "Quantification of protein incorporated into electrospun polycaprolactone tissue engineering scaffolds," *ACS Appl. Mater. Interfaces*, vol. 4, no. 4, pp. 2074–2081, 2012,

doi: 10.1021/am300045y.

[348] H. B. Wang, M. E. Mullins, J. M. Cregg, C. W. McCarthy, and R. J. Gilbert, “Varying the diameter of aligned electrospun fibers alters neurite outgrowth and Schwann cell migration,” *Acta Biomater.*, vol. 6, no. 8, pp. 2970–2978, 2010, doi: 10.1016/j.actbio.2010.02.020.

[349] X. Wen and P. A. Tresco, “Effect of filament diameter and extracellular matrix molecule precoating on neurite outgrowth and Schwann cell behavior on multifilament entubulation bridging device in vitro,” *J. Biomed. Mater. Res. - Part A*, vol. 76, no. 3, pp. 626–637, 2006, doi: 10.1002/jbm.a.30520.

[350] V. Karageorgiou and D. Kaplan, “Porosity of 3D biomaterial scaffolds and osteogenesis,” *Biomaterials*, vol. 26, no. 27, pp. 5474–5491, 2005, doi: 10.1016/j.biomaterials.2005.02.002.

[351] M. F. Meek and J. H. Coert, “US Food and Drug Administration / Conformit Europe-Approved Absorbable Nerve Conduits for Clinical Repair of Peripheral and Cranial Nerves,” *Ann. Plast. Surg.*, vol. 60, no. 1, pp. 110–116, 2008, doi: 10.1097/SAP.0b013e31804d441c.

[352] W. S. Ramsey, W. Hertl, E. D. Nowlan, and N. J. Binkowski, “Surface Treatments and Cell Attachment,” *In Vitro*, vol. 20, no. 10, pp. 802–808, 1984, doi: 10.1007/BF02618296.

[353] N. Rangappa, A. Romero, K. D. Nelson, R. C. Eberhart, and G. M. Smith, “Laminin-coated poly(L-lactide) filaments induce robust neurite growth while providing directional orientation,” *J. Biomed. Mater. Res.*, vol. 51, no. 4, pp. 625–634, 2000, doi: 10.1002/1097-4636(20000915)51:4<625::AID-JBM10>3.0.CO;2-U.

[354] H. Shen, X. Hu, J. Bei, and S. Wang, “The immobilization of basic fibroblast growth factor on plasma-treated poly (lactide- co -glycolide),” *Biomaterials*, vol. 29, no. 15, pp. 2388–2399, 2008, doi: 10.1016/j.biomaterials.2008.02.008.

[355] C. Charbonneau, J. Ruiz, P. Lequoy, G. De Crescenzo, M. R. Wertheimer, and

S. Lerouge, “Chondroitin Sulfate and Epidermal Growth Factor Immobilization after Plasma Polymerization : A Versatile Anti-Apoptotic Coating to Promote Healing Around Stent Grafts,” *Macromol. Biosci.*, vol. 12, no. 6, pp. 812–821, 2012, doi: 10.1002/mabi.201100447.

[356] T. R. Gengenbach and H. J. Griesser, “Aging of 1,3-Diaminopropane Plasma-Deposited Polymer Films: Mechanisms and Reaction Pathways,” *J. Polym. Sci. Part A Polym. Chem.*, vol. 37, no. 13, pp. 2191–2206, 1999, doi: 10.1002/(SICI)1099-0518(19990701)37:13<2191::AID-POLA34>3.0.CO;2-F.

[357] T. R. Gengenbach, R. C. Chatelier, and H. J. Griesser, “Characterization of the ageing of plasma-deposited polymer films: Global analysis of X-ray photoelectron spectroscopy data,” *Surf. Interface Anal.*, vol. 24, no. 4, pp. 271–281, 1996, doi: 10.1002/(SICI)1096-9918(199604)24:4<271::AID-SIA116>3.0.CO;2-J.

[358] T. R. Gengenbach, R. C. Chatelier, and H. J. Griesser, “Correlation of the nitrogen 1s and oxygen 1s XPS binding energies with compositional changes during oxidation of ethylene diamine plasma polymers,” *Surf. Interface Anal.*, vol. 24, no. 9, pp. 611–619, 1996, doi: 10.1002/(SICI)1096-9918(19960916)24:9<611::AID-SIA169>3.0.CO;2-7.

[359] B. N. Johnson *et al.*, “3D Printed Anatomical Nerve Regeneration Pathways,” *Adv. Funct. Mater.*, vol. 25, no. 39, pp. 6205–6217, 2015, doi: 10.1002/adfm.201501760.

[360] H. Fujimaki *et al.*, “Oriented collagen tubes combined with basic fibroblast growth factor promote peripheral nerve regeneration in a 15 mm sciatic nerve defect rat model,” *J. Biomed. Mater. Res. - Part A*, vol. 105, no. 1, pp. 8–14, 2017, doi: 10.1002/jbm.a.35866.

[361] C. Cheng and D. W. Zochodne, “In vivo proliferation, migration and phenotypic changes of schwann cells in the presence of myelinated fibers,” *Neuroscience*, vol. 115, no. 1, pp. 321–329, 2002, doi: 10.1016/S0306-

4522(02)00291-9.

[362] F. Gisbert Roca, F. M. André, J. Más Estellés, M. Monleón Pradas, L. M. Mir, and C. Martínez-Ramos, “BDNF-Gene Transfected Schwann Cell-Assisted Axonal Extension and Sprouting on New PLA–PPy Microfiber Substrates,” *Macromol. Biosci.*, p. 2000391, 2021, doi: 10.1002/mabi.202000391.

[363] K. Kimpinski, R. B. Campenot, and K. Mearow, “Effects of the neurotrophins nerve growth factor, neurotrophin-3, and brain-derived neurotrophic factor (BDNF) on neurite growth from adult sensory neurons in compartmented cultures,” *J. Neurobiol.*, vol. 33, no. 4, pp. 395–410, 1997, doi: 10.1002/(SICI)1097-4695(199710)33:4<395::AID-NEU5>3.0.CO;2-5.

Appendix

Table 20. List of reagents used with information about supplier and catalogue number.

Reagent/Product	Abbreviation	Brand/Supplier	Catalogue no.
Dulbecco's Modified Eagle's Medium	DMEM	Sigma, United Kingdom	6546
Foetal bovine serum	FBS	Pan, Biotech	P30-3033
L-glutamine	--	Sigma, United Kingdom	G5792
Penicillin-streptomycin	P/S	Sigma, United Kingdom	P0781
Amphotericin B	--	Sigma, United Kingdom	A2942
MEM Eagle D-Valine	--	USBiological Life Sciences, USA	38210000
N2 supplement	N2	Invitrogen, United Kingdom	17502001
Bovine pituitary extract	--	Invitrogen, United Kingdom	02-104
Forskolin	--	Sigma, United Kingdom	F3917
Heparin sodium salt from porcine intestinal mucosa	Heparin	Sigma, United Kingdom	H3393
Phosphate buffered saline	PBS	Oxoid, United Kingdom	BR0014G
0.2 µm pore size filter (Filtropur S)	--	Sarstedt AG & Co. KG, Germany	83.1826.001
Recombinant rat β-Nerve growth factor	NGF	R&D systems, United Kingdom	556-NG/CF

Recombinant human/mouse/rat Brain derived neurotrophic factor	BDNF	R&D systems, United Kingdom	248-BD/CF
1 mL syringe	--	Beckton Dickinson, United Kingdom	309628
20-gauge needle, 1 inch long	--	Fisnar, USA	8001098
NGF ELISA Kit (DuoSet Rat βNGF)	--	R&D systems, United Kingdom	DY556
BDNF ELISA Kit (DuoSet Human/Mouse BDNF)	--	R&D systems, United Kingdom	DY248
DuoSet Ancillary reagent kit 2 for ELISA	--	R&D systems, United Kingdom	DY008
NG108-15 neuronal cell line	--	ECACC, United Kingdom	88112302
PC12 adh neuronal cell line	--	ATCC, USA	CRL-1721.1
Trypsin/EDTA	--	Sigma, United Kingdom	T3924
Dimethylsulfoxide	DMSO	Alfa Aesar, United Kingdom	36480
CellTiter 96® AQ_{ueous} One Solution Cell Proliferation Assay	--	Promega, United Kingdom	G3580
Formaldehyde	FA	Sigma-Aldrich, United Kingdom	F8775
Triton X-100	--	Fisher Scientific, United Kingdom	BP151
4′,6-diamidino-2-phenylindole	DAPI	Sigma, United Kingdom	D8417

Phalloidin–Tetramethyl rhodamine B isothiocyanate	Phalloidin TRITC	Sigma-Aldrich, United Kingdom	P1951
Human recombinant Tumor Necrosis Factor-α	TNF- α	Sigma, United Kingdom	T6674
Mouse anti-βIII tubulin monoclonal antibody	--	Abcam, United Kingdom	Ab7751
Rabbit anti- S100-β polyclonal antibody	--	Dako, USA	Z5116
Alexa Fluor 488 goat anti-mouse	--	Life technologies, USA	A11001
Alexa Fluor 546 goat anti-rabbit	-	Life technologies, USA	A11010
Bovine serum albumin	BSA	Sigma, United Kingdom	A7030
Polycaprolactone	PCL	Aldrich, United Kingdom	440744
Dichloromethane	DCM	Fisher Scientific, United Kingdom	10127611
Allylamine	Aam	Aldrich, United Kingdom	145831
Crystal violet	--	Sigma, United Kingdom	C6158
Ethanol	--	Fisher Scientific, United Kingdom	E/0600DF/17
Acetic acid	--	Fisher Scientific, United Kingdom	A/0360/PB17
Toluidine blue powder	TBO	Sigma-Aldrich, United Kingdom	T3260
Hydrochloric acid	HCl	Fisher Scientific, United Kingdom	A481-2112

Sodium hydroxide	NaOH	Sigma-Aldrich, United Kingdom	221455

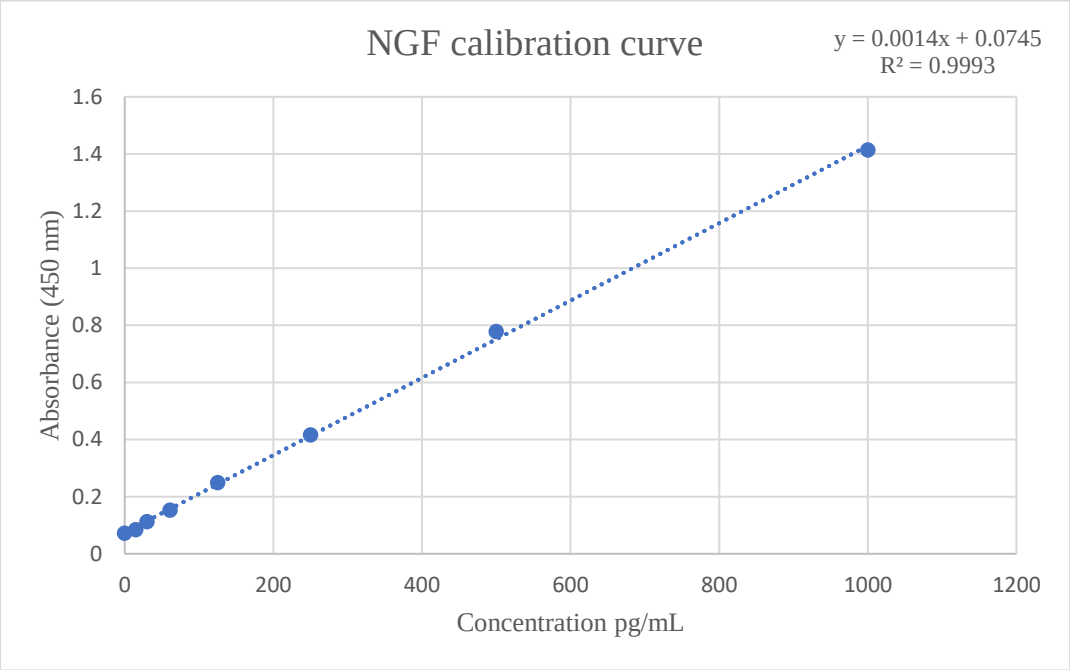

Figure 132. ELISA NGF calibration curve for the quantification of NGF.

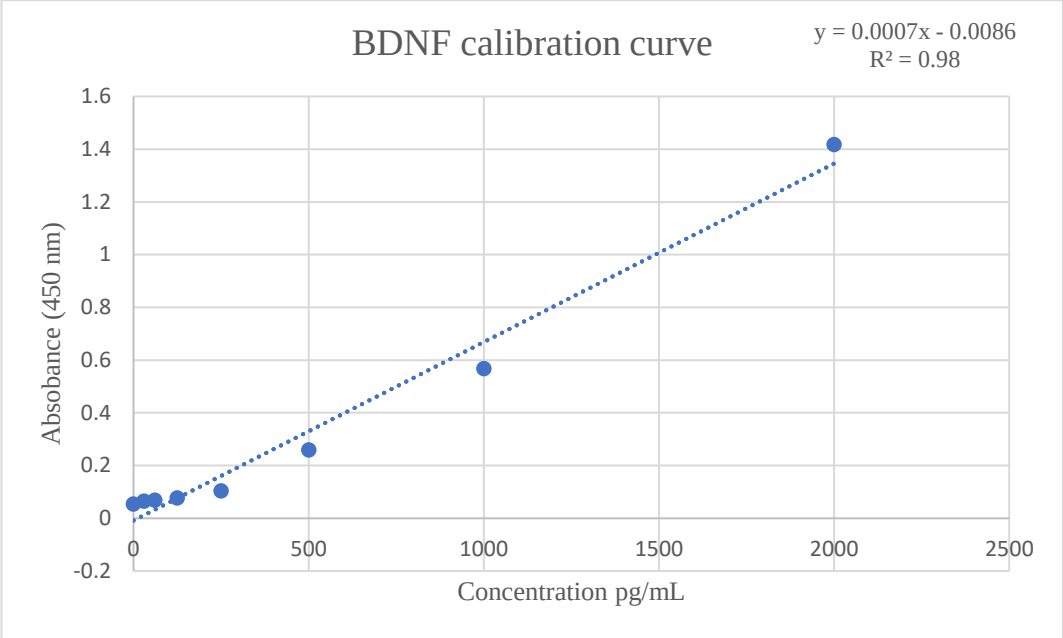

Figure 133. ELISA BDNF calibration curve for the quantification of BDNF.

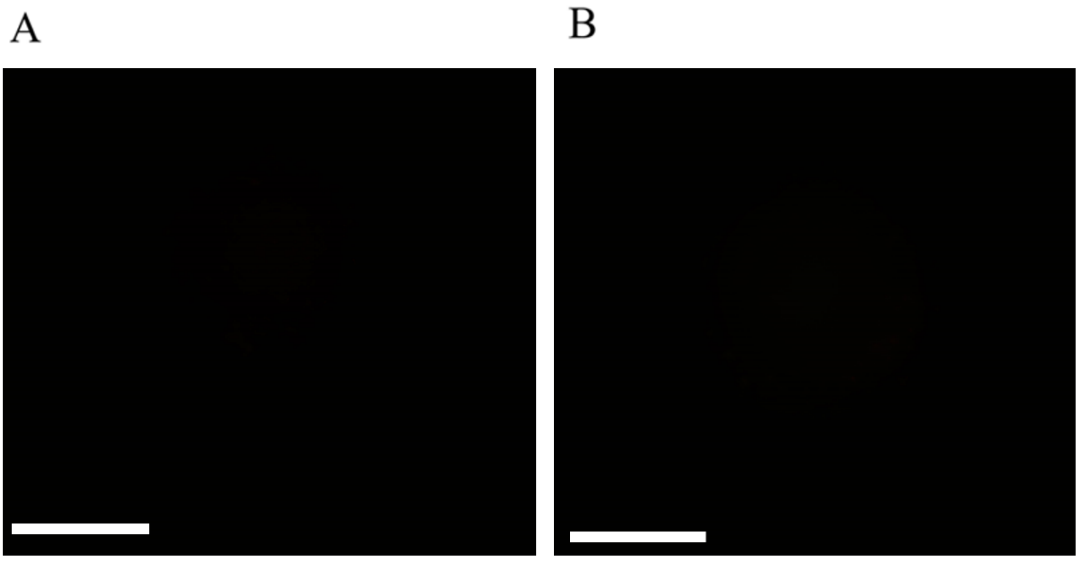

Figure 134. Secondary antibody control groups A) DRG without secondary antibody, and B) DRG with secondary antibody. Scalebar= 200 µm.

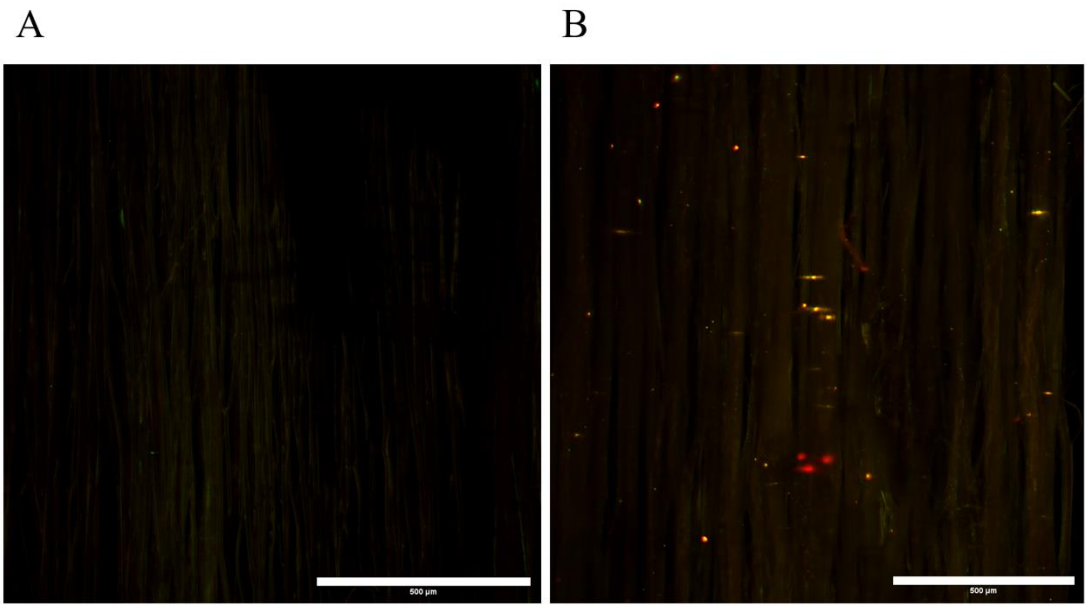

Figure 135. Secondary antibody control groups A) PCL + NH2+ scaffold, and B) PCL + NH2+ + Heparin + Immobilised BDNF scaffold. Scalebar= 500 µm.